

**THIRD-ORDER NONLINEAR OPTICAL STUDIES
OF NOVEL Zn(II) METALLOPORPHYRIN
COORDINATION COMPLEXES AND
BENZO[C]CINNOLINE-CONSISTING COPOLYMERS**

TEO TANG LIN
(B.Sc.(Hons.), NUS)

**A THESIS SUBMITTED
FOR THE DEGREE OF DOCTOR OF PHILOSOPHY
DEPARTMENT OF CHEMISTRY
NATIONAL UNIVERSITY OF SINGAPORE**

2007

ACKNOWLEDGEMENT

This thesis is the result of four years of work whereby I have been accompanied and supported by many people. It is a pleasant aspect that I have now the opportunity to express my gratitude to all of them.

First, let me thank my supervisor, Assoc. Prof. Lai Yee Hing, for giving me an opportunity to be a part of this challenging research project. His advices and constant help kept me moving forward. My co-supervisor, Dr Chen Zhikuan, is always available when I needed advice. Our research collaborators, Dr Marek Samoc and wife, Dr Anna Samoc, for giving me the invaluable opportunity to carry out nonlinear optical measurements at the Australian National University. I am fortunate to grow and develop my research skills under the guidance of these established scientists who have shown immense patience, intellectual guidance, enthusiasm and integral view on research.

I am greatly indebted to the staff of the Chemical, Molecular and Materials Analysis Centre (CMMAC) and laboratory officers of the Chemistry Department for their assistance in various analyses as well as loan of instruments.

Special thanks to my seniors and colleagues in the Department of Chemistry, Mr Cai Liping, Mr Fang Zhen, Mr Lu Yong, Dr Wang Weiling, Dr Vetrichelvan M., Mr Adrian Mak, Ms Junie Tok, Ms Pamela Oon and Mr Wee Chorng Shin. I will always remember the days when we sweat together in the laboratory, the fun, laughter and tears we shed together. I would like to specially thank my senior Dr Wang Fuke for his encouragement, inspirational ideas and for vetting my thesis.

My thanks goes to colleagues in the Institute of Materials Research and Engineering, Ms Su Siew Ping, Ms Chang Soon Yee, Mr Huang Chun, Ms Meili, Mr Zhen Changgua and Ms Yao Junhong for their assistance and generosity in the usage of the sophisticated instruments in the institute as well as for making me feel welcomed in the group.

I would also like to thank my group of close friends who kept me sane during this enduring period. They are Boon Jong, Glenn, Jiangwei, Yew Keong, Guofeng, Felicia, Chang Hong, Ming Hwee, Daniel, Tze Han, Joanna, Guowei and Benjamin.

I am grateful to my parents, grandmother, twin sister Jamie and best friend, Pang Cheng Wan for their unconditional love, support, encouragement and for keeping me spiritually, emotionally, physically and mentally sound.

Last but not least, I am grateful to the Agency for Science, Technology and Research (A*STAR) for awarding me the A*STAR Graduate Fellowship throughout the 4 years of postgraduate studies and the Ang Kok Peng Memorial Fund Committee for the award during my overseas attachment to the ANU.

TABLE OF CONTENTS

Acknowledgement.....	i
Table of Contents.....	iii
List of Abbreviations.....	xi
Summary.....	xviii
List of Figures.....	xxi
List of Scheme.....	xxvii
List of Tables.....	xxix
Chapter 1: Porphyrins and Metalloporphyrins.....	1
1.0 Introduction	1
1.1.0 Porphyrins	4
1.1.1 General Chemistry of Porphyrins	4
1.1.2 Synthesis of Porphyrins	6
1.2 Multiporphyrin Arrays	8
1.3 Porphyrin as Nonlinear Optical Limiting Materials	10
1.4 Importance of Porphyrin as Third-Order Nonlinear Optical Limiting Materials	15
1.5 References	20
Chapter 2: Elements of the Theory of Nonlinear Optics.....	29
2.0 Introduction	29
2.1 Principles and Origin of Nonlinear Optics	30
2.2 Nonlinear Index of Refraction	33

2.3.0	Introduction to Two-Photon Absorption	35
2.3.1	Two-Photon Absorption: the Main Concepts and Theoretical Considerations	39
2.3.2	Single Beam Two-Photon Absorption	42
2.3.3	Parity Selection rule for Two-Photon Transitions	43
2.4	Excited State Absorption	45
2.5	References	48

Chapter 3: The Z-Scan and Degenerate Four-Wave Mixing Techniques.....52

3.0	Transmission Measurements	52
3.1.0	The Z-Scan Technique	52
3.1.1	Advantages and Disadvantages of the Z-Scan Technique	56
3.1.2	Theory of Z-Scan	57
3.1.3	Experimental Technique	62
3.2.0	The Degenerate Four-Wave Mixing (DFWM) Technique	64
3.2.1	Principle of DFWM Measurements	66
3.2.2	The DFWM Technique	69
3.3	References	71

Chapter 4: Synthesis and Characterization of Coordination Driven Self-Assemblies of Zn(II) Metalloporphyrin Complexes with Spatial Geometry Directed by Conformational Diversity.....73

4.0	Introduction	73
4.1.0	Synthesis of Porphyrin Ligand Building Blocks	74
4.1.1	Single Crystal X-Ray Crystallographic Study of 4-6	84

- 4.1.2 Synthesis of 5,15-Bis-3-Methoxymethylphenylporphyrin - 'Meta' Porphyrin
(**4-13** and **4-14**) 86
- 4.1.3 Single Crystal X-Ray Crystallographic Study of **4-13** 88
- 4.2 Synthesis of Coordination Dimers and Polymers of Zn(II) Metalloporphyrins 89
- 4.3.0 Properties of Coordination Complexes 94
 - 4.3.1.0 Properties of Three-Dimensional Coordination Polymer **4-15** 95
 - 4.3.1.1 The Anomalous Time-Dependent ¹H NMR of **4-15** 95
 - 4.3.1.2 The Effect of Solvent and Small Molecules on the Solid State Structure of
4-15 99
 - 4.3.1.3 Optical Properties of **4-15** 102
 - 4.3.2.0 Properties of One-Dimensional Coordination Polymer **4-18** and **4-20** 104
 - 4.3.2.1 Optical Properties of **4-18** and **4-20** 105
 - 4.3.3.0 Properties of One-Dimensional Coordination Dimer **4-16** 107
 - 4.3.3.1 The Anomalous Time-Dependent ¹H NMR of **4-16** 108
 - 4.3.3.2 Optical Properties of **4-16** 110
 - 4.3.4.0 Properties of One-Dimensional Coordination Dimer **4-22** 112
 - 4.3.4.1 Optical Properties of **4-22** 112
 - 4.3.5.1 Comparison of UV-vis Absorption Spectrum of the Free Base Porphyrins,
Zn(II) Metalloporphyrin Dimers and Polymers 113
 - 4.3.6 Thermal Analyses of the Zn(II) Metalloporphyrin Dimers and Polymers
115
- 4.4 Light Harvesting Properties of **4-15** and **4-16** 118
- 4.5.0 X-Ray Crystallographic Studies of a Class of Zn(II) Metalloporphyrin Dimers and
Polymers Formed by Zn-O Coordination Bonds and their Corresponding Ligands
123

4.5.1.1	Single Crystal X-Ray Crystallographic Study of 4-15 Grown in CHCl ₃ /Cyclohexane Solvent Mixture	123
4.5.1.2	Single Crystal X-Ray Crystallographic Study of 4-15 Grown in CHCl ₃ /Ethyl Acetate Solvent Mixture and C ₆ H ₅ NO ₂	128
4.5.2.1	Single Crystal X-Ray Crystallographic Study of 4-16 Grown in CHCl ₃	131
4.5.2.2	Single Crystal X-Ray Crystallographic Study of 4-16 Grown in THF	136
4.5.3	Single Crystal X-Ray Crystallographic Study of 4-18	138
4.5.4	Single Crystal X-Ray Crystallographic Study of 4-20	143
4.5.5.1	Single Crystal X-Ray Crystallographic Study of 4-22 Grown in CHCl ₃ /Toluene	147
4.5.5.2	Single Crystal X-Ray Crystallographic Study of 4-22 Grown in THF	150
4.6	Conclusion	151
4.7	References	152

Chapter 5: Nonlinear Optical Measurements of Zn(II) Metalloporphyrin

	Complexes.....	156
5.0	Introduction	156
5.1.0	Results and Discussions	157
5.1.1	Data Analyses	158
5.1.2	Two-Photon Absorption Cross Section Properties	165
5.1.3	Excited State Absorption (ESA) – Reverse Saturable Absorption (RSA)	168
5.1.4	Three-Level Model	175
5.1.5	Discussions	178
5.1.6	Wavelength Dispersion of the Third-Order Nonlinear Optical Properties of 4-16	181

5.2	Conclusion	187
5.3	References	188

Chapter 6: Conjugated Covalent Porphyrin Systems as Nonlinear Optics

	Materials	190
6.0	Introduction	190
6.1.0	Synthesis of Covalent Porphyrin Systems Consisting of Cis and Trans Porphyrin Monomers	192
6.1.1.0	Characterization of Conjugated Porphyrin Oligomers 6-9 and 6-10	195
6.1.1.1	^1H and ^{13}C NMR Analyses	195
6.1.1.2	Elemental Analyses	196
6.1.1.3	FT-IR Spectroscopy	196
6.1.1.4	Molecular Weight Determination	198
6.1.1.5	Thermal Analyses	198
6.1.1.6	Linear Optical Properties	199
6.1.1.7	Nonlinear Optical Properties	201
6.2.0	Conjugated Porphyrin Systems with Aryl Acetylene Links	204
6.2.1.0	Characterization of Conjugated Porphyrin Systems 6-31 , 6-32 and 6-33 with Aryl Acetylene Links	208
6.2.1.1	^1H and ^{13}C NMR Analyses	208
6.2.1.2	Elemental Analyses	209
6.2.1.3	FT-IR Spectroscopy	210
6.2.1.4	Molecular Weight Determination	212
6.2.1.5	Thermal Analyses	213
6.2.1.6	Linear Optical Properties	214
6.2.1.7	Nonlinear Optical Measurements	215

6.3 Conclusion 217

6.4 References 218

Chapter 7: Third-Order Nonlinear Properties of the Bromo Benzo[c]cinnoline Monomer and Novel Fluorene-Benzo[c]cinnoline Copolymers.....220

7.0 Introduction 220

7.1 Our Work 224

7.2 Benzo[c]cinnoline-based Conjugated Polymers as Nonlinear Optics Materials 226

7.3.0 Results and Discussions 229

7.3.1 Synthesis and Characterization of **7-7** Monomer 229

7.3.2.0 Synthesis and Characterization of Fluorene-Benzo[c]cinnoline Copolymers 232

7.3.2.1 ¹H and ¹³C NMR Analyses 232

7.3.2.2 Elemental Analyses 233

7.3.2.3 Molecular Weight Determination 235

7.3.2.4 Thermal Analyses 235

7.3.2.5 Optical Studies 237

7.4 Nonlinear Optical Properties 240

7.5 Conclusion 247

7.6 References 249

Chapter 8: The Effect of Conformational and Configurational Diversity on the Interaction of Water-Soluble Porphyrin with Nucleotides and their Photobleaching Properties.....252

8.0	Introduction	252
8.1	Target and Approach of our Research Work	253
8.2.0	Results and Discussions	256
8.2.1	Synthesis of Water-Soluble Porphyrin Photosensitizers	256
8.2.2	^1H and ^{31}P Nuclear Magnetic Resonance Studies	259
8.2.3	Optical Studies	265
8.3	Conclusion	271
8.4	References	271
Chapter 9: Conclusion and Future Work.....		274
9.1	Conclusion and Future Work	274
9.2	References	278
Chapter 10: Experimental Results.....		279
10.1	Materials	279
10.2.0	Characterization Techniques	279
10.2.1	Fourier-Transform Infrared (FTIR) Spectroscopy	280
10.2.2	Nuclear Magnetic Resonance (NMR) Spectroscopy	280
10.2.3	Elemental Analysis (EA)	281
10.2.4	Mass Spectrometry (MS)	281
10.2.5	Ultraviolet-Visible Absorption (UV-vis) spectroscopy	282
10.2.6	Photoluminescence Spectroscopy	282
10.2.7	Differential Scanning Calorimetry (DSC)	283
10.2.8	Thermogravimetric Analysis (TGA)	283
10.2.9	Gel Permeation Chromatography (GPC) Analyses	283

10.2.10 X-Ray Crystallography 284

10.2.11 Melting Point 284

10.3 Procedure 285

10.4 References 331

Appendix.....333

LIST OF ABBREVIATIONS

NLO	nonlinear optical
SHG	second harmonic generation
DFWM	degenerate four-wave mixing
TPA	two-photon absorption
PDT	photodynamic therapy
AMP	adenosine monophosphate
ATP	adenosine triphosphate
DNA	deoxyribonucleic acid
3D	three-dimensional
HOMO	highest occupied molecular orbital
LUMO	lowest occupied molecular orbital
OPA	one-photon absorption
ESA	excited state absorption
SA	saturable absorption
RSA	reverse saturable absorption
<i>u</i>	<i>ungerade</i>
<i>g</i>	<i>gerade</i>
FRET	fluorescence resonance energy transfer
ISC	intersystem crossing
GM	Göppert-Mayer
VT	variable temperature
<i>d</i>	deuterated
<i>tert</i>	tertiary
TLC	thin layer chromatography
NBS	N-bromosuccinimide
THF	tetrahydrofuran
NMR	proton nuclear magnetic resonance

IR	infrared
PL	photoluminescence spectroscopy
UV-vis	ultraviolet-visible
GPC	gel-permeation chromatography
PDI	polydispersity index
MALDI-TOF	matrix-assisted laser desorption ionization -time-of-flight
TGA	thermogravimetric analysis
DSC	differential scanning calorimetry
MS	mass spectrometry
EI	electron ionization
ESI	electron spray ionization
CI	chemical ionization
FAB	fast atom bombardment
HR	high resolution
EA	elemental analysis
HPLC	high-performance liquid chromatography
FTIR	Fourier-transform infrared spectroscopy
BuLi	butyl lithium
DIBAL	diisobutylaluminium hydride
EtOH	ethanol
MeOH	methanol
DMF	dimethylformamide
DMSO	dimethylsulfoxide
Ph	phenyl
γ	second hyperpolarizability
γ_{imag}	imaginary component of the second hyperpolarizability
γ_{real}	real component of the second hyperpolarizability
$\chi^{(n)}$	nth-order susceptibility tensors
$\chi_{\text{imag}}^{(3)}$	imaginary component of the third-order nonlinear susceptibility

$\chi_{\text{real}}^{(3)}$	real component of the third-order nonlinear susceptibility
n_2	nonlinear refractive index
$n_{2,\text{imag}}$	Imaginary component of nonlinear refractive index
σ_n	n-photon absorption cross-section
σ_{gr}	ground state absorption cross-section
σ_{ex}	excited state absorption cross section
S_n	nth singlet excited state
S_{nv}	nth singlet vibrational states
T_n	nth triplet excited state
$P_i(t)$	induced polarization with respect to time
$P_{\text{stat},i}$	static polarization
$E_j(t)$	applied electric field with respect to time
$\tilde{p}(t)$	time dependent dipole moment of a molecule
$\mu_1^\circ(t)$	molecular dipole moment
α_{iJ}	linear polarizability
β_{IJK}	first hyperpolarizability
γ_{IJKL}	second hyperpolarizability
Δn	change in the refractive index
n_0	linear refractive index of medium (at low light intensity)
n_2'	nonlinear index intensity coefficient
$I(r,t)$	Intensity of light as a function of time and spatial coordinate
ϵ_0	electric permittivity of free space (8.85×10^{-12} F/m)
ϵ	dielectric constant
c	speed of light in vacuum (3×10^8 m s ⁻¹)
λ	wavelength
λ_{max}	maximum wavelength
ν_i	frequency of the i-th absorbed photon
ω	frequency
ω_e	frequency of pump or excitation beam

ω_p	frequency of probe beam
h	Planck constant
$\hbar\omega$	energy of photons in the incident optical field
E	transition energy
P	probability of multiphoton excitation
I_k	intensity of k -th source of light
n_k	number of photons from the k -th source of light
$\sum_k n_k$	total number of absorbed photons
α	linear absorption coefficient
β	TPA coefficient
z	distance along z-axis
N	number density of molecules
N_0	Avogadro number
N_i	concentrations of molecules of the solution components
L	Length
L_{eff}	effective sample thickness
I_0	incident energies
ψ	wavefunctions
m	intermediate level
z_R	Rayleigh range of the beam in air
$\Delta\varphi(r, z, t)$	nonlinear phase shift
$\Delta\varphi_{\text{real}}$	real component of the nonlinear phase shift
$\Delta\varphi_{\text{imag}}$	imaginary component of the nonlinear phase shift
$I_0(t)$	on-axis intensity at focus
w_0	beam radius at the focus
$\langle\Delta\Phi_0\rangle$	peak on-axis phase shift
T	transmittance
$\Delta T_{\text{p-v}}$	difference in the peak and valley transmittance values
ζ_p	z positions corresponding to the maximum $T(\zeta)$ value

ζ_v	z positions corresponding to the minimum $T(\zeta)$ value
S	low-power aperture transmission
\mathcal{E}_i	measured incident pulse energy corrected for Fresnel reflection
δ_i	weight fraction of a solution component
$n_{2,\text{solute}}$	nonlinear refractive index of solute
$n_{2,\text{solvent}}$	nonlinear refractive index of solvent
L'	local-field factor
M_i	component's molecular weight
M_n	number average molecular weight
ρ	density
$\Delta\phi_0$	change in nonlinear phase shift
$\Delta\phi_{\text{real}}$	real part of the nonlinear phase shift
$\Delta\phi_{\text{imag}}$	imaginary part of the nonlinear phase shift
κ	coupling coefficient
C_{refl}	correction factor for reflection
C_{abs}	correction factor for absorption
Φ_{eff}	fluorescence quantum efficiency
Φ_{unk}	fluorescence quantum efficiency of the sample
Φ_{std}	fluorescence quantum efficiency of the standard
I_{unk}	integrated emission intensities of the sample
I_{std}	integrated emission intensities of the standard
A_{unk}	absorbance of the sample at the excitation wavelength
A_{std}	absorbance of the standard at the excitation wavelength
η_{unk}	refractive indices of the solutions containing the sample
η_{std}	refractive indices of the solution containing the standard
E_i	input energy
E_o	output energy
F_i	input fluence
F_o	output fluence

g'	weight fraction of the solute
g'_i	weight fraction of component in solution
T'	coupling factor
ε'	molar absorptivity
ν	laser excitation frequency
$\bar{\nu}$	Is the laser wavenumber
ν_{mg}	frequency of the $m \leftarrow g$ transition
$\Delta\nu_{mg}$	halfwidth of the transition $m \leftarrow g$
α'	angle between transition dipole moments
Γ_m^{-2}	full width at half maximum of the absorption band
$g(2\nu)$	line shape function as a function of ν
T_d	onset decomposition temperature
T_g	glass transition temperature
$W_{1/2}$	bandwidth at half-height peak
R_f	retention index
m/z	mass/charge
V	volume of unit cell
Z	molecules per unit cell
d_{calc}	calculated density
μ	absorption coefficient
θ_{max}	theta range for data collection
R	refinement indices
$a, b, c, \alpha, \beta, \gamma$	unit cell dimensions
$b.p$	boiling point
$m.p$	melting point
br	broad
s	singlet
d	doublet
t	triplet

<i>m</i>	multiplet
s	seconds
<i>sh</i>	shoulder
ps	picoseconds
fs	femtoseconds
cm	centimeters
mm	millimeters
nm	nanometers
μm	micrometers
Hz	hertz
MHz	mega hertz
W	walts
rad	radians
J	joules
ppm	parts-per-million
mg	milli grams
g	grams
mol	moles
mmol	milli moles
ml	milli litres
cgs	centimetre-gram-second
ⁿ <i>J</i>	n-bond coupling constant
δ	chemical shift

SUMMARY

In recent years, because of the advantages of photodynamic therapy (PDT), we gradually observe the replacement of this medical treatment over conventional cancer treatment. However, current application of PDT is also met with a major disadvantage of limited light penetration which restricts its application to dermatological cancer treatment. Two-photon PDT is able to overcome this limitation.

Two-photon absorption is a third-order nonlinear optical (NLO) phenomenon. The last two decades have witnessed a phenomenal growth of research in nonlinear optical (NLO) properties of various conjugated polymers, molecular solids, organic and organometallic compounds. A collective effort from chemists, physicists and material scientists is in progress to understand the basic processes responsible for optical nonlinearity. Among the various organic materials, porphyrins, metalloporphyrins and their derivatives are one of the most studied groups of molecules. The general strategies taken to amplify their optical nonlinearity were extension of π -conjugation through the formation of covalent and coordination bonds.

However, covalent systems are often more difficult to achieve on a practical scale. Multiporphyrin architectures assembled through various associations and orientations can provide a large class of intriguing coordination complexes that are more synthetically viable. This is clearly demonstrated in our work.

Our research work involves the investigation of the NLO properties of covalently-linked and coordination complexes of Zn(II) metalloporphyrins using Z-scan and

degenerate four-wave mixing (DFWM) techniques. In particular, the third-order nonlinear phenomenon of two-photon absorption (TPA) is highlighted because of their potential application in two-photon photodynamic therapy (PDT). Zn(II) metalloporphyrin dimer formed via Zn-O coordination bonds displayed the largest merit factor (TPA cross section, $\sigma_2/\text{formula weight}$) of 1.61 GM mol g⁻¹ amongst the complexes formed.

In our effort to discover novel compounds with potential application for two-photon PDT, our study reports the first finding of two-photon absorptivity in a series of benzo[c]cinnoline-fluorene copolymer in which the value of σ_2 increased with the composition of benzo[c]cinnoline.

Prior to the discovery of photosensitizers (drugs) for PDT, the study of specific molecular recognition of biomolecules, aggregation in aqueous system and photobleaching properties, is of fundamental importance. Hence, we performed a detailed study on the effects of the conformation and configuration of porphyrin substituents on these properties. Our studies found that water-soluble Zn(II) metalloporphyrins with *ortho* and *para* substituents bind similarly to ATP and AMP. However, the former display greater photostability and higher quantum efficiency than their commonly studied *para* counterparts.

Hence, our work investigates the third-order NLO properties of Zn(II) metalloporphyrin coordination complexes, covalently-linked porphyrin polymers as well as benzo[c]cinnoline-fluorene copolymers. This work provides an insight on the influence of molecular architecture on NLO properties. In another aspect of the work, a detailed study of the conformational and configurational effects of peripheral substituents on

molecular recognition and photobleaching activities shed light on the future design of materials with large σ_2 as photosensitizers for two-photon PDT.

LIST OF FIGURES

- Fig.
- 1.1 A typical UV-vis absorption spectrum of a free base porphyrin
 - 2.1 Optical limiters based on self-focusing. (a) $n_2 > 0$ and (b) $n_2 < 0$
 - 2.2 Illustration of TPA (a) Self-TPA, (b) Pump-probe TPA
 - 2.3 Illustration of TPA and single-photon excited state absorption processes
 - 2.4 An energy diagram of a typical organic molecule
 - 3.1 Schematic setup for the Z-scan measurements with closed- and open-aperture
 - 3.2 Diagram illustrating the theoretical shapes of open- and closed-aperture Z-scans for (A) no nonlinear absorption, (B) induced absorption and (C) absorption saturation
 - 3.3 Picture of the Z-scan setup at the Laser Physics Centre, The Australian National University, Canberra
 - 3.4 Picture of the DFWM setup at the Laser Physics Centre, Australian National University, Canberra
 - 3.5 (a) BOXCARS geometry of the interaction of the beams in the DFWM experiment (top); (b) View on the screen behind the sample (bottom)
 - 3.6 Scheme of the laser system used in nonlinear optical measurements at 800nm
 - 3.7 Scheme of DFWM setup in BOXCARS configuration
 - 4.1 Mechanism for the condensation of pyrrole and **4-4**
 - 4.2 Scrambling reaction during condensation
 - 4.3 Illustration of the possible bond rotations of the methoxymethyl substituents in **4-7**
 - 4.4 ^1H NMR peaks of a mixture of **4-6** and **4-7** (left), ^1H NMR peak of **4-7** (middle), ^1H NMR peak of **4-6** (right)
 - 4.5 Variable temperature ^1H NMR spectrum of **4-6** (-3.20 to -2.00 ppm)
 - 4.6 Rapid tautomerization of porphyrin
 - 4.7 Molecular structure **4-6**; thermal ellipsoids are drawn at 30% probability level

- 4.8 The distance of deviation of the phenyl C attached to the *meso* C of porphyrin with respect to the plane of the porphyrin formed by the four N atoms refers to *x*
- 4.9 Diagram shows absence of π - π interactions between adjacent units of **4-6** in the solid state packing
- 4.10 Molecular structure **4-13**; thermal ellipsoids are drawn at 50 % probability level
- 4.11 Time-dependent ^1H NMR spectra (in CDCl_3) of a freshly isolated sample of 3D coordination polymer **4-15**
- 4.12 Time-dependent ^1H NMR spectra (in $d_5\text{-C}_6\text{D}_5\text{NO}_2$) of a freshly isolated sample of 3D coordination polymer **4-15**
- 4.13 UV-vis absorption spectrum of **4-15** in various solvents. Dotted lines show Q-bands amplified for clarity
- 4.14 Emission spectrum of **4-6** and **4-15** in toluene at concentration of 1×10^{-5} M
- 4.15 UV-vis absorption spectrum of **4-18** in various solvents. Dotted lines show Q-bands amplified for clarity
- 4.16 UV-vis absorption spectrum of **4-20** in various solvents. Dotted lines show Q-bands amplified for clarity
- 4.17 Time-dependent ^1H NMR spectra (in CDCl_3) of a freshly isolated sample of dimer **4-16**
- 4.18 An illustration showing the association of the dimeric unit in **4-15** and a relatively weakly coordinated unit which forms only one Zn-O coordination bond
- 4.19 UV-vis absorption spectrum of **4-16** in various solvents. Dotted lines show Q-bands amplified for clarity
- 4.20 UV-vis absorption spectrum of **4-22** in various solvents. Dotted lines show Q-bands amplified for clarity
- 4.21 UV-vis absorption spectrum of the Zn(II) metalloporphyrin dimers and polymers as well as their corresponding ligands in CHCl_3 . Dotted lines show Q-bands amplified for clarity
- 4.22 DSC plot of Zn(II) metalloporphyrin complexes **4-15**, **4-16** and **4-18**
- 4.23 TGA plot of Zn(II) metalloporphyrin complexes **4-15**, **4-16**, **4-18**, **4-20** and **4-22**
- 4.24 Illustration of FRET from supramolecular porphyrin self-assembly (stores excitation energy) to energy acceptor for example chloranil
- 4.25 Emission spectrum of **4-15**, **4-16** in CHCl_3 (5×10^{-6} M) and Zn(II) tetraphenylporphyrin in toluene at concentration of 1×10^{-5} M

- 4.26 Stern-Volmer plot for **4-15**, **4-16** (note that both lines overlapped) and Zn(II) tetraphenylporphyrin (2×10^{-4} M) with chloranil in CHCl_3
- 4.27 An ORTEP view of the asymmetric unit of complex **4-15**
- 4.28 A segment of the coordination polymer **4-15**
- 4.29 View of **4-15** along *c*-axis. Columns A and B are marked in red and blue respectively (refer to text)
- 4.30 View of **4-15** along *a*-axis
- 4.31 Monomeric unit of **4-15** when grown in ethyl acetate (thermal ellipsoids are drawn at 50 % probability level)
- 4.32 A view showing weak interaction due to the overlap of aryl C-H σ bonding orbital with the aromatic π ring of the porphyrin
- 4.33 Molecular structure **4-16**; thermal ellipsoids are drawn at 50 % probability level
- 4.34 A monomeric unit of **4-16** showing the direction of the methoxy substituents in solid state
- 4.35 ORTEP view showing the two different porphyrin alignments and non-bonded Zn-H interactions (dotted lines)
- 4.36 A side view of **4-16** showing the differences in dihedral angle of the two phenyl rings
- 4.37 ORTEP view showing one tilted Zn(II) metalloporphyrin molecule with one coordinated THF molecule and one molecule of solvent THF; thermal ellipsoids are drawn at 50 % probability level
- 4.38 Molecular structure of **4-18**; thermal ellipsoids are drawn at 50 % probability level
- 4.39 The ORTEP view of **4-18** showing two alignments of the Zn(II) metalloporphyrin units
- 4.40 The zig-zag, step-like infinite structure of **4-18**
- 4.41 A view of the non-bonding H-Br interactions between columns along the *b*-axis
- 4.42 A view of the non-bonding H-Br and Br-Br interactions between columns along the *c*-axis
- 4.43 ORTEP view of **4-20**; thermal ellipsoids are drawn at 50 % probability level
- 4.44 Non-bonding H-Br and Br-Br interactions between units in different columns
- 4.45 Molecular structure of **4-22**; thermal ellipsoids are drawn at 50 % probability level

- 4.46 ORTEP view showing the one porphyrin alignment and non-bonded Zn-Br interactions between the dimers
- 4.47 ORTEP view showing one tilted Zn(II) metalloporphyrin molecule with one coordinated THF molecule; thermal ellipsoids are drawn at 50 % probability level
- 5.1 Example of Z-scan curve fitting to obtain T factor and $\Delta\phi$ values
- 5.2 Typical of closed-aperture scans for (a) 0.398 wt%, (b) 0.220 wt%, (c) 0.110 wt% of **4-6** in CHCl_3 and (d) pure CHCl_3
- 5.3 Concentration dependence of open-aperture Z-scans of **4-6** 0.398 wt% (light red), 0.220 wt% (green), 0.110 wt% (blue) and 0 wt% (black) in CHCl_3 solution
- 5.4 Transmission of **4-6**, **4-7** and 5,15-diphenylporphyrin with increase in input fluence
- 5.5 Transmission of **4-6** and **4-17** with increase in input fluence
- 5.6 Transmission of **4-15** and **4-18** with increase in input fluence
- 5.7 Transmission of Zn(II) 5,15-diphenylporphyrin and **4-15** with increase in input fluence
- 5.7 Three-level model system used for the description of TPA process
- 5.8 Correlation between the σ_2 and a combination of linear absorption parameters for a series of free base porphyrins and Zn(II) metalloporphyrin dimers and polymers
- 5.9 The experimental values of γ_{real} (blue line) and γ_{imag} (red line) for **4-16**. The absorption spectrum of a dilute solution of **4-16** in CHCl_3 is also shown
- 5.10 One photon (black line) and two photon (blue line) absorption spectra in the a) Soret and b) Q band regions
- 6.1 IR spectrum of *trans* oligomer **6-9**. Arrow indicates *cis* C=C bond
- 6.2 IR spectrum of *cis* oligomer **6-10**. Arrow indicates *cis* C=C bond
- 6.3 TGA plots of **6-9** (bold lines) and **6-10** (dotted lines)
- 6.4 UV-vis absorption spectrum of **6-6**, **6-8**, **6-9** and **6-10**. Dotted lines show Q-bands amplified for clarity
- 6.5 Nonlinear transmission response of **6-9**, **6-10** and C_{60} in CH_2Cl_2 . Note that the line are drawn for extrapolation of input fluence at a transmission of 0.375
- 6.6 IR spectrum of **6-31**, **6-32** and **6-33**
- 6.7 TGA plots of **6-31** (red), **6-32** (blue) and **6-33** (black)

- 6.8 UV-vis absorption spectrum of **6-31**, **6-32** and **6-33**
- 6.9 DFWM signal at 800 nm for a film of **6-32** scanned from positive to negative delay times. The increase of the background signal at negative delays is due to formation of permanent grating
- 7.1 Isomerization of azobenzene from *trans* **7-8** (left) to *cis* **7-9** (right) conformations
- 7.2 ORTEP diagram of **7-7**, thermal ellipsoids are drawn at 50 % probability level
- 7.3 ¹H NMR spectrum of **7-12a-e** in CDCl₃
- 7.4 ¹³C NMR spectrum of **7-12a-e** in CDCl₃
- 7.5 TGA plot of the polymers **7-12a-e**
- 7.6 UV-vis absorption spectra of **7-7**, **7-11** and polymers **7-12a-e**
- 7.7 Emission spectra of monomers **7-7** (suppressed) and **7-11** as well as polymers **7-12a-e** in CHCl₃ at concentrations of 1 × 10⁻⁵ M. Inset shows emission of **7-12c-e** at 420 - 590 nm for clarity
- 7.8 Plot of quantum efficiency ϕ_{eff} (%) against benzo[*c*]cinnoline content in polymers **7-12a-e**
- 7.9 An open-aperture scan in 0.0377 wt% solution of **7-12a** in CHCl₃
- 7.10 A closed-aperture scan in 0.0377 wt% solution of **7-12a** in CHCl₃
- 7.11 Concentration dependences of the real and imaginary components of the nonlinear phase shift $\Delta\phi$
- 8.1 Illustration of two possible binding modes of two molecules of ATP with **8-1b** through ligand coordination and electrostatic interactions. The α , β and γ P atoms are labeled in red
- 8.2 Illustration of synergic effect observed in the Zn(II) metalloporphyrin complex with an increase in axial ligand
- 8.3 ¹H NMR spectrum of ATP, **8-1c** and their complexes with variable ATP ratio and time
- 8.4 ³¹P NMR of ATP, **8-1c** and their complexes with variable ATP ratio and time. Broad β -³¹P peaks observed in the 2.5:1 complex at 0 hours sharpened over time. The α , β and γ ³¹P peaks are labeled
- 8.5 ³¹P NMR of ATP, **8-1b** and their complexes with variable ATP ratio and time. Broad β - and γ -³¹P peaks observed in the 2.5:1 complex at 0 hours sharpened over time. The α , β and γ ³¹P peaks are labeled

- 8.6 UV-vis absorption spectrum of **8-1a-c** (1×10^{-5} M) in 2.5 equivalents ATP in H₂O and 10 % methanol before oxygenation and irradiation.* Refers to the same solution after oxygenation and irradiation with Xe lamp for 2 hours
- 8.7 A study of the effect of sodium azide on rate of photobleaching. Negative change in absorbance over time upon oxygenation and irradiation with Xe lamp of solution containing **8-1a-c** with 2.5 equivalents ATP in H₂O and 10 % methanol separately
- 9.1 Modular system (top) and proposed molecular structure (bottom) using known compounds studied in this work for the design of water-soluble porphyrin as photosensitizer for PDT. The functions of each moiety in the proposed structure (bottom) correspond to the colour scheme shown in the diagram above

LIST OF SCHEMES

Scheme

- 1.1 [2+2] Condensation of dipyrromethanes – the MacDonald method
- 4.1 i, Na, CH₃OH, reflux; ii, DIBAL, benzene; iii, MeOH, HCl, H₂O, 0 °C; iv, CF₃COOH/ CH₂Cl₂; v, chloranil, reflux
- 4.2 i, Na, CH₃OH, reflux; ii, Na₂CO₃, DMSO, reflux
- 4.3 i, Na, CH₃OH, reflux; ii, Na₂CO₃, DMSO, reflux; iii, CF₃COOH, CH₂Cl₂; iv, chloranil, reflux
- 4.4 i, Zn(OAc)₂.xH₂O, EtOH
- 4.5 i, Zn(OAc)₂.xH₂O, THF
- 4.6 i, NBS, CHCl₃, 0 °C, pyridine; ii, acetone; iii, Zn(OAc)₂.xH₂O, THF
- 4.7 i, NBS, CHCl₃, 0 °C, pyridine; ii, acetone; iii, Zn(OAc)₂.xH₂O, THF
- 4.8 i, NBS, CHCl₃, 0 °C, pyridine; ii, acetone; iii, Zn(OAc)₂.xH₂O, THF
- 6.1 i, KOH, EtOH, C₁₀H₂₁Br, reflux; ii, Br₂, MeOH, CHCl₃, 0 °C; iii, BuLi, dry THF, -78 °C; iv, DMF, -78 °C
- 6.2 i, HBr, CHCl₃; ii, PPh₃, DMF, 120 °C
- 6.3 i, HBr, CHCl₃; ii, PPh₃, DMF, 120 °C
- 6.4 i, EtONa, CHCl₃
- 6.5 i, EtONa, CHCl₃
- 6.6 i, KOH, EtOH, C₁₀H₂₁Br, reflux; ii, KIO₃, I₂, H₂SO₄, CH₃COOH, 80 °C; iii, Et₃N, PdCl₂(PPh₃)₂, CuI, trimethylsilyl acetylene; iv, THF, MeOH, aq. NaOH
- 6.7 i, KOH, EtOH, C₁₀H₂₁Br, reflux; ii, KIO₃, I₂, H₂SO₄, CH₃COOH, 80 °C; iii, Et₃N, PdCl₂(PPh₃)₂, CuI, trimethylsilyl acetylene; iv, THF, MeOH, aq. NaOH
- 6.8 i, KOH, EtOH, C₁₀H₂₁Br, reflux; ii, KIO₃, I₂, H₂SO₄, CH₃COOH, 80 °C; iii, Et₃N, PdCl₂(PPh₃)₂, CuI, trimethylsilyl acetylene; iv, THF, MeOH, aq. NaOH
- 6.9 i, CF₃COOH/ CH₂Cl₂; ii, chloranil; iii, NBS, CHCl₃, 0 °C; iv, Zn(OAc)₂.xH₂O, THF
- 6.10 i, i-Pr₂NH, PdCl₂(PPh₃)₂, CuI, toluene, 100 °C
- 6.11 i, i-Pr₂NH, PdCl₂(PPh₃)₂, CuI, toluene, 100 °C

- 6.12 i, $i\text{-Pr}_2\text{NH}$, $\text{PdCl}_2(\text{PPh}_3)_2$, CuI , toluene, $100\text{ }^\circ\text{C}$
- 7.1 Possible routes to the formation of benzo[*c*]cinnoline
- 7.2 Synthesis of **7-2**
- 7.3 Synthesis of **7-4**
- 7.4 i, Cu , DMF , 120°C ; ii, Sn , conc. HCl , EtOH , reflux or Zn , aq CaCl_2 , EtOH , reflux
- 7.5 i, $\text{Pd}(\text{PPh}_3)_4$, aq K_2CO_3 , $(n\text{-C}_4\text{H}_9)_4\text{NBr}$, toluene, $100\text{ }^\circ\text{C}$
- 8.1 i, HBr , CHCl_3 ; ii, PPh_3 , DMF ; iii, $\text{Zn}(\text{OAc})_2 \cdot x\text{H}_2\text{O}$, THF
- 8.2 i, Na , CH_3OH , reflux; ii, Na_2CO_3 , DMSO , reflux; iii, CF_3COOH , CH_2Cl_2 ; iv, chloranil, reflux

LIST OF TABLES

Table

- 4.1 Selected proton chemical shifts (ppm) of **4-6** and **4-15**
- 4.2 Selected proton chemical shifts (ppm) of **4-7** and **4-16**
- 4.3 Summary of the T_g (°C) and T_d (°C) [% weight loss] of the Zn(II) metalloporphyrin complexes
- 4.4 Summary of the dihedral angles of the phenyl rings with respect to the plane of the four N atoms for single crystals of **4-15** grown in various solvents
- 5.1 Summary of nonlinear optics parameters of free base and Zn(II) metalloporphyrin complexes
- 6.1 Calculated and experimental elemental analyses of **6-9** and **6-10**
- 6.2 Average molecular weights of oligomers **6-9** and **6-10** determined from GPC, using polystyrene as standard
- 6.3 Calculated and experimental elemental analyses of **6-31**, **6-32** and **6-33**
- 6.4 Molecular weights of **6-31**, **6-32** and **6-33** based on the highest peak measured on MALDI-TOF
- 7.1 Ratio of **7-7**, **7-10** and **7-11** in synthesis of polymers **7-12a-e** of various percentages of benzo[*c*]cinnoline
- 7.2 Summary of the elemental analysis results of **7-12a-e**
- 7.3 Summary of the yield of the polymers **7-12a-e**
- 7.4 Average molecular weights of polymers determined from GPC, using polystyrene as standard
- 7.5 Summary of the T_d (°C) values of **7-12a-e**
- 7.6 Summary of Φ_{eff} (%) of polymers **7-12a-e**
- 7.7 Summary of the third-order nonlinear parameters of **7-7**, **7-12a,e**
- 8.1 Chemical shifts of H of AMP and ATP at C2 and C8 (ppm)
- 8.2 The λ_{max} (nm) and $W_{1/2}$ (nm) of **8-1a-c** obtained from UV-vis spectrum in H₂O, CH₃OH and DMF
- 8.3 Fluorescence quantum efficiencies (Φ_{eff}) of **8-1a-c** with and without ATP

- 10.1 Summary of the quantities of the monomers **7-7**, **7-10** and **7-11** used to synthesize the polymers **7-12a-e**, reaction yields, M_n , PDI, T_d ($^{\circ}\text{C}$), Φ_{eff} (%), elemental analyses as well as ^1H and $^{13}\text{C}\{^1\text{H}\}$ results

CHAPTER 1

PORPHYRINS AND METALLOPORPHYRINS

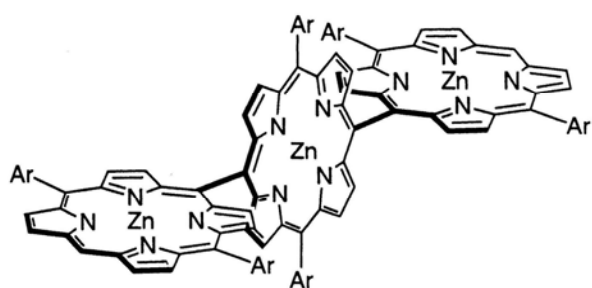
1.0 INTRODUCTION

The basic tetrapyrrole skeleton of porphyrin¹ found in many natural pigments such as hemin, chlorophyll and bacteriochlorophyll, is probably one of the oldest bioorganic structures known to man. These macrocycles play a number of critical biological roles such as molecular binding,² reaction catalysis,³ energy and electron transfers,⁴ and light harvesting.⁵ The importance of these functions provided the impetus for intensive research towards artificial porphyrin systems that may be able to model or mimic their natural counterparts.⁶

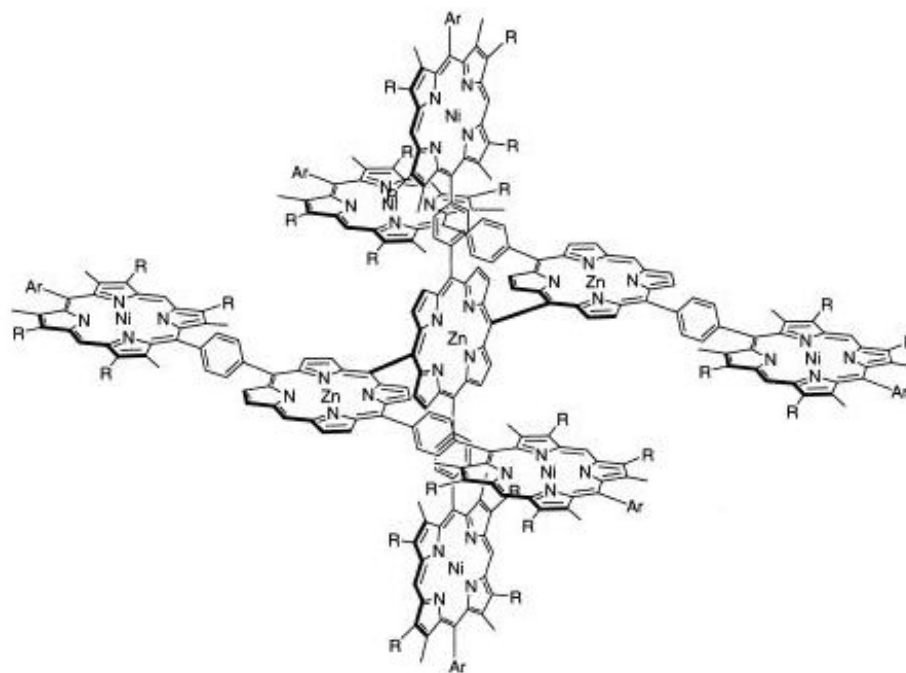
As a consequence of this search for mimic compounds, porphyrins have also been found to have great potential in areas outside mimicking natural systems. These include molecular sensing,⁷ molecular recognition,² medicine (photodynamic therapy (PDT),⁸ boron nuclear capture therapy and DNA cleavage) and optical application (data storage,⁹ nonlinear optics, electrochromism and optical limiting¹⁰). The production of prototypical molecular-scale devices such as wires,¹¹ logic devices,¹² switches¹³ and gates¹⁴ which are essential for the miniaturization of electronic componentry and technology using porphyrin-based materials further increased the stimulus for intensive research towards artificial porphyrin assemblies.

For all the uses mentioned above, it is important that the individual molecules within an array can communicate with each other otherwise the whole will be no better

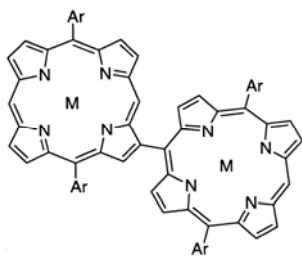
than the sum of the components and the array cannot behave with enhanced effectiveness. This led to the design and synthesis of multiporphyrin arrays that can be formed with covalent type linkages such as *meso-meso* (**1-1**, **1-2**¹⁵), *meso-β* (**1-3**¹⁵) and as well as non-covalent type linkages such as hydrogen bonding (**1-4**¹⁶), metal-metal bonds¹⁷ and the most common in porphyrin chemistry being coordination bond (**1-5**¹⁷). The choice of linker usually complements the functionality of the porphyrin unit and also depends on the availability of materials, research group's expertise and ease of implementation.



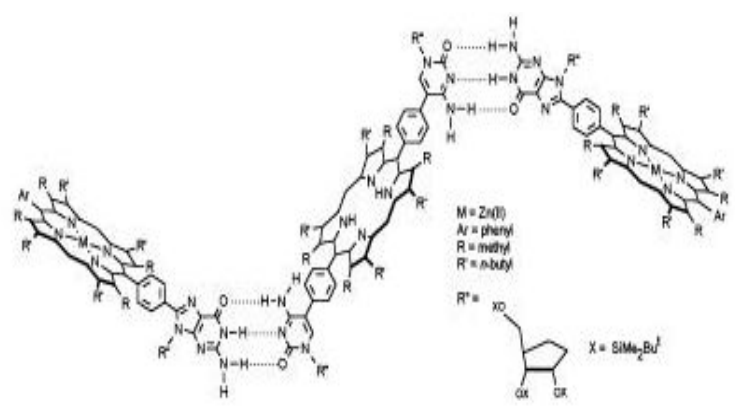
1-1



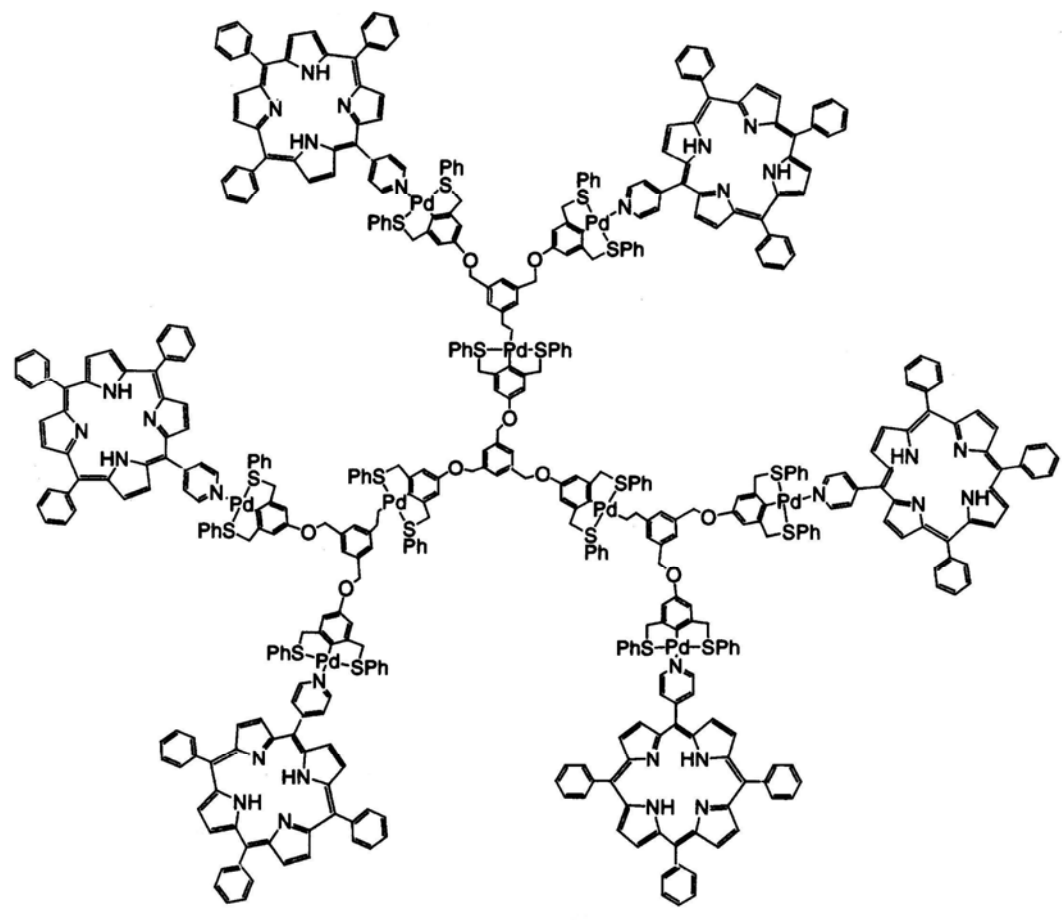
1-2



1-3



1-4

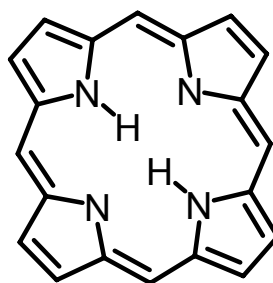


1-5

1.1.0 PORPHYRINS

Porphyryns are atypical biological macrocycles. A macrocycle is a cyclic molecule that contains at least three potential donor atoms in a ring with nine or more atoms.¹⁸ The general criterion for a macrocycle involves having donor atoms to coordinate ions plus having a ring cavity large enough to accommodate these ions. The donor atoms in porphyryns are thus the four N atoms.¹

The porphyryn nucleus consists of four 'pyrrole-type' rings joined by four methine bridges to give the macrocycle (**1-6**). This cyclic porphyryn structure was first suggested by Küster in 1912; at that time it was thought that such a large ring would be unstable and that this structure was not accepted by Fischer, the father of contemporary porphyryn chemistry until much later.¹⁹



1-6

1.1.1 GENERAL CHEMISTRY OF PORPHYRINS

The porphyryn macrocycle is highly conjugated and a number of resonance forms can be written. There are nominally 22 π electrons but only 18 of these are included in any one delocalisation pathway. This conforms to the Hückel's $4n+2$ rule for aromaticity

which is characterized by a unique absorption spectrum of porphyrins. Generally, porphyrins show four absorption bands in the visible region and one very intense band, the Soret band, in the near-ultraviolet (~ 400 nm). A typical UV-vis absorption spectrum of a porphyrin is as shown in Fig. 1.1. The Q-bands are attributed to the lowest energy spin-allowed electronic transition, namely the $S_1 \leftarrow S_0$ transition and its vibronic satellites corresponding to the I-st and II-nd Q-bands. Second spin-allowed electronic transition from the ground state $S_2 \leftarrow S_0$ and its vibronic satellite correspond to the III-rd and IV-th Q-bands.^{1, 20}

If a metal is introduced into the center, then the symmetry of the macrocycle increases, changing the point group from D_{2h} to D_{4h} . This leads to degeneracy of the S_1 and S_2 electronic levels, decreasing the number of Q-bands from 4 to 2.

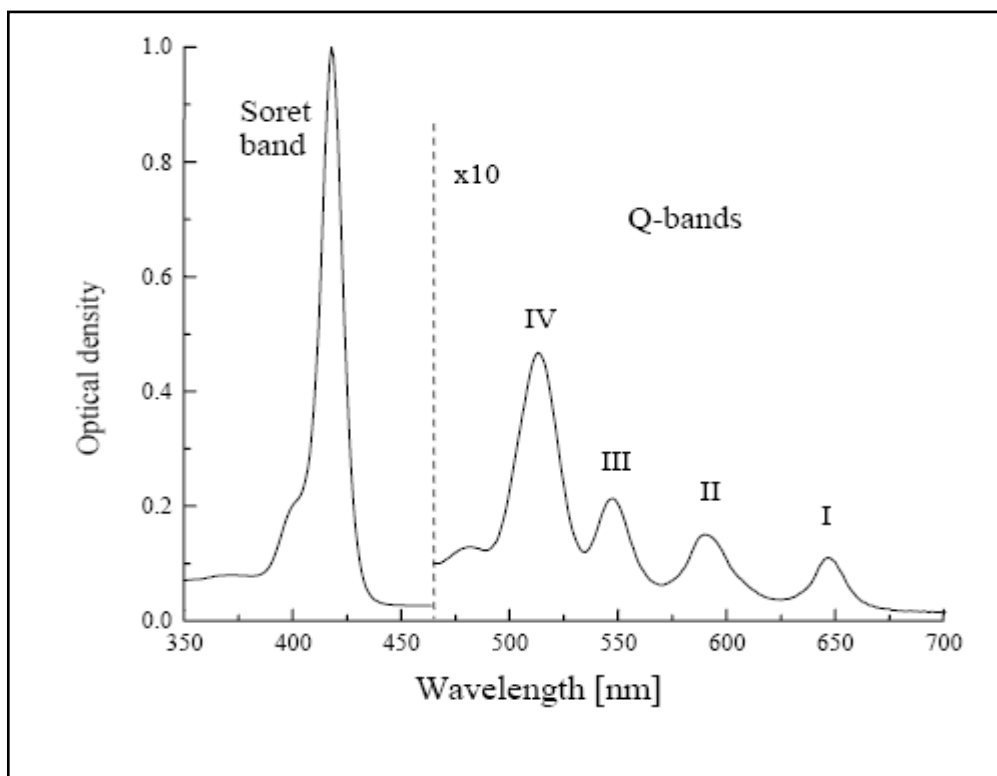


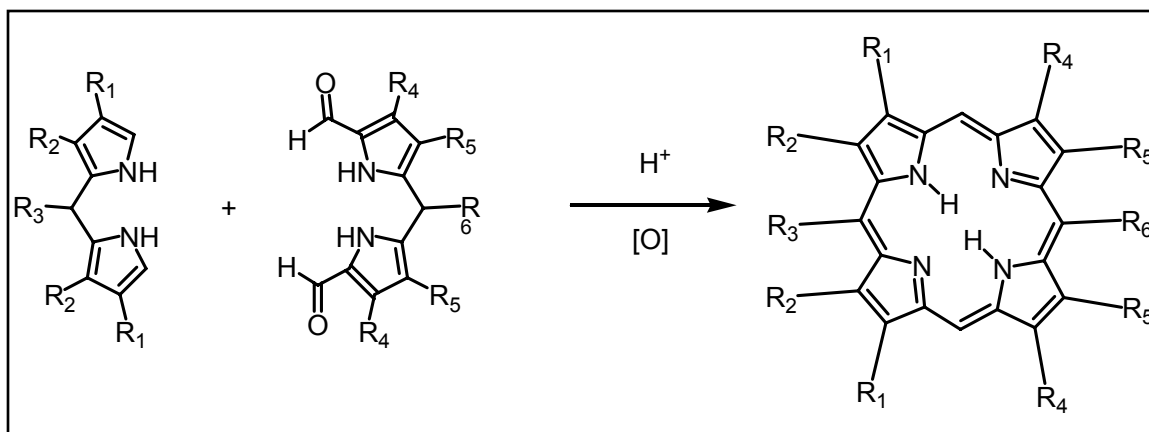
Fig. 1.1 A typical UV-vis absorption spectrum of a free base porphyrin

Formation of a metalloporphyrin complex results, in most cases, in the collapse of the four-banded spectrum to yield two absorption bands in the visible region, while the Soret band usually remains unaltered. The basic planarity of the nucleus that conforms with the basic requirement for aromatic character was confirmed by its X-Ray diagram, the very shielded NH protons (-2 to -4 ppm), as well as deshielded *meso* protons due to the anisotropic ring current effect. The startling abundance of doubly-charged ions and the stability of molecular ion towards fragmentation in the mass spectra of porphyrins and their derivatives also attest to the aromatic nature of the nucleus.^{1, 19}

1.1.2 SYNTHESIS OF PORPHYRINS

Porphyrins can be synthesized by several routes which are generally from monopyrrole, dipyrrolic intermediates, 1,19-dideoxybiladienes and oxabilane intermediates.¹ The strategy to the synthesis of porphyrins depends on the structure of porphyrins. Non-symmetric types require more laborious construction of an open chain intermediate while symmetrically substituted compounds are best synthesized by polymerisation of a suitable monopyrrole.

The synthesis of monomeric porphyrins in this project involves the MacDonald-type [2+2] condensation of dipyrromethane²¹ with an equivalent of aldehyde to yield the 1,15-disubstituted porphyrins. The first example of such a porphyrin was reported by Triebs and Haberle who synthesized 5,15-diphenylporphyrins from benzaldehyde and dipyrromethane. The breakthrough in porphyrin synthesis from dipyrromethanes came with MacDonald's method²² whose research group developed the first dipyrromethane-based porphyrin syntheses as shown in Scheme 1.1.



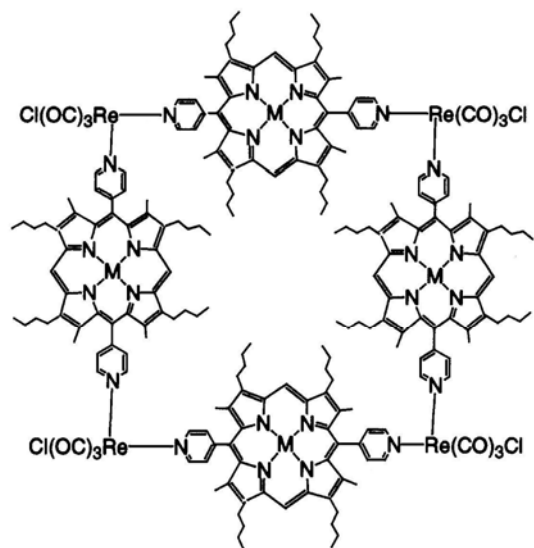
Scheme 1.1 [2+2] Condensation of dipyrromethanes – the MacDonald method²²

Dipyrromethanes represent the partial structure of rubinoid bile pigments. Therefore, much attention has been focussed on the preparation of dipyrromethanes.²³ Synthetic methods for β -substituted-*meso*-substituted dipyrromethane and β -unsubstituted-*meso*-substituted dipyrromethanes are well documented, but that of β , *meso*-unsubstituted dipyrromethane was less developed. Recently, a novel one-step synthetic route to the compound was established with a yield of 40 %, thus making the synthesis of the β , *meso*-unsubstituted dipyrromethane easier. Until today, several groups are continuing their search for better procedures that give higher yield of the compound.^{12a,24} In addition, a diverse range of reaction conditions for the MacDonald-type [2+2] condensation of dipyrromethane and aldehyde had been studied by Lindsey *et al.*²⁵ with the goal of eliminating acid-catalyzed polypyrrolic rearrangement reaction as a function of the acid catalyst, reagent concentration, reagent stoichiometry, solvent salts and temperature.

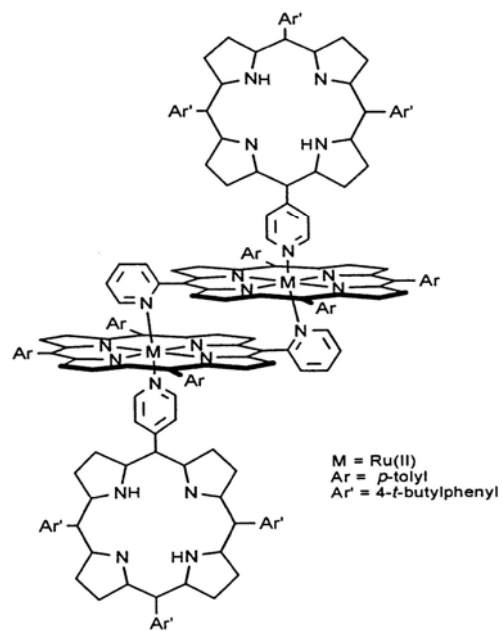
1.2 MULTIPORPHYRIN ARRAYS

Multiporphyrin architectures reveal enormous versatility in photoactivity, electron transfer and redox properties.^{3, 26} In particular, functional assemblies of multiporphyrin arrays have been designed for the development of new molecular electronic devices,²⁷ molecular machines and catalysts.²⁸ Although many elegant structures of such arrays have been constructed via direct covalent bonding, it is difficult to realize the materials into devices on a practical scale.^{22,29} Molecular self-assembly offers a good alternative to a wide variety of one-, two- and three-dimensional arrays.³⁰ The most well-studied Zn(II) metalloporphyrin self-assemblies are formed from Zn-N coordination bonds (**1-7**, **1-8**, **1-9**).^{17d,31} For example, extension into a one-dimensional (1D) network was achieved in a series of tetra(4-pyridyl)-porphyrins. A five-coordinate Zn(II) with one intermolecular Zn-N(pyridyl) coordination was preferred due to steric reasons. Three-dimensional (3D) coordination polymers involving six-coordinate Zn(II) with two axial N (pyridyl)-donors was only formed after more extensive crystallization experiments.³²

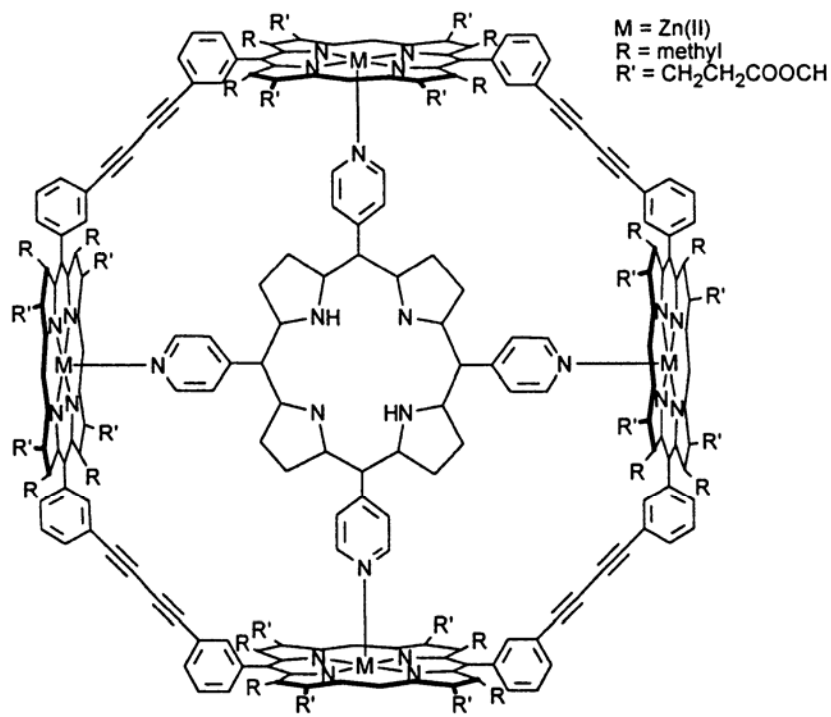
Coordination polymers of Zn(II) metalloporphyrins with O-donor are less studied. For example, axial O-donor from functional groups attached to peripheral phenyl rings has been reported.³³ These examples are, however, limited to five-coordinate Zn(II), thus restricting the formation of only 1D polymer network. To the best of our knowledge, six-coordinate Zn(II) metalloporphyrin complexes with two axial O donors forming a 3D polymer network were not known before our work. The ability of the central metal ion to accommodate two axial ligands is important in obtaining extensive multi-layered arrays. Coordination complexes of Zn(II) metalloporphyrins formed by Zn-O bonds reported in our work will be described in detail in Chapter 5.



1-7



1-8



1-9

A literature survey revealed that the Zn(II) metal atom in the porphyrin center has a marked preference for either four-coordinate square-planar or five-coordinate square-pyramidal environments.³⁴ It binds to the four inner pyrrole N atoms of the porphyrin macrocycle and quite often also to another ligand in the axial direction, revealing a particularly high affinity for N Lewis bases. Hence, ligands with N donor(s) are often used to bridge porphyrin macrocycles. The majority of the ligands are bidentate such as bipyridyl-type functional ligands and diaminoalkane types.³⁵ It is considerably more difficult to construct extended coordination polymers with Zn(II) tetraphenylporphyrin building blocks due to the low affinity of the Zn(II) metal atom for an octahedral ligation environment. A survey of the Cambridge Crystallographic Database by Allen F.H and Kennard O³⁴ indicates that only about 20 % out of 1500 crystal structures of Zn(II) complexes known to date contain a six-coordinate Zn(II) ion. Only scattered examples of monomeric six-coordinate complexes of various Zn(II) metalloporphyrin derivatives with amine axial ligands have been characterized³⁶ and even less so when it comes to extended polymers.³⁷

1.3 PORPHYRINS AS NONLINEAR OPTICAL LIMITING MATERIALS

We witnessed the phenomenal growth of research in nonlinear optical (NLO) properties of conjugated polymers³⁸ and organic/organometallic³⁹ compounds over the last two decades. The current emphasis is placed on the synthesis of novel chemical structures, tailored to optimize the nonlinear response while preserving their chemical, mechanical, optical and thermal stability.

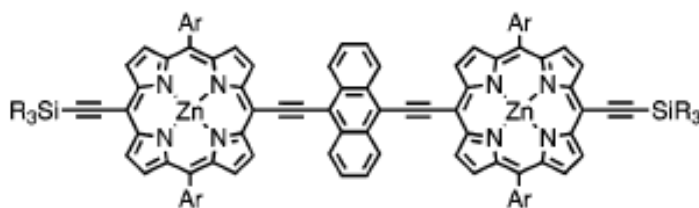
Among the various organic materials, porphyrins and their derivatives are one of the most widely studied class of molecules for NLO applications.^{38a,40} Porphyrins are a

ubiquitous class of naturally occurring compounds found in biological systems. Their derivatives are biological representatives in heme, chlorophyll and vitamin B₁₂.⁴¹ They are also involved in oxygen binding, catalysis, light harvesting and electron transfer processes in biological systems. The Fe(II) and Mg(II) metalloporphyrins are found in heme and chlorophyll respectively. The former is found in blood responsible for the transfer of molecular oxygen to tissues while the latter is required for the decomposition of water via photosynthesis in organisms. Zn(II) metalloporphyrins take part in metabolic processes.

Although porphyrin is a macromolecule, its flexibility allows a large number of metal ions to be inserted into its internal cavity. The versatility of structural changes via the peripheral substituents allows these changes to be introduced without compromising its excellent chemical and thermal stability. In addition, the high electron density and extensive electron delocalization ability makes porphyrins useful for a variety of NLO effects. Their sharp absorption bands in the visible and near-IR can be used for resonance enhancement of the NLO susceptibility tensors of a given medium (refer to Chapter 2 for detailed explanation). Thus, they have enormous potential for applications in optical limiting, optical switching, optical data processing and electronic device fabrication.^{20,21}

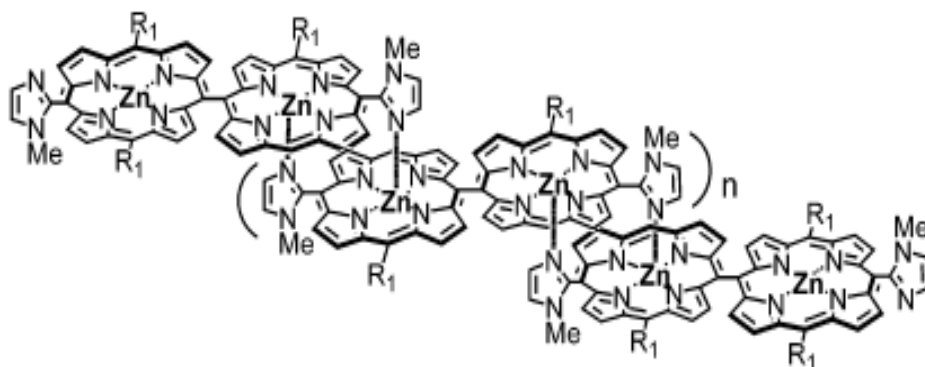
Optical limiting was first reported in porphyrin dyes by Blau *et al.*⁴² in 1985. Laser pulses of 85 ps duration at 532 nm were used to show that the excited state absorption cross section σ_{ex} is larger than the ground state absorption cross-section, σ_{gr} in Zn(II), Co(II) and metal-free tetraphenylporphyrins. Beddard *et al.*⁴³ noted that porphyrins with closed-shell metal atoms have relatively long excited state lifetimes while those with open-shell metal atoms generally have short excited state lifetimes due to rapid charge

transfer from the excited porphyrin to the metal atom. The effect of halogenation on the excited state lifetime and optical limiting performance were also studied.⁴⁴ It was found that Br atoms increase the triplet yield via heavy atom effect. In addition, Br atoms distort the porphyrin structure from planarity via steric hindrance. The distortion broadens the linear absorption features, shifts the position of the Soret and Q-bands to longer wavelengths and increases the triplet yield further by increasing the mixing between singlet and triplet states. However, increasing the triplet yield (rate) also decreases the triplet lifetime and a compromise must be achieved to ensure that the dye is still effective against relatively long microsecond-duration laser pulses. Modified porphyrins have since been extensively studied for their optical limiting properties.



R = C₆H₁₃, Ar = 3,5-di-*tert*-butylphenyl

1-10

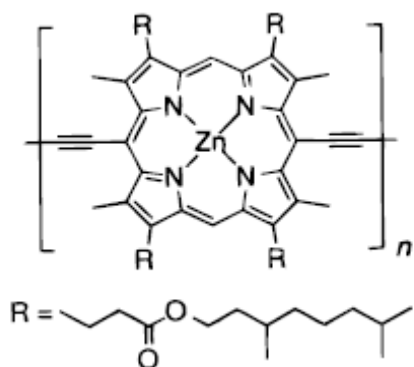


1-11 R = C₇H₅

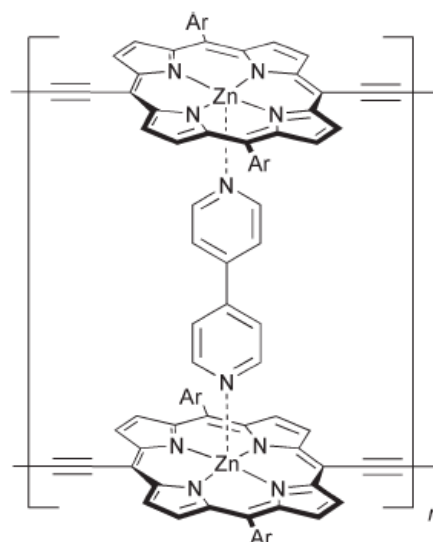
Conjugated porphyrin polymers⁴⁵ such as **1-10** and **1-11** exhibit exceptionally large third-order nonlinear susceptibility ($\chi^{(3)}$) making them relevant to a large variety of NLO applications. High values of $\chi^{(3)}$ are associated with large, polarisable π -systems, long conjugation lengths and small HOMO-LUMO gaps of porphyrins. The impact of molecular design on the magnitude of third-order nonlinear responses of porphyrins has been widely explored. Peripheral substituents with donor/acceptor groups,⁴⁶ dendrimers,⁴⁷ divalent ions with decreasing d-shell occupancy, electronegative axial ligands⁴⁸ and extended conjugation through covalent and coordination bonds^{38a,49} have been found to be important factors in these designs. For instance, **1-12** exhibit very large electronic nonlinearity from the highly conjugated structure when measured by degenerate four-wave mixing (DFWM) technique at 1064 nm with 45 ps pulses.⁵⁰ In addition, it possesses one of the largest nonlinearities of any conjugated organic polymers to date and the largest among those studied off-resonance by over a factor of 10. Efforts have thus been extended to enhance the optical properties through substitution of ethyne with butadiyne linker. However, polydiacetylenes do not offer large enough nonlinearities together with fast response times.

Very recently, double strand ladder complexes **1-13** based on polymers related to **1-12** have been widely studied by means of the DFWM technique.⁵¹ Anderson *et al.* sought to improve the optical properties through the extension of conjugation in two dimensions to increase electronic delocalization. The *meso*-ethynyl substituents were attached perpendicular to the main polymer chain. However, the extension of two-dimensional (2D) conjugation did not increase the optical nonlinearity. Instead, it was later demonstrated that the optical nonlinearity of a conjugated metalloporphyrin can be

amplified by supramolecular self-assembly using ligand coordination as well as change of coordinated metal.

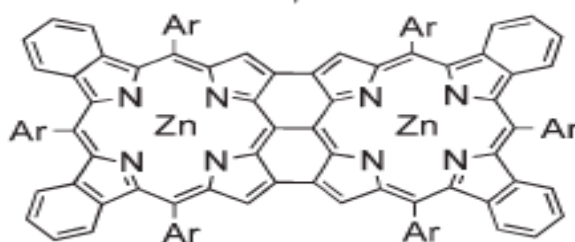


1-12



Ar = 3',5'-di-*tert*-butylphenyl

1-13



(Ar = 4-*tert*-butylphenyl)

1-14

Most recently, it was reported that fused diporphyrins such as **1-14**⁵² have much larger two-photon absorption (TPA) cross-section (σ_2) values (refer to Chapter 3 for

detailed explanation) in comparison to directly linked porphyrin oligomers,⁵³ self-assembled porphyrin tetramers^{49,54} and porphyrin dimers.⁵⁵ However, it is important to highlight that the syntheses of such covalently-linked conjugated systems are tedious and difficult to realize on a practical scale. In addition, such macromolecular structures are hydrophobic and suffer from aggregation problems due to π - π stacking of planar systems. This will most likely result in poor water-solubility, an important property for biological application, even if hydrophilic functional groups were attached.

1.4 IMPORTANCE OF PORPHYRIN AS THIRD-ORDER NONLINEAR OPTICAL LIMITING MATERIALS

Our group is particularly interested in the study of structure-property relationship of porphyrins on their third-order NLO properties. In particular TPA is of interest because of it shows potential practical utility in a variety of areas such as fluorescence microscopy, optical data storage,⁵⁶ laser chemistry, micro-fabrication⁵⁷ and photomedicine.^{55,58} Application of porphyrins is especially attractive in two-photon-based PDT,⁵⁹ where reduced absorption and scattering at near-IR wavelengths allows deeper penetration of light through body tissues to be achieved.

PDT is gaining acceptance worldwide as an alternative treatment of tumors as well as age-related macular degeneration because of its potential ability to treat subcutaneous tumors non-invasively, while at the same time eliminating the adverse physical discomfort associated with traditional chemotherapy and the debilitating effects of actinic radiation treatments. PDT has been used as a clinical treatment of cancer for more than 10 years in Canada, Europe and Asia, and recently in the United States. PDT is currently used for treatment of cancers such as lung, skin, head, neck, throat and

reproductive organs. New photodynamic drugs are currently being studied for treatment of brain cancer, breast cancer, and leukemia.⁶⁰

The accepted mechanism for PDT involves the interaction of an excited state of the drug or dye with the ground state of oxygen. A molecule of the drug absorbs a photon of red light and is excited to the first excited singlet state. If this singlet state is long lived, energy can be transferred from the singlet state to the triplet state through inter-system crossing. This triplet state can react with local oxygen molecules to create an excited state of oxygen called singlet oxygen. Singlet oxygen is cytotoxic and destroys nearby cells. Since the drugs used in PDT are localized on cancer cells, this increases the specificity of the treatment process.⁵⁹

Currently, the drugs that have been approved for PDT are mainly porphyrin derivatives. They are however far from ideal, for instance, the most commonly used Photofrin® suffers from low purity due to the mixture of products formed during synthesis. Serendipitously, porphyrin molecules possess the rare feature of selective accumulation in tumour cells which makes it the obvious choice as core building block for photosensitizers. However, tissue's transmission depends critically on the illumination wavelength and is the largest in the so-called tissue transparency window at 750 - 1000 nm. Porphyrins currently in use for PDT fall short of this transparency window: their absorption varies from 620 - 690 nm, where effective penetration in most tissues is no more than just a few millimeters in depth. Unfortunately, attempts to shift the one-photon absorption band toward longer wavelengths by chemical modification of the porphyrin structure come into conflict with the fundamental requirement that the excitation energy of singlet oxygen is lower than the energy of the state. In addition, long-wavelength shift

of porphyrin's energy levels often aggravates the situation by reducing the compound's stability.

In the view of these challenging difficulties, a proposal to use TPA, a phenomenon of NLO properties, appears as the best alternative way to achieve PDT. It involves the simultaneous absorption of two photons so that the illumination wavelength is twice that of the actual transition wavelength. Thus, TPA allows the use of near-infrared (IR) photons in the tissue transparency window and does not require the red shift of the lowest electronic transition of the porphyrin. Hence, in recent years, research on the two-photon properties of porphyrin-based compounds has been very vibrant. However, so far, in the reports of TPA-PDT, the σ_2 of photosensitizers were very low⁶¹ or not described^{59b,62} until the most recent works of Okura *et al.*⁶³ The group reports a water-soluble porphyrin self-assembly consisting of monoacetylene-linked conjugated bis(imidazolylporphyrin) possessing the largest σ_2 of 7900 GM and photocytotoxicity for HeLa cancer cells. However, the multi-step synthetic route and difficulty of purification pose a major drawback if this compound is to be used as PDT agent. Thus, this demands the continuous investigation of strong two-photon absorbers for PDT applications.

The ultimate success of any of the two-photon-based applications critically depends on the efficiency of TPA, that is, on the value of intrinsic nonlinear cross section, σ_2 . The factors that can lead to the enhancement of NLO properties include (1) the expansion of π -conjugation,^{38a,53, 64} (2) molecular polarization induced by push-pull effects^{65(a), 65} and (3) enhanced exciton interaction through complementary coordination.⁶⁶ Thus, most research so far has been focused on designing extensive

conjugated systems using porphyrin as the core two-photon absorber. Very often, important factors such as water-solubility is neglected in the design of these materials. In addition, the synthetic routes taken to design the porphyrin derivatives such as fused porphyrin dimers⁶⁷ are synthetically challenging and thus pose a problem when they are eventually synthesized on the practical scale.

Thus, the direction of this research work lies in the design and synthesis of compounds with biological relevance, as strong two-photon absorbers. We take the approach of minimizing synthetic steps to obtain parent porphyrin compounds that can derive a wide variety of compounds for practical reasons. Next, we generate a series of compounds generated through further derivation of the parent porphyrin to allow the establishment of structure-property relationships.

It is known that water-solubility is an important property for drugs. However, the planar structure of porphyrin compounds causes π - π stacking and hence aggregation⁶⁸ and in addition, they undergo photobleaching⁶⁹ in aqueous systems which lowers their efficiency as photosensitizers for PDT. This problem is especially significant in most of the water-soluble porphyrin compounds studied. This is because, although the peripheral groups of macrocycle contain water-solubilizing groups, they are attached to the *para* positions and hence do not impose steric effects. Hence, our work aims at designing porphyrin systems to minimize these problems through conformational and configurational modification of the porphyrin structures.

In our in-depth research to study of the structural-NLO property relationship of porphyrin compounds, our results also uncovers the NLO properties of another class of compound, benzo[c]cinnoline, which possess biological applications. Therefore, this

thesis investigates two classes of biologically relevant compounds, namely, porphyrin and benzo[c]cinnoline as two-photon absorbers.

Chapter 2 of the thesis introduces the origin, elements and principles of NLO, as well as the concepts of TPA via a single photon pumped process and excited state absorption.

Chapter 3 introduces the theory and information on the measurement methods used for determining the NLO parameters in this work. These are the Z-scan and DFWM techniques.

Chapter 4 presents the design, synthesis and characterization of a series of free base porphyrins and self-assembled Zn(II) metalloporphyrin coordination complexes. In addition, this chapter provides detailed description of the behaviour of Zn(II) metalloporphyrins coordination dimer and polymer in various solutions gathered from spectroscopic studies (^1H NMR and UV-vis absorption).

Chapter 5 describes the collection, interpretation and analyses of data obtained from Z-scan and excited state absorption (ESA) measurements. The chapter discusses the NLO properties and parameters of the free base porphyrins and Zn(II) metalloporphyrins coordination complexes described in Chapter 4. Different factors leading to TPA enhancement are identified and analyzed. As a result, practical guidelines for design of porphyrin molecules with strongly enhanced TPA are established.

Chapter 6 presents the design, synthesis and characterization of covalently-bonded conjugated systems consisting of porphyrins. Silica plates coated with thin films of the materials were studied for NLO properties using DFWM technique.

Chapter 7 describes two novel, high-yielding and large-scale methods for the synthesis of a class of benzo[*c*]cinnoline compounds. The synthesis, characterization and NLO studies of the copolymers of benzo[*c*]cinnoline and fluorene are described for the first time.

Chapter 8 introduces the molecular recognition of water-soluble porphyrin with nucleotides and highlights the importance of configurational and conformational designs on aggregation and photobleaching properties.

Chapter 9 concludes the thesis and presents future works that can be carried out based on the research findings from this work.

Chapter 10 summarized the experimental procedures, yield, and characterization results of all the compounds synthesized in this work.

1.5 REFERENCES

¹ Dolphin, D. *The Porphyrins, Volume 1, Structure and Synthesis, Part A*, Academic Press, New York, 1978.

² Zheng, J.Y.; Konisi, K.; Aida, T. *Tetrahedron* **1997**, 53, 9115.

³ Collman, J.P.; Wagenknecht, P.S.; Hutchison, J.E. *Angew. Chem. Int. Ed. Engl.* **1994**, 33, 1537.

- ⁴ Gust, D.; Moore, T.A.; Moore, A.L. *Acc. Chem Res.* **1993**, *26*, 198. (b) Wasielewski, M.R. *Chem. Rev.* **1992**, *92*, 435.
- ⁵ Gust, D. *Nature* **1997**, *386*, 21.
- ⁶ Milgrom, L.R. *"The Colours of Life: An Introduction to the Chemistry of Porphyrins and Related Compounds"*, Oxford Univ. Press, 1997.
- ⁷ Konishi, K.; Kimata, S.; Yoshida, K.; Tanaka, M.; Aida, T. *Angew. Chem. Int. Ed. Engl.* **1996**, *35*, 2323.
- ⁸ Okura, I. *"Photosensitization of Porphyrins and Phthalocyanines"*, Amsterdam, Gordon and Breach Science, 2000.
- ⁹ (a) Gryko, D.T.; Zhao, F.; Yasseri, A.A.; Roth, K.M.; Bocian, D.F.; Kuhr, W.G.; Lindsey, J.S. *J. Org. Chem.* **2000**, *65*, 7356. (b) Clausen, C.; Gryko, D.T.; Dabke, R.B.; Dontha, N.; Bocian, D.F.; Kuhr, W.G.; Lindsey, J.S. *J. Org. Chem.* **2000**, *65*, 7363. (c) Li, J.; Gryko, D.; Dabke, R.B.; Diers, J.R.; Bocian, D.F.; Kuhr, W.G.; Lindsey, J.S. *J. Org. Chem.* **2000**, *65*, 7379.
- ¹⁰ (a) Brunel, M.; Chaput, F.; Vinogradov, S.A.; Campagne, B.; Canva, M.; Boilot, J.P.; Brun, A. *Chem. Phys.*, **1997**, *218*, 301. (b) Qureshi, F.M.; Martin, S.J.; Long, X.; Bradley, D.D.C.; Henari, F.Z.; Blau, W.J.; Smith, E.C.; Wang, C.H.; Kar, A.K.; Anderson, H.L. *Chem. Phys.*, **1998**, *231*, 87. (c) McEwan, K.J.; Bourhill, G.; Robertson, J.M. *J. Nonl. Opt. Phy. Mat.* **2000**, *9* (4), 451.
- ¹¹ Wagner, R.W.; Lindsey, R.S.; Seth, J.; Palaniappan, V.; Bocian, D.F. *J. Am. Chem. Soc.* **1996**, *118*, 3996.
- ¹² Nitahara, S.; Akiyama, T.; Inoue, S.; Yamada, S. *J. Phys. Chem. B* **2005**, *109* (9), 3944.
- ¹³ (a) Xiao, X.W.; Xu, W.; Zhang, D.Q.; Xu, H.; Lu, H.Y.; Zhu, D.B. *J. Mater. Chem.* **2005**, *15* (26), 2557. (b) Straight, S.D.; Andreasson, J.; Kodja, G.; Moore, A.L.; Moore, T.A.;

- Gust, D. *J. Am. Chem. Soc.* **2005**, *127* (8), 2717. (c) Li, H.C.; Jeppesen, J.O.; Levillain, E.; Becher, J. *Chem. Comm.* **2003**, *14*, 846. (d) Hembury, G.A.; Borovkov, V.V.; Lintuluoto, J.M.; Inoue, Y. *Chem. Lett.* **2003**, *32* (5), 428. (e) Loppacher, C.; Guggisberg, M.; Pfeiffer, O.; Meyer, E.; Bammerlin, M.; Luthi, R.; Schlittler, R.; Gimzewski, J.K.; Tang, H.; Joachim, C. *Phys. Rev. Lett.* **2003**, *90* (6), 066107-1. (f) Otsuki, J.; Yasuda, A.; Takido, T. *Chem. Comm.* **2003**, *5*, 608.
- ¹⁴ (a) Straight, S.D.; Andreasson, J.; Kodis, G.; Bandyopadhyay, S.; Mitchell, R.H.; Moore, T.A.; Moore, A.L.; Gust, D. *J. Am. Chem. Soc.* **2005**, *127* (6), 9403. (b) Ambroise, A.; Wagner, R.W.; Rao, P.D.; Riggs, J.A.; Hascoat, P.; Diers, J.R.; Seth, J.; Lammi, R.K.; Bocian, D.F.; Holten, D.; Lindsey, J.S. *Chem. Mater.* **2001**, *13* (3), 1023. (c) Kuciauskas, D.; Liddell, P.A.; Moore, A.L.; Moore, T.A.; Gust, D. *J. Am. Chem. Soc.* **1998**, *120* (42), 10880.
- ¹⁵ Aratani, N.; Osuka, A. *Bull. Chem. Soc. Jpn.* **2001**, *74*, 1361.
- ¹⁶ (a) Bhyrappa, P.; Wilson, S.R.; Suslick, K.S. *J. Am. Chem. Soc.* **1997**, *119*, 8492. (b) Harriman, A.; Magda, D.J.; Sessler, J.L. *J. Chem. Soc. Chem. Comm.* **1991**, 345. (c) Harriman, A.; Magda, D.J.; Sessler, J.L. *J. Phys. Chem.* **1991**, *95*, 1530. (d) Sessler, J.L.; Wang, B.; Harriman, A. *J. Am. Chem. Soc.* **1995**, *117*, 704.
- ¹⁷ (a) Wojaczyński, J.; Latos-Grażyński, L. *Coord. Chem. Rev.* **2000**, *204*, 113. (b) Collman, J.P.; Harford, S.T.; Fransen, S.; Eberspacher, T.A.; Shoemaker, R.K.; Woodruff, W.H. *J. Am. Chem. Soc.* **1998**, *120*, 1456. (c) Collman, J.P.; Harford, S.T.; Maldivi, P.; Marchon, J.-C. *J. Am. Chem. Soc.* **1998**, *120*, 7999. (d) Imamura, T.; Fukushima, K. *Coord. Chem. Rev.* **2000**, *198*, 133.
- ¹⁸ Constable, E.C. "Coordination Chemistry of Macrocyclic Compounds", Oxford University Press, New York, 1999.

- ¹⁹ Smith, K.M. "*Porphyrins and Metalloporphyrins*", Elsevier Scientific Publishing Co., 1976.
- ²⁰ (a) Rodriguez, J.; Kirmaier, C.; Holten, D. *J. Am. Chem. Soc.* **1989**, *111*, 6500. (b) Gratz, H.; Penzkofer, A. *Chem. Phys.* **2000**, *254*, 363.
- ²¹ (a) Wang, Q.M.; Bruce, D.W. *Synlett*, **1995**, *12*, 1267. (b) Fan, D.Z.; Taniguchi, M.; Yao, Z.; Dhanalekshmi, S.; Lindsey, J.S. *Tetrahedron* **2005**, *61* (43), 10291. (c) Laha, J.K.; Dhanalekshmi, S.; Taniguchi, M.; Ambroise, A.; Lindsey, J.S. *Org. Prog. Res. Dev.* **2003**, *7* (6), 799. (d) Lin, V.S.Y.; Iovine P.M.; DiMugno, S.G.; Therien, M.J. *Inorg. Syn.* **2002**, *33*, 55. (e) Bruckner, C.; Posakony, J.J.; Johnson, C.K.; Boyle, R.W.; James, B.R.; Dolphin, D. **1998**, *2* (6), 455.
- ²² Burrell, A.K.; Officer D.L.; Plieger, P.G.; Reid, D.C.W. *Chem. Rev.* **2001**, *101*, 2751.
- ²³ (a) Taniguchi, M.; Balakumar, A.; Fan, D.Z.; McDowell, B.E.; Lindsey, J.S. *J. Por. Phthal.* **2005**, *9* (8), 554. (b) Thamyongkit, P.; Bhise, A.D.; Taniguchi, M.; Lindsey, J.S. *J. Org. Chem.* **2006**, *71* (3), 903.
- ²⁴ (a) Orlewska, C.; Maes, W.; Toppet, S.; Dehaen, W. *Tetrahedron Letters* **2005**, *46* (36), 6067. (b) Sessler, J.L.; Katayev, E.; Pantos, G.D.; Scherbakov, P.; Reshetova, M.D.; Khrustalev, V.N.; Lynch, V.M.; Ustynyuk, Y.A. *J. Am. Chem. Soc.* **2005**, *127* (32), 11442. (c) Sharada, D.S.; Muresan, A.Z.; Muthukumaran, K.; Lindsey, J.S. *J. Org. Chem.* **2005**, *70* (9), 3500.
- ²⁵ Littler, B.J.; Ciringh, Y.; Lindsey, J.S. *J. Org. Chem.* **1999**, *64*, 2864.
- ²⁶ Guest, D.; Moore, T.A.; Moore, A.L. *Acc. Chem. Res.* **1993**, *26*, 198.
- ²⁷ Chen, C.; Suslick, K.S. *Coord. Chem. Rev.* **1993**, *128*, 293.
- ²⁸ (a) Taira, I.; Keiko, F. *Coord. Chem. Rev.* **2000**, *198*, 133. (b) Maruoka, K.; Murase, N.; Yamamoto, H. *J. Org. Chem.* **1993**, *58*, 2938.

- ²⁹ (a) Jin, M.-L.; Chen, L.; Yin, J.-J.; Guo, C.-C.; Chen, Q.-Y. *Eur. J. Org. Chem.* **2005**, 3994. (b) Vidal-Ferran, A.; Bampos, N.; Sanders, J.K.M. *Inorg. Chem.* **1997**, 36, 6117. (c) Mackay, L.G.; Wylie, R.S.; Sanders, J.K.M. *J. Am. Chem. Soc.* **1994**, 116, 3141. (d) Prathapan, S.; Johnson, T.E.; Lindsey, J.S. *J. Am. Chem. Soc.* **1993**, 115, 7519. (e) Tsuda, A.; Furuta, H.; Osuka, A. *Angew. Chem. Int. Ed.* **2000**, 39, 2549. (f) Khoury, R.G.; Jaquinod, L.; Smith, K.M. *Chem. Comm.* **1997**, 1057. (g) Shi, X.; Liebeskind, L.S. *J. Org. Chem.* **2000**, 65, 1665.
- ³⁰ (a) Wei, Y.L.; Guo, X.L.; Shuang, S.M.; Dong, C.; Sun, X.H.; Wong, M.S. *J. Photochem. Photobiol. B- Biol.* **2005**, 81 (3), 190. (b) Trabolsi, A.; Elhabiri, M.; Urbani, M.; de la Cruz, J.L.D.; Ajamaa, F.; Solladie, N.; Albrecht-Gary, A.M.; Nierengarten, J.F. **2005**, 46, 5736. (c) Plieger, P.G.; Burrell, A.K.; Hall, S.B.; Officer, D.L. *J. Incl. Phenom. Macrocyclic Chem.* **2005**, 53 (3), 143. (d) Ballester, P.; Costa, A.; Deya, P.M.; Frontera, A.; Gomila, R.M.; Oliva, A.I.; Sanders, J.K.M.; Hunter, C.A. *J. Org. Chem.* **2005**, 70 (17), 6616. (e) Lu, J.Z.; Tan, X.C.; Huang, J.W.; Dong, C.H.; Fu, B.; Yu, H.C.; Ji, L.N. *Trans. Met. Chem.* **2005**, 30 (5), 643. (f) Carlucci, L.; Ciani, G.; Proserpio, D.M.; Porta, F. *Crystengcomm* **2005**, 7, 78. (g) Lauceri, R.; De Napoli, M.; Mammana, A.; Nardis, S.; Romeo, A.; Purrello, R. *Syn. Met.* **2004**, 143 (1-3), 49.
- ³¹ Ikeda, C.; Tanaka, Y.; Fujihara, T.; Ishii, Y.; Ushiyama, T.; Yamamoto, K.; Yoshioka, N.; Inoue, H. *Inorg. Chem.* **2001**, 40, 3395.
- ³² Krupitsky, H.; Stein, Z.; Goldberg, I.; Strouse, C. *J. Incl. Phenom. Macrocycl. Chem.* **1994**, 18, 177.
- ³³ Senge, M.O.; Speck, M.; Wiehe, A.; Dieks, H.; Aguirre, S.; Kurreck, H. *Photochem. Photobiol.* **1999**, 70, 206.
- ³⁴ Diskin-Posner, Y.; Patra, G.K.; Goldberg, I. *J. Chem. Soc., Dalton Trans.* **2001**, 2775.

- ³⁵ Shukla, A.D.; Dave, P.C.; Suresh, E.; Das, A.; Dastidar, P. *J. Chem. Soc., Dalton Trans.* **2000**, 4459.
- ³⁶ Byrn, M.P.; Curtius, C.J.; Hsiou, Y.; Khan, S.I.; Sawin, P.A.; Tendick, S.K.; Terzis, A.; Strouse, C.E. *J. Am. Chem. Soc.*, **1993**, *115*, 9840.
- ³⁷ (a) Krishna Kumar, R.; Balasubramanian, S.; Goldberg, I. *Inorg. Chem.*, **1998**, *37*, 541. (b) Krishna Kumar, R.; Goldberg, I. *Angew. Chem. Int. Ed.*, **1998**, *37*, 3027.
- ³⁸ (a) Zhou, X.; Ren, A.-M.; Feng, J.-F. *Chem. Eur. J.* **2004**, *10*, 5623. (b) Yin, S.C.; Xu, H.Y.; Shi, W.F.; Gao, Y.C.; Song, Y.L.; Wing, J.; Lam, Y.; Tang, B.Z. *Polymer* **2005**, *46* (18), 7670.
- ³⁹ (a) Whittall, I.R., McDonagh, A.M., Humphrey, M.G., Samoc, M. *Adv. Organomet. Chem.* **1998**, *42*, 291. (b) Whittall, I.R., McDonagh, A.M., Humphrey, M.G., Samoc, M. *Adv. Organomet. Chem.* **1999**, *43*, 349.
- ⁴⁰ (a) Annoni, E.; Pizzotti, M.; Ugo, R.; Quici, S.; Morotti, T.; Bruschi, M.; Mussini, P. *Eur. J. Inorg. Chem.* **2005**, *19*, 3857. (b) Calvete, M.; Yang, G.Y.; Hanack, M. **2004**, *141* (3), 231. (c) Yang, G.Y.; Ang, S.G.; Chng, L.L.; Lee, Y.W.; Lau, E.W.P.; Lai, K.S.; Ang, H.G. *Chem. Eur. J.* **2003**, *9* (4), 900. (d) Kandasamy, K.; Shetty, S.J.; Puntambekar, P.N.; Srivastava, T.S.; Kundu, T.; Singh, B.P. *J. Por. Phthal.* **1999**, *3* (2), 81. (e) Sen, A.; Ray, P.C.; Das, P.K.; Krishnan, V. **1996**, *100* (50), 19611.
- ⁴¹ Voet, D.; Voet, J.G.; Pratt, C.W. "*Fundamentals of Biochemistry*", John Wiley & Sons, Inc. USA, 1999.
- ⁴² Blau, W., Byrne, H., Dennis, W.M., Kelly, J.M. *Opt. Comm.* **1985**, *56*, 25.
- ⁴³ Irvine, M.P.; Harrison, R.J.; Strahand, M.A.; Beddard, G.S. *Ber. Bunsenges. Phys. Chem.* **1985**, *89*, 226.

- ⁴⁴ (a) Bonnett, R.; Harriman, A.; Kozyrev, A.N. *J. Chem. Soc. Faraday Trans.* **1992**, *88*, 763. (b) Su, W.; Cooper, T.M.; Nguyen, M.C.; Brant, M.C.; Brandelik, D.; McLean, D.G. *SPIE Proc.* **1998**, *136*, 3472.
- ⁴⁵ (a) Anderson, H.L. *Chem. Comm.* **1999**, 2323. (b) Susumu, S.; Therien, M.J. *J. Am. Chem. Soc.* **2002**, *124*, 8550. (c) Tsuda, A.; Osuka, A. *Science* **2001**, *293*, 79. (c) Thorne, J.R.G.; Kuebler, S.M.; Denning, R.G.; Blake, I.M.; Taylor, P.N.; Anderson, H.L. *Chem. Phys.* **1999**, *248*, 181.
- ⁴⁶ Zhang, T.G.; Zhao, Y.; Asselberghs, I.; Persoons, A.; Clays, K.; Therien, M.J. *J. Am. Chem. Soc.* **2005**, *127*, 9710.
- ⁴⁷ Yan, X.; Goodson III, T.; Imaoka, T.; Yamamoto, K. *J. Phys. Chem. B.* **2005**, *109*, 9321.
- ⁴⁸ Kiran, P.P.; Reddy, D.R.; Maiya, B.G.; Dharmadhikari, A.K.; Kumar, G.R.; Rao, D.N. *Opt. Comm.* **2005**, *252*, 150.
- ⁴⁹ Ogawa, K.; Phashi, A.; Kobuke, Y.; Kamada, K.; Ohta, K. *J. Am. Chem. Soc.* **2003**, *125*, 13356.
- ⁵⁰ Kuebler, S.M.; Denning, R.G.; Anderson, H.L. *J. Am. Chem. Soc.* **2000**, *122*, 339.
- ⁵¹ Screen, T.E.O.; Thorne, J.R.G.; Denning, R.G.; Bucknall, D.G.; Anderson, H.L. *J. Am. Chem. Soc.* **2002**, *124*, 9712.
- ⁵² Kim, D.Y.; Ahn, T.K.; Kwon, J.H.; Kim, D.; Ikeue, T.; Aratani, N.; Osuka, A.; Shigeiwa, M.; Maeda, S. *J. Phys. Chem. A* **2005**, *109* (13), 2996.
- ⁵³ Terazima, M.; Shimizu, H.; Osuka, A. *J. Appl. Phys.* **1997**, *81*, 2946.
- ⁵⁴ Ogawa, K.; Zhang, T.; Yoshihara, K.; Kobuke, Y. *J. Am. Chem. Soc.* **2002**, *124*, 22.
- ⁵⁵ Drobizhev, M.; Stepanenko, Y.; Dzenis, Y.; Karotki, A.; Rebane, A.; Taylor, P.N.; Anderson, H.L. *J. Am. Chem. Soc.* **2004**, *126*, 15352.

- ⁵⁶ Glezer, E.N.; Milosavljevic, M.; Huang, L.; Finlay, R.J.; Her, T.H.; Callan, J.P.; Mazur, E. *Opt. Lett.* **1996**, *21*, 2023.
- ⁵⁷ (a) Sun, H.B.; Kawakami, T.; Xu, Y.; Ye, J.Y.; Matuso, S.; Misawa, H.; Miwa, M.; Kaneko, R. *Opt. Lett.* **2000**, *25*, 1110. (b) Maruo, S.; Kawata, S. *J. Microelectromech. Syst.* **1998**, *7*, 411. (c) Sun, H.B.; Xu, Y.; Juodkazis, S.; Sun, K.; Watanabe, M.; Matsuo, S.; Misawa, H.; Nishii, J. *Opt. Lett.* **2001**, *26*, 325.
- ⁵⁸ So, P.T.C.; Kim, H. *Opt. Exp.* **1998**, *3* (9), 339.
- ⁵⁹ (a) Fisher, W.G.; Partridge, W.R.; Dees, Jr. C.; Wachter, E.A. *Photochem. Photobiol.* **1997**, *66*, 141. (b) Bhawalkar, J.D.; Kumar, N.D.; Zhao, C.F.; Prasad, P.N. *J. Clin. Lasers Med. Surg.* **1997**, *15*, 201. (c) Frederiksen, P.K.; Jorgensen, O.P.R. *J. Am. Chem. Soc.* **2001**, *123*, 1215.
- ⁶⁰ Dougherty, T.J.; Gomer, C.J.; Henderson, B.W.; Jori, G.; Kessel, D.; Korbelik, M.; Moan, J.; Peng, Q. *J. Nat. Cancer. Instit.* **1998**, *90* (12), 889.
- ⁶¹ Liu, J.; Zhao, Y.W.; Zhao, J.Q.; Xia, A.D.; Jiang, L.J.; Wu, S.; Ma, L.; Dong, Y.Q.; Gu, Y.H. *J. Photochem. Photobiol. B* **2002**, *68*, 156.
- ⁶² Wachter, E.A.; Partridge, W.P.; Fisher, W.G.; Dees, H.C.; Petersen, M.G. *Proc. SPIE-Int. Soc. Opt. Eng.* **1998**, *3269*, 68.
- ⁶³ Ogawa, K.; Hasegawa, H.; Inaba, Y.; Kobuke, Y.; Inouye, H.; Kanemitsu, Y.; Kohno, E.; Hirano, T.; Ogura, S.; Okura, I. *J. Med. Chem.* **2006**, *49* (7), 2276.
- ⁶⁴ (a) Rubio-Pons, O.; Luo, Y.; Agren, H. *J. Chem. Phys.* **2006**, *124* (9), Art. No. 094310. (b) Ahn, T.K.; Kim, K.S.; Kim, D.Y.; Noh, S.B.; Aratani, N.; Ikeda, C.; Osuka, A.; Kim, D. *J. Am. Chem. Soc.* **2006**, *128* (5), 1700. (c) Karotki, A.; Drobizhev, M.; Dzenis, Y.; Taylor, P.N.; Anderson, H.L.; Rebane, A. *Phys. Chem. Chem. Phys.* **2004**, *6* (1), 7. (d) Ogawa, K.; Ohashi, A.; Kobuke, Y.; Kamada, K.; Ohta, K. *J. Am. Chem. Soc.* **2003**, *125* (44), 13356.

- ⁶⁵ (a) Ray, P.C.; Leszczynski, J. *Chem. Phys. Lett.* **2006**, *419* (4-6), 578. (b) Monnereau, C.; Blart, E.; Montembault, W.; Fontaine, L.; Odobel, F. *Tetrahedron* **2005**, *61* (42), 10113. (c) Tillekaratne, A.D.; de Silva, R.M.; de Silva, K.M.N. *J. Mol. Struc - Theochem* **2003**, *638*, 169. (d) LeCours, S. M.; Guan, H.-W.; DiMugno, S. G.; Wang, C. H.; Therien, M. J. *J. Am. Chem. Soc.* **1996**, *118*, 15040. (e) LeCours, S. M.; DiMugno, S. G.; Therien, M. J. *J. Am. Chem. Soc.* **1996**, *118*, 11854. (f) Priyadarshy, S.; Therien, M. J.; Beratan, D. N. *J. Am. Chem. Soc.* **1996**, *118*, 1497.
- ⁶⁶ (a) Kiran, P.P.; Reddy, D.R.; Dharmadhikari, A.K.; Maiya, B.G.; Kumar, G.R.; Rao, D.N. *Chem. Phys. Lett.* **2006**, *418* (4-6), 442. (b) Ogawa, K.; Ohashi, A.; Kobuke, Y.; Kamada, K.; Ohta, K. *J. Phys. Chem. B* **2005**, *109* (46), 22003. (c) Screen, T.E.O.; Thorne, J.R.G.; Denning, R.G.; Bucknall, D.G.; Anderson, H.L. *J. Mater. Chem.* **2003**, *13* (11), 2796.
- ⁶⁷ Inokuma, Y.; Ono, N.; Uno, H.; Kim, D.Y.; Noh, S.B.; Kim, D.; Osuka, A. *Chem. Comm.* **2005**, 3782.
- ⁶⁸ Chandrasekhar, V.; Nagendran, S.; Azhakar, R.; Kumar, M.R.; Srinivasan, A.; Ray, K.; Chandrashekar, T.K.; Madhavaiah, c.; Verma, S.; Priyakumar, U.D.; Sastry, G.N. *J. Am. Chem. Soc.* **2005**, *127*, 2410.
- ⁶⁹ Bonnett, R.; Martinez, G. *Org. Lett.* **2002**, *4* (12), 2013.

CHAPTER 2

ELEMENTS OF THE THEORY OF NONLINEAR OPTICS

2.0 INTRODUCTION

The birth of the field of nonlinear optics (NLO) was marked by Kerr's observation in 1875, of a change in the refractive index of CS_2 proportional to the square of the amplitude of an applied field.¹ This is now known as the Kerr effect. Shortly, in 1893, a similar but linear electric field effect in quartz was observed and this process is known as the Pockels effect.¹ These two nonlinear effects flourished after the invention of laser in 1960 and were followed by the observation of the second harmonic generation (SHG) by Franken and co-workers² in quartz a year later. The Pockels (also known as the linear electrooptic) effect is the change in the linear susceptibility and thus refractive index of the material with changes in applied voltage. At the atomic level, the applied voltage is anisotropically distorting the electron density within the material. Thus, application of a voltage to a material causes the optical beam to "see" a different material with a different polarizability and a different anisotropy of the polarizability than in the absence of the voltage.³

The first observation of SHG in an organic compound was made in benzopyrene and was done by Rentzepis and Pao in 1965. This developed explosively throughout the 1960s whereupon the work of Bloembergen (Nobel prize 1981) and co-workers⁴ were highlighted for exploring the full range of NLO responses of materials systems.

Many of the interesting phenomena of NLO derive their behaviour from the nonlinear index of refraction. The phenomena include the optical Kerr effect, four-wave mixing, two-beam coupling, optical bistability and self-focussing.¹ Thus, it has been utilized in a variety of applications such as nonlinear spectroscopy, high resolution photolithography, spatial information processing, temporal signal processing, optical computing and optical limiting.¹

On the other hand, changes in optical properties of a material upon absorption of intense radiation from a laser can lead to nonlinear absorption processes, including multiphoton, reduced (saturable) as well as increased (reverse saturable) absorption and are explained in detail in the following sections.

2.1 PRINCIPLES AND ORIGIN OF NONLINEAR OPTICS

NLO involves the interactions of electromagnetic fields in various media to produce new fields which may be altered in phase, frequency, amplitude or other propagation characteristics from the incident field. When a beam of light is impinged into a material, it causes the electrons in the atoms to oscillate. This occurs for any light but the oscillations are more pronounced for more intense light such as laser. Lasers are sources of coherent light, characterized by a high degree of monochromaticity, high directionality and high intensity or brightness. Today, with optical parametric oscillators and amplifiers, it is possible to cover a large range of wavelengths, including the entire visible spectrum, for instance from 403 nm to 2580 nm continuously, using a Nd:YAG pump laser which beams are focused into a LiB_3O_5 crystal.⁵

For low light intensities, that is, in linear optics domain, the amount of charge displacement is proportional to the instantaneous amplitude of the electric field hence, the charges are driven to oscillate at the same frequency as the frequency of the incident light. The oscillating charges can radiate light at the same frequency or in the presence of material resonances. Energy can be transferred via non-radiative modes that result in material heating or through other energy transfer mechanisms. The displacement of charges from the equilibrium positions gives rise to induced polarization $P_i(t)$, which depends linearly upon the applied electric field in a manner depicted by the relationship

$$(2.1) \quad P_i(t) = P_{\text{stat},i} + \chi_{ij}^{(1)} E_j(t)$$

where $P_i(t)$ is the polarization of the medium with respect to time, $P_{\text{stat},i}$ is the static polarization, $\chi_{ij}^{(1)}$ is the linear susceptibility and $E_j(t)$ is the applied electric field with respect to time. Note that the second term in this equation is a sum over j and the sum symbol is skipped under Einstein's summing convention. The presence of material resonances leads to phase shifts between P and E and to absorption. These are accounted for by allowing $\chi^{(1)}$ to be complex.

When the intensity of light becomes large enough, linear optics is no longer enough to describe the situation observed experimentally. This is due to the interaction of light waves with the optical medium and through the medium with one another and the optical medium. Hence, the theory of linear optics has to be extended to explain the new phenomena. In NLO, $\vec{P}(t)$ should be expressed as a power series of $\vec{E}(t)$ as

$$(2.2) \quad \vec{P}(t) = \vec{P}_0(t) + \chi_{ij}^{(1)} \vec{E}_j(t) + \chi_{ijk}^{(2)} \vec{E}_j(t) \vec{E}_k(t) + \chi_{ijkl}^{(3)} \vec{E}_j(t) \vec{E}_k(t) \vec{E}_l(t) + \dots$$

where $\chi^{(n)}$ are the n^{th} order NLO susceptibility tensors of a given medium respectively and the Einstein's summing convention is used.¹

The above two equations are under the assumption that the polarization at time (t) depends only on the instantaneous value of the electric field.

At the molecular level, the time dependent dipole moment of a molecule $\tilde{p}(t)$ is

$$(2.3) \quad \tilde{p}(t) = \mu_1^0(t) + \alpha_{IJ} \tilde{E}_J(t) + \beta_{IJK} \tilde{E}_J(t) \tilde{E}_K(t) + \gamma_{IJKL} \tilde{E}_J(t) \tilde{E}_K(t) \tilde{E}_L(t) + \dots$$

where $\mu_1^0(t)$ is the molecular dipole moment, α_{IJ} is the linear polarizability, β_{IJK} is the first hyperpolarizability and γ_{IJKL} is the second hyperpolarizability.

The physical processes that occur as a result of the second-order nonlinear polarization⁶ and third-order nonlinear polarization⁷ are distinctly different. Second-order effects are dependent on the first hyperpolarizability tensor term $\chi^{(2)}$ and third-order effects may also be present (for example, three-photon absorption) under high light intensities. For second-order effects,⁸ such interactions can only occur in non-centrosymmetric media. Since liquids, gases, amorphous solids and even most crystals display inversion symmetry, $\chi^{(2)}$ vanishes for such media. On the other hand, third-order NLO interactions occur both for centrosymmetric and non-centrosymmetric media. Basically, all forms of matter exhibit NLO phenomena but to be useful as a NLO device, the material must exhibit a high degree of nonlinearity so it may be operated at a reasonable power level.¹

2.2 NONLINEAR INDEX OF REFRACTION¹³

The general dependence of the refractive index on intensity can be expressed as

$$(2.4) \quad n(r,t) = n_0 + \Delta n[I(r,t)] = n_0 + n_2[I(r,t)]$$

This equation indicates that the change in the refractive index Δn over its value at low intensities n_0 (that is, linear index of refraction), has a functional dependence on the time and spatial coordinate dependent intensity $I(r,t)$ where $I(r,t) = 2\varepsilon_0 n_0 c |A|^2$ with expressions in S.I units and $\varepsilon_0 = 8.85 \times 10^{-12}$ F/mⁱ being the electric permittivity of free space and $c = 3 \times 10^8$ m s⁻¹ is the speed of light in vacuum. A is the electric field amplitude and n_2 is the nonlinear refractive index. Large refractive nonlinearities in materials are commonly associated with a resonant transition which may be of single or multiphoton nature. In this case, $\chi^{(3)}$ is now considered to be a complex quantity:

$$(2.5) \quad \chi^{(3)} = \chi_{\text{real}}^{(3)} + i\chi_{\text{imag}}^{(3)}$$

and n_2 is related to $\chi^{(3)}$ by

$$(2.6) \quad n_2 = \frac{16}{c\varepsilon\pi^2} \chi_{\text{imag}}^{(3)}$$

where ε is the dielectric constant.

The imaginary part of $\chi^{(3)}$ is the origin of two-photon absorption (TPA) in which two photons (same or different frequencies) are simultaneously absorbed in a material. The TPA process will be described in detail shortly. For many applications, $\chi^{(3)}$ should be purely real in order to induce a maximum nonlinear phase-shift without optical loss.

ⁱ F/m is farad/meter (SI); 1 F/m = 1 C V⁻¹m⁻¹ (SI)

Although the imaginary part of $\chi^{(3)}$ is often considered an adverse effect, especially for all-optical signal processing, TPA is nevertheless important for many applications.

Several diverse physical effects contribute to and arise from the nonlinear index of refraction. One area of interest is self-focusing and self-defocusing. These nonlinear phenomena have been applied in some devices, one of the most common being optical limiting. This is illustrated in Fig. 2.1 for both positive and negative n_2 . The nonlinear medium is situated between two lenses. Light of low-intensity is collected by the second lens and imaged through an aperture to a detector. When light of high-intensity is passed through a medium with $n_2 > 0$, the beam will collapse and phase distortion will result such that the light is not focused by the second lens but defocused in the aperture plane. Thus, the power transmitted by the aperture to the detector is limited and the detector is protected from the high-intensity radiation. When $n_2 < 0$, the beam diverges more rapidly from the intermediate focus rather than collapsing. A defocused beam reached the aperture plane also. However, the advantage of this type of limiter over the previous is that it is self-protecting (that is, the light is defocused inside the medium leading to lower intensity there that is less likely to cause laser damage). This is important when the medium is solid and the damage would be permanent.¹

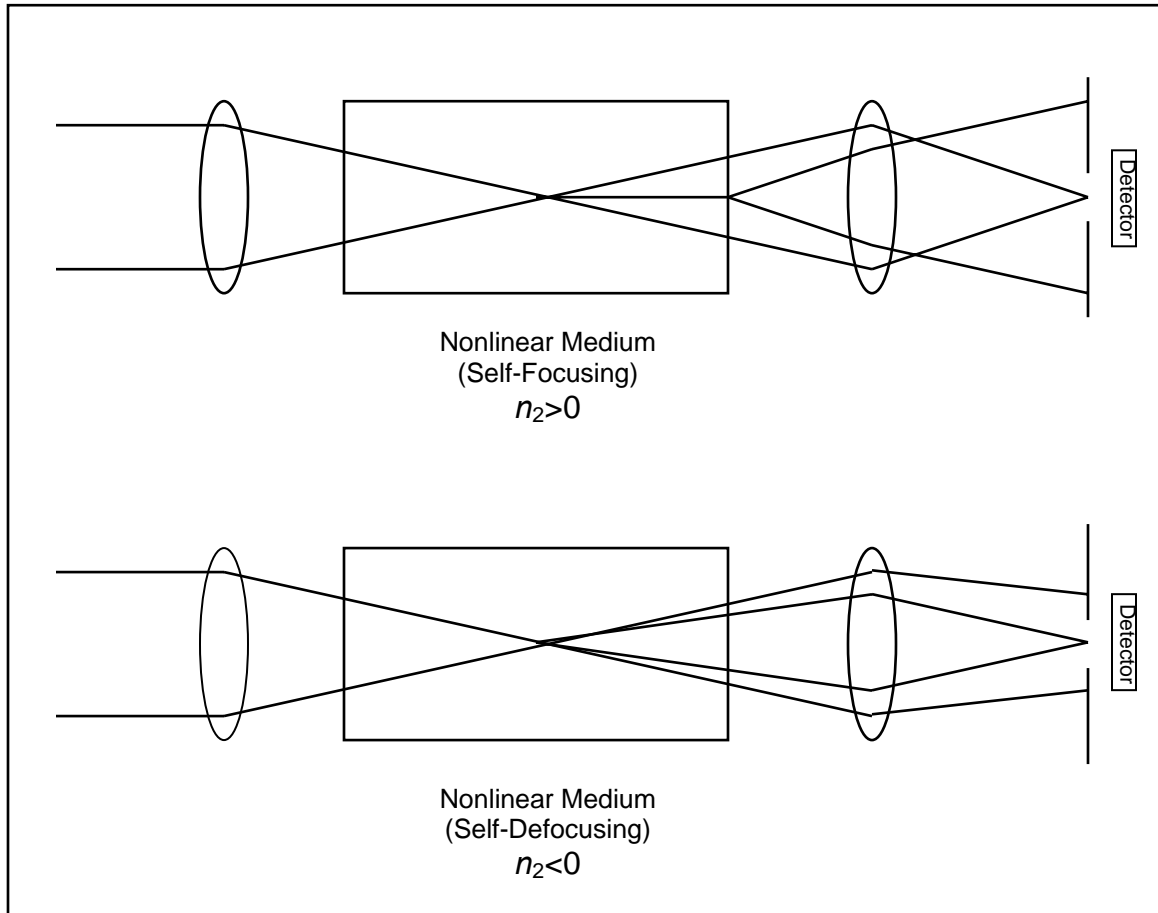


Fig. 2.1 Optical limiters based on self-focusing. (a) $n_2 > 0$ and (b) $n_2 < 0$

2.3.0 INTRODUCTION TO TWO-PHOTON ABSORPTION

The effect of TPA immediately proved to be a particularly useful spectroscopic technique in providing information about atomic and molecular structures since its discovery in the early 1960s.⁹ In the years to follow, applications of TPA flourished and have extended to the fields of high resolution three-dimensional (3D) microscopy,¹⁰ 3D ultrahigh density optical data storage,¹¹ 3D micro- and nanofabrication,¹² optical power limiting,¹³ ultrashort pulse characterization,¹⁴ frequency upconversion lasing¹⁵ and photodynamic therapy (PDT).¹⁶

Today, some 40 years later, the importance of two-photon spectroscopy of organic molecules grew because of two critical factors. First, there is an increasing demand for efficient two-photon absorbers that are compatible with new technologies for biological applications. Second, the development of mode-locked ultrafast lasers in the 1990s provided a source of extremely high peak intensity light pulses that facilitate instantaneous two-photon processes.

The advantage of TPA as a spectroscopic tool arises from the ability to provide additional information on the atomic and molecular structures of compounds especially in centrosymmetric molecules. One-photon absorption (OPA) parity selection rules in such molecules apply where only transitions between states of different parities, that is, *ungerade* ↔ *gerade* (*u* ↔ *g*) are allowed. On the contrary, TPA allows transitions between states of the same parities, that is, *gerade* ↔ *gerade* (*g* ↔ *g*) and *ungerade* ↔ *ungerade* (*u* ↔ *u*) transitions. Since the ground state is usually of *g* parity, TPA facilitates the investigation of excited *g* parity levels that are usually very difficult to access for linear absorption spectroscopy. Hence, TPA spectroscopy greatly enhances our understanding of molecular properties.

The list of unique properties that make TPA attractive for several practical applications are many:

1. instantaneous response;
2. quadratic dependence of absorption rate on the excitation intensity ($\sim I^2$);
3. higher energy emission wavelength as compared to the excitation wavelength;
4. possibility of exciting molecules selectively in a small volume ($\sim \lambda^3$);

5. deeper penetration of near IR light, typically used for two-photon excitation into tissues.

The instantaneous response of TPA allows efficient cutoff of high intensity light even on the femtosecond time scale. While the quadratic dependence on the excitation light intensity can be used for optical power limiting in which an ideal power limiter allows low intensity light to propagate practically without absorption while attenuating high intensity light. Furthermore, the quadratic dependence of TPA on the excitation intensity allows one to measure second order intensity autocorrelation or cross-correlation functions and is used short laser pulse characterization.

Since in two-photon transitions, the energies of two photons are added up, the excitation wavelength is typically much longer and well separated from the fluorescence wavelength. This greatly simplifies the registration of two-photon excited fluorescence because the excitation and fluorescence photons can be easily separated by filters and/or monochromators. This makes two-photon fluorescence microscopy advantageous over its one-photon counterpart in laboratory experiments. Two-photon excited fluorescence is also employed for readout in high density 3D optical data storage.

The ability to confine laser light through focusing allows one to generate light of high enough intensity to observe TPA phenomena. This is particularly important for applications such as 3D microfabrication, high-density 3D optical data storage and two-photon fluorescence microscopy.

The final point mentioned is particularly important for PDT, which is expected to replace the current forms of cancer therapy as it is burdened with many shortcomings. In PDT, near-infrared (near-IR) light is used because this light is less absorbed and scattered by human tissues than visible light. This enables increased penetration of the light into human body which can be used for two-photon excitation of biologically relevant molecules deep inside the tissues. Hence, TPA-based fluorescence microscopy using near-IR light for excitation is able to provide imaging of tissues an order of magnitude deeper than one-photon confocal fluorescence microscopy using visible light. Similar advantage can be gained by two-photon-based PDT which uses excitation of a photosensitizer (the drug) inside the body to initiate photophysical and photochemical processes for tumor destruction. Current PDT uses OPA that can only treat tumors close to the surface of tissues or accessible by endoscope. The use of near-IR light for two-photon excitation of photosensitizers can thus greatly increase the efficiency of PDT in future.

In this respect, the study of TPA properties of organic molecules especially those compatible with biological and medical applications is of great importance. The ultimate success of any two-photon-based applications depends critically on the efficiency of TPA of the molecules, which includes the ability to perform specialized photophysical, photochemical and photobiological function and in particular, on the value of intrinsic nonlinear cross section (or TPA cross section), σ_2 . Hence, the biologically relevant tetrapyrrolic molecules, porphyrins, are particularly well suited for these applications. Porphyrins perform several crucial functions in nature, such as oxygen transportation and photosynthesis and are widely used in one-photon-based PDT.

The TPA properties of porphyrins were ignored until recently. Rebane *et al.* have investigated the intrinsic TPA spectra of many tetrapyrrolic compounds using 100 fs pulses.¹⁷ Typically, the TPA σ_2 is generally low in the Q-band with a value of $\sigma_2 = 1 - 10$ GM while in the vicinity of the Soret band, it can be enhanced up to $\sigma_2 = 1 \times 10^3$ GM, by different mechanisms, including resonance enhancement, electron-donating or -accepting substitutions and *g* parity excited states.

2.3.1 TWO-PHOTON ABSORPTION: THE MAIN CONCEPTS AND THEORETICAL CONSIDERATIONS

TPA is a NLO process in which two photons are absorbed simultaneously, such that the energy of the photons add up to the energy of the excited atom or molecule:

$$(2.7) \quad \hbar\nu_1 + \hbar\nu_2 = E$$

where $\hbar = \frac{h}{2\pi}$ and h is the Planck constant, ν_i is the frequency of the *i*-th absorbed photon, E is the transition energy. It involves a transition from the ground state of a system to a higher-lying state. The absorption of all the photons is simultaneous in the sense that there are real intermediate energy levels that are populated in this process. The absorption takes place through so-called virtual levels, whose existence is allowed by quantum mechanics. This effect is completely different from stepwise absorption. In this case, no real intermediate levels are populated during absorption. The process also involves different selection rules from those of OPA hence TPA spectroscopy complements linear absorption spectroscopy in studying the excited states of systems.

Two possible situations are illustrated in Fig. 2.2. In the first, two photons from the same optical field oscillating at frequency ω are absorbed to make the transition which is approximately resonant at 2ω . This is known as single-beam TPA. In the second situation, two optical fields at frequencies ω_e and ω_p are present and one photon from each field is absorbed for the transition which is approximately resonant at $\omega_e + \omega_p$. The ω_e can be thought of as the pump or excitation beam while ω_p can be considered as the probe beam. In this case, the process occurs in two-beam TPA.

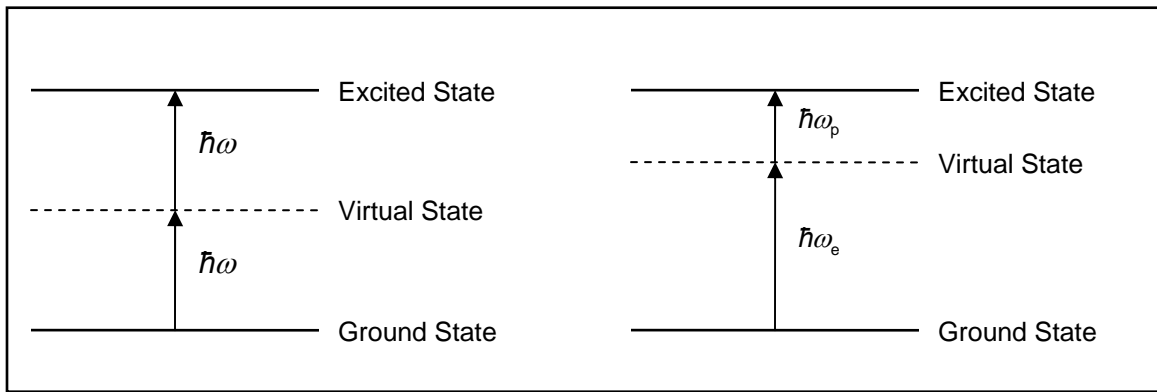


Fig. 2.2 Illustration of TPA (a) Self-TPA, (b) Pump-probe TPA

In the case where real intermediate energy levels are populated, single-photon excited state absorption (ESA, described in detail in Section 2.4) process is said to have taken place. As illustrated in Fig. 2.3, the excited state (3) is populated in TPA and the single-photon excited state processes, but in the latter, the symmetry of the intermediate state (2) must be opposite to both the upper and lower levels. While TPA is an instantaneous process, stepwise excitations may be separated by a period determined by the lifetime of level (2). The two photons involved in either process may have different frequencies (ω_1, ω_2). The cross sections σ_2 , $\sigma_{(12)}$ and $\sigma_{(23)}$ correspond to the two-photon, single-photon and excited state absorption processes respectively.^{9a}

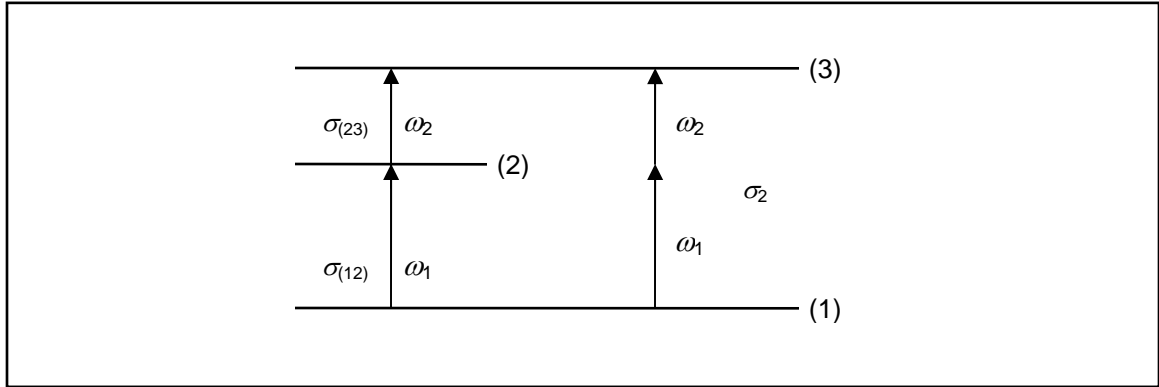


Fig. 2.3 Illustration of TPA and single-photon excited state absorption processes

TPA was predicted theoretically by M. Göppert-Mayer¹⁸ in 1931 for transitions between discrete energy states and was later applied for transitions between band states in dielectrics and semiconductors. The probability of multiphoton absorption on excitation light intensity follows the power law:

$$(2.8) \quad P \propto I_1^{n'_1} I_2^{n'_2} \dots I_k^{n'_k}$$

where P is the probability of multiphoton excitation, I_k is the intensity of k -th source of light and n'_k is the number of photons from the k -th source of light participating in a single act of simultaneous multiphoton absorption so that the sum $\sum_k n'_k$ is equal to the total number of absorbed photons. In the case of one excitation source (laser), equation 2.8 simplifies to:

$$(2.9) \quad P = \frac{1}{n'} \sigma_{n'} I^{n'}$$

where $\sigma_{n'}$ is the n' -photon absorption cross section and coefficient $1/n'$ takes into account the fact that n' photons are required for n' -photon excitation of one atom (molecule).

The unit for σ_2 is $\text{cm}^4 \text{ s photon}^{-1} \text{ molecule}^{-1}$ or GM (called Göppert-Mayer) where $1 \text{ GM} = 10^{-50} \text{ cm}^4 \text{ s photon}^{-1} \text{ molecule}^{-1}$, to honor the woman who theoretically predicted

TPA. As the units suggest, the cross section may be defined by the simple expression for the decay in an incident light flux, F , along a propagation direction, z , due solely to TPA:

$$(2.10) \quad -\frac{dF}{dz} = N\sigma_2 F^2$$

where N is the number density of molecules.

2.3.2 SINGLE BEAM TWO-PHOTON ABSORPTION

The nonlinear absorption in this case is proportional to the square of the instantaneous intensity I . The differential equation describing the optical loss is given by:

$$(2.11) \quad \frac{dI}{dz} = -\alpha I - \beta I^2$$

where α is the linear absorption coefficient due to the presence of impurities and β is the TPA coefficient.

The TPA coefficient β is a macroscopic parameter characterizing the material. Often there is interest in the individual molecular TPA property that is described by σ_2 . The relation between β and σ_2 is given as:

$$(2.12) \quad \sigma_2 = \frac{\hbar\omega\beta}{N}$$

where $\hbar\omega$ is the energy of photons in the incident optical field.

The β is also related to the third order susceptibility:

$$(2.13) \quad \beta = \frac{3\pi}{\epsilon_0 n^2 c \lambda} \chi_{\text{imag}}^{(3)} \quad (\text{S.I.})$$

$$\beta = \frac{48\pi^3}{n^2 c \lambda} \chi_{\text{imag}}^{(3)} \quad (\text{cgs})$$

where $\chi_{\text{imag}}^{(3)}$ is the imaginary third-order nonlinear susceptibility, λ is wavelength. Note that it is the imaginary part of $\chi^{(3)}$ that determines the strength of the nonlinear absorption.

The principal quantity of interest in a measurement is the net transmittance of the material to light at ω . The physical quantity usually measured for a sample with length L is the optical energy thus the transmittance T ¹⁹ is defined as the ratio of transmitted I_{tr} and incident energies I_0 .

$$(2.14) \quad \frac{1}{T} = \frac{I_0}{I_{\text{tr}}} = 1 + \beta I_0 L$$

This equation predicts a linear dependence between the inverse of T and I_0 . The β may be simply determined from the slope of the inverse T of the sample as a function of I_0 . However, corrections are needed because of the fact that one deals with spatial and temporal dependencies of the light intensities.

2.3.3 PARITY SELECTION RULES FOR TWO-PHOTON TRANSITIONS

According to the electric dipole approximation, the efficiency of TPA between the ground state and upper final state is determined by the energy eigenstate that plays a role of intermediate level and the electric-dipole energy in the electric field. If the molecule is centrosymmetric, then the wavefunctions corresponding to different energy

levels also possess some degree of symmetry which limits the number of radiation transitions between the energy levels. In particular, wavefunctions ψ of centrosymmetrical molecules can have either even (g parity) or odd symmetry (u parity) in which case the following relations are obeyed:

$$(2.15) \left\{ \begin{array}{l} \psi_g(r) = \psi_g(-r) \quad \text{gerade} \\ \psi_u(r) = -\psi_u(-r) \quad \text{ungerade} \end{array} \right\}$$

Two different cases are possible: 1) ground and final levels have different parity, 2) ground and final levels have the same parity. In the first case, no matter what the parity of the intermediate level m is, one of the multipliers will always be zero. In the second case, if the symmetry of the intermediate level is different from the symmetry of the ground and final excited levels then both multipliers are different from zero. Correspondingly, in centrosymmetric molecules, TPA can take place only when the initial and final levels have the same parity, that is $g \leftarrow g$ or $u \leftarrow u$ transitions. Two-photon transitions between levels with different parity are prohibited in the dipole approximation.

As the ground level typically has g parity, the two-photon transitions from the ground levels are allowed only into other g parity levels. Since allowed transitions are always much stronger than the prohibited transitions (prohibited transition can always be slightly allowed for example through quadrupole approximation) $g \leftarrow g$ TPA bands have large σ_2 .

Since selection rules for OPA are opposite, that is, only $g \leftarrow u$ or $u \leftarrow g$ transitions are allowed, TPA spectroscopy is complimentary to OPA spectroscopy as the former allows the investigation of otherwise inaccessible energy levels. For non-

centrosymmetric molecules, the symmetry of the energy levels cannot be precisely defined and both types of transition are allowed between different levels.

Higher order absorption spectroscopy is also very useful technique. For instance, three-photon absorption has the same parity selection rules as OPA but the former can reveal even more information about molecules than the latter. In centrosymmetric molecules, there are $g \leftarrow u$ transitions that are parity allowed for OPA but still forbidden due to other symmetry considerations. In that case, these transitions become allowed in higher order absorption, like simultaneous absorption of three photons. Three-photon spectroscopy also permits observation of a greater manifold of vibronic transitions than are accessible to one-photon spectroscopy.²⁰

2.4 EXCITED STATE ABSORPTION¹

As mentioned earlier, TPA mechanism involves the absorption of a second photon from a virtual state. On the other hand, excited state absorption (ESA) involves a real intermediate state. When the incident intensity of light is high and close to so-called saturation intensity, the excited state of the molecules can become significantly populated. The excited molecules rapidly make a transition to one of the excited states before it eventually transitions back to the ground state. However, there are also a number of highly-lying states that may be radiatively coupled to these intermediate states and for which the energy differences are in near-resonance with the incident photon energy. Therefore, before the molecule completely relaxes to the ground state, it may experience absorption that promotes it to a higher-lying state and this process is called the ESA. This is observable when the incident intensity is sufficient to deplete the ground state significantly.

When the σ_2 of the excited state is smaller than that of the ground state, the transmission of the system will be increased when the system is highly excited. This process is called saturable absorption (SA). On the other hand, when the σ_2 of the excited state is larger than that of the ground state, the system will be less transmissive when excited. This gives the opposite result as saturable absorption and is thus called reverse saturable absorption (RSA).

Within each electronic state of a molecule, there exists a manifold of very dense vibrational-rotational states. When the molecule absorbs electromagnetic radiation, it will generally undergo transition to one of these vibrational-rotational states. After collision, it drops to the lowest vibrational-rotational level within the electronic manifold of states whereupon, it experiences absorption of another photon or relax to any of a number of lower-energy states.

The ground electronic state (S_0) is called a singlet state which has a pair of electrons with anti-parallel spins. Selection rules disallow parallel spins in the same state hence absorption from S_0 only allows transition to another singlet electronic state. However, it is possible to produce a spin flip by external processes such as collisions with paramagnetic ions or internal processes such as spin-orbit coupling. Under such conditions, the first excited electronic state may make a radiationless transition to a lower-lying triplet state, that is, a state with a pair of electrons having parallel spins. A radiative transition from this state is allowed by selection rules if the transition is to another triplet state. Transitions between singlet-singlet and triplet-triplet states are spin-allowed.

The process of absorption can be explained using an energy diagram as shown in Fig. 2.4. The absorption of an incident photon at low incident fluences causes most of the molecules within the illuminated volume occupy low absorbent ground state S_0 , while at higher incident fluences, significant number of molecules is pumped into the excited state with higher absorption coefficient. Thus, the overall absorption by the system increases. A necessary condition for this effect is thus the wavelength overlap between the absorption bands for both states. Depending on the type of molecular system and efficiency of the intramolecular transitions such as intersystem crossing (explained below), the participating excited state can be singlet state, triplet state or in some cases, both states can be involved.²¹

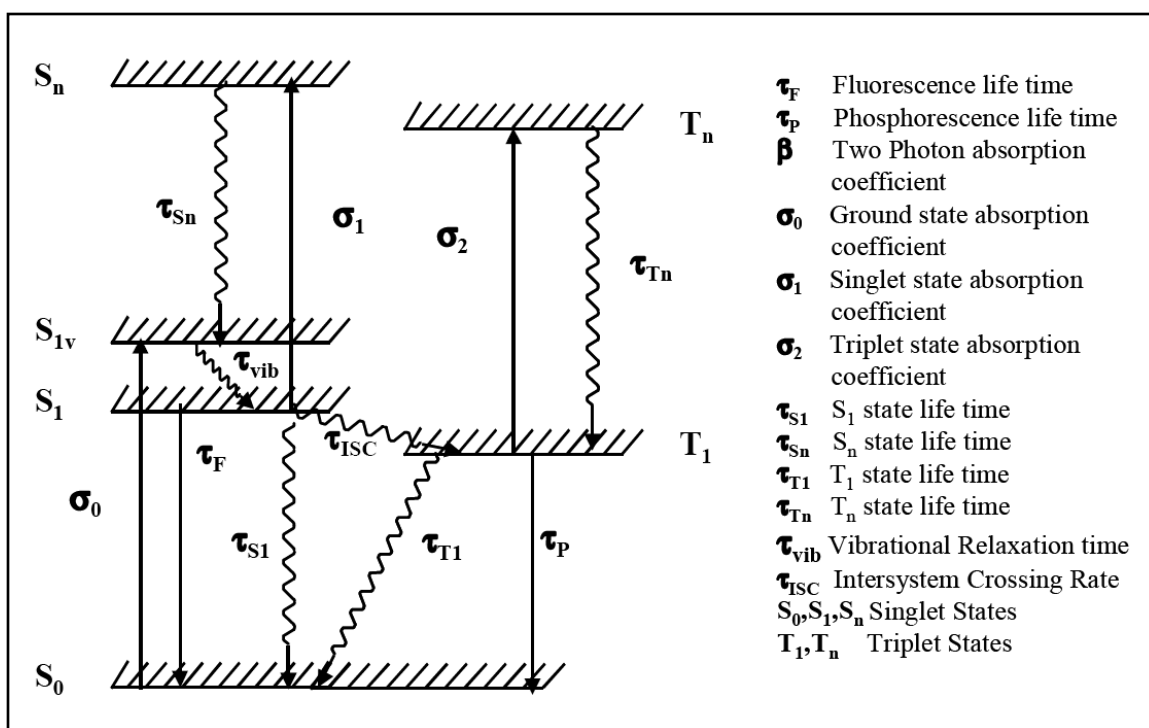


Fig. 2.4 An energy diagram of a typical organic molecule

When a laser pulse is incident, the molecules are excited from the lowest levels of the ground state S_0 to the higher vibrational states of S_1 (S_{1v}). The decay from S_{1v} to S_1 is non-radiative and occurs within few ps. From S_1 , the molecules can relax back to the ground state radiatively or non-radiatively or crossover to T_1 via intersystem crossing. The radiative decay, which is spontaneous, from S_1 to S_0 is known as fluorescence and is governed by the lifetime of the S_1 state. For organic molecules, the lifetime is typically of the order of a few ns. The energy difference between absorption and emission processes is taken by the non-radiative decay in the S_1 and S_0 states and the relaxation of the molecules from S_1 to the lowest triplet state T_1 is governed by the intersystem crossing rate. The intersystem crossing rate constant is typically 10^{11} to 10^7 s^{-1} due to spin restriction factor. Another important process of deactivation of the S_1 state is the internal conversion, which is the non-radiative decay of S_1 to S_0 . The decay from T_1 to S_0 can be radiative or non-radiative and is termed as phosphorescence if it is the former type. Typical phosphorescence lifetimes are in the range of ms to μ s. The lifetime of T_1 is generally large since the triplet-singlet transition is dipole forbidden. Hence, a molecule can absorb another photon from the excited singlet or triplet states before it relaxes back to ground state. Thus, this explains the process of ESA which gives rise to effective third-order nonlinearity and holds implications on optical limiting. The parameter describing an optical limiter in this study is the value of nonlinear threshold. It is defined as the linear transmission at 50 % of the initial one.

2.5 REFERENCES

- ¹ (a) Sutherland, R.L.; McLean, D.G.; Kirkpatrick, S. *“Handbook of Nonlinear Optics”*, Basel, N.Y., Marcel Dekker, Inc., 2003, U.S.A. (b) Butcher, P.N.; Cotter, D.; Knight, P. L.;

Miller A. *"The Elements of Nonlinear Optics"*, Cambridge, N.Y., Cambridge University Press, 1990. (c) Sauter, E.G. *"Nonlinear Optics"*, N.Y. Wiley, 1996.

² Franken, P.A. *Phys. Rev. Lett.* **1961**, 7(1), 18.

³ Yesodha, S.K.; Pillai, C.K.S.; Tsutsumi, N. *Prog. Polym. Sci.* **2004**, 29, 45.

⁴ Bloembergen, N. *"Encounters in Nonlinear Optics"*, River Edge, N.J., World Scientific, 1996, Singapore.

⁵ Krause, H.J.; Daum, W. *Appl. Phys. Lett.* **1992**, 60, 2180.

⁶ Stucky, G.D.; Marder, S.R.; Sohn, J.E.; Editors; Williams, D.J. *"Materials for Nonlinear Optics, Chemical Perspectives"*, Chapter 2, ACS Symposium Series 455.

⁷ Stucky, G.D.; Marder, S.R.; Sohn, J.E.; Editors; Prasad, P.N. *"Materials for Nonlinear Optics, Chemical Perspectives"*, Chapter 3, ACS Symposium Series 455.

⁸ Prasad, P.N.; Williams, D.J. *"Introduction to Nonlinear Optical Effects in Molecules and Polymers"*, N.Y., Wiley, 1991.

⁹ (a) Kuzyk, M.G.; Dirk, C.W. *"Characterization Techniques and Tabulations for Organic Nonlinear Optical Materials"*, Marcel Dekker, N.Y., 1998. (b) Wagniere, G.H. *"Linear and Nonlinear Optical Properties of Molecules"*, VCH, N.Y., 1993.

¹⁰ (a) Denk, W.; Strickler, J.H.; Webb, W.W. *Science* **1990**, 248, 73. (b) Shear, J.B. *Anal. Chem.* **1999**, 71, 598A.

¹¹ (a) Parthenopoulos, D.A.; Rentzepis, P.M. *Science* **1989**, 245, 843. (b) Cumpston, B.H.; Ananthavel, S.P.; Barlow, S.; Dyer, D.L.; Ehrlich, J.E.; Erskine, L.L.; Heikal, A.A.; Kuebler, S.M.; Lee, I.-Y.S.; McCord-Maughon, D.; Qin, J.; Röckel, H.; Rumi, M.; Wu, X.-L.; Marder, S.R.; Perry, J.W. *Nature* **1999**, 398, 51. (c) Gu, M.; Amistoso, J.O.; Toriumi, A.; Irie, M.; Kawata, S. *Appl. Phys. Lett.* **2001**, 79, 148.

¹² (a) Kawata, S.; Sun, H.-B.; Tanaka, T.; Takada, K. *Nature*, **2001**, 412, 697. (b) Zhou, W.; Kuebler, S.M.; Braun, K.L.; Yu, T.; Cammack, J.K.; Ober, C.K.; Perry, J.W.; Marder,

S.R. *Science* **2002**, 296, 1106. (c) Yu, T.; Ober, C.K.; Kuebler, S.M.; Zhou, W.; Marder, S.R.; Perry, J.W. *Adv. Mater.* **2003**, 15, 517.

¹³ (a) Silly, M.G.; Porrès, L.; Mongin, O.; Chollet, P.-A.; Blanchard-Desce, M. *Chem. Phys. Lett.* **2003**, 379, 74. (b) Spangler, C.W. *J. Mater. Chem.* **1999**, 9, 2013. (c) Desroches, C.; Parola, S.; Vocanson, F.; Ehlinger, N.; Miele, P.; Lamartine, R.; Bouix, J.; Eriksson, A.; Lindgren, M.; Lopes, C. *J. Mater. Chem.* **2001**, 11, 3014.

¹⁴ (a) Sekikawa, T.; Kanai, T.; Watanabe, S. *Phys. Rev. Lett.* **2003**, 91, 103902. (b) Rasmusson, M.; Tarnovsky, A.N.; Åkesson, E.; Sundström, V. *Chem. Phys. Lett.* **2001**, 335, 201.

¹⁵ He, G.S.; Markowicz, P.P.; Lin, T.-C.; Prasad, P.N. *Nature* **2002**, 415, 767.

¹⁶ (a) Frederiksen, P.K.; Jørgensen, O.P.R. *J. Am. Chem. Soc.* **2001**, 123, 1215. (b) Liu, J.; Zhao, Y.W.; Zhao, J.Q.; Xia, A.D.; Jiang, L.J.; Wu, S.; Ma, L.; Dong, Y.Q. Gu, Y.H. *J. Photochem. Photobiol. B: Biol.* **2002**, 68, 156. (c) Meshalkin, Y.P.; Alfimov, E.E.; Vasil'ev, N.E.; Denisov, A.N.; Makukha, V.K.; Ogirenko, A.P. *Quant. Electron.* **1999**, 29, 1066.

¹⁷ (a) Drobizhev, M.; Karotki, A.; Kruk, M.; Rebane, A. *Chem. Phys. Lett.* **2002**, 355, 175. (b) Drobizhev, M.; Karotki, A.; Kruk, M.; Mamardashvili, N. Zh.; Rebane, A.; *Chem. Phys. Lett.* **2002**, 361, 504. (c) Drobizhev, M.; Karotki, A.; Kruk, M.; Krivokapic, A.; Anderson, H.L.; Rebane, A. *Chem. Phys. Lett.* **2003**, 370, 690. (d) Karotki, A.; Drobizhev, M.; Dzenis, Y.; Taylor, P.N.; Anderson, H.L.; Rebane, A. *Phys. Chem. Chem. Phys.* **2004**, 6, 7, 2004. (e) Karotki, A.; Drobizhev, M.; Kruk, M.; Spangler, C.; Nickel, E.; Mamardashvili, N.; Rebane, A. *J. Opt. Soc. Am. B* **2003**, 20, 321. (f) Drobizhev, M.; Stepanenko, Y.; Dzenis, Y.; Karotki, A.; Rebane, A.; Taylor, P.N.; Anderson, H.L. *J. Am. Chem. Soc.* **2004**, 126, 15352.

¹⁸ Göppert-Mayer, M. *Ann. Phys.* **1931**, 9, 273.

¹⁹ Wise, D.L.; Wnek, G.E.; Trantolo, D.J.; Cooper, T.M.; Gresser, J.D. *“Photonic Polymer Systems”*, Marcel Dekker, Inc., N.Y., Basel, H.K., 1998.

²⁰ Friedrich, D.M. *J. Chem. Phys.* **1981**, *75*, 3258.

²¹ (a) Giuliano, C.R.; Hess, L.D. *IEEE J. Quant. Electron* **1967**, *QE-3*, 358. (b) Huff, L.; DeShazer, L.G. *J. Appl. Phys.* **1969**, *40*, 4336. (c) Huff, L.; DeShazer, L.G. *J. Opt. Soc. Am.* **1970**, *60*, 157.

CHAPTER 3

THE Z-SCAN AND DEGENERATE FOUR-WAVE MIXING TECHNIQUES

3.0 TRANSMISSION MEASUREMENTS

The most obvious effect of nonlinear absorption is a change in the transmission of a material with increasing intensity or fluence. Thus, transmission measurements can be used to obtain various nonlinear parameters including the two-photon absorption (TPA) coefficient (β) and excited state cross section σ_{ex} . Other techniques used for investigations of nonlinear absorption include three-wave mixing¹, two-photon fluorescence,² photothermal techniques,³ degenerate four-wave mixing (DFWM),⁴ heterodyned Kerr effect⁵ measurements and chirped-pulse pump-probe technique.⁶ The advantage of the transmission method includes its straightforwardness and it is directly amenable to pump-probe methods⁷ for studying wavelength and time dependencies. However, its chief disadvantage is that it involves measuring a small change in a large background since the nonlinear transmittance change is generally a small fraction of the linear transmittance. In our work, transmittance measurements using mainly the Z-scan and the DFWM techniques are carried out and will be further elaborated⁸.

3.1.0 THE Z-SCAN TECHNIQUE

The Z-scan technique was first developed in 1989 by Sheik-bahae *et al.*⁹ to be a sensitive measurement technique for investigation of nonlinear absorption and refraction. The schematic setup for the Z-scan measurements with closed- and open-

aperture is shown in Fig. 3.1.¹¹ A sample is scanned along the path of a laser beam which is focused by a lens. The far-field on-axis light intensity is monitored with a detector with an aperture in front of it. The nonlinear behaviour of the sample is equivalent to the formation of an induced positive or negative lens. The positive lens results in self-focusing while the negative causes self-defocusing effects, changing the beam intensity at the aperture plane.^{9,10}

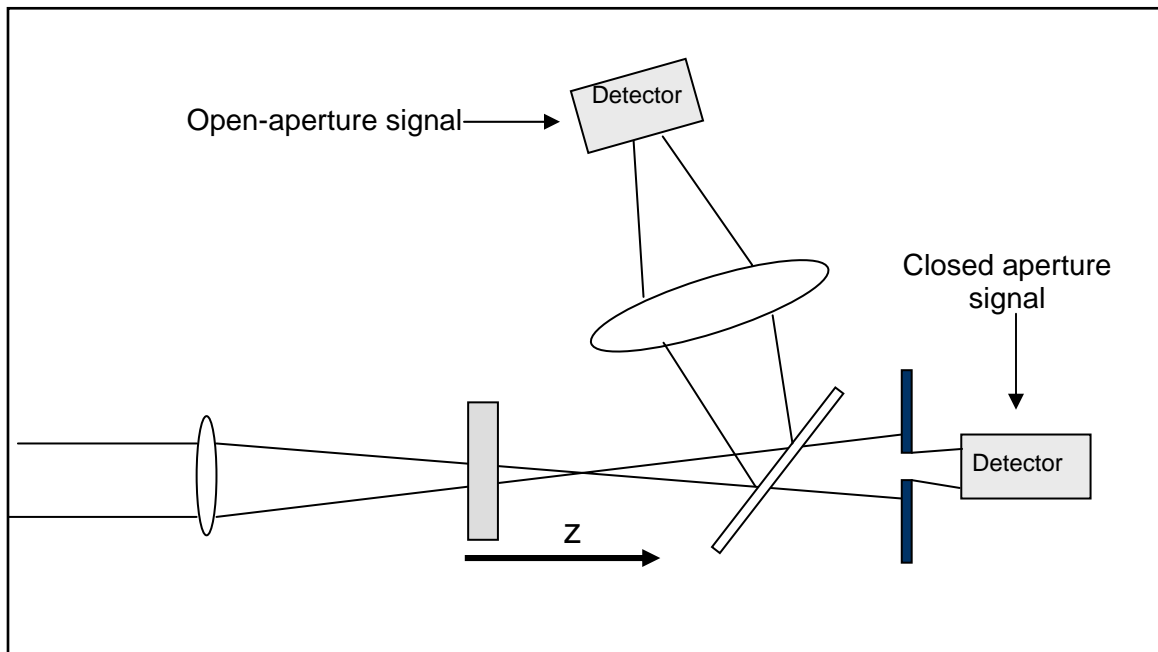


Fig. 3.1 Schematic setup for the Z-scan measurements with closed- and open-aperture¹¹

The sample acts like an intensity dependent lens. As it is scanned along the beam path, its effective focal length will change since the incident intensity is changing. This change will be reflected in the intensity distribution at the aperture in the far field. The amount of energy transmitted by the aperture will thus depend on the sample location along the z -axis and the sign of the nonlinear index of refraction n_2 .

The principle of the measurement for the case of $n_2 > 0$ (self-focusing) is shown in Fig. 3.2. Because light intensity varies due to the focusing action of the linear lens, the nonlinear lens strength induced in the sample varies with the position of the sample with respect to the focused beam waist. Starting the scan from a distance far away from the focus (negative z), the beam irradiance is low and negligible nonlinear refraction occurs. Hence the transmittance remains relatively constant. As the sample is brought closer to focus, the beam irradiance increases, leading to self-focusing in the sample. A positive self-focusing prior to focus tends to broaden the beam at the aperture and thus leads to decrease in transmittance. As the scan in z direction continues and the sample passes the focal plane to the right (positive z), the same self-focusing collimates the beam, causing a beam narrowing at the aperture which results in increase in the measured transmittance. This suggests that there is a null as the sample crosses the focal plane. The Z-scan is completed as the sample is moved away from focus (positive z) such that the transmittance becomes linear since irradiance is again low. A prefocal transmittance minimum (valley) followed by a postfocal transmittance maximum (peak) is the Z-scan signature of a positive refractive nonlinearity.

On the other hand, the opposite applies to negative nonlinear refraction in which the peak-valley configuration is obtained instead. The S-shape resulting from scanning of the sample can then be analyzed using calculation techniques described by Sheik-Bahae *et al.*⁹ and the nonlinear properties of the sample can be derived.

The increase and decrease of the intensity of the beam shows the focusing and defocusing effects of the sample and is thus a measure of the refractive component of nonlinearity when no absorptive nonlinearities (such as multiphoton or saturation of absorption) are present. Qualitatively, multiphoton absorption ($n_{2,\text{imag}} > 0$) suppresses the

peak and enhances the valley while saturation absorption ($n_{2,imag} < 0$) produces the opposite effect. The sensitivity to nonlinear refraction is entirely due to the aperture and the removal of the aperture completely eliminates the effect. However, in this case, the Z-scan will still be sensitive to nonlinear absorption. Nonlinear absorption coefficients can be extracted from such open-aperture experiments. We will show in Chapter 5 how the data from the two Z-scans with and without the aperture can be used to separately determine both the nonlinear absorption and the nonlinear refraction. In the open-aperture Z-scan, all the light transmitted through the sample is collected.

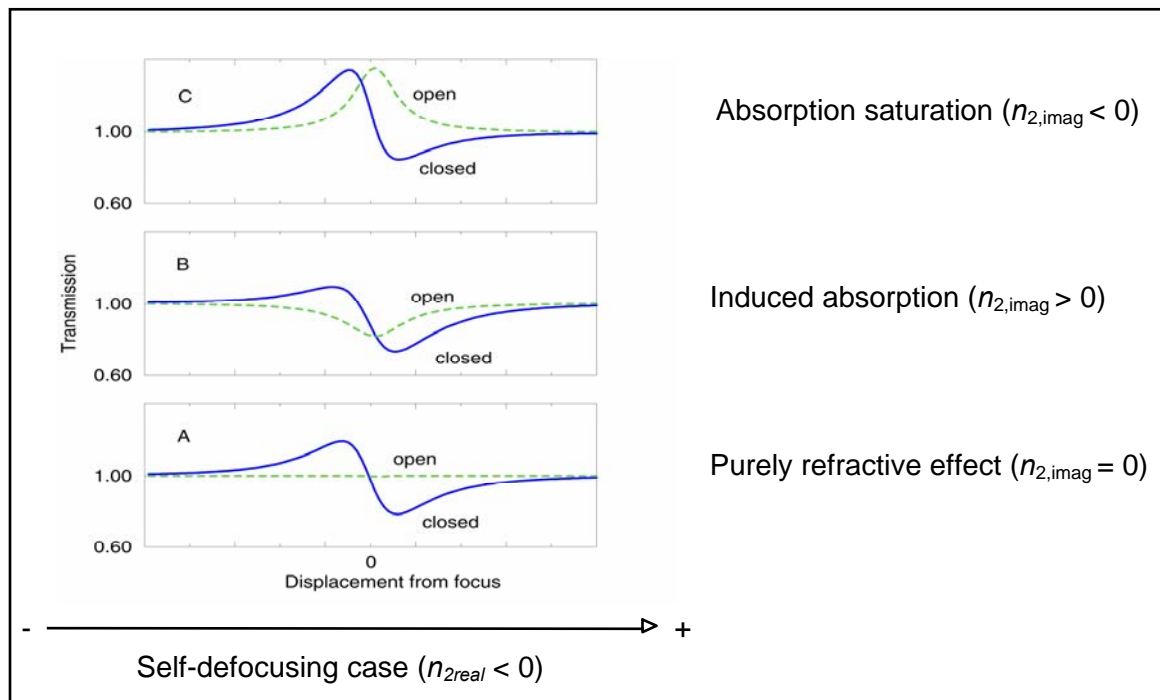


Fig. 3.2 Diagram illustrating the theoretical shapes of open- and closed-aperture Z-scans for (A) no nonlinear absorption, (B) induced absorption and (C) absorption saturation

Hence, the aperture transmittance as a function of sample position depends on the magnitude and the sign of nonlinear refractive index (n_2). This is the basis of the Z-

scan technique. The nonlinear medium impresses a phase distortion on the electric field of the transmitted light and modifies its amplitude through nonlinear absorption.

3.1.1 ADVANTAGES AND DISADVANTAGES OF THE Z-SCAN TECHNIQUE

The Z-scan has several advantages. Among these is its simplicity. As a single-beam technique, the alignment of beam is not difficult although it is to be kept centered on the aperture. It can be used to determine both the magnitude and the sign of n_2 . The sign is obvious from the shape of the transmittance curve. Generally, data analysis is quick and simple, making it a good method for screening new nonlinear materials. Under certain conditions, it is possible to isolate the nonlinear refractive and nonlinear absorptive contributions to the far-field transmittance. Thus, unlike most DFWM methods, the Z-scan can determine both the real and the imaginary parts of $\chi^{(3)}$. The technique is also highly sensitive, capable of resolving a phase distortion of $\sim \frac{\lambda}{300}$ in samples of high optical quality. Finally, the Z-scan can also be modified to study nonlinearities on different time scales as well as higher order contributions.

Disadvantages of the technique include the fact that it requires a high quality Gaussian TEM₀₀ beam for absolute measurements. The analysis must be different if the beam is non-Gaussian. It is possible to relax the requirements on beam shape when relative measurements against a standard material are performed. Sample distortions or wedges, or a tilting of the sample during translation, can cause the beam to walk off the far-field aperture. This produces unwanted fluctuations in the detected signal. Even if these are kept under control, beam jitter will produce the same effect. A second reference arm can be employed to subtract out the effects of beam jitter. The technique

cannot be used to measure off-diagonal elements of the susceptibility tensor except when a second non-degenerate frequency beam is employed. Such a technique is useful for measuring the time dependence of nonlinearities but this detracts from the simplicity and elegance of the method. The introduction of a second beam of a different frequency requires careful alignment of the two beams, taking into account difference in spot sizes and focal positions due to chromatic aberration, and physical separation and filtering of the beams prior to detection.

3.1.2 THEORY OF Z-SCAN

It is assumed that a Gaussian TEM₀₀ beam is incident on a thin nonlinear medium (that is, $L \ll z_R$, where z_R is the Rayleigh range of the beam in air). Hence, the amplitude of the beam is unchanged by linear or nonlinear absorption. However, the phase of the incident wave is distorted and the nonlinear phase $\Delta\varphi(r, z, t)$ impressed on the wave follows the shape of the incident beam

$$(3.1) \quad \Delta\varphi(r, z, t) = \Delta\varphi(z, t) \exp\left[-\frac{2r^2}{w^2(z)}\right],$$

where

$$(3.2) \quad w(z) = w_0 \sqrt{1 + \left(\frac{z}{z_R}\right)^2}$$

$$(3.3) \quad \Delta\varphi(z, t) = \frac{\Delta\Phi_0(t)}{1 + \left(\frac{z}{z_R}\right)^2}$$

$$(3.4) \quad \Delta\Phi_0(t) = \frac{2\pi}{\lambda} n_2' I_0(t) L_{\text{eff}}$$

$$(3.5) \quad L_{\text{eff}} = \frac{1 - \exp(-\alpha L)}{\alpha}$$

$I_0(t) = I(0,0,t)$ is the on-axis intensity at focus, w_0 is the $\frac{1}{e^2}$ beam radius at the focus, α is the linear absorption coefficient, n_2' is the nonlinear index intensity coefficient (where $n_2' = \Delta n / I$; Δn is the change in refractive index) and L_{eff} is the effective sample thickness.⁸

The quantity of interest is the optical power transmitted by the aperture. An expression for this can be obtained in terms of the peak on-axis phase shift $\langle \Delta \Phi_0 \rangle$. Sheik-bahae *et al.*⁹ have shown that a useful experimental parameter that is proportional to $\langle \Delta \Phi_0 \rangle$ is the difference in the peak and valley transmittance values: $\Delta T_{\text{p-v}} = T(\zeta_p) - T(\zeta_v)$ where ζ_p and ζ_v give the z positions corresponding to the maximum and minimum $T(\zeta)$ values. Sheik-bahae *et al.* have determined through numerical analysis that for $|\Delta \Phi_0| < \pi$, the following approximation is valid to within 3%:

$$(3.6) \quad \Delta T_{\text{p-v}} \cong 0.405(1-S)^{0.25} \langle \Delta \Phi_0 \rangle$$

where S is the low-power aperture transmission. For a Gaussian-shaped pulse, $\langle \Delta \Phi_0 \rangle = \frac{\Delta \Phi_0}{\sqrt{2}}$ where $\Delta \Phi_0$ is now the peak on-axis phase shift. Then n_2' is determined by

$$(3.7) \quad n_2' \cong a \frac{\lambda \omega_0^2 t_{\text{FWHM}}}{L_{\text{eff}} \epsilon_i} \langle \Delta \Phi_0 \rangle,$$

where t_{FWHM} is the measured pulse width (full width at half maximum), ϵ_i is the measured incident pulse energy corrected for Fresnel reflection at the front sample surface and $a = 0.38$.¹²

As mentioned earlier, the presence of nonlinear absorption will distort the shape of the Z-scan transmittance curve. TPA will enhance the valley and reduce the peak while saturable absorption produces the opposite effect.

When TPA is present, it reduces the intensity in the sample as a function of the z-position of the sample. It also distorts the amplitude which further affects the beam shape in the far field. To account for TPA, the previous theoretical expressions have to be slightly modified and β has to be determined from another measurement.

One technique for determining β is to perform an open-aperture Z-scan. Open-aperture implies that all the energy transmitted by the sample is collected and detected. Thus in this case, the nonlinear transmittance is due to absorption loss only. By performing both an open- and a closed-aperture Z-scan the results obtained were analyzed with expressions to yield the real part of the nonlinear phase shift $\Delta\varphi_{\text{real}}$ induced by the third-order nonlinearity and the T factor (defined here as

$$T = \frac{4\pi\Delta\varphi_{\text{imag}}}{\Delta\varphi_{\text{real}}}, \text{ where } \Delta\varphi_{\text{imag}} \text{ is the imaginary part of the nonlinear phase shift) for a}$$

given sample. Roughly, the amplitude of a closed-aperture Z-scan (peak-to-valley difference in transmission values) is proportional to $\Delta\varphi_{\text{real}}$, where the asymmetry of a closed-aperture scan depends on the T factor (for $T = 0$, the scan is essentially S shaped and symmetric). The $\Delta\varphi_{\text{imag}}$ can be obtained either from the asymmetry of the

closed-aperture scan (with $\Delta\varphi_{\text{imag}} = \frac{T\Delta\varphi_{\text{real}}}{4\pi}$) or from the dip in the open-aperture scan

that is directly related to the value of $\Delta\varphi_{\text{imag}}$. Alternatively, in some cases, we used a procedure consisting of dividing the closed-aperture scan by the open-aperture scan to

resolve information on the real part of the phase shift. Such a procedure gives a scan that is essentially free from the influence of $\Delta\varphi_{\text{imag}}$, that is, free from the TPA effect.

The relationship between the $\Delta\varphi$ and the n_2 can be written as

$$(3.8) \quad \Delta\varphi = \frac{2\pi n_2 I L_{\text{eff}}}{\lambda},$$

Knowledge of the light intensity can be used for conversion from phase shift values to nonlinearity values. However, it is more convenient to perform measurements in a relative manner. Hence, we calibrated the values of the NLO parameters by performing measurements of the $\Delta\varphi$ for a silica plate for which $n_2 = 3 \times 10^{-16} \text{ cm}^2 \text{ W}^{-1}$ was assumed. For measurements of solutions, we assume that the complex n_2 of a dilute solution can be approximated by the linear expression

$$(3.9) \quad n_2 = \delta n_{2,\text{solute}} + (1 - \delta) n_{2,\text{solvent}}$$

where δ is the weight fraction of the solute, $n_{2,\text{solute}}$ is the compound's (extrapolated) nonlinear refractive index, and $n_{2,\text{solvent}}$ is the nonlinear refractive index of the solvent.

It should be noted that the value of $n_{2,\text{solute}}$ determined from the slope of the n_2 - versus- δ_{solute} dependence, in principle, be substantially different from the value of n_2 for the pure polymer in the solid phase. Two main factors to consider are the difference in density between the solute and the solvent and the difference in the local field factors, which we can formally interpret by taking into account that

$$(3.10) \quad n_2 = \frac{C_1 \chi^{(3)}}{n^2},$$

where the constant C_1 depends on the definition of $\chi^{(3)}$ and on the system of units adopted: in the cgs system, $C_1 = \frac{12\pi^2}{c}$ can be used.

In mixed system, for the conversion from $\chi^{(3)}$ in esu units to n_2 in square centimeters per watt, the numerical value of C_1 is ~ 0.039 and

$$(3.11) \quad \chi^{(3)} = L'^4 \sum N_i \gamma_i,$$

where L' is the local-field factor, often approximated by the Lorentz expression

$$L' = \frac{(n^2 + 2)}{3}$$

and γ is the hyperpolarizability which we assume to be concentration independent.

N_i are concentrations of molecules of the solution

components $N_i = \frac{N_0 \delta_i \rho_{\text{solution}}}{M_i}$, where N_0 is the Avogadro number, δ_i is the weight fraction

of a solution component, M_i is the component's molecular weight and ρ_{solution} is the

solution density. For dilute solutions, one can assume that $n_{\text{solution}} = n_{\text{solvent}}$ and

$\rho_{\text{solution}} = \rho_{\text{solvent}}$. We conclude that the

$$(3.12) \quad \frac{n_{2,\text{extrapol}}}{n_2} = \left(\frac{L_{\text{solvent}}}{L_{\text{solute}}} \right)^4 \left(\frac{n_{\text{solute}}}{n_{\text{solvent}}} \right)^2 \left(\frac{\rho_{\text{solvent}}}{\rho_{\text{solute}}} \right) C_{\text{or}}$$

where C_{or} is the correction for the possible difference in the orientational order of molecules in solution and in the solid.

3.1.3 EXPERIMENTAL TECHNIQUE

The Z-scan measurements⁹ were performed on solutions of the coordination complexes in CHCl_3 . The experimental setup (Fig. 3.3) comprised of a Ti:sapphire regenerative amplifier (CPA-2001, Clark, MXR) which typically produces 150 fs duration pulses of 250 Hz at wavelength of 775 nm. These pulses have energy of about 1 mJ/pulse. The fundamental pulses from the regenerative amplifier were parametrically down-converted in an optical parametric amplifier (TOPAS, Quantronix) and where necessary, frequency-doubled, which yielded 100 - 150 fs long pulses (FWHM) with tunable wavelength at 520 - 1600 nm.



Fig. 3.3 Picture of the Z-scan setup at the Laser Physics Centre, The Australian National University, Canberra

The measurements were conducted using a simple arrangement that allowed us to record the open-aperture Z-scan and the closed-aperture Z-scan simultaneously. The travel range of the table was generally chosen to be $z = -35$ to $z = 35$ mm. The focussed spot sizes were in the range of $w_0 = 30 - 40$ μm .

For convenience, the measurements were performed in a relative manner hence, we calibrated the values of the NLO parameters by performing measurements of the $\Delta\varphi$ of the solvent in 1 mm cell and adjusting the light intensity to obtain a change in nonlinear phase shift ($\Delta\phi_0$) value in the range of 0.7 - 1.0 rad for the cell with the solvent and of a 1 mm thick silica plate for which $n_2 = 3 \times 10^{-16}$ $\text{cm}^2 \text{W}^{-1}$ was assumed.

3.2.0 THE DEGENERATE FOUR-WAVE MIXING (DFWM) TECHNIQUE



Fig. 3.4 Picture of the DFWM setup at the Laser Physics Centre, Australian National University, Canberra

Four-wave mixing refers to the interaction of four waves in a nonlinear medium via the third order polarization. When the waves have different frequencies, the process can be used to generate new frequencies. However, interesting effects are observed when all the waves have the same frequency. This is referred to as the degenerate case.¹³

In DFWM, one laser is used and the beam is split to provide the pump beams and the probe beam. The beam is initially collimated using two convex lenses and an aperture is used to cut the scattered background before splitting it into three beams. The three coherent waves are incident on a nonlinear medium and a fourth wave (the phase conjugate) is generated. The strength of this phase conjugate wave is dependent on a coupling coefficient κ that is proportional to the effective $\chi^{(3)}$ for the interaction. Hence measurements of the phase conjugate intensity can yield the $\chi^{(3)}$ tensor components of the medium. The DFWM technique is now much less popular than the experimentally simpler Z-scan technique.

In DFWM (Fig. 3.4), two coherent “pump” beams interact within a material creating an interference pattern of light intensity.^{1a} A refractive index grating results from the change in refractive index of a third-order material depends on the intensity of the applied field, and this can be described by the dependence $\Delta n(r) = n_2(r)$. When a third beam is incident on this grating, a fourth beam is generated, the intensity of which is proportional to the product of all the input intensities and to the square of the absolute value the molecules third-order susceptibility, i.e $I_4 = |\chi^{(3)}|^2 I_1 I_2 I_3$.

DFWM has several advantages: one can measure all the independent $\chi^{(3)}$ tensor components of an isotropic medium by using various combinations of polarizations for the four beams employed in the experiment, absolute and relative measurements of $\chi^{(3)}$ are possible and the time dependence of the nonlinear response can be studied. The last mentioned is significant because off-resonance electronic

nonlinearities show a practically instantaneous response and these can be separated from slower processes that also contribute to n_2 .

Due to the difficulty of distinguishing the contributions from $\chi_{\text{real}}^{(3)}$ and $\chi_{\text{imag}}^{(3)}$ in DFWM,⁴ one must perform a series of measurements on solutions of a compound with varying concentrations in a non-absorbing solvent. The concentration dependence of the DFWM signal is

$$(3.13) \quad I_{\text{DFWM}} \propto |\chi^{(3)}|^2 \propto [N_{\text{solute}} \gamma_{\text{real,solute}} + N_{\text{solvent}} \gamma_{\text{real,solvent}}]^2 + [N_{\text{solute}} \gamma_{\text{imag,solute}}]^2$$

It is assumed here that the solvent contributes only to the real part of the solution susceptibility whereas the solute can contribute to both the real (refractive) and imaginary (absorptive) components.¹⁴

Despite its experimental complexity, DFWM forms a useful technique to the technically less difficult Z-scan in that it can be used to verify that the origin of the observed nonlinearity is electronic in nature.

3.2.1 PRINCIPLE OF DFWM MEASUREMENTS

The geometry of the beams is as shown (Fig. 3.5). Three pump beams, coincident from one side of the sample, were obtained by splitting of the main beam of approximately equal intensity. Two of the beams (1 and 2) were timed to arrive at the sample at the same time while the delay of the beam 3 was scanned between the negative values (corresponding to beam 3 arriving at the sample before the pump beams 1 and 2) and positive values (corresponding to beam 3 arriving at the sample after the beams). They were then focused with a 75 cm focal length plane-convex lens.

The samples were placed at a distance of 72 cm from the lens being about one Rayleigh range shifted from the focal plane. The beam waist spot radius was approximately $w_0 = 200 \mu\text{m}$. The BOXCARS arrangement of the beams leads to the emergence of a phase-matched DFWM signal in the fourth corner of the rectangle formed by the three intersecting beams.^{13b,13d,13e} Most of the measurements were done with the pulse energy about 3 uJ/pulse, the total beam intensity being about 30 GW cm^{-2} . The effective nonlinearity of the materials measured using DFWM was related to effective nonlinearity of neat CHCl_3 , which in turn referenced to the n_2 of fused silica.

The phase matched diffraction signal, generated in the sample through the nonlinear interaction was monitored with a photodiode whose output was fed into a boxcar (Fig. 3.5). Another photodiode monitored the amplitude of the input pulses and the data collection program was setup to accept only laser pulses with the amplitudes falling within a prescribed range. The delay of one of the beams with respect to the two remaining beams varied with a computer controlled delay line, providing the temporal resolution of the DFWM signal.¹

As mentioned earlier, the DFWM signal intensity is proportional to the square of the transient susceptibility change. In fact, as both the real (“refractive”) and imaginary (“absorptive”) parts of the susceptibility may be involved, the intensity of the instantaneous part of the DFWM signal can be written as

$$(3.14) \quad I_{\text{DFWM}} \propto (\chi_{\text{real}}^{(3)})^2 + (\chi_{\text{imag}}^{(3)})^2$$

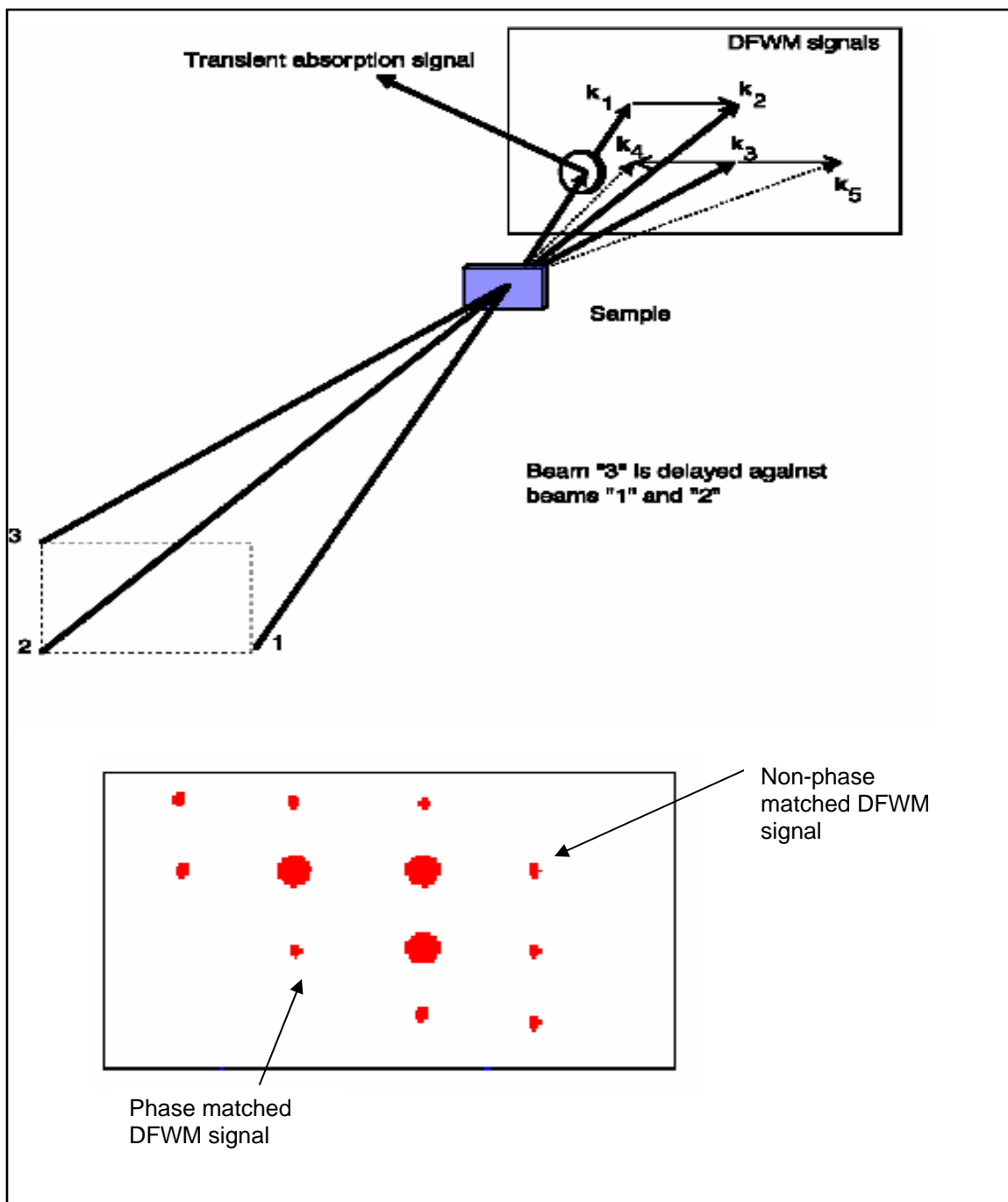


Fig. 3.5 (a) BOXCARS geometry of the interaction of the beams in the DFWM experiment (top); (b) View on the screen behind the sample (bottom)¹

This relation allows one to determine the modulus of the third-order susceptibility, $|\chi^{(3)}|$ or rewriting the equations in terms of a complex nonlinear refractive index n_2 , the modulus of the nonlinear refractive index, $|n_2|$. In our case, we determine the nonlinearity of our sample in CHCl_3 solution contained in a 1 mm glass cell so a convenient way of determining its nonlinearity is by comparing the DFWM signal from the material from the pure solvent contained in the same cell. The nonlinearity can then be calculated as

$$(3.15) \quad \left| n_2^{\text{sample}} \right| = C_{\text{refl}} C_{\text{abs}} n_2^{\text{silica}} \frac{L_{\text{silica}}}{L_{\text{sample}}} \left(\frac{I_{\text{DFWM}}^{\text{sample}}}{I_{\text{DFWM}}^{\text{silica}}} \right)^{\frac{1}{2}}$$

where C_{refl} and C_{abs} are correction factors taking into account the differences in the reflection and absorption for the sample and silica respectively.¹⁵

3.2.2 THE DFWM TECHNIQUE

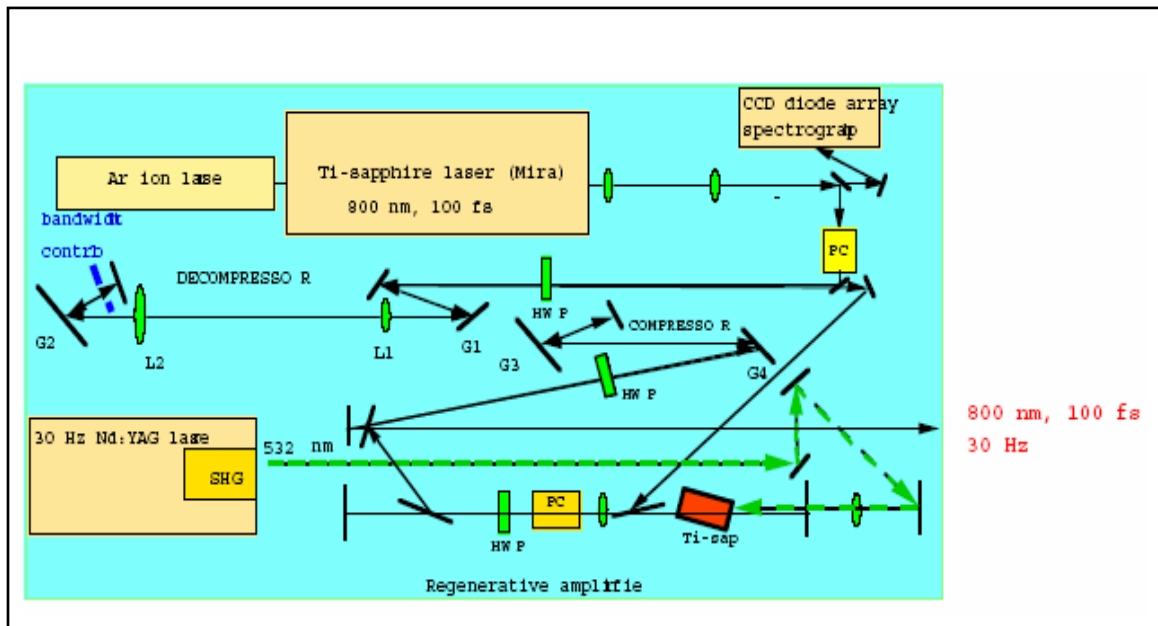


Fig. 3.6 Scheme of the laser system used in nonlinear optical measurements at 800 nm

The laser system (Fig. 3.6) used in the experiments consisted of a Coherent Verdi pumped Coherent Mira 900D femtosecond Ti-sapphire oscillator providing a train of nominally 100 fs pulses which were then amplified in a Ti-sapphire regenerative amplifier with diffraction grating decompression and compression stages, pumped at 30 Hz with the second harmonic of a Spectra Physics GCR Nd:YAG laser. After recompression, autocorrelation measurements showed the amplified pulses to be transform-limited with a FWHM of 125 fs and maximum pulse energy of 500 μ J pulses which were attenuated and directed into a folded BOXCARS (forward) DFWM system (Fig. 3.7).^{1a,16}

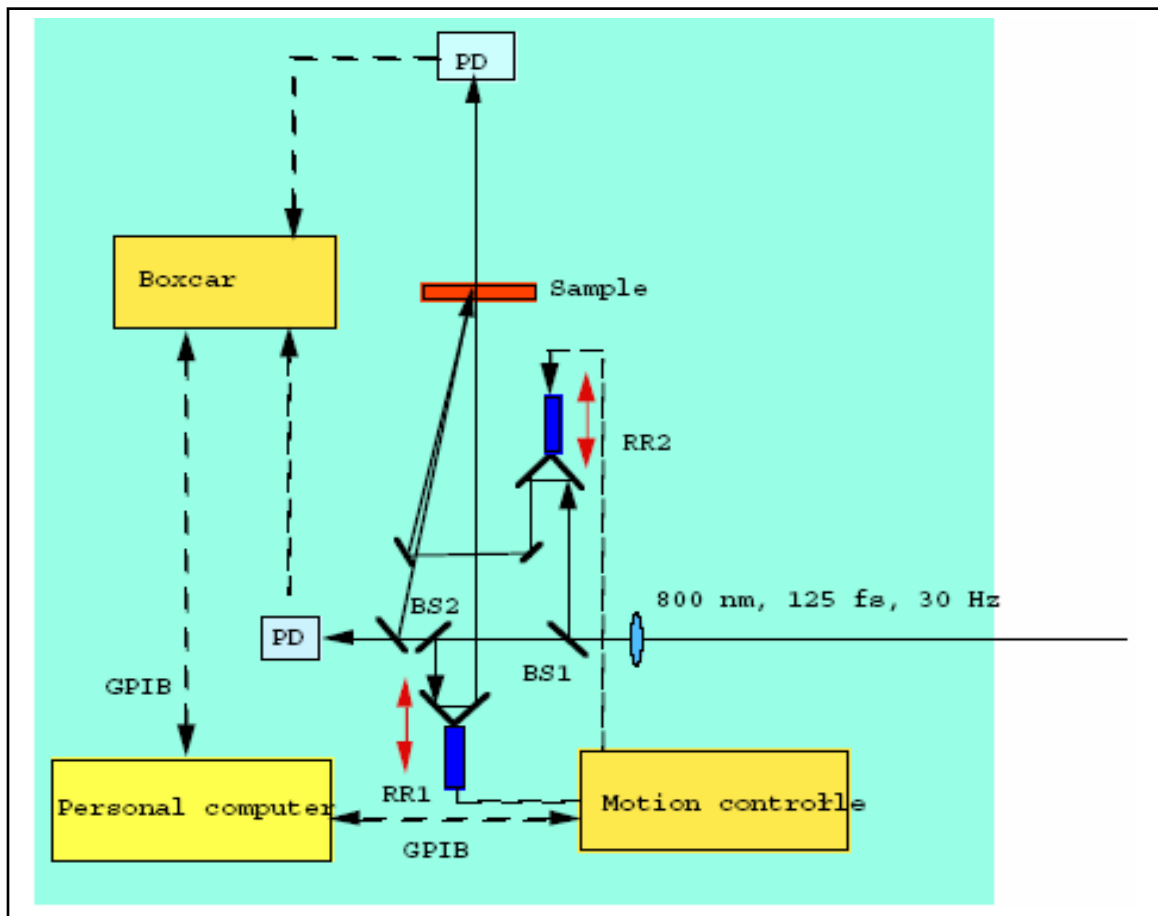


Fig. 3.7 Scheme of DFWM setup in BOXCARS configuration

3.3 REFERENCES

- ¹ (a) Adair, R.; Chase, L.L.; Payne, S.A. *J. Opt. Soc. Am. B* **1987**, *4*, 875. (b) Anderson, R.J.M.; Holtom, G.R.; McClain, W.M. *J. Chem. Phys.* **1979**, *70*, 4310.
- ² (a) Swofford, R.L.; McClain, W.M. *Rev. Sci. Instrum.* **1975**, *46*, 246. (b) Bennett, J.A.; Birge, R.R. *J. Chem. Phys.* **1980**, *73*, 4234. (c) Holtom, G.R.; McClain, W.M. *Chem. Phys. Lett.* **1976**, *44*, 436. (d) Fang, H.L.; Thrash, R.J.; Leroi, G.E. *Chem. Phys. Lett.* **1978**, *57*, 59.
- ³ (a) Long, M.E.; Swofford, R.L.; Albrecht, A.C. *Science* **1976**, *191*, 183. (b) Twarowski, A.J.; Kliger, D.S. *Chem. Phys.* **1977**, *20*, 253. (c) Twarowski, A.J.; Kliger, D.S. *Chem. Phys.* **1977**, *20*, 259. (d) Fang, H.L.; Gustafson, T.L.; Swofford, R.L. *J. Chem. Phys.* **1983**, *78*, 1663.
- ⁴ (a) Sutherland, R.L.; Rea, E.; Natarajan, L.V.; Pottenger, T.; Fleitz, P.A. *J. Chem. Phys.* **1993**, *98*, 2593. (b) Fleitz, P.A.; Sutherland, R.L.; Natarajan, L.V.; Pottenger, T.; Fernelius, N.C. *Opt. Lett.* **1992**, *17*, 716.
- ⁵ (a) Sheik-Bahae, M.; Hagan, D.J.; Van Stryland, E.W. *Phys. Rev. Lett.* **1990**, *65* (1), 96. (b) Butcher, P.N.; Cotter, D.; Knight, P. L.; Miller A. *"The Elements of Nonlinear Optics"*, Cambridge, N.Y., Cambridge University Press, 1990. (c) Sauter, E.G. *"Nonlinear Optics"*, N.Y.' Wiley, 1996.
- ⁵ Franken, P.A. *Phys. Rev. Lett.* **1961**, *7* (1), 18.
- ⁶ Tang, N.; Sutherland, R.L. *J. Opt. Soc. Am. B* **1997**, *14*, 3412.
- ⁷ Rasmusson, M.; Tarnovsky, A.N.; Åkesson, E.; Sundström, V. *Chem. Phys. Lett.* **2001**, *335*, 201.
- ⁸ Sutherland, R.L.; *"Handbook of Nonlinear Optics"*, 2nd ed. New York, N.Y.: Marcel Dekker, 2003, 627.

- ⁹ Sheik-bahae, M.; Said, A.A.; Wei, T.-H.; Hagan, D.J.; Van Stryland, E.W. *IEEE J. Quant. Electron.* **1990**, *26* (4), 760.
- ¹⁰ (a) Soileau, M.J.; Williams, W.F.; Van Stryland, E.W. *IEEE J. Quant. Electron.* **1975**, *19*, 731. (b) Soileau, M.J.; Williams, W.F. Van Stryland, E.W. *IEEE J. Quant. Electron.* **1983**, *QE-19*, 731.
- ¹¹ Samoc, A.; Samoc, M.; Woodruff, M.; Luther-Davies, B. *"Photonic Polymer Systems"*, N.Y., Basel, Hong Kong, Marcel Dekker, Inc., 1998, 373.
- ¹² Sheik-bahae, M.; Wang, J.; DeSalvo, R.; Hagan, D.J.; Van Stryland, E.W. *Opt. Lett.* **1992**, *17*, 258.
- ¹³ (a) Friberg, S.R.; Smith, P.W. *IEEE J. Quant. Electron.* **1987**, *QE-23*, 2089. (b) Carter, G.M. *J. Opt. Soc. Am. B* **1987**, *4*, 1018. (c) Cao, X.F.; Jiang J.P.; Bloch, D.P.; Hellwarth, R.W.; Yu, L.P.; Dalton, L. *J. Appl. Phys.* **1989**, *65*, 5012. (d) Pang, Y.; Samoc, M.; Prasad, P.N. *J. Chem. Phys.* **1991**, *94*, 5282. (e) Strohkendl, F.P.; Dalton, L.R.; Hellwarth R.W.; Sarkas, H.W.; Kafafi, Z.H. *J. Opt.Soc. Am. B* **1997**, *14*, 92.
- ¹⁴ Zhao, M.; Cui, Y.; Samoc, M.; Prasad, P.M.; Unroe, M.; Reinhardt, B.A. *J. Chem. Phys.* **1991**, *95*, 3991.
- ¹⁵ Prasad, P.N.; Williams, D.J. *"Introduction to Nonlinear Optical Effects in Molecules and Polymers"*, John Wiley, N.Y., 1991, 218.
- ¹⁶ (a) Samoc, A.; Samoc, M.; Luther-Davies, B.; Freydank, A.C.; Lucas, N.T. *J. Nonlinear Opt. Phys Mat.* **2003**, *12* (2), 235.

CHAPTER 4

SYNTHESIS AND CHARACTERIZATION OF COORDINATION DRIVEN SELF-ASSEMBLIES OF Zn(II) METALLOPORPHYRIN COMPLEXES WITH SPATIAL GEOMETRY DIRECTED BY CONFORMATIONAL DIVERSITY

4.0 INTRODUCTION

Molecular self-assembly offers a good alternative pathway to a wide variety of one-, two- and three-dimensional arrays through various associations and orientations.² It not only allows the derivation of supramolecules with interesting and sometimes unexpected structures, it is also generally less tedious than the approach taken to form covalent compounds. The practical aspect of this work when applied on a large scale synthesis basis was taken into consideration.

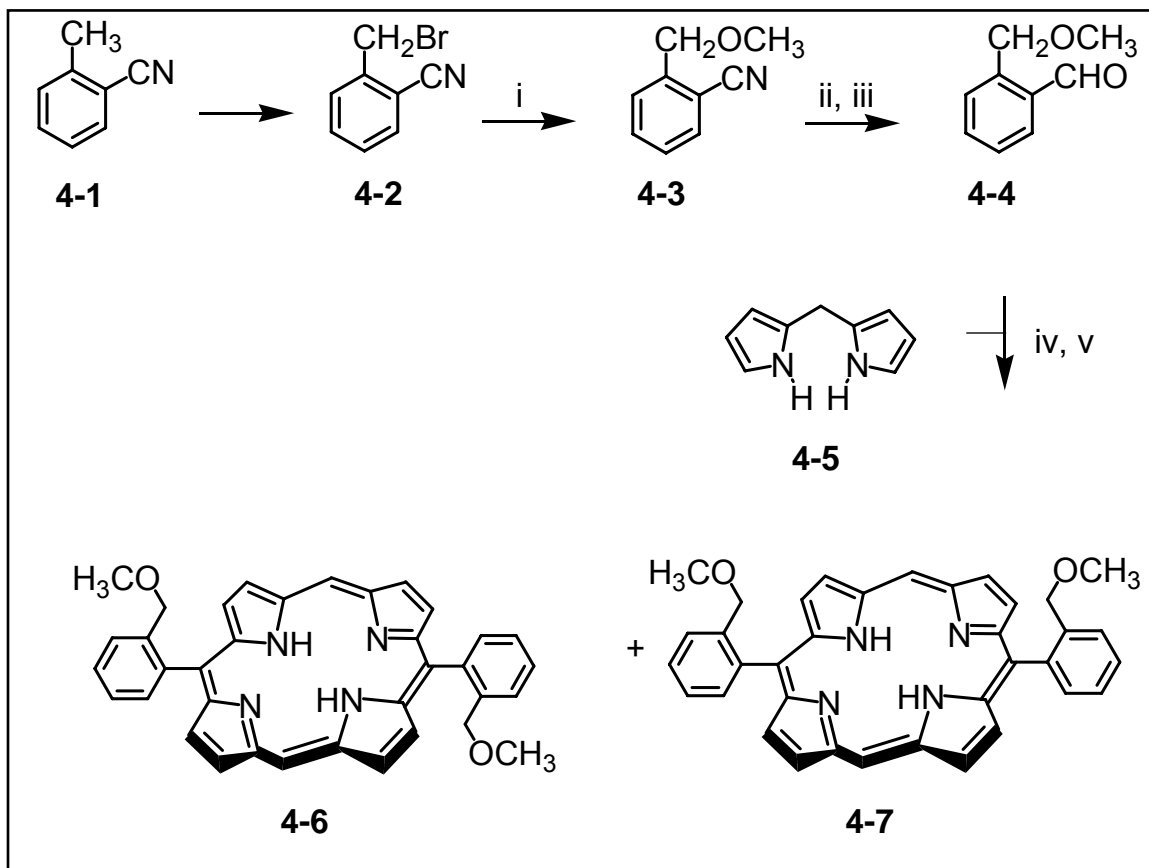
Therefore, in our work, we designed and synthesized porphyrin with phenyl rings as peripheral side groups. The latter possess *ortho* methoxymethyl substituents which contain O donor atoms for the formation of coordination bonds. Also, the *ortho* substituents on the phenyl rings confer greater some rigidity to the structure. This is advantageous as it allows the separation of the atropisomers and more importantly, leads to the formation of a larger variety of coordination complexes described in this chapter.

The series of coordination complexes are characterized and studied for their spectroscopic behaviour in solutions prior to the analyses of their nonlinear optical (NLO) properties using Z-scan technique. We can then establish the structure-property relationship; in particular, the influence of their overall molecular geometries on their third-order nonlinear responses (described in Chapter 5).³ Through this approach, we discover new molecular designs that allow us to gain more insight into improving third-order NLO properties of metalloporphyrin complexes.

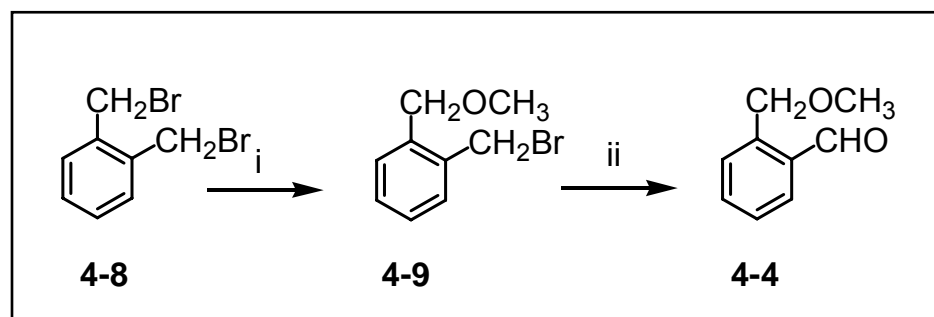
Therefore, in this chapter, we describe the syntheses and characterization of a variety of self-assembled Zn(II) metalloporphyrin complexes.

4.1.0 SYNTHESIS OF PORPHYRIN LIGAND BUILDING BLOCKS

The synthesis of the porphyrin building blocks **4-6** and **4-7** from **4-1** to **4-5** for the class of self-assembled coordination Zn(II) metalloporphyrin complexes described in this chapter is shown in Scheme 4.1 below.



Scheme 4.1 i, Na, CH₃OH, reflux; ii, DIBAL, benzene; iii, MeOH, HCl, H₂O, 0 °C; iv, CF₃COOH/ CH₂Cl₂; v, chloranil, reflux



Scheme 4.2 i, Na, CH₃OH, reflux; ii, Na₂CO₃, DMSO, reflux

The porphyrin building blocks are compounds **4-6** and **4-7** and their syntheses involved a 5-steps reaction pathway. Free radical bromination of the methyl group in 2-

methylbenzotrile (**4-1**) gave 2-(bromomethyl)benzotrile (**4-2**). The methoxymethyl group in 2-(methoxymethyl)benzotrile (**4-3**) was then introduced by nucleophilic substitution reaction in **4-2**. The latter was reduced by diisobutylaluminium hydride (DIBAL) to provide the aldehyde function in 2-(methoxymethyl)benzaldehyde (**4-4**) needed for the construction of the porphyrin template. The other building block, namely dipyrromethane (**4-5**), was formed by a condensation reaction between pyrrole and paraformaldehyde according to literature method.⁴ The porphyrins **4-6** and **4-7** were prepared from **4-4** and **4-5** via a MacDonald [2+2] condensation reaction⁵ and subsequent oxidation of the intermediate porphyrinogens by chloranil.

In a second route, we were able to obtain the porphyrins **4-6** and **4-7** in two steps. First, the nucleophilic substitution of one of the benzylic carbons of 1,2-bis(bromomethyl)benzene (**4-8**) to form 1-(bromomethyl)-2-(methoxymethyl)benzene (**4-9**). The latter then undergoes oxidation in NaHCO₃ and DMSO to form 2-(methoxymethyl)benzaldehyde (**4-4**).⁶ The formation of the porphyrin **4-6** and **4-7** via this route is preferable as it involves one reaction less and uses less expensive and less dangerous reagents (DIBAL is highly flammable) as compared to the previously reported route.⁷

The novel 1,15-disubstituted porphyrin **4-6** and **4-7** were synthesized by acid-catalyzed condensation of **4-4** and **4-5**. The porphyrins are symmetrical but they cannot be synthesized by the simple pathway to the formation of symmetrical porphyrin such as tetraarylporphyrins by the acid-catalyzed condensation reaction of the aldehydes and 2 equivalents of pyrrole. This was because of the reaction as shown in Fig. 4.1 below. The aldehyde will condense with pyrrole to form a linear intermediate that cyclizes to give the porphyrinogen first. Subsequent oxidation of the latter will yield four possible products. It

will be impossible to obtain the desired porphyrin building blocks which lack alternative *meso* substitution. Even with the condensation of 1:1:2 of **4-4**/paraformaldehyde/pyrrole, the reaction will yield an even larger number of products due to random condensation. Low yield of the desired product will be obtainable only after extensive chromatography and characterization. However, with the development of dipyrromethane,⁴ the synthesis of 1,15-disubstituted porphyrins is made possible.

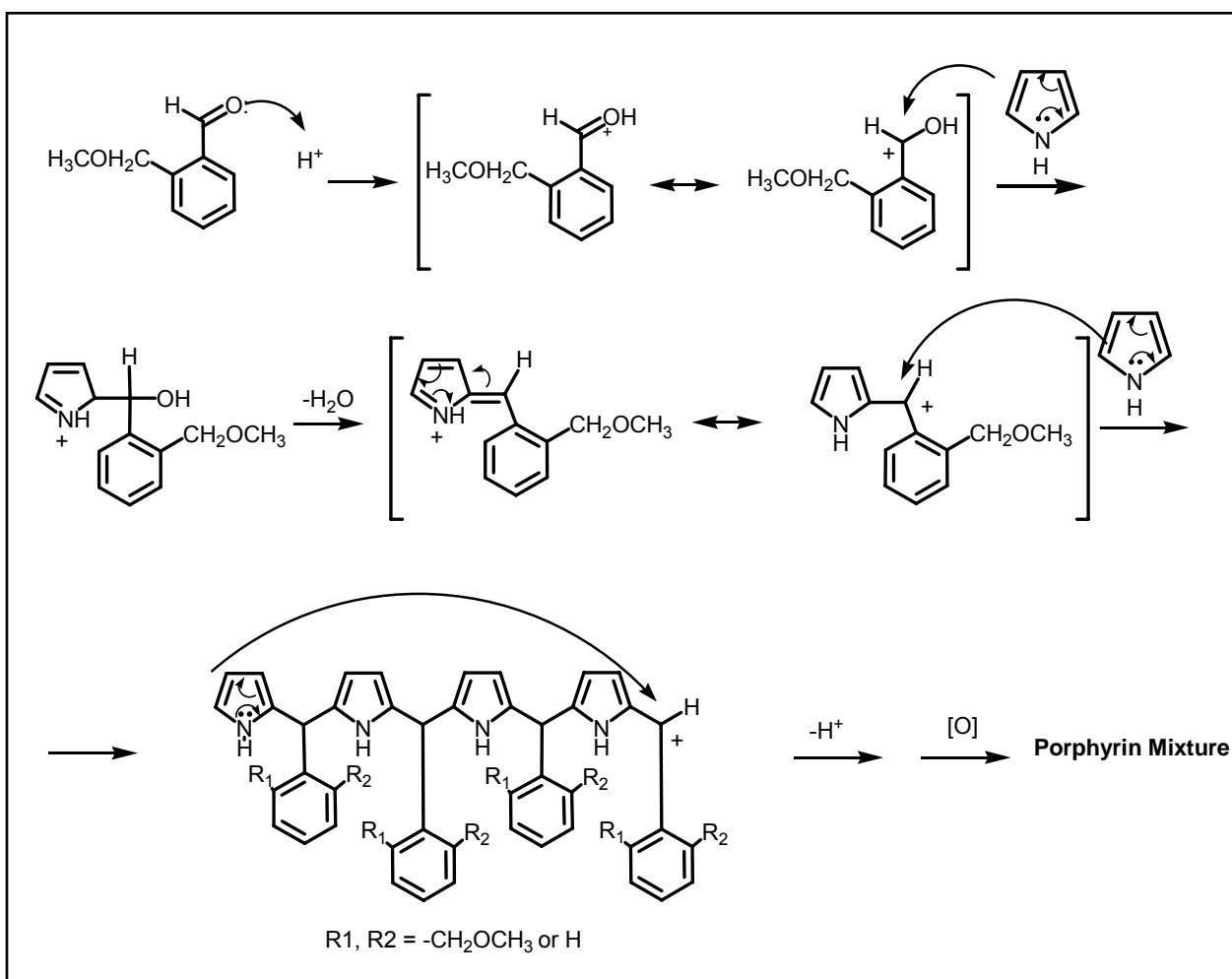


Fig. 4.1 Mechanism for the condensation of pyrrole and **4-4**

Compounds **4-6** and **4-7** were synthesized using the reported procedures by Manka and Lawrence⁸ who prepared similar porphyrins in high yield (73 - 92 %) and under mild reaction conditions that thermodynamically favour the formation of the intermediate porphyrinogens. However, only modest yield of 12 % and 11 % **4-6** and **4-7** were obtained respectively. The synthesis of the porphyrin using the procedure by Manka and Lawrence⁸ follows closely to the conditions which minimize scrambling as studied by Lindsey and co-workers.⁹ These conditions include the use of trifluoroacetic acid as catalyst, CH₂Cl₂ as solvent, stringent control of stoichiometry (1:1), use of dipyrromethane and aldehyde concentration less than 10 mM. Scrambling, which means rearrangement catalyzed by the acid will lead to the formation of 5,10-disubstituted porphyrin when the intermediate D in Fig. 4.2 condenses with another aldehyde, thus giving rise to by-product, lowering yield of the desired 5,15-disubstituted porphyrin.

It is noteworthy that the reaction gave comparable yields of the two atropisomers. The two methoxymethyl substituents in **4-7** are in *cis* conformation but they do not experience significant steric hindrance due to the ability to freely rotate in solution, as illustrated in Fig. 4.3 below. This is confirmed later in the X-Ray Crystallographic structure of the Zn(II) metalloporphyrins of **4-7** (refer to Section 4.5.2.1) where we observe the projection of the methoxy substituents away from the porphyrin core. Hence, the formation of **4-6** and **4-7** during condensation reaction is equally favourable.

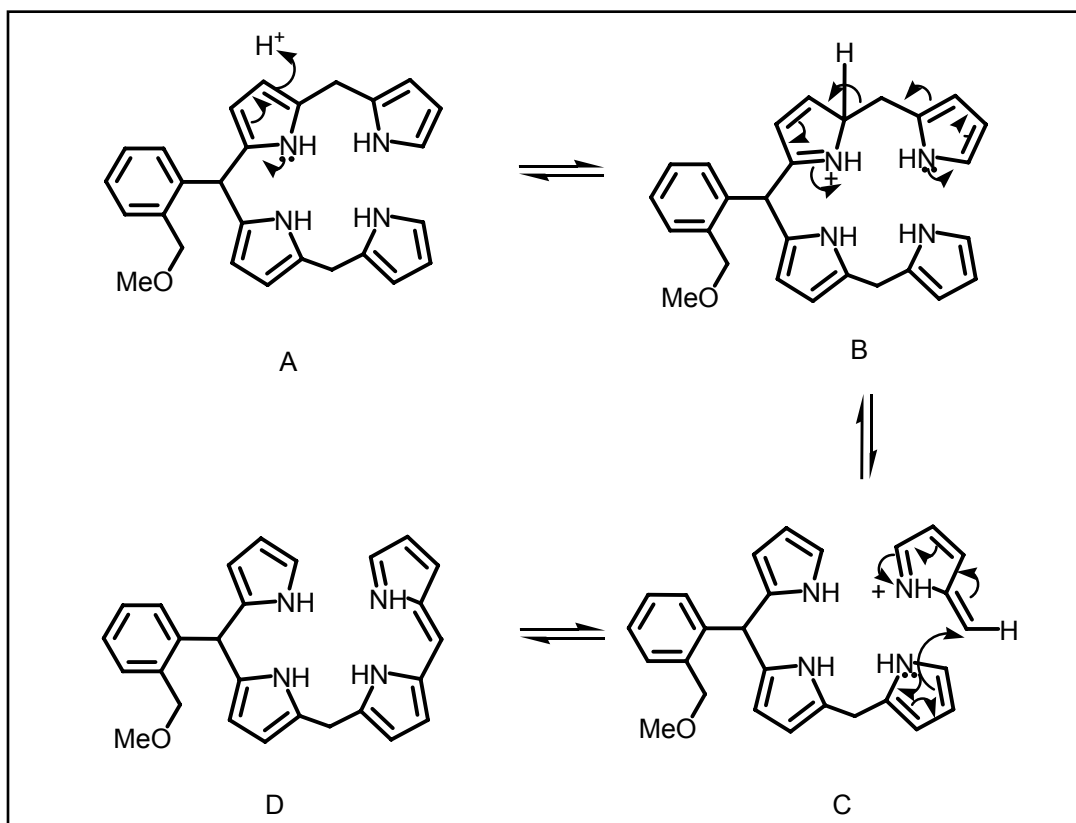


Fig. 4.2 Scrambling reaction during condensation⁸

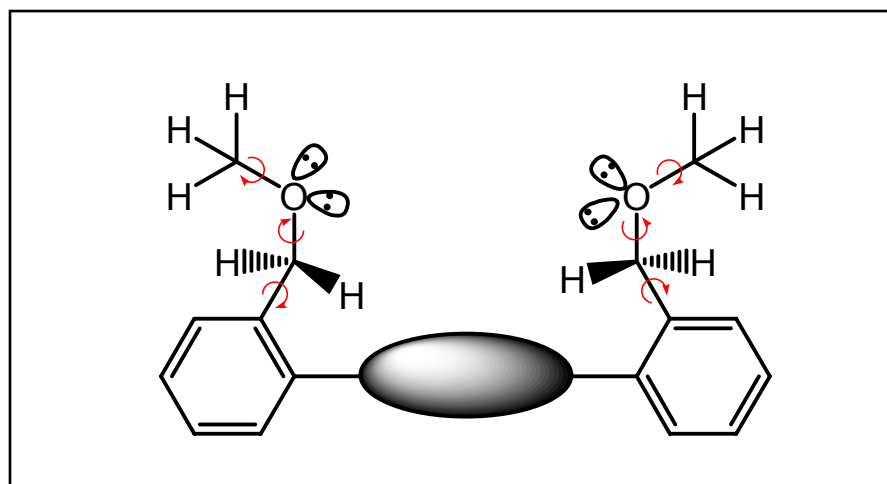


Fig. 4.3 Illustration of the possible bond rotations of the methoxymethyl substituents in 4-7

The ^1H NMR (CDCl_3) spectrum of the product mixture immediately isolated from the reaction between **4-4** and **4-5** clearly suggested the presence of *trans* **4-6** and *cis* **4-7** porphyrin isomers. Two separate signals 0.07 ppm apart in a ratio of approximately 1:1 were observed for the methylene protons of the two isomers, respectively. The corresponding pairs of other proton signals are identical. These isomers could be separated by column chromatography. The isomers elute as two very close red bands and they have similar ^1H NMR, ^{13}C NMR and EI-mass spectra. A clean separation of the two isomers can be easily observed in their ^1H NMR spectra wherein the benzylic protons have different chemical shifts as shown in Fig. 4.4. The benzylic protons of the *trans* isomer **4-6** are slightly more deshielded than that of the *cis* isomer **4-7**.

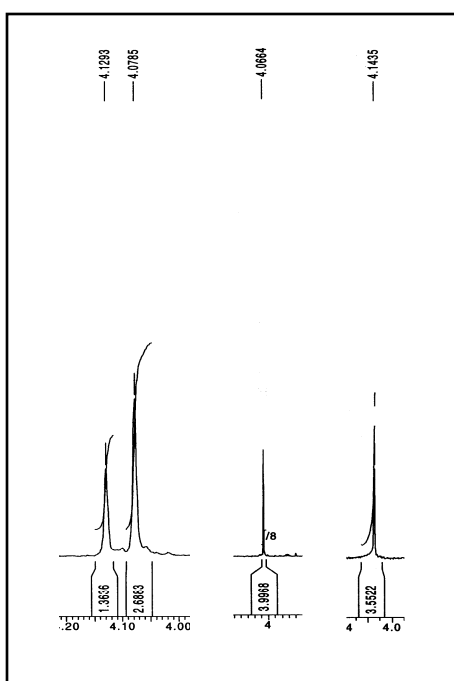


Fig. 4.4 ^1H NMR peaks of a mixture of **4-6** and **4-7** (left), ^1H NMR peak of **4-7** (middle), ^1H NMR peak of **4-6** (right)

X-Ray Crystallography was used to differentiate the isomers. Only one of the isomers crystallizes out to give single crystals suitable for the analysis. In a solvent mixture of 1:1 cyclohexane/CHCl₃, single crystals of the *trans* isomer **4-6** (refer to Section 4.1.1) were obtained and it corresponds to the band that eluted first during separation using column chromatography (CHCl₃ as eluent).

Since **4-6** was found to crystallize in 1:1 cyclohexane/CHCl₃ mixture but not **4-7**, the mixture of the two isomers was first separated by fractional crystallization to obtain the pure **4-6**. The mother liquor was then concentrated and purified using column chromatography to separate **4-6** and **4-7**. The isomers were obtained in similar yields. This shows that the substituents on the phenyl rings did not pose significant steric hindrance to disfavour the formation of the *cis* isomer, probably due to free rotation of the former. This is in contrast to the atropisomers reported by Uemori *et al.*¹⁰ in which their obtained *trans* isomer is in excess of the *cis* isomer by 22 % because of steric hindrance from the long side chains of the peripheral group.

A conformational study of **4-6** was carried out in order to investigate the temperature at which free rotation of the phenyl ring to yield **4-7** occurs. This is detrimental in temperature control of the following reaction. Variable temperature (VT)-NMR of **4-6** at 30, 80, 90 and 100 °C in toluene-*d*₈ showed that the aryl rings did not rotate to give **4-7** up to 100 °C because there was no appearance of additional singlet from the benzylic protons of **4-7**.

However, more rapid tautomerization of the NH protons at higher temperature was evident (Fig. 4.5). Tautomerism (illustrated in Fig. 4.6) is generally fast on the NMR scale which explains the broad and sometimes unobserved peaks of the N-H protons.

The most stable form of porphyrin is that in which the two inner H atoms are bonded to opposite N atoms. The less symmetrical form with H atoms bonded to adjacent N is considerably less stable because of the penetration of the atoms into the van der Waals sphere of each other. The appearance of the peak attributed to these protons differs. It may appear sharp, broad or may be completely absent. The appearance is subjected to temperature changes which in turn affects the dynamic N-H tautomerism process. This observed phenomenon is in fact very important since photoinduced tautomerization of free-base tetrapyrroles is useful for optical memory applications.¹¹

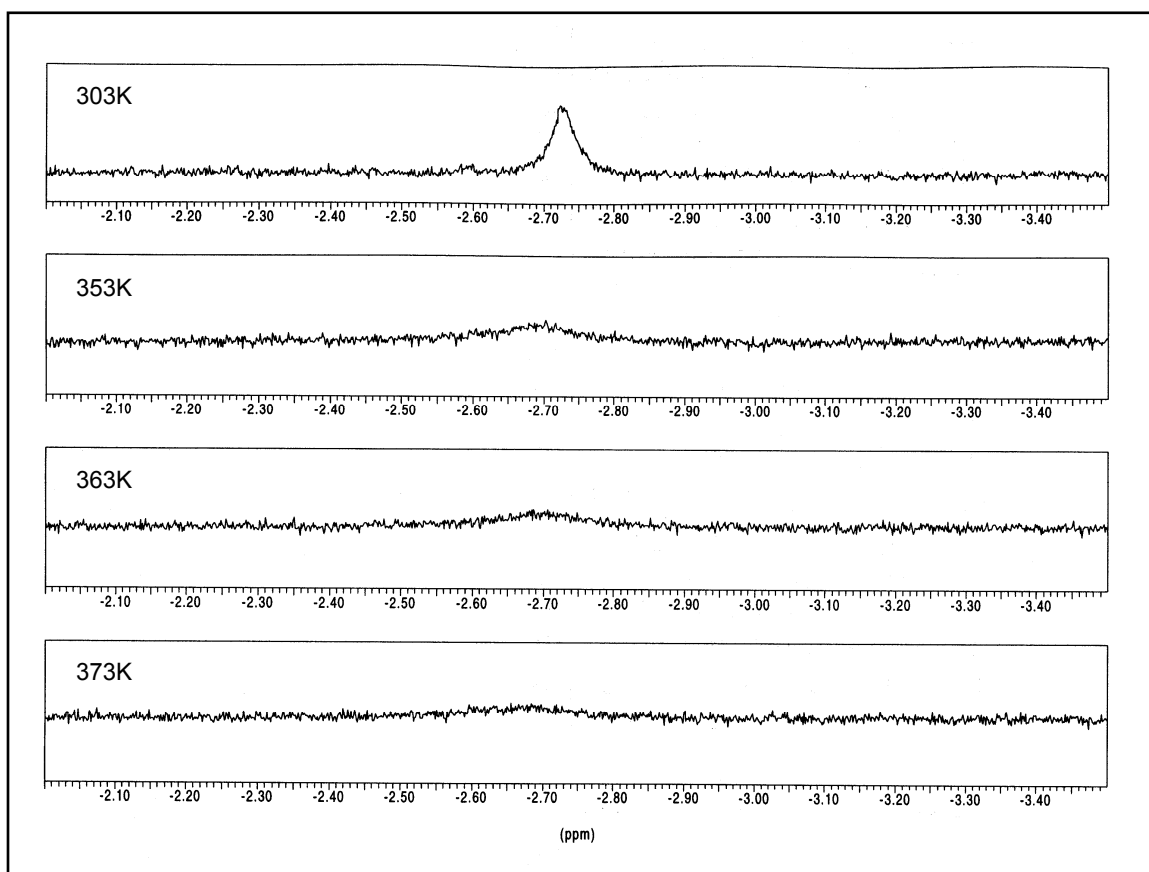


Fig. 4.5 Variable temperature ¹H NMR spectrum of 4-6 (-3.20 to -2.00 ppm)

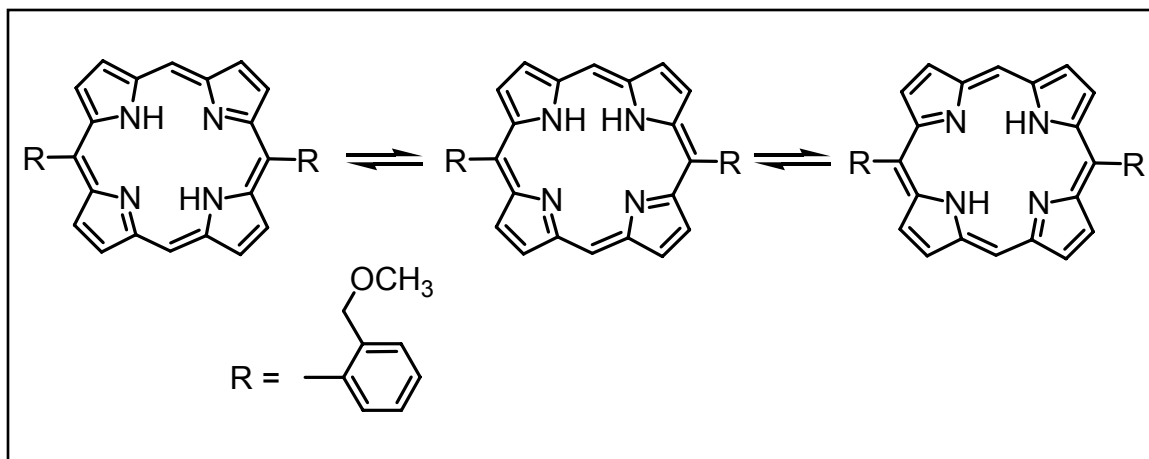


Fig. 4.6 Rapid tautomerization of porphyrin

Earlier works^{8,12} on the synthesis of 5,15-diarylporphyrins also indicated the presence of atropisomers in examples involving *ortho* substituents in the aryl rings. More recently, discrete atropisomers of a series of *meso* tetraarylporphyrins having *ortho* aryl rings were successfully separated by chromatography.¹³ Due to the presence of *ortho* substituents, restricted rotation about the *meso* C-aryl C bond gives rise to the formation of two atropisomers. Hence, the conformational rigidity conferred by the *ortho* substituents of **4-6** and **4-7** (even up to 100 °C) probably accounts for the difference in their polarity which aid in the separation of the isomers. This was further proven by the synthesis of the *meta* isomer described in Section 4.1.2.

4.1.1 SINGLE CRYSTAL X-RAY CRYSTALLOGRAPHIC STUDY OF 4-6ⁱ

Single crystals of **4-6** were grown by slow evaporation of a solution of **4-6** in a cyclohexane/CHCl₃ mixture. The asymmetric unit consists of half of the molecule. The ORTEP diagram of the ligand is shown in Fig. 4.7. The porphyrin ring is perfectly planar (with respect to four pyrrolic C atoms and four N atoms) and the two substituted aromatic rings are in *anti* conformation. All H atoms were located directly, and the thermal ellipsoids indicate a relatively rigid core structure with somewhat dangling side chains. The flexible ether substituents are not rotated above or away from the porphyrin ring. A 70.6 ° orientation of the phenyl rings was observed with respect to the perfect plane of the porphyrin ring and the pair on the porphyrin ring have slight deviation of 0.011 Å (in opposite directions, refer to Fig. 4.8). This orientation is comparable with the tetra-substituted porphyrin systems. In the solid state packing, no π - π interactions was observed between the aromatic rings. One of the phenyl rings of one adjacent unit lie above the plane of the porphyrin ring as shown in Fig. 4.9.

ⁱ Refer to **Appendix** for crystal refinement data, selected bond lengths and angles for all X-Ray Crystal structures in this thesis

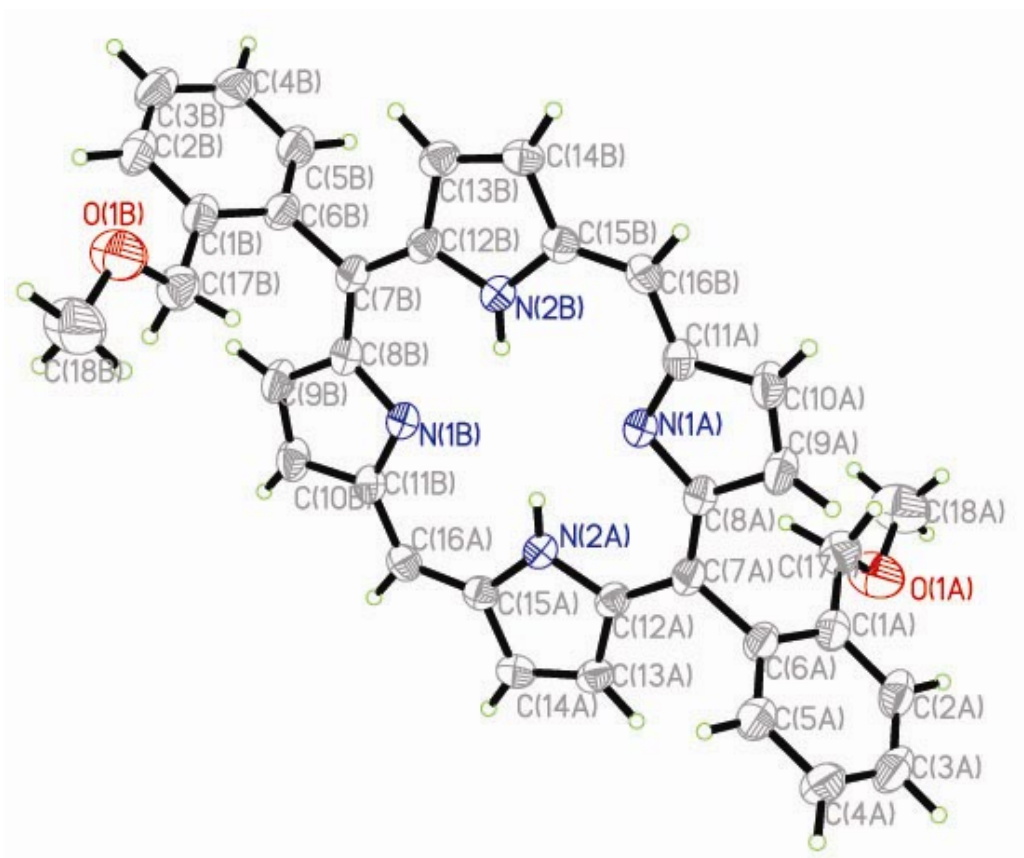


Fig. 4.7 Molecular structure **4-6**; thermal ellipsoids are drawn at 30 % probability level

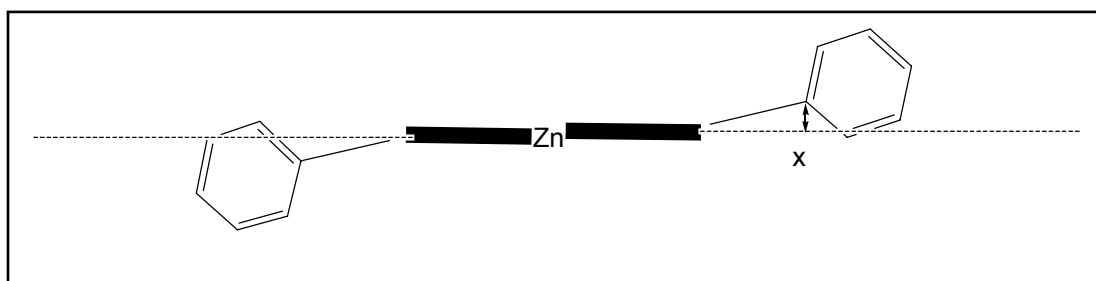


Fig. 4.8 The distance of deviation of the phenyl C attached to the *meso* C of porphyrin with respect to the plane of the porphyrin formed by the four N atoms refers to x

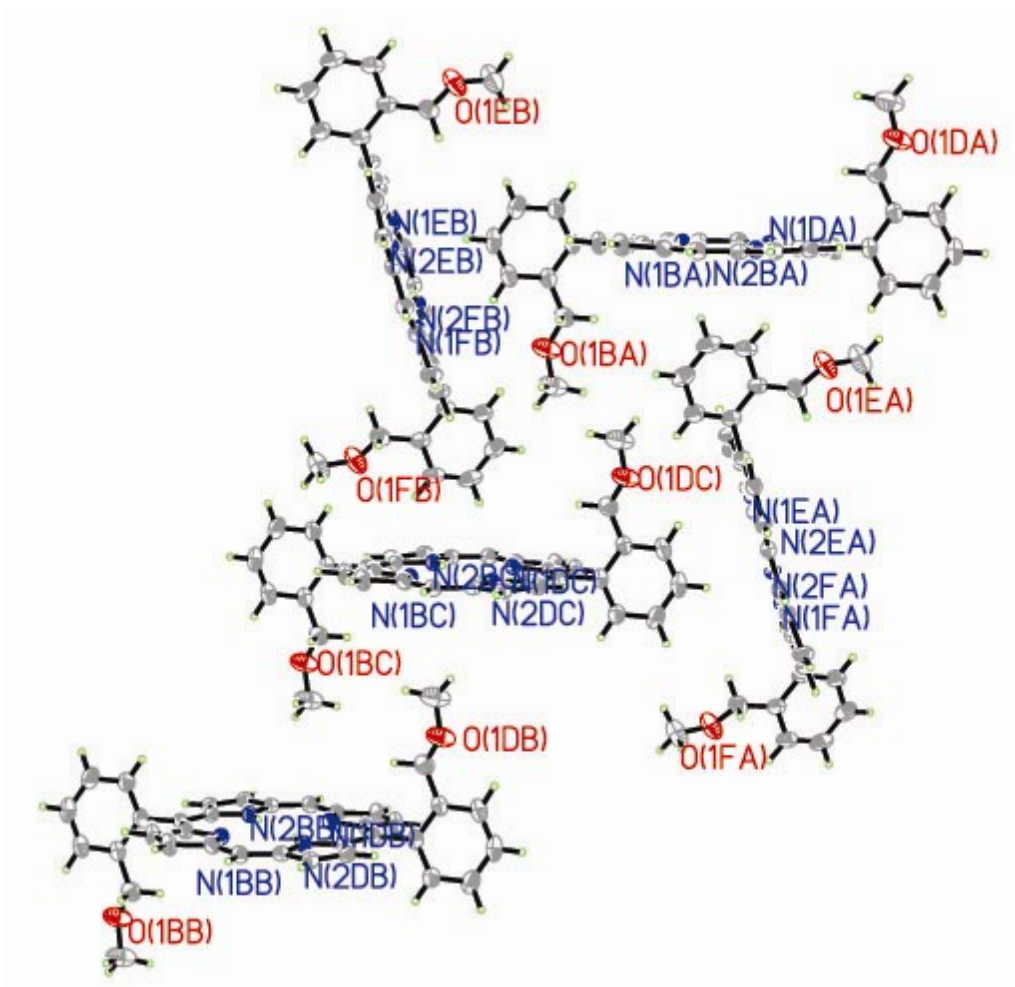
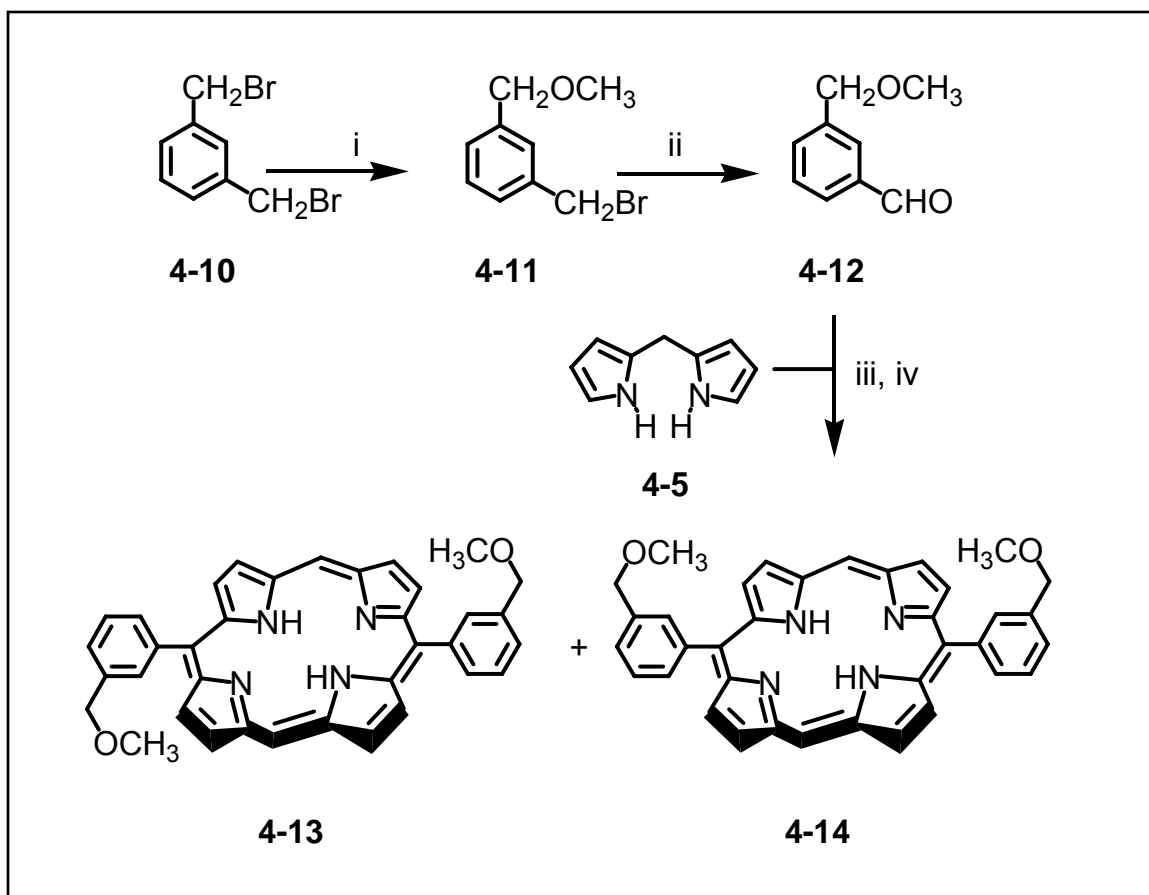


Fig. 4.9 Diagram shows absence of π - π interactions between adjacent units of **4-6** in the solid state packing

4.1.2 SYNTHESIS OF 5,15-BIS-3-METHOXYMETHYLPHENYLPORPHYRIN – 'META' PORPHYRIN (4-13 and 4-14)

Using the same synthetic route for the synthesis of the *ortho* ligands (**4-6** and **4-7**), the *meta* porphyrins were prepared from the 3-methoxymethylbenzaldehyde precursor as shown in the scheme below. Several purification techniques were

performed on the crude porphyrin. However, we were unable to separate the *cis* and *trans* isomers on the column unlike in the *ortho* counterparts despite trying various solvent mixtures and crystallization techniques. The isomers displayed identical chemical shifts on ^1H NMR and even resolution of the benzylic proton peaks using the 500 MHz NMR spectrometer was unsuccessful. This can be attributed to the absence of a large group at the *ortho* position and hence lack of torsional strain to prevent free rotation of the phenyl rings at room temperature in solution.



Scheme 4.3 i, Na, CH₃OH, reflux; ii, Na₂CO₃, DMSO, reflux;
iii, CF₃COOH, CH₂Cl₂; iv, chloranil, reflux

4.1.3 SINGLE CRYSTAL X-RAY CRYSTALLOGRAPHIC STUDY OF 4-13

Single crystals of a mixture of **4-13** and **4-14** were grown by slow evaporation of a solution of ethyl acetate/ CHCl_3 solvent mixture. The ORTEP diagram (Fig. 4.10) of the porphyrin that was elucidated turned out to be the *trans* isomer, which is not surprising since the *trans* isomer formed single crystals more easily in the case of their *ortho* counterparts **4-6** too.

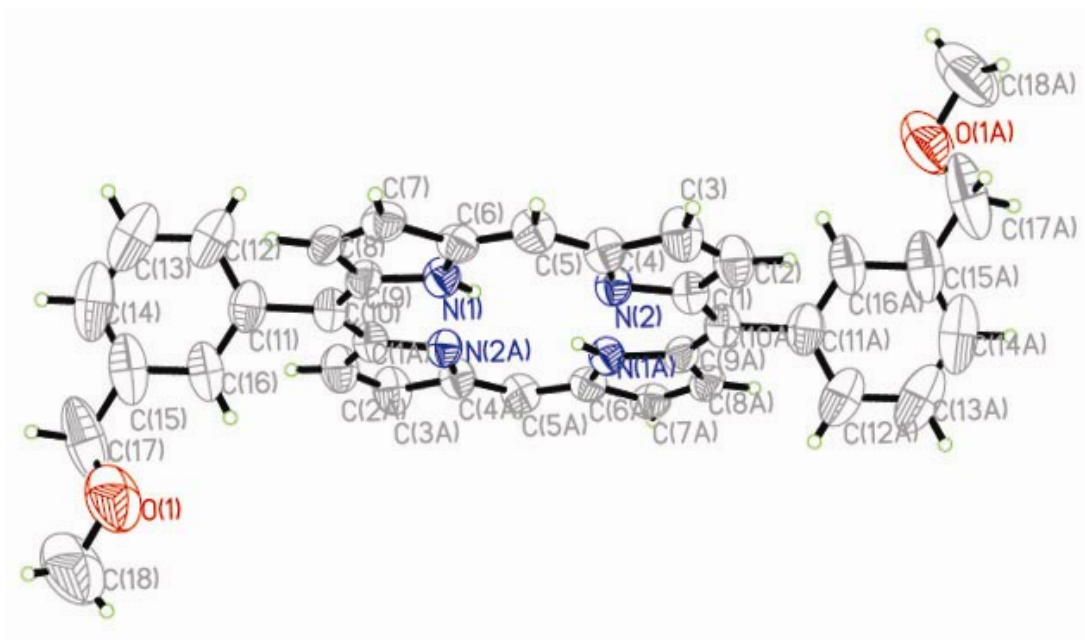


Fig. 4.10 Molecular structure **4-13**; thermal ellipsoids are drawn at 50 % probability level

The asymmetric unit consists half of the molecule. The porphyrin ring is planar with the four N atoms lying on a perfect plane and the two substituted aromatic rings are in *anti* conformation. The phenyl rings orientate by 63.0° with respect to the perfect plane of the porphyrin ring and deviation of 0.023 \AA (in opposite directions).

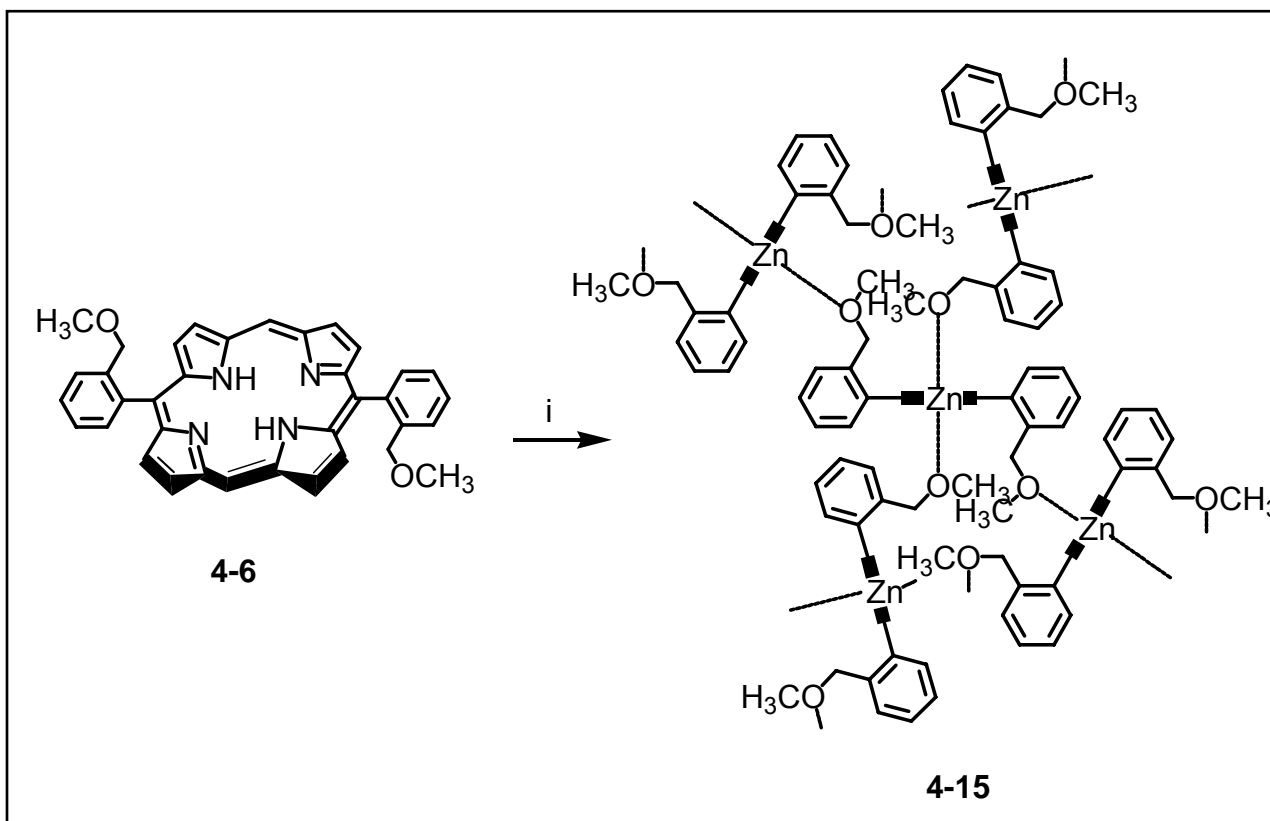
Hence, from the above study on 'meta' porphyrin, we are able to highlight the importance of having two *ortho* methoxymethyl substituents in the structure of the parent porphyrin ligand. These substituents allow the separation of the individual atropisomers. This in turn allows the synthesis and further derivation of the parent porphyrin ligands to produce a series of coordination dimers and polymers with distinct coordination geometries and architectures that can be characterized by single crystal X-Ray Crystallographic techniques. The advantageous features of the designed parent porphyrin ligand will be illustrated in the remaining chapters of the thesis.

4.2 SYNTHESIS OF COORDINATION DIMERS AND POLYMERS OF Zn(II) METALLOPORPHYRINS

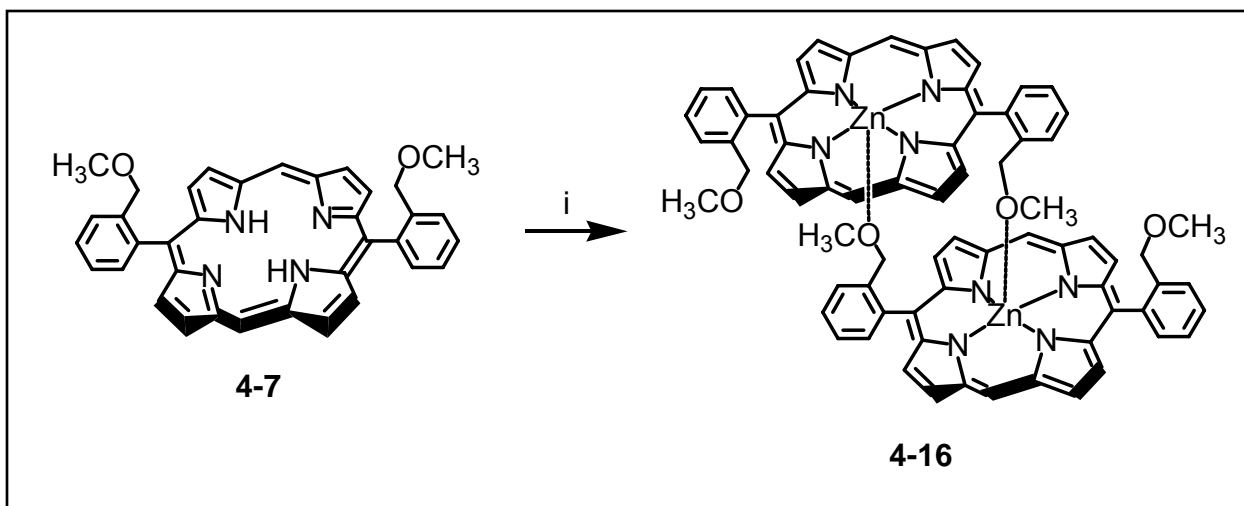
The *trans* ligand **4-6** obtained after purification from its *cis* counterpart was stirred in an ethanolic solution of $Zn(OAc)_2 \cdot xH_2O$ (Scheme 4.4). The product **4-15** isolated was purified on a short chromatographic column using a mixture of hexane/ CH_2Cl_2 as eluent. Structural elucidation of the complex using X-Ray Crystallography yielded a 3D coordination polymer in which each metalloporphyrins contain a hexa-coordinated Zn metal atom and formed Zn-O coordination bonds with four other identical units.⁷ The *cis* ligand **4-7** was stirred in a THF solution of $Zn(OAc)_2 \cdot xH_2O$ and similarly purified to yield **4-16** which was elucidated as a dimer with two Zn-O coordination bonds (Scheme 4.5).

The porphyrins **4-6** and **4-7** were brominated using stoichiometric amounts of recrystallized NBS and a few drops of pyridine as catalyst in $CHCl_3$ at 0 °C and the reactions were closely monitored by TLC (Scheme 4.6 - 4.8). For dibromination of the porphyrins **4-6** and **4-7**, 2.1 equivalents of NBS was added in a single portion with slight excess further added when TLC showed the presence of starting material and

monobrominated species. Care was taken against adding excess NBS as more side product will form. The monobromination reaction had to be carried out with slow addition of NBS and less pyridine to reduce further bromination of the monobrominated species. The reaction was quenched with the addition of acetone as soon as all the starting materials were consumed. When the reaction was allowed to stir for longer period of time (more than 1 hour), more side products formed. The products were purified by precipitation of a CHCl_3 solution of the crude product using methanol then redissolved and reprecipitated using the same method to yield the pure brominated compounds.

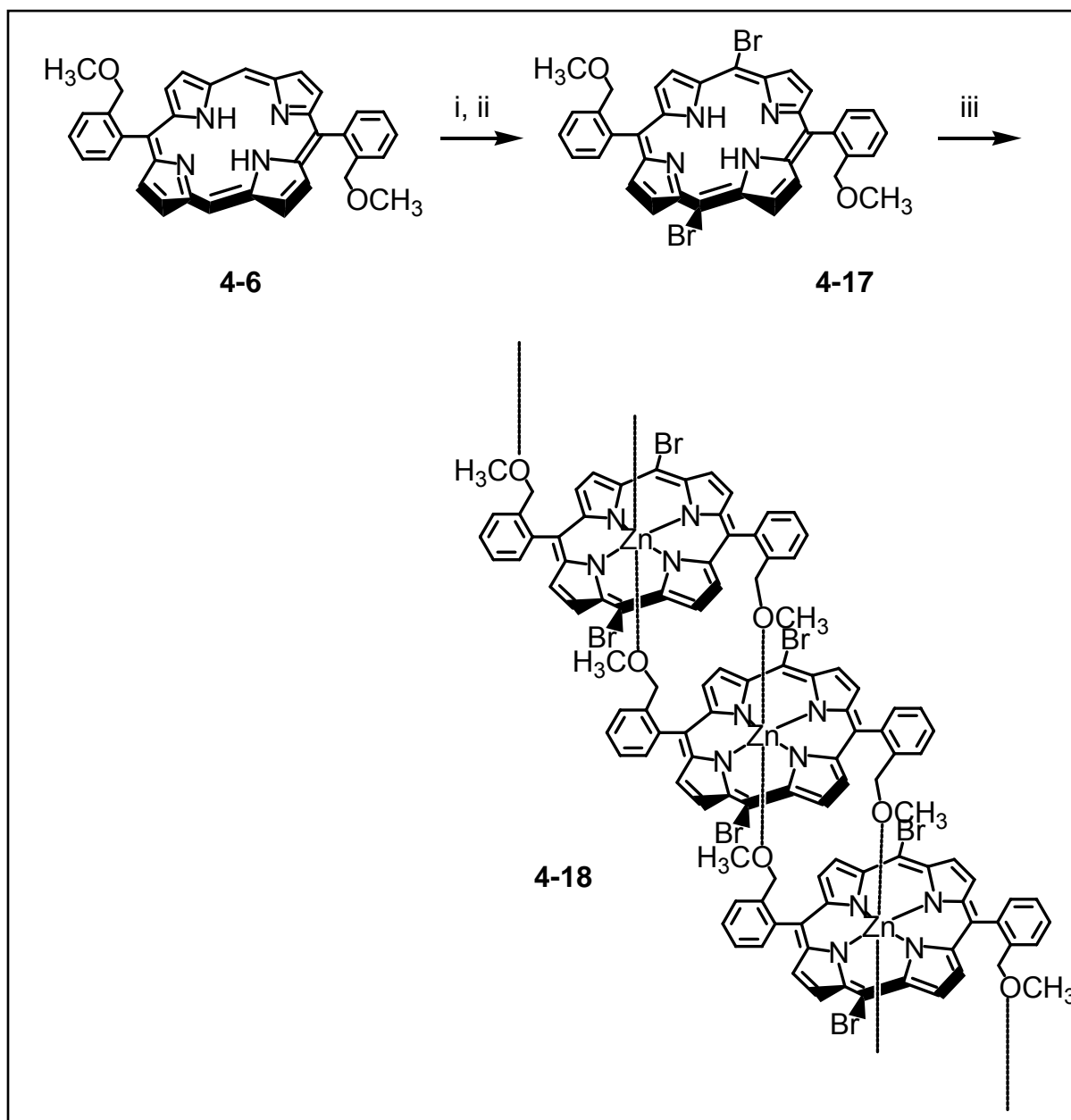


Scheme 4.4 i, $\text{Zn}(\text{OAc})_2 \cdot x\text{H}_2\text{O}$, EtOH

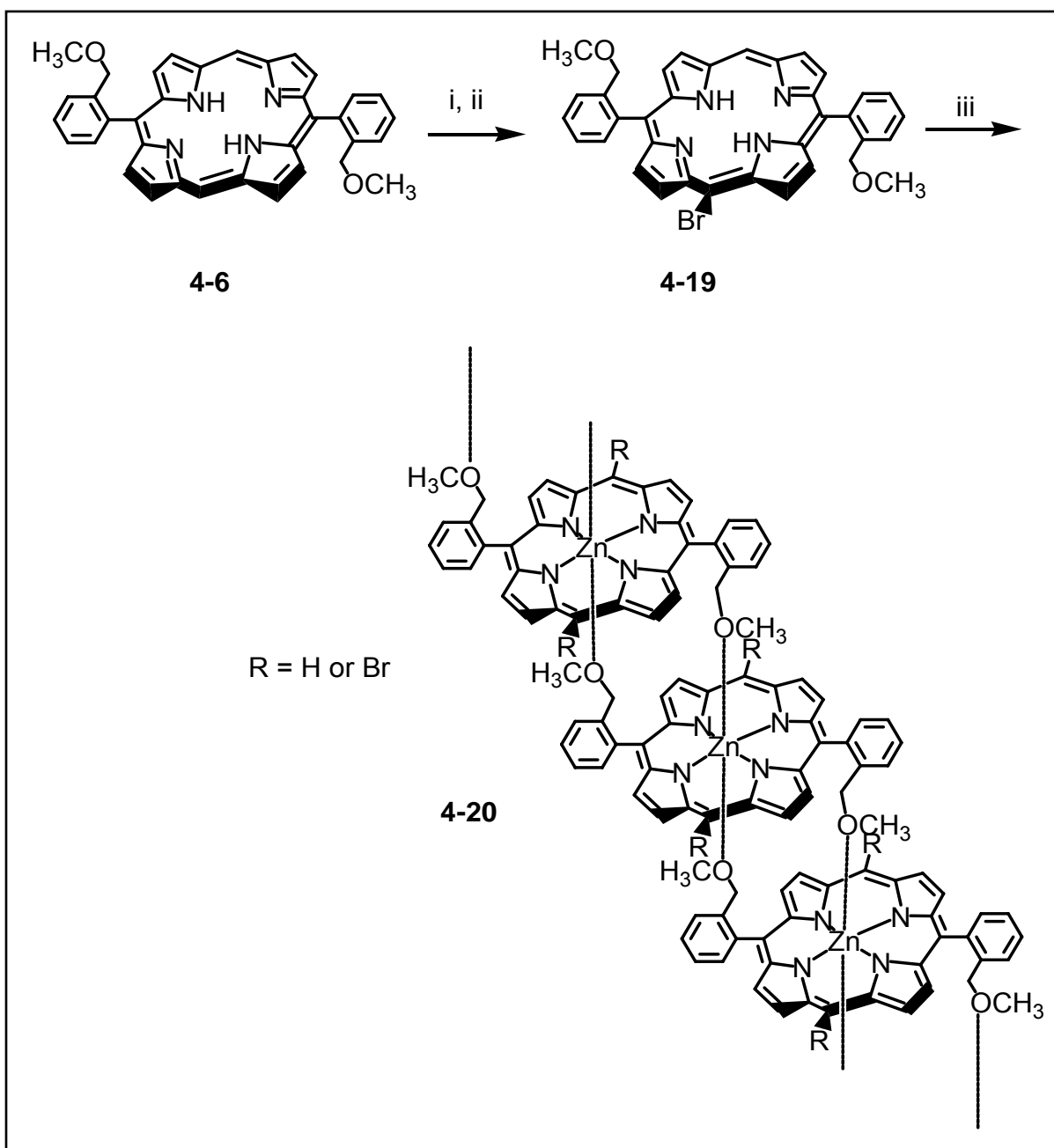


Scheme 4.5 i, $\text{Zn}(\text{OAc})_2 \cdot x\text{H}_2\text{O}$, THF

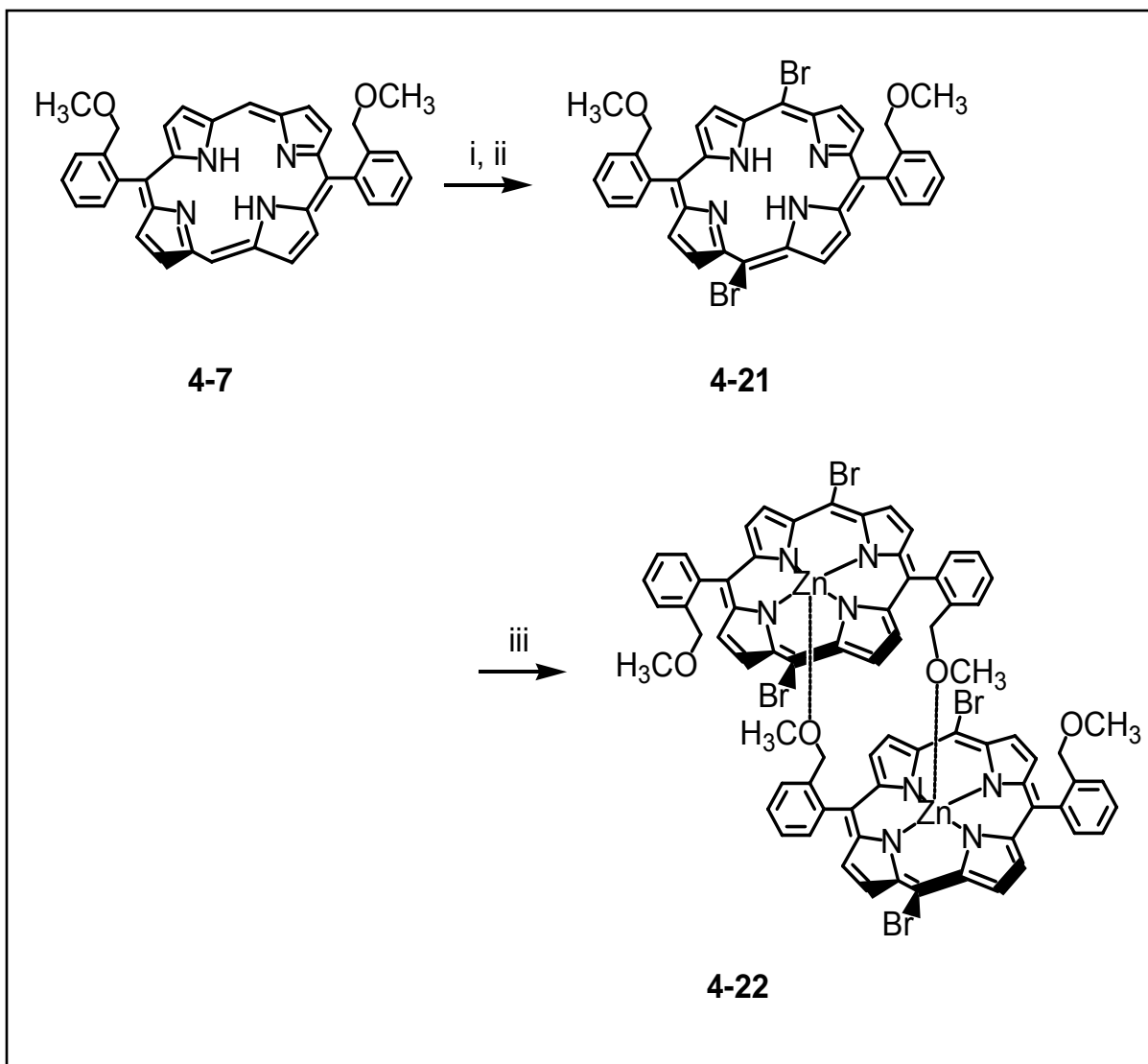
Complexes of the brominated porphyrins **4-17**, **4-19** and **4-21** were stirred in THF solution of $\text{Zn}(\text{OAc})_2 \cdot x\text{H}_2\text{O}$ due to their insolubility in ethanol. The complexes were purified on a short chromatographic column using a mixture of hexane/ CH_2Cl_2 as eluent.



Scheme 4.6 i, NBS, CHCl₃, 0 °C, pyridine; ii, acetone; iii, Zn(OAc)₂.xH₂O, THF



Scheme 4.7 i, NBS, CHCl_3 , 0°C , pyridine; ii, acetone; iii, $\text{Zn}(\text{OAc})_2 \cdot x\text{H}_2\text{O}$, THF



Scheme 4.8 i, NBS, CHCl_3 , 0°C , pyridine; ii, acetone; iii, $\text{Zn}(\text{OAc})_2 \cdot x\text{H}_2\text{O}$, THF

4.3.0 PROPERTIES OF COORDINATION COMPLEXES

As described above, we have synthesized and characterized a variety of self-assembled Zn(II) porphyrin coordination complexes. They are constructed out of the ligands as building block, obtained from a single step reaction that generates a pair of

atropisomers with *cis* and *trans* stereochemistry. Interestingly, each of these ligands gave coordination complexes of Zn(II) with completely different architectures upon insertion of the metal ion which are described in detail as follows.

4.3.1.0 PROPERTIES OF THREE-DIMENSIONAL COORDINATION POLYMER 4-15

This thesis reports the first 3D polymeric complex of six-coordinate Zn(II) metalloporphyrin with two axial O-donors.⁷ Each metalloporphyrin unit in the complex is linked to four other identical complexes through 1-point via Zn-O coordination chemistry. The metalloporphyrin core is the acceptor building block while the substituent appended on the peripheral phenyl ring is the donor block. The formation of **4-15** is entropically unfavourable but its formation suggests that there must be considerable cooperativity between the addition of the first and subsequent donor blocks.

Coordination polymers of Zn(II) porphyrins with one axial O-donor from functional groups attached to peripheral phenyl rings have also been reported.¹⁴ *Ortho* substituted benzylic O donors (earlier examples involved phenolic O donors) have been reported but the ether function is preferred to a hydroxyl group as the latter may favor intermolecular hydrogen-bonding instead of metal-coordination.¹⁵

4.3.1.1 THE ANOMALOUS TIME-DEPENDENT ¹H NMR of 4-15

It was noted that the 3D network of **4-15** had a cavity with the shortest and longest non-hydrogen atomic distances across the channel of about 4.81 Å and 9.27 Å respectively. These cavities and channels should be involved in the phenomenon observed in time-dependent ¹H NMR study as illustrated in Fig. 4.11. The initial

spectrum showed that the benzylic, methyl, one of the pyrrolic and phenyl protons appeared as significantly broadened signals. As time progressed, these signals shifted to higher fields and sharpened. There were essentially no further changes observed after the final spectrum was taken after 10 hours. In fact this spectrum was reproducible even after solvent removal and redissolving the residue in the same solvent. A similar phenomenon was observed in experiments using deuterated toluene as a solvent. The above could have involved a slow diffusion of solvent into the cavities of the polymeric network. This was associated with slow conformational changes of the molecular framework which propagated from the exterior of the 3D network into the interior as the solvent diffusion progressed. Upon attaining equilibrium, the optimum 3D molecular framework allowed rapid diffusion of solvents in and out of the network resulting in sharp averaged signals in the ^1H NMR spectrum. Total removal of the solvent was possible (refer to the next section for discussion on X-Ray Crystallographic analysis) but the optimum molecular conformation was maintained. Thus, redissolving the dried sample in the same solvent gave an identical ^1H NMR spectrum.

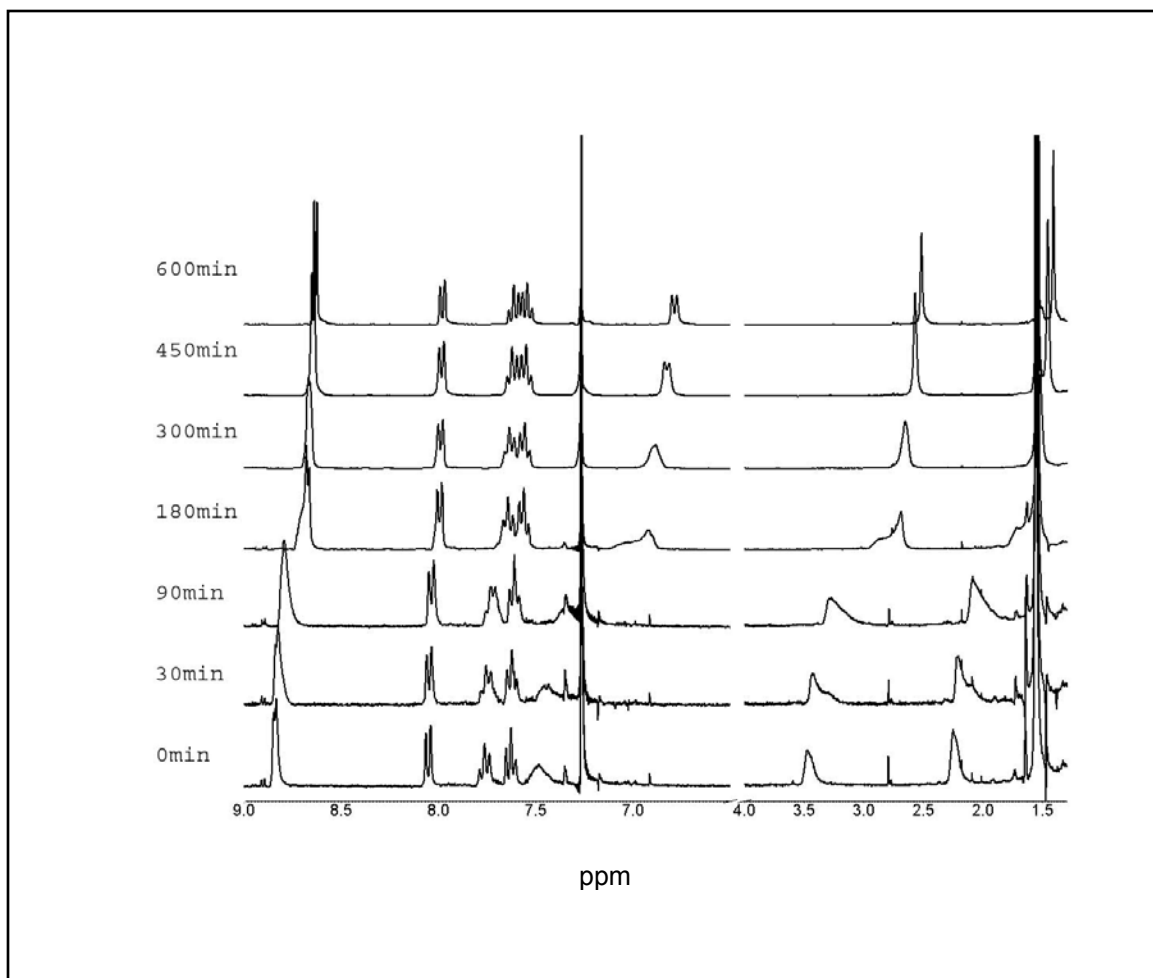


Fig. 4.11 Time-dependent ^1H NMR spectra (in CDCl_3) of a freshly isolated sample of 3D coordination polymer **4-15**

A comparison of the ^1H NMR spectra of the free ligand **4-6** and **4-15** (optimized conformation) shows that the methylene and methyl protons, and the aryl proton on carbon next to that carrying the CH_2OCH_3 group are significantly shifted upfield (Table 4.1). In addition to the fact that the O atom is coordinated to Zn(II) in **4-15**, these protons are all located within the shielding zone of the adjacent aromatic porphyrin macrocycle accounting for the strong shielding effect observed.

Table 4.1 Selected proton chemical shifts (ppm) of **4-6** and **4-15**

Proton	Chemical shifts (ppm)					
	PhH ⁱⁱ		CH ₂ O		OCH ₃	
Solution Concentration ⁱⁱⁱ × 10 ⁻³ (M)	3.60	0.36	3.60	0.36	3.60	0.36
4-6	7.80	7.80	4.11	4.11	2.80	2.80
4-15	6.92	7.48	2.70	3.44	1.61	2.23

The effect of concentration changes to the observed phenomenon was tested. ¹H NMR analyses were carried out on *d*₁-CDCl₃ solutions of **4-6** and **4-15** with concentrations of 3.6 × 10⁻³ M and 3.6 × 10⁻⁴ M. It was observed that upon dilution by 10-folds, the benzylic, methyl, one of the pyrrolic and phenyl protons do not exhibit changes in chemical shifts for **4-6** but that of **4-15** shifted upfield without broadening of the peaks. Hence, peak broadening can be attributed to the diffusion of solvent in the 3D network leading to conformational changes in the molecules while the shift in peaks is due to concentration changes. As more of the compounds dissolved, concentration increased. Hence, the molecules become compressed and moved closer into the anisotropic field of its neighbouring metalloporphyrin (shielded region). The interaction was predetermined by the Zn-O bonds formed in the complex.

In *d*₅-C₆D₅NO₂ solution, there is no obvious shift of the peaks but only a change in shape from broad to sharp over time. Equilibrium was attained faster in *d*₅-C₆D₅NO₂ than in *d*₁-CDCl₃. As concluded earlier, since concentration effects only cause changes

ⁱⁱ Proton on carbon adjacent to carbon carrying CH₂OCH₃.

ⁱⁱⁱ Concentration of **4-15** used for Z-scan measurement = 7.9 × 10⁻³ M (Refer to Chapter 5 for discussion on Z-scan measurement of **4-15**).

in the chemical shifts, the observation made in $d_5\text{-C}_6\text{D}_5\text{NO}_2$ solution may be due to the opening up of the 3D network polymer **4-15** to form monomers. This is supported by the X-Ray Crystallographic results which show the existence of **4-15** as monomers in solid state when grown in $\text{C}_6\text{H}_5\text{NO}_2$ solution.

As the concentration of **4-15** in CHCl_3 is lower than that used in Z-scan measurement, the significant downfield shift of **4-15** as compared to its ligand **4-6** confirm that the three-dimensional network of **4-15** is maintained at the concentration of the NLO measurements.

4.3.1.2 THE EFFECT OF SOLVENT AND SMALL MOLECULES ON THE SOLID STATE STRUCTURE OF 4-15

According to calculations, the cavities within **4-15** were expected to be large enough to hold small molecular species. We tested this possibility by using small molecular weight solvents. Crystals of **4-15** were dissolved in sufficient amounts of a solvent mixture of CHCl_3 /cyclohexane (1:1) and solvents such as CHCl_3 , acetonitrile, ethyl acetate and THF separately before the solutions were allowed to slowly evaporate off to regenerate single crystals suitable for X-Ray Crystallographic analyses. The results show that identical single crystals of **4-15** were obtained whether it was grown in CHCl_3 /cyclohexane (1:1) solvent mixture, CHCl_3 , acetonitrile, or THF.

Hence, it can be deduced that in solution, the cavity of the coordination polymer may have (i) contracted and hence the solvent molecules are unable to penetrate, or (ii) the sizes of the molecules is too large to fit into the cavity or (iii) the molecules are so

small that they are able to freely move in and out of the cavities and channels and thus be removed from the network when evaporated.

Interestingly, when $C_6H_5NO_2$ and ethyl acetate were separately diffused into the crystals of **4-15**, the 3D architecture of the coordination polymer opened up to give monomeric units of the Zn(II) metalloporphyrin complex as elucidated from the single crystal X-Ray Crystallographic analyses. In addition, no solvent residue was trapped in the single crystal. Hence, these solvent molecules caused the polymer to “break up” by diffusing through the cavities. The possibility of this occurrence caused by the coordination of the N atom of $C_6H_5NO_2$ or O atom of ethyl acetate in substitution of the existing O atoms is expelled because the single crystal of the monomer did not contain any residual solvent molecules.

In addition, similar downfield shift of the benzylic, methyl, one of the pyrrolic and phenyl protons in the 1H NMR spectrum of **4-15** in $d_5-C_6D_5NO_2$ (Fig. 4.12) show that despite the contraction of the cavities and channels, the solvent was able to pass through them. Since $C_6H_5NO_2$ is larger in size relative to the other solvents mentioned and yet exhibit high accessibility into the cavities and channels, the first and second postulations suggested earlier cannot be valid. Thus, that leaves the possibility that the small molecules are able to move in and out of the cavity so easily that they cannot be trapped in the 3D network in solid state.

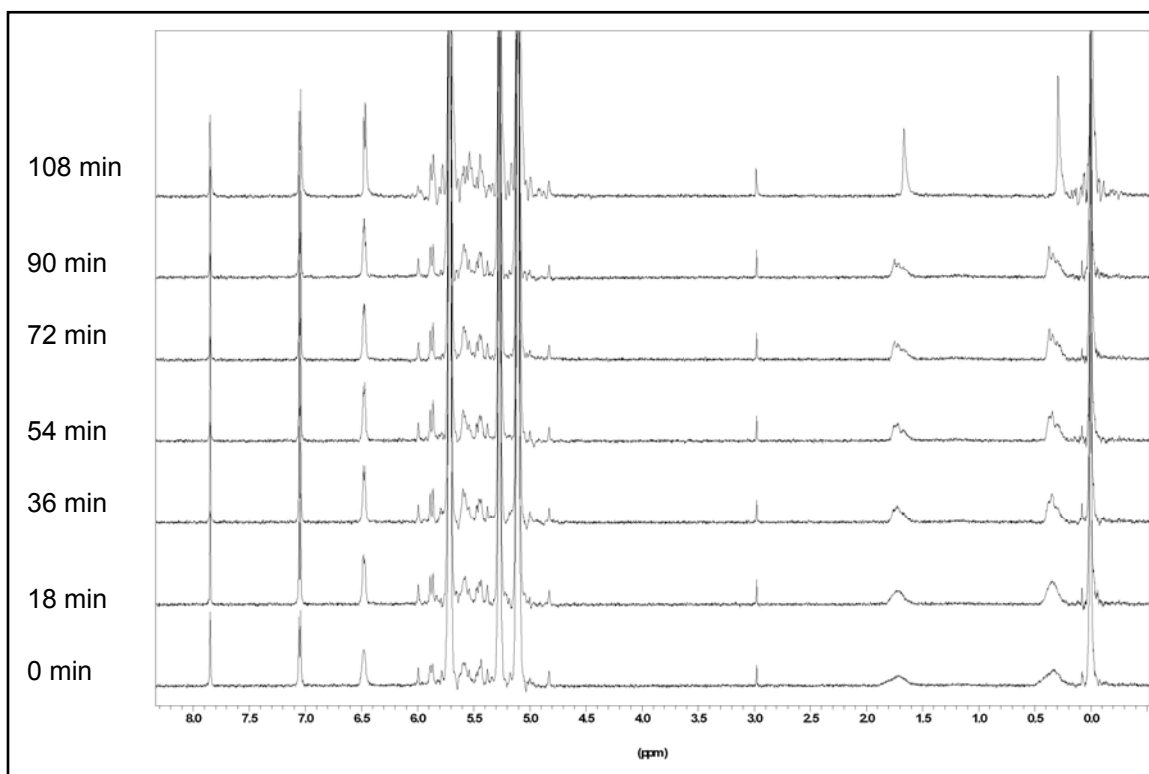


Fig. 4.12 Time-dependent ^1H NMR spectra (in $d_5\text{-C}_6\text{D}_5\text{NO}_2$) of a freshly isolated sample of 3D coordination polymer **4-15**

We studied the association of highly electron-deficient molecules chloranil¹⁶ and 1,4-benzoquinone with electron-rich **4-15**. When the ligand was stirred in a CHCl_3 solution with excess $\text{Zn}(\text{OAc})_2 \cdot x\text{H}_2\text{O}$ and chloranil/1,4-benzoquinone separately, the ^1H NMR spectrum of the purified compound reveals that a similar 3D coordination polymer had formed and the absorption spectrum does not show the presence of chloranil nor 1,4-benzoquinone. Purification was carried out by solvent extraction to wash away the excess $\text{Zn}(\text{OAc})_2 \cdot x\text{H}_2\text{O}$ using deionized water followed by column chromatography. Clearly, in addition to the bands attributed to chloranil and 1,4-benzoquinone, there was only one relatively broad dark pink band which eluted at the same rate as **4-15**.

In addition, after **4-15** was stirred in a CHCl_3 solution of chloranil and 1,4-benzoquinone separately for 2 days, the purified product obtained was the starting material. These observations lead to the conclusion that the 3D polymeric network of **4-15** is very closely knitted. Hence, the stability of the coordination complex is not disturbed by the association of electronically deficient foreign species with the Zn(II) porphyrins at the surface of the array.

4.3.1.3 OPTICAL PROPERTIES OF 4-15

Typical Soret and Q-bands, characteristic of a free-base and the corresponding Zn(II) metalloporphyrin in various solvents were recorded. These bands shift depending on the type of solvent used as shown from its UV-vis spectra (Fig. 4.13).

The emission spectra were taken in CH_2Cl_2 by exciting the sample at 407 nm. The emission spectra (Fig. 4.14) of the free ligand **4-6** and the 3D coordination polymer **4-15** are dominated by two main features, namely the Q(0,0) and Q(0,1) bands. The Q(0,0) and Q(0,1) emission bands occur near 640 - 650 and 675 - 725 nm, respectively, for **4-6** and 560 - 595 and 595 - 660 nm, respectively for **4-15**. The quantum efficiency of **4-15** was determined to be 0.058 using Zn(II) tetraphenylporphyrin ($\Phi_{\text{eff}} = 0.033$) as standard in the same solvent toluene. The higher quantum efficiency of **4-15** relative to its standard is probably due to less fluorescence quenching as a result of π - π stacking, because the monomeric units are coordinated in a tilted angle relative to each other.

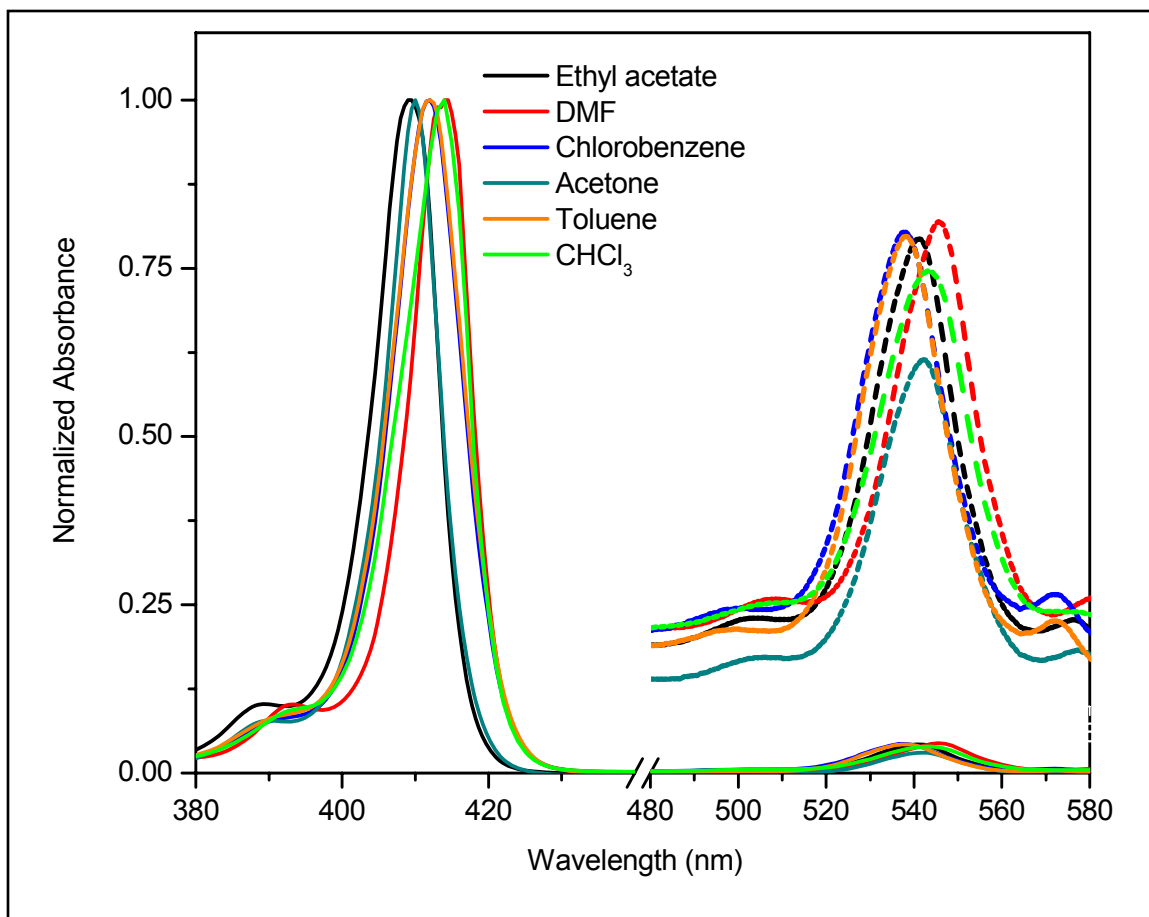


Fig. 4.13 UV-vis absorption spectrum of **4-15** in various solvents. Dotted lines show Q-bands amplified for clarity

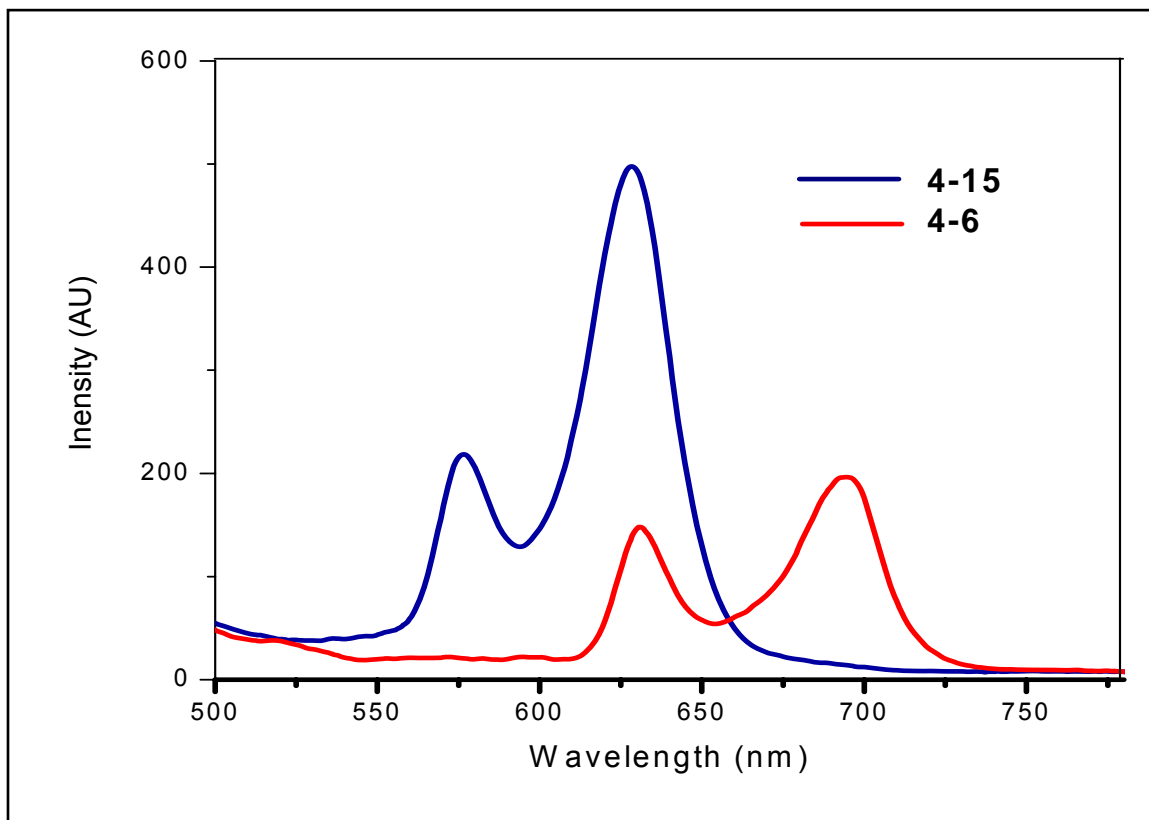


Fig. 4.14 Emission spectrum of **4-6** and **4-15** in toluene at concentration of 1×10^{-5} M

4.3.2.0 PROPERTIES OF ONE-DIMENSIONAL COORDINATION POLYMER **4-18** AND **4-20**

Calculation of the size of Br atom using AM1 shows that a Br atom which has a calculated van der Waals' radius of 2.33 Å is small enough to occupy the cavity in the 3D coordination polymer **4-15**. Hence, we attempted to construct architectures with incorporated Br atom by substituting the one and two *meso* H on the free base **4-6** to yield **4-17** and **4-19**. We can thus determine the effect of the number of Br atoms on the NLO properties of the resulting coordination complexes. Surprisingly, structural elucidation of the single crystal of **4-18** and **4-20** after it was synthesized from a THF

solution of $\text{Zn}(\text{OAc})_2 \cdot x\text{H}_2\text{O}$ and the corresponding free base ligands gave a coordination polymer with totally different architecture from **4-15**. One-dimensional linearly stacked coordination polymers were obtained. Each $\text{Zn}(\text{II})$ metalloporphyrins are coordinated to two adjacent units via two Zn-O coordination bonds, thus forming an infinite 'wire' of $\text{Zn}(\text{II})$ metalloporphyrins with apical donor blocks on the two opposite faces. Since the units stack on each other in a slipped cofacial manner, each row resembles a step-like infinite structure. In addition, all the 'wires' stack one after the other in a zig-zag fashion.

The presence of an additional coordination bond in **4-18** and **4-20** compared to **4-15** causes each unit in the former to be held to each other in a more rigid manner hence, free rotation of about a single Zn-O bond is more restricted. Also, the additional bond causes every unit to be in slipped cofacial geometry while in **4-15**, each unit is tilted at an angle. The single Br atom on each building block is randomly orientated in the coordination polymer **4-20** and the single Br renders the monomer and overall polymer asymmetrical.

4.3.2.1 OPTICAL PROPERTIES OF 4-18 AND 4-20

Typical Soret and Q-bands, characteristic of $\text{Zn}(\text{II})$ metalloporphyrin of **4-18** and **4-20** in various solvents were recorded. The chromophoric interactions between adjacent units were not exhibited in their UV-vis spectra (Fig. 4.15 and Fig. 4.16) even though the porphyrin chromophores are more cofacially oriented than in **4-15**. The absorption spectrum of **4-20** in different solvents closely resembles that of **4-10** although the geometries of the polymers are completely different. However, the absorption spectrum of **4-18** is clearly different from the former polymers. The Soret band of **4-18** is more red-shifted in the same solvents. Since the relatively large Br atom causes steric

hindrance and is known to result in distortion of planarity of the porphyrin ring, the red-shift in absorption spectrum is not likely to be attributed to increase in conjugation but rather due to electronic effects. Both polymers **4-18** and **4-20** do not exhibit fluorescence which is expected because of the heavy atom effect of Br. Heavy atoms promote mixing of singlet and triplet states due to spin-orbit coupling, thus enhancing intersystem crossing from $S_1 \rightarrow T_1$.¹⁷

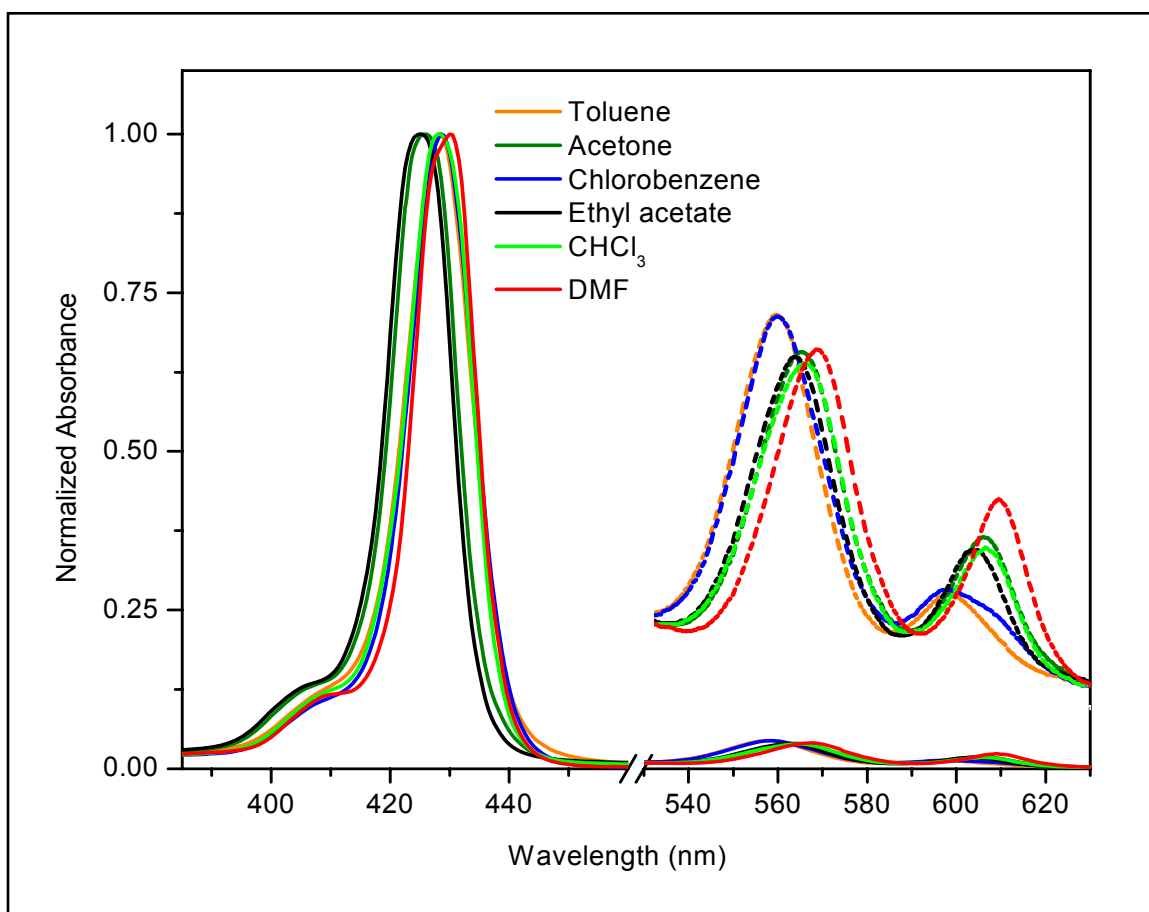


Fig. 4.15 UV-vis absorption spectrum of **4-18** in various solvents. Dotted lines show Q-bands amplified for clarity

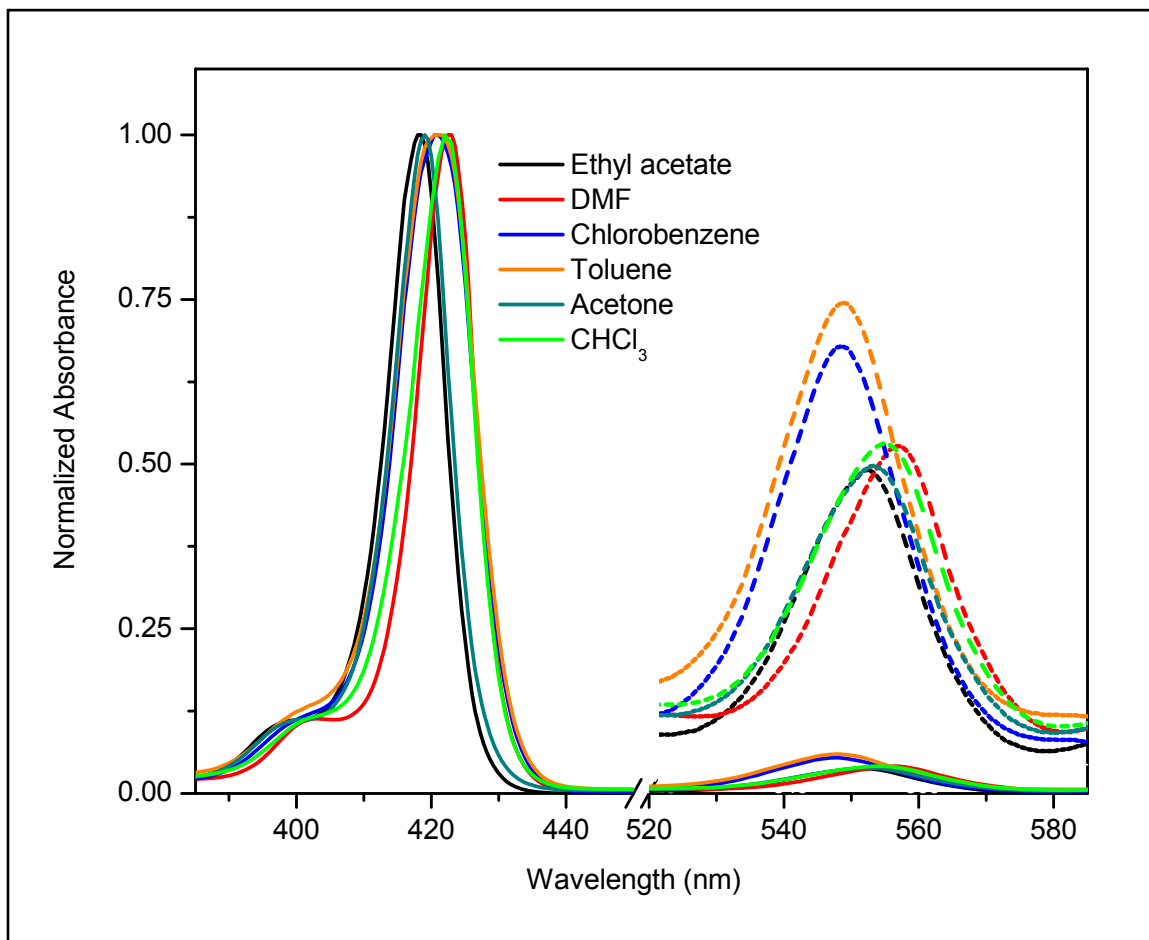


Fig. 4.16 UV-vis absorption spectrum of **4-20** in various solvents. Dotted lines show Q-bands amplified for clarity

4.3.3.0 PROPERTIES OF ONE-DIMENSIONAL COORDINATION DIMER 4-16

The *cis* ligand **4-7** gave a completely different coordination complex when stirred in a THF solution of $\text{Zn}(\text{OAc})_2 \cdot x\text{H}_2\text{O}$. Interestingly, a dimer which resembles the bacteria photosynthetic reaction centres was obtained. The bacteria contains the ‘special pairs’ of bacteriochlorophyll¹⁸ molecules in which the whole rings are laterally offset by approximately 6 Å. In the coordination dimer **4-16**, the units are oriented such that their

edge-over-edge overlap involves only one phenyl ring interacting with the Zn(II) metal atom at the porphyrin and possess a vertical separation $\sim 5.6 \text{ \AA}$.

4.3.3.1 THE ANAMOLOUS TIME-DEPENDENT ^1H NMR of 4-16

A comparison of the ^1H NMR spectra of **4-7** and **4-16** show that the methylene, methyl and the aryl proton on carbon next to that carrying the CH_2OCH_3 group of **4-16** are significantly shifted upfield (Table 4.2). The ^1H NMR shows the appearance of only one set of broad benzylic and methyl protons which sharpened after 507 minutes (Fig. 4.17).

Table 4.2 Selected proton chemical shifts (ppm) of **4-7** and **4-16**

	Chemical shift (ppm)					
	PhH ⁱⁱ		CH ₂ O		OCH ₃	
Solution Concentration^{iv} $\times 10^{-3}$ (M)	3.60	0.36	3.60	0.36	3.60	0.36
4-7	7.69	7.69	4.07	4.07	2.81	2.81
4-16	6.74	6.91	2.47	3.23	1.44	2.11

At higher concentration, we observed sharp shoulder peak adjacent to the broad peaks of benzylic and methyl protons in the lower field. These sharp shoulder peaks do not shift over time and are thus attributed to the methoxymethyl substituents with uncoordinated O atoms in the dimer. This shows that at lower concentration, the chromophores may have moved further from each other in the dimer. However, the

^{iv} Concentration of **4-16** used for Z-scan measurement = 4.9×10^{-3} M. (Refer to Chapter 5 for discussion on Z-scan measurement of **4-16**).

significant upfield shift as compared to the free ligands show that each unit is still in close proximity to be affected by the anisotropic field of each other.

The relative geometry of the pair is almost coplanar also. Unlike the 3D coordination polymer **4-5**, another monomeric unit of **4-16** did not coordinate to either of the two units in the dimer probably because the lack of another bond renders the association energetically unfavourable. This is illustrated in Fig. 4.18.

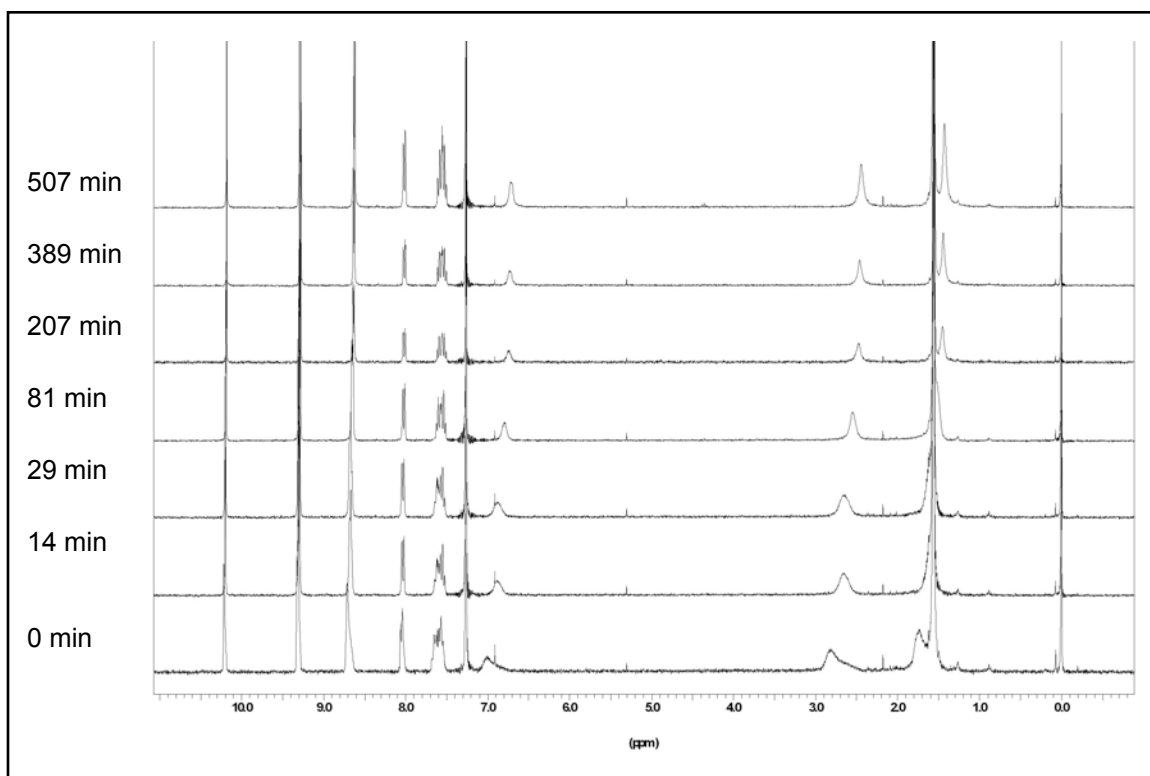


Fig. 4.17 Time-dependent ¹H NMR spectra (in CDCl₃) of a freshly isolated sample of dimer **4-16**

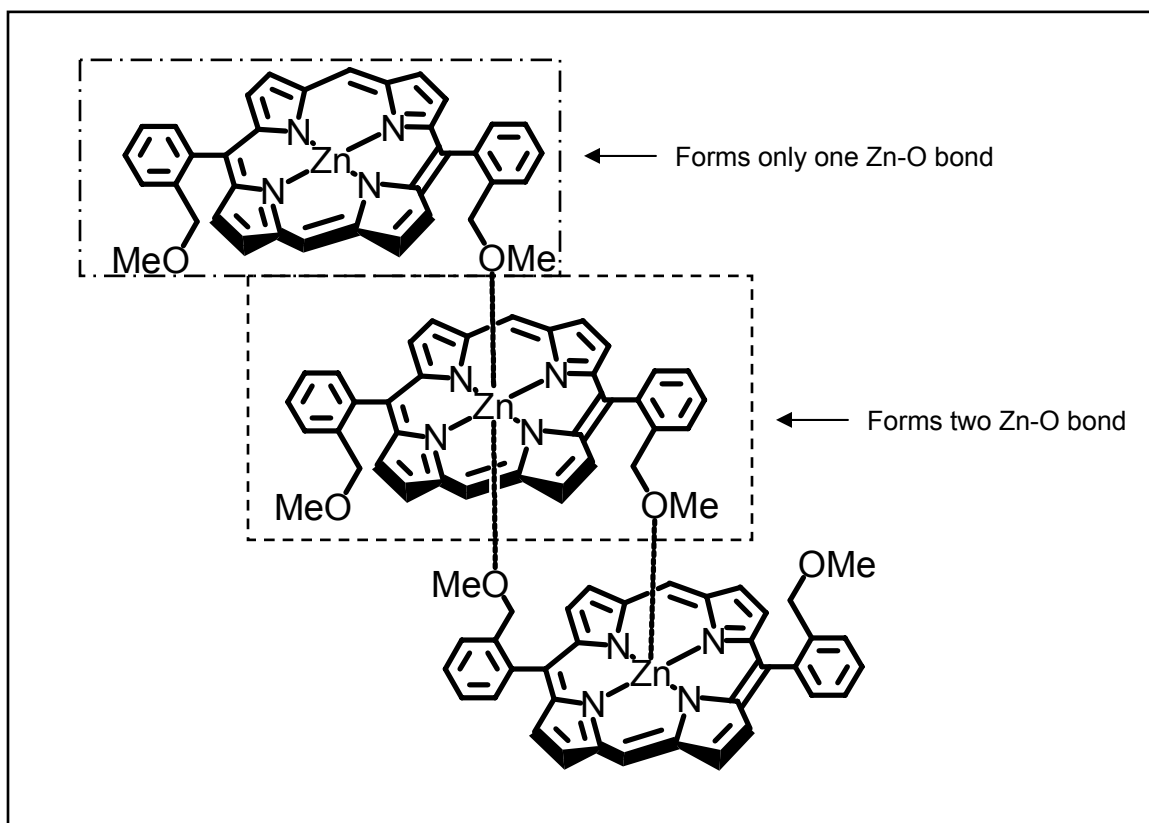


Fig. 4.18 An illustration showing the association of the dimeric unit in **4-15** and a relatively weakly coordinated unit which forms only one Zn-O coordination bond

4.3.3.2 OPTICAL PROPERTIES OF 4-16

Typical Soret and Q-bands, characteristic of a Zn(II) metalloporphyrin in various solvents were recorded. Similar to 3D coordination polymer **4-15**, the dimer **4-16** does not show chromophoric interactions in its optical spectrum even though the chromophores are closer (Fig. 4.19).

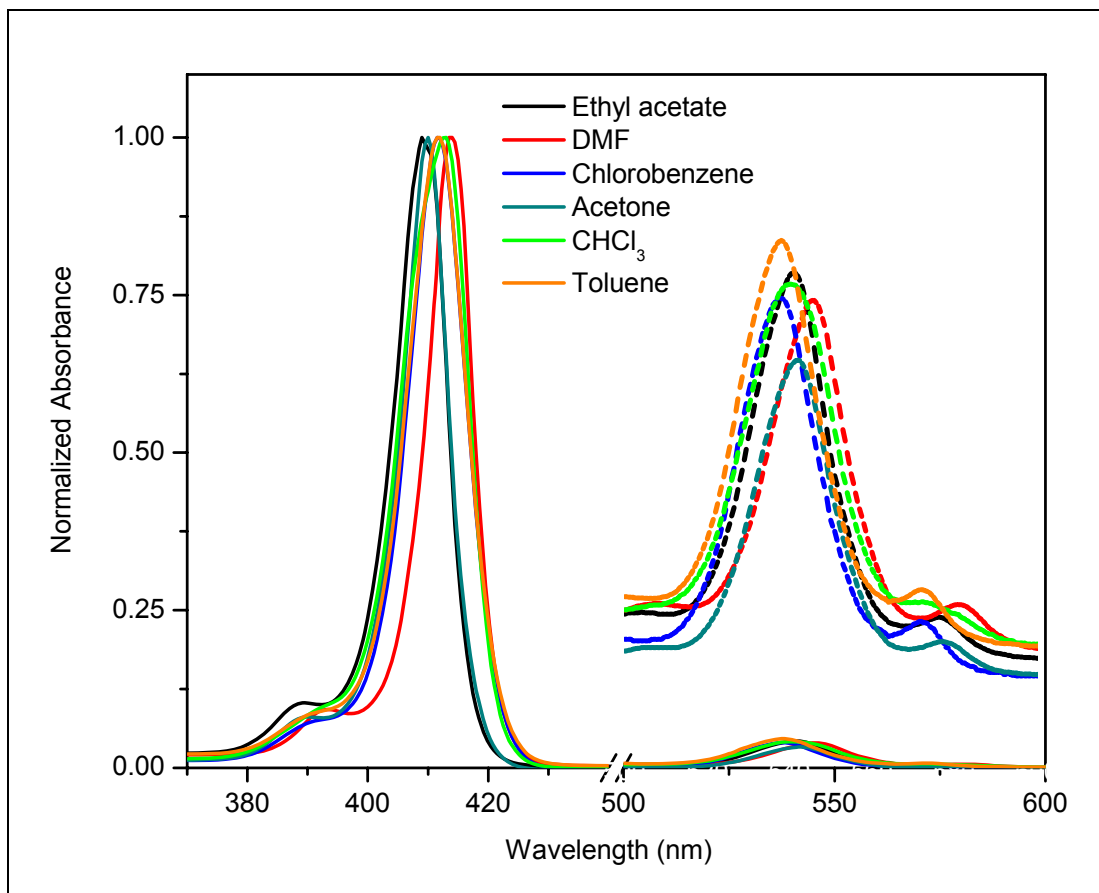


Fig. 4.19 UV-vis absorption spectrum of **4-16** in various solvents. Dotted lines show Q-bands amplified for clarity

The emission spectra were taken in CHCl_3 exciting the sample at 413 nm. The emission spectra of the free ligand **4-7** and the coordination dimer **4-16** are similar to those of **4-6** and **4-15** and are dominated by two main features, namely the Q(0,0) and Q(0,1) bands. The quantum efficiency of **4-16** in CHCl_3 was determined to be 0.039 using Zn(II) tetraphenylporphyrin ($\phi_{\text{eff}} = 0.033$) as standard in toluene. The lower quantum efficiency of **4-16** relative to **4-15** is probably due to larger extent of aggregation of the **4-16** because of the cofacial packing of **4-16** whereas those in the polymer **4-15** are coordinated in a tilted angle relative to each other.

4.3.4.0 PROPERTIES OF ONE-DIMENSIONAL COORDINATION DIMER 4-22

The monobrominated *trans* ligand **4-19** gave a coordination polymer **4-20** with random orientation of the Br substituent which allows the overall effect of the atom on the polarization of the large supramolecular architecture to be averaged out. However, this approximation cannot be made for a dimeric coordination complexes hence only the dibromo ligand **4-21** was synthesized from the *cis* ligand **4-7** for the formation of Zn(II) metalloporphyrin complex. Unlike the *trans* ligand series, the brominated *cis* ligand **4-21** gave a similar dimeric complex **4-22** when stirred in an THF solution of Zn(OAc)₂.xH₂O.

4.3.4.1 OPTICAL PROPERTIES OF 4-22

Typical Soret and Q-bands, characteristic of a Zn(II) metalloporphyrin in various solvents were recorded. Similar to the coordination dimer **4-16**, **4-22** does not show chromophoric interactions (Fig. 4.20).

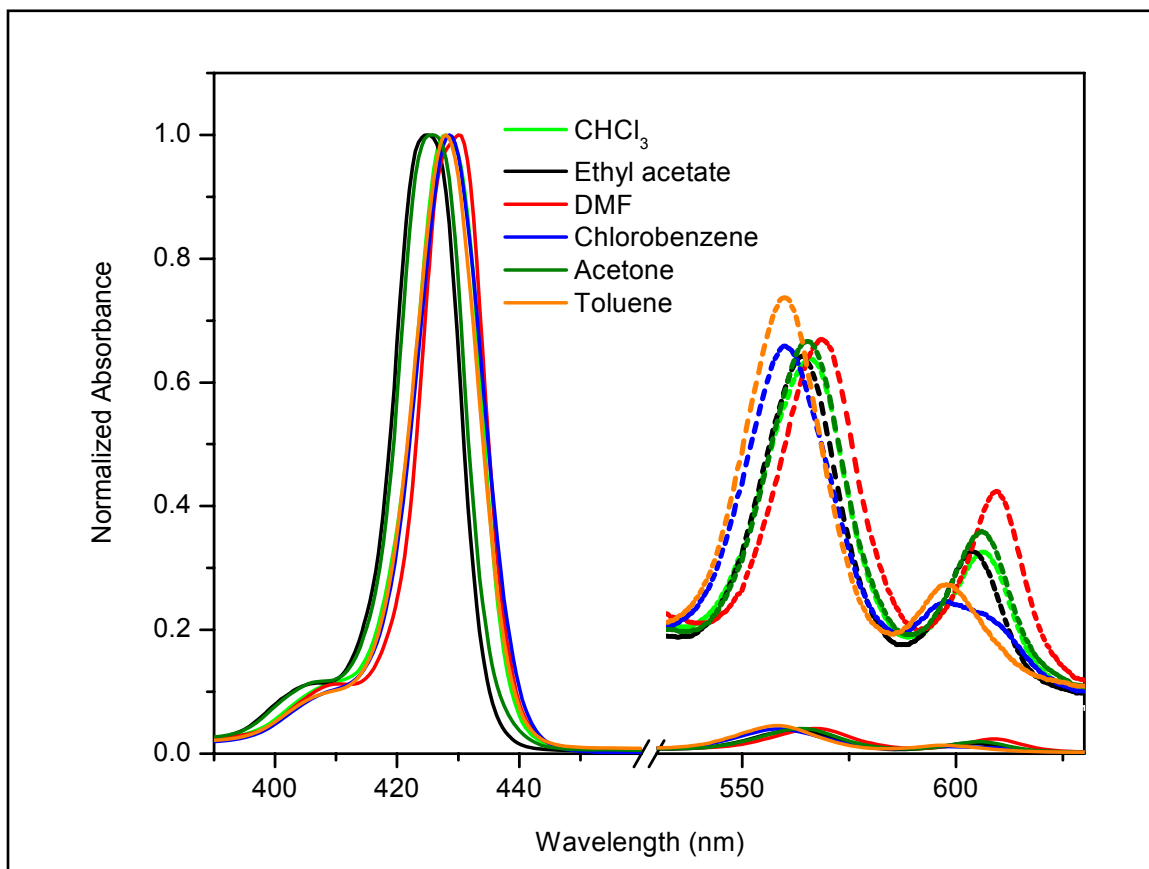


Fig. 4.20 UV-vis absorption spectrum of **4-22** in various solvents. Dotted lines show Q-bands amplified for clarity

4.3.5 COMPARISON OF UV-VIS ABSORPTION SPECTRUM OF THE FREE BASE PORPHYRINS, Zn(II) METALLOPORPHYRIN DIMERS AND POLYMERS

Generally, the coordination complexes gave similar shifts in the various solvents chosen shown in the previous figures. The Fig. 4.21 clearly illustrates the effect of bromination and complexation on the optical properties of the porphyrin derivatives. The absorption peaks of brominated ligands **4-17**, **4-19** and **4-21** are more red-shifted than the unbrominated ligands **4-6** and **4-7** due to electronic effects of the Br atom. The

coordination complexes also exhibit hypsochromic shifts relative to their ligands. This is attributed to the increase in conjugation of the metalloporphyrin upon insertion of the Zn(II) metal atom.

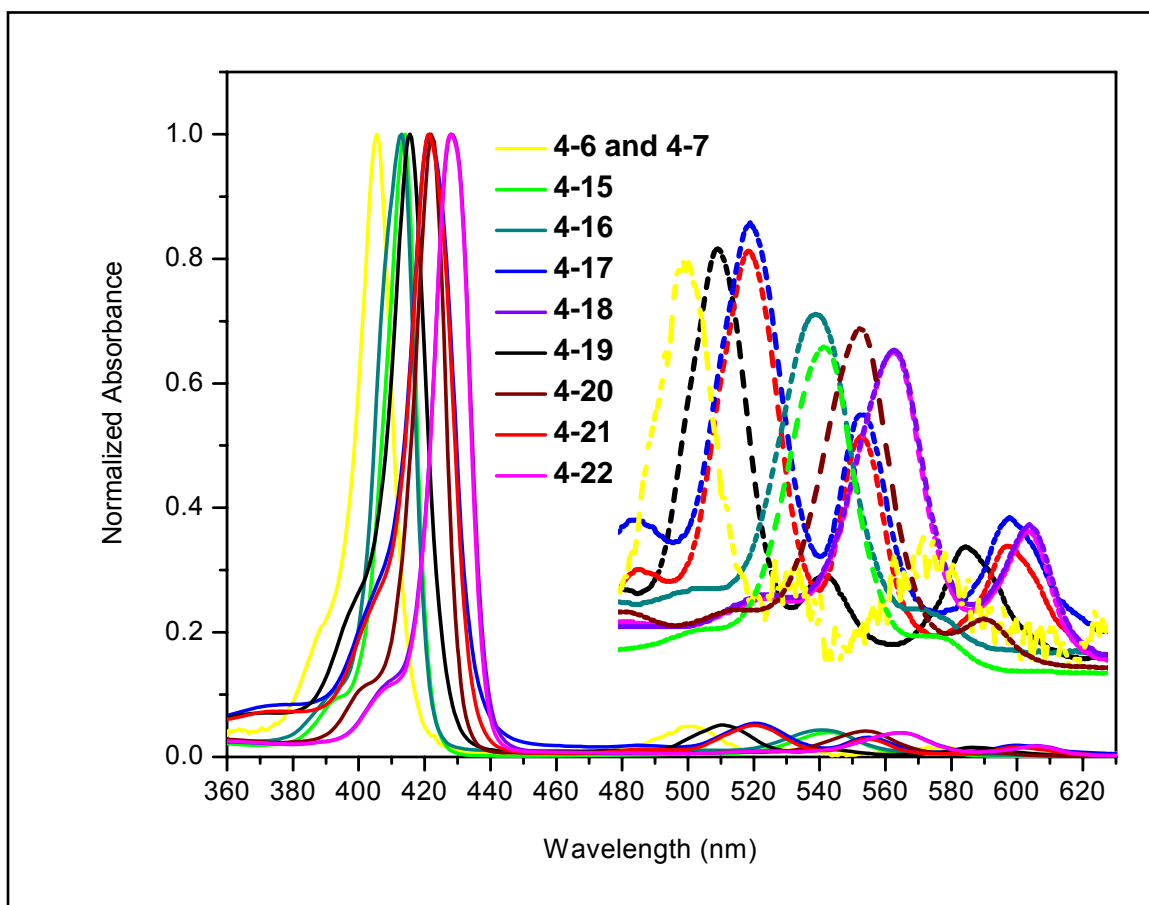


Fig. 4.21 UV-vis absorption spectrum of the Zn(II) metalloporphyrin dimers and polymers as well as their corresponding ligands in CHCl_3 . Dotted lines show Q-bands amplified for clarity

4.3.6 THERMAL ANALYSES OF THE ZN(II) METALLOPORPHYRIN DIMERS AND POLYMERS

The thermal stability of the Zn(II) metalloporphyrin complexes were studied. Their thermally induced phase transition behaviours were investigated with differential scanning calorimetry (DSC) and reflected by the glass transition temperatures (T_g) (Fig. 4.22). The onset of decomposition temperatures (T_d) (Fig. 4.23) were investigated with thermogravimetric analyses (TGA). The values are summarized in Table 4.3 below.

The Zn(II) metalloporphyrin complexes **4-20** and **4-22** do not exhibit distinct glass transition temperatures. The higher Br content could have reduced ring mobility due to the steric bulkiness of the two Br atoms,¹⁹ thus increasing the value of T_g . All the Zn(II) metalloporphyrin complexes T_d values of above 196 °C, signifying high thermal stability.

Table 4.3 Summary of the T_g (°C) and T_d (°C) [% weight loss] of the Zn(II) metalloporphyrin complexes

	T_g (°C)	T_d (°C) [% weight loss]
4-15	148.7	346 [17.1]
4-16	177.3	329 [18.1]
4-18	133.4	196 [10.0], 242 [9.9], 289 [18.1]
4-20	-	204 [10.6]
4-22	-	239 [11.9], 297 [20.6]

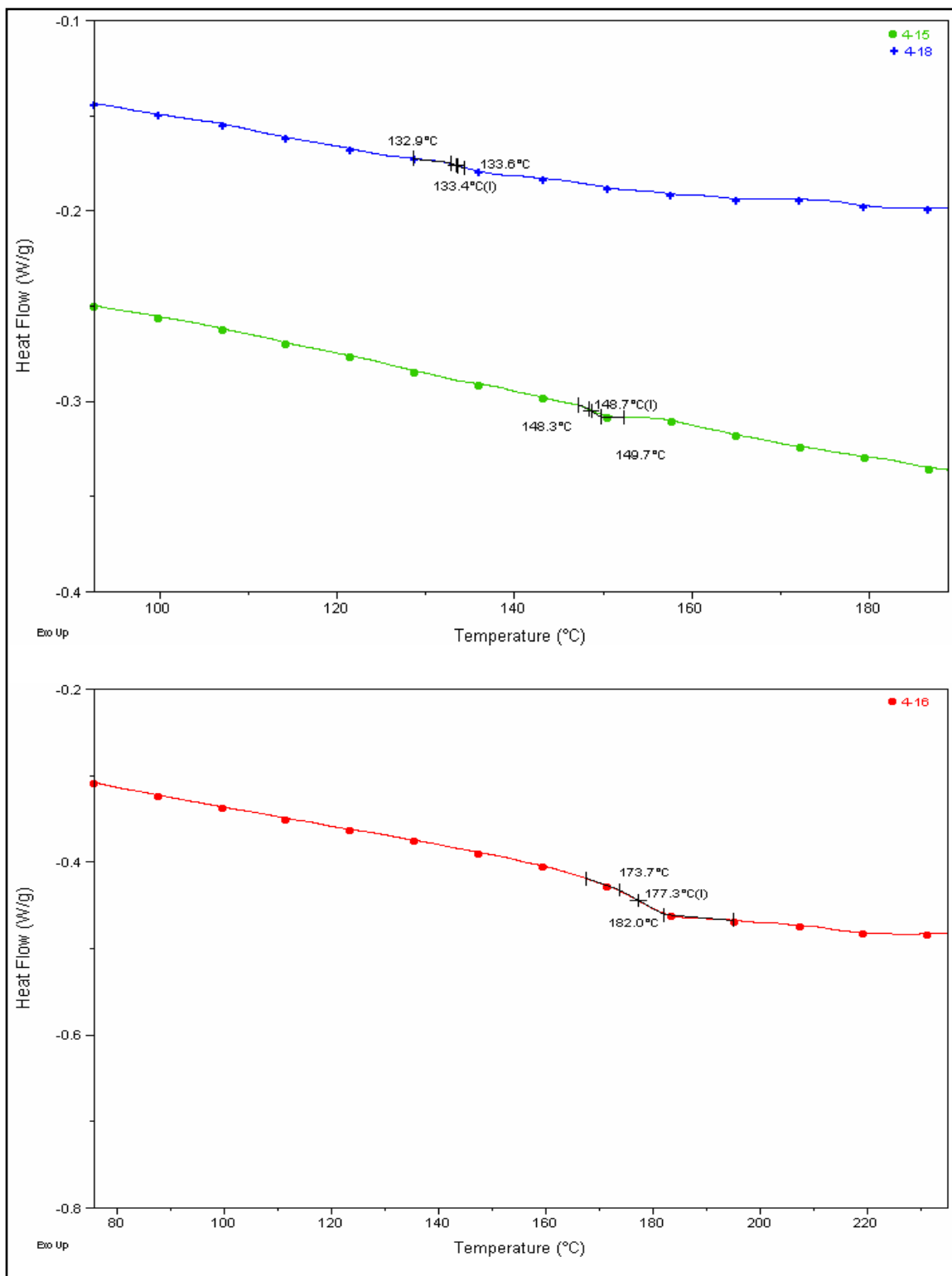


Fig. 4.22 DSC plot of Zn(II) metalloporphyrin complexes **4-15**, **4-16** and **4-18**

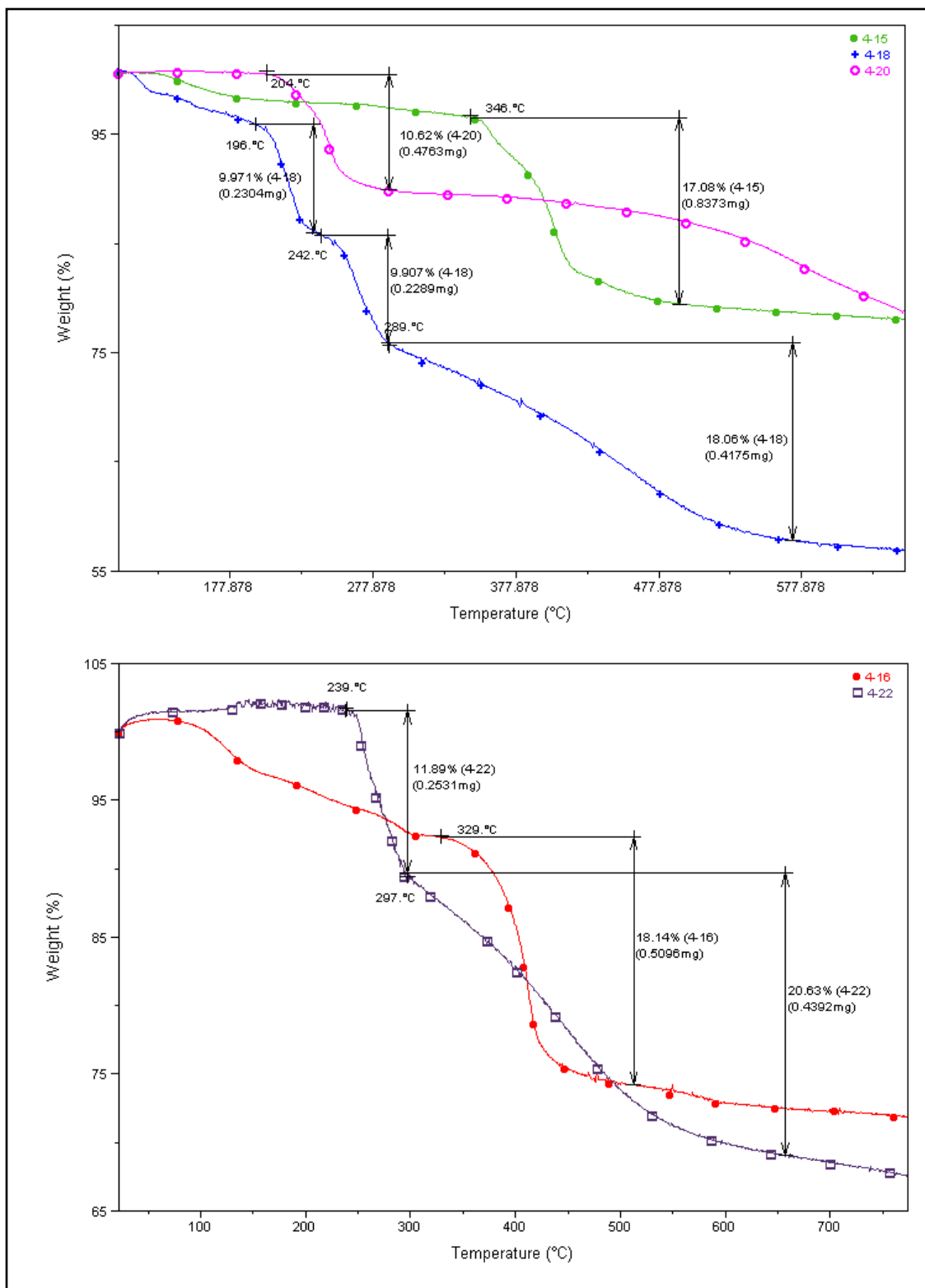


Fig. 4.23 TGA plot of Zn(II) metalloporphyrin complexes **4-15**, **4-16**, **4-18**, **4-20** and **4-22**

4.4 LIGHT HARVESTING PROPERTIES OF 4-15 AND 4-16

The strategic use of non-covalent self-assembly of molecular units has been developed as highly promising means for the construction of multi-dimensional architectures that have specific structures, properties and functions.²⁰ Initially inspired by the non-covalent nature of photosynthetic systems found in Nature, this approach has been increasingly attempted in the mimicry of light-harvesting and charge separation systems.²¹ This in turn led to the discovery of more application of such assemblies such as in molecular-scale electronics and optical applications.

Among the many molecular modules used as construction elements of chromophore assemblies in light harvesting antenna functions of photosynthesis, porphyrins are one of the most attractive building blocks. They offer a variety of desirable features such as high chemical and thermal stability, ease of structural modification through chemical reactions, flexible tunability of optical and redox properties through metallation with wide variety of metal ions and small HOMO-LUMO energy gap.

Interesting examples reported thus far include arrays formed by purely coordination bonds and combination of additional covalent bonds. For instance, the giant porphyrin arrays and wheels formed by hydrogen-bonding through the peripheral imidazolyl ligand reported by Kobuke *et al.*^{19,22} and the windmill arrays developed by Osuka *et al.*²³ serve as models of light-harvesting antennas. The oligomeric conjugated porphyrin ladders developed by Anderson *et al.*²⁴ exhibit very large two-photon absorption (TPA) cross-sections (σ_2).

The design of efficient light harvesting materials remains an important goal, considering the need for effectively using renewable energy sources.²⁵ Nature has already evolved an effective pathway for harvesting sunlight in to useful chemical energy that is stored in the form of ATP. Nature's light harvesting assembly, as exemplified in purple photosynthetic bacteria,¹⁸ consists of a multichromophore array that is capable of absorbing photons of a broad spectral range. These chromophores are well-ordered and arranged in slipped cofacial array. In contrast to these well-organized structures in bacteria antennae, antenna complexes from plants are disordered.

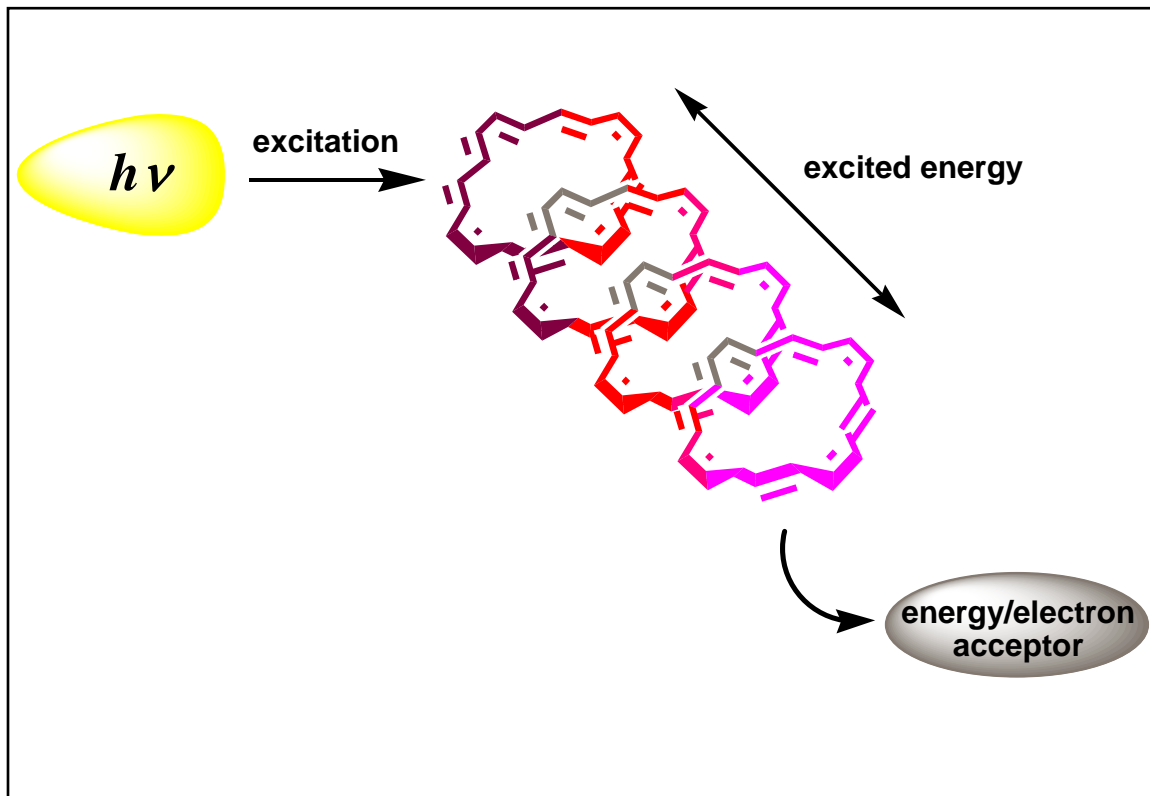


Fig. 4.24 Illustration of FRET from supramolecular porphyrin self-assembly (stores excitation energy) to energy/energy acceptor for example chloranil

The porphyrin-porphyrin interaction is sensitively reflected in their efficiency to transfer energy and electron to external acceptors which can be monitored by fluorescence quenching experiments. Hence, a fluorescence quenching²⁶ study of **4-15** and **4-16** with chloranil as energy/electron acceptor in CHCl_3 solution was carried out (refer to Fig. 4.24 for illustration). The typical emission spectrum of **4-15**, **4-16** and Zn(II) tetraphenylporphyrin is shown in Fig. 4.25. It was observed that fluorescence quenching increased with increase in the concentration of chloranil.

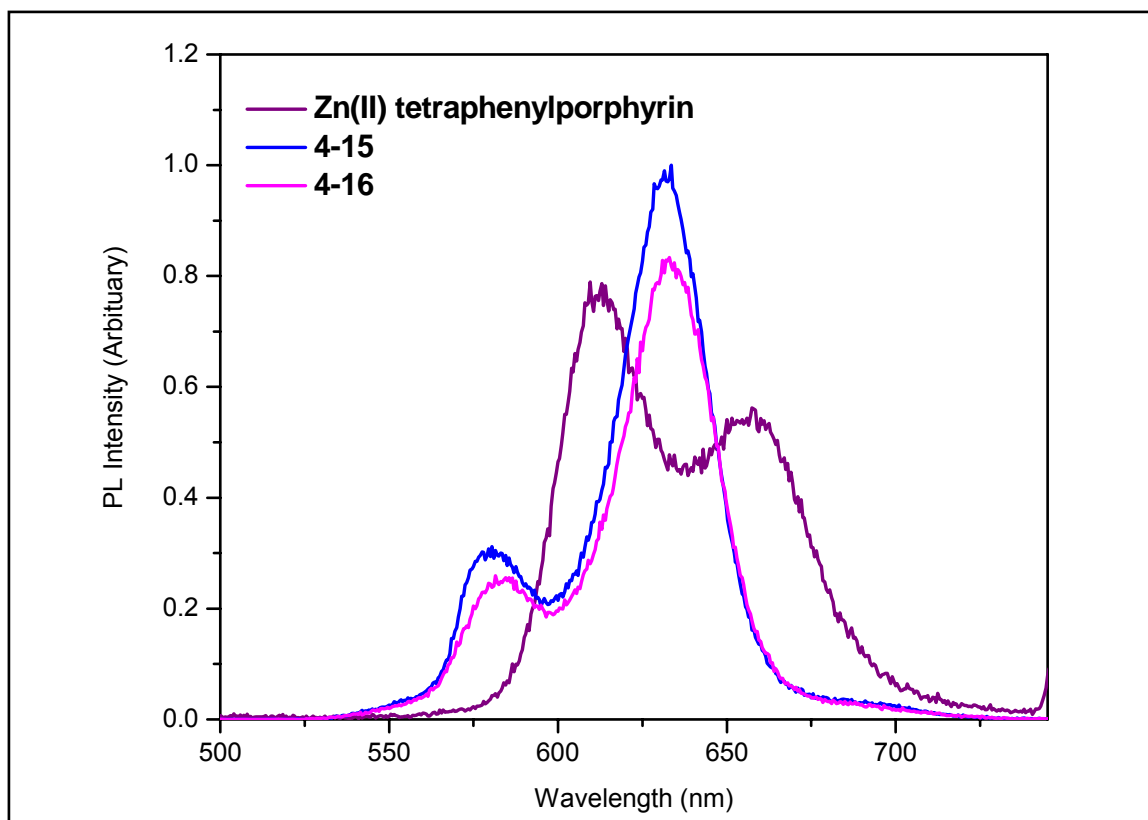


Fig. 4.25 Emission spectrum of **4-15**, **4-16** in CHCl_3 (5×10^{-6} M) and Zn(II) tetraphenylporphyrin in toluene at concentration of 1×10^{-5} M

The quenching of fluorescence can be described by the Stern-Volmer equation²⁶,

$$(4.1) \quad \frac{I_0}{I} = 1 + k_q \tau_0 [Q] = 1 + K_{SV} [Q]$$

where I_0 and I are the fluorescence intensities in the absence and presence of the quencher, respectively, k_q is the bimolecular quenching constant, τ_0 is the lifetime of the fluorophore in the absence of the quencher and $[Q]$ is the concentration of the quencher. The Stern-Volmer quenching constant, K_{SV} is represented by $k_q \tau_0$. The bimolecular quenching constant k_q reflects the efficiency of quenching or the accessibility of the fluorophores to the quencher.

The Stern-Volmer plot (Fig. 4.26) clearly shows that **4-15** and **4-16** have the same rates of fluorescence quenching (K_{SV}) from the slope of the graph. Their rates are 2.2 times faster than that of Zn(II) tetraphenylporphyrin. This implies that the energy-electron process occurs more efficiently in the coordination complexes as compared to monomeric species. This difference in rate (considering the use of only approximately 10 equivalents of the acceptor) is significant. In the reported works of Kobuke *et al.*, a similar study was carried out on a 5,15-bis(imidazol-4-yl)-10,20-bis(4-dodecyloxyphenyl)porphyrin supramolecular assembly and a higher energy-electron transfer rate of 2.9 was observed as compared to the reported monomer. However, this was achieved by using a large excess (10^{10} equivalents) of chloranil.¹⁶

The small K_{SV} value suggests that energy-electron transfer takes place mainly by diffusion and collision of the excited state molecules to the quencher via the mechanism called dynamic quenching.²⁷ A possible explanation for the more efficient energy transfer and/or electron transfer observed in **4-15** and **4-16** may be due to the high migration of

photoinduced excitons (along the conjugated backbone) from one monomer to the other in the supramolecular assembly to the acceptors. Hence, the coordination complexes **4-15** and **4-16** exhibit potential as light harvesting compounds.

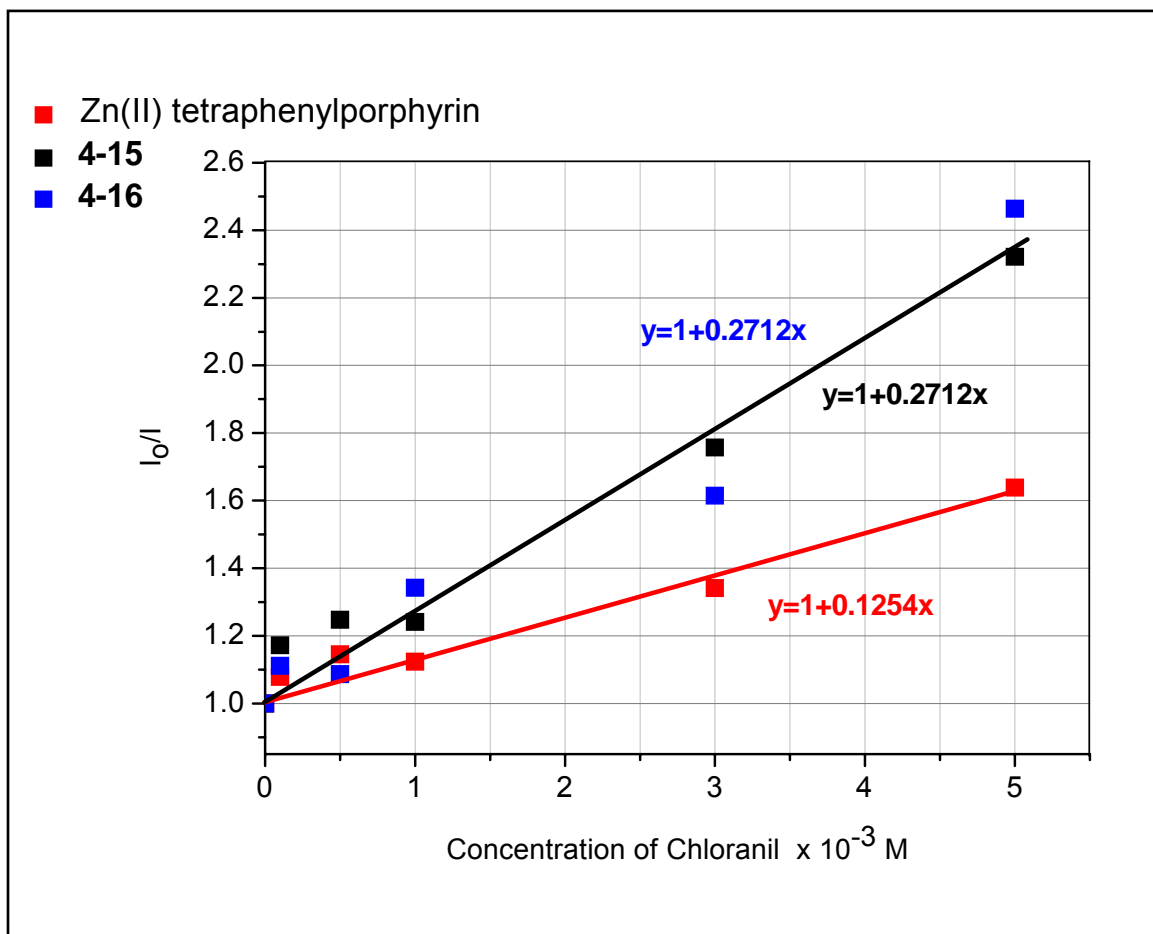


Fig. 4.26 Stern-Volmer plot for **4-15**, **4-16** (note that both lines overlapped) and Zn(II) tetraphenylporphyrin (5×10^{-6} M) with chloranil in CHCl_3

Additionally, this study provides important information to prove that in CHCl_3 solution, the Zn-O coordination bonds continue to hold each unit closely in the coordination complexes (at concentration of 5×10^{-6} M, which is an order of magnitude lower than that used for NLO measurements in Chapter 5). This explains the faster rate

of energy-electron transfer when the individual chromophores are closer in the coordination complexes than in the monomers in solution.

4.5.0 X-RAY CRYSTALLOGRAPHIC STUDIES OF A CLASS OF Zn(II) METALLOPORPHYRIN DIMERS AND POLYMERS FORMED BY Zn-O COORDINATION BONDS AND THEIR CORRESPONDING LIGANDSⁱ

4.5.1.1 SINGLE CRYSTAL X-RAY CRYSTALLOGRAPHIC STUDY OF 4-15 GROWN IN CHCl₃/CYCLOHEXANE SOLVENT MIXTURE

Single crystals of **4-15** were grown by slow evaporation of a solution of **4-15** in a cyclohexane/CHCl₃ solvent mixture. The asymmetric unit consists of half the molecule. There are four different porphyrin alignments. The complex **4-15** is a 3D coordination polymer and the ORTEP drawing of its fundamental building unit is shown in Fig. 4.27. Each Zn(II) metal atom forms a square plane (angles are perfect at 180.0 °) and sits on the perfect plane with the four pyrrolic N atoms. The former coordinates to two neighboring O atoms of the methoxymethyl functions and hence gives a hexa-coordinated Zn(II) atom. The apical O atom coordinates to the metal atom with angle of 87.6 - 92.4 ° to the plane of the four N atoms. Thus, the Zn(II) atom possess a distorted octahedral geometry. The axial methoxy groups of phenyl rings are in *trans* orientation with a Zn-O bond distance of 2.434 Å and the average equatorial Zn-N distance is 2.049 Å. Both these values are very similar to those reported for related porphyrin systems thus indicating that there are little geometric strain/changes in the porphyrin units of the polymeric framework of **4-15**. A segment of the coordination polymer is shown in Fig. 4.28.

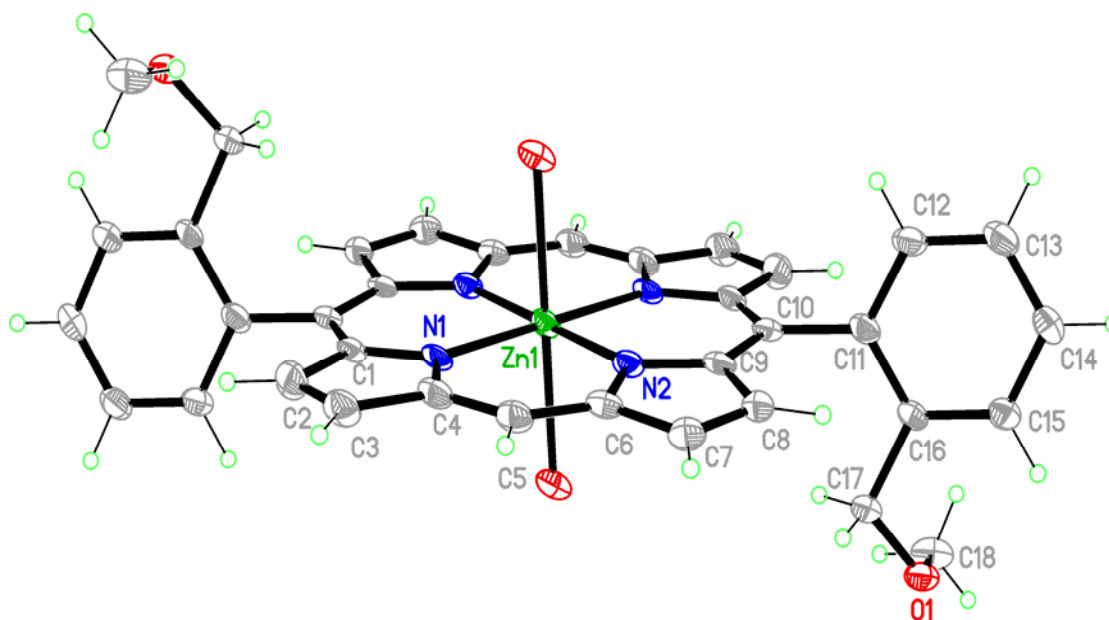


Fig. 4.27 An ORTEP view of the asymmetric unit of complex **4-15**

For Zn(II) metalloporphyrins, five-coordinate are common examples^{1b,13,18c, 28} while the Zn(II) polymer **4-15** with six-coordinate Zn(II) atoms, is the first Zn(II) porphyrin 3D framework successfully assembled through two axial Zn-O coordination.⁷ Examples reported earlier involved phenoxy functions with a Zn-O distance too short for building up a 3D framework. However, the oxygen function at the methoxymethyl group in the *ortho* position gave the [Zn(II)-O]-[Zn(II)-O]' coordination from two adjacent units, adopting an ideal "square planar" arrangement with appropriate Zn-O distances. This is clearly confirmed in the crystallographic 3D framework of **4-15** (Fig. 4.29) along the *c*-axis. Compared to **4-6**, the phenyl rings in **4-15** has a slightly larger dihedral angle of 76.7 ° with respect to the plane of the four N atoms. The pair of phenyl rings on the porphyrin ring are parallel but have a deviation of 0.086 Å (in opposite directions) with respect to the N atoms on the perfect plane of the porphyrin.

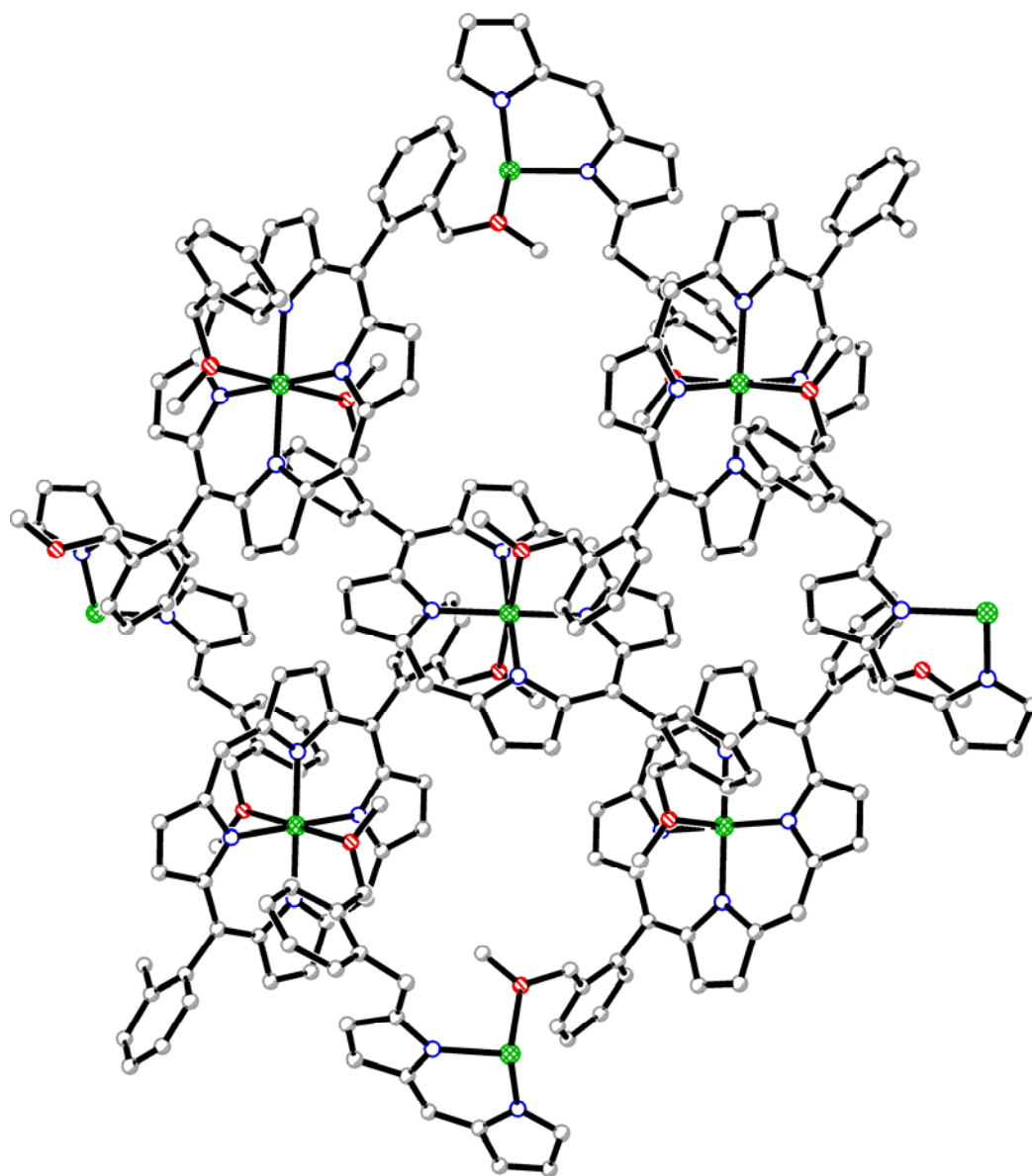


Fig. 4.28 A segment of the coordination polymer **4-15**

Along the *c*-axis, the packing creates the flower-like cavities as shown in Fig. 4.29. The shortest and longest non-hydrogen atomic distances across the channel are about 4.81 Å and 9.27 Å respectively. These cavities and channels should be involved in

the solvent diffusion phenomenon observed in the time-dependent NMR study described earlier. Interestingly, the porphyrins along each column have the same tilt angle such that they overlap perfectly. The porphyrins in one column (for example 'A' marked in red on Fig. 4.29) have four identical and adjacent neighbours (for example 'B' marked in blue on Fig. 4.27). The chromophores in the corresponding columns 'bow' in different directions as they possess different tilt angles. This generates a regular alternating ABAB pattern and gives rise to the cavities observed.

Along the *a*-axis of the polymeric structure of **4-15** (Fig. 4.30), two different alignments of the units are visible. One array is flat and another array is slanted and thus results in the formation of a 3D-coordination network polymer. There is no appreciable aromatic interaction in the chains based on the estimated inter-ring distances.

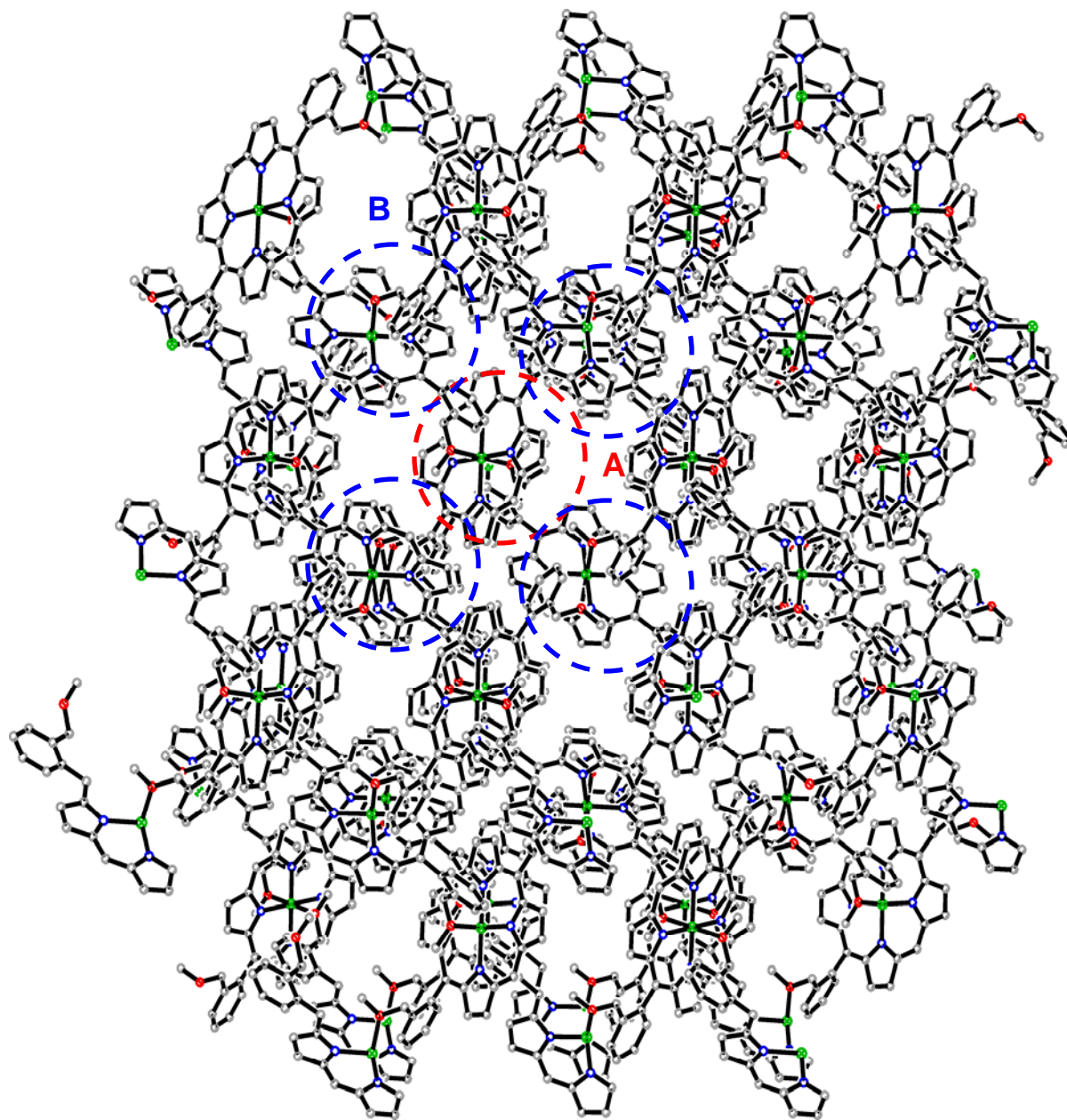


Fig. 4.29 View of **4-15** along *c*-axis. Columns A and B are marked in red and blue respectively (refer to text)

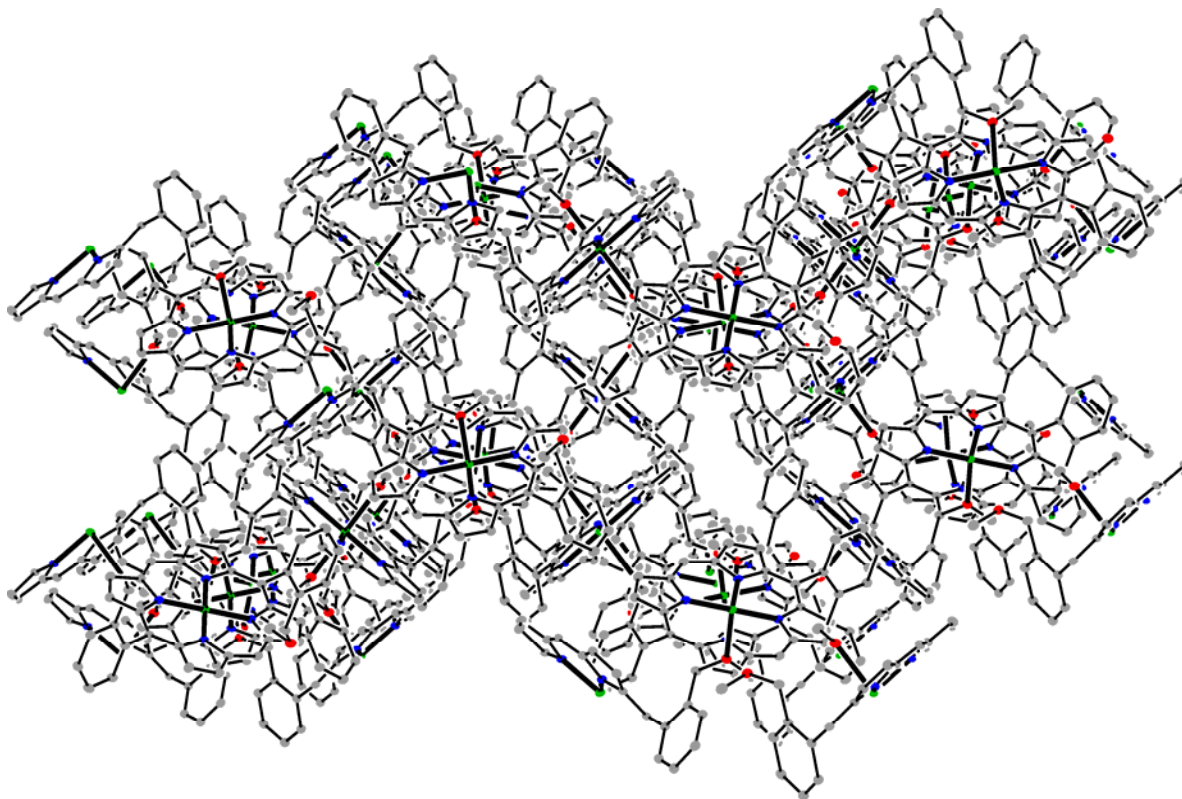


Fig. 4.30 View of **4-15** along *a*-axis

4.5.1.2 SINGLE CRYSTAL X-RAY CRYSTALLOGRAPHIC STUDY OF **4-15** GROWN IN CHCl_3 /ETHYL ACETATE SOLVENT MIXTURE AND $\text{C}_6\text{H}_5\text{NO}_2$

Single crystals of **4-15** were grown by slow evaporation of a solution of **4-15** in CHCl_3 /ethyl acetate solvent mixture and $\text{C}_6\text{H}_5\text{NO}_2$ separately. The single crystal X-Ray Crystallographic studies show that the Zn(II) metalloporphyrins exist as monomers instead of 3D coordination polymers (Fig. 4.31). This could be attributed to the coordination of the solvent to the Zn metal, resulting in the cleavage of the original Zn-O coordination bond between the Zn(II) metalloporphyrins. Hence, this result provided us

with important information on the choice of solvent when we carry out the NLO measurements in solution (Refer to Chapter 5).

Analysis of the single crystals grown in CHCl_3 /ethyl acetate and $\text{C}_6\text{H}_5\text{NO}_2$ are similar and the asymmetric unit of both consists of half of the tilted molecule. The four pyrrolic C atoms and four N atoms of the porphyrin macrocycle lie on a perfect plane and the Zn(II) metal atom sits on the perfect plane of the porphyrin core. The Zn(II) metal atom also forms a square plane (angles are perfect 180.00°) with the four pyrrole N atoms on a perfect plane. The average equatorial Zn–N distance of 2.029 Å is similar to that of **4-15** grown in CHCl_3 /cyclohexane. The phenyl rings have a slightly larger dihedral angle of 81.8° with respect to the plane of the four N atoms and are parallel to each other. The phenyl rings have a deviation of 0.046 Å (in opposite directions) with respect to the four N atoms on the perfect plane of the porphyrin. The monomeric units possess a larger dihedral angle between the phenyl and porphyrin rings as compared to that in the polymeric system (Refer to Table 4.4).

Table 4.4 Summary of the dihedral angles of the phenyl rings with respect to the plane of the four N atoms for single crystals of **4-15** grown in various solvents

Dihedral angle ($^\circ$) for single crystals grown in		
CHCl_3 /Cyclohexane	$\text{C}_6\text{H}_5\text{NO}_2$	CHCl_3 /Ethyl acetate
76.7	81.7	81.8

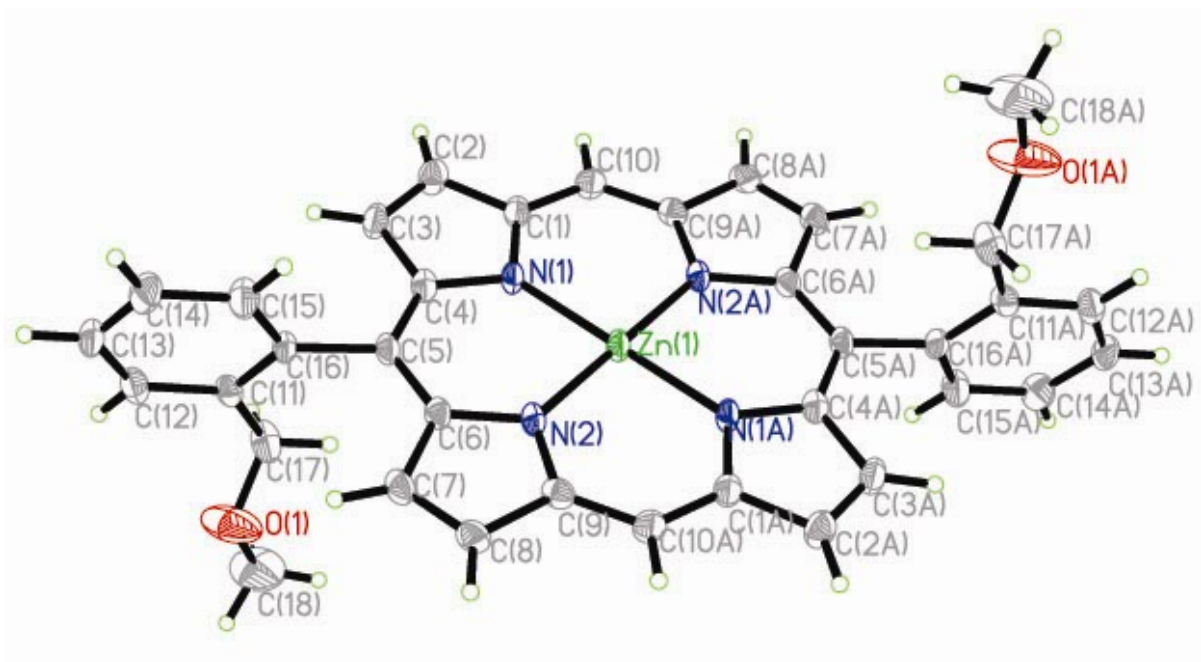


Fig. 4.31 Monomeric unit of **4-15** when grown in ethyl acetate (thermal ellipsoids are drawn at 50 % probability level)

In contrast to its ligand **4-6**, one of the phenyl rings of two adjacent units lie in a tilted cofacial angle above and below each porphyrin ring in the solid state packing with an approximate distance of 2.624 Å from the H (C12A) to the plane of the Zn(II) and four N atoms shown by the two monomers in Fig. 4.32. These indicate the presence of weak interaction due to the overlap of aryl C-H σ bonding orbital with the aromatic π ring of the porphyrin. This is similarly observed in the work of Suslick *et al.*¹⁵ The porphyrins are basically arranged in two dimensions with insignificant π - π interaction between the two macrocycles due to the relatively large tilt angle.

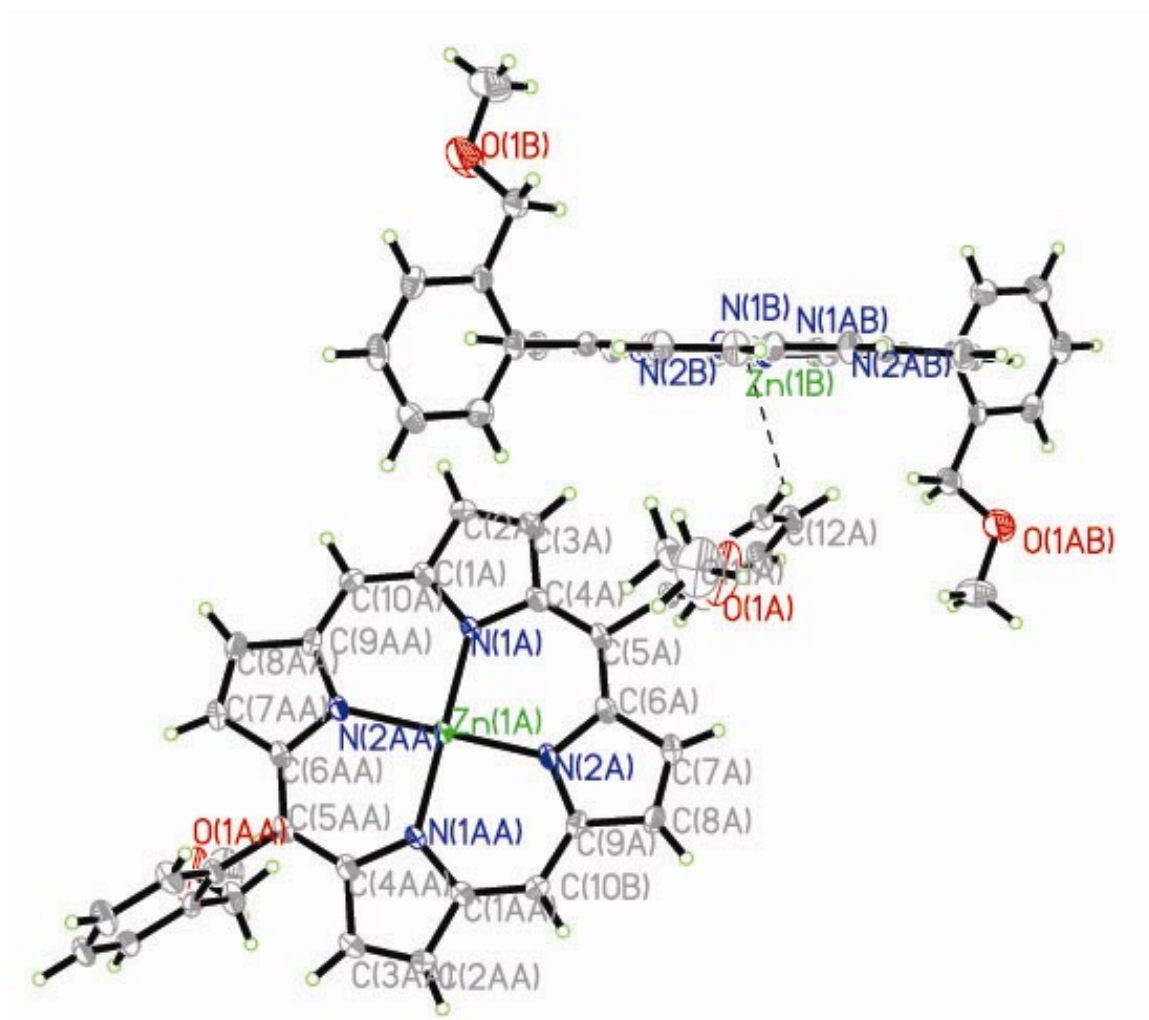


Fig. 4.32 A view showing weak interaction due to the overlap of aryl C-H σ bonding orbital with the aromatic π ring of the porphyrin

4.5.2.1 SINGLE CRYSTAL X-RAY CRYSTALLOGRAPHIC STUDY OF 4-16 GROWN IN CHCl_3

Single crystals of **4-16** were grown by slow evaporation of a solution of **4-16** in CHCl_3 (Fig. 4.33). The asymmetric unit consists of half the molecule also. There are two different porphyrin alignments. The complex is a coordination dimer with two

coordination points per monomer and the ORTEP drawing of the dimer is shown in Fig. 4.33. The four N atoms and the four outer pyrrolic C atoms in the porphyrin forms a distorted plane with deviation of 0.009 Å and 0.037 Å respectively. The Zn(II) metal atom sits above the distorted plane of a four pyrrolic N atoms with a deviation of 0.180 Å (towards the coordinated O atom). The N-Zn-N angles are 170.36 ° and 169.42 ° and deviate significantly from the perfect 180.00 ° found in previous complexes. Thus, this indicates that there are geometric strain/changes in the porphyrin units of the dimeric framework.

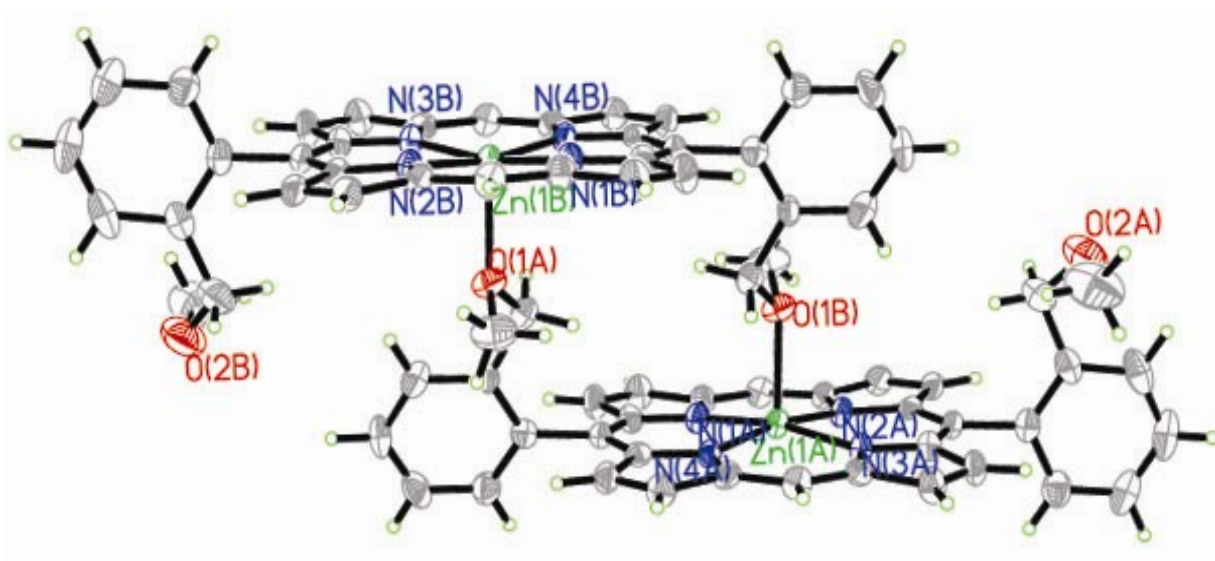


Fig. 4.33 Molecular structure **4-16**; thermal ellipsoids are drawn at 50 % probability level

The Zn(II) metal atom coordinates to one of the neighbouring O atoms of the methoxymethyl functions and hence gives a penta-coordinated Zn(II) atom. It bends towards the opposite porphyrin in the dimer. The apical O atom coordinates to the metal atom with angle of 93.17 - 96.47 ° to the four N atoms. Thus Zn(II) atom possess a

distorted square pyramidal geometry. The axial methoxy groups of phenyl rings are in *cis* orientation with a Zn-O bond distance of 2.209 Å and the average equatorial Zn-N distance is 2.046 Å. It is noteworthy that the methoxy substituents point in the same direction but away from the porphyrin core (Fig. 4.34).

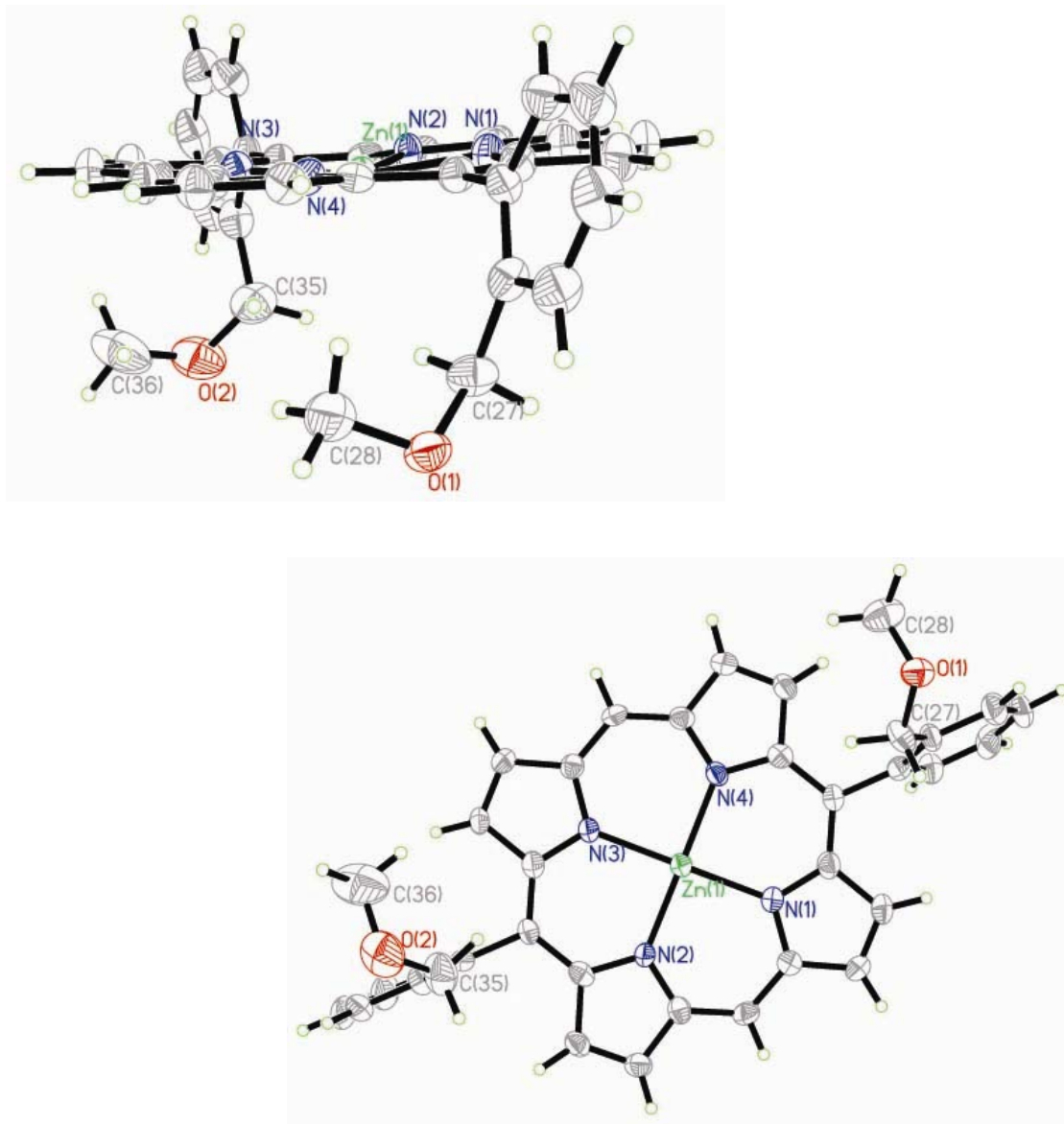


Fig. 4.34 A monomeric unit of **4-16** showing the direction of the methoxy substituents in solid state

The dimers 'connect' via non-bonding interaction of 3.19 Å between the Zn(II) metal atom and a β pyrrolic proton. There is probably weak interaction due to the overlap of aryl C-H σ bonding orbital with the aromatic π ring of the porphyrin (Fig. 4.35).¹⁵

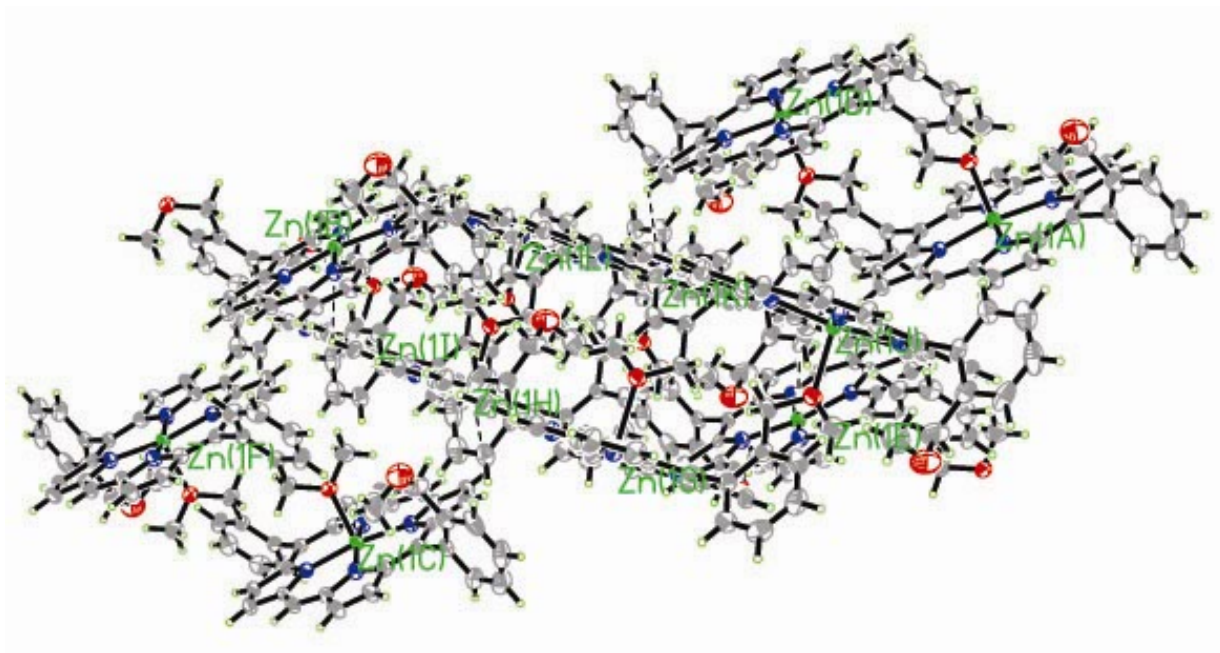


Fig. 4.35 ORTEP view showing the two different porphyrin alignments and non-bonded Zn-H interactions (dotted lines)

The two phenyl rings on a monomeric unit possess different dihedral angles and are tilted in opposite directions (Fig. 4.36). Their relative dihedral angle is 15.8°. Due to the distortion of the plane of the porphyrin, it is difficult to determine accurately the dihedral angle and deviation of aryl C-*meso* C bond (in terms of distance and angle). From the ORTEP diagram above, it can be estimated that the inner phenyl ring (with O donor atom) has a smaller dihedral angle of 73.2° than that of the outer phenyl ring

which is 88.9° . Also, the inner phenyl ring has aryl C-*meso* C bond bent towards the opposite porphyrin in the dimer due to the presence of some strain during coordination by 0.158 \AA while the outer phenyl ring bent away by a comparatively smaller distance of 0.036 \AA (with respect to the plane of the four pyrrolic N atoms).

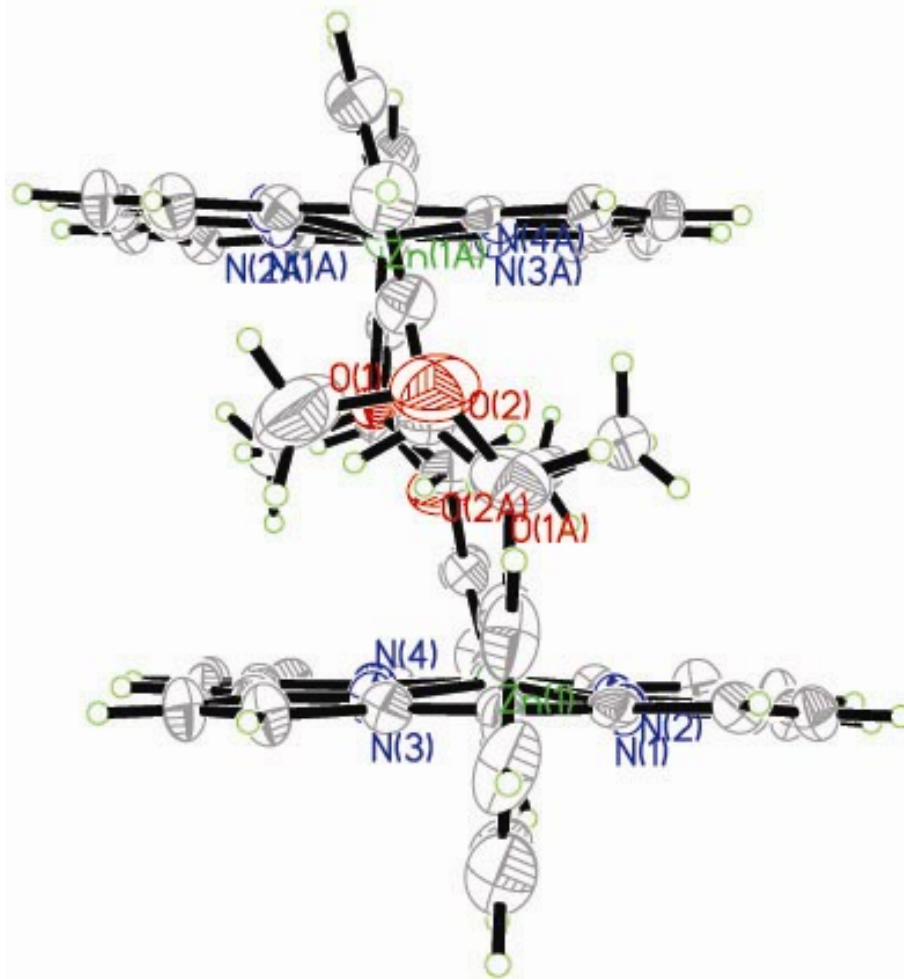


Fig. 4.36 A side view of **4-16** showing the differences in dihedral angle of the two phenyl rings

This Zn-O bond (2.209 \AA) is significantly shorter than the hexa-coordinated Zn(II) complexes of **4-15** (2.434 \AA), **4-18** (2.428 \AA) and **4-20** (2.417 \AA), which probably

explains the porphyrin ring distortion and difference in the deviation of aryl *C-meso* C bond in **4-16**. The two macrocycles in the dimer are arranged in a slipped cofacial pattern and are almost parallel with respect to each other. The distance between the two adjacent porphyrin planes is 5.595 Å (from Zn atom of adjacent unit to the plane of the four N atoms).

4.5.2.2 SINGLE CRYSTAL X-RAY CRYSTALLOGRAPHIC STUDY OF 4-16 GROWN IN THF

When **4-16** was grown in THF solvent, analysis of the asymmetric unit of the single crystal shows that it contains one tilted Zn(II) metalloporphyrin molecule and one molecule of solvent THF. The dimer separated into monomeric units as the O atom of the solvent molecule coordinated to the Zn(II) metal atom (Fig. 4.37). In contrast, the coordination polymer **4-15** did not possess any axial ligands after ethyl acetate and nitrobenzene evaporated off (Refer to Section 4.5.1.2). This could be attributed to the formation of stronger coordination bond between the more electron rich O atom of THF as compared to ethyl acetate and nitrobenzene. Hence, it is important to avoid the use of solvents with donor atoms that can form coordination bonds with Zn metal atom for subsequent NLO measurements.

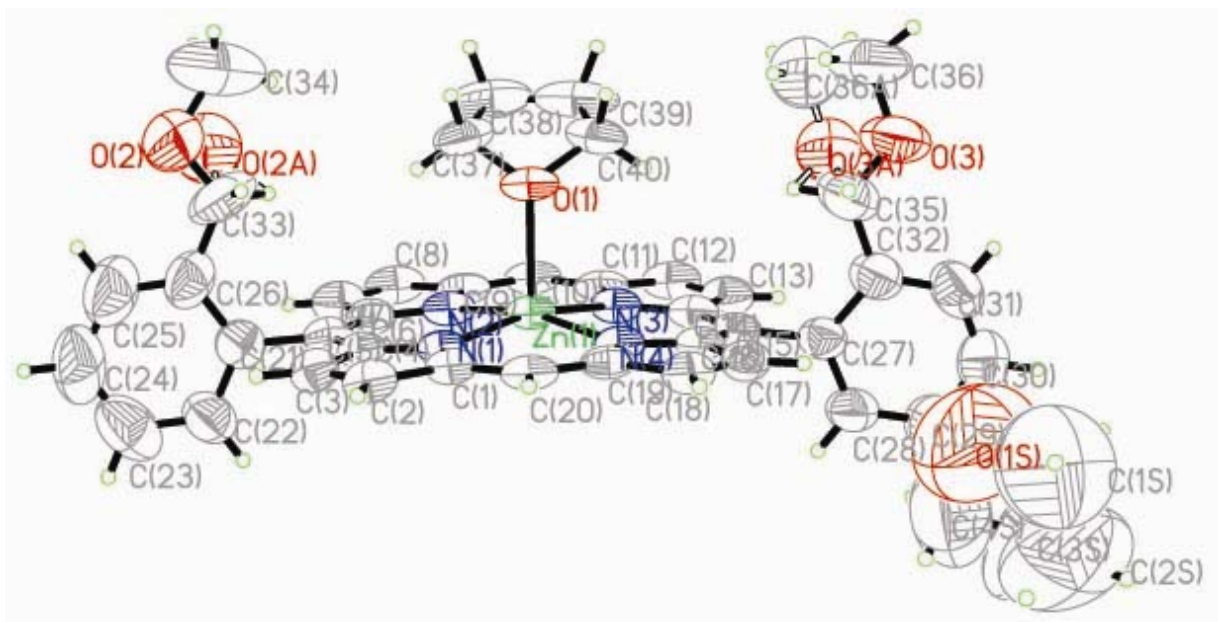


Fig. 4.37 ORTEP view showing one tilted Zn(II) metalloporphyrin molecule with one coordinated THF molecule and one molecule of solvent THF; thermal ellipsoids are drawn at 50 % probability level

From the ORTEP diagram (Fig. 4.37), we see that the two methoxy side chains of the metalloporphyrin are slightly disordered (O3 -C36 and O2) with occupancy factor of 0.60 for the major part. The four N atoms and the four outer pyrrolic C atoms in the porphyrin forms a less distorted plane with deviation of 0.003 Å and 0.016 Å respectively. The Zn(II) metal atom sits above the distorted plane of a four pyrrolic N atoms with a larger deviation of 0.238 Å and a similar Zn-O bond length of 2.212 Å. The N-Zn-N angles are 166.48 ° and 166.92 ° and deviate significantly from the perfect 180.00° found in previous complexes. The average equatorial Zn-N distance is 2.053 Å. Thus, the Zn(II) atom possess a distorted square pyramidal geometry. Thus, this indicates that there is geometric strain/changes in the porphyrin.

4.5.3 SINGLE CRYSTAL X-RAY CRYSTALLOGRAPHIC STUDY OF 4-18

Single crystals of **4-18** were grown by slow evaporation of its solution in CH_2Cl_2 as shown in Fig. 4.38. There are two different porphyrin alignments (Fig. 4.39). The complex is a one dimensional coordination polymer and the ORTEP drawing of its fundamental building unit is shown Fig. 4.38. In the one-dimensional linearly stacked coordination polymer, each Zn(II) metalloporphyrins are coordinated to two adjacent units via two-points Zn-O coordination bonds, thus forming an infinite 'wire' of Zn(II) metalloporphyrins. The units stack on each other in a slipped cofacial manner and each row resembles a step-like infinite structure. In addition, all the 'wires' stack one after the other in a zig-zag fashion (Fig. 4.40).

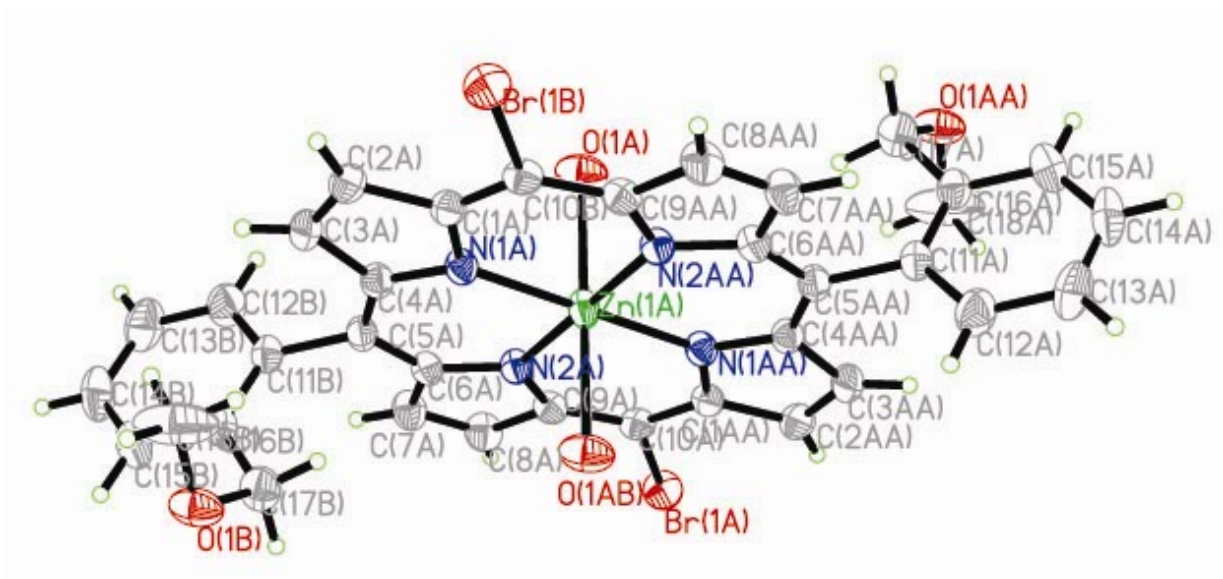


Fig. 4.38 Molecular structure of **4-18**; thermal ellipsoids are drawn at 50 % probability level

Each Zn(II) metal atom forms angle of 180.00° with two diagonal N atoms and sits on the perfect plane of the four pyrrolic N atoms. The Zn(II) metal atom coordinates to two neighboring O atoms of the methoxymethyl functions at 180.00° (Fig. 4.38) and hence gives an overall distorted hexa-coordination geometry. The apical O atom coordinates to the metal atom with angle of $88.11 - 92.36^\circ$ to the plane of the four N atoms which is identical to that in **4-15**. The axial methoxy groups of phenyl rings are in *trans*-orientation with a Zn-O bond distance of 2.428 \AA and the average equatorial Zn-N distance is 2.051 \AA . Both these values are very similar to those reported for related porphyrin systems, thus indicating that there is little geometric strain/changes in the porphyrin units of the polymeric framework of **4-18**.

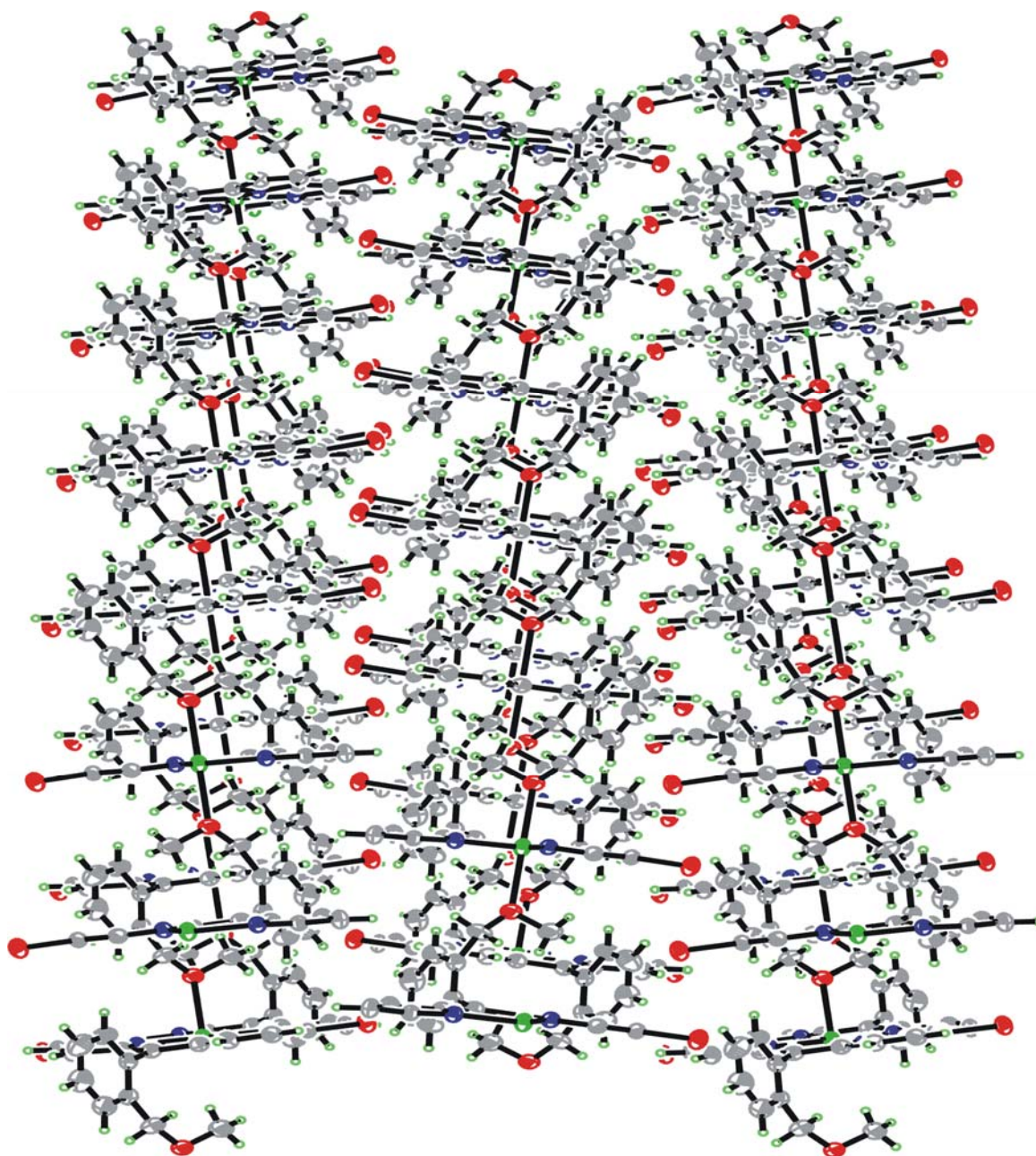


Fig. 4.39 The ORTEP view of **4-18** showing two alignments of the Zn(II) metalloporphyrin units

The phenyl rings have a dihedral angle of 81.8° and deviation of 0.238 \AA (in opposite directions) with respect to the perfect plane of the four N atoms. The distance

between the two adjacent porphyrin planes is 5.972 Å (from the Zn atom of an adjacent unit to the plane of the four N atoms).

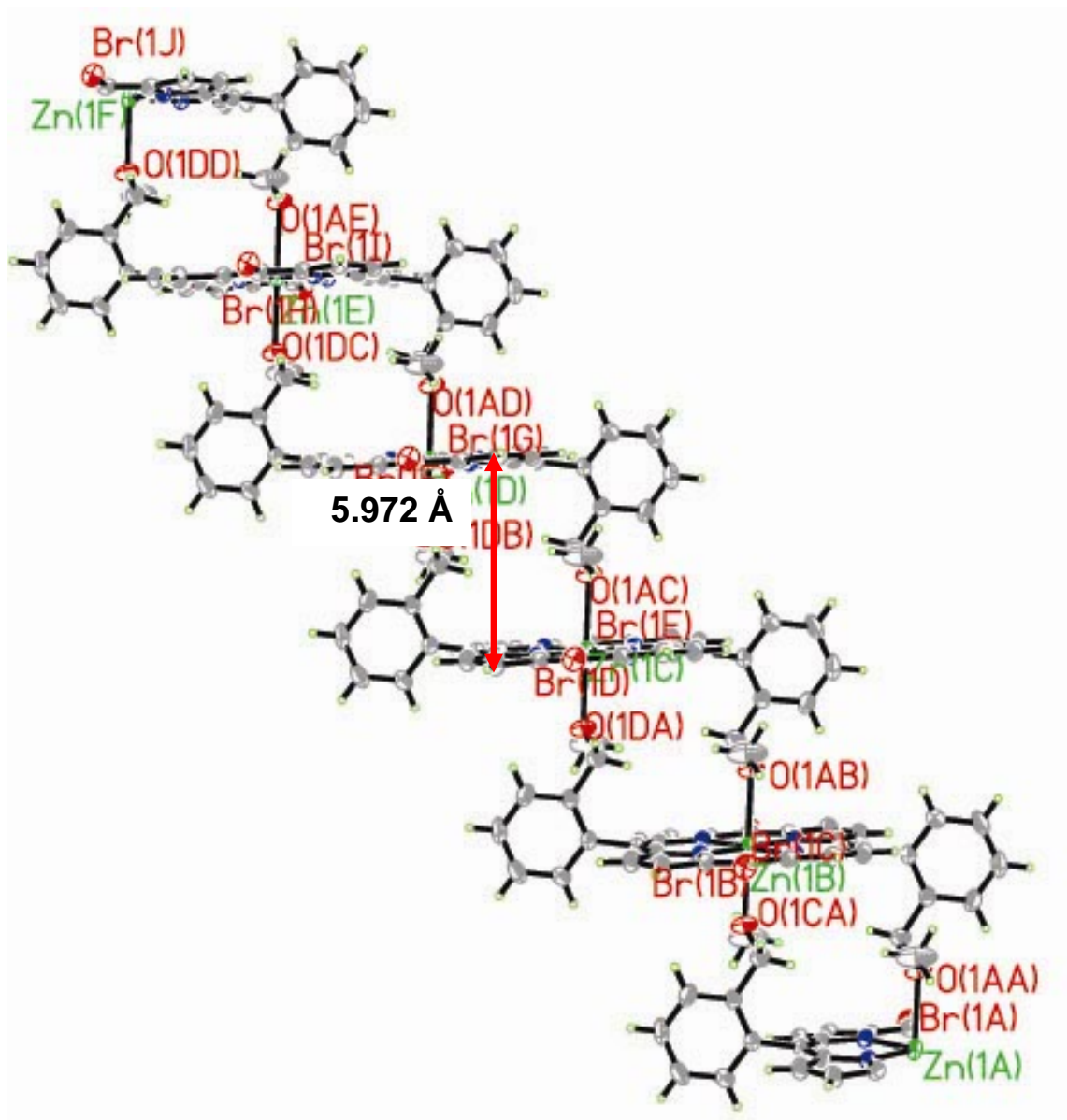


Fig. 4.40 The zig-zag, step-like infinite structure of **4-18**

Each linear slipped-stacked chain of the polymer possesses a herringbone structure. The one-dimensional structure has changed to a multi-dimensional structure

with the presence of non-bonding interaction between the Br atoms on the *meso* C with a phenyl H on the adjacent polymer chain. These non-bonding interaction range from 3.116 - 3.421 Å. In addition, there is non-bonding Br-Br interaction of 3.981 Å. As seen in Fig. 4.41 and 4.42, four columns 'bind' to one another indirectly through the non-bonding H-Br and Br-Br interactions due to close proximity.

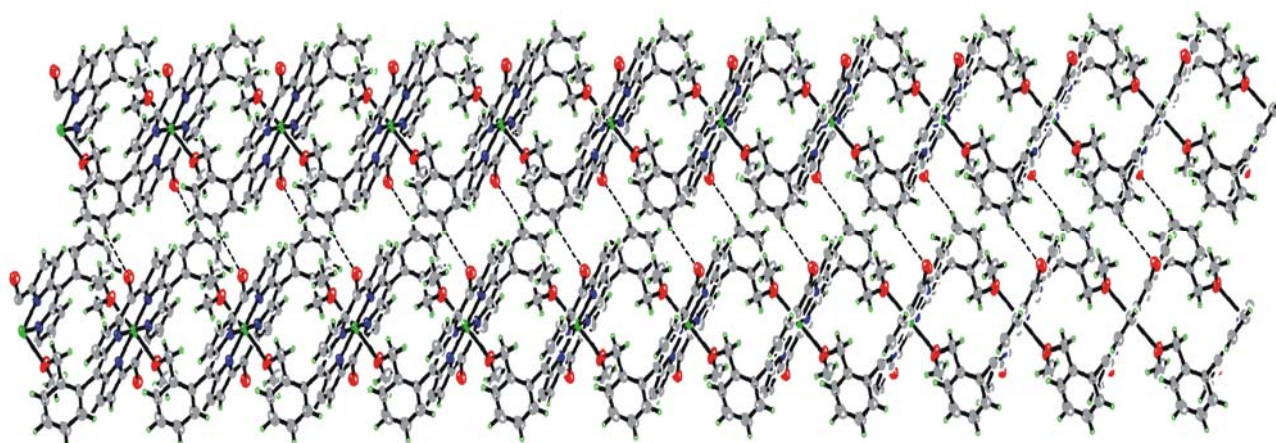


Fig. 4.41 A view of the non-bonding H-Br interactions between columns along the *b*-axis

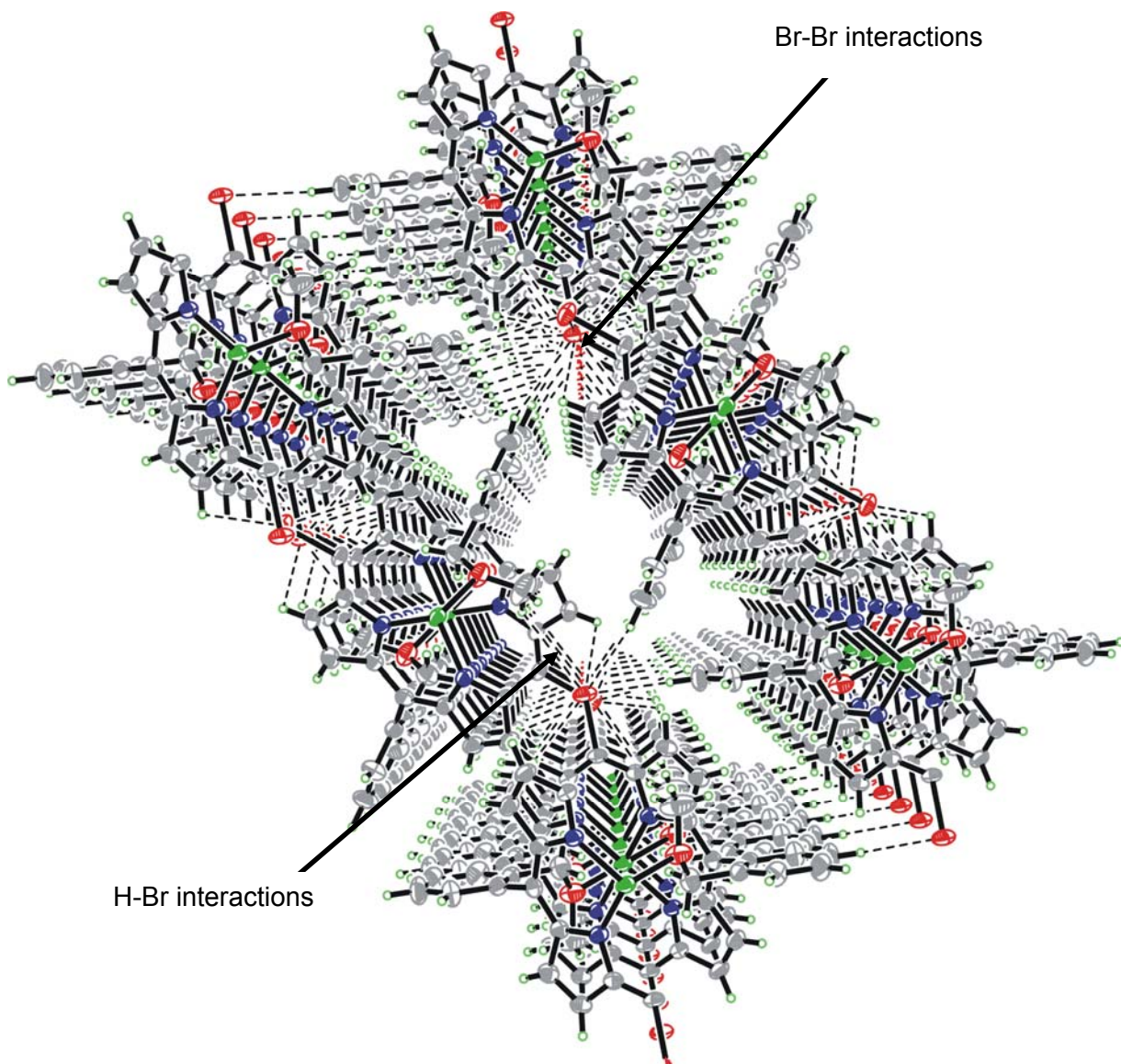


Fig. 4.42 A view of the non-bonding H-Br and Br-Br interactions between columns along the *c*-axis

4.5.4 SINGLE CRYSTAL X-RAY CRYSTALLOGRAPHIC STUDY OF 4-20

Single crystals of **4-20** were grown by slow evaporation of its solution in THF. There are two different porphyrin alignments identical to that in **4-18**. The complex **4-20**

resembles **4-18** and is a one dimensional coordination polymer with the ORTEP drawing shown Fig. 4.43.

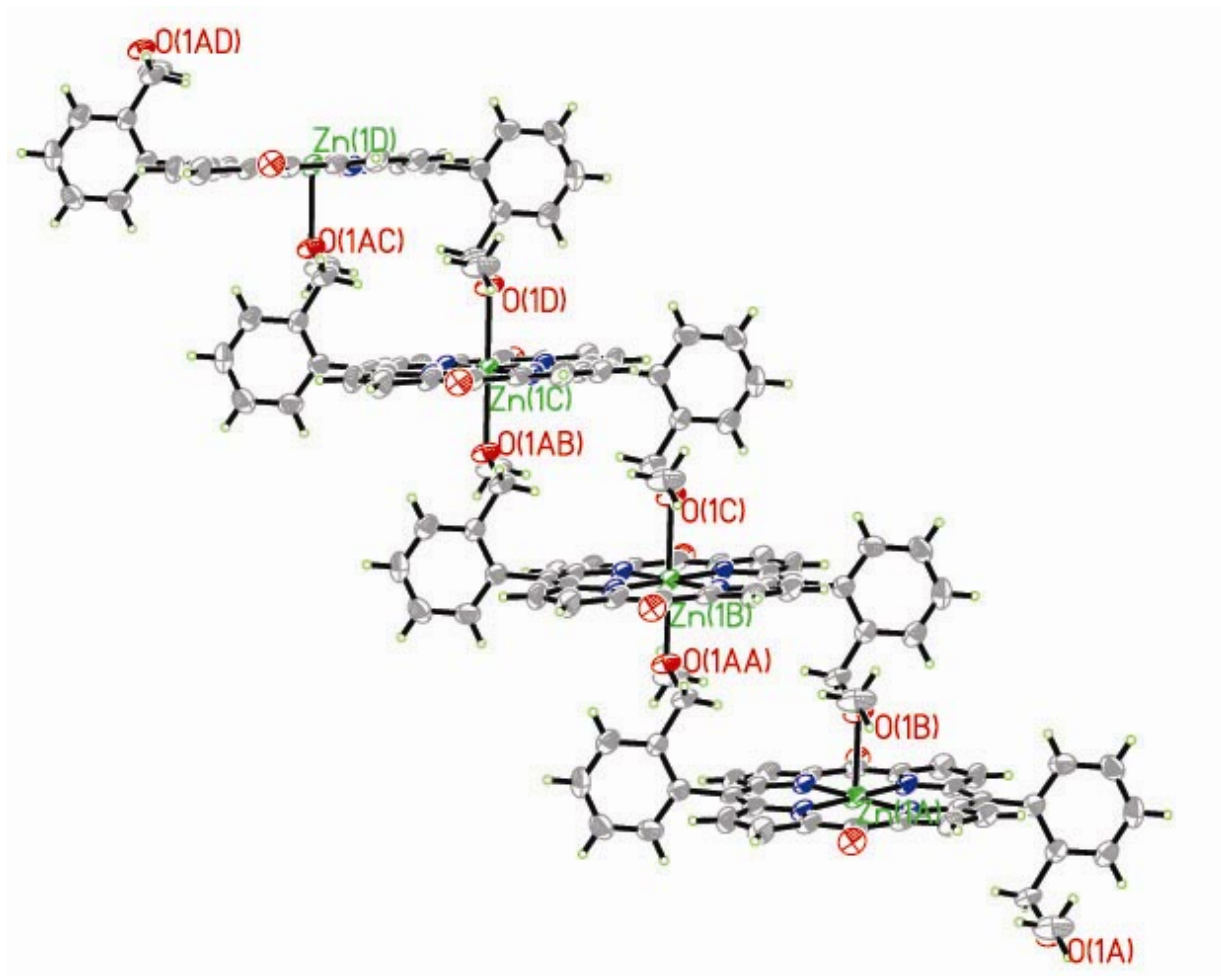


Fig. 4.43 ORTEP view of **4-20**; thermal ellipsoids are drawn at 50 % probability level

Each Zn(II) metal atom forms angle of 180.0° with two diagonal N atoms. The Zn(II) metal atom coordinates to two neighboring O atoms of the methoxymethyl functions at 180.00° . The Zn(II) metal atom coordinates to two neighboring O atoms of the methoxymethyl functions at 180.00° . The apical O atom coordinates to the metal

atom with angle of 88.02 - 91.98 ° to the plane of the four N atoms. The axial methoxy groups of phenyl rings are in *trans* orientation with a Zn-O bond distance of 2.417 Å and the average equatorial Zn-N distance is 2.053 Å. Both these values are very similar to those reported for related porphyrin systems thus indicating that there is little geometric strain/changes in the porphyrin units of the polymeric framework of **4-20**. The single Br atom at the *meso* C is distorted at two equivalent positions of 50:50 random occupancy.

The phenyl rings on the porphyrins are parallel to each other. They have a dihedral angle of 79.5 °, deviation of 0.194 Å (in opposite direction) with respect to the plane of the four N atoms. The distance between the two adjacent porphyrin planes is 5.896 Å (from Zn atom of adjacent unit to the plane of the four N atoms).

Each linear slipped-stacked chain of polymer also possesses a herringbone structure. The one-dimensional structure has changed to a multi-dimensional structure with the presence of non-bonding interaction between the Br atoms on the *meso* C with a phenyl H on the adjacent polymer chain. The non-bonding interaction in **4-20** is very similar to that in **4-18** except that the H-Br non-bonding interactions are generally shorter. These non-bonding interaction ranges from 2.899 - 3.264 Å. The Br-Br non-bonding interaction is 4.031 Å (Fig. 4.44).

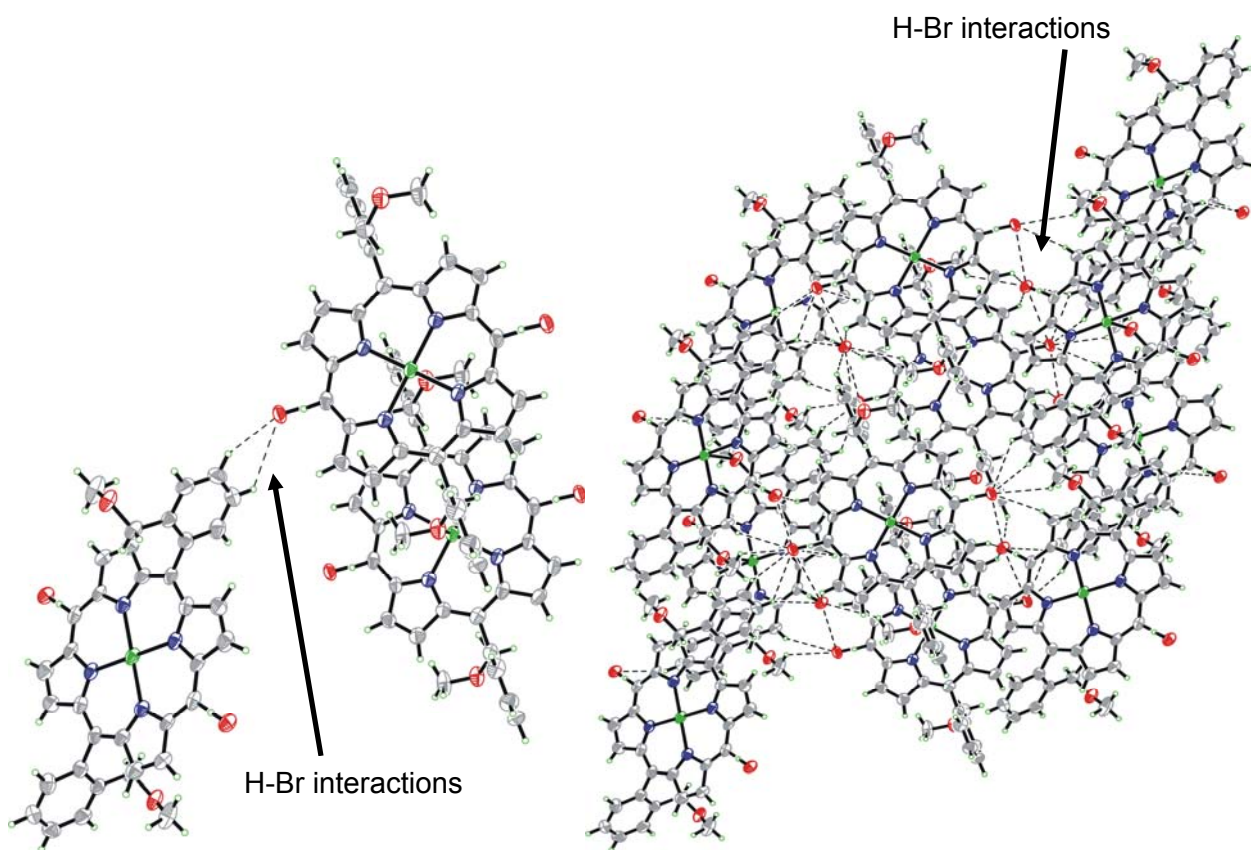


Fig. 4.44 Non-bonding H-Br and Br-Br interactions between units in different columns

4.5.5.1 SINGLE CRYSTAL X-RAY CRYSTALLOGRAPHIC STUDY OF 4-22 GROWN IN CHCl₃/TOLUENE

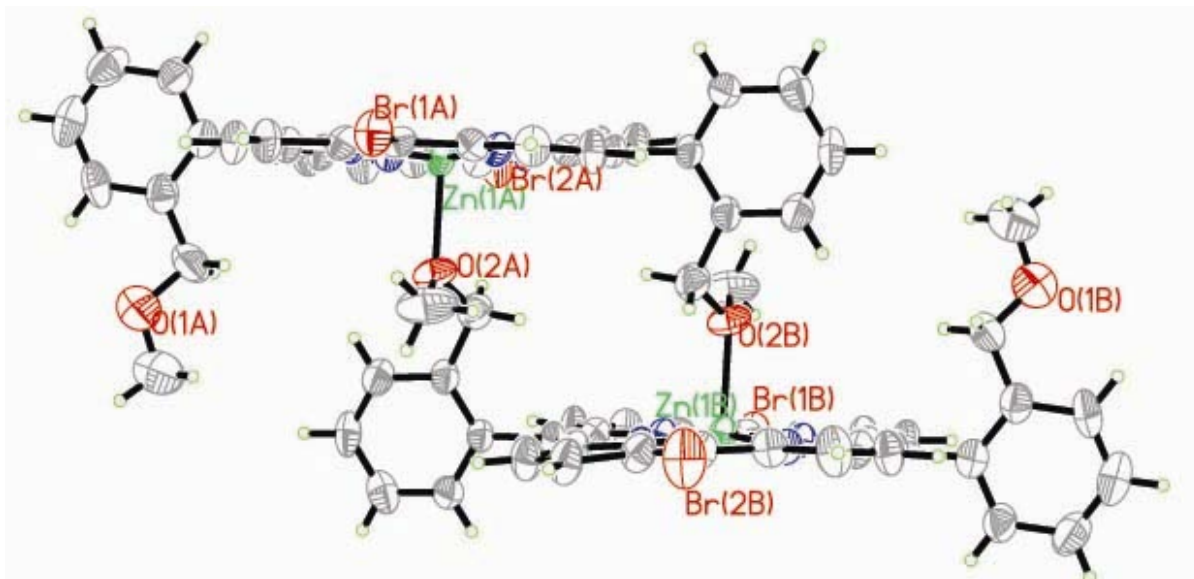


Fig. 4.45 Molecular structure of **4-22**; thermal ellipsoids are drawn at 50 % probability level

Single crystals of **4-22** were grown by slow evaporation of a solution in CHCl₃ and toluene (Fig. 4.45). The asymmetric unit consists of half the molecule also. The dimers pack in a single alignment (Fig. 4.46, unlike in one alignment in **4-16**) one stacked above the other in a slipped cofacial alignment. The complex is a coordination dimer with two coordination points per monomer. The porphyrin rings show greater distortion from planarity than **4-16**. The four pyrrolic N atoms in a porphyrin forms a distorted plane with deviation of 0.021 Å which is about twice that of **4-16** while the outer pyrrolic C atoms in the porphyrin form a distorted plane of 0.103 Å. The Zn(II) metal atom sits above the distorted plane of a four pyrrolic N atoms with deviation of 0.1561 Å. The average equatorial Zn-N distance is 2.047 Å.

The coordination chemistry of **4-22** is very similar to that of **4-16**. The apical O atom coordinates to the metal atom with angle of 92.85 - 96.92 ° to the plane of the four N atoms. The N-Zn-N angles are 172.41 and 170.08 ° and deviate significantly from the perfect 180.00 ° found in previous complexes. Thus, this indicates that there is geometric strain/changes in the porphyrin units of the dimeric framework. The Zn(II) metal atom possess a distorted square pyramidal geometry. The axial methoxy groups of phenyl rings are in *cis* orientation with a Zn-O bond distance of 2.252 Å which is slightly longer than that in **4-16** which is probably due to the mesomeric effect of the two Br atoms.

The two phenyl rings on a monomeric unit possess different dihedral angles tilted towards opposite directions. Their relative dihedral angle is 6.2 °. The inner (with O donor atom) and outer phenyl rings have dihedral angle of 99.5 ° and 94.2 ° from the plane of the porphyrin ring formed by the four N atoms, respectively. Also, the inner phenyl ring has aryl C-*meso* C bond bent towards the opposite porphyrin in the dimer due to the presence of some strain during coordination by 0.028 Å while the outer bent away by 0.199 Å with respect to the plane of the four N atoms.

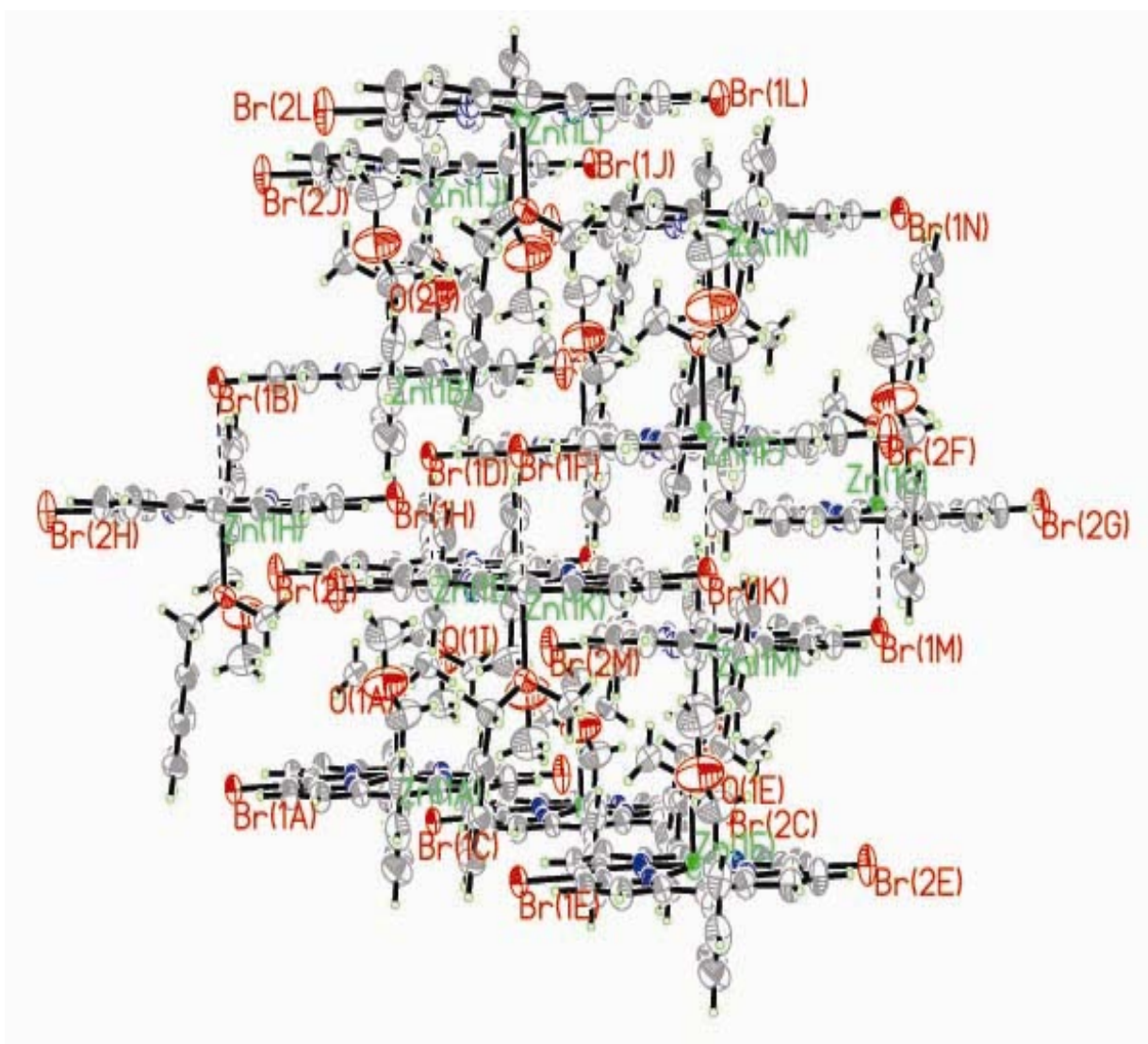


Fig. 4.46 ORTEP view showing the one porphyrin alignment and non-bonded Zn-Br interactions between the dimers

The distance between the two adjacent porphyrin planes in **4-22** is 5.499 Å (from Zn atom of adjacent unit to the plane of the four N atoms) and this is about 0.1 Å shorter than that in **4-16**. The dimers 'connect' via non-bonding interaction of 3.439 Å between the Zn(II) metal atom and a Br atom from adjacent dimer (Fig. 4.46).

4.5.5.2 SINGLE CRYSTAL X-RAY CRYSTALLOGRAPHIC STUDY OF 4-22 GROWN IN THF

Similar to **4-16**, when **4-22** was grown in THF solvent, the dimer separated into monomer units with a THF molecule coordinated to the Zn(II) metal atom (Fig. 4.47). The porphyrin plane is almost planar. The four N atoms and the four outer pyrrolic C atoms show minor deviation of 0.001 Å and 0.006 Å respectively. The Zn(II) metal atom is displaced from the plane of the four N atoms towards the THF molecule by 0.246 Å. The Zn-O bond length of 2.161 Å is slightly shorter than that in the dimer and the Zn(II) atom possess a distorted square pyramidal geometry.

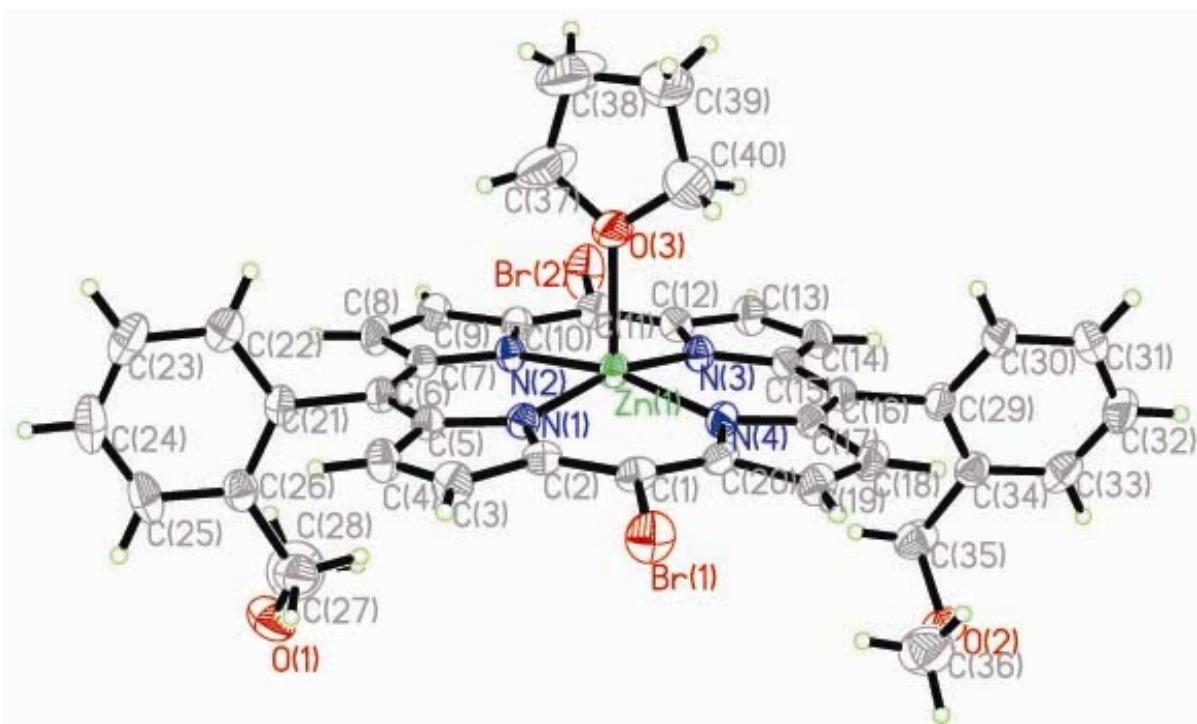


Fig. 4.47 ORTEP view showing one tilted Zn(II) metalloporphyrin molecule with one coordinated THF molecule; thermal ellipsoids are drawn at 50 % probability level

4.6 CONCLUSION

The McDonald [2+2] condensation of dipyrromethane **4-5** and aromatic aldehydes successfully yielded corresponding 5,15-diarylporphyrins. A single step condensation of **4-5** and 2-methoxymethylbenzaldehyde **4-4** gave a pair of atropisomers **4-6** and **4-7** (with *ortho trans* and *cis* methoxymethyl substituents respectively) in comparable yields. These compounds were purified and separated using fractional crystallization and column chromatography (CHCl₃ as eluent). They were characterized and differentiated using X-Ray Crystallography where single crystals of the *trans* isomer **4-6** was identified. The ability to separate the pair of atropisomers (**4-6** and **4-7**) has led to subsequent derivatization (through mono- and dibromination) as well as the generation of a series of five Zn(II) metalloporphyrin complexes derived from the pure isomer. The isolation of the atropisomers was made possible due to the steric bulkiness of the *ortho* methoxymethyl substituents which restricted free rotation about the C-C bond. This was proven by the inability to separate their *meta* counterparts (**4-13** and **4-14**).

The Zn(II) metalloporphyrin complexes with variable architectural structures were obtained by stirring their corresponding free base ligands in a solution of Zn(OAc)₂.xH₂O. Their solid state structures were revealed by X-Ray Crystallographic studies. The *trans* free base ligand **4-6** gave a 3D polymeric network **4-15** while the *cis* counterpart **4-7** gave a slipped cofacial dimer **4-16**. Both coordination complexes demonstrated time-dependent ¹H NMR spectrum due to their fluxionality in various solvents. Spectroscopic studies in CHCl₃ solution show that these arrays display more efficient electron-energy transfer than the monomeric Zn(II) tetraphenylporphyrin complex which signifies the retention of the supramolecular structure even at a low concentration of 1×10⁻⁶ M.

Further, bromination of the free base ligands **4-6** and **4-7** at the *meso* C gave three ligands. The insertion of Zn(II) metal atom yielded two infinite step-like polymeric complexes of Zn(II) metalloporphyrin (**4-18** and **4-20**) and a dimer (**4-22**) with similar structure as **4-16**.

The overall solid state architecture of the complexes was found to be determined by (1) the conformation of the free base ligand which is in turn dependent on the spatial distribution of the side chains on the peripheral phenyl rings, (2) the presence of a large atom on the *meso* position of the free base ligand and (3) the solvent in which the single crystals were grown.

In conclusion, this Chapter summarizes the design, synthesis and characterization of ten free base porphyrin ligands and Zn-O metalloporphyrins coordination dimers and polymers obtained with practical ease from derivation of the parent porphyrins **4-6** and **4-7**.

The third-order NLO properties of the characterized free base porphyrin ligands and Zn(II) metalloporphyrins coordination complexes are studied and the results are summarized in Chapter 5.

4.7 REFERENCES

² (a) Lauceri, R.; De Napoli, M.; Mammana, A.; Nardis, S.; Romeo, A.; Purrello, R. *Synth. Met.* **2004**, *147*, 49. (b) Krupitsky, H.; Stein, Z.; Goldberg, I.; Strouse, C.E. *J. Includ. Phenom. Mol. Recog. Chem.* **1994**, *18*, 177. (c) Wojaczyński, J.; Latos-Grażyński, L. *Coord. Chem. Rev.* **2000**, *204*, 113. (d) Kumar, R.K.; Goldberg, I. *Angew. Chem.. Int. Ed.*

1998, 37 (21), 3027. (e) Bhyrappa, P.; Wilson, S.R.; Suslick, K.S. *J. Am. Chem. Soc.* **1997**, 119, 8492. (f) Min, K.S.; Suh, M.P. *Chem. Eur. J.* **2001**, 7 (1), 303. (g) Kumar, A.A.; Giribabu, L.; Reddy, D.R.; Maiya, B.G. *Inorg. Chem.* **2001**, 40, 6757. (h) Plater, M.J.; Aiken, S.; Bourhill, G. *Tetrahedron Lett.* **2001**, 42, 2225. (i) D'Souza, F.; Ito, O. *Coord. Chem. Rev.* **2005**, 249 (13-14), 1410.

³ (a) Zhou, X.; Ren, A.-M.; Feng, J.-K.; Liu, X.-J.; Zhang, Y.-D. *Chem. Phys. Chem.* **2003**, 4, 991. (b) Ogawa, K.; Zhang, T.; Yoshihara, K.; Kobuke, Y. *J. Am. Chem. Soc.* **2002**, 124 (1), 22.

⁴ (a) Weast, R.C.; Grasselli, J.G. "CRC Handbook of Data on Organic Compounds", Vol 2, 2nd ed, CRC Press, Inc., 1989. (b) Lee, C.H.; Lindsey, J.S. *Tetrahedron* **1994**, 50 (39), 11427.

⁵ Arsenault, G.P.; Bullock, E.; MacDonald, S.F. *J. Am. Chem. Soc.* **1960**, 82, 4384.

⁶ Nace, M. *J. Org. Chem.* **1959**, 24, 1792.

⁷ Teo, T.L.; Vetrichevan, M., Lai, Y.H. *Org. Lett.* **2003**, 5 (22), 4207.

⁸ Manka, J.S.; Lawrence, D.S. *Tetrahedron Lett.*, **1989**, 30 (50), 6989.

⁹ (a) Geier, G.R.; Lindsey, J.S. *Tetrahedron* **2004**, 60, 11435. (b) Balakumar, A.; Methukumar, K.; Lindsey, J.S. *J. Org. Chem.* **2004**, 69 (15), 5112. (c) Geier, G.R.; Littler, B.J.; Lindsey, J.S. *J. Chem. Soc. Per. Trans 2*, **2001**, 2 (5), 701. (d) Littler, B.J.; Ciringh, Y.; Lindsey, J.S. *J. Org. Chem.* **1999**, 64 (8), 2864.

¹⁰ Munakata, H.; Kanzaki, T.; Nakagawa, S.; Imai, H.; Uemori, Y. *Chem. Pharm. Bull.* **2001**, 49 (12), 1573.

¹¹ Tian, M.; Zhang, J.; Lorgere, I.; Galaup, J.P.; Le Gouet, J.L. *J. Opt. Soc. Am. B- Opt. Phys.* **1998**, 15 (8), 2216.

¹² Osuka, A.; Nagata, T.; Kobayashi, F.; Maruyama, K. *J. Heterocyclic Chem.* **1990**, 27, 1657.

- ¹³ Setsune, J.; Hashimoto, M.; Shiozawa, K.; Hayakawa, J.; Ochi, T.; Masuda, R. *Tetrahedron* **1998**, *54*, 1407.
- ¹⁴ Senge, M.O.; Speck, M.; Wiehe, A.; Dieks, H.; Aguirre, S.; Kurreck, H. *Photochem. Photobiol.* **1999**, *70*, 206.
- ¹⁵ Bhyrappa, P.; Wilson, S.R.; Suslick, K.S. *J. Am. Chem. Soc.* **1997**, *119*, 8492.
- ¹⁶ Nagata, N.; Kugimiya, S-ichi.; Kobuke, Y. *Chem. Comm.* **2000**, 1389.
- ¹⁷ Chandra, A.K.; Turro, N.J.; Lyons, Jr. A.L.; Stone, P. *J. Am. Chem. Soc.* **1978**, *100* (16), 4964.
- ¹⁸ (a) Wasielewski, M.R. *Chem. Rev.* **1992**, *92*, 435. (b) Prathapan, S.; Johnson, T.E.; Lindsey, J.S. *J. Am. Chem. Soc.* **1993**, *115*, 7519. (c) Seth, J.; Palaniappan, V.; Johnson, T.E.; Prathapan, S.; Lindsey, J.S.; Bocian, D.F. *J. Am. Chem. Soc.* **1994**, *116*, 10578. (d) Papagiannakis, E.; Kennis, J.T.M.; van Stokkum, I.H.M.; Cogdell, R.J.; van Grondelle, R. *PNAS*, **2002**, *99* (9), 6017. (e) Tamiaki, H.; Miyatake, T.; Tanikaga, R.; Holzwarth, A.R.; Schaffner, K. *Angew. Chem. Int. Ed. Engl.* **1996**, *35*, 772. (f) Franzen, S.; Goldstein, R.F.; Boxer, S.G. *J. Phys. Chem.* **1993**, *97*, 3040. (g) Chamorovsky, C.S.; Chamorovsky, S.K.; Semenov, A.Y. *Biochemistry (Moscow)*, **2005**, *70* (2), 257. (h) Franl, H.A.; Violette, C.A.; Trautman, J.K.; Shreve, A.P.; Owens, T.G.; Albrecht, A.C. *Pure Appl. Chem.* **1991**, *63* (1), 109.
- ¹⁹ Mukherjee, A.K.; Mohan, A. *J. Applied Polymer Sci.* **1992**, *44*, 773.
- ²⁰ (a) Lehn, J.-M. *Science* **2002**, *295*, 2400. (b) Hollingsworth, M.D. *Science* **2002**, *295*, 2410.
- ²¹ (a) Campbell, W.M.; Burrell, A.K.; Officer, D.L.; Jolley, K.W. *Coord. Chem. Rev.* **2004**, *248* (13-14), 1363. (b) Hayashi, T.; Ogoshi, H. *Chem. Soc. Rev.* **1997**, *26*, 355. (c) Imamura, T.; Fukushima, K. *Coord. Chem. Rev.* **2000**, *198*, 133. (d) Flamigni, L.;

Johnson, M.R. *New J. Chem.* **2001**, 25, 1368. (e) Hartnell, R.D.; Arnold, D.P. *Organometallics* **2004**, 23, 391.

²² (a) Ogawa, K.; Kobuke, Y. *Angew. Chem., Int. Ed.* **2000**, 39, 4070. (b) Takahashi, R.; Kobuke, Y. *J. Am. Chem. Soc.* **2003**, 125, 2372.

²³ Aratani, N.; Osuka, A. *Bull. Chem. Soc. Jpn.* **2001**, 74, 1361.

²⁴ (a) Screen, T.E.O; Thorne, J.R.G.; Denning, R.G.; Bucknall, D.G.; Anderson, H.L. *J. Mater. Chem.* **2003**, 13, 2796. (b) Screen, T.E.O; Thorne, J.R.G.; Denning, R.G.; Bucknall, D.G.; Anderson, H.L. *J. Am. Chem. Soc.* **2002**, 124, 9712. (c) Wilson, G.S.; Anderson, H.L. *Chem. Commun.* **1999**, 1539.

²⁵ Hoffert, M.I.; Caldeira, K.; Jain, A.K.; Haites, E.K.; Harvey, L.D.D.; Potter, S.D.; Schlessinger, M.E.; Schnedier, S.H.; Watts, R.G.; Wigley, T.M.; Wuebbles, D.J. *Nature* **1998**, 395, 881.

²⁶ Lakowicz, J.R.; *"Principles of Fluorescence Spectroscopy"*, N.Y., 2nd ed., Kluwer Academic/Plenum, 1999.

²⁷ Ciardelli, F.; Tsuchida, E.; Wohrle, D. *"Macromolecule-Metal Complexes"*, Springer-Verlag Berlin Heidelberg, 1996.

²⁸ Ikeda, C.; Tanaka, Y.; Fujihara, T.; Ishii, Y.; Ushiyama, T.; Yamamoto, K.; Yoshioka, N.; Inoue, H. *Inorg. Chem.* **2001**, 40, 3395.

CHAPTER 5

NONLINEAR OPTICAL MEASUREMENTS OF Zn(II) METALLOPORPHYRIN COMPLEXES

5.0 INTRODUCTION

The Z-scan measurements were performed on solutions of the coordination complexes in CHCl_3 . The experimental setup used a Ti:sapphire regenerative amplifier (CPA-2001, Clark, MXR) which typically produces ~ 1 mJ, 150 fs duration pulses with the repetition rate of 250 Hz at the wavelength of 775 nm. The fundamental pulses from the regenerative amplifier are then parametrically down-converted in an optical parametric amplifier (TOPAS, Quantronix) to yield 100 - 150 fs long pulses (FWHM) with a wavelength of 650 nm.

The measurements were conducted using a simple arrangement that allowed us to record the open-aperture Z-scan and the closed-aperture Z-scan simultaneously. The travel range of the table was generally chosen to be $z = -35$ to $z = 35$ mm. The focussed spot sizes were in the range of $w_0 = 30 - 50 \mu\text{m}$.

For convenience, the measurements were performed in a relative manner, hence, the values of the nonlinear optical (NLO) parameters were calibrated by performing measurements of the nonlinear phase shift, $\Delta\phi_0$ of the solvent in a 1 mm glass cell and adjusting the light intensity to obtain $\Delta\phi_0$ value in the range of 0.5 - 1.0 rad for the cell

with the solvent and comparing that with a phase shift obtained on 1 mm thick silica plates for which $n_2 = 3 \times 10^{-16} \text{ cm}^2 \text{ W}^{-1}$ was assumed.

The excited state absorption (ESA) measurements were performed on solutions of the coordination complexes in CH_2Cl_2 using a frequency-doubled Q-switched Nd:YAG laser operating at 532 nm with a temporal pulse of 7 ns (FWHM) and a repetition rate of 10 Hz or single shot. The laser pulses were focused at the center of the sample cell (thickness = 1 mm) by a 25-cm-focal-length lens giving a spot radius of $\sim 35 \mu\text{m}$. The laser beam was divided into two beams, one was used to monitor the incident laser energy, and the other was focused into the sample cell. The nonlinear transmission curve was obtained by varying the input energy (E_i) with a half-wave plate and polarizer combination and by monitoring input energy (E_i) and output energy (E_o) with two RJP-735 series energy detectors.

The input energy was in the range of 0.2 to 50 μJ . According to the formula $F_{i/o} = 2E_{i/o} / (\pi w_0^2)$, where $E_{i/o}$ is the input/output energy, $F_{i/o}$ is the input/output fluence and $w_0 \sim 35 \mu\text{m}$ is the spot radius at the focus point, the input fluence was in the range of 0.01 to 2.6 J cm^{-2} .

5.1.0 RESULTS AND DISCUSSIONS

All the samples used in this study show linear absorption features typical of the free base porphyrins and metalloporphyrins namely, the high energy B- (Soret) and the low energy Q-bands. The reproducibility of the absorption spectra before and after exposure to laser confirmed the photostability of the compounds.

Note that maximum concentrations are needed because nonlinear transmittance-based methods are not sensitive by their nature hence a large concentration of the studied molecules is required to obtain signal from the strong background. High solubility of the compounds ensured that there were no undissolved particles that can cause significant scattering of laser light.

5.1.1 DATA ANALYSES

The Z-scans obtained were analyzed with expressions derived by Sheikh-Bahae *et al.*¹ to yield the real part of the nonlinear phase shift $\Delta\phi_{\text{real}}$ induced by the third-order nonlinearity and the T factor defined here as

$$(5.1) \quad T = 4\pi \Delta\phi_{\text{imag}} / \Delta\phi_{\text{real}}$$

for a given sample. The analyses were performed by comparing the shapes of the closed-aperture and open-aperture scans with those computed theoretically. In the absence of nonlinear absorption, the amplitude of a closed-aperture Z-scan measured as the difference in transmission values from peak-to-valley is proportional to the real part of the nonlinear phase shift $\Delta\phi_{\text{real}}$. However, the presence of nonlinear absorption causes the asymmetry of a closed-aperture scan which depends on the T factor.

The imaginary part of the nonlinear phase shift $\Delta\phi_{\text{imag}}$ can be obtained from the asymmetry of the closed-aperture scan by direct fitting or from the depth of a dip in the open-aperture scan that is directly related to $\Delta\phi_{\text{imag}}$ using the Z-scan fitting software as shown in Fig. 5.1. Alternatively, we also used a procedure consisting of dividing the closed-aperture scan by the open-aperture scan to resolve information on the real part of

the phase shift to give a scan that is essentially free from the influence of the imaginary part of the phase shift [that is, free from two-photon absorption (TPA) effect].

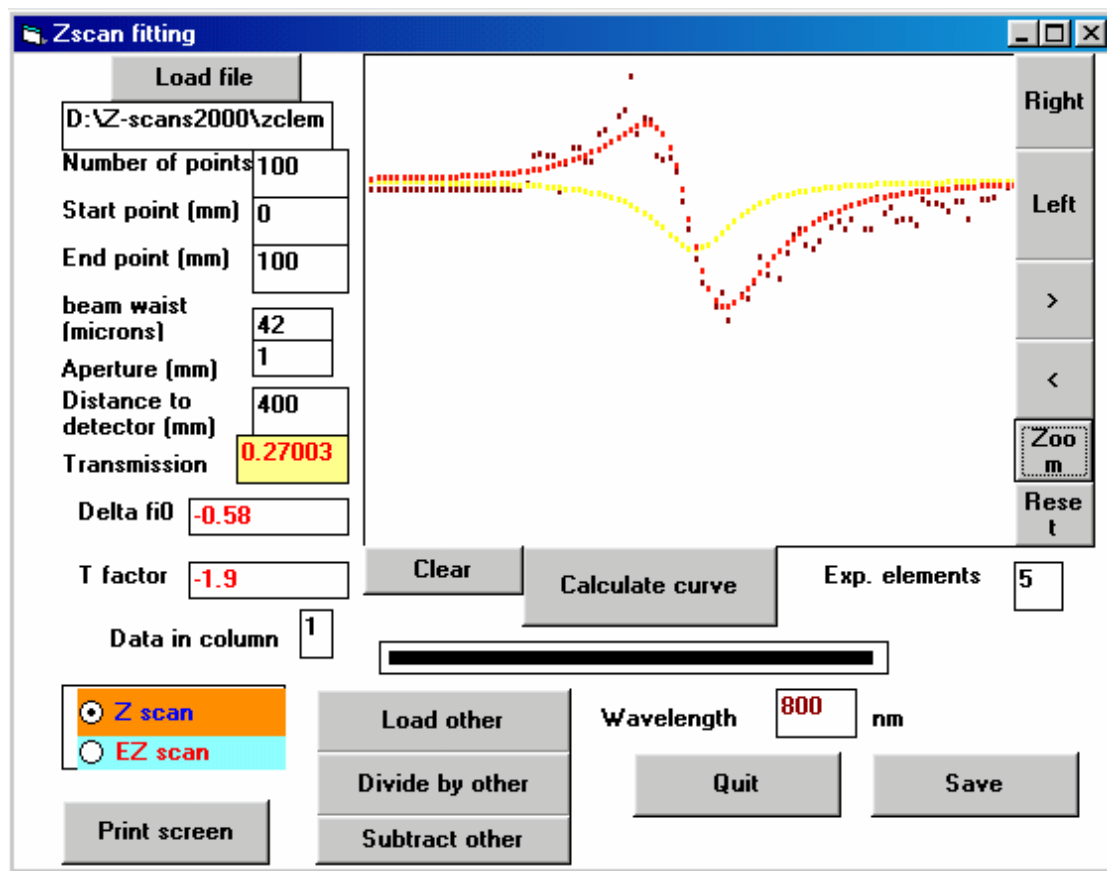


Fig. 5.1 Example of Z-scan curve fitting to obtain T factor and $\Delta\phi$ values

The Fig. 5.2 shows examples of closed-aperture scans for a series of solutions of the soluble compounds in CHCl_3 . The amplitudes of the scans decrease with increasing concentration indicating that the real part of the nonlinearity of the solute is opposite in sign to that of the solvent. There is an increasing asymmetry of the scans indicating also the presence of the imaginary part of the nonlinearity. The dependence of $\Delta\phi_{\text{mag}}$ and $\Delta\phi_{\text{real}}$ on concentration can be analyzed to extract information on the NLO properties of

the solute. The relation between the nonlinear phase shift and the nonlinear refractive index can be written as

$$(5.2) \quad \Delta\phi = (2 \pi n_2 I L_{\text{eff}}) / \lambda$$

where L_{eff} is the thickness of the sample corrected for one-photon absorption (OPA) in cm, n_2 is nonlinear refractive index, I is light intensity and λ is wavelength. Hence, knowledge of the light intensity can be used for the conversion of phase shift values to nonlinearity values. In practice, we derived the intensity values from $\Delta\phi$ measured for silica samples. The complex n_2 of a dilute solution is approximated by the following linear expression

$$(5.3) \quad n_2 = g' n_{2,\text{solute}} + (1-g') n_{2,\text{solvent}}$$

where g' is the weight fraction of the solute, $n_{2,\text{solute}}$ is the solute (extrapolated) nonlinear refractive index and $n_{2,\text{solvent}}$ is the nonlinear refractive index of the solvent.

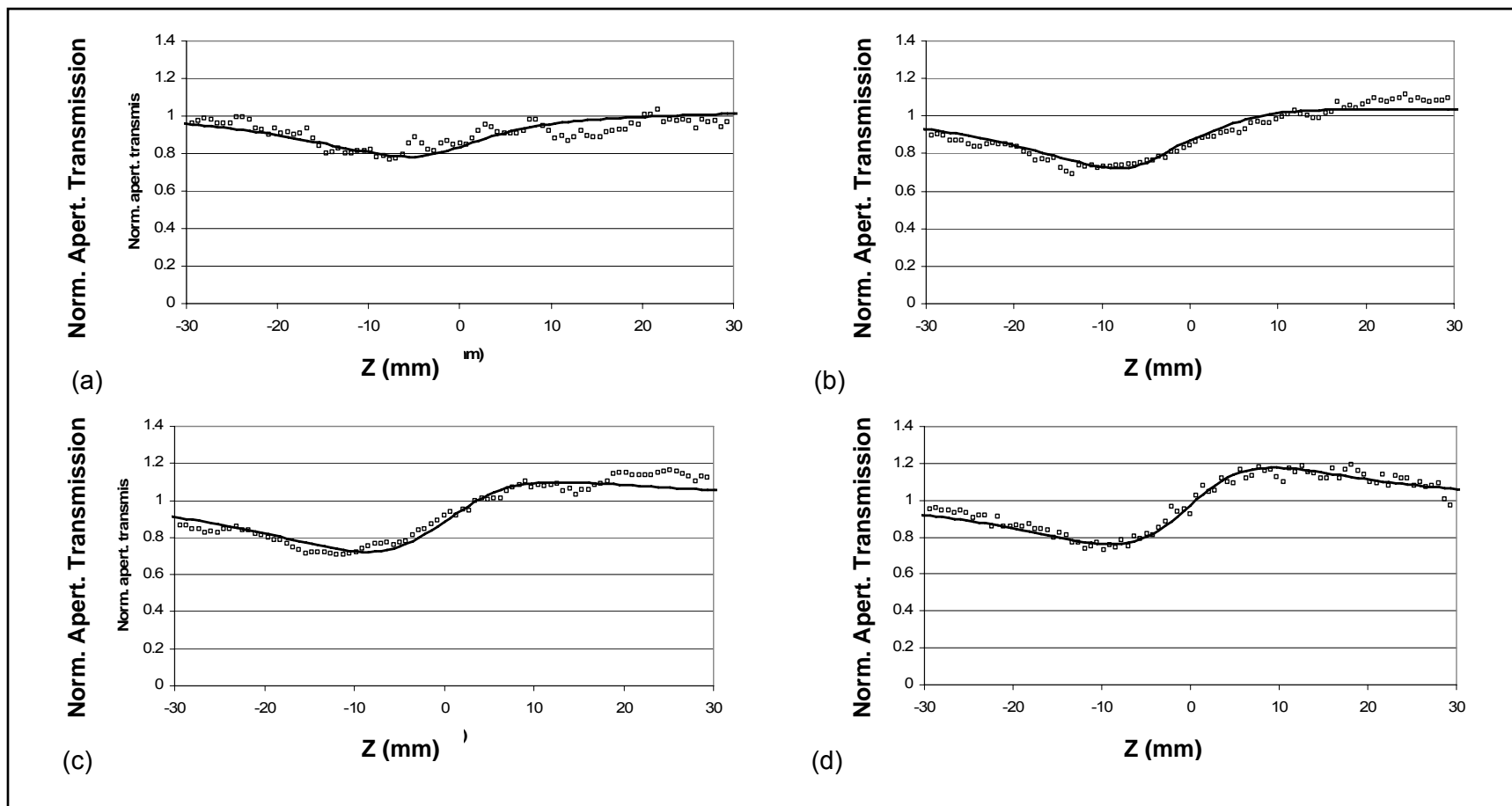


Fig. 5.2 Typical of closed-aperture scans for (a) 0.398 wt%, (b) 0.220 wt%, (c) 0.110 wt% of **4-6** in CHCl_3 and (d) pure CHCl_3

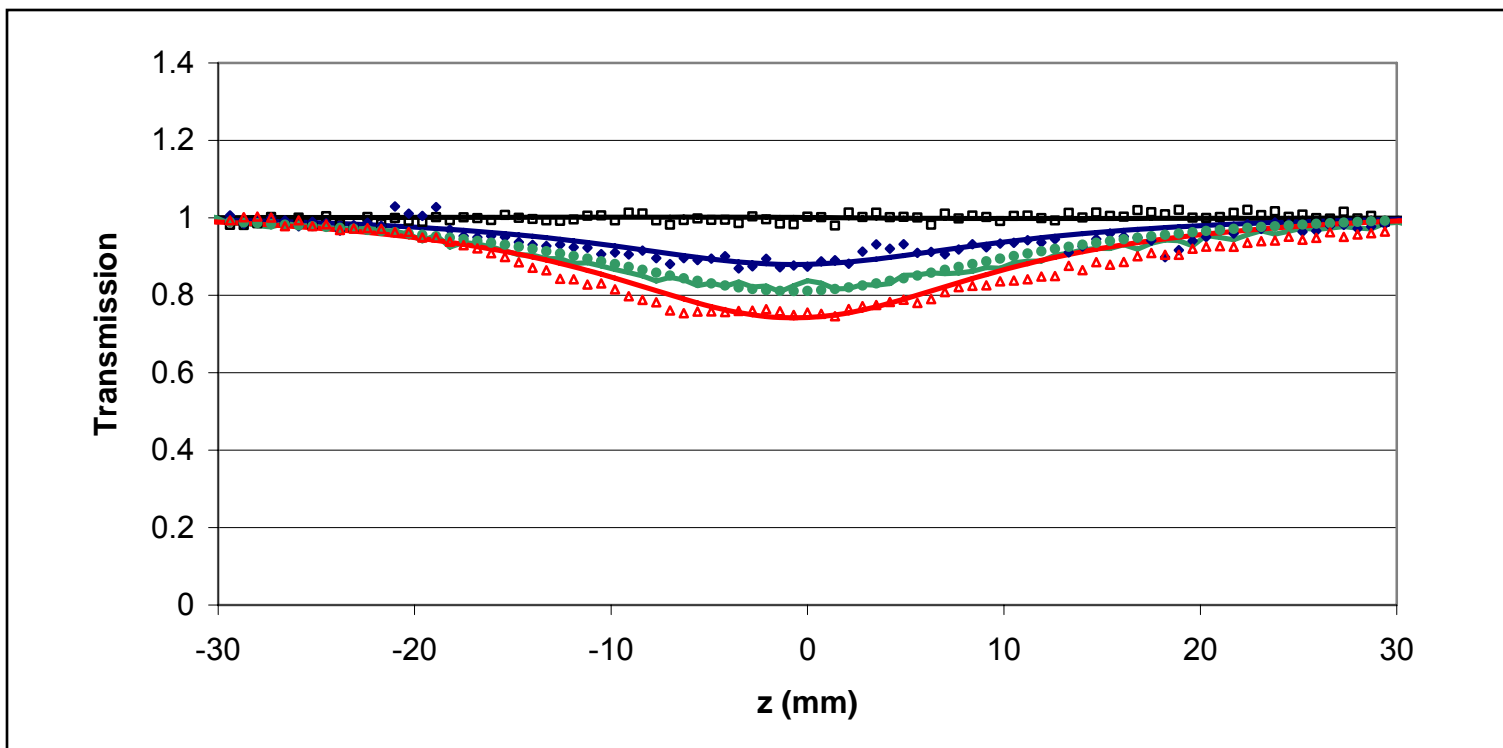


Fig. 5.3 Concentration dependence of open-aperture Z-scans of **4-6** 0.398 wt% (light red), 0.220 wt% (green), 0.110 wt% (blue) and 0 wt% (black) in CHCl_3 solution

From the open-aperture scan, the dip in the curve increases with increase in concentration of the solution of **4-6** (applies to other porphyrin-based compounds also) in CHCl_3 as shown in Fig. 5.3 while the linear transmission of the solutions found from the UV-vis spectra of each of these solutions is approximately = 1. Hence, qualitatively, the TPA of **4-6** solution increases with increase in the concentration of the compound.

Quantitatively, the variation of the TPA coefficient, β with concentration changes can be determined from the coupling factor T' obtained from curve fitting. Since $T' = \beta\lambda / n_2$ where λ is the laser wavelength and n_2 is the nonlinear index of refraction, the values of β for various concentrations can be obtained.

The slopes of the linear relations of $\Delta\phi_{\text{real}}$ and $\Delta\phi_{\text{mag}}$ on concentration of the solutions are used to calculate the real and the imaginary parts of $n_{2,\text{solute}}$. Since g' is small, $1-g' \cong 1$, equation 5.3 becomes

$$(5.4) \quad n = g' n_{2,\text{solute}} + n_{2,\text{solvent}}$$

by substituting equation 5.2 into 5.4, we obtain

$$(5.5) \quad \frac{\lambda \Delta\phi}{2\pi I L_{\text{eff}}} = g' n_{2,\text{solute}} + n_{2,\text{solvent}}$$

which rearranges to give

$$(5.6) \quad \Delta\phi = \frac{2\pi I L_{\text{eff}}}{\lambda} g' n_{2,\text{solute}} + \frac{2\pi I L_{\text{eff}}}{\lambda} n_{2,\text{solvent}}$$

Treating $\Delta\phi$ as complex, one assumes that equation 5.6 holds for dependences of both $\Delta\phi_{\text{real}}$ and $\Delta\phi_{\text{mag}}$ vs g' . Dividing the gradient of the plot of $\Delta\phi_{\text{real}}$ against concentration by the y-intercept, one gets

$$(5.7) \quad \frac{2 \pi l L_{\text{eff}} n_{2,\text{solute}}}{\lambda} / \frac{2 \pi l L_{\text{eff}} n_{2,\text{solvent}}}{\lambda}$$

$$= \frac{n_{2,\text{solute}}}{n_{2,\text{solvent}}}$$

Thus, multiplication of the value of slope/intercept by $n_{2,\text{solvent}}$ gives the extrapolated nonlinear refractive index of the solute. However, it should be noted that the value of $n_{2,\text{solute}}$ determined from this method may be substantially different from the value of n_2 for the neat substance in its solid phase because of the differences in densities between the solute and the solvent, local field factors and solvent influences on the nonlinear parameters of the solute molecules.

An alternative way of presenting the cubic nonlinearity is by quoting the value of the cubic susceptibility $\chi^{(3)}$ which can be calculated from n_2 using

$$(5.8) \quad \chi^{(3)} = \frac{n^2}{C_1} n_2$$

where C_1 is a constant which depends on the definition of $\chi^{(3)}$ and on the system of units adopted. For the conversion of n_2 in $\text{cm}^2 \text{W}^{-1}$ (SI units) to $\chi^{(3)}$ in esu (cgs units), the value of C_1 is approximately 0.039.² To calculate molecular parameters from macroscopic ones, one uses

$$(5.9) \quad \chi^{(3)} = L^4 \sum N_i \gamma_i$$

where L is the local-field factor, often approximated by the Lorentz expression $L = (n_0^2 + 2) / 3$ and n_0 is the linear index of refraction. In addition, γ_i are the hyperpolarizabilities of the components of the system (assumed to be independent of concentration). $N_i = N_0 g'_i \rho_{\text{solution}} / M_i$, where N_0 is the Avogadro's number, g'_i is the weight fraction of a solution component, M_i is the component's molecular weight and

ρ_{solution} is the density of solution. Finally, the TPA cross sections (σ_2) in $\text{cm}^4 \text{s photon}^{-1}$ molecule⁻¹ are defined as

$$(2.12) \quad \sigma_2 = \frac{\hbar\omega\beta}{N}$$

which also leads to the following relation between σ_2 and γ_{imag} ,³

$$(5.10) \quad \sigma_2 = \frac{0.039 \hbar\omega L^4}{\lambda n^2} 4\pi\gamma_{\text{imag}}$$

where N is the number density of molecules, \hbar is Planck's constant = $h/2\pi$, ω is frequency, λ is wavelength and γ_{imag} is the imaginary component of the second hyperpolarizability.

Analyses of the nonlinear index of refraction of solutions of the porphyrin compounds at 650 nm showed that $n_{2,\text{real}}$ are negative in all of them except **4-6**. Thus, the former show self-defocusing properties while the latter show self-focusing properties at this wavelength. As mentioned in Chapter 2, self-defocusing materials are usually more desirable in power limiting applications than those showing self-focusing because the latter often leads to laser damage.⁴ The former possess self-protecting ability because the beam diverges rapidly from the intermediate focus. This property is particularly important for solid materials.

5.1.2 TWO-PHOTON ABSORPTION CROSS SECTION PROPERTIES

The σ_2 of the porphyrin compounds synthesized in this work and determined at 650 nm are summarized in Table 5.1. They possess relatively high σ_2 as the excitation wavelength is in two photon resonance with the Soret band. It is interesting to note that

the free base porphyrins, **4-6** and **4-7** exhibit significant differences in σ_2 . This is likely to arise from the geometry and dipole moment of the molecules.

The coordination polymer, **4-15** as well as the dimer **4-16** exhibit larger TPA merit factor (σ_2 / formula weight (FW) of the monomeric unit) than their corresponding free bases. This could be attributed to the improved π - π conjugation in the metalloporphyrin with the insertion of the Zn(II) metal atom.

However, it was observed that the TPA merit factors of **4-18** and **4-20** are lower than those of the other coordination complexes. In addition, there is no significant difference in the TPA merit factors when the free base ligand is mono- or dibrominated in **4-20** and **4-18** respectively. A clearer comparison of the effect of Br atom on σ_2 can be done using the geometrically similar dimers **4-16** and **4-22** formed by two-points coordination. It was found that the unbrominated dimer **4-16** gave a larger merit factor as compared to **4-22**.

In an attempt to study the effect of the coordination bonds formed in the self-assemblies on their TPA properties, a comparison of this property with Zn(II) 5,15-diphenylporphyrin was carried out. We observed a larger σ_2 for this monomeric metalloporphyrin. However, the results obtained for this complex contain a large uncertainty. The Z-scans indicate a possibility of other mechanisms contributing to variations in the absorption and refraction in the solutions of this complex. Although femtosecond pulses were used, which usually minimizes the possibility of contributions from ESA, this mechanism can still occur in the presence of sufficiently strong laser light.

Table 5.1 Summary of nonlinear optics parameters of free base and Zn(II) metalloporphyrin complexes

Compound	FW (g/mol)	λ_{\max} (nm) [ϵ' (mM ⁻¹ cm ⁻¹)]	$n_{2,\text{real}}$ (cm ² W ⁻¹)	$n_{2,\text{imag}}$ (cm ² W ⁻¹)	γ_{real} (10 ⁻³⁶ esu)	γ_{imag} (10 ⁻³⁶ esu)	σ_2 (GM)	Merit Factor σ_2/FW (GM mol g ⁻¹)
4-6	550.65	404 [19.54]	7.9E-15	1.9E-13	0±500	1850±300	700±100	1.27
4-7	550.65	406 [45.96]	-8.7E-14	1.2E-13	-800±400	1200±200	450±70	0.82
4-15	614.02	412 [30.19]	-2.2E-13	2.3E-13	-2300±1500	2500±800	930±300	1.51
4-16	614.02	412 [61.56]	-3.5E-13	2.5E-13	-3600±1400	2600±600	990±230	1.61
4-18	692.92	422 [16.37]	-2.5E-13	9.1E-14	-1000±1000	1200±400	460±160	0.66
4-20	767.97	424 [36.34]	-8.5E-14	1.0E-13	-3200±1000	1200±350	460±130	0.59
4-22	767.97	426 [59.26]	-2.8E-13	2.1E-13	-800±2000	2700±800	1030±300	1.34
Zn(II) 5,15-diphenylporphyrin	524.10	409 [61.68]	-1.3E-13	3.1E-13	-1200±500	2800±2000	1060±600	2.02

The measured σ_2 may be strongly dependent on the duration of laser pulses used for two-photon excitation due to additional photon losses caused by the one-photon ESA process.⁵ Molecules excited by TPA by the front of the pulse can participate in OPA by the rest of the pulse from their excited states which is especially important if pulses are in nanoseconds range. Since the efficiency of one-photon excitation is usually much larger than the efficiency of two-photon excitation, an overestimation of the σ_2 will result. In particular, ESA is critical for the nonlinear transmittance-based method adopted in our study because OPA from the excited state contributes to the decrease of the transmittance signal. Hence, we believe a reliable method of measuring TPA is through the use of sufficiently short laser pulses of few picoseconds or less. It is generally agreed among the experimental groups in this area that ESA will not pose significant problem if the two-photon excitation is performed by femtosecond laser pulses.

5.1.3 EXCITED STATE ABSORPTION (ESA) – REVERSE SATURABLE ABSORPTION (RSA)

The nonlinear absorption of the solutions of porphyrin derivatives is well known to contain contributions from ESA.⁶ Such contributions are very important for nonlinear absorption occurring in the range of OPA but may also be contributing when the initial absorption step is a two-photon process. We attempt to determine the contribution of this mechanism on the transmission results obtained earlier. For this study, our measurement is limited to the laser excitation wavelength of 532 nm.

A comparison of the optical limiting measurements of **4-6** and **4-7** show that the two atropisomers display similar reverse saturable absorption (RSA) property although

they differ in conformation (Fig. 5.4). This may be due to the dominance of other mechanisms such as thermal effects. Hence, the difference in TPA merit factor may be mainly contributed by the difference in the transition dipole moment of the molecules. Comparison of **4-6** and **4-7** with 5,15-diphenylporphyrin (Fig. 5.4) shows that this optical limiting property is not affected by the presence of the two methoxymethyl substituents.

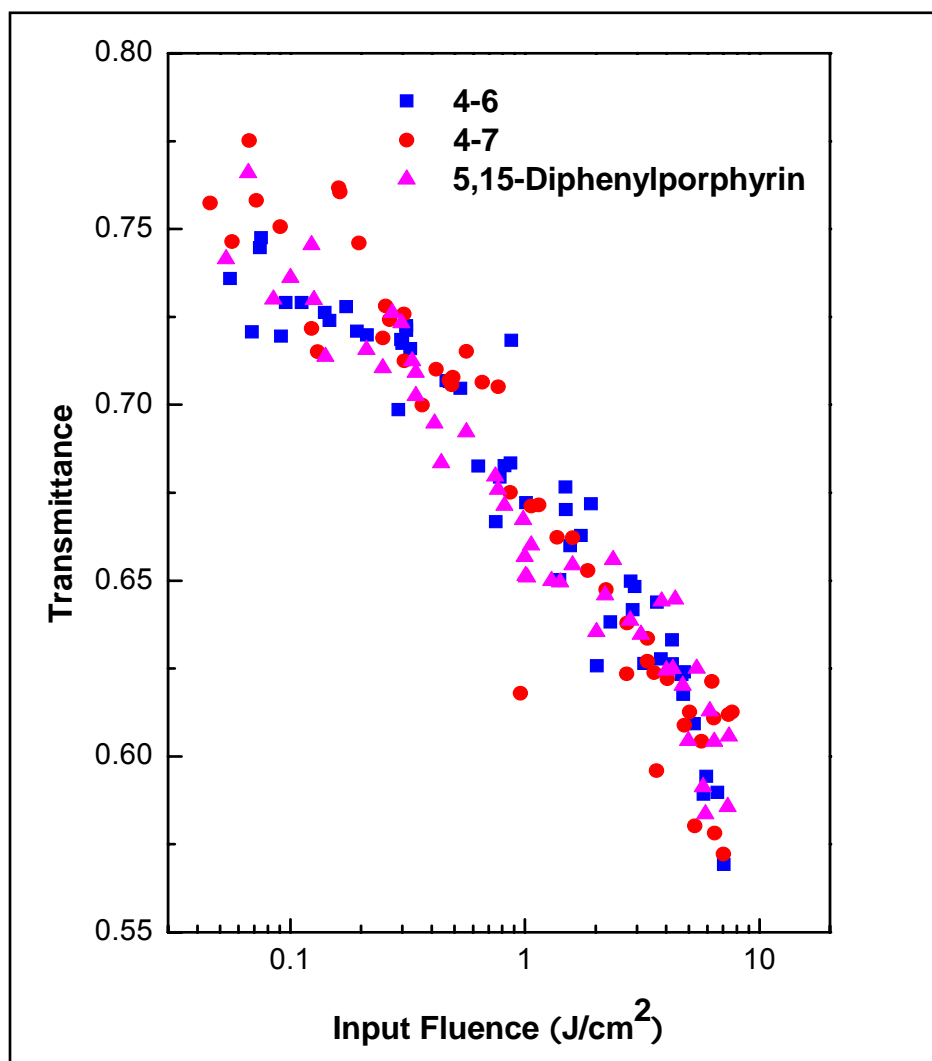


Fig. 5.4 Transmission of **4-6**, **4-7** and 5,15-diphenylporphyrin with increase in input fluence

The substitution of Br atoms on the two *meso* positions of **4-6** to give **4-17** resulted in an increase in the threshold of optical limiting (Fig. 5.5). The compound **4-17** shows minimal saturable absorption while **4-6** exhibits relatively strong RSA. The UV-vis absorption spectrum of the porphyrin after bromination red-shifted by 15 nm implying that although the atoms distort the porphyrin structure from planarity via steric hindrance, the mesomeric effect of the atoms causes the position of the Soret and Q-bands to shift to longer wavelengths. This may increase the triplet yield further by increasing the mixing between singlet and triplet states, having influence on the efficiency of RSA occurring through triplet-triplet ESA. However, increasing the rate of intersystem crossing from $S_1 \rightarrow T_1$ also decreases the triplet lifetime due to faster rate of relaxation from $T_1 \rightarrow S_1$. On the other hand, the insertion of Zn(II) metal atom into the brominated ligand resulted in a stronger ESA of **4-18** as compared to **4-15** (Fig. 5.6). The insertion of Zn(II) metal atom into the cavity of porphyrin is known to increase the planarity of the porphyrin ring. Also, metalloporphyrins with closed shell atom generally have longer excited state lifetimes.⁷ Porphyrins with open shell metal atoms generally have short excited state lifetimes due to rapid charge transfer from the excited porphyrin to the metal atom. This is confirmed by the results showing a lower threshold for optical limiting of Zn(II) 5,15-diphenylporphyrin as compared to its free base. Hence, the overall geometry of the self-assembled coordination complex affects the nonlinear absorption of the supramolecule.

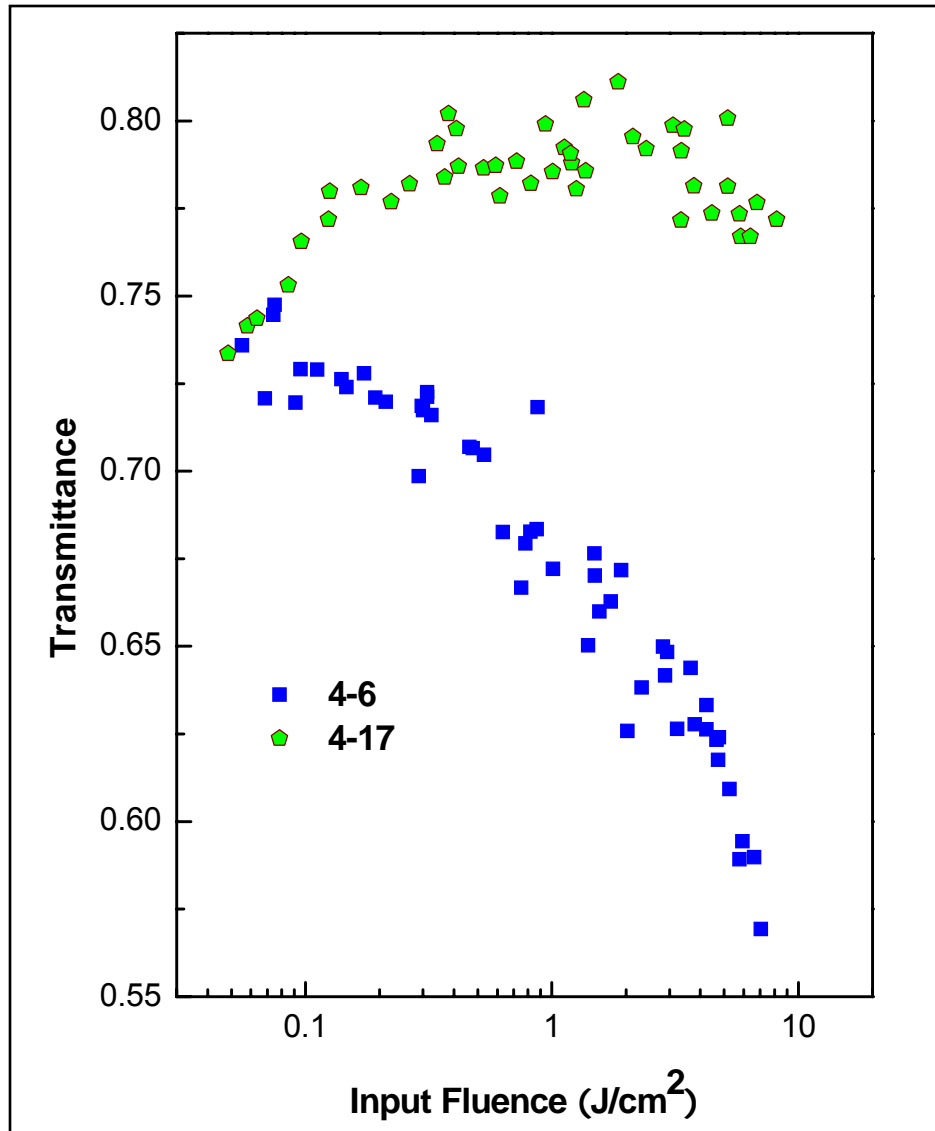


Fig. 5.5 Transmission of 4-6 and 4-17 with increase in input fluence

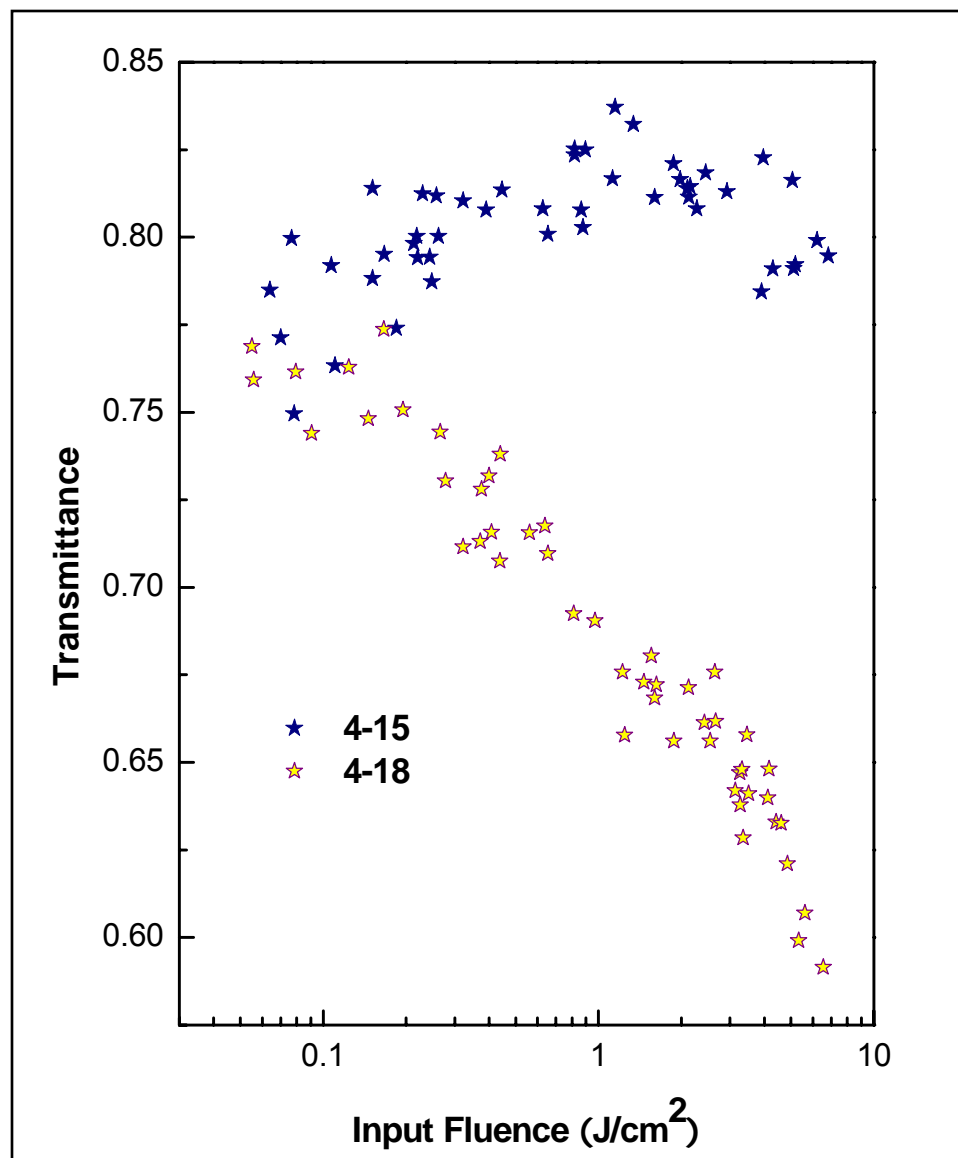


Fig. 5.6 Transmission of **4-15** and **4-18** with increase in input fluence

As mentioned before, the large σ_2 for Zn(II) 5,15-diphenylporphyrin may be partly attributed to some contribution of ESA or influence of photochemical instability. A comparison of Zn(II) 5,15-diphenylporphyrin without coordinating side arm with **4-15** (which shows negligible RSA) clearly shows that the large contribution of the σ_2 of the

former could be due to the combination of RSA and TPA mechanisms (Fig. 5.7). Also, it can be commented that the contribution of σ_2 in **4-15** is largely due to the nonlinear absorption mechanism rather to ESA. Hence, uncertainties arise about the role of both processes in Zn(II) 5,15-diphenylporphyrin. The compound **4-15** exhibits negligible RSA probably because of the close proximity of the monomers linked by Zn-O coordination bond which allows the molecules to undergo relaxation at a faster rate, resulting in the decrease of ESA. Zn(II) 5,15-diphenylporphyrin exist as monomeric units in solution hence lowering the rate of relaxation.

Therefore, for optical limiting applications, uncoordinated Zn(II) metalloporphyrins without heavy atoms may be favoured as they exhibit lower thresholds for optical limiting. However, for other applications of TPA, it is important to avoid the occurrence of RSA which can complicate the nonlinear properties of the former.

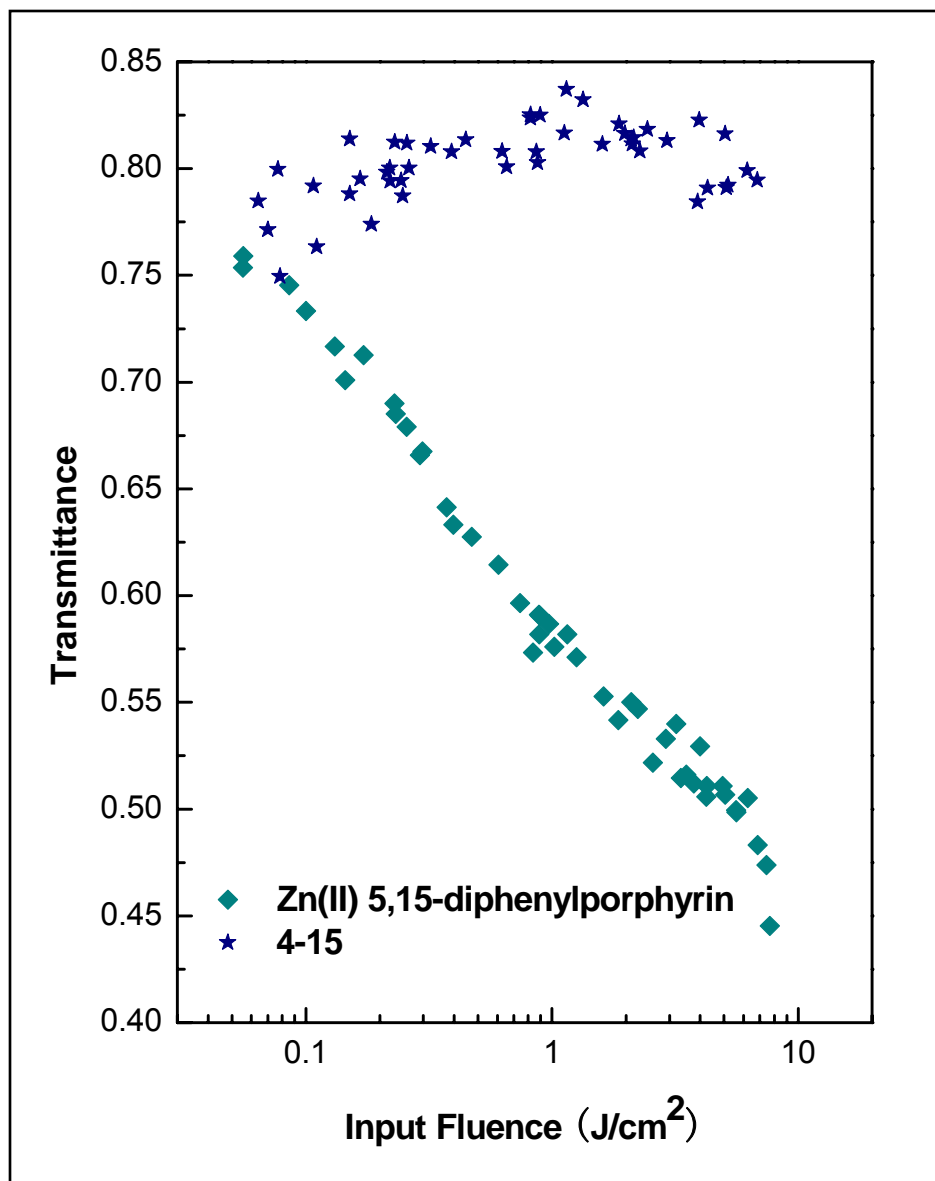


Fig. 5.7 Transmission of Zn(II) 5,15-diphenylporphyrin and 4-15 with increase in input fluence

5.1.4 THREE-LEVEL MODEL

The values of σ_2 determined in this work were all obtained at the wavelength of 650 nm, which limits the possibility of a full analysis of their variations. In fact, our measurements of the full TPA spectrum of **4-16** indicate that σ_2 has a broad maximum around 700 - 800 nm (Refer to section 5.1.6 for detailed discussion). However, some preliminary insight into the factors influencing the values of σ_2 can be obtained by analyzing the trends obtained here without taking into account the individual shifts of the TPA spectra. It is known that, if the frequency detuning between the laser and a transition becomes small, a single resonance term may dominate over the contribution of all the other levels combined. In this case, a three-level model can be used to describe the TPA process.⁸ In this model, three energy levels of a molecule are considered, namely, the ground level (*g*), the two-photon excited level (*f*) and a single intermediate level (*m*).

The free bases and Zn(II) metalloporphyrins coordination complexes studied in our project contain centre of symmetry. For such molecules, the σ_2 reduces to just one term corresponding to the resonance intermediate level:⁹

$$(5.11) \quad \sigma_{fg}^{(2)}(\nu) = 2 \frac{[2\cos^2(\alpha') + 1] (2\pi)^4 \nu^2 L^4}{15 h^2 n^2 c^2} \frac{|\mu_{fm}|^2 |\mu_{mg}|^2}{(\nu_{mg} - \nu)^2 + \Gamma_m^2(\nu)} g(2\nu)$$

where $\sigma_{fg}^{(2)}(\nu)$ is the two photon absorption cross section expressed as a function of laser excitation frequency ν , ν_{mg} is the frequency of the $m \leftarrow g$ transition in s^{-1} , α' is the angle between transition dipole moments μ_{fm} and μ_{mg} of the transitions $f \leftarrow m$ and $m \leftarrow g$ respectively, c refers to the speed of light in $cm\ s^{-1}$, Γ_m^2 is the full width at half maximum

of the absorption band $m \leftarrow g$ in cm represented as a function of ν and $g(2\nu)$ is the line shape function in cm.

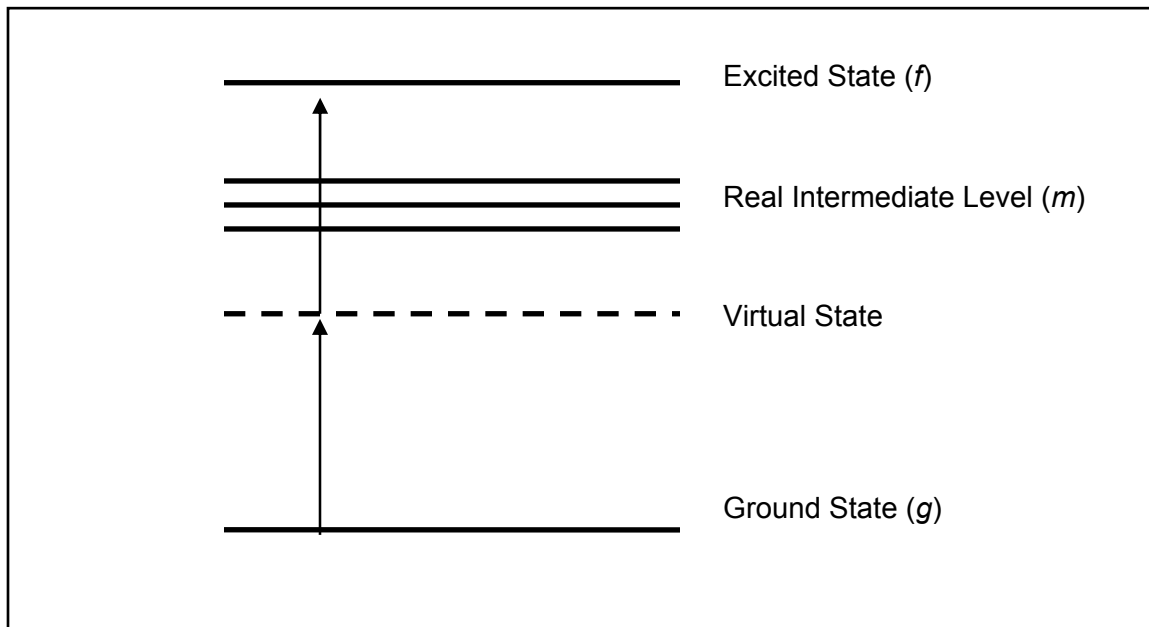


Fig. 5.7 Three-level model system used for the description of TPA process

The lowest energy transition in the OPA spectrum of porphyrins is the Q-band. If one supposes that the σ_2 at 650 nm for all the porphyrins are mainly determined by a resonance enhancement mechanism, then equation 5.12 predicts that σ_2 should be proportional to the linear transition dipole moment squared over the frequency detuning squared:

$$(5.12) \quad \sigma_2 \sim \frac{|\mu_{mg}|^2}{(\nu_{mg} - \nu)^2}$$

One can assume that $|\mu_{mg}|^2 g(2\nu)$ does not vary much amongst the molecules. This assumption is rather reasonable considering that the absorption coefficient which is related to the transition dipole of the molecules is of the same order of magnitude for all

the molecules investigated. The analyses can be carried out between free base porphyrins as well as Zn(II) metalloporphyrin dimers and polymers because it is evident that their values of the absorption coefficient do not vary significantly.

The following relation holds between the product $|\mu_{fm}|^2 g(2\nu)$ and the extinction coefficient ε_{fm} of one-photon transition $f \leftarrow m$ as a function of $2\bar{\nu} - \bar{\nu}_{mg}$:

$$(5.13) \quad |\mu_{fm}|^2 g_{\text{TPA}}(2\nu) = \frac{\varepsilon_{fm}(\bar{\nu} - \bar{\nu}_{mg})}{1.07 \times 10^{38} \bar{\nu}_{fm} c}$$

where $\bar{\nu}$ is the laser wavenumber, $\bar{\nu}_{mg}$ is the wavenumber of the $m \leftarrow g$ transition, $\bar{\nu}_{fm}$ is the wavenumber of the $f \leftarrow m$ transition. Thus, the variation of $|\mu_{fm}|^2 g(2\nu)$ from one molecule to another can be expected to follow that of the product $\varepsilon_{fm}(2\bar{\nu} - \bar{\nu}_{mg})$.⁹

To make a plot of σ_2 as a function of $|\mu_{fm}|^2 g(2\nu)$, we note that

$$(5.14) \quad \sigma_2 \sim \frac{|\mu_{mg}|^2}{(\nu_{mg} - \nu)^2} \sim \frac{\varepsilon_{\text{max}}(\bar{\nu}_{mg}) \Delta\bar{\nu}_{mg}}{\bar{\nu}_{mg} (\bar{\nu}_{mg} - \bar{\nu})^2}$$

where $\varepsilon_{\text{max}}(\bar{\nu}_{mg})$ and $\Delta\bar{\nu}_{mg}$ are the maximum absorption coefficient and halfwidth of the transition $m \leftarrow g$, respectively.

Fig. 5.8 shows the σ_2 of the series of free base porphyrins and Zn(II) metalloporphyrins measured at 650 nm plotted as a function of linear absorption parameters $\varepsilon_{\text{max}}(\bar{\nu}_{mg}) \Delta\bar{\nu}_{mg} / \bar{\nu}_{mg} (\bar{\nu}_{mg} - \bar{\nu})^2$ [cm mM⁻¹]. For simplicity, it is assumed that $\Delta\bar{\nu}_{mg}$ is constant since the systems are similar and the concentration of the solutions (influencing the broadening of the absorption profiles) are of the same order.

Considering the simplification of the equation, a rather linear dependence of the σ_2 on the resonance factor comprising of a combination of linear absorption parameters (Refer to Fig. 5.8) was obtained for the series of free bases and Zn(II) metalloporphyrin complexes except for Zn(II) 5,15-diphenylporphyrin. The deviation of Zn(II) 5,15-diphenylporphyrin from the dependence for other porphyrin compounds further confirms the presence of additional factors contributing to the nonlinear absorption like the ESA as explained earlier. This result substantiates the conclusion that there is indeed a quantitative relation between σ_2 and the resonance enhancement factor, $|\mu_{mg}|^2 / (\nu_{mg} - \nu)^2$. This also confirms the validity of the three-level model and supports our conclusion that there is small variation of $|\mu_{fm}|^2 g(2\nu)$ for the molecules studied.

5.1.5 DISCUSSIONS

All the porphyrin compounds (summarized in Table 5.1) except **4-5** analyzed at 650 nm in CHCl_3 solutions exhibit self-defocusing (n_2 is negative). Such materials are usually more desirable in power limiting applications than self-focusing types because the latter often leads to laser damage.⁴

The Zn(II) metalloporphyrin coordination complexes assembled from unbrominated ligands show larger merit factor than those derived from the brominated ligands. The overall conformation of the molecules also plays a role in affecting the TPA properties of the molecules which was clearly shown by the significant differences in the σ_2 of the free base porphyrins, **4-6** and **4-7**. The optical nonlinearity of the coordination complexes is affected by the overall architecture even though there is no direct conjugation between the monomeric units. This can be attributed to the presence of

some π - π interactions between the monomers in solution especially in the cofacial dimer **4-16** which exhibits the largest merit factor in the series studied. This was clearly illustrated by comparison of the NLO studies of Zn(II) 5,15-diphenylporphyrin as reference compound which nonlinear absorption property was determined to be partly complicated by the presence of RSA mechanism. This study reveals the stability of the architecture of the coordination complexes in CHCl_3 solution which was supported by time-variable ^1H NMR studies. Therefore, the Zn(II) metalloporphyrin coordination complexes formed by Zn-O bonds show great potential as TPA core for photosensitizing applications.¹⁰ The TPA properties of these complexes are expected to be further enhanced through the incorporation of photoactive moieties (refer to Chapter 9 for illustration) which serve to excite the porphyrin core through fluorescence resonance energy transfer (FRET).¹¹ This can be carried out by chemical modification of the porphyrin core at the unsubstituted *meso* C, since facile bromination can be carried out at these atoms.

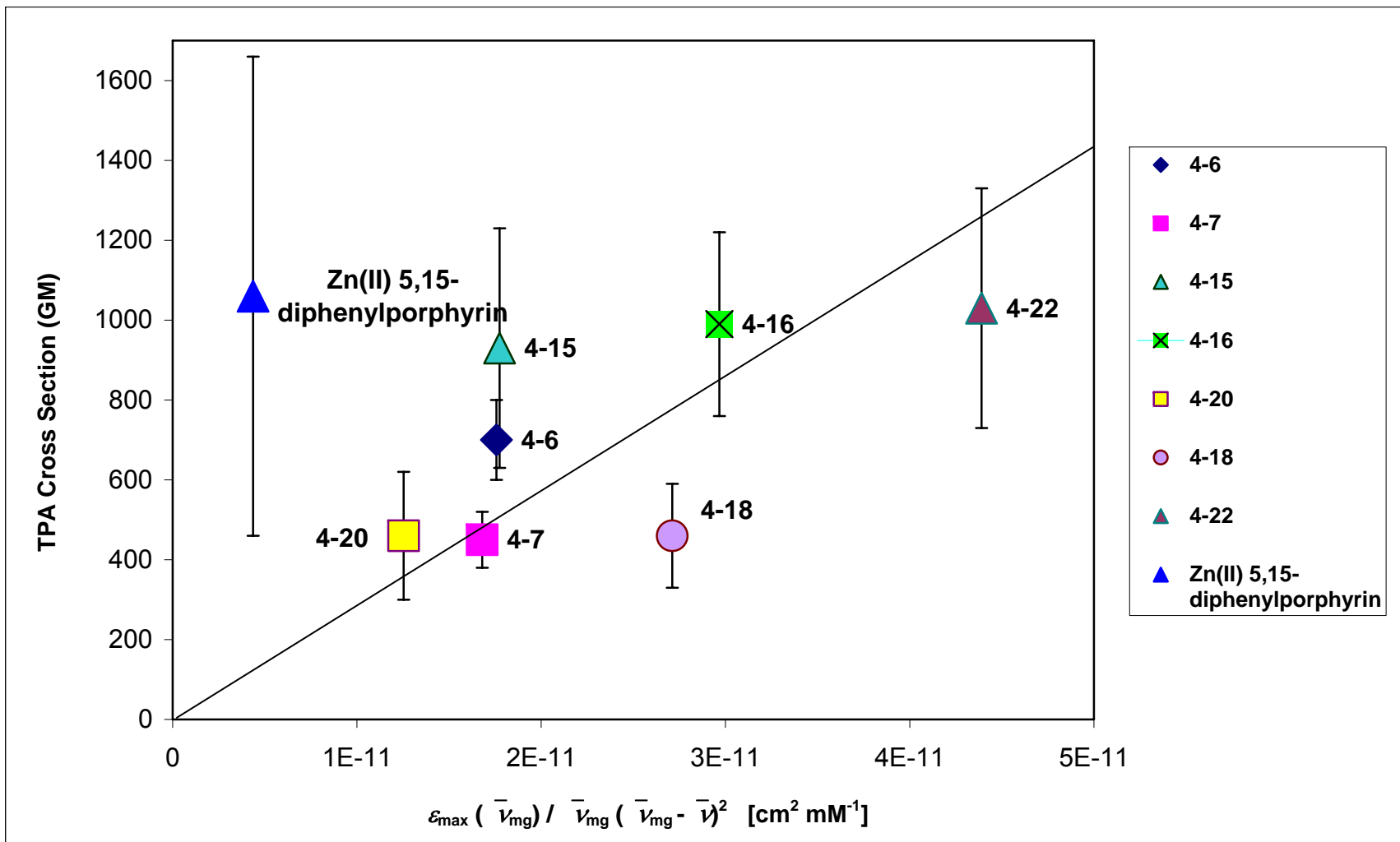


Fig. 5.8 Correlation between the σ_2 and a combination of linear absorption parameters for a series of free base porphyrins and Zn(II) metalloporphyrin dimers and polymers

5.1.6 WAVELENGTH DISPERSION OF THE THIRD-ORDER NONLINEAR OPTICAL PROPERTIES OF 4-16

Although the third-order NLO properties of porphyrins have been widely investigated, many reports provide information on the σ_2 at a fixed wavelength only. Studies of the spectral dependences of σ_2 provide additional information on the atomic and molecular structures of compounds especially in centrosymmetric molecules since TPA allows transitions between states of the same parity.

Information on the nonlinear absorption can be extracted in an indirect way, by monitoring action spectra of upconverted fluorescence, or, by direct measurements, e.g. from open-aperture Z-scan experiments in solutions of investigated compounds.² The wavelength-dependent Z-scan experiments, while laborious help to achieve deeper understanding of the structure-property relationships because the dispersion study of the γ_{imag} and γ_{real} of the compound can be carried out concurrently.^{8c} Therefore, we conducted the study using the Zn(II) metalloporphyrins dimer with the largest σ_2 .

A saturated solution of **4-16** with a concentration of 4.86 mM (0.20 wt%) was prepared for Z-scan measurements. It was confirmed that the complex exist in dimeric form at this concentration by ¹H NMR analysis at different concentrations (Chapter 4, Section 4.3.3.1). At lower concentrations of 3.6 and 0.36 mM, the benzylic, methyl, one of the pyrrolic and phenyl protons are significantly shifted to higher fields as compared to its ligand.

Our spectral range was limited from 650 nm to 1180 nm (corresponding to the longest wavelength of the signal that the optical parametric amplifier can generate). The presence of OPA even by the tail of the first absorption band (first Q-band) can cause significant reduction of the transmittance of laser.

The Fig. 5.9 shows the experimental results obtained in the NLO studies. The χ_{real} and χ_{imag} values are plotted against wavelength. The sign of the β (and therefore χ_{imag}) is positive throughout the whole range, thus corresponding to nonlinear absorption. The values of χ_{real} are negative in most of the wavelength range. It needs to be stressed that the error margins are generally higher for χ_{real} than for χ_{imag} because the nonlinear absorption of the solvent is negligible in the wavelength and intensity ranges used in this work and thus, the nonlinear absorption of the dimer can be determined against null background. In contrast, the refractive nonlinearity of **4-16** is always measured as an increment to the sum of refractive nonlinearity of the solvent and of glass walls of the cuvette. In addition, the nonlinear refraction may contain contributions from slower (cumulative) effects due to the presence of two-photon excited states and their relaxation while the nonlinear absorption may contain higher order contributions in addition to the TPA. Nevertheless, it can be commented that the data points in Fig. 5.9 follow the Kramers-Kronig integral-type relation between the real and imaginary parts of susceptibilities to a certain extent.

To illustrate the resonance enhancement effect, a plot of σ_2 data points as a function of the transition frequency (rather than the laser frequency) is overlapped with the corresponding OPA in the Soret band region and in the Q-band regions shown in Fig. 5.10 The data shows that σ_2 in the Soret band region is considerably larger than that in

the Q-band region. However, the TPA spectrum of **4-16** does not reproduce the linear Soret band. The maximum σ_2 value of 1400 GM occurs at a higher frequency than the OPA Soret $B_x(0-0)$ transition. This may be explained by the fact that the dimer is centrosymmetric (or nearly centrosymmetric) in CHCl_3 solution, that is, the two porphyrins rings in the dimer are almost coplanar unlike in solid state. For centrosymmetric molecules, the selection rules for one- and two-photon dipole transitions are mutually exclusive.

At 800 nm, the dimer shows a large $\sigma_2 = 1400 \pm 350$ GM which gives σ_2/FW value of $2.3 \text{ GM mol g}^{-1}$. This value is likely to be resonantly enhanced. Also, it is the largest value obtained for a self-assembled cofacial Zn(II) metalloporphyrin coordination dimer bound by two Zn-O coordination bonds. As highlighted in Chapter 1, such self-assembled arrays have an advantage over structures constructed via direct covalent bonding as the latter are relatively difficult to realize on a practical scale and pose a problem if eventually used for real applications.

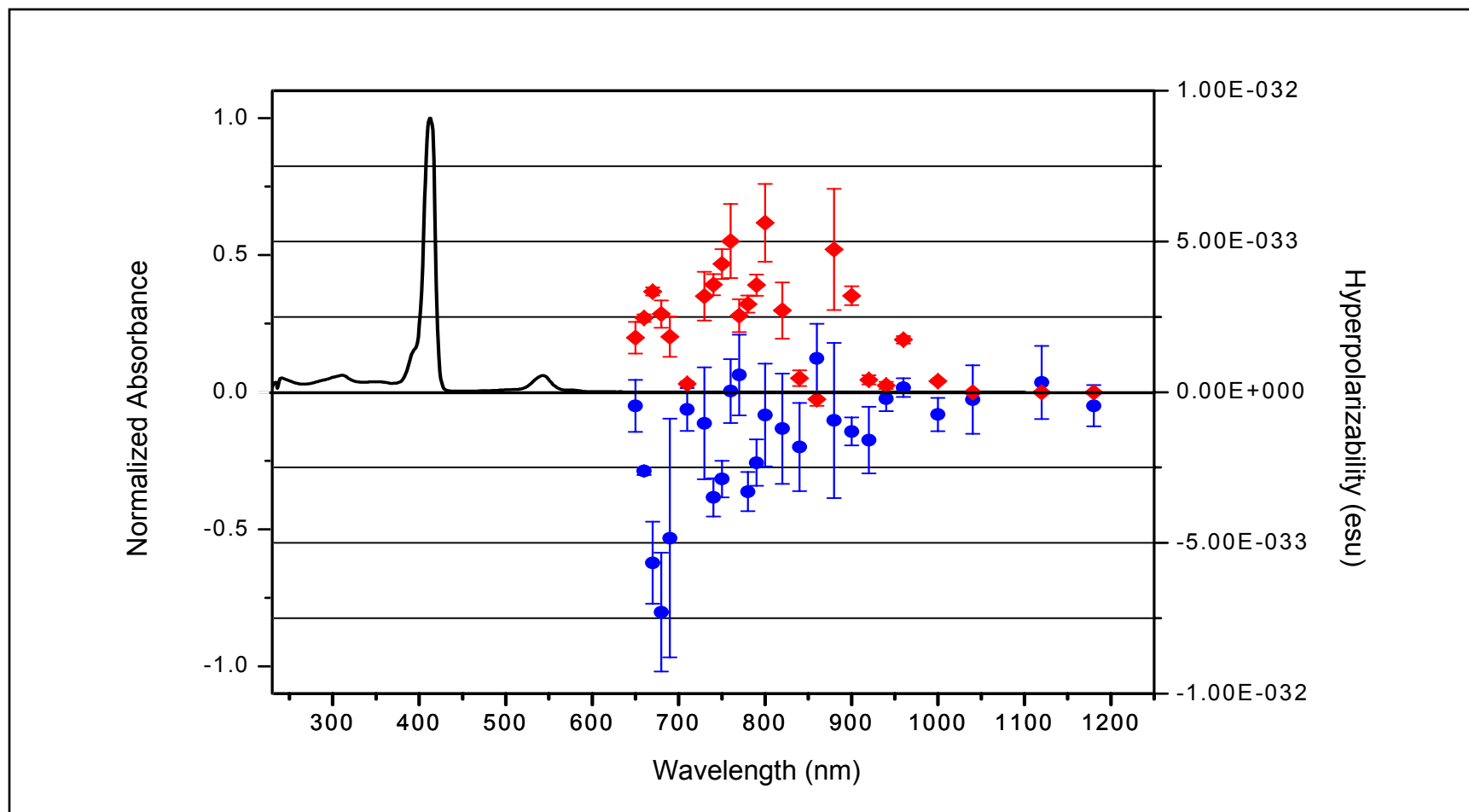


Fig. 5.9 The experimental values of γ_{real} (blue line) and γ_{imag} (red line) for **4-16**.
The absorption spectrum of a dilute solution of **4-16** in CHCl_3 is also shown

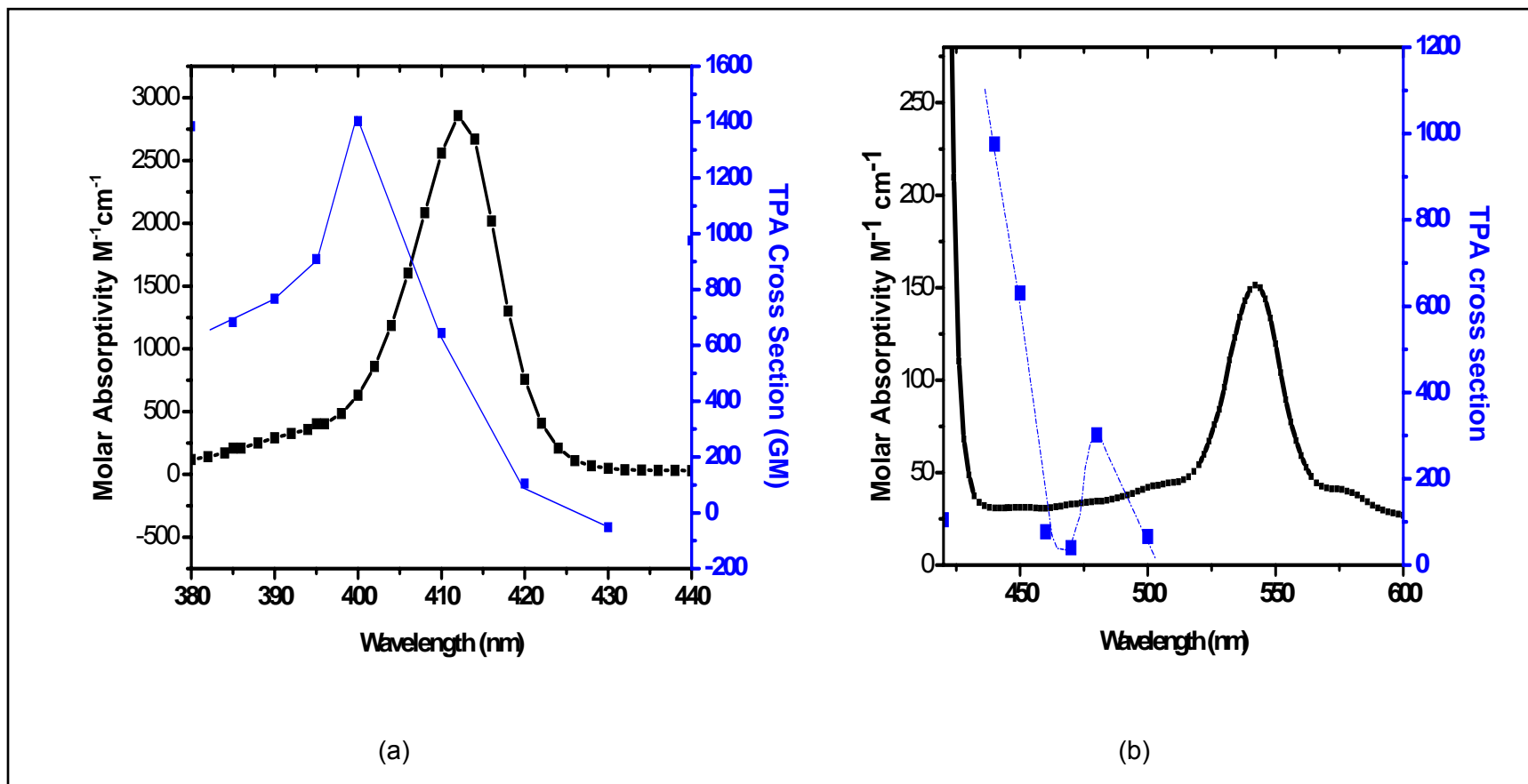


Fig. 5.10 One photon (black line) and two photon (blue line) absorption spectra in the a) Soret and b) Q-band regions

Since the ground level has g parity and the two-photon transitions from the ground levels are allowed only into other g parity levels, the described observation can be qualitatively explained by the presence of two-photon allowed g states lying higher in energy than the Soret transition (Fig. 5.10). The σ_2 values at a frequencies close to (but higher than) the OPA Q(0-0) transition are significantly lower than those near the Soret band and this pattern has been similarly observed in other tetrapyrrolic compounds. The strong TPA in the dimer excited at 800 nm is thus strongly resonance enhanced and largely contributed by the $B_x(0-0)$ transition rather than the Q(0-0) transition.

In order to explain the large σ_2 in Soret region, one has to take into account that if the laser excitation frequency ω is close to the frequency of some real intermediate transition ω_{mg} , then strong resonance enhancement of two-photon absorption takes place. From observation of Fig. 5.9, the large σ_2 and broad two-photon absorption band of the dimer at around 800 nm suggests that there are one-photon forbidden but two-photon allowed transitions in the Soret band region which are not observable in the linear absorption spectrum. Hence, the large σ_2 is probably due to strong $g \leftarrow g$ transitions.

In comparison to a self-assembled Zn(II) metalloporphyrin comprising of bis(imidazolylporphyrin), which reportedly possess the highest σ_2 for a measured with femtosecond pulses),¹² the dimer **4-16** shows a poorer two photon absorptivity. The σ_2/FW value of 2.3 GM mol g^{-1} is 2.4 times lower than that value of 5.64 GM mol g^{-1} (calculated based on the reported value of σ_2). However, it should be highlighted that the reported compound requires purification by GPC, which possess a great difficulty in the large scale preparation of the compound. Whereas, all the compounds synthesized in

our thesis can be purified using column chromatography. Hence, further exploration can be carried out to optimize the TPA properties of the Zn(II) metalloporphyrins (elaborated in Chapter 9) based on the structure-property relationships established in this work.

5.2 CONCLUSION

A variety of unique architectural structures of Zn(II) metalloporphyrin coordination complexes formed by self-assembly were obtained through the formation of Zn-O coordination bonds from their respective free bases. Structural modifications to the porphyrin rings yielded coordination complexes with different architectures that affected their overall optical nonlinearity. The architectures of all the coordination complexes have been established prior to the determination of their NLO properties, unlike studies involving cooperative enhancement through random aggregates formation in solutions. Some groups have attempted to increase the σ_2 through cooperative effects by forming molecular aggregates in solutions and ligation.¹³ In addition, the retention of the supramolecular architecture in CHCl_3 solution was confirmed from their ^1H NMR studies.

These Zn(II) metalloporphyrin complexes and unbrominated free bases exhibit negative χ_{real} when at 650 nm in CHCl_3 solution. The factors that affect the σ_2 include the polarity of the molecules, presence of Zn(II) metal atom and the heavy Br atom, as well as the overall geometry of the coordination complexes. The relatively higher σ_2 of monomeric Zn(II) 5,15-diphenylporphyrin as compared to the Zn(II) metalloporphyrin coordination complexes is found to be influenced by the strong ESA process, which complicated the nonlinear absorption processes of the former. This is evident from the deviation of the theoretical three-level model that relates σ_2 to OPA parameters and the

experimental errors that accompanied the open aperture measurements. The well-fitted dependence of these parameters for the whole series of centrosymmetric compounds studied in this work shows the validity of the simple model which can be adopted for future studies of a similar class of compounds.

The wavelength dispersion study of **4-16** demonstrates the TPA spectrum of the dimer. The largest σ_2 of 1400 ± 350 GM corresponding to the laser excitation wavelength of 800 nm, is close to the one-photon absorption Q(0-0) transition and was attributed to strong $g \leftarrow g$ transitions. This study also revealed the centrosymmetry of the dimer in solution.

5.3 REFERENCES

¹ Sheikh-Bahae, M.; Said, A.A. Wei, T.; Hagan, D.J. Van Stryland, E.W. *IEEE J. Quant. Electron.* **1990**, *26*, 760.

² Samoc, M.; Samoc, A.; Luther-Davies, B.; Bao, Z.; Yu, L.; Hsieh, B.; Scherf, U. *J. Opt. Soc. Am. B.* **1998**, *15* (2), 817.

³ (a) Butcher, P.N.; Cotter, D. “*The Elements of Nonlinear Optics*”, 1990, Cambridge University Press, Cambridge. (b) Boyd, R.W. “*Nonlinear Optics*”, 1992, San Diego, Academic Press.

⁴ Hagan, D.J., Van Stryland, E.W., Soileau, M.J., Wu, Y.Y., Guhu, S. *Opt. Lett.* **1988**, *13*, 315.

⁵ Kiran, P.P.; Reddy, D.R.; Dharmadhikari, A.K.; Maiya, B.G.; Kumar, G.R.; Rao, D.N. *Chem. Phys. Lett.* **2006**, *418*, 442.

- ⁶ (a) McEwan, K.; Lewis, K.; Yang, G.; Chng, L.; Lee, Y.; Lau, W.; Lai, K. *Adv. Funct. Mater.* **2003**, *13*, 863. (b) Ai, X.; Jin, R.; Ge, C.; Wang, J.; Zou, Y.; Zhou, X.; Xiao, X. *J. Chem. Phys.* **1997**, *106*, 3387.
- ⁷ Irvine, M.P.; Harrison, R.J.; Strahand, M.A.; Beddard, G.S. *Ber. Bunsenges. Phys. Chem.* **1985**, *89*, 226.
- ⁸ (a) Drobizhev, M.; Stepanenko, Y.; Dzenis, Y.; Karotki, A.; Rebane, A.; Taylor, P.N.; Anderson, H.L. *J. Phys. Chem. B* **2005**, *109* (15), 7223. (b) Drobizhev, M.; Stepanenko, Y.; Dzenis, Y.; Karotki, A.; Rebane, A.; Taylor, P.N.; Anderson, H.L. *J. Am. Chem. Soc.* **2004**, *126* (47), 15352. (c) Powell, C.E.; Morrall, J.P.; Ward, S.A.; Cifuentes, M.P.; Notaras, E.G.A.; Samoc, M.; Humphrey, M.G. *J. Am. Chem. Soc.* **2004**, *126* (39), 12234.
- ⁹ Drobizhev, M.; Karotki, A.; Kruk, M.; Rebane, A. *Chem. Phys. Lett.* **2002**, *355*, 175.
- ¹⁰ (a) Frederiksen, P.K.; McIlroy, S.P.; Nielson, C.B.; Nikolajsen, L.; Skovsen, E.; Jørgensen, M.; Mikkelsen, K.V.; Ogilby, P.R. *J. Am. Chem. Soc.* **2005**, *127*, 255. (b) Niedre, M.; Patterson, M.S.; Wilson, B.C. *Photochem. Photobiol.* **2002**, *75* (4), 382.
- ¹¹ (a) Dichtel, W.R.; Serin, J.M.; Edder, C.; Fréchet, J.M.J.; Matuszewski, M.; Tan, L-S.; Ohulchansky, T.Y.; Prasad, P.N. *J. Am. Chem. Soc.* **2004**, *126*, 5380. (b) Oar, M.A.; Serin, J.M.; Dichtel, W.R.; Fréchet, J.M.J.; Ohulchansky, T.Y.; Prasad, P.N. *Chem. Mater.* **2005**, *17*, 2267.
- ¹² (a) Ogawa, K.; Ohashi, A.; Kobuke, Y.; Kamada, K.; Ohta, K. *J. Am. Chem. Soc.* **2003**, *125*, 13356. (b) Ogawa, K.; Ohashi, A.; Kobuke, Y.; Kamada, K.; Ohta, K. *J. Phys. Chem. B* **2005**, *109*, 22003.
- ¹³ (a) Collini, E.; Ferrante, C.; Bozio, R. *J. Phys. Chem. B* **2005**, *109*, 2. (b) McRae, E.G.; Kasha, M. *J. Chem. Phys.* **1958**, *28*, 721. (c) Screen, T.E.O.; Thorne, J.R.G.; Denning, R.G.; Bucknall, D.G.; Anderson, H.L. *J. Mater. Chem.* **2003**, *13*, 2796.

CHAPTER 6

CONJUGATED COVALENT PORPHYRIN SYSTEMS AS NONLINEAR OPTICS MATERIALS

6.0 INTRODUCTION

Conjugated systems comprising of porphyrin as building block are of interest because such π -systems are highly polarizable and possess the advantages of the molecule of porphyrin as nonlinear optical (NLO) materials. Thus, large values of third-order susceptibility $\chi^{(3)}$ can be achievable. In our work, we have designed and synthesized a series of conjugated systems consisting of porphyrins as building blocks. The porphyrins are configurational and conformational isomers of one another. A comparison study between the conjugated systems comprising of the conformational isomers is of interest because of the differences in the polarities of the isomers that in turn affect their overall NLO properties.

Till date, linear porphyrin arrays linked by butadiyne are shown to exhibit high $\chi^{(3)}$ values which are among one of the largest for organic materials.¹ Several modifications have since been carried out, such the extension of the two-dimensional conjugation to improve the NLO properties.^{1b} However, one of the important characteristics of a molecule that influence the $\chi^{(3)}$ is its polarity which is characterized by the dipole moment. Hence, the geometry of the monomers in the conjugated system with respect to each other can in fact be varied and studied for their difference in NLO properties. For instance, in the recent works of Osuka *et al.*² where they demonstrated a strong

correlation between the dihedral angle of porphyrin units in a conjugated system with their two-photon absorption (TPA) properties. However, most research has been focused on the studies of linear porphyrins arrays linked via single³ or triple bonds¹ from opposite *meso* C atoms or via their peripheral phenyl rings at the *para* positions of the latter. This is partly because of the ease of purifying the synthesized porphyrins since isomers do not form.

Although acetylene-linked porphyrin polymers remain as one of intensively studied compounds for NLO applications because of their high $\chi^{(3)}$, most research works are still concentrated on linear conjugated systems. Hence, it is of interest to study acetylene-linked systems with conjugation that projects in greater through space dimensions.

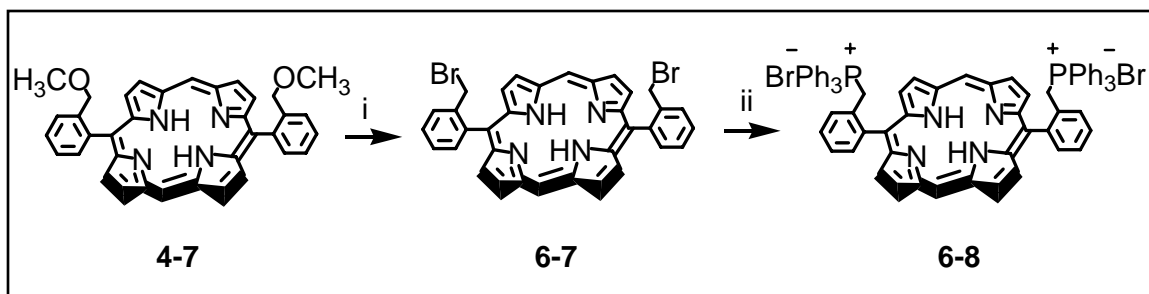
In our work, the broad absorption bands of porphyrin-based conjugated compounds render them unsuitable for Z-scan measurements, as the latter is a transmission technique. The degenerate four-wave mixing (DFWM) technique was thus adopted to study the third-order NLO property of these polymers in the form of thin films. The disadvantage of using such a technique is the necessity to use relatively larger amounts of sample to obtain thin films of the sample. Also, obtaining homogeneous thin films of the material pose a challenge, especially when the processability of the polymers is low and the evaporation of solvent often leads to formation of solid particles on the glass support. In addition, the glass support itself exhibits optical nonlinearity. Hence, this property of the material has to be sufficiently stronger in order for the measurements to be taken. This can be overcome by spin-coating a thick sample of the material but it also increases the possibility of light scattering through the sample as the laser light passes through it.

6.1.0 SYNTHESIS OF COVALENT PORPHYRIN SYSTEMS CONSISTING OF *CIS* AND *TRANS* PORPHYRIN MONOMERS

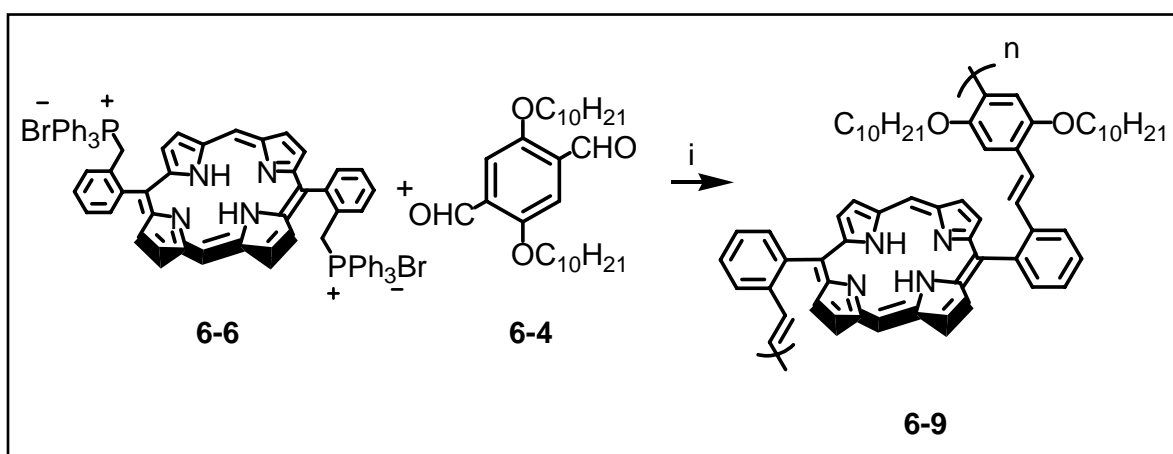
Two conjugated porphyrin systems are synthesized via Wittig coupling reaction of the phosphonium salt of porphyrin (**6-6**, **6-8**) and aromatic dialdehyde 2,5-bisdecyloxy-1,4-diformylbenzene (**6-4**) consisting of solubilizing long alkyl chains. The compound **6-4** was synthesized according to Scheme 6.1. The attachment of long alkyl chain to the phenyl rings was to aid their solubility in organic solvents for characterization and spin-coating of the materials. The porphyrin phosphonium salts, were first synthesized from **4-6** and **4-7** by nucleophilic substitution of the methoxy group to form **6-5** and **6-7** respectively. This was carried out by using excess gaseous HBr. Several attempts had been carried out. In aqueous HBr (48 %), the reaction did not occur even after the mixture was refluxed overnight and this was attributed to the insolubility of the macrocycle in aqueous medium. However, by dissolving in toluene and through vigorous stirring at room temperature for 24 hours, the reaction yielded only 61 % and 26 % of the mono and disubstituted compounds respectively.

The reaction of **6-5** and **6-7** with triphenylphosphine yielded the corresponding **6-6** and **6-8** phosphonium salts. Excess triphenylphosphine (4 equivalents) had to be added for the complete substitution of two Br atoms, otherwise a mixture of mono and disubstituted phosphonium salt will be obtained. Also, the reaction reached completion only after 3 days of stirring at a high temperature of 120 °C (Scheme 6.2, 6.3).

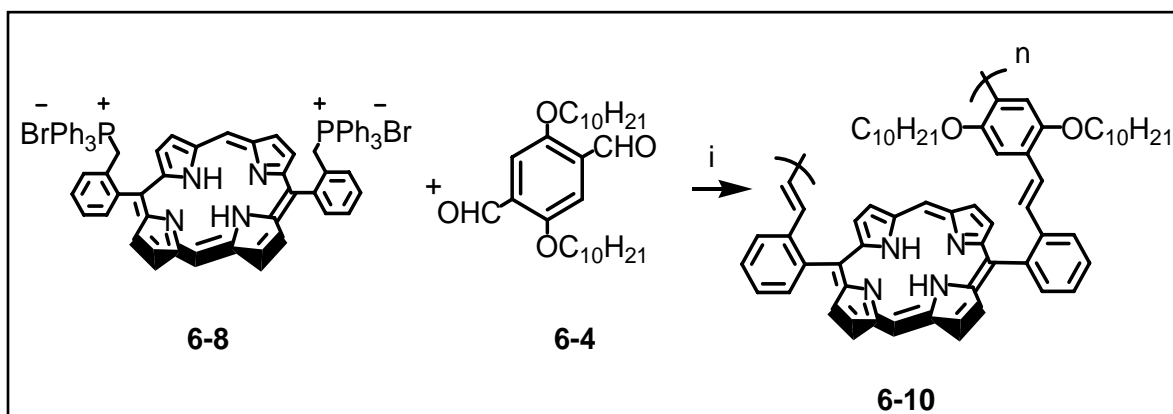
We attempted to prepare the conjugated system by switching the functionalities between the monomers. However, the conversion of the bromomethyl functionality on the phenyl ring of the porphyrin to aldehyde functional group was not successful. The



Scheme 6.3 i, HBr, CHCl₃; ii, PPh₃, DMF, 120 °C



Scheme 6.4 i, EtONa, CHCl₃



Scheme 6.5 i, EtONa, CHCl₃

6.1.1.0 CHARACTERIZATION OF CONJUGATED PORPHYRIN OLIGOMERS 6-9 AND 6-10

6.1.1.1 ^1H AND ^{13}C NMR ANALYSES

^1H NMR and ^{13}C NMR spectroscopy were used for the characterization of the molecular structures of the monomers and the conjugated *trans* (**6-9**) and *cis* (**6-10**) conjugated systems. From the ^1H NMR spectrum of **6-9**, we observe the presence of –PPh₃ end group. The –CH₂PPh₃ (δ 5.14) benzylic protons of the terminal group are shifted upfield compared to its monomer (δ 5.41). The broad multiplets (δ -0.20 – 3.74) in the high field region confirmed the presence of the aromatic phenyl monomer with solubilizing alkyl side chains. The –OCH₂– (δ 3.49, 3.72) side chain on the aromatic aldehyde is more shielded than in the monomer (δ 4.07) most probably because the protons lie above the anisotropic ring of the porphyrin. The singlets in the most shielded region of δ -3.22, -3.08 confirmed the presence of porphyrin due to the –NH protons in the inner core of the ring. The ^{13}C NMR spectrum of **6-9** revealed the presence of terminal –CHO (δ 189.8) group.

The ^1H NMR study of **6-10** displayed a similar spectrum with its *trans* counterpart. We observe the presence of –PPh₃ end group and the –CH₂PPh₃ (δ 5.11) benzylic protons of the terminal group are also shifted upfield compared to its monomer (δ 5.36). The broad multiplets (δ -0.20 – 3.46) in the high field region confirmed the presence of the aromatic phenyl monomer with solubilizing alkyl side chains. In addition, the –OCH₂– (δ 3.46) side chain is more shielded in the conjugated system than in the monomer (δ 4.07). The singlets in the most shielded region of δ -3.24, -3.19 confirmed the presence

of porphyrin due to the –NH protons in the inner core of the ring. The ^{13}C NMR spectrum of **6-10** confirmed the presence of terminal –CHO (δ 189) group.

6.1.1.2 ELEMENTAL ANALYSES

Elemental analyses were employed as the most accurate method to determine the purities of the obtained products. The experimental results showed that the conjugated systems agree well with the expected values of H and N contents as summarized in Table 6.1. The elements P and Br were too little to be traced.

Table 6.1 Calculated and experimental elemental analyses of **6-9** and **6-10**

	Elements [Calculated (%) / Found (%)]		
	C	H	N
6-9	82.63 / 80.16	7.61 / 7.25	6.22 / 6.11
6-10	82.63 / 82.64	7.61 / 7.67	6.22 / 6.29

6.1.1.3 FT-IR SPECTROSCOPY

The IR spectra of the *trans* conjugated system clearly shows the presence of *cis* alkene bond because of the relatively strong C=C stretching at around 1672 cm^{-1} (Fig. 6.1). The *cis* conjugated system shows the presence of *cis* alkene bond at C=C stretching of around 1680 cm^{-1} (Fig. 6.2).

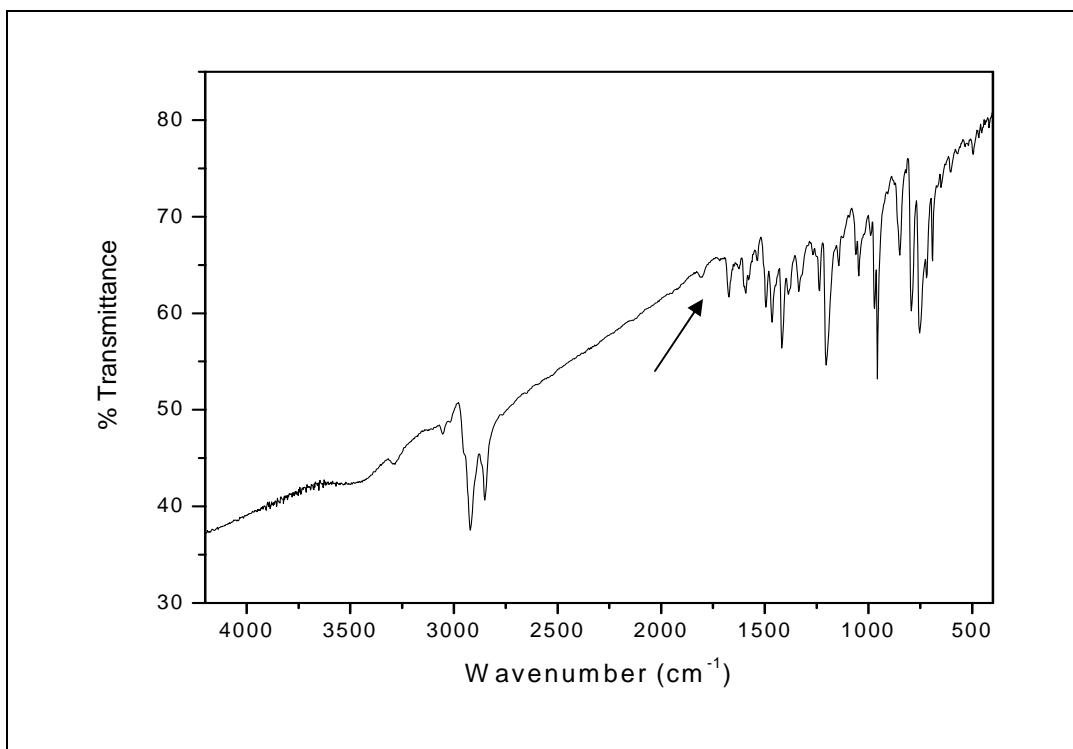


Fig. 6.1 IR spectrum of *trans* oligomer **6-9**. Arrow indicates *cis* C=C bond

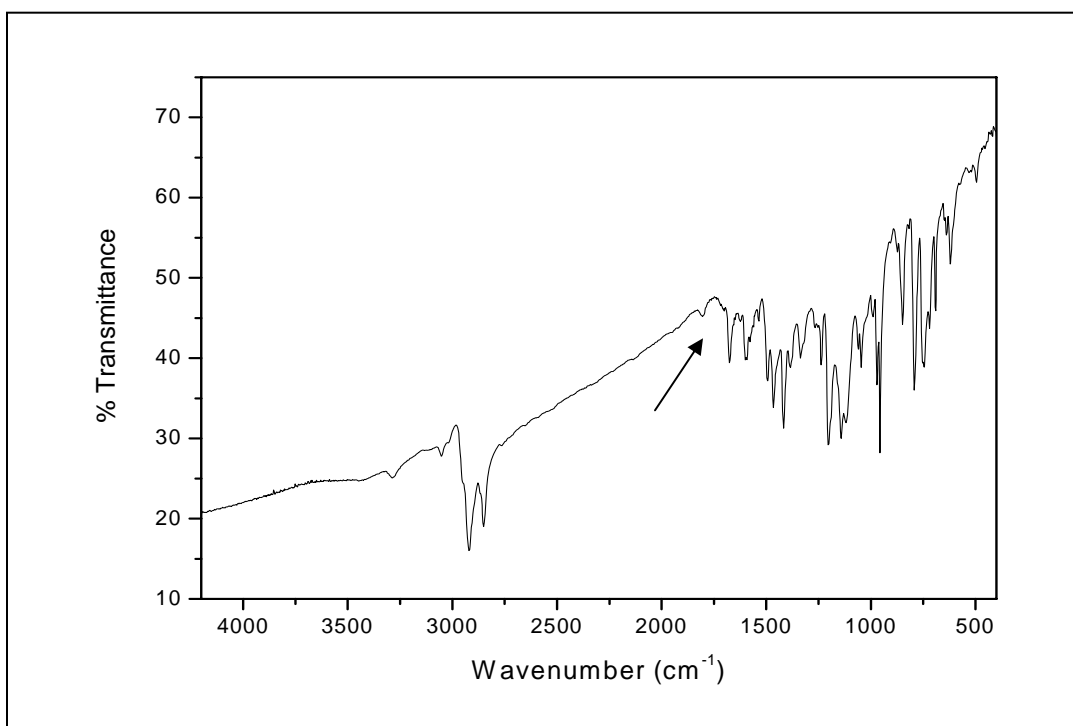


Fig. 6.2 IR spectrum of *cis* oligomer **6-10**. Arrow indicates *cis* C=C bond

6.1.1.4 MOLECULAR WEIGHT DETERMINATION

The molecular weights of the *trans* and *cis* systems were measured by means of gel-permeation chromatography (GPC) using THF as eluent and polystyrene as standard. A summary of their molecular weights and polydispersity indices (PDI) are listed in Table 6.2.

Table 6.2 Average molecular weights of oligomers **6-9** and **6-10** determined from GPC, using polystyrene as standard

	M_w	M_n	PDI
6-9	5800	5500	1.05
6-10	6000	5200	1.15

From the above results, both compounds have similar chain length and hence are suitable for comparison in further studies. Calculations show that the results corresponds to an average of around 5-6 repeating units in both compounds and can be considered as oligomers.

6.1.1.5 THERMAL ANALYSES

The thermal stability of the oligomers was studied. The oligomers **6-9** and **6-10** showed an onset decomposition temperature (T_d) of 291 °C and 213 °C respectively (Fig. 6.3). The thermally induced phase transition behaviour of the oligomers was also investigated with DSC but there was no detection of a distinct glass transition temperature (T_g) for both oligomers. The oligomer **6-10** starts to show weight loss before the temperature rises above 380 °C in nitrogen, indicating that thermal decomposition

occurred. However, there was no significant weight loss displayed by the oligomer **6-9** until the temperature was raised above 290 °C. In addition, the residual weight retention at 600 °C for both oligomers are approximately 55 %, implying that the oligomers possess relatively high thermal stability.⁴

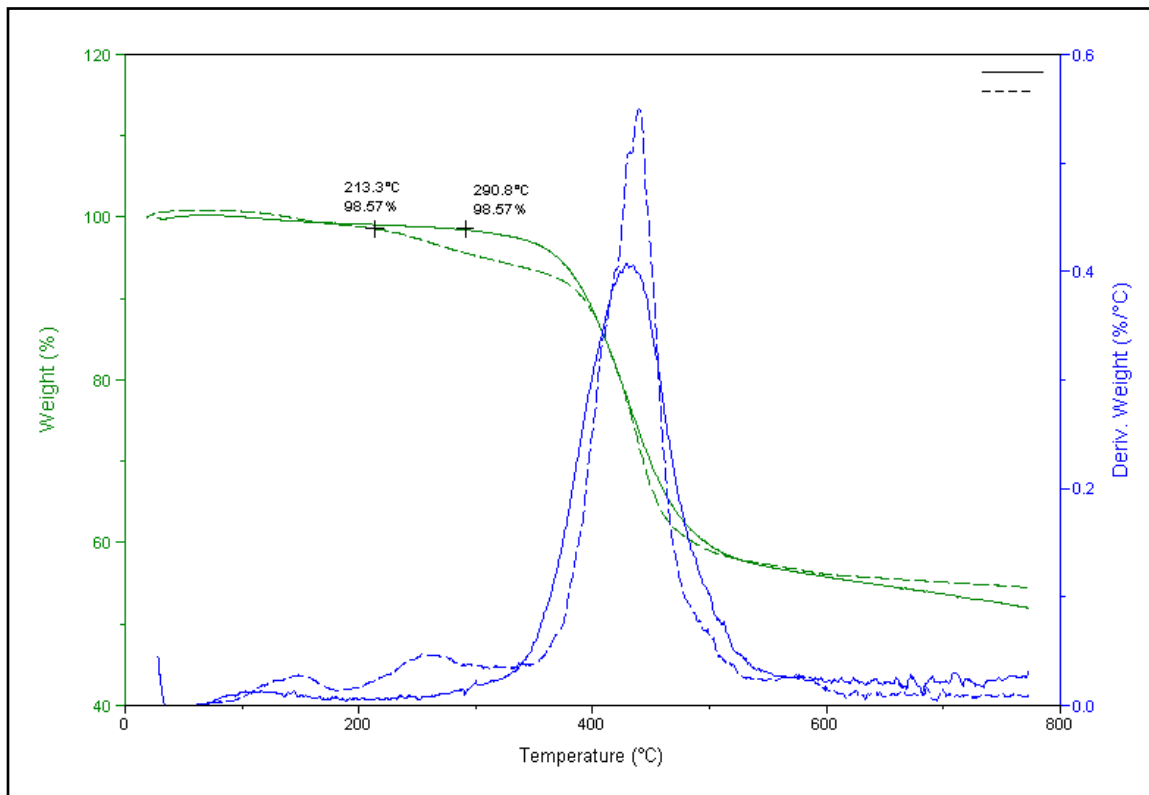


Fig. 6.3 TGA plots of **6-9** (bold lines) and **6-10** (dotted lines)

6.1.1.6 LINEAR OPTICAL PROPERTIES

The optical properties of the materials were investigated by UV-vis absorption and photoluminescence (PL) spectroscopy. The UV-vis spectrum of the oligomers (Fig. 6.4) in CHCl_3 displays a slight red-shift and intensification of the Q-band and a

broadening of the Soret band as compared to the porphyrin monomers at similar concentrations. This is associated with the strong electronic communication between the porphyrins. The oligomers do not exhibit significant fluorescence in solution.

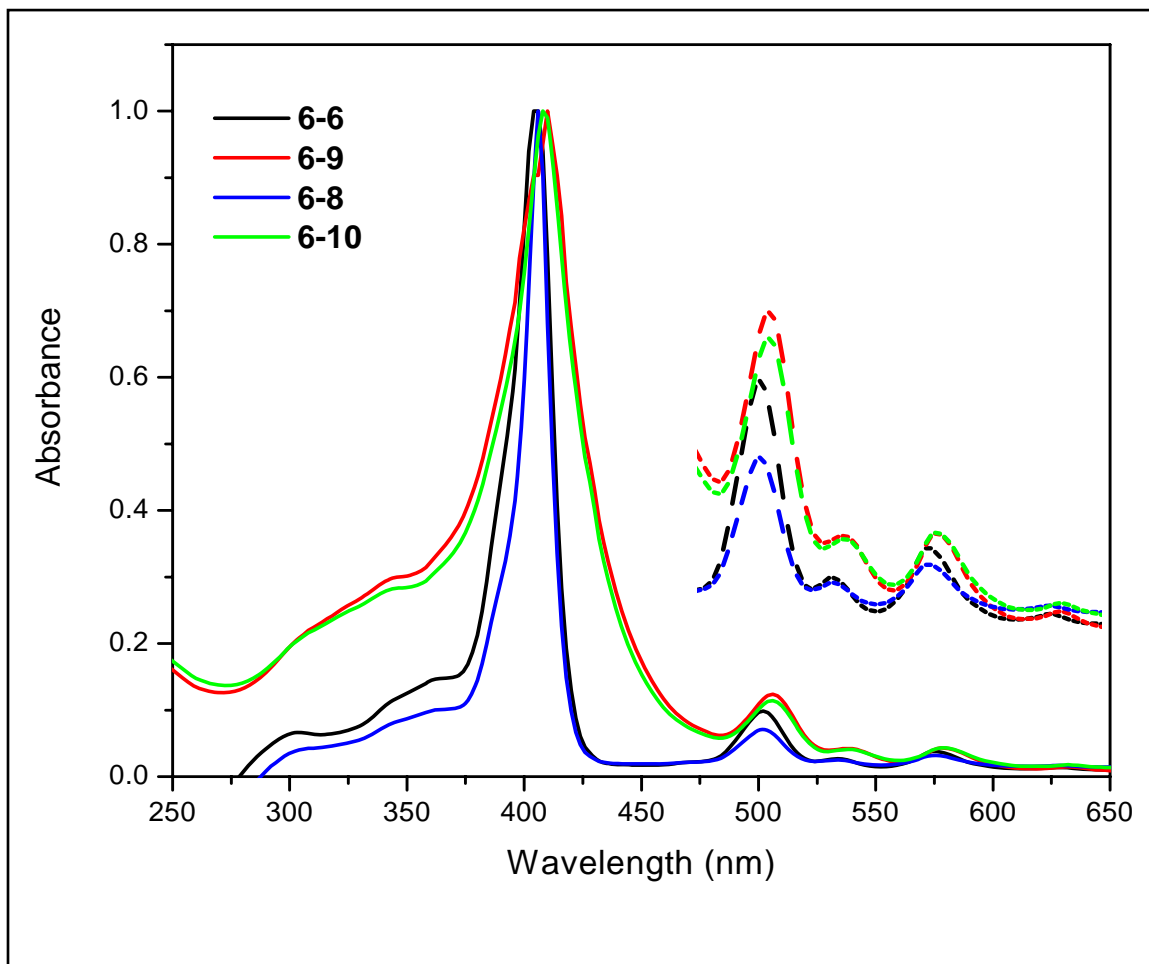


Fig. 6.4 UV-vis absorption spectrum of **6-6**, **6-8**, **6-9** and **6-10**.
Dotted lines show Q-bands amplified for clarity

The oligomers **6-9** and **6-10** have similar conjugation pattern but may vary slightly because of the difference in the dihedral angles of the peripheral phenyl rings. This is in turn affected by steric factors arising from the spatial arrangement of the phenyl rings. Steric hindrance is expected to be more predominant in the oligomer **6-10**

which comprise of the porphyrins in *cis* conformation. Hence, it is interesting to study the effect of porphyrin conformation on the overall NLO properties of a conjugated system.

An attempt was made to carry out the NLO measurement of these two conjugated systems. The Z-scan technique involves transmission measurement and requires a highly concentrated solution of the compound with low absorption in the laser excitation wavelength. The CHCl_3 solutions of these two compounds show large absorption even up to 1000 nm and hence were unsuitable for transmission measurements. Due to the small molecular weight of the oligomers, these compounds are not easily processable and do not form a homogeneous film with thickness suitable for DFWM measurements. Measurements of the sample at different thickness and higher laser light intensity did not yield results that is significantly different from the glass support. Hence, the technique was found to be unsuitable for the third-order NLO measurements of the materials. Therefore, nonlinear excited state measurements of the oligomers in diluted solutions were carried out and at an excitation wavelength of 532 nm where the absorption of the solution is low.

6.1.1.7 NONLINEAR OPTICAL PROPERTIES

The nonlinear transmission results obtained for the oligomers **6-9** and **6-10** using C_{60} as reference are presented in Fig 6.5. The compound C_{60} and its derivatives are often chosen as reference material because they are known to exhibit strong excited state absorption (ESA) and have been extensively studied.⁵ The transmission of the oligomers **6-9** and **6-10** decreases with input fluence, which is similar to that of C_{60} . Hence, the oligomers exhibit reverse saturable absorption (RSA).

Through extrapolation of the results shown in Fig. 6.5, we can see that with increase in input fluences, **6-10** exhibits significantly lower threshold for optical limiting (the input fluence where the linear transmission is 50 % of the initial one) as compared to **6-9**. Hence, the conformation of the porphyrin in the oligomer indeed affects the overall NLO properties. The more polar *cis* porphyrin moiety in **6-10** probably has a longer excited state lifetime than the *trans* counterpart in **6-9**. It is noteworthy to comment that the threshold of optical limiting of **6-10** is lower than that of C₆₀ and the latter is one of the best optical limiting materials known to this date.⁵

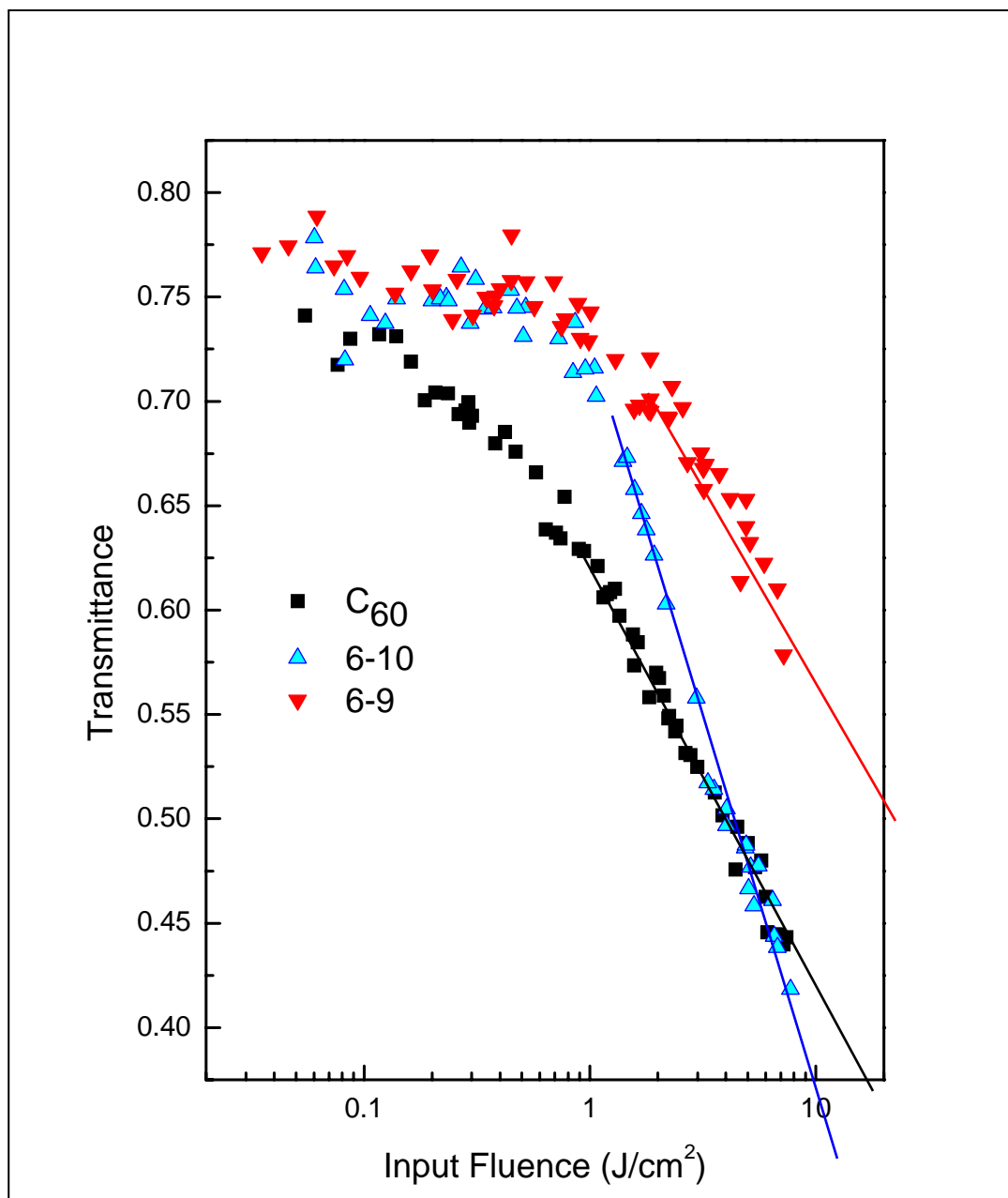
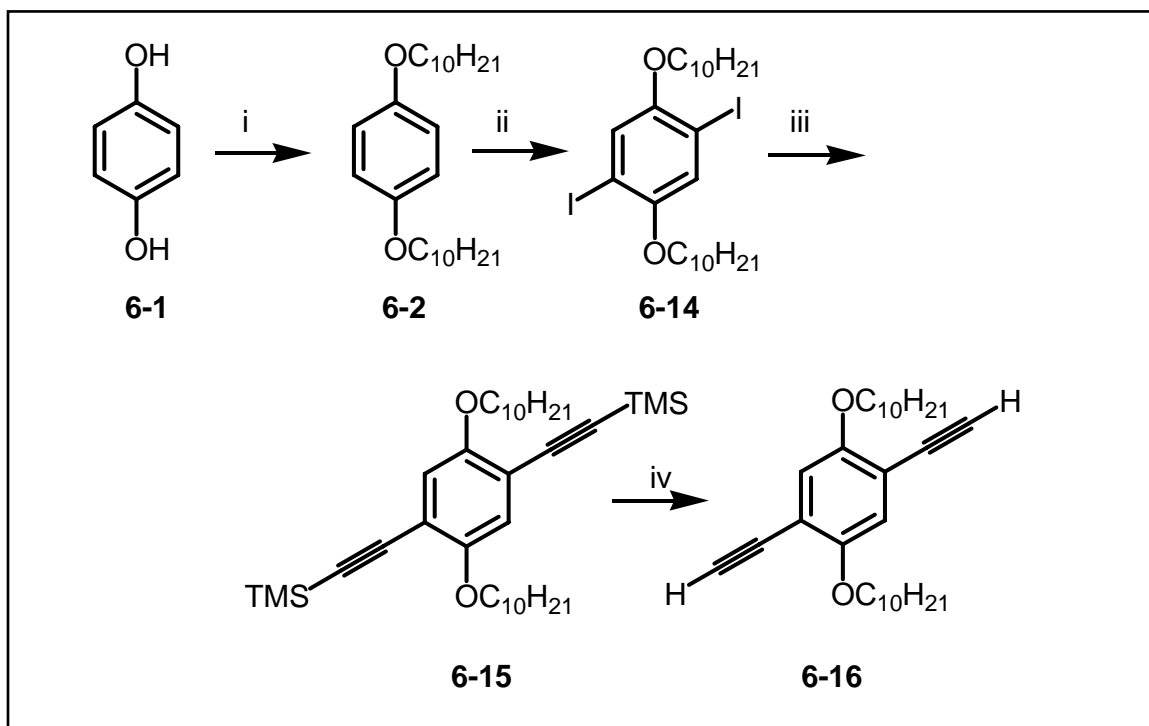


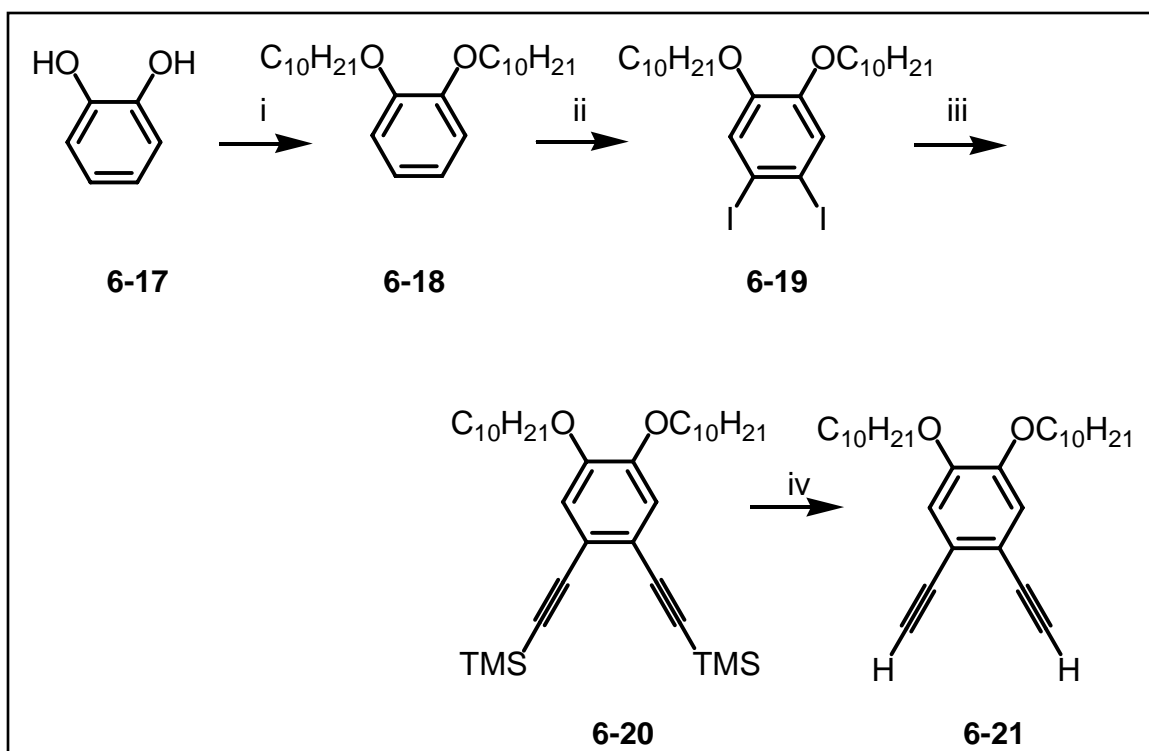
Fig. 6.5 Nonlinear transmission response of **6-9**, **6-10** and C_{60} in CH_2Cl_2 . Note that the line are drawn for extrapolation of input fluence at a transmission value of 0.375

6.2.0 CONJUGATED PORPHYRIN SYSTEMS WITH ARYL ACETYLENE LINKS

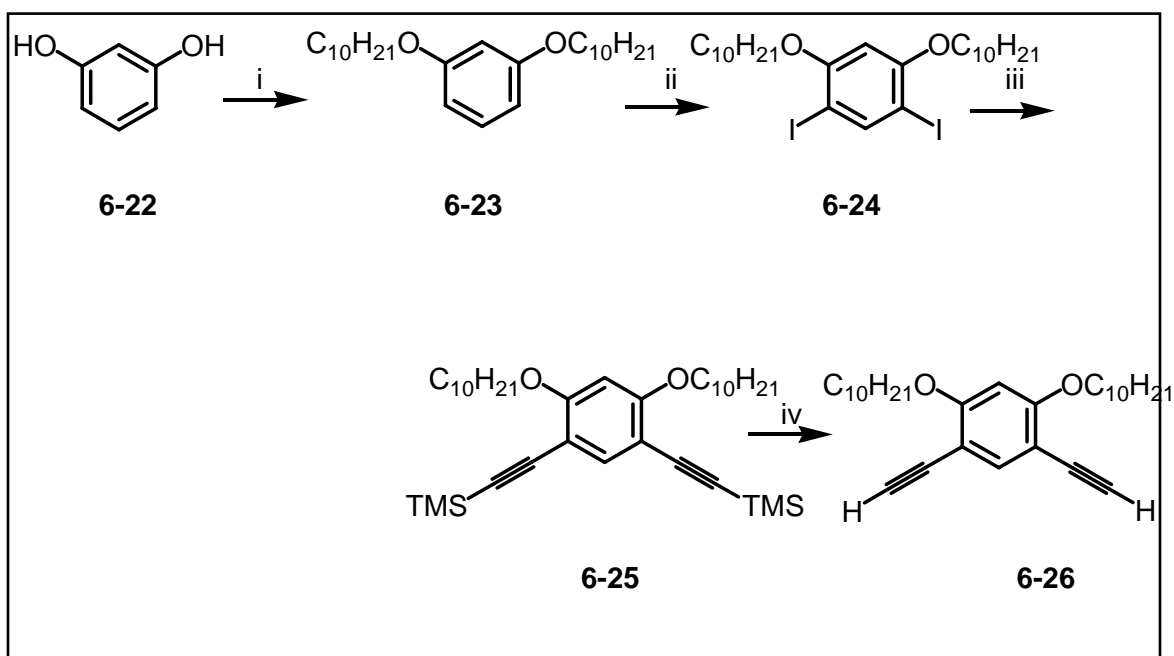
As mentioned earlier, acetylene-linked conjugated polymers of porphyrins are widely studied because of their exceptionally high value of $\chi^{(3)}$. Some examples of which has been cited in Chapter 1.^{1b,6} It will be interesting to investigate if the propagation of conjugation in space via covalent links will affect the overall NLO properties of the conjugated system. The direction of conjugation is varied by changing the attachment of acetylene bonds on the benzenoid monomer. The *para*, *ortho* and *meta* acetylene-directed benzenoid monomers are synthesized according to Schemes 6.6, 6.7 and 6.8 respectively. The Zn(II) metal atom was inserted into the porphyrin cavity before the polymerization step to avoid the possible insertion of Pd(II) metal atom from the catalyst into the cavity.



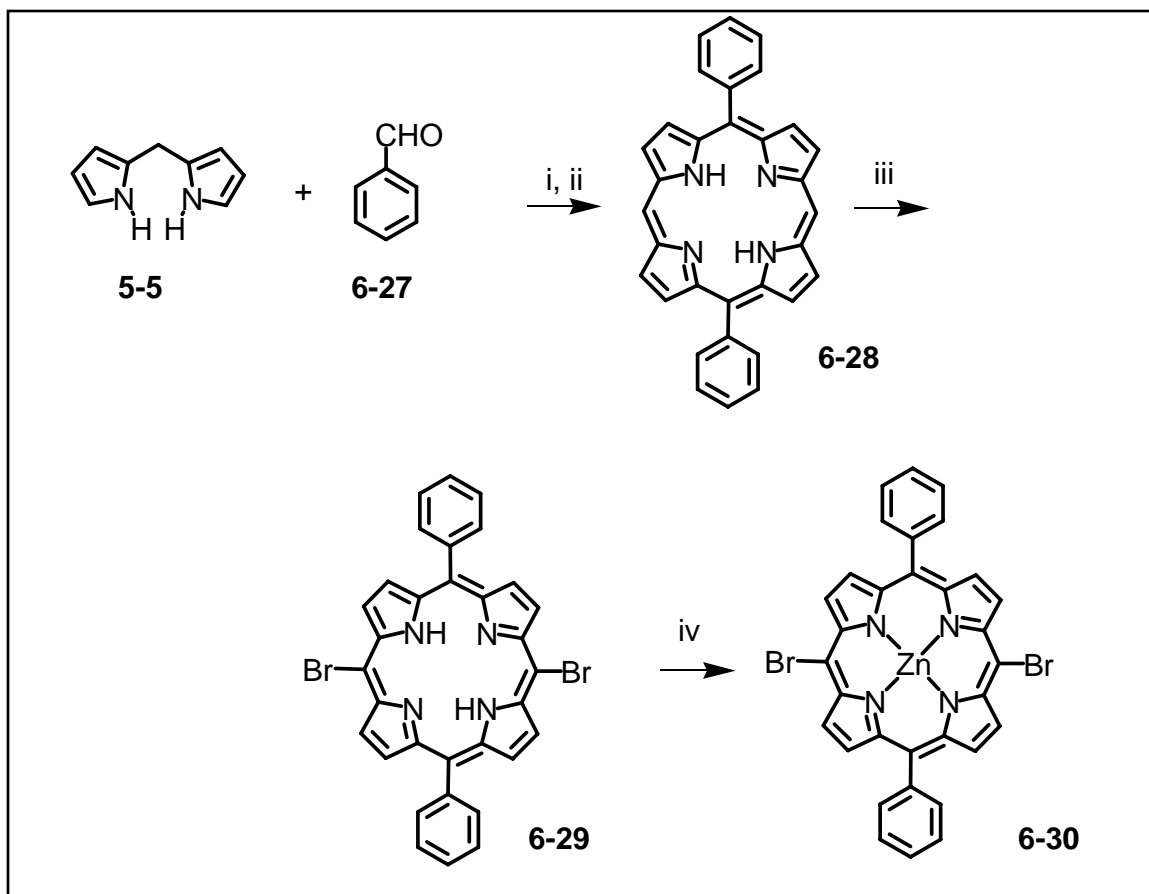
Scheme 6.6 i, KOH, EtOH, $C_{10}H_{21}Br$, reflux; ii, KIO_3 , I_2 , H_2SO_4 , CH_3COOH , 80 °C; iii, Et_3N , $PdCl_2(PPh_3)_2$, CuI , trimethylsilyl acetylene; iv, THF, MeOH, aq. NaOH



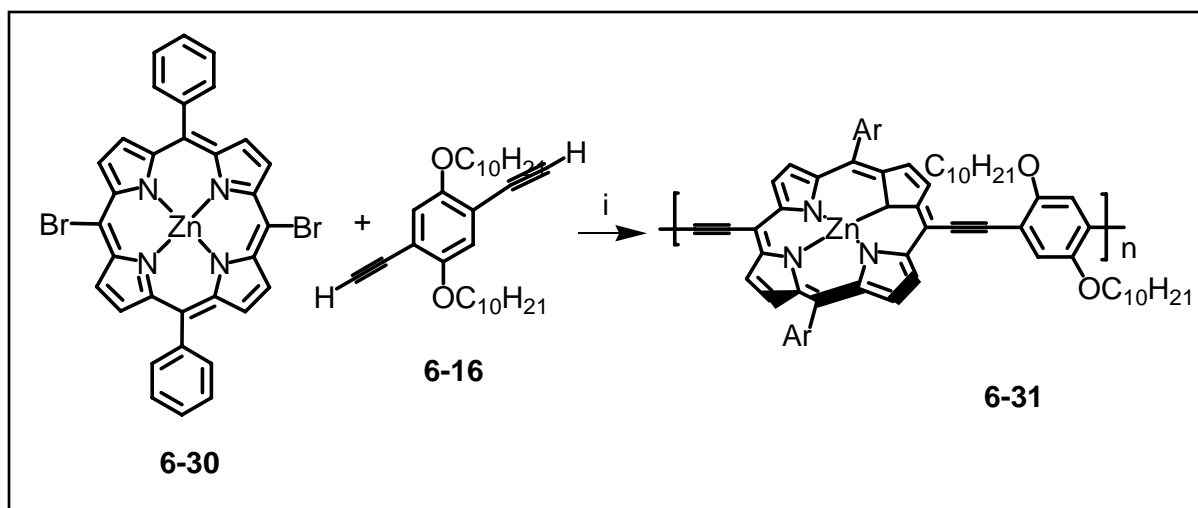
Scheme 6.7 i, KOH, EtOH, C₁₀H₂₁Br, reflux; ii, KIO₃, I₂, H₂SO₄, CH₃COOH, 80 °C; iii, Et₃N, PdCl₂(PPh₃)₂, CuI, trimethylsilyl acetylene; iv, THF, MeOH, aq. NaOH



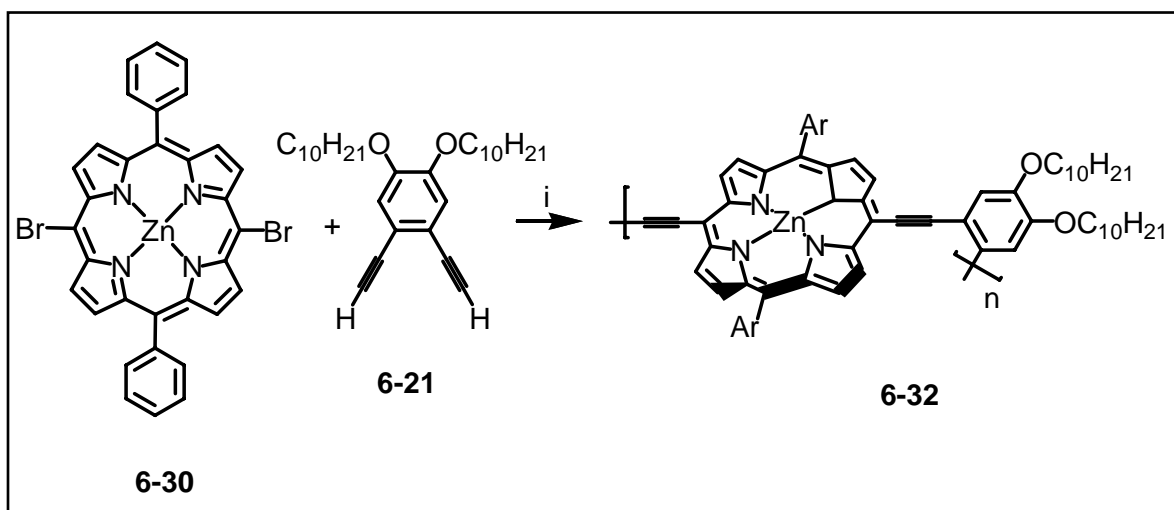
Scheme 6.8 i, KOH, EtOH, C₁₀H₂₁Br, reflux; ii, KIO₃, I₂, H₂SO₄, CH₃COOH, 80 °C; iii, Et₃N, PdCl₂(PPh₃)₂, CuI, trimethylsilyl acetylene; iv, THF, MeOH, aq. NaOH



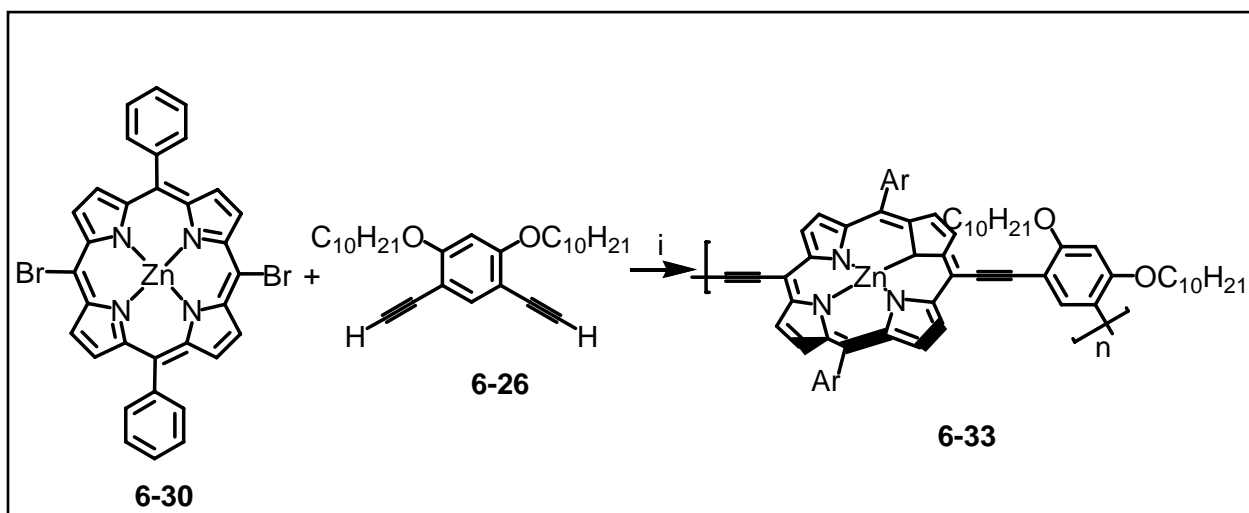
Scheme 6.9 i, $\text{CF}_3\text{COOH}/\text{CH}_2\text{Cl}_2$; ii, chloranil; iii, NBS, CHCl_3 , 0°C ; iv, $\text{Zn}(\text{OAc})_2 \cdot x\text{H}_2\text{O}$, THF



Scheme 6.10 i, $i\text{-Pr}_2\text{NH}$, $\text{PdCl}_2(\text{PPh}_3)_2$, CuI , toluene, 100°C



Scheme 6.11 i, *i*-Pr₂NH, PdCl₂(PPh₃)₂, CuI, toluene, 100 °C



Scheme 6.12 i, *i*-Pr₂NH, PdCl₂(PPh₃)₂, CuI, toluene, 100 °C

6.2.1.0 CHARACTERIZATION OF CONJUGATED PORPHYRIN SYSTEMS 6-31, 6-32 AND 6-33 WITH ARYL ACETYLENE LINKS

6.2.1.1 ^1H AND ^{13}C NMR ANALYSES

The ^1H NMR of the conjugated systems **6-31**, **6-32** and **6-33** are obtained by dissolving the compounds in CS_2 and d_5 -pyridine. Pyridine was added to ligate the Zn metalloporphyrin to prevent aggregation and aid in solubilizing the compounds. The spectra are consistent with the proposed structure. The ^1H NMR of **6-31** in CS_2 and d_5 -pyridine clearly shows the presence of porphyrin and phenyl constituents. The proton peaks in the conjugated system are broadened as compared to the monomers (note that the ^1H NMR spectrum of the monomers are measured in CDCl_3). The pyrrolic protons of the porphyrin in the conjugated system have shifted upfield because of the substitution of electron-withdrawing Br atom by acetylene. There are two singlets at δ 3.77 and 3.66 which can be attributed to the H of terminal acetylene group. There are no peaks in the shielded region below δ 1.00 hence the porphyrin did not undergo demetallation during the coupling reaction.

The ^1H NMR of **6-32** in CS_2 and d_5 -pyridine also shows the presence of porphyrin and phenyl constituents. The proton peaks in the conjugated system are less defined as compared to **6-31** probably because of the less rigid backbone of this system due to larger steric hindrance. The pyrrolic protons of the porphyrin in the conjugated system are broad but nevertheless, the phenyl proton peaks can be identified. There is one singlet at δ 3.58 which may be attributed to the H of terminal acetylene group. There are

no peaks in the shielded region below δ 1.00 hence the porphyrin also did not undergo demetallation during the coupling reaction.

The ^1H NMR of **6-33** in CS_2 and d_5 -pyridine clearly resembles that of **6-31** except in the protons of the phenyl ring. The proton peaks in the conjugated system are broadened as compared to the monomers. The pyrrolic protons of the porphyrin in the conjugated system have shifted upfield because of the substitution of electron-withdrawing Br atom by acetylene. There are two singlets at δ 3.76 and 3.67 which may be attributed to the H of terminal acetylene group. Similarly, the absence of ^1H peaks below δ 1.00 implies that the porphyrin did not undergo demetallation during the coupling reaction.

6.2.1.2 ELEMENTAL ANALYSES

The experimental formula showed that the conjugated systems agree within 3.2 % from the expected values of C, H, N and Zn contents. Trace amount of Br atom was detected for **6-33**.

Table 6.3 Calculated and experimental elemental analyses of **6-31**, **6-32** and **6-33**

	Elements [Expected (%) / Found (%)]				
	C	H	N	Zn	Br
6-31	77.52/74.35	6.51/6.74	5.83/5.41	6.81/4.86	Not detected
6-32	77.52/75.37	6.51/6.90	5.83/5.97	6.81/4.42	Not detected
6-33	77.52/77.06	6.51/6.29	5.83/5.85	6.81/4.42	2.59

6.2.1.3 FT-IR SPECTROSCOPY

The IR spectra of the conjugated system (Fig. 6.6) clearly show the presence of the alkyne bond. The relatively strong absorption of the C≡C stretching clearly shows that the disubstituted triple bond is not symmetrical and the conjugated system is alternating. The C≡C stretchings appear at 2184 and 2189 cm⁻¹ for **6-31** and **6-33** respectively but that of **6-32** is too weak to be observed. However, terminal *sp* C-H stretch at above 3300 cm⁻¹ is observed for all three compounds although the peaks are slightly obscured by O-H stretching from H₂O.

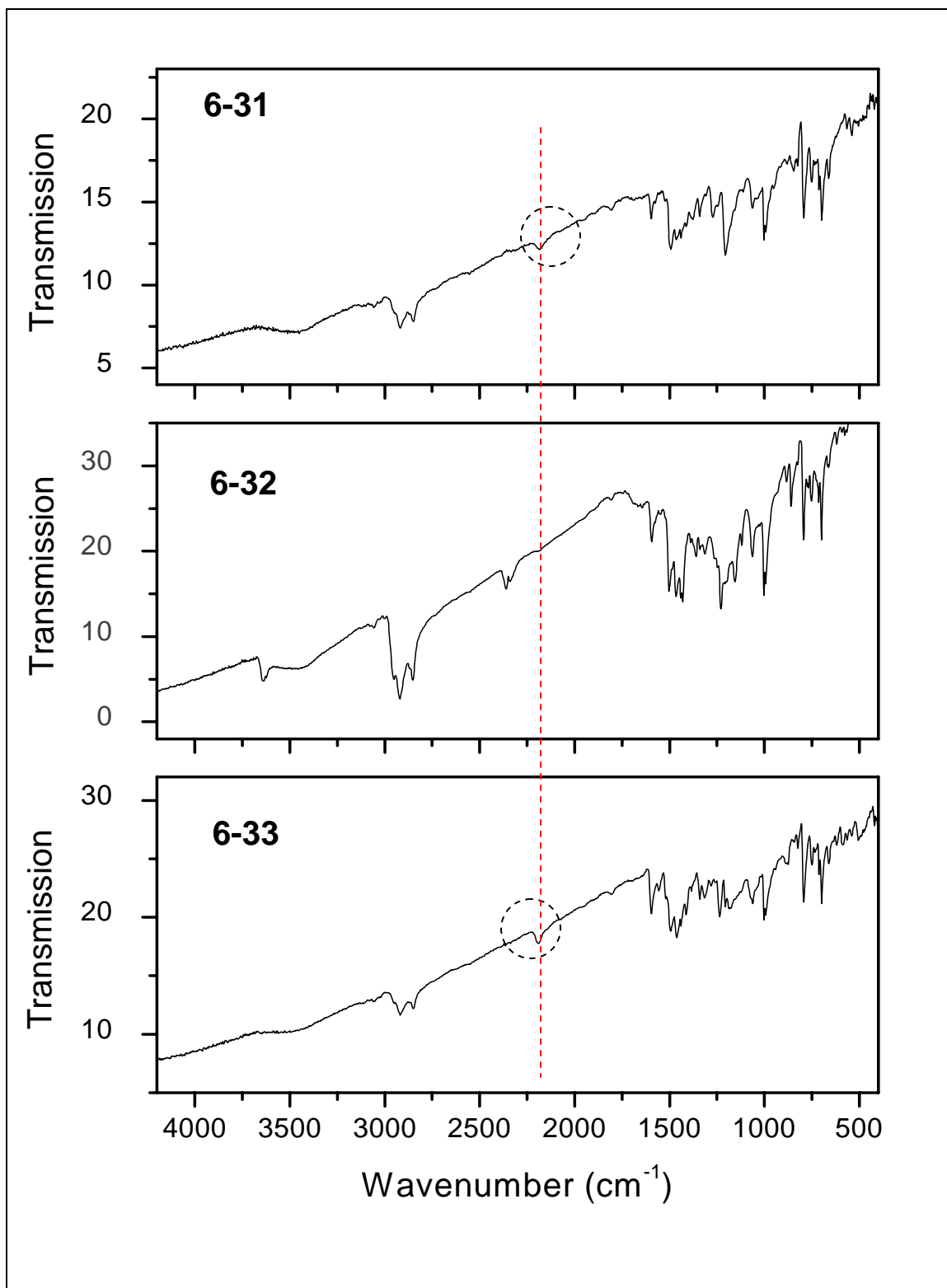


Fig. 6.6 IR spectrum of **6-31**, **6-32** and **6-33**

6.2.1.4 MOLECULAR WEIGHT DETERMINATION

The main advantage of **6-32** compared to **6-31** is the higher solubility. The conjugated system **6-31** is known to aggregate through π - π stacking hence resulting in insolubility. The insolubility of the compounds in common solvents prevented the determination of chain length by GPC. Hence, MALDI-TOF was used to determine the molecular weight of the compounds instead. The conjugated compounds were prepared in CS₂ and pyridine and added with dithranol matrix. A preliminary study on **6-32** shows that there is no significant change with or without pyridine hence, it may be assumed that evaporation of solvents involve the evaporation of pyridine and hence does not coordinate permanently to the Zn(II) metal atom in the compounds. Qualitatively, the compounds have similar molecular weight M_n of 4900 - 5300 g mol⁻¹ (Table 6.4) which comprise of about five repeating units and hence are oligomers. From the above results, the oligomers have similar chain lengths.

Table 6.4 Molecular weights of **6-31**, **6-32** and **6-33** based on the highest peak measured on MALDI-TOF

Compound	Molecular weight M _n (g mol ⁻¹)
6-31	5300
6-32	4900
6-33	5000

6.2.1.5 THERMAL ANALYSES

The thermal stability of the oligomers was studied and the TGA plots are shown in Fig. 6.7 below. The oligomer **6-32** started to show decomposition first with increase in temperature. The oligomers showed similar weight loss of 1 - 6 % before showing an onset decomposition of 281, 288 and 301 °C for **6-31**, **6-32** and **6-33** respectively. The residual weight retention at 600 °C for all three oligomers was above 60 %, which is an indication of good thermal stability.⁴ The thermally induced phase transition behaviour of the oligomers was investigated with DSC but they do not exhibit clear glass transition probably due to the low molecular weight of the compounds.

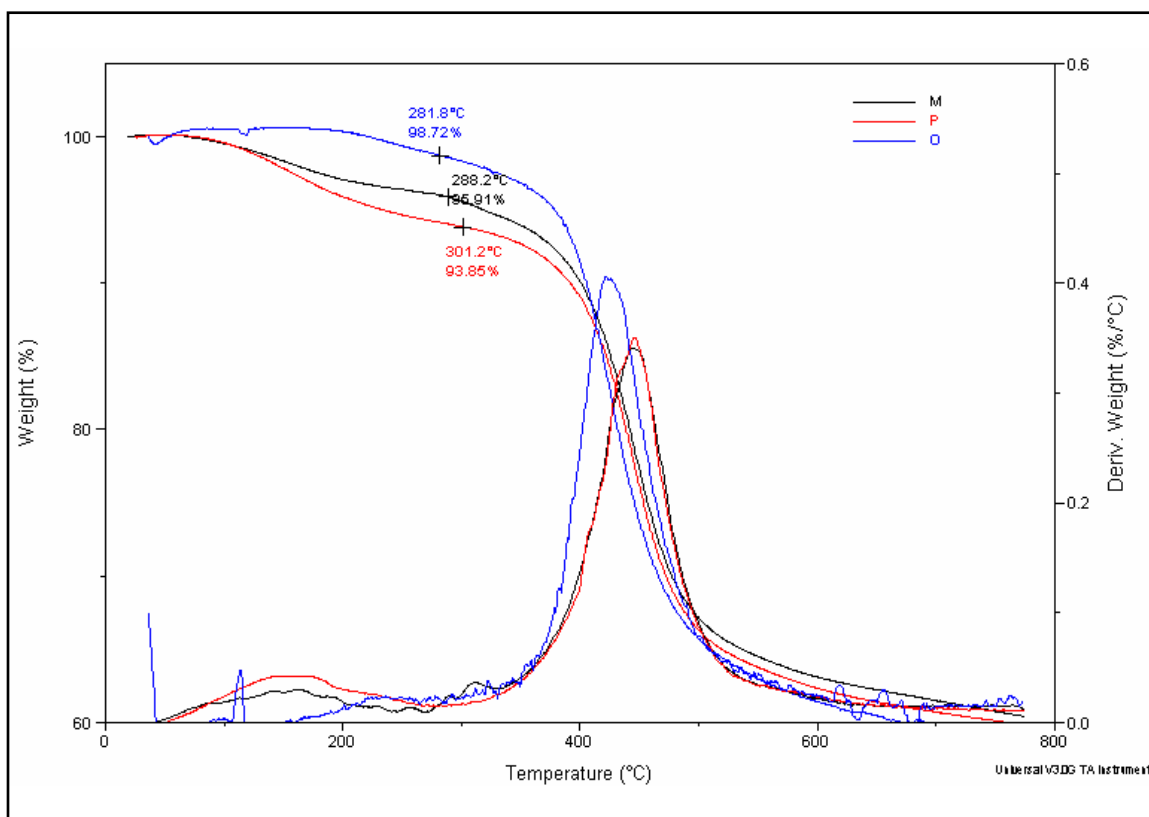


Fig. 6.7 TGA plots of **6-31** (red), **6-32** (blue) and **6-33** (black)

6.2.1.6 LINEAR OPTICAL PROPERTIES

The UV-vis spectrum of the oligomers (Fig. 6.8) was obtained in CS₂ and pyridine solutions. They display a slight red-shift of the Soret and Q-bands in comparison to their porphyrins monomers. The broad absorption band exhibited by **6-31** and **6-32** reveal the significant aggregation of the oligomers even in the presence of pyridine. The λ_{max} of the oligomer **6-32** showed the least red-shift, which implies poorer conjugation in the conjugated system. This is expected to be due to steric factors. The oligomers do not fluoresce and is most probably due to aggregation.

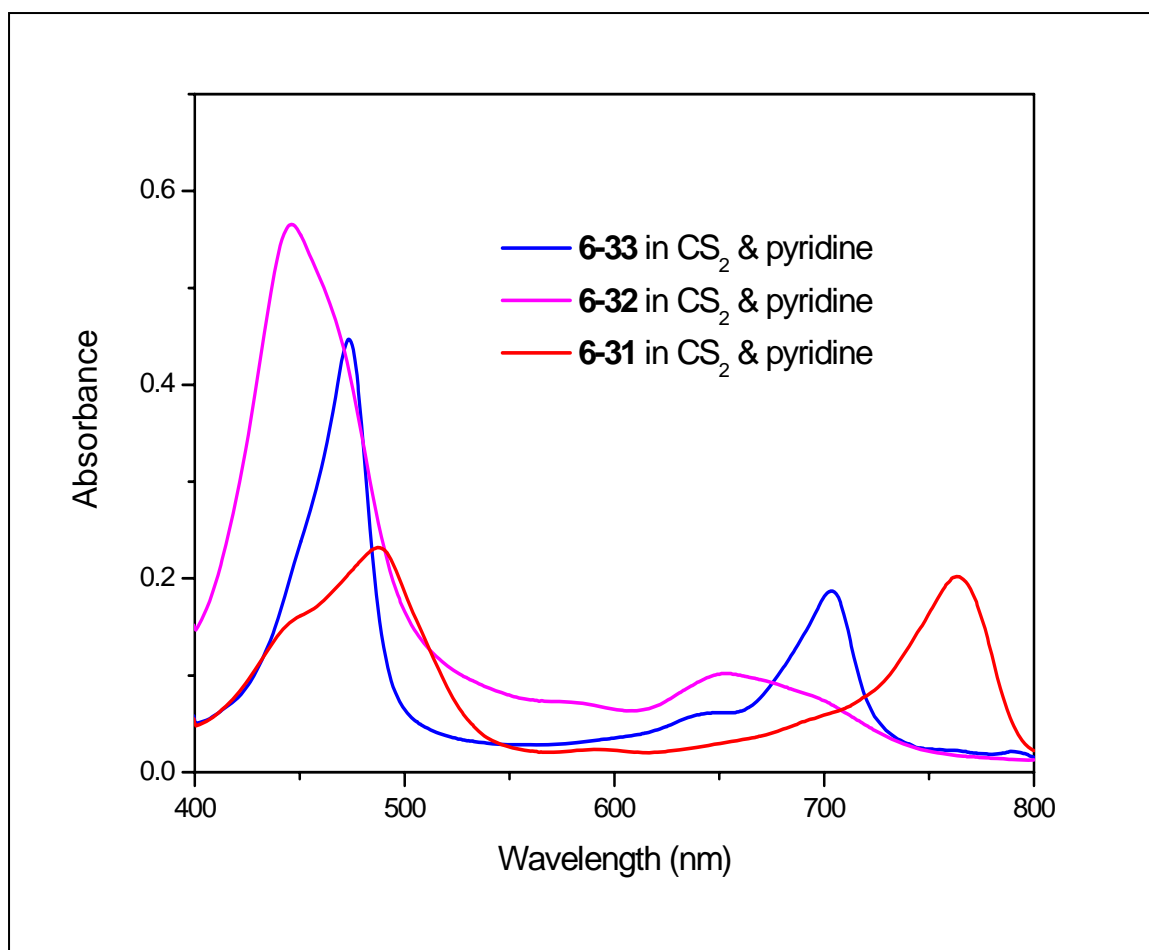


Fig. 6.8 UV-vis absorption spectrum of **6-31**, **6-32** and **6-33**

6.2.1.7 NONLINEAR OPTICAL MEASUREMENTS

As the oligomers **6-31**, **6-32** and **6-33** show strong absorption in the UV-vis region similar to that of **6-9** and **6-10**, the former are not suitable for Z-scan measurements using the available instruments also. However, thin films could be prepared could be prepared by drip-dry method where a concentrated CS₂/pyridine solution was introduced onto 1 mm thick silica plates and the solvents was allowed to evaporate off under nitrogen atmosphere.

The nonlinear measurements reveal the nonlinear responses of the oligomers which contain a delayed part. This is most probably attributed to nonlinear absorption or relatively long excitations that decay on a ps time scale. With the increase of the input power, the tail becomes more prominent. However, as the intensity increases further, the material showed signs of material burning (Fig. 6.9). Therefore, the nonlinear absorption properties and the photochemical instability of such acetylene-linked covalent oligomers of porphyrin and benzene are exhibited in all three systems under the measurement conditions. As the oligomers are only soluble in CS₂/pyridine solutions and CS₂ is known to show large nonlinear properties,⁷ the latter is likely to mask the signal from the oligomers, thus, nonlinear measurements of the solutions using Z-scan⁸ and DFWM techniques cannot be carried out.

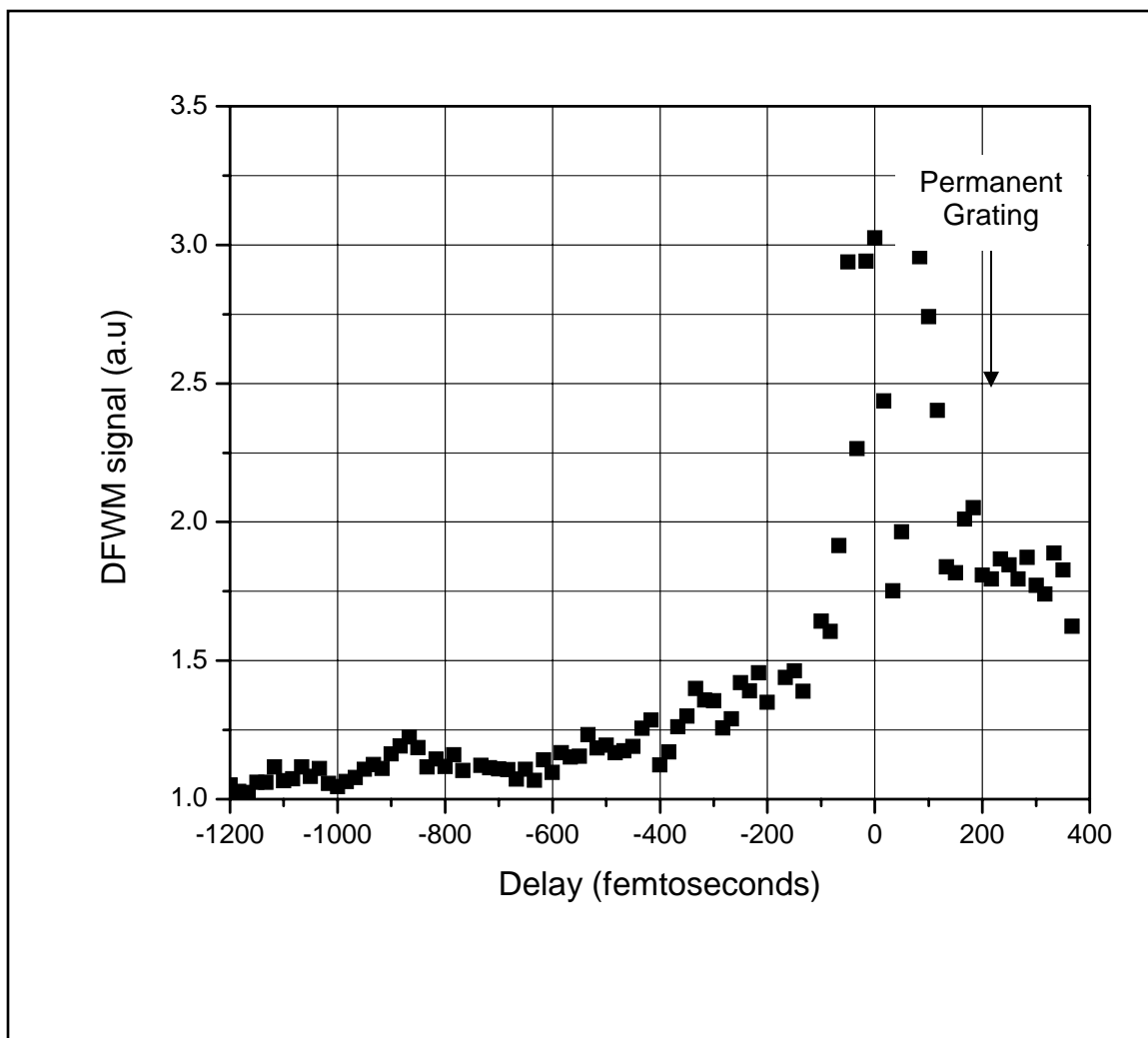


Fig. 6.9 DFWM signal at 800 nm for a film of **6-32** scanned from positive to negative delay times. The increase of the background signal at negative delays is due to formation of permanent grating

6.3 CONCLUSION

Section 1

Two conjugated oligomers consisting of porphyrin and aromatic ring with long alkoxy side chains linked by alkene double bonds have been synthesized and characterized using ^1H NMR, ^{13}C NMR, GPC, elemental analyses, FT-IR and UV-vis absorption spectroscopy. These two conjugated systems have similar conjugation pattern but differ in the spatial projection of the π -electron cloud due to the difference in the conformation of the porphyrin monomer. The excited state measurements of the oligomers in CH_2Cl_2 reveal that the conformation of the peripheral group on the porphyrin moiety in the conjugated system affects the nonlinear properties of the overall conjugated system. The oligomer **6-10** was found to exhibit lower threshold of limiting than **6-9** and C_{60} in CH_2Cl_2 solution.

Section 2

Three conjugated oligomers consisting of porphyrin and aromatic ring with long alkoxy side chains are linked by acetylene triple bonds that differ in the position at which the acetylene bonds are attached on the aromatic ring. These oligomers are not stable under laser light and show signs of burning and formation of permanent grating.

In conclusion, the oligomers presented in this chapter are not suitable for transmission measurements using Z-scan technique because the concentrated solutions of these oligomers absorb strongly in the excitation wavelength range of the laser, which limited the use of this technique. The poor processability of **6-9** and **6-10** made the

formation of thin film thick enough or DFWM measurements impossible. Although the oligomers **6-31**, **6-32** and **6-33** can form thin films on silica plates using drip-dry method, the materials exhibit poor photostability. Hence, the porphyrin-consisting oligomers presented in this Chapter are found to be less favourable for NLO measurements than the coordination complexes presented earlier in Chapter 4 and 5.

6.4 REFERENCES

¹ (a) Thorne, J.R.G.; Kuebler, S.M.; Denning, R.G.; Blake, I.M.; Taylor, P.N.; Anderson, H.L. *Chem. Phys.* **1999**, *248*, 181. (b) Screen, T.E.O.; Lawton, K.B.; Wilson, G.S.; Dolney, N.; Ispasoiu, R.; Goodson III, T.; Martin, S.J.; Bradley, D.D.C.; Anderson, H.L. *J. Mater. Chem.* **2001**, *11*, 312. (c) Ogawa, K.; Hasegawa, H.; Inabe, Y.; Kobuke, Y.; Inouye, H.; Kanemitsu, Y.; Kohno, E.; Hirano, T.; Ogura, S.; Okura, I. *J. Med. Chem. Art. No.* 10.1021/jm0506423. (d) Ogawa, K.; Ohashi, A.; Kobuke, Y.; Kamada, K.; Ohta, K. *J. Am. Chem. Soc.* **2003**, *125*, 13356. (e) Ogawa, K.; Ohashi, A.; Kobuke, Y.; Kamada, K.; Ohta, K. *J. Phys. Chem. B* **2005**, *109*, 22003.

² Ahn, T.K.; Kim, K.S.; Kim, D.Y.; Noh, S.B.; Aratan, N.; Ikeda, C.; Osuka A.; Kim, D. *J. Am. Chem. Soc.* **2006**, *128*, 1700.

³ Aratani, N.; Osuka, A.; Kim, Y.H.; Jeong, D.H.; Kim, D. *Angew. Chem. Int. Ed.* **2000**, *112*, 1517.

⁴ Ge, Z.Y.; Yin, D.X.; Liu, J.G.; Fan, L.; Yang, S.Y. *IEEE 6th Int. Conf. Elec. Packaging Tech.* **2005**.

⁵ (a) Meth, J.S.; Vanherzeele, H.; Wang, Y. *Chem. Phys. Lett.* **1992**, *197*, 26. (b) Kafali, Z.H.; Lindle, J.R.; Pong, R.G.S.; Bartoli, F.J.; Lingg, L.J. Milliken, J. *Chem. Phys. Lett.* **1992**, *188*, 492. (c) Harigaya, K.; Abe, S. *J. Luminescence* **1994**, *60-61*, 380. (d) Bindhu,

C.V.; Harilal, S.S.; Nampoory, V.P.N.; Vallabhan, C.P.G. *Appl. Phys. B* **2000**, *70*, 429. (e)

Elim, H.I.; Oyang, J.Y.; Goh, S.H.; Ji, W. *Thin Solid Films* **2005**, *477* (1-2), 63.

⁶ (a) Kuebler, S.M.; Denning, R.G.; Anderson, H.L. *J. Am. Chem. Soc.* **2000**, *122*, 339.

(b) Screen, T.E.O.; Thorne, J.R.G.; Denning, R.G.; Bucknall, D.G.; Anderson, H.L. *J. Am. Chem. Soc.* **2002**, *124*, 9712.

⁷ (a) Gnoli, A.; Razzari, L.; Righini, M. *Opt. Express*, **2005**, *13* (20), 7976. (b) Breitzer, J.G.; Dlott, D.D.; Iwaki, L.K.; Kirkpatrick, S.M.; Rauchfuss, T.B. *J. Phys. Chem. A* **1999**, *103*, 6930. (c) Fischer, G.L.; Boyd, R.W.; Moore, T.R.; Sipe, J.E. *Opt. Lett.* **1996**, *21* (20), 1643.

⁸ (a) Gnoli, A.; Razzari, L.; Righini, M. *Optics Express* **2005**, *13* (20), 7976. (b) Ganeev, R.A.; Ryasnyanskii, A.I.; Kuroda, H. *Optics Spec.* **2006**, *100* (1), 108.

CHAPTER 7

THIRD-ORDER NONLINEAR PROPERTIES OF THE BROMO BENZO[C]CINNOLINE MONOMER AND NOVEL FLUORENE- BENZO[C]CINNOLINE COPOLYMERS

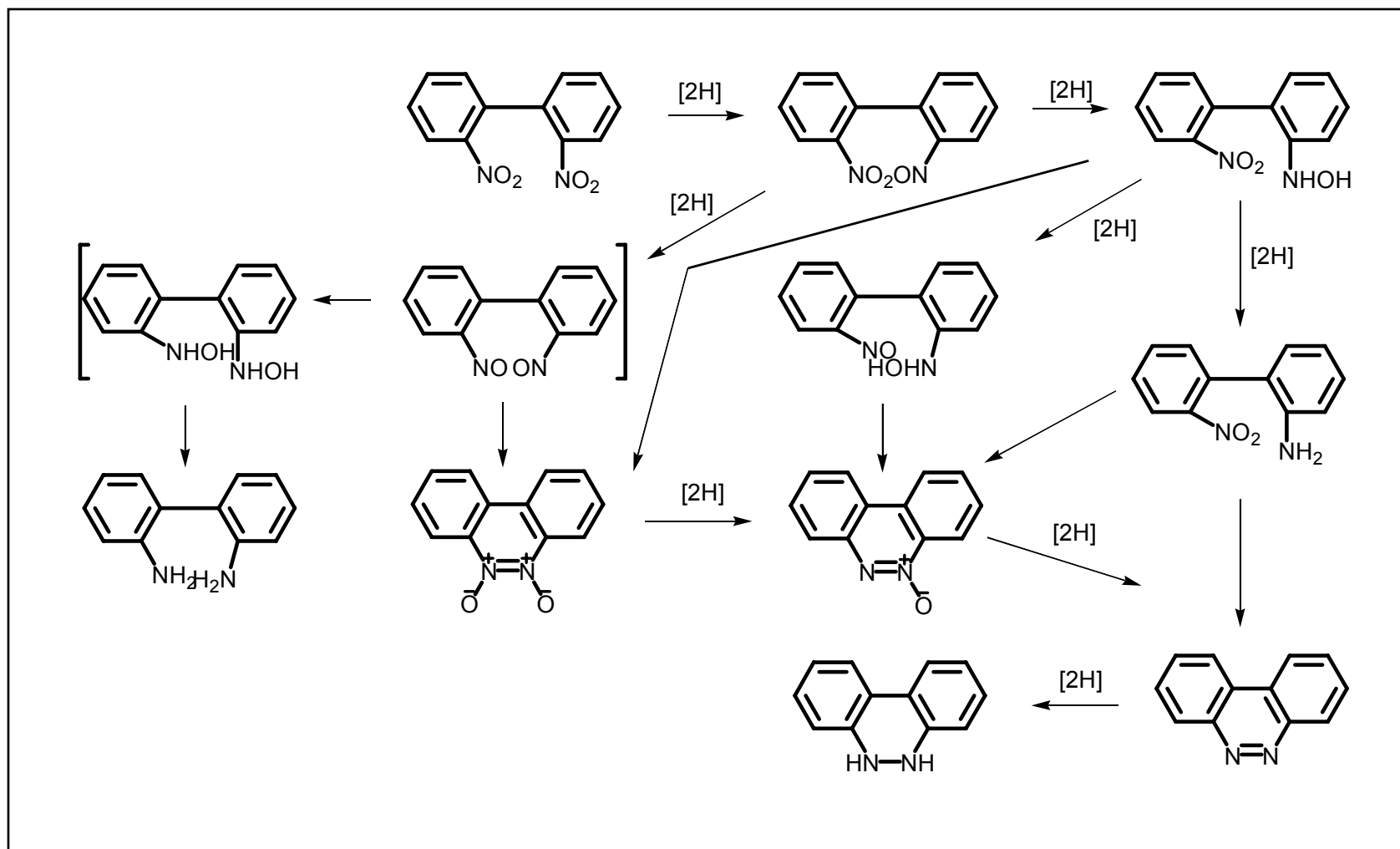
7.0 INTRODUCTION

Recently, there has been renewed interest in benzo[c]cinnolines as they provide an interesting class of compound due to their variety of biological activities, for example, as topoisomerase I inhibitors¹ and compounds with fungicidal effects.² Several groups are thus interested in investigating novel processes to build the framework of this class of *N*-heteroarenes and functionalize them in various ways.

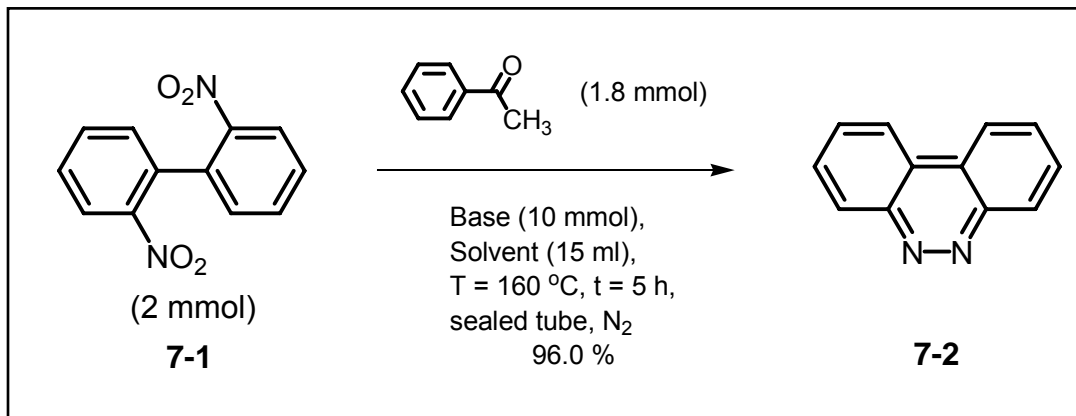
The most widely used method of preparing benzo[c]cinnolines is through the reduction of 2,2'-dinitrobiphenyls. 2,2'-Disubstituted biphenyls undergo intramolecular cyclization reactions with particular feasibility because of the close spatial proximity of the interacting substituents. Cyclization concomitant with the reduction of 2,2'-disubstituted biphenyls is very common and in cases involving nitro groups, is almost impossible to avoid. For instance, the conversion of 2,2'-dinitrobiphenyl (**7-1**) to benzo[c]cinnoline (**7-2**) can be accomplished by zinc³, lithium aluminium hydride⁴, reduced iron⁵, ferrous oxalate⁶, triethyl phosphite⁷ and iron carbonyl⁸ and electrolytically.⁹ Catalytic hydrogenation with Raney nickel¹⁰ and palladium on carbon is reported to give **7-2** but reduction to 2,2'-diaminobiphenyl also has been reported.¹¹ The compound **7-2** is formed in the reduction of **7-1** with tin or stannous chloride in

hydrochloric acid.¹⁰ *N,N'*-Dioxides or *N*-oxides may be formed as intermediates in these reactions, depending on the stage at which N-N bond formation takes place (Scheme 7.1) and on the vigor of the subsequent reduction. By suitable choice of reaction conditions these may be isolated.¹²

In the most recent attempt, Bjørsvik *et al.*¹³ developed a novel synthetic process to synthesize benzo[*c*]cinnoline **7-2** (Scheme 7.2) and its derivatives. The process is a one-step reaction conducted with an alcohol as solvent and alkoxide as base in a sealed tube purged with nitrogen. A high temperature of 160 °C and reaction time of 5 hours were maintained. Although high reaction yields of 96 % were attainable for unsubstituted benzo[*c*]cinnoline using NaOH as base as well as acetophenone and ethanol as solvents, the drastic reaction condition in a sealed tube renders the procedure undesirable, limits the scale of reaction and increases the danger of the reaction.

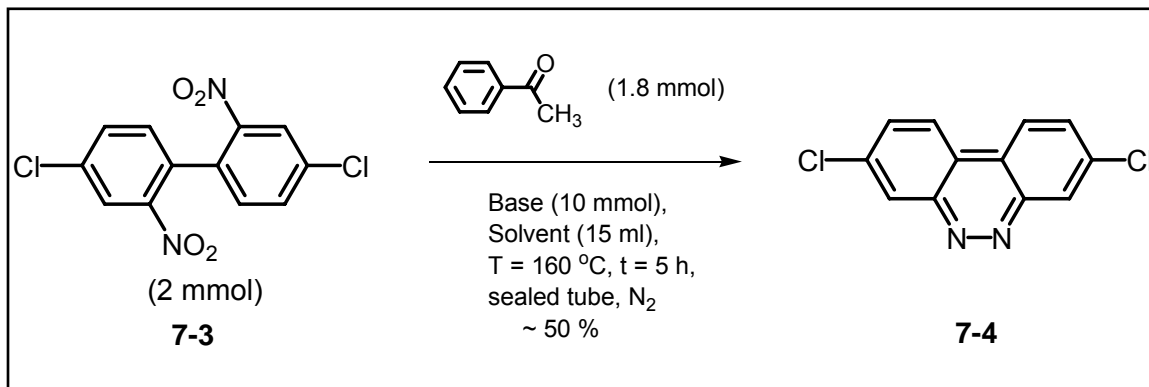


Scheme 7.1 Possible routes to the formation of benzo[c]cinnoline¹²



Scheme 7.2 Synthesis of **7-2**¹³

In addition, the high yield was no longer achievable for all substituted benzo[c]cinnolines. For instance, chloro functionalized benzo[c]cinnoline **7-4** (Scheme 7.3) could only be attained in 50 % yield.



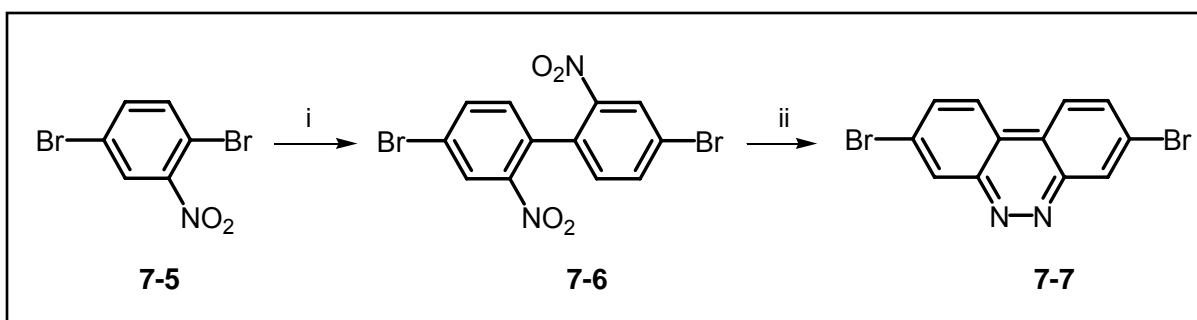
Scheme 7.3 Synthesis of **7-4**¹³

7.1 OUR WORK

In our endeavour to improve the synthetic process, we discovered two approaches that can derive benzo[c]cinnoline and their derivatives by a simpler

approach (Scheme 7.3). For comparison, we chose to synthesize **7-2** and **7-4** via these two approaches to determine the advantage of this synthetic method over the literature method.¹³

For our work, the bromo substituted benzo[*c*]cinnoline derivative is preferred over the chloro counterpart because the Br atom on the aromatic ring of the former is generally more feasibly removed in subsequent coupling reactions via substitution reactions. Therefore, **7-7** was also synthesized according to Scheme 7.4.



Scheme 7.4 i, Cu, DMF, 120 °C; ii, Sn, conc. HCl, EtOH, reflux or Zn, aq CaCl₂, EtOH, reflux

Although the reported procedure by Bjørsvik *et al.*¹³ possesses the advantages of using relatively non-hazardous and cheap reagents and does not require heavy or transition metals for reaction, it suffers from some obvious drawbacks. For instance, the operation has to take place at high temperature of 160 °C. Below 140 °C, the redox process will not operate while at 170 °C, decomposition takes place readily. The high reaction temperature requires the use of high boiling solvent acetophenone (b.p 201.7 °C) which can be difficult to remove after the reaction. Stringent conditions on the choice of base and solvent used are required as the redox processes involve a “cage re-

bonding” step. Such reaction mechanism is very dependent on the solvent properties, especially solvent viscosity and thereby reaction temperature.

7.2 BENZO[C]CINNOLINE-BASED CONJUGATED POLYMERS AS NONLINEAR OPTICS MATERIALS

The third-order nonlinear optical (NLO) properties of benzo[c]cinnoline based conjugated polymeric systems has not been reported to the best of our knowledge. Heterocyclic rings such as thiazole¹⁴ or thiophene¹⁵ have been introduced to replace benzene in NLO materials but such five-membered heterocyclic rings have poor bond alternation. The aromatic benzo[c]cinnoline possess two six-membered rings with better bond alternation and additional conjugation through the N=N double bond and aryl C-C bond.

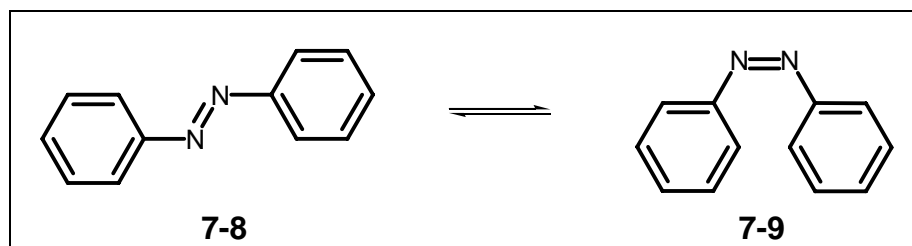


Fig. 7.1 Isomerization of azobenzene from *trans* 7-8 (left) to *cis* 7-9 (right) conformations

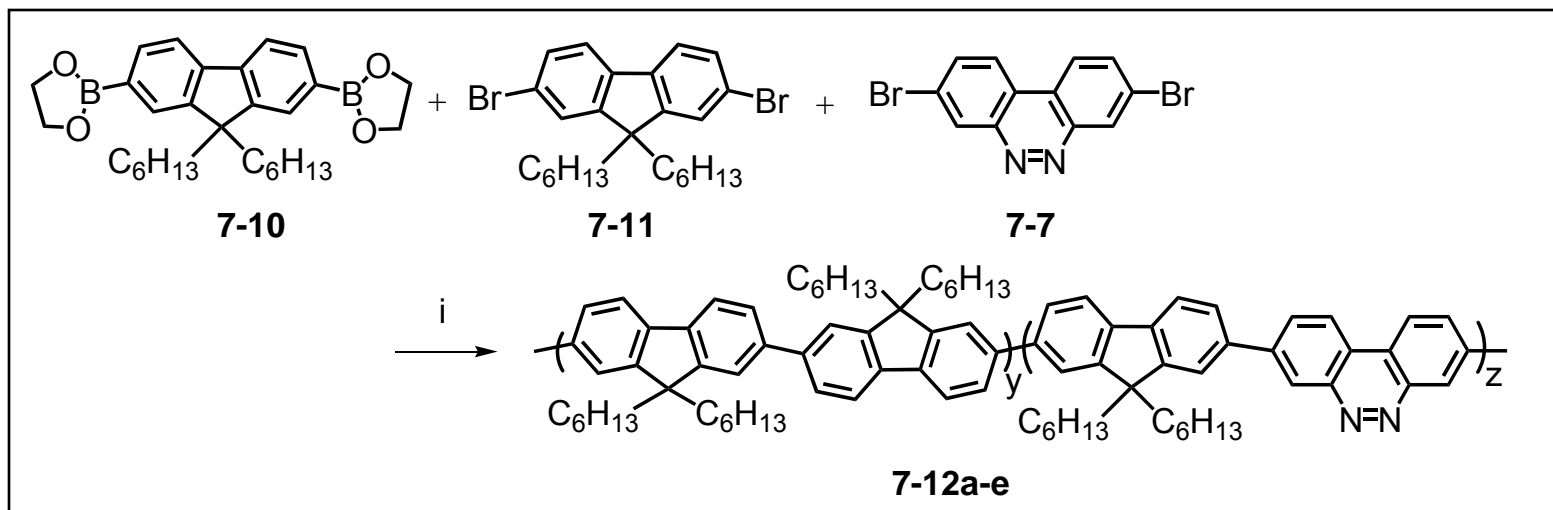
Benzo[c]cinnolines structurally resemble azobenzenes. The latter can exist in two isomeric forms namely the *E* (*trans*) 7-6 and *Z* (*cis*) 7-7, and possess the advantages of high optical nonlinearities due to photoinduced *trans-cis* isomerization (Fig. 7.1), molecular reorientation and nonlinear absorption and thus, are interesting because they combine the properties of anisotropy with photoresponsive behaviour that give rise to

applications in areas such as LC displays, NLO materials and information storage devices.¹⁶

Benzo[c]cinnolines resemble the *cis* isomer of azobenzene **7-9** but in a 'locked' conformation. Hence, we are interested in designing materials which incorporate the benzo[c]cinnoline moiety and investigate their potential for third-order NLO applications, in conjunction with our search for materials with large two-photon absorption (TPA). In order to enhance their third-order NLO properties, conjugated polymeric systems with extensive conjugation are designed.

During our search for highly efficient third-order NLO materials that can enhance the properties of benzo[c]cinnoline, we are particularly attracted by the structural features of the well conjugated, planar and rigid ring of fluorene. Fluorene π -systems have proven to be an efficient building block for chromophores with high two-photon absorptivities, as well as excellent thermal and photochemical stabilities.¹⁷ Also, fluorene chemistry is one of the fortes of our group, hence, we designed the synthesis of soluble conjugated co-polymers of fluorene and the key organic compound, benzo[c]cinnoline via Suzuki coupling reaction as shown in Scheme 7-5.¹⁸

In order to investigate the effect of benzo[c]cinnoline composition in a fluorene-benzo[c]cinnoline copolymers on the optoelectronic properties, the relative compositions of benzo[c]cinnoline and fluorene derivative monomers are varied (Table 7.1). The composition of the polymer is designed to comprise 10, 20, 30, 40 and 50 % of benzo[c]cinnoline. In the first 4 compositions (10 - 40 %), the monomers are randomly arranged while in the 50 % polymer, the monomers are arranged in alternating pattern in the polymer. The synthetic scheme is shown below (Scheme 7.5).



Scheme 7.5 i, Pd(PPh₃)₄, aq K₂CO₃, (n-C₄H₉)₄NBr, toluene, 100 °C

Table 7.1 Ratio of **7-7**, **7-10** and **7-11** in synthesis of polymers **7-12a-e** of various percentages of benzo[*c*]cinnoline

Polymer	Percentage of 7-7 (%)	Ratio		
		Fluorene		Benzo[<i>c</i>]cinnoline
		7-10 (x)	7-11 (y)	7-7 (z)
7-12a	10	5	4	1
7-12b	20	5	3	2
7-12c	30	5	2	3
7-12d	40	5	1	4
7-12e	50	1	0	1

7.3.0 RESULTS AND DISCUSSIONS

7.3.1 SYNTHESIS AND CHARACTERIZATION OF 7-7 MONOMER

In our work, we attempted two methods to synthesize **7-7**. The precursor, **7-6** was synthesized from **7-5** by Ullmann coupling reaction using Cu in DMF at 120 °C coupling followed by reduction of the former. In the first attempt, **7-6** was reduced using Sn and concentrated HCl in refluxing ethanol for 30 minutes. The cooled reaction mixture was quenched in ice cold water then basified before usual work-up. This reaction does not require inert condition, completes in a shorter time at lower temperature of less than 100 °C and gave high yield of 79.2 %. In addition, the scale of our reaction is 20 times higher as compared to the reported works of Bjørsvik *et al.*¹³ However, the usage of toxic Sn and the generation of hazardous by-product made the disposal and treatment of the reaction products difficult. The reduction of **7-6** was carried out with 4 equivalents of Sn and the reaction was quenched in 30 minutes. The addition of excess Sn (10 equivalents) and longer reaction time of 3 hours will result in further reduction of the intermediate to 2,2'-diamino-4,4'-dibromoniphenyl. This will yield only 17 % of the **7-7** and 63 % of the by-product.¹⁹ It is also interesting to note that Olah *et al.*²⁰ carried out the reaction using the same reagent but with gradual addition of Sn. This yielded 2,2'-diamino-4,4'-dibromoniphenyl as the major product with a yield of 95.5 % instead.

Due to the toxicity of Sn, the reduction of **7-6** was carried out using Zn powder and CaCl₂ as base in ethanolic solution under reflux conditions for 2 hours instead. The advantage of this method over the previous two is the usage of less toxic Zn metal as reducing agent and eliminated the usage of concentrated acid which in turn simplified

the purification process. The Zn powder and CaCl_2 reducing agents are also much easier to handle and are less expensive than the tin reduction method. The yield of this reaction (78.5 %) is only marginally lower than the Sn reduction method.

Therefore, we have accomplished two synthetic processes that (i) have shorter reaction time (ii) lower reaction temperature, (iii) does not require sealed tube and so lowers experimental risk that may be due to shattering of glass and thus, (iv), can be carried out in larger scale and not limited by size of vessel, (v) uses only ethanol as solvent, which is easy to remove after reaction unlike acetophenone, (vi) does not require inert condition and most importantly, (vii) gives high yield in the synthesis of **7-7**.

The structure of **7-7** was indirectly determined from the single crystal X-Ray structure of its salt (Fig. 7.2). A saturated CHCl_3 solution of the compound was added with some drops of iodomethane (excess) and left aside for slow evaporation. Dark crystals of the salt formed and were sent for X-ray analysis. The structure of the targeted halogenated benzo[*c*]cinnoline was thus confirmed.

The benzo[*c*]cinnoline skeleton is slightly distorted from planarity. The torsional angles C(12)-N(2)-N(1)-C(1) and C(8)-C(7)-C(6)-C(5) are 1.4° . The dihedral angles N(2)-N(1)-C(1) and N(1)-N(2)-C(12) are 124.9° and 118.1° respectively. All the bond distances are very similar to those of the parent compound.²¹

The crystal lattice consists of infinite chain of benzo[*c*]cinnoline units. Each unit on one layer interacts through non-bonded I-Br and I-H interactions. The non-bonded I-Br interactions are 3.621 and 3.756 Å and the I-H interactions range from 2.919 - 3.197

Å. The H is attached to the C atom at C(1). The units which form a layer are not completely planar because of the non-bonded interactions. The adjacent layers comprise of antiparallel units and are off-centered. There are no interactions between the layers.

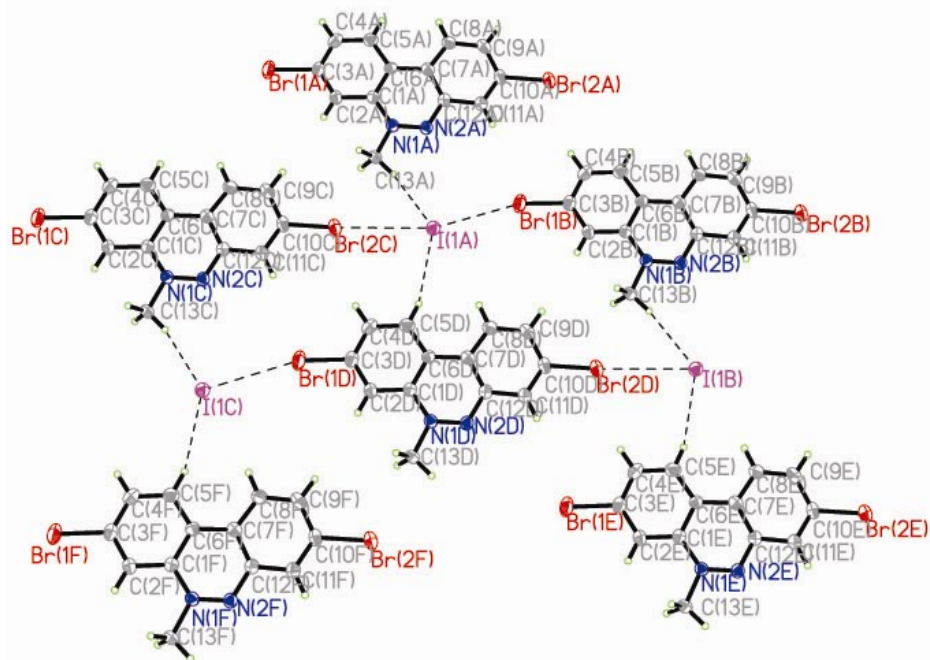


Fig. 7.2 ORTEP diagram of **7-7**, thermal ellipsoids are drawn at 50 % probability level

The syntheses of **7-2** and **7-4** were carried out using the second method of reduction from their respective precursors 2-bromonitrobenzene and 2-bromo-5-chloronitrobenzene. The compounds **7-2** and **7-4** were obtained in yields of 16.5 % and 45.1 % while literature values¹³ are 94 % and 50 % (this value was estimated from GC-MS analysis) respectively. Although the parent compound was obtained in much lower yield than the literature method, the more useful halogenated derivative **7-4** was isolated in comparable yield to the literature method. In addition, the pure isolated product of **7-4** was obtained in our work

7.3.2.0 SYNTHESIS AND CHARACTERIZATION OF FLUORENE-BENZO[C]-CINNOLINE COPOLYMERS

7.3.2.1 ^1H AND ^{13}C NMR ANALYSES

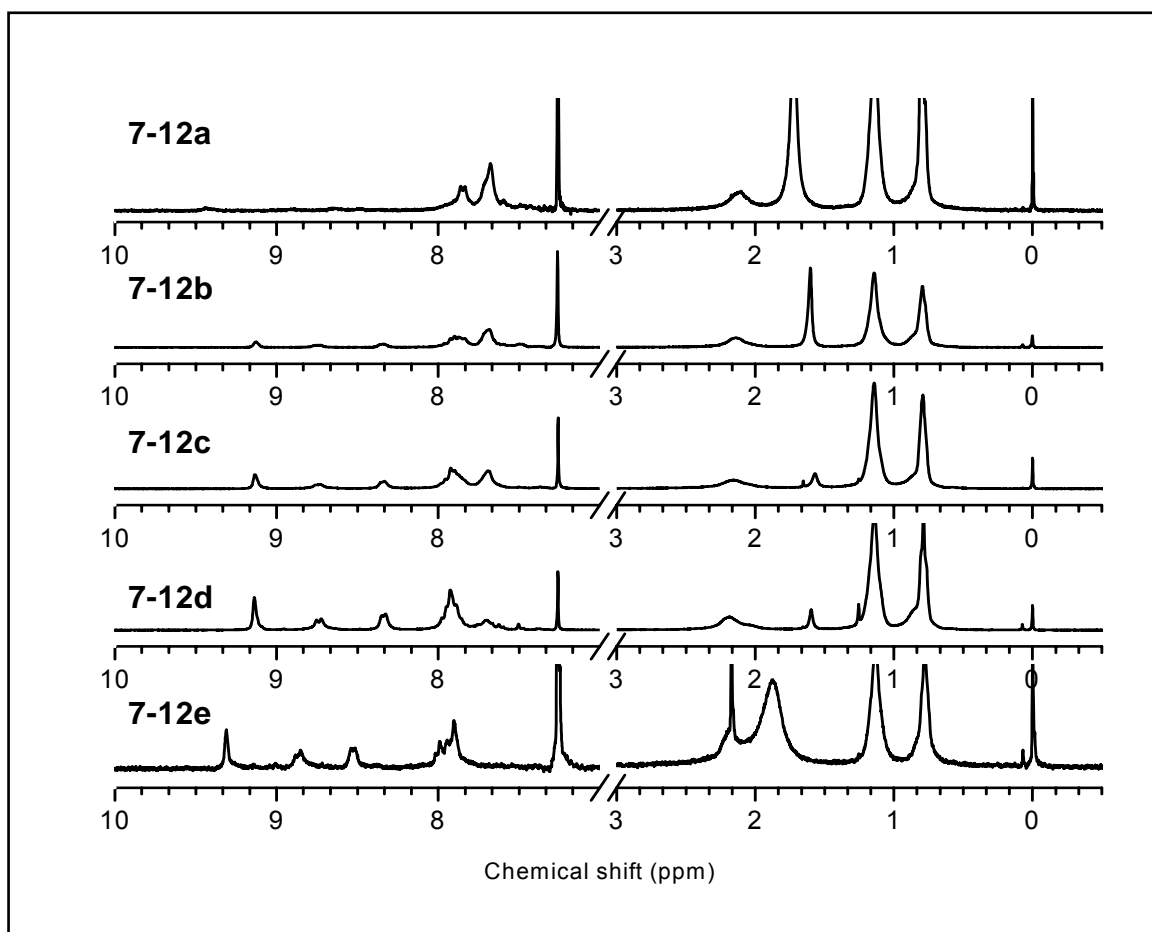


Fig. 7.3 ^1H NMR spectrum of **7-12a-e** in CDCl_3

The ^1H NMR spectrum (Fig. 7.3) of the random polymers containing 20 - 50 % benzo[c]cinnoline gave proton peaks of the benzo[c]cinnoline units and fluorene units that are well resolved from one another hence, the ratio of the units in the polymer was precisely determined. However, the ^1H NMR spectrum of the polymer containing 10 %

benzo[c]cinnoline do not clearly show the benzo[c]cinnoline peaks because of the low content in the polymer. The ^{13}C NMR spectrum (Fig. 7.4) of polymers containing 20 - 50 % benzo[c]cinnoline were also well resolved.

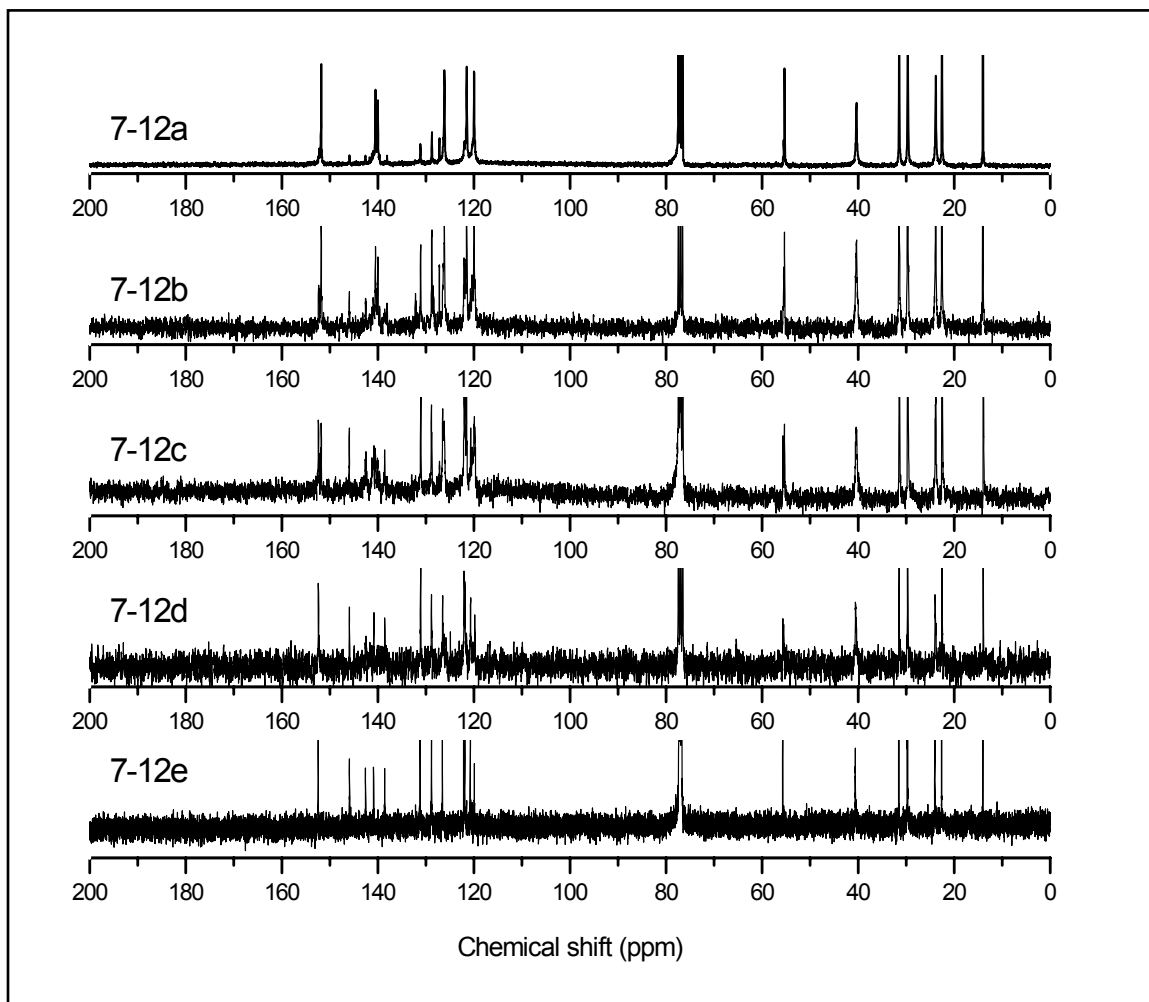


Fig. 7.4 ^{13}C NMR spectrum of 7-12a-e in CDCl_3

7.3.2.2 ELEMENTAL ANALYSES

The elemental analyses of the polymers confirmed the C, H and N contents in the polymers and the experimental results agree relatively well with the calculated

values. The experimental results for C, H and N contents are summarized in Table 7.2. The Pd catalyst was not trapped in any of the polymers. Terminal Br and boronic ester were not detected which could be due to the low content with respect to the long polymer backbone or the cleavage of these groups during the polymerization reactions. The percentage of benzo[c]cinnoline in the polymers can be calculated from the N content and is found to agree within 3.7 % of the expected value. The polymers were obtained in high yields summarized in Table 7.2 below. The yields range from 47.0 - 63.6 % (Table 7.3).

Table 7.2 Summary of the elemental analysis results of **7-12a-e**

Percentage of 7-7 added (%)	Elements [Expected (%) / Found (%)]			Percentage of benzo[c]cinnoline in polymer product from elemental analyses studies (calculated from N content, %)
	C	H	N	
10	89.77 / 89.86	9.35 / 8.51	0.88 / 0.55	6.3
20	89.19 / 90.36	8.95 / 8.08	1.86 / 1.88	20.2
30	88.54 / 90.59	8.52 / 8.65	2.94 / 2.70	27.6
40	87.82 / 87.36	8.04 / 7.64	4.14 / 4.49	43.4
50	87.02 / 87.39	7.50 / 7.42	5.49 / 5.55	50.5

Table 7.3 Summary of the yield of the polymers **7-12a-e**

Percentage of 7-7 added (%)	Percentage of benzo[c]cinnoline in polymer product from elemental analyses studies (calculated from N content, %)	Yield (%)
10	6.3	63.6
20	20.2	53.5
30	27.6	60.0
40	43.4	47.0
50	50.5	51.1

7.3.2.3 MOLECULAR WEIGHT DETERMINATION

The molecular weights of the polymers were measured by means of gel-permeation chromatography (GPC) using THF as eluent and polystyrene as standard. The molecular weights (M_n) and polydispersity indices (PDI) range from 6765 - 39728 g mol⁻¹ and <2.0 respectively Table 7.4. From the results, polymers **7-12a** and **7-12e** have similar chain length and hence are suitable for comparison in further studies.

Table 7.4 Average molecular weights of polymers determined from GPC, using polystyrene as standard

Polymer	M_w	M_n	PDI
7-12a	20100	10600	1.90
7-12b	34300	20100	1.71
7-12c	54800	39700	1.38
7-12d	18300	14600	1.25
7-12e	7100	6770	1.05

7.3.2.4 THERMAL ANALYSES

The thermal stability of the polymers was studied. The TGA plots are shown in Fig. 7.5 below. The polymers showed similar weight loss starting from above temperature range of 325 - 358 °C which is an indication of good thermal stability. Thermally induced phase transition behaviour of the polymers was also investigated with DSC but they do not exhibit clear glass transition, probably due to the rigidity of the polymer backbone.

Table 7.5 Summary of the T_d ($^{\circ}\text{C}$) values of **7-12a-e**

Polymer	T_d ($^{\circ}\text{C}$)
7-12a	356
7-12b	329
7-12c	358
7-12d	347
7-12e	325

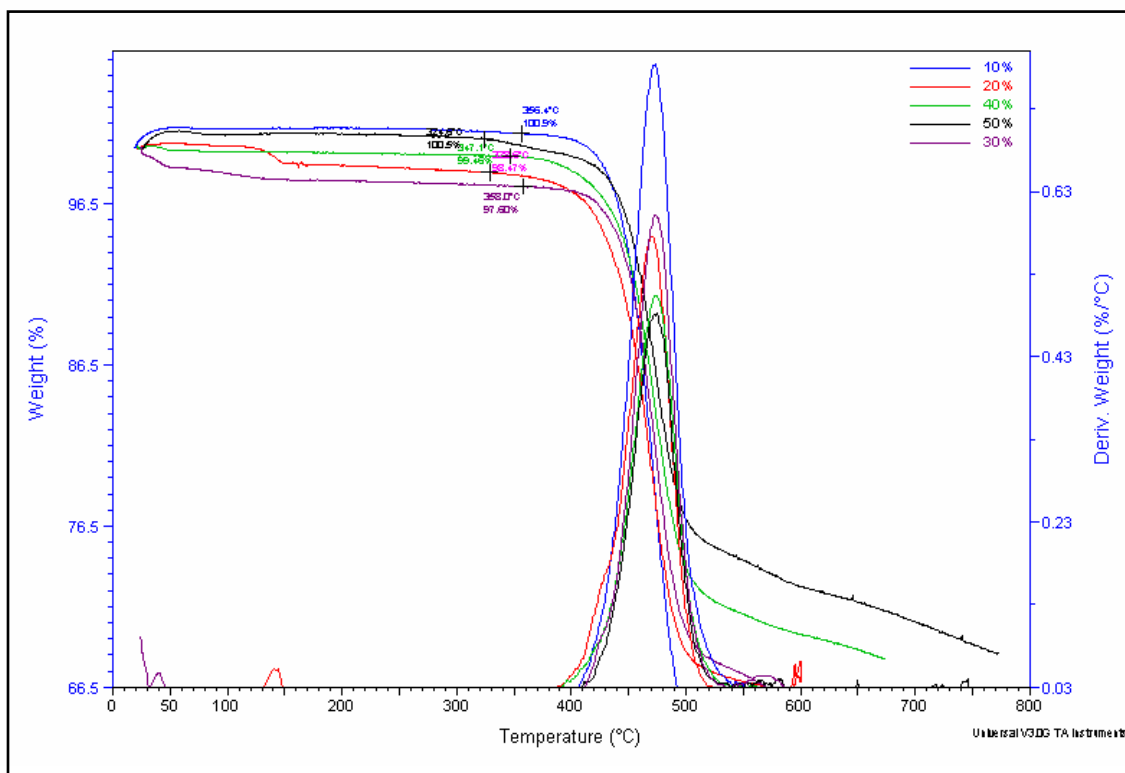


Fig. 7.5 TGA plot of the polymers **7-12a-e**

7.3.2.5 OPTICAL STUDIES

The UV-vis absorption spectra for the **7-7** and polymers **7-12a-e** in with various compositions of benzo[*c*]cinnoline are shown in Fig. 7.6. The UV-vis absorption maxima (λ_{max}) values lie between 264 nm and 388 nm. The spectra of the polymers are significantly red-shifted as compared to those of the monomers and this is attributed to the extensive conjugation of the polymer. With higher composition of benzo[*c*]cinnoline, the spectrum becomes more blue-shifted ($\Delta\lambda = \lambda_{\text{max},7-12a} - \lambda_{\text{max},7-12e} = 11 \text{ nm}$).

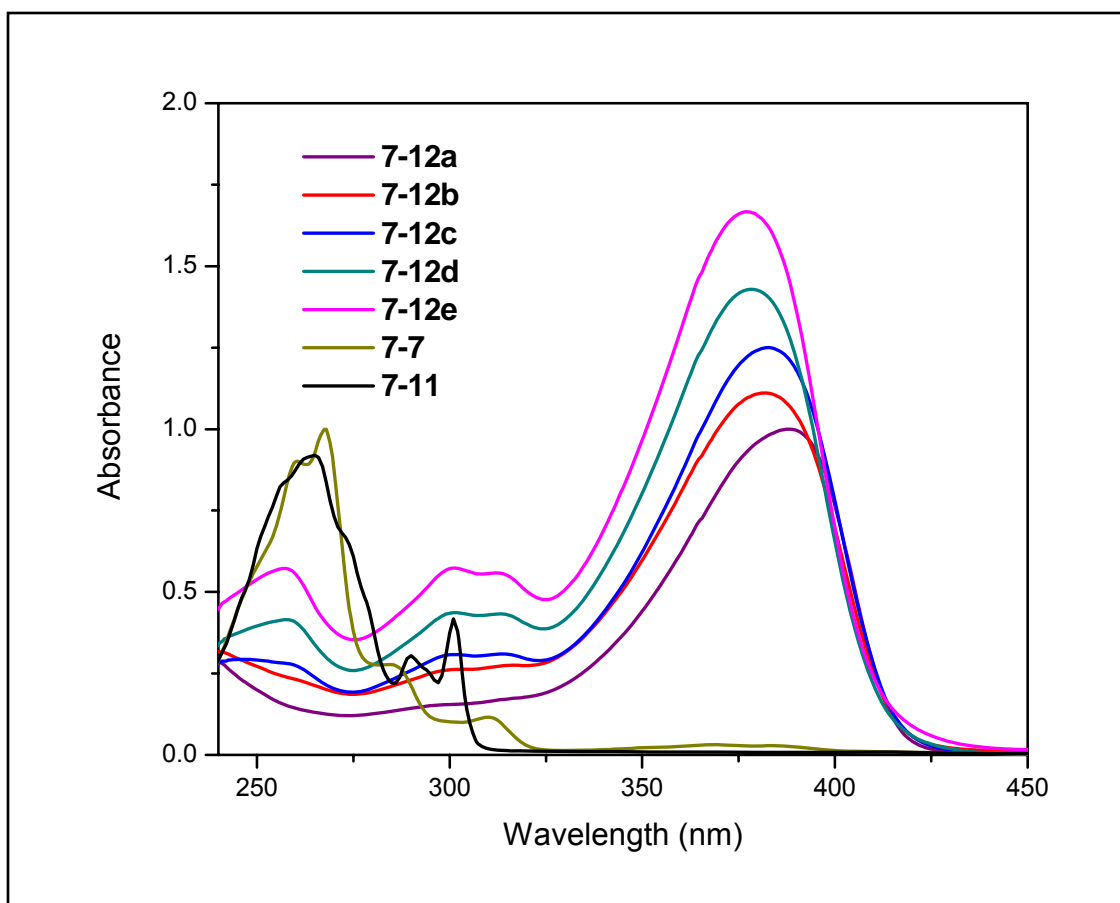


Fig. 7.6 UV-vis absorption spectra of **7-7**, **7-11** and polymers **7-12a-e**

The emission spectra of the polymers are shown in Fig. 7.7. The measurements were carried out in CHCl_3 solution using quinine sulphate in 0.1N sulphuric acid (fluorescence quantum efficiency, $\Phi_{\text{eff}} = 55\%$) as standard. With increasing compositions of benzo[*c*]cinnoline, the Φ_{eff} of the polymer decreases (summarized in Table 7.6). Since the concentration of the solutions are low, fluorescence quenching could have resulted from more efficient intrachain rather than interchain energy trapping.

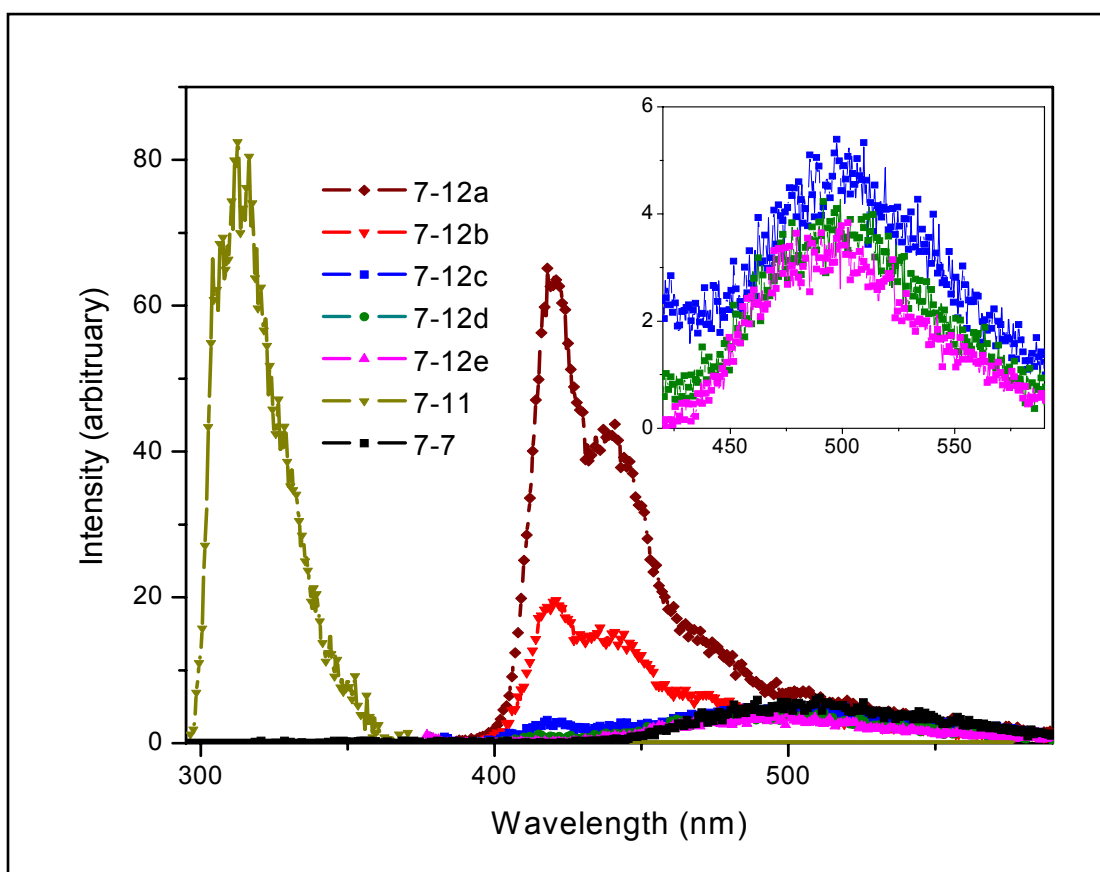


Fig. 7.7 Emission spectra of monomers **7-7** (suppressed) and **7-11** as well as polymers **7-12a-e** in CHCl_3 at concentrations of 1×10^{-5} M. Inset shows emission of **7-12c-e** at 420 - 590 nm for clarity

Table 7.6 Summary of Φ_{eff} (%) of polymers **7-12a-e**

Polymer	Φ_{eff} (%)
7-12a	1.05
7-12b	0.57
7-12c	0.45
7-12d	0.26
7-12e	0.19

We observe a relatively linear decrease in the Φ_{eff} of the polymers with increasing amounts of benzo[c]cinnoline which can be clearly illustrated in Fig. 7.8.

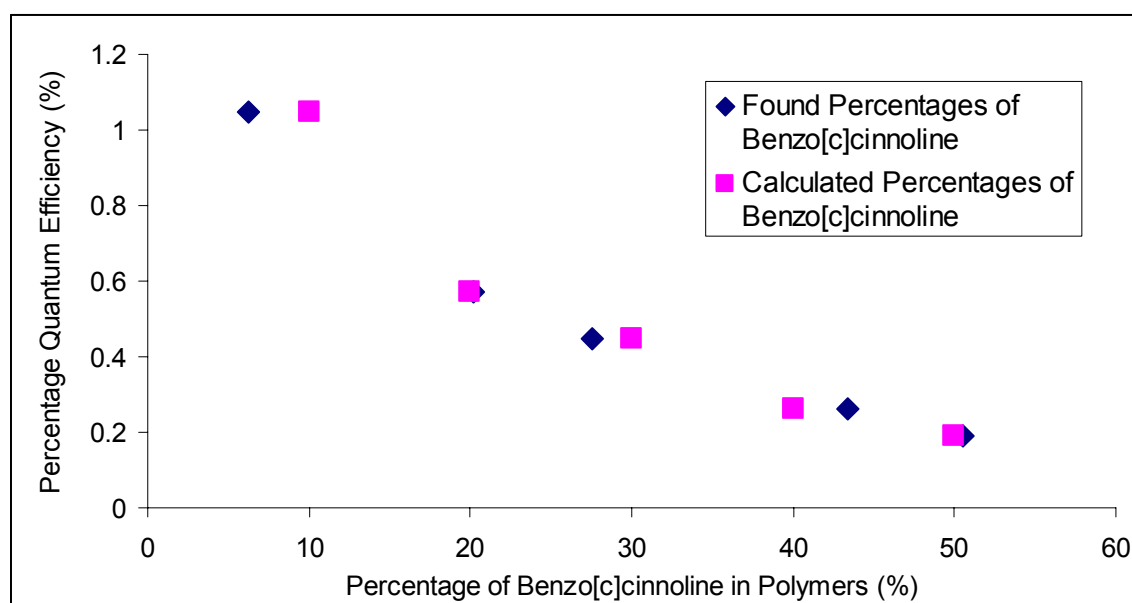


Fig. 7.8 Plot of quantum efficiency Φ_{eff} (%) against benzo[c]cinnoline content in polymers **7-12a-e**

7.4 NONLINEAR OPTICAL PROPERTIES

All the NLO measurements were performed by the Z-scan technique at 650 nm in CHCl_3 solutions. The closed aperture scans of the solutions exhibit the typical prefocal transmittance minimum (valley) followed by a postfocal transmittance maximum (peak) with changes in the position (Z) of the sample, indicating a positive nonlinear refraction²². The enhanced valley as compared to the peak of the closed aperture scan also shows the presence of multiphoton absorption. Fig. 7.9 shows the typical closed aperture Z-scan curve (nonlinear refraction measurement) for **7-12a**. The open aperture curves (see Fig. 7.10) show minima attributed to nonlinear absorption. The lines are fitted curves with the parameters: $\omega_0 = 45$ mm, $\Delta\phi = 1.3$ rd, $T = 1.5$.

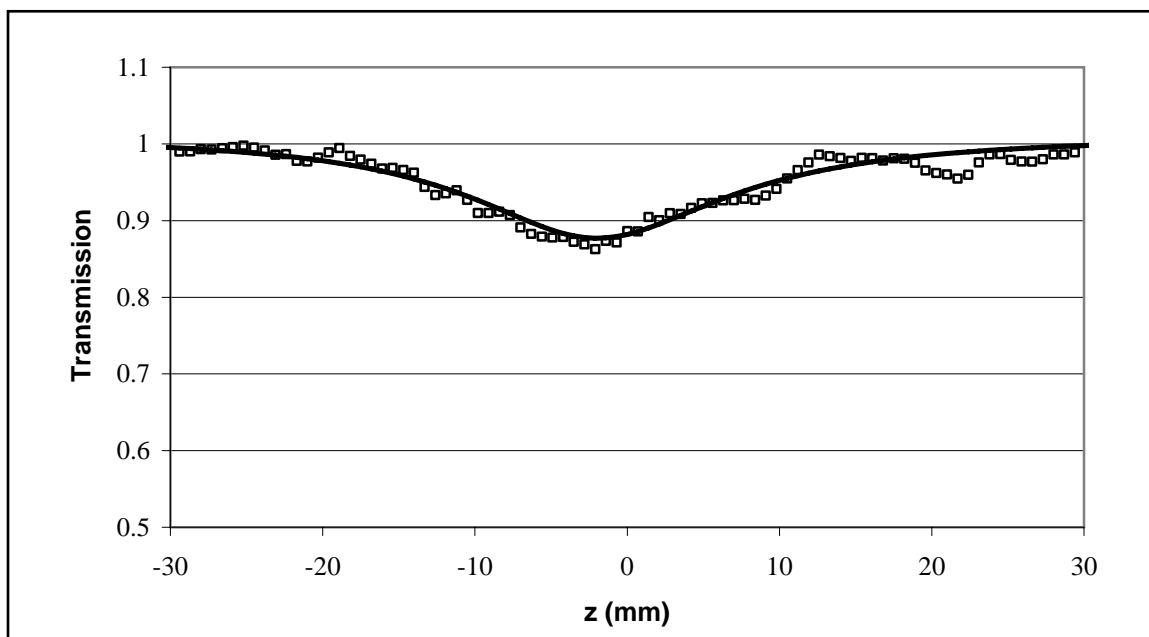


Fig. 7.9 An open-aperture scan in 0.0377 wt% solution of **7-12a** in CHCl_3

The NLO data which included the real and imaginary part of the complex nonlinear refractive index ($n_{2,\text{real}}$ and $n_{2,\text{imag}}$), real and imaginary components of the third-order susceptibility ($\chi_{\text{real}}^{(3)}$, $\chi_{\text{imag}}^{(3)}$), real and imaginary components of hyperpolarizability (γ_{real} , γ_{imag}) and the TPA cross section (σ_2) are summarized in Table 7.7. The concentration dependencies of $\Delta\phi_{\text{real}}$ and $\Delta\phi_{\text{imag}}$ of **7-7**, **7-12a** and **7-12e** were analyzed and a typical plot is shown in Fig. 7.11 for **7-7**. The results for the three compounds reveal the real (refractive) part of the nonlinearity to be positive (self-focusing) and the imaginary part of the nonlinearity to be positive, corresponding to nonlinear (two-photon) absorption.

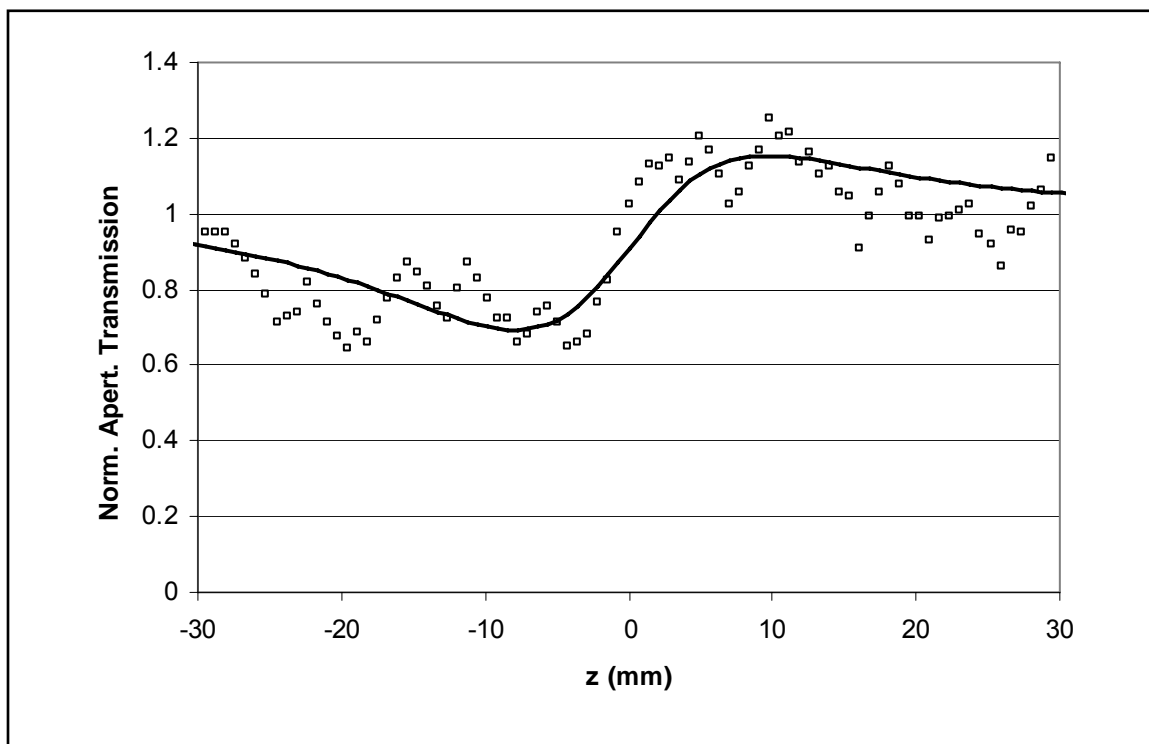


Fig. 7.10 A closed-aperture scan in 0.0377 wt% solution of **7-12a** in CHCl_3

The extrapolated $n_{2,\text{real}}$ values for **7-7**, **7-12a** and **7-12e** are 3.9×10^{-14} , 5.5×10^{-14} and $4.3 \times 10^{-13} \text{ cm}^2 \text{ W}^{-1}$ respectively. Hence, these compounds exhibit self-focusing properties at 650 nm. It is interesting to note that the polymer **7-12a** does not show significant difference in the $n_{2,\text{real}}$ value as compared to its monomer while the polymer **7-12e** which consists of a 40 % increment of benzo[c]cinnoline content exhibit $n_{2,\text{real}}$ value which is an order of magnitude larger.

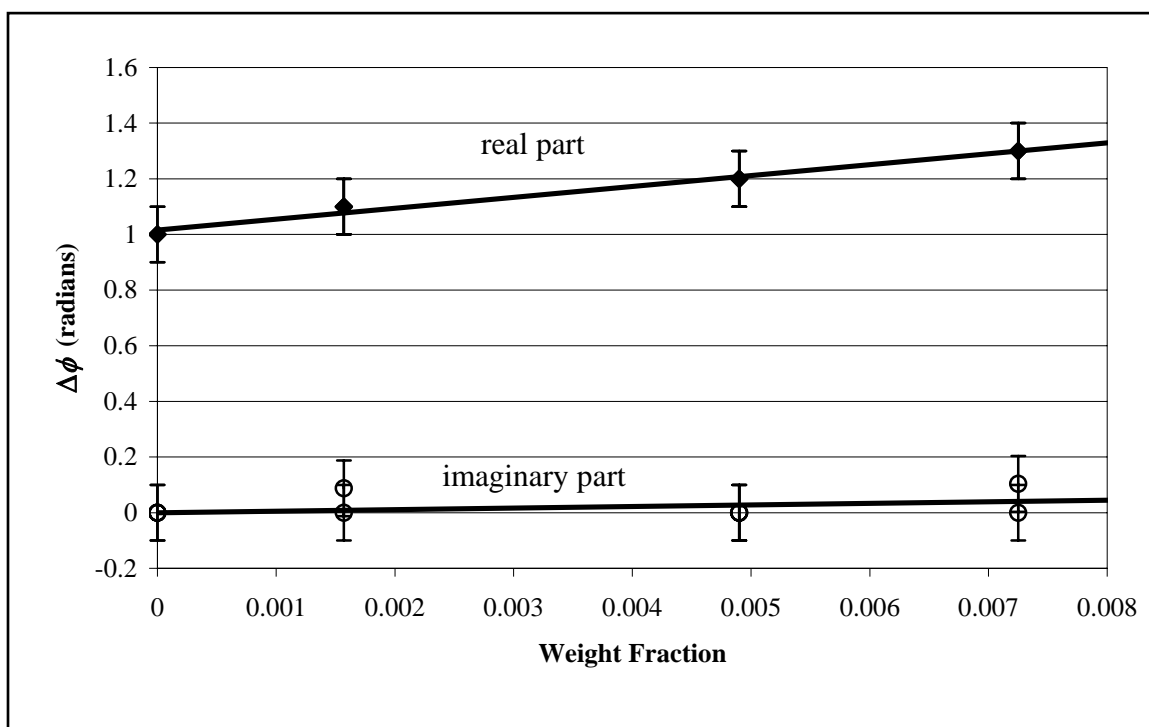
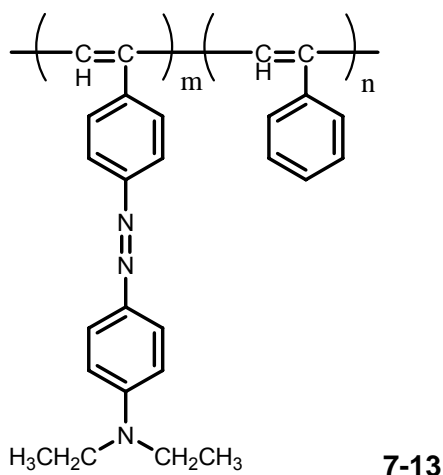


Fig. 7.11 Concentration dependences of the real and imaginary components of the nonlinear phase shift $\Delta\phi$

Table 7.7 Summary of the third-order nonlinear parameters of 7-7, 7-12a,e

Compound	$n_{2,\text{real}}^2$ ($\text{cm}^2 \text{W}^{-1}$)	$n_{2,\text{imag}}^2$ ($\text{cm}^2 \text{W}^{-1}$)	$\chi_{\text{real}}^{(3)}$ (esu)	$\chi_{\text{imag}}^{(3)}$ (esu)	γ_{real} (esu)	γ_{imag} (esu)	σ_2 (GM)
7-7	3.9×10^{-14}	5.5×10^{-15}	2.1×10^{-12}	3.0×10^{-13}	$2.3 \times 10^{-34} \pm$ 2.8×10^{-35}	$3.2 \times 10^{-35} \pm$ 4.1×10^{-35}	12 ± 16
7-12a	5.5×10^{-14}	1.2×10^{-13}	3.0×10^{-12}	6.2×10^{-12}	$6.0 \times 10^{-34} \pm$ 1.5×10^{-33}	$1.3 \times 10^{-33} \pm$ 5.0×10^{-34}	480 ± 180
7-12e	4.3×10^{-13}	3.1×10^{-13}	2.3×10^{-11}	1.6×10^{-11}	$3.8 \times 10^{-33} \pm$ 5.3×10^{-33}	$2.7 \times 10^{-33} \pm$ 1.1×10^{-33}	1020 ± 400

From the open aperture scans of the separate CHCl_3 solution of **7-7**, **7-12a** and **7-12e**, and comparison with the signal from the same cell containing the solvent CHCl_3 , the values of $\chi_{\text{imag}}^{(3)} = 3.2 \times 10^{-35} \pm (4.1 \times 10^{-35})$, $1.3 \times 10^{-33} \pm (5.0 \times 10^{-34})$ and $2.7 \times 10^{-33} \pm (1.1 \times 10^{-33})$ esu measured at 650 nm were respectively determined. This corresponds to $\chi_{\text{imag}}^{(3)}$ values of 3.0×10^{-13} , 6.2×10^{-12} and 1.6×10^{-11} esu respectively. The $\chi_{\text{imag}}^{(3)}$ of **7-12e** calculated according to our experimental data and calculation method is found to be of the same order of magnitude to polyacetylenes bearing poly[4-ethynyl-4'-(*N,N*-diethylamino)azobenzene-co-phenylacetylene] as chromophoric pendants (**7-13**). The latter was in turn cited to possess $\chi_{\text{imag}}^{(3)}$ with two orders of magnitude larger than those of polyacetylenes and larger than those of poly(*N*-carbazoylacetylene) and poly(1-naphthylacetylene).²³



The TPA property is evident from the transmission signal which is reflected by the deep valley ($\Delta T \propto \beta$).²² The compounds show increasing order of TPA property from **7-7**, **7-12a** to **7-12e** as the depth increased. The compound **7-7** shows a low σ_2 value on the order of 10 GM which is typical for a low molecular weight molecule. The polymers **7-**

12a and **7-12e** gave σ_2 values of 480 ± 190 and 1020 ± 400 GM respectively. These correspond to approximately 40- and 80-folds increase in the TPA property from a benzo[c]cinnoline monomer to a conjugated polymer. This increase is understandable in terms of large change in the one-photon absorption spectrum. A low σ_2 value of **7-7** is obtained because this chromophore has a one-photon absorption maximum at 268 nm and absorption cut-off at approximately 500 nm, thus the operating laser wavelength of 650 nm does not lead to a strong two-photon resonance at 325 nm. On the other hand, 325 nm is well above the main one-photon resonances for **7-12a** and **7-12e**, thus the presence of strong TPA is most probably due to resonance enhancement.

It can be concluded from the results above that the conjugated system containing fluorene and benzo[c]cinnoline show larger σ_2 with an increase in the benzo[c]cinnoline content. The large increase in the σ_2 of the polymers **7-12a** and **7-12e** from its monomer **7-7** can be explained by two-photon resonance enhancement effect. As the one-photon absorption maxima of these polymers **7-12e** and **7-12a** are red-shifted by 120 and 109 nm respectively, from the monomer **7-7**, the λ_{\max} lies closer to $2\lambda_{\text{ex}}$. As λ_{\max} of **7-12e** is closer to $2\lambda_{\text{ex}}$, the TPA enhancement effect on **7-12e** is larger which accounts for the higher σ_2 .

7.5 CONCLUSION

In our work, benzo[c]cinnoline and its halogenated derivatives were synthesized using two methods with obvious advantages over the reported works of Bjørsvik *et al.*¹³ Some of the highlighted advantages include shorter reaction time, lower reaction temperature, larger scale and high yields of the halogenated derivatives.

The NLO properties of **7-7** were measured at 650 nm and a solution of this chromophore in CHCl_3 was found to exhibit minor TPA properties and self-focusing phenomenon. This chromophore was then linked to fluorene monomers via Suzuki coupling reaction to generate a series of random polymers **7-12a-d** and alternating polymer **7-12e**.

The polymers were characterized using ^1H NMR, ^{13}C NMR, elemental analysis, TGA, GPC, FT-IR, UV-vis and emission spectroscopic techniques. The exact content of benzo[c]cinnoline in the random polymers **7-12a-d** was determined using elemental analyses of the N content. The compound **7-7** fluoresces weakly hence, an increase in the composition of benzo[c]cinnoline in the polymers **7-12a-e** decrease the fluorescence of the polymers. The parent compound was thus determined to be unfavourable for light-emitting applications.

The polymers **7-12a** and **7-12e** containing 10 and 20 % of benzo[c]cinnoline were investigated for their nonlinear properties. Both polymers were found to exhibit self-focusing properties and the latter with higher benzo[c]cinnoline content possess an order of magnitude higher n_2 . The latter also exhibits the largest σ_2 and hence strongest TPA property among the three compounds studied. Therefore, this work, to the best of our knowledge, is the first in its discovery of a benzo[c]cinnoline chromophores and a polymer with a significant TPA property.

7.6 REFERENCES

- ¹ Singh, S.K.; Yu, Y.; Ruchelman, A.; Sim, S.-P.; Liu A.; Leroy, F.; LaVoie, E.J. *Abstract of Papers*; 222nd ACS National Meeting, Chicago, August 26-30, 2001; American Chemical Society; Washington, DC, 2001.
- ² Weaver, L.J. (Monsanto Chemical Co.). US Patent 3012909, 1959.
- ³ Radell, J.; Spialter, L.; Hollander, J. *J. Org. Chem.* **1956**, *21*, 1051.
- ⁴ Badger, G.M.; Seidler, J.H.; Thomson, B. *J. Chem. Soc.* **1951**, 3207.
- ⁵ Slack, P.Z.; Slack, R. *Nature* **1947**, *160*, 437.
- ⁶ Banthorpe, D.V.; Hughes, E.D.; Ingold, C. *J. Chem. Soc.* **1962**, 2386.
- ⁷ Cadogan, J.I.G.; Cameron-Wood, M.; Mackie, R.K.; Searle, R.J.G. *J. Chem. Soc.* **1965**, 4831.
- ⁸ Kmiecik, J.E. *J. Org. Chem.* **1965**, *30*, 2014.
- ⁹ Braithwaite, R.S.W.; Holt, P.F.; Hughes, A.N. *J. Chem. Soc.* **1958**, 4073.
- ¹⁰ Everett, J.L.; Ross, W.C. *J. Chem. Soc.* **1949**, 1972.
- ¹¹ Ross, S.D.; Kahan, G.J.; Leach, W.A. *J. Am. Chem. Soc.*, **1952**, *74*, 4122.
- ¹² Barton, J.W. *Adv. Heterocyclic Chem.* **1963**, *24*, 151.
- ¹³ Bjørsvik, H.R.; González, R.R.; Liguori, L. *J. Org. Chem.* **2004**, *69*, 7720.
- ¹⁴ Wang, Y.K.; Shu, C.F.; Breitung, E.M.; McMahon, R.J. *J. Mater. Chem.* **1999**, *9* (7), 1449.
- ¹⁵ (a) Zhan, C.L.; Li, Y.J.; Li, D.H.; Wang, D.Y.; Nie, Y.X. *Opt. Mater.* **2006**, *28* (3), 289. (b) Rigaut, S.; Perruchon, J.; Guesmi, S.; Fave, C.; Touchard, D.; Dixneuf, P.H. *Euro. J. Inorg. Chem.* **2005**, *3*, 447. (c) Wu, W.; Zhang, Z.L.; Zhang, X.Y. *J. Chem. Res. -S*, **2004**, *9*, 617.
- ¹⁶ (a) Yesodha, S.K.; Pillai, C.K.S.; Tsutsumi, N. *Prog. Polym. Sci.* **2004**, *29*, 45. (b) Delaire, J.A.; Nakatani, K. *Chem Rev.* **2000**, *100*, 1817. (c) Kawata, S.; Kawata, Y.

Chem. Rev. **2000**, *100*, 1777. (d) Ledoux, I.; Zyss, J.; Barni, E.; Barolo, C.; Diulgheroff, B.N.; Quagliotto, P.; Viscardi, G. *Synth. Met.* **2000**, *115*, 213. (e) Kułakowska, J.; Kucharski, S. *Eur. Polym. J.* **2000**, *36*, 1805.

¹⁷ (a) Reinhardt, B.A.; Brott, L.L.; Clarson, S.J.; Dillard, A.G.; Bhatt, J.C.; Kannan, R.; Yuan, L.; He, G.S.; Prasad, P.N. *Chem. Mater.* **1998**, *10* (7), 1863. (b) Belfield, K.D.; Hagan, D.J.; Van Stryland, E.W.; Schafer, K.J.; Negres, R.A. *Org. Lett.* **1999**, *1* (10), 1575. (c) Kannan, R.; He, G.S.; Yuan, L.; Xu, F.; Prasad, P.N.; Dombroskie, A.G.; Reinhardt, B.A.; Baur, J.W.; Vaia, R.A.; Tan, L-S. *Chem. Mater.* **2001**, *13* (5), 1896. (d) Lee, K-S; Lee, J.H.; Choi, H.; Cha, M.; Chung, M-A; Kim, Y.J.; Jung, S-D. *Mol. Cryst. Liq. Cryst. Sci. Technol., Sect. A* **2001**, *370*, 155. (e) Belfield, K.D.; Morales, A.R.; Kang, B-S.; Hales, J.M.; Hagan, D.J.; Van Stryland, E.W.; Chapela, V.M.; Percino, J. *Chem. Mater.* **2004**, *16*, 4634. (f) Belfield, K.D.; Morales, A.R.; Hales, J.M.; Hagan, D.J.; Van Stryland, E.W.; Chapela, V.M.; Percino, J. *Chem. Mater.* **2004**, *16* (11), 2267. (g) Kannan, R.; He, G.S.; Lin, T-C; Prasad, P.N.; Vaia, R.A.; Tan, L-S. *Chem. Mater.* **2004**, *16*, 185. (h) Belfield, K.D.; Bondar, M.V.; Przhonska, O.V.; Schafer, K.J. *J. Photochem. Photobiol., A* **2004**, *162* (2-3), 489. (i) Kawamata, J.; Akiba, M.; Tani, T.; Harada, A.; Inagaki, Y. *Chem. Lett.* **2004**, *33* (4), 448. (j) Hales, J.M.; Hagan, D.J.; Van Stryland, E.W.; Schafer, K.J.; Morales, A.R.; Belfield, K.D.; Pacher, P.; Kwon, O.; Zojer, E.; Bre´das, J.L. *J. Chem. Phys.* **2004**, *121* (7), 3152. (k) Belfield, K.D.; Bondar, M.V.; Hernandez, F.E.; Morales, A.R.; Przhonska, O.V.; Schafer, K.J. *Appl. Opt.* **2004**, *43* (34), 6339. (l) Kawamata, J.; Akiba, M.; Inagaki, Y.; Tani, T.; Harada, A. *J. Nonlinear Opt. Phys. Mater.* **2004**, *13* (3-4), 475. (m) Werts, M.H. V.; Gmouh, S.; Mongin, O.; Pons, T.; Blanchard-Desce, M. *J. Am. Chem. Soc.* **2004**, *126* (50), 16294. (n) Day, P.N.; Nguyen, K.A.; Pachter, R. *J. Phys. Chem. B* **2005**, *109* (5), 1803. (o) Cohanoschi, I.; Belfield, K.D.; Hernandez, F.E. *Chem. Phys. Lett.* **2005**, *406* (4-6), 462.

- ¹⁸ Yu, L.P.; Dalton, L.R. *Synth. Met.* **1989**, *29*, E463.
- ¹⁹ Patrick, D.A.; Boykin, D.W.; Wilson, W.D.; Tanious, F.A.; Sychala, J.; Bender, B.C.; Hall, J.E.; Dykstra, C.C.; Ohemeng, K.A.; Tidwell, R.R. *Eur. J. Med. Chem.* **1997**, *32*, 781.
- ²⁰ Yamato, T.; Hideshima, C.; Suehiro, K.; Tashiro, M.; Prakash, G.K.S.; Olah, G.A. *J. Org. Chem.* **1991**, *56*, 6248.
- ²¹ Benin, V.; Kaszynski, P.; Pink, M.; Young, V.G. Jr. *J. Org. Chem.* **2000**, *65*, 6388.
- ²² (a) Chérioux, F.; Audebert, P.; Maillotte, H.; Grossard, L.; Hernandez, F.E.; Lacourt, A. *Chem. Mater.* **1997**, *9*, 2921. (b) Sheik-Bahae, M.; Said, A.A.; Wei, T.H.; Hagan, D.J.; Van Stryland, E.W. *IEEE J. Quant. Electron.* **1990**, *26*, 760.
- ²³ Yin, S.; Xu, H.; Shi, W.; Gao, Y.; Song, Y.; Wing, J.; Lam, Y.; Tang, B.Z. *Polymer* **2005**, *46*, 7670.

CHAPTER 8

THE EFFECT OF CONFORMATIONAL AND CONFIGURATIONAL DIVERSITY ON THE INTERACTION OF WATER-SOLUBLE PORPHYRIN WITH NUCLEOTIDES AND THEIR PHOTBLEACHING PROPERTIES

8.0 INTRODUCTION

Positively charged porphyrins have attracted considerable attention since they were first reported almost three decades ago¹ because of their remarkable ability to form complexes with and cleave nucleic acids as described in the pioneering works of Fiel *et al.*² Molecular recognition of DNA is of fundamental importance to life hence the analysis of the interaction of small molecules with DNA is of considerable interest. Potential applications of these systems include photodynamic therapy of cancer (PDT), design of telomerase inhibitors,³ antiviral agent development⁴ and molecular biology applications such as DNA footprinting.⁵ Water-soluble porphyrin derivatives have been shown to possess great potential as therapeutic agents for PDT because of their antiviral activity⁶ and the ability to cleave DNA⁷ and RNA⁸ selectively. Hence, porphyrins with charged peripheral groups have attracted considerable attention, in particular, the positively charged species, because of their additional ability to form complexes with and cleave nucleic acids described in pioneer works by Fiel *et al.*² Several positively charged porphyrins that show strong ability to

bind to DNA included those bearing pyridinium, ammonium,¹ trialkylammonium,⁹ trialkyl- and triarylphosphonium moieties.¹⁰ In particular, a variety of alkyl/arylphosphonium tetratolylporphyrins have been extensively studied to investigate the effect of the size of the substituents on the degree of aggregation and DNA binding affinity. However, no study was carried out to probe the effect of substituents proximity on these factors that affect PDT.

8.1 TARGET AND APPROACH OF OUR RESEARCH WORK

Prior to the study of how porphyrins interact with DNA,¹¹ it is important to perform a fundamental study of their interaction with nucleotides. The complexes can be formed by coordination bonds between the metal ions in the porphyrin and nucleophilic N atoms on the nucleotides, as well as electrostatic interactions between the positively charged substituents on the porphyrin periphery and the negatively charged phosphate oxygen atoms of nucleotides.

The binding of porphyrins containing hydrophobic substituents is often complicated by aggregation in aqueous solution which lowers their fluorescence quantum efficiency (Φ_{eff}), posing a detrimental effect on photosensitization and reduces their ability to cleave nucleic acids. However, through proper design of the steric bulk and polar properties of these substituents, the porphyrins can be fine-tuned to suit medical applications. Lipophilic substituents like phenyl enhance the ability of

porphyrins to pass through or accumulate biomembranes while charged sites improve their water-solubilities.¹²

Photoexcitation of a nucleotide-bound porphyrin can lead to photosensitized cleavage of the nucleotide initiated by electron and/or energy transfer between the excited porphyrin and the adjacent base pair. The photoactivity of these photosensitizers depends on their quantum yields and stability towards oxidative degradation known as photobleaching. Photobleaching of the chromophore which refers to the loss of absorption or emission intensity caused by light occurs during PDT.¹³ It is considered as a disadvantageous property in a tumor photosensitizer because the source of the active species is being destroyed.

Porphyrins with *para* substituted phenyl rings on the *meso* carbon are commonly studied but such compounds usually suffer from aggregation due to π - π stacking of porphyrins.^{11b} Hence, *ortho* substituted isomers are designed and synthesized. These compounds are expected to exhibit less aggregation due to greater steric hindrance but are less well investigated.

Hence, the objective of this work is to design novel water-soluble porphyrins with triphenylphosphonium substituents at different positions and spatial arrangement to investigate the importance of these variables on (1) their interaction with nucleobases, (2) aggregation properties and (3) photobleaching activities. Since it is

well known that a drastic decrease in adenosine triphosphate (ATP) occurs in tumors shortly after PDT treatment with Photofrin II,¹⁴ our study will make use of nucleotides such as ATP and adenosine monophosphate (AMP).

The three isomers designed for this study are **8-1a-c** and they are novel. The Zn(II) metalloporphyrin complexes possess methylene bridges linking the phosphonium substituents to the phenyl ring. The electronic effect of the cationic centre on the π -system of the phenyl and porphyrin chromophores is thus eliminated, which leaves steric and proximity as factors that affect the binding properties with nucleotides. We have chosen to study metalloporphyrins as they undergoes photooxidation more easily due to their lower redox potential and Zn(II) metal atom provides an additional point of binding for the ATP and AMP through the N donor atom (most nucleophilic) of the purine. This is illustrated in Fig. 8.1. The insertion of Zn(II) metal atom into the porphyrin cavity is important in increasing an additional site for the binding of ligand and also increases the Φ_{eff} of the porphyrin. In addition, Zn(II) is an important cofactor. Hence, its biological existence in our body makes it a suitable choice for metallation of porphyrin. Compounds **8-1a,b** are marked by an increase of Φ_{eff} by 50-60 fold while that of **8-1c** is about 20 fold only relative to their free ligands.

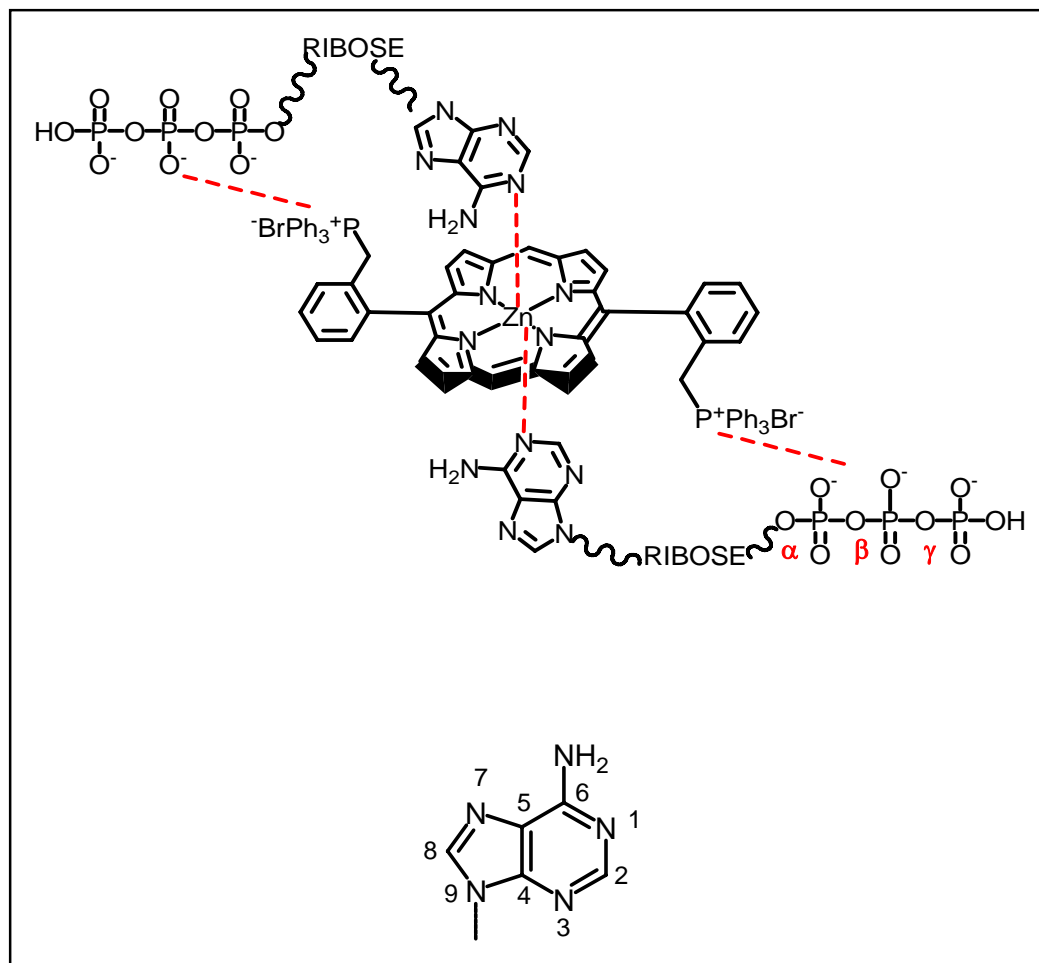


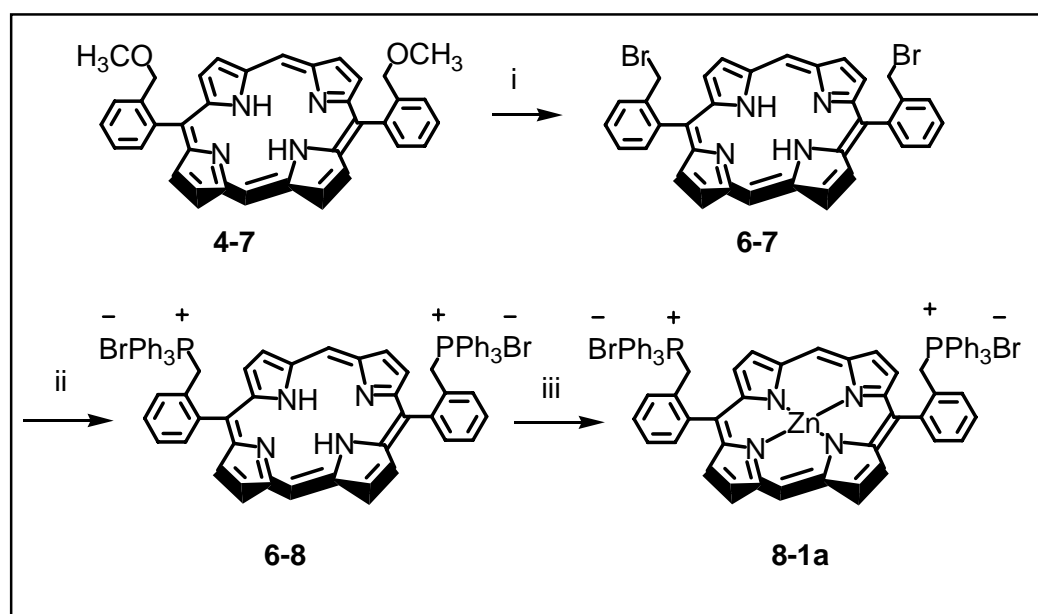
Fig. 8.1 Illustration of two possible binding modes of two molecules of ATP with **8-1b** through ligand coordination and electrostatic interactions. The α , β and γ P atoms are labeled in red

8.2.0 RESULTS AND DISCUSSIONS

8.2.1 SYNTHESIS OF WATER SOLUBLE PORPHYRIN PHOTSENSITIZERS

Ethers **4-7** and **4-6** were hydrolyzed and then substituted using hydrobromic acid to afford **6-7** and **6-5** respectively. Treated with triphenylphosphine, compounds **6-7** and **6-5** were converted to phosphonium salts **6-8** and **6-6**. Zn(II) metal atoms

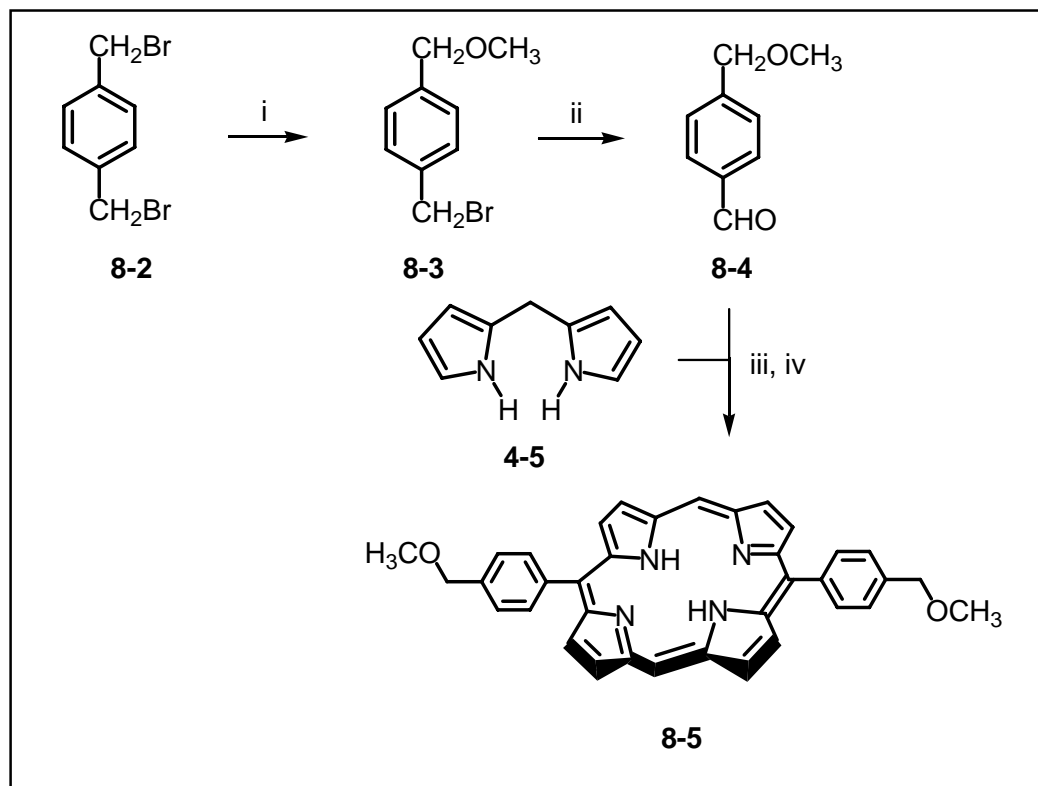
were inserted into the porphyrin rings of **6-6** and **6-8** to form metalloporphyrins **8-1a** and **8-1b** that were used for further analysis after purification (Scheme 8.1). For the purpose of comparison, the *para* isomer **8-1c** was prepared via the similar procedure to compound **8-1a** and **8-1b** except that the starting material in the synthesis of **8-1c** is 1,4-bis-bromomethylbenzene **8-2** (Scheme 8.2).



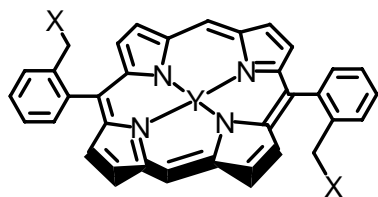
Scheme 8.1 i, HBr, CHCl_3 ; ii, PPh_3 , DMF; iii, $\text{Zn(OAc)}_2 \cdot x\text{H}_2\text{O}$, THF

Porphyrinoid sensitizers form a number of complexes with nucleic acids, proteins, and other biomolecules as a result of electronic and hydrophobic nature. The investigation of the interaction between porphyrinoid photosensitizers and biomolecules allows people to have a better understanding of the mechanism of PDT and open a new way to increase the efficiency of the photosensitization. Here, we first

use ^1H NMR to study the interaction of AMP and ATP with positively-charged porphyrins.



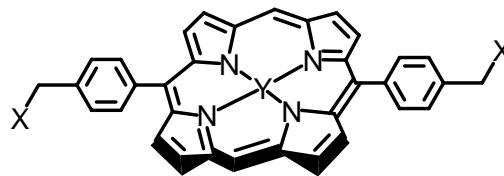
Scheme 8.2 i, Na, CH_3OH , reflux; ii, Na_2CO_3 , DMSO, reflux;
iii, CF_3COOH , CH_2Cl_2 ; iv, chloranil, reflux



6-5: X = Br, Y = 2H

6-8: X = $^+\text{PPh}_3\text{Br}^-$, Y = 2H

8-1b: X = $^+\text{PPh}_3\text{Br}^-$, Y = Zn^{2+}



8-5: X = OCH₃, Y = 2H

8-6: X = Br, Y = 2H

8-7: X = $^+\text{PPh}_3\text{Br}^-$, Y = 2H

8-1c: X = $^+\text{PPh}_3\text{Br}^-$, Y = Zn^{2+}

8.2.2 ^1H AND ^{31}P NUCLEAR MAGNETIC RESONANCE STUDIES

In the ^1H NMR spectrum, for all compounds **8-1a-c**, addition of 1 equivalent of AMP in D_2O (2.7 mM) to the respective Zn(II) metalloporphyrin complexes in CD_3OD (2.7 mM), resulted in upfield shifts of the protons on the purine ring. This comparison is made relative to the uncomplexed AMP in the same concentration and solvents. In all cases, the proton at C2 of the purine ring shifted the most, indicating that the nucleotide binds to the porphyrin through the nucleophilic N at the 6-membered ring and N1 is the most likely N atom to bind to the central metal because of its highest nucleophilicity on the purine ring. This is similar to a study which results suggested the coordination of N1 atom also.¹⁵ Compared to the uncomplexed AMP, protons at C2 on the purine ring shifted upfield for the 1:1 AMP:**8-1a-c** complexes. This was similarly observed in the 1:1 ATP:**8-1a-c** complexes (Refer to Table 8.1).

Table 8.1 Chemical shifts of H of AMP and ATP at C2 and C8 (ppm)

Compound	Chemical Shift of H at C2, C8 (ppm)			
	8.33, 8.63		8.39, 8.68	
Pure nucleotide	1 equiv AMP	2.5 equiv AMP	1 equiv ATP	2.5 equiv ATP
8-1a	8.25, 8.56	8.27, 8.59	7.97, 8.51	merged ⁱ , 8.56
8-1b	8.17, 8.58	8.27, 8.60	8.01, 8.53	8.20, 8.60
8-1c	8.26, 8.58	8.29, 8.60	8.11, 8.57	8.21, 8.60

The upfield shifts of the proton at C2 was most significantly observed in the AMP:**8-1b** and ATP:**8-1a,b** complexes which may imply that the nucleotide is more strongly coordinated to the metal centre of these *ortho* porphyrins. This was confirmed by the fact that when 2.5 equivalents of AMP or ATP were added in their respective solutions, protons at C2 shifted downfield more in these complexesⁱⁱ. This can be attributed to the synergic effect in which extra coordination of the purine N atom to the central metal centre caused the bases to be pushed further from the porphyrin ring as illustrated in Fig. 8.2. An example of the observed spectrum change of **8-1c** with variable ATP ratio and time is shown in Fig. 8.3.

ⁱ Peak overlapped

ⁱⁱ Observation does not apply to 2.5:1 ATP:**7a** complex

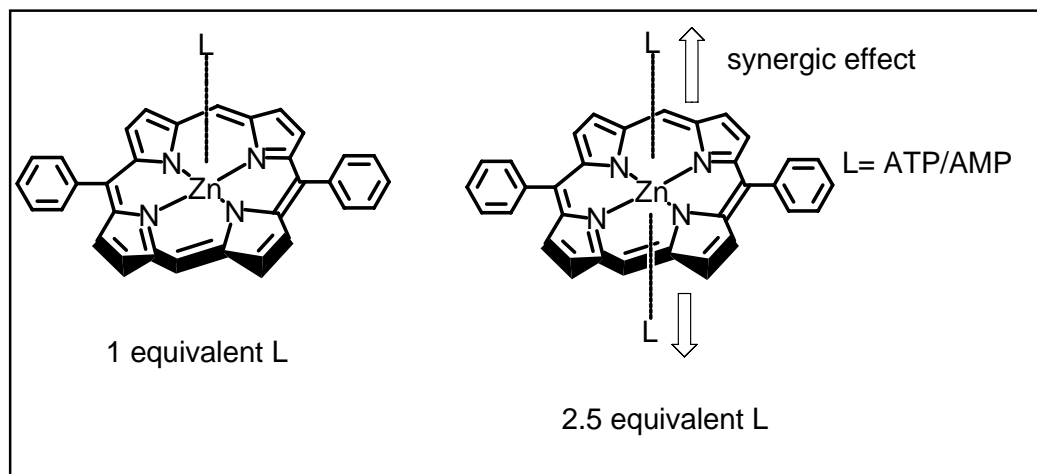


Fig. 8.2 Illustration of synergic effect observed in the Zn(II) metalloporphyrin complex with an increase in axial ligand

Interestingly, the ATP and AMP complexes of **8-1a-c** (both 1:1 and 2.5:1 ratios) exhibit significant differences in their ^1H NMR spectrum. Generally, the upfield shifts for protons at C2 were greater in the ATP:**8-1a-c** than AMP:**8-1a-c** complexes (1:1). The upfield shifts for protons at C2 are 0.42, 0.38 and 0.28 ppm in the 1:1 ATP complexes of **8-1a**, **8-1b** and **8-1c**, respectively, when compared to the uncomplexed ATP. Whereas, the upfield shifts for protons at C2 are 0.08, 0.16 and 0.07 ppm in the 1:1 AMP complexes of **8-1a**, **8-1b** and **8-1c**, respectively, when compared to the uncomplexed AMP.

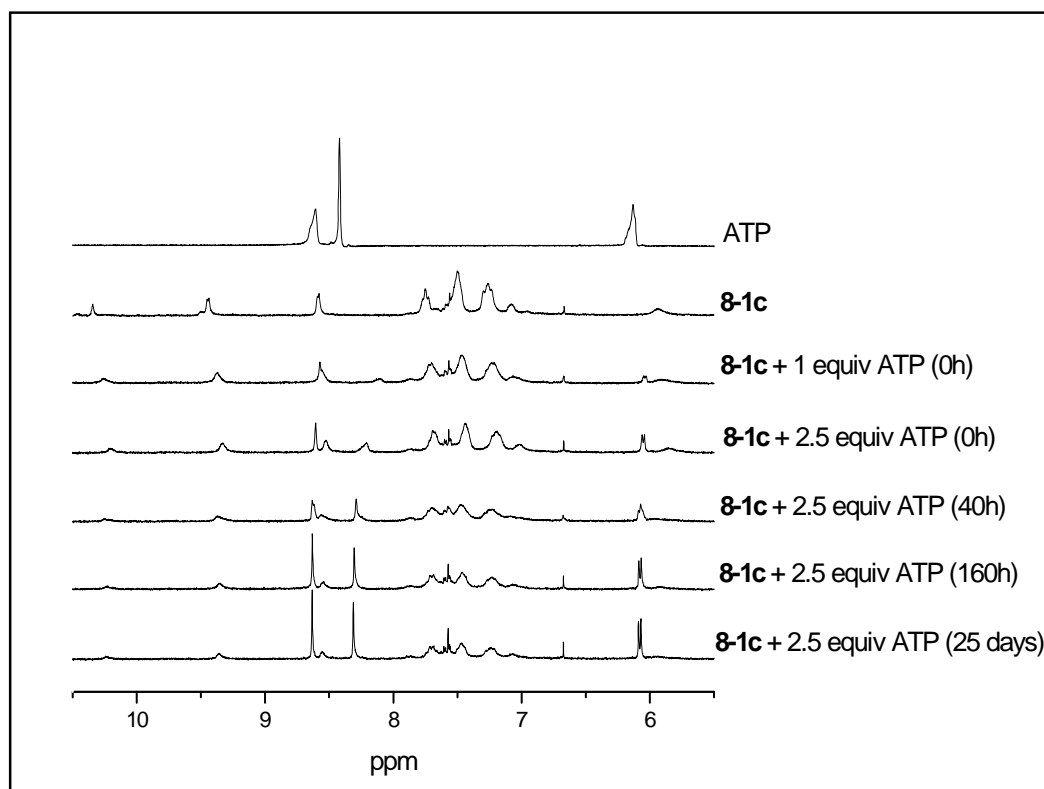


Fig. 8.3 ^1H NMR spectrum of ATP, **8-1c** and their complexes with variable ATP ratio and time

These results may imply that two additional phosphate groups of ATP cause the purine base to bind more tightly to porphyrin. This was also confirmed by the observation that the *meso* and pyrrolic protons of the ATP complexes shifted more upfield than the AMP complexes. The stronger interaction in ATP:**8-1a-c** complexes was attributed to electrostatic interaction(s) between the charged phosphorus at the substituents extended from the phenyl ring of porphyrin and the oxygen of phosphate. Hence, ^{31}P NMR was used to probe for the presence of such interactions.

The ^{31}P -NMR spectrum of the AMP complexes do not show any obvious changes in the phosphorus peaks even upon addition of 2.5 equivalents of the nucleotide and after long hours. However, the ATP:**8-1c** (2.5:1) complex exhibit additional splitting of the β -ATP and **8-1c** phosphorus peaks after 40 hours (Fig. 8.4) while the β -ATP and γ -ATP peaks broadened only in the ATP:**8-1b** (2.5:1) complex which sharpened after 40 hours (Fig. 8.5). These observations reveal that the positively-charged P atoms of *para* phosphonium substituents on **8-1c** have electrostatic interaction with the O atom of phosphate at the β -position. On the other hand, the P atoms of *trans* phosphonium at the *ortho* position in **8-1b** are in close proximity to interact with two O atoms of ATP. The interaction of **8-1b** and **8-1c** with nucleotides is therefore determined by steric and proximity factors.

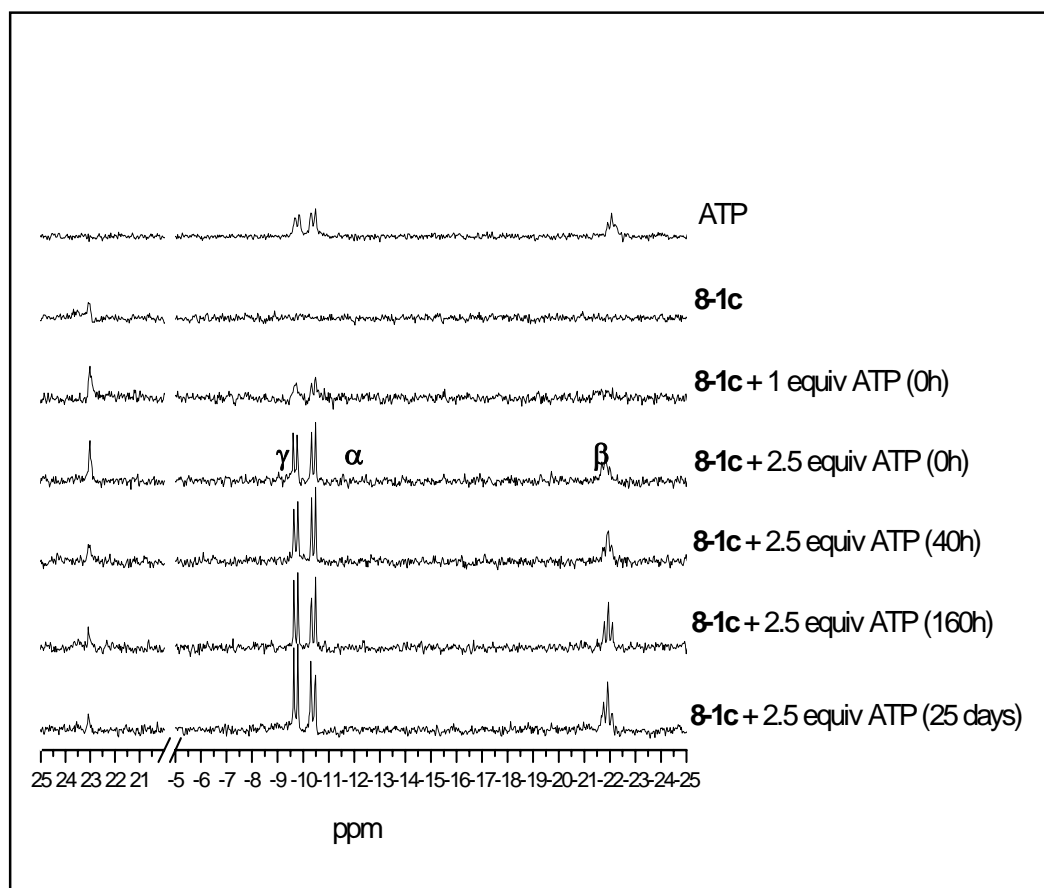


Fig. 8.4 ^{31}P NMR of ATP, **8-1c** and their complexes with variable ATP ratio and time. Broad β - ^{31}P peaks observed in the 2.5:1 complex at 0 hours sharpened over time. The α , β and γ ^{31}P peaks are labeled

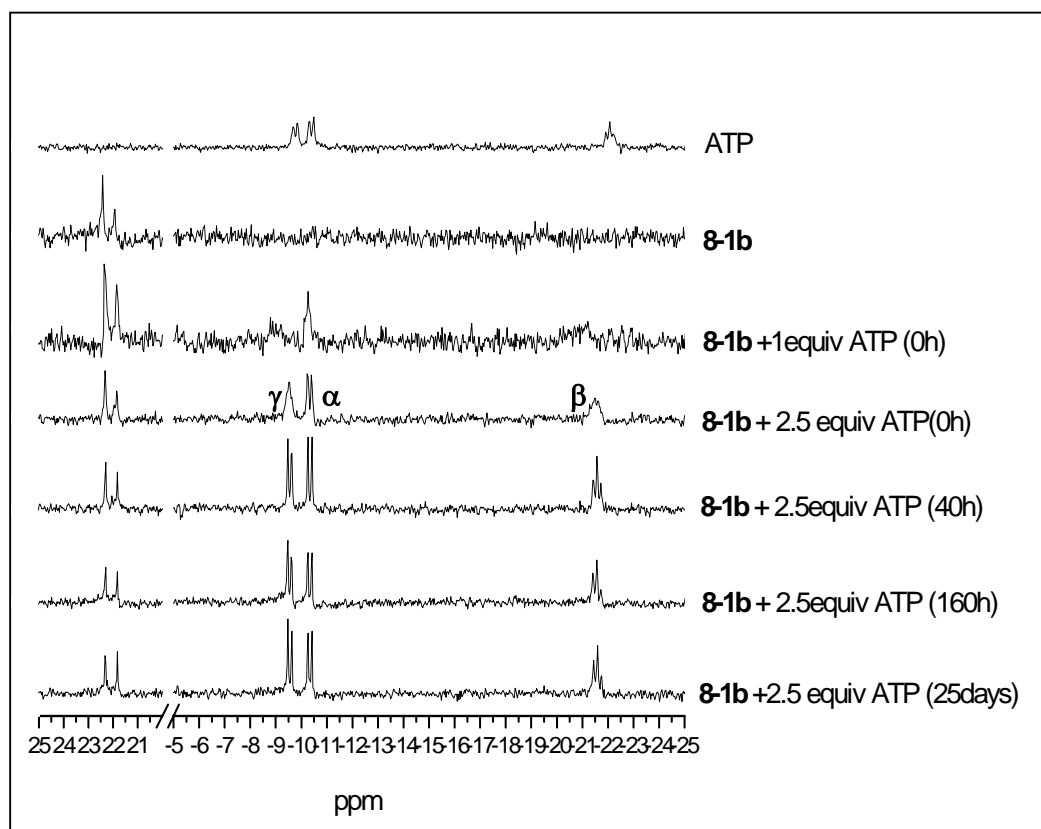


Fig. 8.5 ^{31}P NMR of ATP, **8-1b** and their complexes with variable ATP ratio and time. Broad β - and γ - ^{31}P peaks observed in the 2.5:1 complex at 0 hours sharpened over time. The α , β and γ ^{31}P peaks are labeled

8.2.3 OPTICAL STUDIES

UV-vis absorption spectroscopy is one of the more powerful techniques to study the interaction of ATP with porphyrins. Thus, time course measurement of the UV-vis absorption of **8-1a-c** with and without the nucleotides using UV-vis absorption spectroscopy was carried out. For comparison, the spectroscopic changes of the blank solutions of **8-1a-c** over time were also measured.

We use a simple and effective approach to determine the stoichiometry of the porphyrins to AMP and ATP by plotting the absorbance of the solutions with varying ratios of the two compounds while keeping the total number of moles constant. This is known as a Job's plot.¹⁶ The results show that 1 mole of porphyrin binds to 2 equivalents of nucleotide because the absorbance do not change much with further increase in the proportion of the latter based on their UV-vis spectrum.

Water soluble porphyrins have a tendency to form intermolecular aggregates in aqueous solution. Aggregation complicates the binding of porphyrins to nucleotides and decreases their ϕ_{eff} . The latter lowers photosensitizing activities. UV-vis spectroscopy is a simple tool to gain information on the aggregates. Porphyrin aggregates have large $W_{1/2}$ (bandwidth at half-height peak) of the Soret band. The UV-vis spectra of **8-1a** in H₂O, methanol and DMF were obtained (Refer to Table 8.2). Each porphyrin has a Soret band with large $W_{1/2}$ in H₂O while in DMF each has a Soret band with small $W_{1/2}$. The Soret band of **8-1c** has the largest $W_{1/2}$ in the same solvent and is more red-shifted than that of **8-1a** and **8-1b** which do not differ much in conjugation pattern. This shows that **8-1c**, the most commonly studied porphyrin as a photosensitizer, exists mostly as aggregates in the same concentration and solvent. This highlights the advantage of *ortho* derivatized water-soluble porphyrins **8-1a** and **8-1b** over the *para* types.

Table 8.2 The λ_{\max} (nm) and $W_{1/2}$ (nm) of **8-1a-c** obtained from UV-vis spectrum in H₂O, CH₃OH and DMF

Compound	Solvent { λ_{\max} (nm) [$W_{1/2}$ (nm)]}		
	H ₂ O	CH ₃ OH	DMF
8-1a	416.5 [14]	416 [11]	416 [9.5]
8-1b	416 [15]	416 [11]	416 [12]
8-1c	411 [26]	411 [16]	415.5 [16]

In a lightly degassed solution of the porphyrin and their complexes (2.5 equivalents) in H₂O and 10 % methanol, measured at room temperature and normal room lighting, the absorption changes of these complexes over 7 hours were similar to the blank solutions except for the ATP:**8-1c** complex. The latter complex showed a broadened and red-shifted UV-vis absorption. A blank solution of **8-1c** decreased in absorbance more rapidly over time than the blank solutions of **8-1a** and **8-1b**. Since the change in absorbance of the AMP:**8-1a-c** and ATP:**8-1a,b** is similar to that of the blank, the observation cannot be attributed to the slow coordination of the nucleotide over time but possibly due to the photobleaching of the porphyrins and its complexes.

A detailed investigation of the photobleaching properties of the porphyrins and their complexes was carried out. Solutions of **8-1a-c** in H₂O and 10 % methanol were irradiated with a Xe lamp and purged with a constant flow of oxygen. A rapid photobleaching of the porphyrins was noticed which revealed the chemical degradation of the chromophore and hence lower potential for photosensitization. The

rate of decrease was faster than in the absence of the oxygen, which shows that the oxygen species are responsible for the photobleaching of porphyrins.

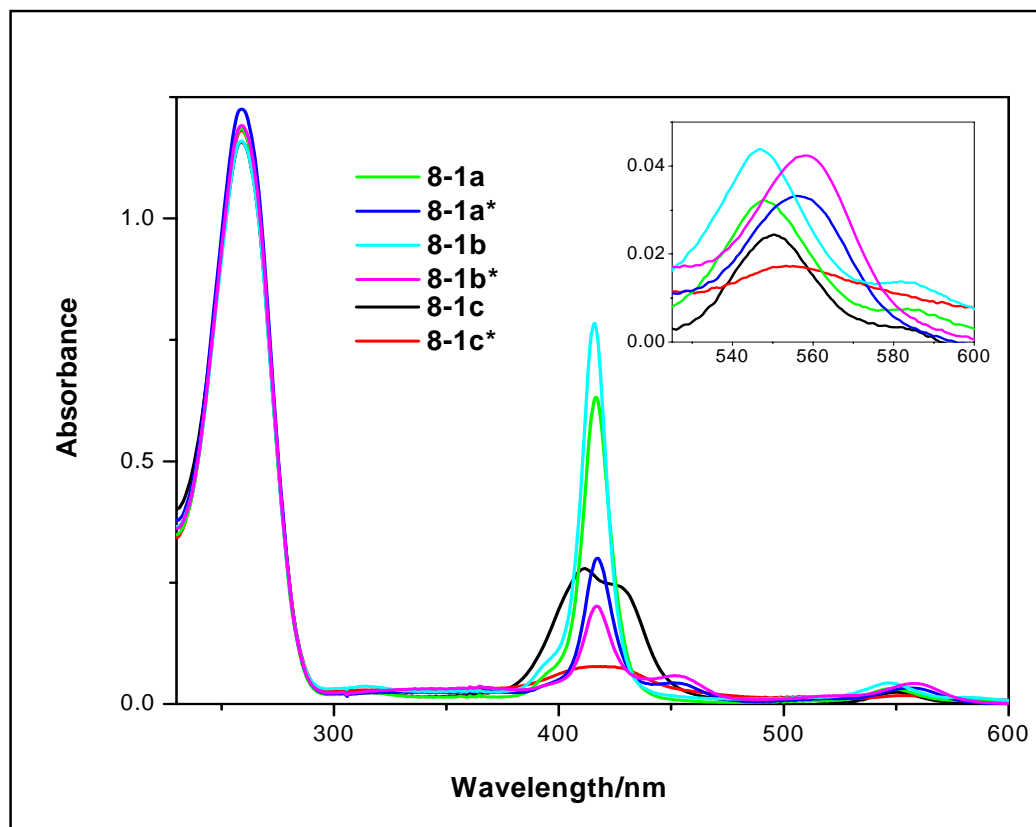


Fig. 8.6 UV-vis absorption spectrum of **8-1a-c** (1×10^{-5} M) in 2.5 equivalents ATP in H_2O and 10 % methanol before oxygenation and irradiation.* Refers to the same solution after oxygenation and irradiation with Xe lamp for 2 hours

The photosensitivity of **8-1c** is shown by the rapid photodegradation even under normal room lighting and sunlight. At the same concentration, **8-1c** shows the lowest molar absorptivity and largest $W_{1/2}$ in H_2O and 10 % methanol solution before irradiation. After oxygenation and irradiation for 2 hours, the optical spectra of the ATP complexes of **8-1a-c** show a loss in absorbance. It can be highlighted that **8-1c** exhibit an almost total loss of absorbance of the Soret band signifying the photodegradation

after 2 hours of the original Zn(II) phosphonium salt. The spectra of **8-1a,b** show the appearance of a band at higher wavelength upon oxygenation and irradiation, indicating both complexes underwent photomodification. While the spectroscopic changes underwent by **8-1c** is less obvious due to the broad Soret band.

The Φ_{eff} of pure **8-1a,b** are about twice that of **8-1c** while that of the ATP complexes of **8-1a,b** is about 4.5 - 5 times that of **8-1c** as summarized in Table 8.3. That is, the Φ_{eff} of **8-1a** and **8-1b** increased upon addition of 2.5 equivalents of ATP while that of **8-1c** quenched by a significant 0.9 % (which is a 50 % decrease of Φ_{eff}). The latter may be attributed to a charge transfer process. The higher Φ_{eff} of the ATP complexes of **8-1a** and **8-1b** reflect the higher potential of these complexes in photosensitizing activities over that of **8-1c** because under the same concentration, ATP:**8-1a,b** are likely to get excited and transfer their energies to $^3\text{O}_2$ more readily. Upon addition of 5 equivalents of ATP, their Φ_{eff} changed only marginally.

Table 8.3 Fluorescence quantum efficiencies (Φ_{eff}) of **8-1a-c** with and without ATP

Compound	$\Phi_{\text{eff}}^{\text{iii}}$	
	Without ATP	Addition of 2.5
8-1a	4.2	4.5
8-1b	3.6	4.1
8-1c	1.8	0.9

ⁱⁱⁱ Zn(II) tetraphenylporphyrin as reference ($\Phi_{\text{eff}} = 3.3\%$ in toluene)

To investigate the species responsible for the photobleaching mechanism, sodium azide (singlet oxygen scavenger) was added to the solutions of the ATP:**8-1a-c** complexes separately. The photobleaching rates decreased in the presence of sodium azide for ATP complexes of **8-1a,b** but occurred for the complex of ATP:**8-1c** only after 53 minutes as shown in Fig. 8.7. This demonstrates the involvement of singlet oxygen in photoproduct formation of the *ortho* isomers whereas the ATP:**8-1c** complex probably underwent another mechanism of photobleaching at the initial stage. The formation of photoproducts of ATP:**8-1a,b** were also revealed clearly in their UV-vis absorption spectrum at higher wavelength (454 nm).

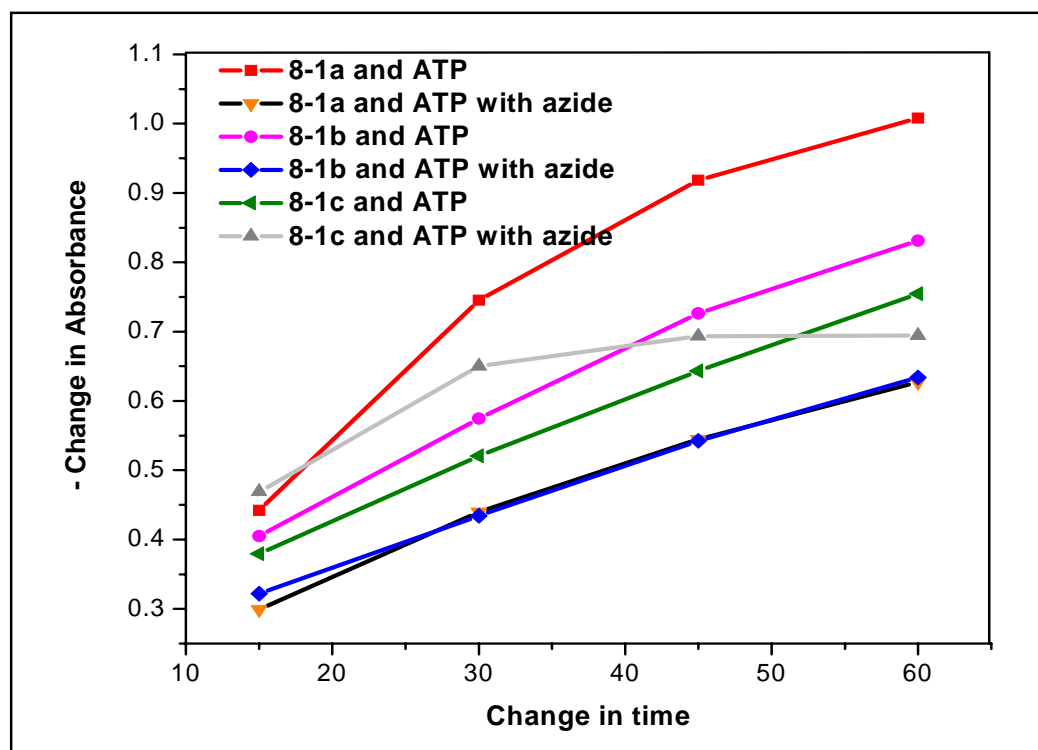


Fig. 8.7 A study of the effect of sodium azide on rate of photobleaching. Negative change in absorbance over time upon oxygenation and irradiation with Xe lamp of solution containing **8-1a-c** with 2.5 equivalents ATP in H₂O and 10% methanol separately

8.3 CONCLUSION

The Zn(II) metalloporphyrin complexes **8-1a,b** with triphenylphosphine substituents at the *ortho* positions are found to overcome the consequence of aggregation posed by their *para* counterparts **8-1c** due to greater steric hindrance of the former. The ^1H and ^{31}P NMR, UV-vis absorption and fluorescence studies show that AMP and ATP complexed with **8-1a-c**. Compounds **8-1a,b** were determined to possess greater potential as photosensitizers because these compounds and their ATP complexes exhibit higher ϕ_{eff} due to lower aggregation in aqueous solution and they exhibit relatively higher stability towards photobleaching compared to **8-1c** and its ATP complex. Through structural modification, two Zn(II) metalloporphyrin complexes with *ortho* substituents are found to possess greater potential as photosensitizers than their more commonly studied *para* counterparts.

8.4 REFERENCES

- ¹ (a) Fleischer, E.B. *Inorg. Chem.* **1962**, *1*, 493. (b) Hambright, P.; Fleischer, E.B. *Inorg. Chem.* **1970**, *9*, 1757. (b)Wynter, C.I.; Hambright, P.; Cheek, C.H. *Nature*, **1967**, *216*, 1105.
- ² (a) Fiel, R.J.; Beerman, T.A.; Mark, E.H.; Datta-Gupta, N. *Biochem. Biophys. Res. Commun.* **1982**, *108*, 1067. (b) Musser, D.A.; Datta-Gupta, N.; Fiel, R.J. *Biochem. Biophys. Res. Comm.* **1982**, *108*, 66. (c) Fiel, R.J.; Howard, J.C.; Mark, E.H.; Datta-Gupta, N. *Nucleic Acids Res.* **1979**, *6*, 3039.

- ³ (a) Seenisamy, J.; Bashyam, S.; Gokhale, V.; Vankayalapati, H.; Sun, D.; Siddiqui-Jain, A.; Streiner, N.; Shin-ya, K.; White, E.; Wilson, W.D.; Hurley, L.H. *J. Am. Chem. Soc.* **2005**, *127* (9), 2944. (b) Ohyama, T.; Mita, H.; Yamamoto, Y. *Biophys. Chem.* **2005**, *113* (1), 53. (c) Laine, M.; Richard, F.; Tarnaud, E.; Bied-Charreton, C.; Verchere-Beaur, C. *J. Bio. Inorg. Chem.* **2004**, *9* (5), 550. (d) Maraval, A.; Franco, S.; Vialas, C.; Pratviel, G.; Blasco, M.A.; Meunier, B. *Org. Biomol. Chem.* **2003**, *1* (6), 921.
- ⁴ (a) Liu, J.; Li, J.N.; Mei, W.J. *Prog. Chem.* **2004**, *16* (6), 969. (b) Song, R.; Witvrouw, M.; Schols, D.; Robert, A.; Balzarini, J.; DeClercq, E.; Bernadou, J.; Meunier, B. *Antiviral Chem Chemotherapy*, **1997**, *8* (2), 85. (c) Neurath, A.R.; Strick, N.; Debnath, A.K. *J. Mol. Recog.* **1995**, *8* (6), 345.
- ⁵ Ford, K.G.; Neidle, S. *Bioorg. Med. Chem.* **1995**, *3* (6), 671.
- ⁶ Bejune, S.A.; Shelton, A.H.; McMillin, D.R. *Inorg. Chem.* **2003**, *42* (25), 8465.
- ⁷ Han, G.Y.; Yang, P. *J. Inorg. Biochem.* **2002**, *91* (1), 230.
- ⁸ Sen, D.; Geyer, C.R. *Curr. Opin. Chem. Bio.* **1999**, *2* (6), 680.
- ⁹ Robic, N.; Bied-Charreton, C.; Perrée-Fauvet, M.; Verchère-Béaur, C.; Salmon, L.; Gaudemer, A.; Pasternack, R.F. *Tetrahedron Lett.* **1995**, *36*, 4227.
- ¹⁰ (a) Kubát, P.; Lang, K.; Král, V.; Anzenbacher, P., Jr. *Phys. Chem. B* **2002**, *106*, 6784. (b) Kubát, P.; Lang, K.; Anzenbacher, P., Jr.; Král, V.; Ehrenberg, B. *J. Chem. Soc., Perkin Trans. 1* **2000**, 933. (c) Jin, R.; Aoki, S.; Shima, K. *J. Chem. Soc., Faraday Trans.* **1997**, *93*, 3945.

- ¹¹ (a) Jasuja, R.; Jameson, D.M.; Nishijo, C.K.; Larsen, R.W. *J. Phys. Chem. B* **1997**, *101*, 1444. (b) Munakata, H.; Kanzaki, T.; Nakagawa, S.; Imai, H.; Uemori, Y. *Chem. Pharm. Bull.* **2001**, *49* (12), 1573. (c) Uno, T.; Aoki, K.; Shikimi, T.; Hiranuma, Y.; Tomisugi, Y.; Ishikawa, Y. *Biochemistry* **2002**, *41*, 13059.
- ¹² Chandrasekhar, V.; Nagendran, S.; Azhakar, R.; Kumar, M.R.; Srinivasan, A.; Ray, K.; Chandrashekar, T.K.; Madhavaiah, c.; Verma, S.; Priyakumar, U.D.; Sastry, G.N. *J. Am. Chem. Soc.* **2005**, *127*, 2410.
- ¹³ (a) Bonnett, R.; Martínez, G. *Tetrahedron* **2001**, *57* (47), 9513. (b) Bonnet, R.; Martínez, G. *Org. Lett.* **2002**, *4* (12), 2013.
- ¹⁴ (a) Ceckler, T.L.; Bryant, R.G.; Oenny, D.P.; Cibson, S.L.; Hilf, R. *Biochem. Biophys. Res. Comm.* **1986**, *140*, 273. (b) Naruse, S.; Horikawa, Y.; Tanaka, C.; Hagashi, T.; Sekimoto, H.; Ueda, S.; Hirakawa, K. *Radiology* **1986**, *160*, 827. (c) Chopp, M.; Farmer, H.; Hetzel, F.; Schaap, A.P. *Photochem. Photobiol.* **1987**, *46*, 819. (d) Hilf, R.; Penney, D.P.; Ceckler, T.L.; Bryant, R.G. *Photochem. Photobiol.* **1987**, *46*, 809. (e) Chapman, J.D.; McPhee, M.S.; Walz, N.; Chemer, M.P.; Stobbe, C.C.; Soderlind, K.; Arnfield, M.; Meeker, B.E.; Trimble, L.; Allen, P.S. *J. Nat. Cancer Inst.* **1991**, *83*, 1650.
- ¹⁵ Ogoshi, H.; Hatakeyama, H.; Kotani, J.; Kawashima, A.; Kuroda, Y. *J. Am. Chem. Soc.* **1991**, *113*, 8181.
- ¹⁶ Kim, J.; Raman, B.; Ahn, K.H. *J. Org. Chem.* **2006**, *71*, 38.

CHAPTER 9

CONCLUSIONS AND FUTURE WORK

9.1 CONCLUSIONS AND FUTURE WORK

This thesis presents conclusions for four main areas of our research. It includes the design, syntheses, characterization and nonlinear optics (NLO) studies of (1) free base porphyrins and Zn(II) metalloporphyrins coordination complexes, (2) covalently-linked conjugated systems consisting of porphyrins, (3) benzo[c]cinnoline-fluorene copolymers and (4) investigation of the molecular recognition, aggregation and photobleaching properties of water-soluble Zn(II) metalloporphyrins which differ in conformation and configuration.

For the first time, two-photon absorption (TPA) properties of a series of Zn(II) metalloporphyrin coordination complexes formed by Zn-O coordination bonds are investigated using the Z-scan technique. Our studies have established that the overall architecture of the coordination complex affects the TPA cross section (σ_2). Higher σ_2 is achieved for Zn(II) metalloporphyrins complexes as compared to their free base ligands, as well as in the absence of heavy Br atoms in the porphyrin ligand. The conformation of the peripheral substituents and hence overall polarity of the macrocycle also plays a role in influencing the TPA property. A wavelength dispersion study of the Zn(II) metalloporphyrins coordination complex **4-16** reveals its centrosymmetry and hence retention of the dimeric structure in CHCl_3 solution.

The excited state measurements of two ethene-linked oligomers **6-9** and **6-10** in CH₂Cl₂ solution reveal that the conformation of the peripheral group on the porphyrin moiety in the polymer affects the nonlinear properties of the overall conjugated system. The oligomer **6-10** was found to exhibit lower threshold of limiting comparable to that of C₆₀.

Water-solubility is an important feature for most drugs. However, it is known that porphyrins tend to aggregate and undergo photobleaching in aqueous systems and these features lower their efficiency as photosensitizers. Hence, we have undertaken the design and study of novel water-soluble porphyrins and found solutions to minimize these problems through structural modification of the *para* substituted compound **8-1c**. Steric hindrance provided by large groups in the *ortho* positions of the peripheral phenyl rings of **8-1a,b** were found to prevent aggregation. These water-soluble Zn(II) metalloporphyrin complexes also show binding to AMP and ATP and compounds **8-1a,b** exhibit greater photostability in aqueous solutions upon oxygenation and irradiation.

Our work reports TPA property exhibited by benzo[*c*]cinnoline monomer as well as copolymer of benzo[*c*]cinnoline and fluorene for the first time. Our first discovery of the TPA property in benzo[*c*]cinnoline as well as the structure-property relationship established in the works of porphyrin-based compounds form the basis of rational designs and jump start to the new materials for two-photon absorption application, in particular, photosensitizers for photodynamic therapy (PDT).

The approach requires modification of the porphyrin core while preserving the desirable properties of the molecule (explained in Chapter 1, Section 1.4). This can be achieved via the indirect excitation of a chromophore with two-photon absorbing property

and strong electron donating properties (donor). Through fluorescence resonance energy transfer (FRET)¹ from the donor to the porphyrin core, the TPA σ_2 of the latter can be significantly enhanced. The energy is effectively concentrated on the first excited singlet level of the porphyrin core. Recently, this approach has successfully shown the enhancement of TPA efficiency in a water-soluble dendrimer.²

However, the design of this modular system can be further improved to incorporate intersystem crossing helper so that most of the photosensitizer molecules will end up in the triplet state and transfer the energy to $^3\text{O}_2$ more effectively (Refer to Chapter 2, Section 2.4). Since triplet lifetimes are longer than singlet lifetimes, the excitation of singlet oxygen from triplet (ground) to singlet (excited) state occurs more efficiently.³

Therefore, the proposed modular system shall comprise of four main parts: the porphyrin core, two-photon absorber, intersystem crossing helper and water-solubilizing moieties. A possible design of such a modular system is proposed as shown in Fig. 9.1 below. The core consist of a Zn(II) metalloporphyrin dimer which structurally resemble that of the coordination dimer (**4-16**) with the largest σ_2 measured at 650 nm. The peripheral phenyl ring carries *ortho* phosphonium group for water-solubility and prevent aggregation. The dichlorinated phenyl ring appended to the *meso* carbon acts as an intersystem crossing helper while the benzo[c]cinnoline and fluorene moieties serve to enhance the two-photon absorptivity of the porphyrin core through energy transfer after two-photon excitation. Hence, this newly designed chromophore may exhibit enhanced two-photon absorptivity and possess properties with potential application for PDT.

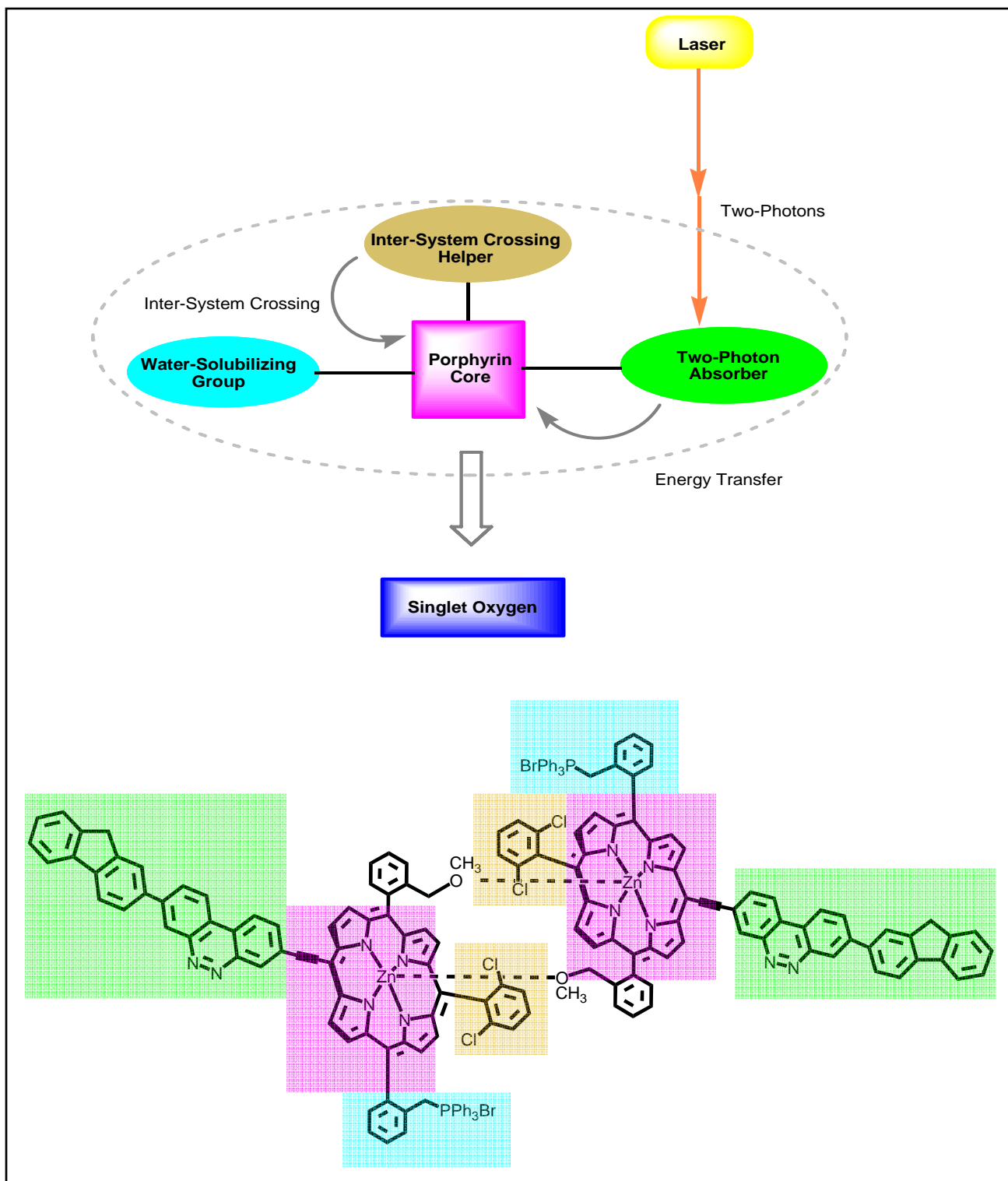


Fig. 9.1 Modular system (top) and proposed molecular structure (bottom) using known compounds studied in this work for the design of water-soluble porphyrin as photosensitizer for PDT. The functions of each moiety in the proposed structure (bottom) correspond to the colour scheme shown in the diagram above

9.2 REFERENCES

¹ Lakowicz, J.R. “ *Principles of Fluorescence Spectroscopy*”, 2nd ed., N.Y., Kluwer Academic/Plenum, 1999.

² Oar, M.A.; Serin, J.M.; Dichtel, W.R.; Frechet, J.M.J.; Ohulchansky, T.Y.; Prasad, P.N. *Chem Mater.* **2005**, *17*, 2267.

³ DeRosa, M.C.; Crutchley, R.J. *Cood. Chem Rev.* **2002**, 233-234, 351.

CHAPTER 10

EXPERIMENTAL RESULTS

10.1 MATERIALS

Solvents, reagents and chemicals were obtained from various chemical companies including Sigma-Aldrich, Merck, TCI, Acros Organics and Fluka and were used without further purification. Argon and nitrogen used in the experiments were obtained directly from gas cylinders.

Anhydrous tetrahydrofuran (THF) was collected by distillation over sodium and benzophenone under nitrogen atmosphere. Anhydrous toluene was also obtained by distillation over sodium. Triethylamine and diisopropylamines were dried over CaH_2 and distilled before used.

10.2.0 CHARACTERIZATION TECHNIQUES

The compounds were characterized by several instrumental techniques namely proton (^1H) and carbon (^{13}C) nuclear magnetic resonance (NMR) spectroscopy, mass spectrometry (MS), elemental analysis (EA) and Fourier-transform infrared (FTIR) spectroscopy. The techniques are used to characterize the structures of the synthesized compounds as well as to give an indication of their purities.

The above mentioned techniques can be broadly classified as methods for the measurement of the molecular structure, attributes which are characteristic of the

compounds. In addition to the above techniques, the properties of the polymer were also determined by gel permeation chromatography (GPC), thermogravimetric analysis (TGA), differential scanning calorimetry (DSC), ultraviolet-visible spectroscopy (UV-vis) and photoluminescence spectroscopy (PL). All the characterization techniques used in this work are as follows.

10.2.1 FOURIER-TRANSFORM INFRARED (FTIR) SPECTROSCOPY¹

FTIR is used where information on chemical, structural and conformational aspects of the compound is required. The FTIR spectra of compounds in KBr disks were determined by scanning from 400 cm^{-1} to 4200 cm^{-1} on a Bio-Rad FTS 165 spectrometer. The spectra were measured at room temperature of 25°C. Peaks in the IR spectrum correlate to specific vibrational modes of the various functional groups or bonds in the molecule. The region between 1300 cm^{-1} and 900 cm^{-1} , known as the “fingerprint” region of an IR spectrum. It is unique for every molecular species and hence aids in the identification of the unknown compounds.

10.2.2 NUCLEAR MAGNETIC RESONANCE (NMR) SPECTROSCOPY²

¹H NMR, ¹³C NMR and ³¹P NMR spectra are collected on the Bruker DPX300 (300 MHz), Bruker ACF300 (300 MHz) and Bruker AMX500 (500 MHz) spectrometers with chloroform-*d*, tetrahydrofuran-*d*, dimethylsulfoxide-*d*, *N,N*-dimethylformamide-*d*, nitrobenzene-*d* or toluene-*d* as solvent and tetramethylsilane (TMS) as internal standard depending on the solubility of compound being tested. Most of the compounds in this thesis are measured with the 300 MHz spectrometers unless otherwise stated.

10.2.3 ELEMENTAL ANALYSIS (EA)³

Perkin-Elmer PE 2400 CHN and CHNS Elemental Analyzers were used for rapid simultaneous determination of the C, H, N and S contents in organic and other types of materials.

A high sensitivity instrument, Thermal Jarrell Ash Duo Iris Inductively Coupled Plasma-Optical Emission Spectrometer was used for analyzing metallic analytes in solutions. A microcomputer-controlled atomic absorption/emission spectrometer, Perkin-Elmer 1100B Atomic Absorption Spectrophotometer, was dedicated to ppm level analysis by the flame technique (absorption and emission). A graphite furnace spectrophotometer, Perkin-Elmer Zeeman Atomic Absorption Spectrophotometer 4100ZL, provides the means to determine some metals at ppb levels. A Flow Injection Device enables the instrument to determine elements that form gaseous hydrides.

For halogen determination which includes the analysis of F, Cl, Br and I, the Schöninger combustion method/oxygen flask method which involves the decomposition of the sample and the conversion of the halogen into a form which can be determined by manual titration were used.

10.2.4 MASS SPECTROMETRY (MS)⁴

The mass spectra of the compounds were analyzed using a high resolution (60,000), 5KV Double Focusing Reversed Nier-Johnson Geometry Mass Spectrometer (Finnigan/MAT 95XL-T) with an effective mass range of 1 - 3,500 m/z. It is coupled with a HP6890 GC system for performing GC/MS analysis with library search. The

MAT95XL-T is also equipped with an Ion Trap for performing MS/MS analysis as well as MS. The available ionization techniques are EI, CI, FAB and ESI and including positive and negative modes. Target compound analysis can be performed by HRGC/HRMS measurement at a resolution of 10,000. MALDI-TOF mass spectra were recorded on Bruker Autoflex TOF/TOF.

10.2.5 ULTRAVIOLET-VISIBLE ABSORPTION (UV-vis) SPECTROSCOPY

The UV-vis spectra of the compounds were measured on a Shimadzu UV-3101PC UV-vis scanning spectrophotometer. The solvents used for the solutions include CHCl_3 , CH_2Cl_2 , THF, nitrobenzene, chlorobenzene, DMF, DMSO, acetone, ethyl acetate, toluene, CS_2 and pyridine.

10.2.6 PHOTOLUMINESCENCE SPECTROSCOPY

The PL spectra of our compounds were measured on a Perkin-Elmer LS55 luminescence spectrometer with a Xe lamp as the light source. The fluorescence quantum efficiency (Φ_{eff}) of the compounds in solutions was estimated using quinine sulphate (1×10^{-5} M in 0.1 M H_2SO_4) as standard, which has a Φ_{eff} of 55 %. The other standard used was Zn(II) tetraphenylporphyrin (1×10^{-5} M in toluene), which has a Φ_{eff} of 3.3 %. The Φ_{eff} is calculated according to the following equation 10.1:

$$(10.1) \quad \Phi_{\text{unk}} = \Phi_{\text{std}} (I_{\text{unk}} / A_{\text{unk}}) (A_{\text{std}} / I_{\text{std}}) (\eta_{\text{unk}} / \eta_{\text{std}})^2$$

where Φ_{unk} and Φ_{std} are the fluorescence quantum efficiencies, I_{unk} and I_{std} are the integrated emission intensities, n_{unk} and n_{std} are the refractive indices of the solutions while A_{unk} and A_{std} are the absorbance at the excitation wavelength of the sample and the standard respectively.

10.2.7 DIFFERENTIAL SCANNING CALORIMETRY (DSC)⁵

The DSC curves of the oligomers and polymers were run on the DuPont thermal analyst system. A heating rate of 20 °C/min was employed in nitrogen.

10.2.8 THERMOGRAVIMETRIC ANALYSIS (TGA)

TGA data were collected on a Du Pont Thermal analyst 2100 system with a TGA 2950 thermogravimetric analyzer in air or nitrogen. A heating rate of 20 °C/min with airflow of 75 cm³/min was used with the runs being conducted from room temperature to 800 °C.

10.2.9 GEL PERMEATION CHROMATOGRAPHY (GPC) ANALYSES⁶

Molecular weights were determined on a Waters 600E HPLC System with PhenogelTM M × L and M × M columns (300 mm × 4.6 mm i.d) using polystyrene as standards and THF as eluent.

10.2.10 X-RAY CRYSTALLOGRAPHY

The diffraction experiments were carried out on a Bruker SMART CCD diffractometer with Mo K α sealed tube at 223(2) K. SMART software was used for collecting frames of data, indexing reflection and determining lattice parameters; SANIT was used for integrating intensity of reflections and scaling; SADABS was used for correcting absorption, SHELXTL was used for determining space group and structure, least-square-refining of F^2 and reporting graphics and structure. All the C-H atoms were placed in their calculated positions and included in the structure factor calculations.

10.2.11 MELTING POINT

The melting points for all the synthesized compounds were measured on a Buchi melting apparatus.

10.3 PROCEDURES

2-BROMOMETHYLBENZONITRILE (4-2)

o-Tolunitrile **4-1** (15.5 mmol, 2.0 ml) and recrystallized NBS (17.1 mmol, 3.04 g) were added into CCl₄ (50 ml). The reaction mixture was irradiated and refluxed gently under Ar gas. After the reaction mixture had started to reflux, a spatula of benzoyl peroxide was added. The reaction was completed in about 3 hours. The mixture was then extracted with CH₂Cl₂, washed with deionised water, dried over anhydrous calcium sulphate, filtered then evaporated. The residue was chromatographed over silica gel (250 - 400 mesh) and 3:1 distilled hexane/CH₂Cl₂ as eluent to give the white crystalline product **4-2**.

Yield: 1.76 g (58 %). Melting point: 71.0 - 71.5°C {lit. 72 - 74°C}.⁷ ¹H NMR (CDCl₃): δ 7.68 (d, 1H, Ph-H proton, ³J = 8.0 Hz), 7.57 (m, 2H, Ph-H protons), 7.42 (td, 1H, Ph-H proton, ³J = 7.2 Hz, ⁴J = 7.9 Hz), 4.64 (s, 2H, Ph-CH₂Br protons). ¹³C {¹H} NMR (CDCl₃): δ 141.0 (1C, -CN), 133.2, 133.1, 130.4, 128.9 (4C, aromatic CH); 116.7, 112.3 (2C, aromatic C); 29.3 (1C, Ph-CH₂Br). El-mass spectrum: 195 (70 %), 197 (70 %).

2-METHOXYMETHYLBENZONITRILE (4-3)

Sodium (326.7 mmol, 7.51 g) was dissolved in dry methanol (1 L) under Ar gas. The reaction mixture was cooled in an ice-bath before a solution of **4-2** (81.6 mmol, 16.00 g) in methanol was added using a dropping funnel. The mixture was refluxed gently for another 2 - 3 hours. After which, the mixture was cooled and methanol was removed *in*

vacuo. The mixture was extracted with CH₂Cl₂, washed with deionised water, dried over anhydrous sodium sulphate, filtered then evaporated. The residue was chromatographed over silica gel (60 - 250 mesh) using 1:1 distilled hexane/CH₂Cl₂ as eluent to yield **4-3** as yellow oil.

Yield: 11.84 g (99 %). ¹H NMR (CDCl₃): δ 7.65 (d, 1H, Ph-H proton, ³J = 7.7 Hz), 7.56 (m, 2H, Ph-H protons), 7.38 (m, 1H, Ph-H proton), 4.64 (s, 2H, Ph-CH₂O- protons), 3.47 (s, 3H, -OCH₃ protons). ¹³C {¹H} NMR (CDCl₃): δ 141.8 (1C, -C_N); 132.8, 132.6, 128.4, 128.0 (4C, aromatic CH); 117.1, 111.3 (2C, aromatic C); 72.0 (1C, Ph-CH₂O-); 58.7 (1C, -OCH₃). El-mass spectrum: 147.0 (40 %). m/z calcd: 147.0684, HRMS: 147.0680 (30 %).

2-METHOXYMETHYLBENZALDEHYDE (4-4)

Method 1

Diisobutylaluminium hydride (DIBAL, 50.0 mol, 50 ml) was added under nitrogen over 30 minutes to a solution of **4-3** (26.5 mmol, 3.90 g) in dried benzene (1 L). The mixture was stirred overnight at room temperature. The viscous pale yellow solution was decomposed slowly (using ice bath cooling) by firstly adding methanol (10 ml), methanol and water (1:1, 15 ml) and finally with conc. HCl (16 ml) and H₂O (30ml) mixture successively and the mixture was stirred for another 2 hours. The benzene layer was separated, washed with deionised water, dried over anhydrous sodium sulphate, filtered then evaporated. The residue was chromatographed over silica gel (60 - 250 mesh)

using 2:1 distilled hexane/CH₂Cl₂ as eluent to yield **4-4** as yellow oil. Yield: 1.42 g (39 %).

Method 2⁸

Bromomethyl-2-methoxymethylbenzene **4-9** (93.0 mmol, 19.90 g) and sodium bicarbonate (930.0 mmol, 78.10 g) were added into DMSO (100 mL) and refluxed under inert condition for 24 hours. Water was added to the cooled mixture to dissolve the sodium bicarbonate suspension. The crude product was extracted with ethyl acetate and washed several times with deionized water until neutral. The organic layer was then dried over anhydrous sodium sulphate, filtered then evaporated. The residue was chromatographed over silica (60 - 250 mesh) using 1:8 ethyl acetate/hexane as eluent to yield **4-4** as yellow oil. Yield: 9.00 g (66 %).

¹H NMR (CDCl₃): δ 10.22 (s, 1H, -CHO proton), 7.86 (d, 1H, Ph-H proton, ³J = 7.2 Hz), 7.60 (m, 2H, Ph-H protons), 7.48 (m, 1H, Ph-H proton), 4.87 (s, 2H, Ph-CH₂- protons), 3.48 (s, 3H, -OCH₃ protons). ¹³C {¹H} NMR (CDCl₃): δ 192.5 (1C, -CHO); 133.6, 132.1, 127.9, 127.6 (4C, aromatic CH); 140.7, 133.3 (2C, aromatic C); 71.6 (1C, Ph-CH₂O-); 58.4 (1C, -OCH₃). EI-mass spectrum: 150.0 (90 %). m/z calcd: 150.1775, HRMS: 150.0682 (14 %).

DIPYRRROMETHANE (4-5)

A solution of pyrrole (144.9 mmol, 10.0 ml) and paraformaldehyde (3.6 mmol, 108 mg) was treated with glacial acetic acid (15 ml) and methanol (5 ml) at room temperature

under Ar gas. The mixture was stirred for 20 hours then diluted with 50 ml of CH₂Cl₂, washed with deionised water (2 x 30 ml), aqueous KOH (0.1 M, 2 x 30 ml) and then deionised water (2 x 250 ml) again. It was dried over anhydrous sodium sulphate, filtered and evaporated to yield a dark solution. The mixture was chromatographed over silica gel (250 - 400 mesh) under N₂, using distilled CH₂Cl₂ and 1 % triethylamine as eluent. Colourless oil crystallized under vacuum to give white solid product **4-5**.

Yield: 80 mg (37 %) {lit. yield 41 %}.⁹ Melting point: 72.0 - 73.0 °C {lit. 73.0 °C}.⁹ ¹H NMR (CDCl₃): δ 7.93 (br s, 2H, NH protons), 6.68 (m, 2H, pyrrolic protons), 6.15 (m, 2H, pyrrolic protons), 6.04 (m, 2H, pyrrolic protons), 3.99 (s, 2H, CH₂ protons). ¹³C {¹H} NMR (CDCl₃): δ 129.0, 117.3, 108.3, 106.4 (8C, pyrrolic C); 26.3 (1C, CH₂). El-mass spectrum: 146. Elemental Analysis (Calc.) for C₉H₁₀N₂: C, 73.94; H, 6.89; N, 19.16 % (Found): C, 73.74; H, 6.83; N, 18.86 %.

TRANS- AND CIS-5,15-DI(2-METHOXYMETHYLPHENYL)PORPHYRIN (4-6 AND 4-7)

Compound **4-4** (3.3 mmol, 500 mg) and **4-5** (3.3 mmol, 487 mg) were dissolved in dried CH₂Cl₂ (500 ml) and 2 drops of trifluoroacetic acid was added. The mixture was stirred under Ar at room temperature for 15 hours. After which, chloroanil (13.2 mmol, 3.25 g) was added and the solution was heated to reflux for 1 hour. The mixture was allowed to cool and the solvent was removed *in vacuo*. The dark solid was chromatographed using CHCl₃ to separate to isolate the isomers. Purple crystals of **4-6** were partially isolated the mixture using fractional crystallization in 2:1 cyclohexane/CHCl₃. The mother liquor was further evaporated to remove the solvent and chromatographed over silica gel (250 - 400 mesh) using CH₂Cl₂ as eluent to obtain **4-6** which eluted first followed by **4-7**.

Yield of **4-6**: 12 mg (13 %). ^1H NMR (CDCl_3) of **4-6**: δ 10.32 (s, 2H, meso protons), 9.39 (d, 4H, pyrrolic protons, $^3\text{J} = 4.4$ Hz), 8.93 (d, 4H, pyrrolic protons, $^3\text{J} = 4.4$ Hz), 8.09 (d, 2H, Ph-H protons, $^3\text{J} = 7.2$ Hz), 8.00 (d, 2H, Ph-H protons, $^3\text{J} = 7.7$ Hz), 7.89 (t, 2H, Ph-H protons, $^3\text{J} = 7.6$ Hz), 7.70 (t, 2H, Ph-H protons, $^3\text{J} = 7.2$ Hz), 4.14 (s, 4H, Ph- CH_2O -protons), 2.83 (s, 6H, $-\text{OCH}_3$ protons), unobserved (2H, NH protons). ^{13}C $\{^1\text{H}\}$ NMR (CDCl_3) of **4-6**: δ 146.9, 145.4, 140.1, 139.4, 134.0, 131.6, 130.6, 128.7, 126.7, 125.6, 116.5, 105.2 (32C, meso C, pyrrolic C and phenyl C); 72.7 (2C, Ph- CH_2O -); 58.0 (2C, $-\text{OCH}_3$). El-mass spectrum: 550.0 (90 %). m/z calcd: 550.2369, MALDI-TOF m/z : 550.3020 (100 %). Elemental Analysis (Calc.) for $\text{C}_{36}\text{H}_{30}\text{N}_4\text{O}_2$: C, 78.52; H, 5.49; N, 10.17 % (Found): C, 78.07; H, 5.43; N, 9.92 %.

Crystal data for **4-6** grown in CHCl_3 and cyclohexane: $\text{C}_{36}\text{H}_{30}\text{N}_4\text{O}_2$. $M = 550.64$. Monoclinic. $P2(1)/n$, $a = 8.3509(6)$ Å, $b = 15.5894(12)$ Å, $c = 11.0918(8)$ Å, $\alpha = 90^\circ$, $\beta = 98.646(2)^\circ$, $\gamma = 90^\circ$, $V = 1427.58(18)$ Å 3 , $Z = 2$, $d_{\text{calc}} = 1.281$ mg/m 3 , $\mu = 0.081$ mm $^{-1}$, $\theta_{\text{max}} = 30.04^\circ$, 11517 reflections collected, 4081 independent reflections, $R_{\text{int}} = 0.0374$, 4081 reflections with $I > 2\sigma(I)$, 250 parameters, $R1$ (all data) = 0.0838, $wR2$ (all data) = 0.1304.

Yield of **4-7**: 11 mg (12 %). ^1H NMR (CDCl_3) of **4-7**: δ 10.30 (s, 2H, meso protons), 9.36 (d, 4H, pyrrolic protons, $^3\text{J} = 4.8$ Hz), 8.90 (d, 4H, pyrrolic protons, $^3\text{J} = 4.4$ Hz), 8.12 (d, 2H, Ph-H protons, $^3\text{J} = 7.2$ Hz), 7.97 (d, 2H, Ph-H protons, $^3\text{J} = 7.7$ Hz), 7.87 (t, 2H, Ph-H protons, $^3\text{J} = 7.6$ Hz), 7.69 (t, 2H, Ph-H protons, $^3\text{J} = 7.4$ Hz), 4.07 (s, 4H, Ph- CH_2O -protons), 2.81 (s, 6H, $-\text{OCH}_3$ protons), -3.13 (br s, 2H, NH protons). ^{13}C $\{^1\text{H}\}$ NMR (CDCl_3) of **4-7**: δ 146.9, 145.5, 140.2, 139.3, 134.0, 131.7, 130.6, 128.7, 126.6, 125.6, 116.5, 105.2 (32C, meso C, pyrrolic C and phenyl C); 72.7 (2C, Ph- CH_2O -); 58.0 (2C, $-\text{OCH}_3$). El-mass spectrum of **4-7**: 550.0 (100 %). m/z calcd: 550.2369, MALDI-TOF m/z :

550.3110 (100 %). Elemental Analysis (Calc.) for $C_{36}H_{30}N_4O_2$: C, 78.52; H, 5.49; N, 10.17 % (Found): C, 78.24; H, 5.65; N, 9.92 %.

1-BROMOMETHYL-2-METHOXYMETHYLBENZENE (4-9)

1,2-Bis-bromomethylbenzene **4-8** (189.0 mmol, 49.50 g) was dissolved in methanol (500 mL). Sodium (189.0 mmol, 4.35 g) was added to dry methanol (300 mL) to form sodium methoxide then cooled. The solution of **4-8** was added dropwise from a dropping funnel into sodium methoxide over 4 hours under reflux. The mixture was stirred under the same condition for an additional hour. After it has cooled, methanol was removed *in vacuo* and the crude product was extracted with ethyl acetate, washed twice with deionized water then dried over anhydrous calcium sulphate, filtered then evaporated. The residue was chromatographed over silica gel using 1:50 ethyl acetate/hexane as eluent to yield **4-9** as pale yellow oil.

Yield: 11.00 g (27 %). 1H NMR ($CDCl_3$): 7.24 - 7.36 (m, 4H, Ph-H protons), 4.61 (s, 2H, Ph- CH_2O - protons), 4.59 (s, 2H, Ph- CH_2Br protons), 3.42 (s, 3H, $-OCH_3$ protons). ^{13}C { 1H } NMR ($CDCl_3$): 136.7 (1C, aromatic C- CH_2O), 136.2 (1C, aromatic C- CH_2Br), 130.7, 129.6, 128.8, 128.5 (4C, aromatic CH), 72.2 (1C, Ph- CH_2O -), 58.4 (1C, $-OCH_3$), 31.0 (1C, Ph- CH_2Br). EI-mass spectrum: 214 (40 %), 216 (40 %). m/z calcd: 213.9993, 215.9973; HRMS: 213.9996 (100 %), 215.9977 (100 %).

1-BROMOMETHYL-3-METHOXYMETHYLBENZENE (4-11)

Refer to procedure on synthesis of **4-9** from **4-8**. Compound 1,3-dibromomethylbenzene (**4-10**) was used as starting material for the synthesis of **4-11**. The product is pale yellow oil.

Yield: 34.7 %. ^1H NMR (CDCl_3): δ 7.26 - 7.37 (m, 4H, Ph-H protons), 4.49 (s, 2H, Ph- CH_2O - protons), 4.44 (s, 2H, Ph- CH_2Br protons), 3.39 (s, 3H, $-\text{OCH}_3$ protons). ^{13}C $\{^1\text{H}\}$ NMR (CDCl_3): δ 138.9 (1C, aromatic **C-CH₂O**), 137.9 (1C, aromatic **C-CH₂Br**), 128.9, 128.3, 128.2, 127.6 (4C, aromatic **CH**), 74.3 (1C, Ph-**CH₂O**-), 58.2 (1C, $-\text{OCH}_3$), 33.4 (1C, Ph-**CH₂Br**). EI-mass spectrum: 214.0 (40 %), 215.0 (30 %). m/z calcd: 213.9993, HRMS: 213.9987 (100 %), 215.9964 (100 %).

3-METHOXYMETHYLBENZALDEHYDE (4-12)

Refer to procedure on synthesis of **4-4** from **4-9** (Method 2). Compound **4-11** was used as starting material for the synthesis of **4-12**. The product is pale yellow oil.

Yield: 40.8 %. ^1H NMR (CDCl_3): δ 10.02 (s, 1H, $-\text{CHO}$ proton), 7.82 (m, 2H, Ph-H protons), 7.61 (d, 1H, Ph-H proton, $^3J = 7.3$ Hz), 7.51 (t, 1H, Ph-H proton, $^3J = 7.7$ Hz), 4.53 (s, 2H, Ph- CH_2O - protons), 3.42 (s, 3H, $-\text{OCH}_3$ protons). ^{13}C $\{^1\text{H}\}$ NMR (CDCl_3): δ 192.2 (1C, $-\text{CHO}$); 133.4, 129.1, 128.9, 128.6 (4C, aromatic **CH**); 139.5, 136.5 (2C, aromatic **C**); 73.8 (Ph-**CH₂O**-); 58.3 ($-\text{OCH}_3$). EI-mass spectrum: 150.0 (90 %). m/z calcd: 150.1775, HRMS: 150.0676 (4 %).

TRANS- AND CIS-5,15-DI(3-METHOXYMETHYLPHENYL)PORPHYRIN (4-13 AND 4-14 RESPECTIVELY)

Refer to procedure on synthesis of **4-6** and **4-7** from **4-4** and **4-5**. Compounds **4-12** and **4-5** were used as starting materials for the synthesis of **4-13** and **4-14**.

Yield: 15 %. ^1H NMR (CDCl_3 , 500MHz): δ 10.31 (s, 2H, meso protons), 9.39 (d, 4H, pyrrolic protons, $^3\text{J} = 4.6$ Hz), 9.07 (d, 4H, pyrrolic protons, $^3\text{J} = 4.7$ Hz), 8.25 (s, 2H, Ph-H protons), 8.21 (m, 2H, Ph-H protons), 7.81 (m, 4H, Ph-H protons), 4.80 (s, 4H, Ph- CH_2O - protons), 3.59 (s, 6H, - OCH_3 protons), unobserved (2H, NH protons). ^{13}C $\{^1\text{H}\}$ NMR (CDCl_3): δ 147.1, 145.2, 141.4, 137.0, 134.2, 134.1, 131.6, 131.0, 127.0, 118.9, 105.2 (32C, meso C, pyrrolic C and phenyl C)ⁱ, 74.9 (2C, - CH_2OCH_3); 58.4(2C, - CH_2OCH_3). El-mass spectrum: 551. m/z calcd: 550.2369, MALDI-TOF m/z : 550.2870 (100 %).

Crystal data of **4-13** grown in ethyl acetate and CHCl_3 : $M = 550.64$. $\text{C}_{36}\text{H}_{30}\text{N}_4\text{O}_2$. Monoclinic. $P2(1)/n$, $a = 8.7154(19)$ Å, $b = 13.750(3)$ Å, $c = 12.896(3)$ Å, $\alpha = 90^\circ$, $\beta = 108.057(5)^\circ$, $\gamma = 90^\circ$, $V = 1469.3(5)$ Å³, $Z = 2$, $d_{\text{calc}} = 1.245$ mg/m³, $\mu = 0.078$ mm⁻¹, $\theta_{\text{max}} = 25.00^\circ$, 8200 reflections collected, 2587 independent reflections, $R_{\text{int}} = 0.0692$, 2587 reflections with $I > 2\sigma(I)$, 195 parameters, $R1$ (all data) = 0.1500, $wR2$ (all data) = 0.2113.

ⁱ One missing carbon peak probably due to overlapping

COMPOUND 4-15

Compound **4-6** (0.2 mmol, 110 mg) and Zn(OAc)₂.xH₂O (4.0 mmol, 880 mg) were stirred in absolute ethanol (5 ml) contained in a 5 ml single-neck round-bottom flask for 5 days. The solvent was removed under vacuum. The residue was dissolved in CH₂Cl₂ and washed with deionized water (2 x 10 ml), dried over anhydrous sodium sulphate, filtered then evaporated. The residue was chromatographed over silica gel (60 - 250 mesh) using 1:5 distilled hexane/CH₂Cl₂ as eluent to yield **4-15** as purple solid.

Yield: 60 mg (54 %). ¹H NMR (CDCl₃): δ 10.17 (s, 2H, meso protons), 9.28 (d, 4H, pyrrolic protons, ³J = 4.5 Hz), 8.65 (d, 4H, pyrrolic protons, ³J = 4.5 Hz), 7.99 (d, 2H, Ph-H protons, ³J = 7.3 Hz), 7.62 (t, 4H, Ph-H protons, ³J = 7.5 Hz), 7.54 (t, 4H, Ph-H protons, ³J = 7.3 Hz), 6.89 (br, 2H, Ph-H protons), 2.61 (s, 4H, Ph-CH₂ protons), 1.50 (s, 6H, -OCH₃ protons). ¹³C {¹H} NMR (CDCl₃): δ 149.44, 149.36, 140.6, 138.9, 116.6 (14C, unprotonated meso C, pyrrolic C and phenyl C); 133.5 (2C, phenyl C), 131.8, 131.5 (8C, pyrrolic C); 128.1 (2C, phenyl C); 125.6, 125.2 (4C, phenyl C), 105.9 (2C, meso C); 70.8 (2C, Ph-CH₂O-); 56.0 (2C, -OCH₃). Elemental Analysis (Calc.) for (C₃₆H₂₈N₄O₂Zn)_n: C, 70.42; H, 4.60; N, 9.12; Zn, 10.65 % (Found): C, 68.99; H, 4.83; N, 8.84; Zn, 8.60 %. m/z calcd (monomer): 612.1504, MALDI-TOF m/z: 612.2687 (100 %). T_g: 148.7 °C. T_d: 346 °C.

Crystal data of **4-15** grown in CHCl₃ and cyclohexane: (C₃₆H₂₈N₄O₂Zn)_n. M = (613.99)_n. Tetrahedral. I4(1)/a, a = 22.812(3) Å, b = 22.812(3) Å, c = 11.423(3) Å, α = 90 °, β = 90 °, γ = 90 °, V = 5944.3(18) Å³, Z = 8, d_{calc} = 1.372 mg/m³, μ = 0.866 mm⁻¹, θ_{max} = 25.00 °,

16293 reflections collected, 2613 independent reflections, $R_{int} = 0.1324$, 2613 reflections with $I > 2\sigma(I)$, 196 parameters, $R1$ (all data) = 0.1022, $wR2$ (all data) = 0.1338.

Crystal data of **4-15** grown in ethyl acetate: $C_{36}H_{28}N_4O_2Zn$. $M = 613.99$ Monoclinic. $P2(1)/c$, $a = 9.2323(8) \text{ \AA}$, $b = 10.3641(10) \text{ \AA}$, $c = 15.0985(14) \text{ \AA}$, $\alpha = 90^\circ$, $\beta = 101.860(2)^\circ$, $\gamma = 90^\circ$, $V = 1413.9(2) \text{ \AA}^3$, $Z = 2$, $d_{calc} = 1.442 \text{ mg/m}^3$, $\mu = 0.910 \text{ mm}^{-1}$, $\theta_{max} = 27.50^\circ$, 9655 reflections collected, 3228 independent reflections, $R_{int} = 0.0508$, 3228 reflections with $I > 2\sigma(I)$, 197 parameters, $R1$ (all data) = 0.0799, $wR2$ (all data) = 0.1327.

Crystal data of **4-15** grown in nitrobenzene: $C_{36}H_{28}N_4O_2Zn$. $M = 613.99$ Monoclinic. $P2(1)/c$, $a = 9.236(6) \text{ \AA}$, $b = 10.424(6) \text{ \AA}$, $c = 15.167(10) \text{ \AA}$, $\alpha = 90^\circ$, $\beta = 102.302(13)^\circ$, $\gamma = 90^\circ$, $V = 1426.6(15) \text{ \AA}^3$, $Z = 2$, $d_{calc} = 1.429 \text{ mg/m}^3$, $\mu = 0.902 \text{ mm}^{-1}$, $\theta_{max} = 27.50^\circ$, 9531 reflections collected, 3264 independent reflections, $R_{int} = 0.0593$, 3264 reflections with $I > 2\sigma(I)$, 196 parameters, $R1$ (all data) = 0.0864, $wR2$ (all data) = 0.1465.

COMPOUND 4-16

Compound **4-7** (0.2 mmol, 100 mg) and $Zn(OAc)_2 \cdot xH_2O$ (4.0 mmol, 880 mg) were stirred in THF at room temperature for 5 days. The solvent was removed *in vacuo* then extracted with $CHCl_3$ and washed with water. The organic layer was then dried with anhydrous sodium sulphate, filtered then evaporated. Purification via column chromatography over silica gel (60 - 250 mesh) using CH_2Cl_2 /hexane (5:1) as eluent yielded purple crystals of **4-16**.

Yield: 81 mg (73 %). ^1H NMR (CDCl_3): δ 10.18 (s, 2H, meso protons), 9.29 (d, 4H, pyrrolic protons, $^3\text{J} = 4.5$ Hz), 8.63 (d, 4H, pyrrolic protons, $^3\text{J} = 4.2$ Hz), 8.01 (d, 2H, Ph-H protons, $^3\text{J} = 6.6$ Hz), 7.55 (m, 4H, Ph-H protons), 6.73 (br s, 2H, Ph-H protons), 2.46 (br s (sh), 4H, Ph- CH_2O - protons), 1.55 (br s (sh), 6H, $-\text{OCH}_3$ protons). ^{13}C $\{^1\text{H}\}$ NMR (CDCl_3): δ 149.4, 140.6, 138.9, 133.4, 131.8, 131.5, 128.1, 125.4, 125.2, 116.5, 105.9 (32C, meso C, pyrrolic C and phenyl C)ⁱⁱ, 70.9 (2C, Ph- CH_2O -), 56.0 (2C, $-\text{OCH}_3$). Elemental Analysis (Calc.) for $(\text{C}_{36}\text{H}_{28}\text{N}_4\text{O}_2\text{Zn})_n$: C, 70.42; H, 4.60; N, 9.12; Zn, 10.65 % (Found): C, 70.06; H, 4.59; N, 8.97; Zn, 9.49 %. m/z calcd: 550.2369, MALDI-TOF m/z : 550.2870 (100 %). m/z calcd (monomer): 612.1504, MALDI-TOF m/z : 612.2678 (100 %). T_g : 177.3 °C. T_d : 329 °C.

Crystal data of **4-16** grown in CHCl_3 : $(\text{C}_{36}\text{H}_{28}\text{N}_4\text{O}_2\text{Zn})_2$. $M = 2(613.99)$. Monoclinic. $P2(1)/n$, $a = 14.3395(11)$ Å, $b = 10.2698(8)$ Å, $c = 19.7425(14)$ Å, $\alpha = 90^\circ$, $\beta = 99.468(2)^\circ$, $\gamma = 90^\circ$, $V = 2867.8(4)$ Å³, $Z = 4$, $d_{\text{calc}} = 1.422$ mg/m³, $\mu = 0.898$ mm⁻¹, $\theta_{\text{max}} = 25.00^\circ$, 16389 reflections collected, 5043 independent reflections, $R_{\text{int}} = 0.1086$, 5043 reflections with $I > 2\sigma(I)$, 390 parameters, $R1$ (all data) = 0.1187, $wR2$ (all data) = 0.1222.

Crystal data of **4-16** grown in THF: $M = 758.20$. $\text{C}_{44}\text{H}_{44}\text{N}_4\text{O}_4\text{Zn}$. Monoclinic. $P2(1)/c$, $a = 17.8424(17)$ Å, $b = 18.7939(18)$ Å, $c = 11.8706(11)$ Å, $\alpha = 90^\circ$, $\beta = 101.134(2)^\circ$, $\gamma = 90^\circ$, $V = 3905.6(6)$ Å³, $Z = 4$, $d_{\text{calc}} = 1.289$ mg/m³, $\mu = 0.676$ mm⁻¹, $\theta_{\text{max}} = 1.59 - 27.50^\circ$, 29735 reflections collected, 8969 independent reflections, $R_{\text{int}} = 0.0493$, 8969 reflections with $I > 2\sigma(I)$, 493 parameters, $R1$ (all data) = 0.1012, $wR2$ (all data) = 0.1672.

ⁱⁱ One missing peak due to poor resolution

TRANS-5,15-BISBROMO-10,20-DI(2-METHOXYMETHYLPHENYL)PORPHYRIN (4-17)

Compound **4-6** (1.0 mmol, 550 mg) was dissolved in dry CHCl_3 (20 ml) and cooled to 0 °C. NBS (2.1 mmol, 372 mg) and pyridine (0.3 ml) were added into the solution and the reaction progress was monitored using TLC. When all the starting material has reacted, the reaction was quenched with acetone. All the solvents were removed *in vacuo* and recrystallization using CHCl_3 and methanol yielded purple crystals.

Yield: 608 mg (86 %). ^1H NMR (CDCl_3): δ 9.58 (d, 4H, pyrrolic protons, $^3\text{J} = 4.9$ Hz), 8.70 (d, 4H, pyrrolic protons, $^3\text{J} = 4.9$ Hz), 7.98 (d, 2H, Ph-H protons, $^3\text{J} = 7.7$ Hz), 7.94 (d, 2H, Ph-H protons, $^3\text{J} = 7.3$ Hz), 7.86 (t, 2H, Ph-H protons, $^3\text{J} = 7.7$ Hz), 7.67 (t, 2H, Ph-H protons, $^3\text{J} = 7.3$ Hz), 4.07 (s, 4H, Ph- CH_2O - protons), 2.83 (s, 6H, $-\text{OCH}_3$ protons), -2.64 (s, 2H, NH protons). ^{13}C $\{^1\text{H}\}$ NMR (CDCl_3): δ 140.0, 139.4, 133.9, 132.4, 129.4, 129.3, 129.0, 126.8, 125.7, 118.9 (32C, aromatic C),ⁱⁱⁱ 72.7 (2C, Ph- CH_2O -), 58.2 (2C, $-\text{OCH}_3$). EI-mass spectrum: 706.1 (15 %), 708.1 (45 %), 710.1 (20 %). m/z calcd: 708.4411, MALDI-TOF m/z : 706.1680 (40 %), 708.1680 (100 %), 710.1680 (40 %). Elemental Analysis (Calc.) for $\text{C}_{36}\text{H}_{28}\text{Br}_2\text{N}_4\text{O}_2$: C, 61.03; H, 3.98; N, 7.91 % (Found): C, 57.28; H, 3.24; N, 7.02 %.

COMPOUND 4-18

Compound **4-17** (0.1 mmol, 100 mg) and $\text{Zn}(\text{OAc})_2 \cdot x\text{H}_2\text{O}$ (2 mmol, 440 mg) were stirred in THF at room temperature for 5 days (refluxing for 3 hours yielded same product). The solvent was removed *in vacuo* then extracted with CHCl_3 and washed with water. The

ⁱⁱⁱ Two peaks missing due to poor resolution

organic layer was then dried with anhydrous sodium sulphate, filtered then evaporated. Purification via column chromatography over silica gel (60 - 250 mesh) using CH₂Cl₂/hexane (5:1) as eluent yielded purple powdery solid **4-18**.

Yield: 74 mg (68 %). ¹H NMR (CDCl₃): δ 9.59 (d, 4H, pyrrolic protons, ³J = 4.9 Hz), 8.44 (d, 4H, pyrrolic protons, ³J = 4.9 Hz), 7.90 (d, 2H, Ph-H protons, ³J = 6.6 Hz), 7.56 (m, 4H, Ph-H protons), 6.62 (br, 2H, Ph-H protons), 2.31 (br s, 4H, Ph-CH₂O- protons), 1.31 (br s, 6H, -OCH₃ protons). ¹³C {¹H} NMR (CDCl₃): δ 150.2, 139.9, 139.7, 138.6, 138.4, 133.4, 133.3, 132.8, 132.5, 128.6, 128.4, 125.3 (32C, meso C, pyrrolic C and phenyl C), 70.9 (2C, Ph-CH₂O-), 56.1 (2C, -OCH₃). Elemental Analysis (Calc.) for (C₃₆H₂₆Br₂N₄O₂Zn)_n: C, 56.02; H, 3.40; N, 7.26; Zn, 8.47 % (Found): C, 54.69; H, 3.12; N, 7.23; Zn, 7.80 %. m/z calcd (monomer): 769.9694, MALDI-TOF m/z: 770.1916 (100 %). T_g: 133.4 °C. T_d: 196, 242, 289 °C.

Crystal data of **4-18** grown in CH₂Cl₂: (C₃₆H₂₆Br₂N₄O₂Zn)_n. M = (771.80)n. Monoclinic. P2(1)/n, a = 10.5664(15) Å, b = 18.505(3) Å, c = 7.9175(11) Å, α = 90 °, β = 103.580(3) °, γ = 90 °, V = 1504.8(4) Å³, Z = 2, d_{calc} = 1.703 mg/m³, μ = 3.513 mm⁻¹, θ_{max} = 27.50 °, 19462 reflections collected, 3455 independent reflections, R_{int} = 0.0241, 3455 reflections with I > 2σ(I), 206 parameters, R1 (all data) = 0.0309, wR2 (all data) = 0.0689.

TRANS-5-BROMO-10,20-DI(2-METHOXYMETHYLPHENYL)PORPHYRIN (4-19)

Compound **4-6** (1 mmol, 550 mg) was dissolved in dry CHCl₃ (20 ml) and cooled to 0 °C. NBS (1.1 mmol, 186 mg) and pyridine (0.3ml) were added into the solution and the reaction progress was monitored using TLC. When all the starting material has reacted,

the reaction was quenched with acetone. All the solvent is removed *in vacuo* and purification via column chromatography over silica gel (60 - 250 mesh) using CH₂Cl₂/hexane (3:2) as eluent yielded purple crystals of **4-19** after drying.

Yield: 440 mg (70 %). ¹H NMR (CDCl₃): δ 10.17 (s, 1H, meso protons), 9.70 (d, 2H, pyrrolic protons, ³J = 4.9 Hz), 9.27 (d, 2H, pyrrolic protons, ³J = 4.9 Hz), 8.80 (d, 4H, pyrrolic protons, ³J = 4.9 Hz), 8.02 (dd, 2H, Ph-H protons, ³J = 7.3 Hz, ⁴J = 0.7 Hz), 7.96 (d, 2H, Ph-H protons, ³J = 7.3 Hz), 7.88 (td, 2H, Ph-H protons, ³J = 7.7 Hz, ⁴J = 1.1 Hz), 7.67 (td, 2H, Ph-H protons, ³J = 7.7 Hz, ³J = 1.0 Hz), 4.09 (s, 4H, Ph-CH₂O- protons), 2.82 (s, 6H, -OCH₃ protons), -2.96 (s, 2H, NH protons). ¹³C {¹H} NMR (CDCl₃): δ 146.8 (br) 140.1, 139.4, 134.0, 132.7, 131.6 (br), 128.9, 126.8, 125.7, 117.7, 105.6, 103.6 (32C, meso C, pyrrolic C and phenyl C),^{iv} 72.8 (2C, Ph-CH₂O-), 58.2 (2C, -OCH₃). EI-mass spectrum: 628.1 (100 %), 630.1 (100 %). *m/z* calcd: 628.1474, MALDI-TOF *m/z*: 628.3301 (100 %), 630.3829 (80 %). Elemental Analysis (Calc.) for C₃₆H₂₉BrN₄O₂: C, 68.68; H, 4.64; N, 8.90; Br, 12.69 % (Found): C, 70.07; H, 4.60; 8.87; Br, 13.38 %.

COMPOUND 4-20

Refer to the procedure on synthesis of **4-18**. Compound **4-19** (0.2 mmol, 100 mg) was used as starting materials for the synthesis of **4-20**.

Yield: 77 mg (70 %). ¹H NMR (CDCl₃): δ 9.96 (s, 1H, meso protons), 9.61 (d, 2H, pyrrolic protons, ³J = 4.9 Hz), 9.12 (d, 2H, pyrrolic protons, ³J = 4.5 Hz), 8.37 (overlapping d, 4H, pyrrolic protons), 7.87 (m, 2H, Ph-H), 7.47 (m, 4H, Ph-H), 6.14 (br s, 2H, Ph-H), 1.71 (br

^{iv} One peak missing due to poor resolution

s, 4H, Ph-CH₂), 0.75 (br s, 6H, OCH₃). ¹³C {¹H} NMR (CDCl₃): δ 150.2, 139.9, 138.6, 133.8, 133.6, 133.4, 133.3, 132.8, 132.5, 128.6, 128.4, 125.3, 105.0 (32C, meso C, pyrrolic C and phenyl C), 70.9 (2C, -CH₂OCH₃), 56.1 (2C, -CH₂OCH₃). Elemental Analysis (Calc.) for (C₃₆H₂₇BrN₄O₂Zn)_n: C, 62.40; H, 3.93; N, 8.09; Zn, 9.44 % (Found): C, 62.69; H, 3.70; N, 8.05; Zn, 6.43 %. m/z calcd (monomer): 692.0588, MALDI-TOF m/z:692.2155 (100 %). T_g: 121.2 °C. T_d: 204 °C.

Crystal data of **4-20** grown in THF: (C₃₆H₂₇BrN₄O₂Zn)_n. M = (693.90)n. Monoclinic. P2(1)/n, a = 10.2123(8) Å, b = 18.4943(15) Å, c = 8.0320(6) Å, α = 90 °, β = 104.387(2) °, γ = 90°, V = 1469.4(2) Å³, Z = 2, d_{calc} = 1.568 mg/m³, μ = 2.237 mm⁻¹, θ_{max} = 25.00 °, 8454 reflections collected, 2586 independent reflections, R_{int} = 0.0500, 2586 reflections with I > 2σ(I), 206 parameters, R1 (all data) = 0.0762, wR2 (all data) = 0.1268.

CIS-5,15-BISBROMO-10,20-DI(2-METHOXYMETHYLPHENYL)PORPHYRIN (4-21)

Refer to the procedure on synthesis of **4-17**. Compound **4-7** (1 mmol, 550 mg) was used as starting materials for the synthesis of **4-21**.

Yield: 532 mg (89 %). ¹H NMR (CDCl₃): δ 9.58 (d, 4H, pyrrolic protons, ³J = 4.9 Hz), 8.71 (d, 4H, pyrrolic protons, ³J = 4.9 Hz), 8.03 (d, 2H, Ph-H protons, ³J = 7.3 Hz), 7.94 (d, 2H, Ph-H protons, ³J = 7.7 Hz), 7.87 (m, 2H, Ph-H protons), 7.68 (t, 2H, Ph-H protons, ³J = 7.3 Hz), 4.03 (s, 4H, Ph-CH₂O- protons), 2.83 (s, 6H, -OCH₃ protons), -2.65 (s, 2H, NH protons). ¹³C {¹H} NMR (CDCl₃): δ 140.1, 139.4, 133.9, 132.4, 132.2, 131.9, 129.0, 126.8, 125.7, 120.5, 118.9, 103.7, 132.4 (32C, aromatic C), 72.7 (2C, Ph-CH₂O-), 58.1 (2C, -

OCH_3). *El-mass spectrum*: 706.0 (40 %), 708.0 (80 %), 710.0 (45 %). *m/z calcd*: 708.4411, *MALDI-TOF m/z*: 706.2396 (50 %), 708.2381 (100 %), 710.2381 (50 %).

COMPOUND 4-22

Refer to the procedure on synthesis of **4-20**. Compound **4-16** (1 mmol, 100 mg) was used as starting materials for the synthesis of **4-22**. Purification via column chromatography over silica gel (60 - 250 mesh) using CH_2Cl_2 /hexane (6:1) as eluent yielded purple crystals.

Yield: 77mg (71 %). $^1\text{H NMR}$ (CDCl_3): δ 9.60 (d, 4H, pyrrolic protons, $^3\text{J} = 4.5$ Hz), 8.43 (d, 4H, pyrrolic protons, $^3\text{J} = 4.9$ Hz), 7.91 (d, 2H, Ph-H protons, $^3\text{J} = 7.0$ Hz), 7.53 (m, 4H, Ph-H protons), 6.52 (br s, 2H, Ph-H protons), 2.30 (br s, 4H, Ph- CH_2O - protons), 1.37 (br s, 6H, $-\text{OCH}_3$ protons). ^{13}C $\{^1\text{H}\}$ NMR (CDCl_3): δ 150.19, 150.15, 140.0, 138.7, 133.5, 133.4, 132.5, 128.3, 125.43, 125.36, 104.9 (32C, meso C, pyrrolic C and phenyl C)^v, 71.1 (2C, Ph- CH_2O -), 56.2 (2C, $-\text{OCH}_3$). *Elemental Analysis (Calc.) for* $(\text{C}_{36}\text{H}_{26}\text{Br}_2\text{N}_4\text{O}_2\text{Zn})_n$: C, 56.02; H, 3.40; N, 7.26; Br, 20.71; Zn, 8.47 % (*Found*): C, 56.48; H, 3.13; N, 7.33; Br, 20.41; Zn, 6.65 %. *m/z calcd (monomer)*: 769.9694, *MALDI-TOF m/z*: 770.1808 (100 %). T_g : 122.7 °C. T_d : 239, 297 °C.

Crystal data of 4-22 grown in CHCl_3 and toluene: $(\text{C}_{36}\text{H}_{26}\text{Br}_2\text{N}_4\text{O}_2\text{Zn})_2$. $M = (771.80)n$. *Triclinic. P-1*, $a = 11.636(3)$ Å, $b = 12.421(3)$ Å, $c = 12.520(3)$ Å, $\alpha = 61.526(4)$ °, $\beta = 83.202(4)$ °, $\gamma = 88.852(4)$ °, $V = 1578.1(6)$ Å³, $Z = 2$, $d_{\text{calc}} = 1.624$ mg/m³, $\mu = 3.350$ mm⁻¹, $\theta_{\text{max}} = 27.50$ °, 20559 reflections collected, 7251 independent reflections, $R_{\text{int}} = 0.1031$,

^v One peak missing due to poor resolution

7251 reflections with $I > 2\sigma(I)$, 408 parameters, $R1$ (all data) = 0.1723, $wR2$ (all data) = 0.1583.

Crystal data of **4-22** grown in THF: $C_{40}H_{34}Br_2N_4O_3Zn$. $M = 843.90$. Monoclinic. $P2(1)/c$, $a = 17.9019(8) \text{ \AA}$, $b = 13.9986(6) \text{ \AA}$, $c = 14.8998(6) \text{ \AA}$, $\alpha = 90^\circ$, $\beta = 111.3870(10)^\circ$, $\gamma = 90^\circ$, $V = 3476.8(3) \text{ \AA}^3$, $Z = 4$, $d_{calc} = 1.612 \text{ mg/m}^3$, $\mu = 3.051 \text{ mm}^{-1}$, $\theta_{max} = 27.50^\circ$, 24329 reflections collected, 7982 independent reflections, $R_{int} = 0.0306$, 7982 reflections with $I > 2\sigma(I)$, 453 parameters, $R1$ (all data) = 0.0545, $wR2$ (all data) = 0.1025.

1,4-BISDECYLOXYBENZENE (6-2)

Potassium hydroxide (220 mmol, 12.31 g) was stirred in absolute ethanol (1 L) and the solution was degassed for 30 minutes. Hydroquinone (**6-1**) (100 mmol, 11.00 g) in degassed absolute ethanol (250 ml) was added dropwise into the solution and stirred for 1 hour. 1-Bromodecane (250 mmol, 55.02 g) was then added dropwise over 30 minutes and the solution was refluxed for 24 hours. After the mixture has cooled to room temperature, ethanol was removed *in vacuo*. The solid was dissolved in ethyl acetate and the organic extract was washed with deionized water until the aqueous layer turned neutral. The organic extract was dried using anhydrous sodium sulphate, filtered then dried. The crude product was recrystallized using ethanol to yield white flaky solids of **6-2**.

Yield: 28.88 g (74 %). Melting point: 66.5 - 67.0 °C {lit. 67-68 °C}¹⁰. 1H NMR ($CDCl_3$): δ 6.81 (s, 4H, Ph-H protons), 3.89 (t, 4H, Ph-OCH₂ protons, $^3J = 5.9$ Hz), 1.27 - 1.75 (m, 32H, -CH₂- protons), 0.88 (s, 6H, -CH₃ protons). ^{13}C { 1H } NMR ($CDCl_3$): δ 153.2 (2C,

aromatic C-O), 115.4 (4C, aromatic CH), 68.6 (2C, Ph-OCH₂-), 14.1, 22.6, 26.0, 29.1, 29.2, 29.3, 29.4, 29.5, 31.9 [18C, -(CH₂)₈CH₃]. El-mass spectrum: 390.2 (40 %). *m/z* calcd: 390.3498, HRMS: 390.3495 (100 %).

1,4-DIBROMO-2,5-BISDECYLOXYBENZENE (6-3)

Compound **6-2** (50 mmol, 19.52 g) was dissolved in methanol and CHCl₃ (600 ml) and cooled to 0°C. Bromine (110 mmol, 17.36 g) in glacial acetic acid (150 ml) was added dropwise into the solution then stirred for additional 24 hours at room temperature. After removing most of the solvent *in vacuo*, the pale yellow solid was filtered and washed several times with water until the filtrate turned neutral and the solid becomes white. The solid was finally washed once with cold ethanol then vacuum dried.

Yield: 24.66 g (90 %). Melting point: 76.0 - 77.5 °C {72 - 76 °C}¹¹. ¹H NMR (CDCl₃): δ 7.08 (s, 2H, Ph-H protons), 3.94 (t, 4H, Ph-OCH₂- protons), 1.79, (quintet, 4H, -CH₂- protons, ³J = 7.1 Hz), 1.27 - 1.49 (m, 28H, -CH₂- protons), 0.88 (t, 6H, -CH₃ protons, ³J = 6.6 Hz). ¹³C {¹H} NMR (CDCl₃): δ 150.0 (2C, aromatic C-O), 118.4 (2C, aromatic C-H), 111.1 (2C, aromatic C-Br), 70.3 (2C, Ph-OCH₂-), 14.1, 22.7, 25.9, 29.1, 29.28, 29.29, 29.5, 31.9 [18C, -(CH₂)₈CH₃]^{vi}. El-mass spectrum: 546.0 (10 %), 548.0 (20 %), 550.0 (10 %). *m/z* calcd: 548.1688, HRMS: 546.1706 (50 %), 548.1691 (100 %), 550.1679 (50 %).

^{vi} One missing ¹³C peak due to poor resolution

2,5-BISDECYLOXY-1,4-DIFORMYLBENZENE (6-4)

Compound **6-3** (10 mmol, 5.46 g) was added into a single-neck RBF which was degassed then sealed and purged with N₂ gas. Dry THF (20 ml) was added and the flask was cooled to -78°C. n-BuLi (40 mmol, 1.6 M, 25 ml) was added dropwise and the temperature was raised to room temperature slowly. The mixture was allowed to stir for another 2 hours at room temperature before it was cooled to -78 °C again. Dry DMF (50 mmol) was purged into the reaction mixture. The flask was allowed to reach room temperature slowly and stirred overnight. The reaction mixture was added to water, extracted with ether, washed with deionized water, dried with anhydrous sodium sulphate, filtered then dried. The crude product was purified by column chromatography over silica gel (60 - 250 mesh) using hexane/ethyl acetate (50:1) as eluent to yield bright yellow solid.

Yield: 4.05 g (91 %). Melting point: 87.0 - 88.0°C {88 - 90°C}¹². ¹H NMR (CDCl₃): δ 10.52 (s, 2H, -CHO protons), 7.43 (s, 2H, Ph-H protons), 4.08 (t, 4H, Ph-OCH₂- protons, ³J = 6.5 Hz), 1.82 (q, 4H, -CH₂- protons, ³J = 7.1 Hz), 0.90 - 1.49 (br s & m, 28H, -CH₂- protons), 0.88 (t, 6H, -CH₃ protons, ³J = 6.5 Hz). ¹³C {¹H} NMR (CDCl₃): δ 189.4 (2C, -CHO), 111.7, 129.2, 155.2 (6C, aromatic C), 69.2 (2C, Ph-OCH₂-), 14.1, 22.6, 26.0, 29.0, 29.3, 29.5, 31.8 [18C, -(CH₂)₈CH₃]^{vii}. El-mass spectrum: 446.3 (15 %). m/z calcd: 446.6624, HRMS: 446.3398 (100 %).

^{vii} Two missing ¹³C peak due to poor resolution

TRANS-5,15-DI(2-BROMOMETHYLPHENYL)PORPHYRIN (6-5)

Aqueous HBr (48 %, 25 ml) was added dropwise into a two-neck round-bottom flask half-filled with phosphorous pentoxide. The HBr gas generated was bubbled into a 100 ml one-neck round-bottom flask solution of **4-6** (500 mg, 0.9 mmol) dissolved in CHCl₃ (50 ml). After which, the mixture was stoppered tightly and stirred for an additional 24 hours. The mixture was washed with sodium bicarbonate, deionized water, dried over anhydrous sodium sulphate, filtered and evaporated. The compound was recrystallized using CHCl₃/hexane mixture to obtain **6-5** as purple solid.

Yield: 490 mg (83 %). ¹H NMR (CDCl₃): δ 10.31 (s, 2H, meso protons), 9.37 (d, 2H, pyrrolic protons, ³J = 4.5 Hz), 8.89 (d, 2H, pyrrolic protons, ³J = 4.5 Hz), 8.07 (dd, 2H, Ph-H protons, ³J = 7.7 Hz, ⁴J = 1.1 Hz), 7.96 (dd, 2H, Ph-H protons, ³J = 7.7 Hz, ⁴J = 1.1 Hz), 7.88 (td, 2H, Ph-H protons, ³J = 7.7 Hz, ⁴J = 1.4 Hz), 7.69 (td, 2H, Ph-H protons, ³J = 7.7 Hz, ⁴J = 1.4 Hz), 4.28 (s, 4H, Ph-CH₂Br protons), -3.13 (s, 2H, NH protons). ¹³C {¹H} NMR (CDCl₃): δ 146.9, 145.6, 139.3, 134.7, 131.7, 130.9, 129.9, 129.3, 126.7, 119.8, 115.5, 105.5 (32C, meso C, pyrrolic C and phenyl C); 31.8 (2C, Ph-CH₂Br). EI-mass spectrum: 648 (5 %). Elemental Analysis (Calc.) for C₃₄H₂₄N₄Br₂: C, 62.98; H, 3.73; N, 8.64; Br, 24.65 % (Found): C, 62.85; H, 3.62; N, 8.29; Br, 24.50 %.

COMPOUND 6-6

Compound **6-5** (500 mg, 0.8 mmol), triphenylphosphine (759 mg, 3 mmol) were dissolved in DMF (20 mL) then heated to 120 °C under inert condition and stirred for 3 days. The solution was cooled then ether was added to precipitate the phosphonium salt.

The residue was filtered, washed several times with ether then dried to yield purple solid of **6-6**.

Yield: 456 mg (50 %). ^1H NMR (CDCl_3): δ 10.32 (s, 2H, meso protons), 9.35 (br, 4H, pyrrolic protons), 8.86 (br, 4H, pyrrolic protons), 8.19 (d, 2H, Ph-H protons, $^3\text{J} = 6.6$ Hz), 7.93 (m, 2H, Ph-H protons), 7.72 (m, 4H, Ph-H protons), 6.62 - 7.05 (m, 30H, Ph-H protons), 5.36 (d, 4H, Ph- CH_2P - protons), unobserved (2H, NH protons). ^{13}C $\{^1\text{H}\}$ NMR (DMF): δ 147.8, 146.6, 137.3, 135.2, 134.5, 134.4, 134.1, 132.9, 131.4, 131.1, 130.2, 130.1, 129.7, 128.1, 119.2, 118.0, 116.6 (62C, meso C, pyrrolic C and phenyl C); 107.2 (2C, Ph- CH_2P -). ESI-mass spectrum: 1011.1 [(M-2Br) $^+$, 10 %]. m/z calcd: 1012.3824, HRMS: 1011.3750 [(M-2Br) $^+$, 100 %].

CIS-5,15-DI(2-BROMOMETHYLPHENYL)PORPHYRIN (6-7)

Refer to the procedure on synthesis of **6-5**. Compound **4-7** was used as starting materials for the synthesis of **6-7**.

Yield: 472 mg (80 %). ^1H NMR (CDCl_3): δ 10.31 (s, 2H, meso protons), 9.37 (d, 4H, pyrrolic protons, $^3\text{J} = 4.8$ Hz), 8.89 (d, 4H, pyrrolic protons, $^3\text{J} = 4.4$ Hz), 8.13 (d, 2H, Ph-H protons, $^3\text{J} = 7.2$ Hz), 7.95 (d, 2H, Ph-H protons, $^3\text{J} = 7.6$ Hz), 7.85 (m, 2H, Ph-H protons), 7.68 (m, 2H, Ph-H protons), 4.21 (s, 4H, Ph- CH_2Br protons), -3.12 (s, 2H, NH protons). ^{13}C $\{^1\text{H}\}$ NMR (CDCl_3): δ 146.9, 145.6, 140.6, 139.3, 134.6, 131.8, 130.9, 129.9, 129.3, 126.7, 115.5, 105.5 (32C, meso C, pyrrolic C and phenyl C); 31.7 (2C, Ph- CH_2Br). EI-mass spectrum: 648.0 (50 %). m/z calcd: 648.3892, MALDI-TOF m/z : 647.1605 (30

%), 649.1616 (100 %), 651.1744 (25 %). Elemental Analysis (Calc.): C, 62.98; H, 3.73; N, 8.64; Br, 24.65 % (Found): C, 62.83; H, 3.60; N, 8.24; Br, 23.64 %.

COMPOUND 6-8

Refer to the procedure on synthesis of **6-6**. Compound **6-7** was used as starting materials for the synthesis of **6-8**.

Yield: 456 mg (50 %). ^1H NMR (CDCl_3): δ 10.33, 10.35 (2s, 2H, meso protons); 9.31, 9.36 (2d, 4H, pyrrolic protons); 8.84, 8.70 (2d, 4H, pyrrolic protons); 7.32 - 8.13 (m, 8H, Ph-H protons), 6.62 - 7.08 (m, 30H, Ph-H protons), 5.36 (2s, 4H, Ph-CH₂P- protons); -3.29, -3.19 (2s, 2H, NH protons). ^{13}C $\{^1\text{H}\}$ NMR (CD_3OD): δ 142.5, 141.3, 137.3, 137.2, 132.0, 129.9, 129.2, 129.1, 128.9, 127.7, 126.1, 125.8, 125.0, 124.9, 124.84, 124.77, 124.3, 122.8, 113.9, 113.7, 112.7, 112.6, 111.3, 111.2 (62C, meso C, pyrrolic C and phenyl C); 101.9 (2C, Ph-CH₂P-). ESI-mass spectrum: 1011.2 [(M-2Br)⁺, 60 %]. *m/z* calcd: 1012.382, HRMS: 1011.3762 [(M-2Br)⁺, 100 %]. Elemental Analysis (Calc.) for C₇₀H₅₄N₄P₂Br₂: C, 71.68; H, 4.64; N, 4.78; Br, 13.62; P, 5.28 %. (Found): C, 71.64; H, 4.31; N, 4.43; Br, 15.40; P, 5.22 %

OLIGOMER 6-9

In a 5ml one-neck RBF, compounds **6-6** (1 mmol, 1.17 g) and **6-4** (1 mmol, 0.45 g) was added and degassed then purged with Ar gas trice. Degassed CHCl₃ (2.5 ml) and sodium ethoxide (5 mmol) in ethanol (1.5 ml) were added and the reaction mixture was allowed to stir at room temperature for 5 days. It was then washed with water, dried and

solvent removed *in vacuo*. The crude product was reprecipitated in methanol. The residue was filtered and washed with acetone using Soxhlet extraction.

Yield: 0.78 g (48 %). ^1H NMR (CDCl_3): δ 10.11, 9.96, 9.90, 9.25, 9.16, 9.07, 8.93, 8.74, 8.23, 7.95, 7.68, 7.54, 7.02, 6.84, 6.68, 6.28 (aromatic and -CHO protons); 5.51, 5.16, 5.12 (alkene protons); 3.72, 3.51, 3.48, -0.20 – 2.21(alkyl protons); -3.08, -3.22 (NH protons). ^{13}C $\{^1\text{H}\}$ NMR (CDCl_3): δ 188.8 (-CHO), 155.4, 151.6, 150.1, 149.7, 147.3, 145.1, 140.5, 139.9, 139.7, 139.6, 135.8, 135.2, 134.3, 132.0, 131.6, 131.4, 131.1, 130.5, 130.3, 128.5, 128.3, 128.1, 126.3, 126.1, 125.6, 125.4, 124.6, 124.2, 123.8, 123.4, 117.4, 117.1, 116.7, 110.6, 109.9, 109.4, 105.1, 104.9, 68.6, 67.5, 34.3, 31.9, 30.4, 29.5, 29.2, 28.9, 29.7, 28.3, 28.0, 27.5, 25.4, 25.2, 24.7, 22.7, 21.2, 14.2. M_w / PDI: 5775 / 1.05. T_g : 110 °C. T_d : 291 °C. Elemental Analysis (Calc.) for $(\text{C}_{62}\text{H}_{68}\text{N}_4\text{O}_2)_n$: C, 82.63; H, 7.61; N, 6.22% (Found): C, 80.16; H, 7.25; N, 6.11%.

OLIGOMER 6-10

Refer to the procedure on the synthesis of **6-9**. Compounds **6-8** and **6-4** were used as starting materials for the synthesis of **6-10**.

Yield: 0.73 g (45 %). ^1H NMR (CDCl_3): δ 10.11, 9.96, 9.88, 9.24, 9.16, 9.06, 8.92, 8.87, 8.76, 7.92, 7.67, 7.53, 6.96, 6.82, 6.66, 6.27 (aromatic and -CHO protons); 5.50, 5.11, (alkene protons); 3.46, 2.88, 0 - 2.20 (alkyl protons); -3.10, -3.19, -3.24 (NH protons). ^{13}C $\{^1\text{H}\}$ NMR (CDCl_3): δ 189.0, 149.7, 147.3, 145.2, 139.9, 135.2, 131.5, 128.5, 128.0, 125.3, 124.1, 117.1, 109.8, 105.0, 67.5, 31.8, 29.2, 28.3, 27.5, 24.6, 14.1, 22.6. M_w / PDI:

6035 / 1.17. T_g : 89 °C. TGA: 213 °C. Elemental Analysis (Calc.) for $(C_{62}H_{68}N_4O_2)_n$: C, 82.63; H, 7.61; N, 6.22 % (Found): C, 82.64; H, 7.67; N, 6.29 %.

1,4-BISDECYLOXY-2,5-DIODOBENZENE (6-14)

To a solution of **6-2** (31.25 g 80 mmol), acetic acid (180 ml), water (14 ml) and concentrated sulfuric acid (6 ml) were added potassium periodate (20.53 g, 96 mmol) and iodine (26.20 g, 96 mmol). The reaction mixture was stirred at 80 °C for 24 hours, cooled to room temperature then acetic acid was removed *in vacuo*. Aqueous sodium thiosulphate (20 %) was added to the solution until the brown colour of iodine disappeared. The mixture was poured into ice water with sodium carbonate (500 ml) and extracted with hexane. The organic layer was washed with sodium chloride solution, dried with anhydrous sodium sulphate, filtered then dried to give white crystals of **6-14** that were recrystallized with ethanol.

Yield: 24.67 g (48 %). Melting point: 58.0 - 59.0 °C {62 - 63 °C}¹⁰. 1H NMR ($CDCl_3$): δ 7.17 (s, 2H, Ph-H protons), 3.92 (t, 4H, Ph-OCH₂- protons, $^3J = 6.5$ Hz), 1.80, (quintet, 4H, -CH₂- protons, $^3J = 6.6$ Hz), 1.28 - 1.51 (br s & m, 28H, -CH₂- protons), 0.88 (t, 6H, -CH₃ protons, $^3J = 6.6$ Hz). ^{13}C { 1H } NMR ($CDCl_3$): δ 152.9 (2C, aromatic C-O), 122.9 (2C, aromatic CH), 86.3 (2C, aromatic C-I), 70.4 (2C, Ph-OCH₂-), 14.0, 22.6, 26.0, 29.0, 29.1, 29.2, 29.5, 29.5, 31.9 [18C, -(CH₂)₈CH₃]. EI-mass spectrum: 642.0 (55 %). m/z calcd: 642.1431, HRMS: 642.1420 (100 %).

1,4-BISDECYLOXY-2,5-TRIMETHYLSILYLETHYNYLBENZENE (6-15)

Compound **6-14** (15 mmol, 9.63 g) was added to freshly distilled triethylamine (100 ml) contained in a two-neck RBF and fitted with a condenser. The mixture was degassed for 30 minutes then dichlorobis(triphenylphosphine) palladium (II) (0.8 mmol, 0.56 g) and copper (I) iodide (0.8 mmol, 0.15 g) were added to the flask which was stoppered and kept under inert atmosphere. Trimethylsilylacetylene (38 mmol, 3.68g) was injected into the flask and the reaction mixture was refluxed for 1 hour. After the mixture had cooled, triethylamine was removed *in vacuo*. The crude product was passed through a short column of silica gel (60 - 250 mesh) using CH₂Cl₂/hexane (2:3) as eluent. After removing the solvent, the solid was recrystallized with ethanol to yield yellow solid of **6-15**.

*Yield: 5.94 g (68 %). Melting point: 69.0 - 71.5 °C {72 - 73 °C}¹⁰. ¹H NMR (CDCl₃): δ 6.90 (s, 2H, Ph-H protons), 3.92 (t, 4H, Ph-OCH₂- protons, ³J = 6.4 Hz), 1.78 (quintet, 4H, -CH₂- protons, ³J = 6.3 Hz), 1.27 - 1.54 (m, 28H, -CH₂- protons), 0.88 (t, 6H, -CH₃ protons, ³J = 6.6 Hz), 0.25 (s, 18H, -Si(CH₃)₃ protons). ¹³C {¹H} NMR (CDCl₃): δ 154.0 (2C, aromatic C-O); 113.9, 117.2, (4C, aromatic C & CH); 101.0 (2C, Ph-C≡C-H), 100.0 (2C, Ph-C≡C-H), 69.4 (2C, Ph-OCH₂), 14.1, 22.6, 26.0, 29.3, 29.4, 29.56, 29.60, 31.9 [18C, -(CH₂)₈CH₃]^{viii}, 0 [6C, -Si(CH₃)₃]. EI-mass spectrum: 582.3 (100 %). *m/z* calcd: 582.4288, HRMS: 582.4285 (100 %).*

^{viii} One missing peak due to poor resolution

1,4-BISDECYLOXY-2,5-DIETHYNYLBENZENE (6-16)

Compound **6-15** (5 mmol, 2.91 g) was dissolved in THF (15 ml) and methanol (15 ml). Aqueous sodium hydroxide (1.7 ml, 5 N) was then added to the solution which was stirred for 2 hours. The solvent was removed *in vacuo* and the product was extracted with hexane, washed with brine then water. After drying, the dark orange solid product was found to be pure enough for subsequent reaction.

Yield: 2.17 g (99 %). Melting point: 75.0 - 76.5 °C {70 - 72 °C}.¹⁰ ¹H NMR (CDCl₃): δ 6.95 (s, 2H, Ph-H protons), 3.97 (t, 4H, Ph-OCH₂- protons, ³J = 6.5 Hz), 3.33 (s, 2H, -C≡C-H protons), 1.80 (br, 4H, -CH₂- protons), 1.27 - 1.46 (m, 28H, -CH₂- protons), 0.86 (br, 6, -CH₃ protons). ¹³C {¹H} NMR (CDCl₃): δ 154.0 (2C, aromatic C-O); 113.3, 117.8 (4C, aromatic C & CH); 82.3 (2C, Ph-C≡C-H), 79.8 (2C, Ph-C≡C-H), 69.7 (2C, Ph-OCH₂-), 14.0, 22.6, 25.9, 29.1, 29.3, 29.5, 31.9 [18C, -(CH₂)₈CH₃]^x. EI-mass spectrum: 438.2 (90 %). m/z calcd: 438.3498, HRMS: 438.3493 (100 %).

1,2-BISDECYLOXYBENZENE (6-18)

Refer to the procedure on synthesis of **6-2**. Catechol **6-17** was used as starting material for the synthesis of **6-18**. The product obtained is white solid.

Yield: 8.20 g (21 %). Melting point: 40.0 - 41.0 °C {40 - 41 °C}¹³. ¹H NMR (CDCl₃): δ 6.88 (s, 4H, Ph-H protons), 3.99 (t, 4H, Ph-OCH₂- protons, ³J = 6.6 Hz), 1.79 (m, 4H, -CH₂- protons), 1.27-1.49 (br s & m, 28H, -CH₂- protons), 0.88 (t, 6H, -CH₃ protons, ³J = 6.6

^x Two missing peak due to poor resolution

Hz). ^{13}C $\{^1\text{H}\}$ NMR (CDCl_3): δ 114.1, 121.0, 149.2 (6C, aromatic C & CH), 69.3 (2C, Ph-OCH₂-), 14.1, 22.7, 26.0, 29.3, 29.4, 29.57, 29.62, 31.9, [18C, -(CH₂)₈CH₃]^x. EI-mass spectrum: 390.3. *m/z* calcd: 390.3498, HRMS: 390.3498.

1,2-BISDECYLOXY-4,5-DIODOBENZENE (6-19)

Refer to the procedure on synthesis of **6-14**. Compound **6-18** was used as starting material for the synthesis of **6-19**. The product obtained is white solid.

Yield: 28.78 g (56 %). Melting point: 40.0 - 42.0 °C {45.6 - 47.2 °C}¹⁴. ^1H NMR (CDCl_3): δ 7.25 (s, 2H, Ph-H protons), 3.92 (t, 4H, Ph-OCH₂- protons, $^3\text{J} = 6.6$ Hz), 1.79, (quintet, 4H, -CH₂- protons, $^3\text{J} = 7.0$ Hz), 1.27 - 1.44 (br s & m, 28H, -CH₂- protons), 0.88 (t, 6H, -CH₃ protons, $^3\text{J} = 6.6$ Hz). ^{13}C $\{^1\text{H}\}$ NMR (CDCl_3): δ 95.9, 123.8, 149.8 (6C, aromatic C & CH), 69.5 (2C, Ph-OCH₂-), 14.1, 22.7, 25.9, 29.0, 29.1, 29.3, 29.45, 29.53, 31.9 [18C, -(CH₂)₈CH₃]. EI-mass spectrum: 641.9 (80 %). *m/z* calcd: 642.1431, HRMS: 642.1413 (100 %).

1,2-BISDECYLOXY-4,5-BISTRIMETHYLSILYLETHYNYLBENZENE (6-20)

Refer to the procedure on synthesis of **6-15**. Compound **6-19** was used as starting material for the synthesis of **6-20**. The product is orange oil.

Yield: 4.72 g (54 %). ^1H NMR (CDCl_3): δ 6.91 (s, 2H, Ph-H protons), 3.97 (t, 4H, Ph-OCH₂- proton, $^3\text{J} = 6.6$ Hz), 1.81 (quintet, 4H, -CH₂- protons, $^3\text{J} = 7.0$ Hz), 1.27-1.47 (m,

^x One peak missing due to poor resolution

28H, -CH₂- protons), 0.88 (t, 6, -CH₃ protons, ³J = 6.5 Hz), 0.25 (s, 18H, -Si(CH₃)₃ protons). ¹³C {¹H} NMR (CDCl₃): δ 149.0 (2C, aromatic C-O); 116.1, 118.7 (4C, aromatic C & CH); 103.6 (2C, Ph-C≡C-H), 96.3 (2C, Ph-C≡C-H), 69.0 (2C, Ph-OCH₂-), 14.1, 22.7, 25.9, 29.0, 29.3, 29.5, 29.6, 31.9 [18C, (CH₂)₈CH₃]^{xi}, 0.1 [6C, -Si(CH₃)₃]. EI-mass spectrum: 582.3 (100 %). m/z calcd: 582.2488, HRMS: 582.4284 (100 %).

1,2-BISDECYLOXY-4,5-DIETHYNYLBENZENE (6-21)

Refer to the procedure on synthesis of **6-16**. Compound **6-20** was used as starting material for the synthesis of **6-21**. The product is dull orange solid.

Yield: 2.13 g (97 %). Melting point: 55.5 - 56.0 °C {52.0 - 53.8 °C}. ¹⁴ ¹H NMR (CDCl₃): δ 6.95 (s, 2H, Ph-H protons), 3.98 (t, 4H, Ph-OCH₂- protons, ³J = 6.6 Hz), 3.25, (s, 2H, -C≡C-H protons), 1.82 (quintet, 4H, -CH₂- protons, ³J = 7.0 Hz), 1.27 - 1.47 (m, 28H, -CH₂- protons), 0.88 (t, 6, -CH₃ protons, ³J = 6.8 Hz). ¹³C {¹H} NMR (CDCl₃): δ 149.5 (2C, aromatic C-O); 116.7, 117.8 (4C, aromatic C & CH); 82.2 (2C, Ph-C≡C-H), 79.3 (2C, Ph-C≡C-H), 69.2 (2C, Ph-OCH₂-), 14.0, 22.6, 25.9, 29.0, 29.3, 29.49, 29.53, 31.8 [18C, -(CH₂)₈CH₃]^{xii}. EI-mass spectrum: 438.3 (70 %). m/z calcd: 438.3498, HRMS: 438.3495 (100 %).

^{xi} Two missing peaks due to poor resolution

^{xii} One missing peak due to poor resolution

1,3-BISDECYLOXYBENZENE (6-23)

Refer to the procedure on synthesis of **6-2**. Resorcinol **6-22** was used as starting material for the synthesis of **6-23**. The product obtained after recrystallization is white flaky solid.

Yield: 14.83 g (38 %). Melting point: 50.5 - 51.0 °C. ¹H NMR (CDCl₃): δ 7.14 (t, 1H, Ph-H protons, ³J = 8.0 Hz), 6.46 - 6.49 (m, 3H, Ph-H proton), 3.92 (t, 4H, Ph-OCH₂- protons, ³J = 6.6 Hz), 1.76 (quintet, 4H, -CH₂- protons, ³J = 7.0 Hz), 1.27 - 1.46 (br s & m, 28H, -CH₂- protons), 0.88 (t, 6H, -CH₃ protons, ³J = 6.6 Hz). ¹³C {¹H} NMR (CDCl₃): δ 160.4 (2C, aromatic C-O), 101.4, 106.6, 129.7 (4C, aromatic C & CH); 67.9 (2C, Ph-OCH₂-), 14.1, 22.7, 26.0, 29.25, 29.29, 29.4, 29.5, 31.9, 40.0 [18C, -(CH₂)₈CH₃]. EI-mass spectrum: 390.3 (55 %). m/z calcd: 390.3498, HRMS: 390.3495 (100 %).

1,5-BISDECYLOXY-2,4-DIODOBENZENE (6-24)

Refer to the procedure on synthesis of **6-14**. Compound **6-23** was used as starting material for the synthesis of **6-24**. The product obtained is cream-coloured solid.

Yield: 27.24 g (53 %). Melting point: 61.0 - 63.0 °C. ¹H NMR (CDCl₃): δ 8.02 (s, 1H, Ph-H proton), 6.32 (s, 1H, Ph-H proton), 3.98 (t, 4H, Ph-OCH₂- protons, ³J = 6.4 Hz), 1.83, (quintet, 4H, -CH₂- protons, ³J = 7.0 Hz), 1.27 - 1.51 (br s & m, 28H, -CH₂- protons), 0.88 (t, 6H, -CH₃ protons, ³J = 6.8 Hz). ¹³C {¹H} NMR (CDCl₃): δ 159.0 (2C, aromatic C-O); 76.0, 97.9, 146.6 (4C, aromatic C & CH); 69.5 (2C, Ph-OCH₂-), 14.1, 22.7, 26.0, 29.0,

29.3, 29.5, 31.9 [18C, $-(\text{CH}_2)_8\text{CH}_3$]^{xiii}. *El-mass spectrum*: 641.9 (65 %). *m/z calcd*: 642.1431, *HRMS*: 642.1423 (100 %).

1,5-BISDECYLOXY-2,4- BISTRIMETHYLSILYLETHYNYLBENZENE (6-25)

Refer to the procedure on synthesis of **6-15**. Compound **6-24** was used as starting material for the synthesis of **6-25**. The product obtained is cream-coloured solid.

Yield: 4.19 g (48 %). *Melting point*: 59.0 - 60.0 °C. ¹H NMR (CDCl₃): δ 7.49 (s, 1H, Ph-H proton), 6.29 (s, 1H, Ph-H proton), 3.99 (t, 4H, Ph-OCH₂- protons, ³J = 6.3 Hz), 1.80 (quintet, 4H, -CH₂- protons, ³J = 6.6 Hz), 1.27 - 1.54 (m, 28H, -CH₂- protons), 0.88 (t, 6, -CH₃ protons, ³J = 6.8 Hz), 0.22 (s, 18H, -Si(CH₃)₃ protons). ¹³C {¹H} NMR (CDCl₃): δ 161.7 (2C, aromatic C-O); 96.7, 96.77, 96.84, 100.5, 138.3 (2C, Ph-C≡C-H; 2C, Ph-C≡C-H; 4C, aromatic C & CH); 68.8 (2C, Ph-OCH₂-), 14.1, 22.6, 26.0, 29.1, 29.3, 29.4, 29.5, 29.6, 31.9 [18C, $-(\text{CH}_2)_8\text{CH}_3$], 0.1 [6C, -Si(CH₃)₃]. *El-mass spectrum*: 582.4 (100 %). *m/z calcd*: 582.4288, *HRMS*: 582.4284 (100 %).

1,5-BISDECYLOXY-2,4- BIS-ETHYNYLBENZENE (6-26)

Refer to the procedure on synthesis of **6-16**. Compound **6-25** was used as starting material for the synthesis of **6-26**. The product obtained is cream-coloured solid.

Yield: 2.17 g (99 %). *Melting point*: 64.0 - 66.5 °C. ¹H NMR (CDCl₃): δ 7.52 (s, 1H, Ph-H proton), 6.36 (s, 1H, Ph-H proton), 4.05 (t, 4H, Ph-OCH₂- protons, ³J = 6.6 Hz), 3.16, (s,

^{xiii} Two missing peak due to poor resolution

2H, $-C\equiv C-H$ protons), 1.84 (quintet, 4H, $-CH_2-$ protons, $^3J = 6.6$ Hz), 1.27 - 1.55 (m, 28H, $-CH_2-$ protons), 0.88 (t, 6, $-CH_3$ protons, $^3J = 6.6$ Hz). ^{13}C $\{^1H\}$ NMR ($CDCl_3$): δ 96.9, 139.0, 161.9 (6C, aromatic C & CH), 79.8 (2C, Ph-C \equiv C-H), 79.1 (2C, Ph-C \equiv C-H), 69.0 (2C, Ph-OCH $_2-$), 14.1, 22.6, 25.8, 28.9, 29.3, 29.5, 31.9 [18C, $-(CH_2)_8CH_3$]^{xiv}. EI-mass spectrum: 438.3 (80 %). m/z calcd: 438.3498, HRMS: 438.3490 (100 %).

5,15-DIPHENYLPORPHYRIN (6-28)

Benzaldehyde **6-27** (10 mmol, 1.06 g) and **4-5** (10 mmol, 1.46g) were dissolved in dried, degassed CH_2Cl_2 (1 L) and 2 drops of trifluoroacetic acid was added. The mixture was stirred under Ar at room temperature for 15 hours. After which, chloroanil (40 mmol, 9.31 g) was added and the solution was heated to reflux for 2 hours. The mixture was allowed to cool and the solvent was removed *in vacuo*. The dark solid was chromatographed over silica gel (60 - 250 mesh) using $CHCl_3$ as eluent to separate the porphyrins from the byproducts of chloranil first followed by hexane/toluene (2:1) to isolate the pure product which forms purple crystals after drying.

Yield: 1.23 g (26.5 %). 1H NMR ($CDCl_3$): δ 10.32 (s, 1H, meso protons), 9.39 (d, 4H, pyrrolic protons, $^3J = 4.5$ Hz), 9.09 (d, 4H, pyrrolic protons, $^3J = 4.5$ Hz), 8.29 (m, 4H, Ph-H protons), 7.81 (m, 6H, Ph-H protons), -3.10 (br s, 2H, NH protons). ^{13}C $\{^1H\}$ NMR ($CDCl_3$): δ 147.2, 145.2, 141.4, 134.8, 131.6, 131.0, 127.7, 126.9, 119.1, 105.2 (32C, meso C, pyrrolic C and phenyl C). EI-mass spectrum: 462.3 (25 %). m/z calcd: 462.185, MALDI-TOF m/z : 462.214 (100 %).

^{xiv} Two missing peak due to poor resolution

5,15-BISBROMO-10,20-DIPHENYLPORPHYRIN (6-29)

Compound **6-28** (1 mmol, 551 mg) was dissolved in dry CHCl_3 (20 ml) and cooled to 0°C . NBS (2.1 mmol, 372 mg) and pyridine (0.3 ml) were added into the solution and the reaction progress was monitored using TLC. When all the starting material has reacted, the reaction was quenched with acetone. All the solvent is removed *in vacuo* and recrystallization using CHCl_3 and methanol yielded purple crystals.

Yield: 58 mg (79 %). $^1\text{H NMR}$ (CDCl_3): δ 9.62 (d, 4H, pyrrolic protons, $^3J = 4.9$ Hz), 8.84 (d, 4H, pyrrolic protons, $^3J = 4.9$ Hz), 8.16 (m, 4H, Ph-H protons), 7.78 (m, 6H, Ph-H protons), -2.70 (br s, 2H, NH protons). ^{13}C $\{^1\text{H}\}$ NMR (CDCl_3): δ 147.0, 144.9, 138.9, 134.5, 130.4, 129.3, 129.1, 128.5, 128.0, 126.8 (32C, meso C, pyrrolic C and phenyl C). EI-mass spectrum: 619.9 (80 %). m/z calcd: 618.0054, MALDI-TOF m/z : 618.1330 (30 %). Elemental Analysis (Calc.) for $\text{C}_{32}\text{H}_{20}\text{N}_4\text{Br}_2$: C, 61.96; H, 3.25; N, 9.03; Br, 25.76 % (Found): C, 63.27; H, 3.10; N, 8.76; Br, 25.31 %.

Zn(II) 5,15-BISBROMO-10,20-DIPHENYLPORPHYRIN (6-30)

Compound **6-29** (500 mg, 0.8 mmol) was stirred in large excess of $\text{Zn}(\text{OAc})_2 \cdot x\text{H}_2\text{O}$ in THF at room temperature for 5 days. The solvent was removed *in vacuo* then the solid was transferred into a buchner funnel. The residue was washed with large amount of water then finally rinsed with cold ethanol then dried in vacuum. Purple crystals were obtained.

Yield: 513 mg (93 %). ^1H NMR (d_6 -DMSO): δ 10.26 (d, 4H, pyrrolic protons, $^3J = 4.9\text{Hz}$), 9.41 (d, 4H, pyrrolic protons, $^3J = 4.9\text{ Hz}$), 8.77 (m, 4H, Ph-H protons), 8.43 (m, 6H, Ph-H protons). ^{13}C $\{^1\text{H}\}$ NMR (d_6 -DMSO): δ 151.2, 150.4, 142.9, 135.3, 134.4, 134.0, 128.9, 127.8, 122.9, 105.1 (32C, meso C, pyrrolic C and phenyl C). EI-mass spectrum: 681.9 (20 %). m/z calcd: 681.9169, MALDI-TOF m/z : 682.0840 (95 %). Analysis (Calc.) for $\text{C}_{32}\text{H}_{18}\text{N}_4\text{Br}_2\text{Zn}$: C, 56.21; H, 2.65; N, 8.19; Zn, 9.56 % (Found): C, 56.68; H, 2.65; N, 8.10; Zn, 7.23 %.

OLIGOMER 6-31

Compounds **6-30** (0.3 mmol, 0.21 g), **6-16** (0.3 mmol, 0.13g), dichlorobis(triphenylphosphine) palladium(II) (0.03 mmol, 21 mg) and copper(I) iodide (0.03 mmol, 6 mg) were added into a 20 ml one-neck RBF and fitted with a condenser. The setup was degassed and purged with Ar gas trice then kept under inert condition. Degassed toluene (2 ml) and diisopropylamine (1.2 ml) were added to the mixture and then heated to 100 °C for 24 hours. After the mixture had cooled, all the solvent was removed *in vacuo*. The residue were transferred into a Buchner funnel and rinsed with water. The residue was then transferred into a Soxhlet thimble, washed with methanol for 3 days, with acetone for another 3 days then THF to remove the porphyrins monomer in the thimble. The insoluble portions can dissolve in CS_2 and pyridine.

Yield: 0.24 g (71 %). ^1H NMR ($\text{CS}_2 + d_5\text{-C}_6\text{H}_5\text{N}$): 10.24, 9.10 (pyrrolic protons); 8.51, 8.39, 7.92, 7.52, 7.14 (phenyl protons); 3.66, 3.77 (-OCH₂ protons); 0 - 2.50 (m, alkyl protons). Elemental Analysis (Calc.): C, 77.52; H, 6.51; N, 5.83; Zn, 6.81 % (Found): C, 74.35; H, 6.74; N, 5.41; Zn, 4.61 %. MALDI-TOF m/z (most abundant): 5337 (100 %). T_d : 281 °C.

OLIGOMER 6-32

Refer to the procedure for the synthesis of **6-31**. Compounds **6-30** and **6-21** were used as starting materials. The residue was then transferred into a Soxhlet thimble, washed with methanol for 3 days then with acetone for another 3 days. The soluble portions of the oligomer were extracted using THF.

Yield: 0.17 g (51 %). ¹H NMR (CS₂ + d₅-C₆H₅N): 10.22, 8.96, 8.37, 7.86, 7.48, 7.27, 6.94 (pyrrolic and phenyl protons); 3.58, 0.94 - 2.03 (m, alkyl protons). Elemental Analysis (Calc.): C, 77.52; H, 6.51; N, 5.83; Zn, 6.81 % (Found): C, 75.37; H, 6.90; N, 5.97; Zn, 4.42 %. MALDI-TOF m/z (most abundant): 4931 (100 %). T_d: 288 °C.

OLIGOMER 6-33

Refer to the procedure for the synthesis of **6-31**. Compounds **6-30** and **6-26** were used as starting materials. The residue was then transferred into a Soxhlet thimble, washed with methanol for 3 days, with acetone for another 3 days then THF to remove the porphyrins monomer in the thimble. The soluble portions of the polymer were extracted using THF.

Yield: 0.18 g (53 %). ¹H NMR (CS₂ + d₅-C₆H₅N): 10.26, 9.13 (pyrrolic protons); 8.41, 7.92, (phenyl protons); 3.67, 3.76 (-OCH₂ protons); 0.80 - 2.50 (m, alkyl protons). Elemental Analysis (Calc.): C, 77.52; H, 6.51; N, 5.83; Zn, 6.81 % (Found): C, 77.06; H, 6.29; N, 5.85; Zn, 4.42; Br, 2.59 %. MALDI-TOF m/z (most abundant): 5008 (100 %). T_d: 301 °C.

4,4'-DIBROMO-2,2'-DINITROBIPHENYL (7-6)

2,5-Dibromonitrobenzene **7-5** (30 mmol, 12.00 g) and copper powder (90 mmol, 5.72 g) and DMF (80 ml) were added into a one-neck RBF and heated to 120 °C for 2 hours. The reaction mixture was then cooled to room temperature and filtered to remove the residue. Toluene was used to rinse any crude product trapped in the residue. The filtrate was washed with water, dried and solvent evaporated *in vacuo*. Recrystallization in ethanol yield bright yellow crystals of the pure product.

Yield: 7.73 g (45 %). Melting point: 153.4 - 154.5 °C {lit. 150 °C}¹⁵. ¹H NMR (CDCl₃): δ 8.38 (d, 2H, 3 and 3' aromatic protons, ⁴J = 1.7 Hz), 7.83 (dd, 2H, 5 and 5' aromatic protons, ³J = 8.4 Hz, ⁴J = 1.7 Hz), 7.16 (d, 2H, 6 and 6' aromatic protons, ³J = 8.4 Hz). ¹³C {¹H} NMR (CDCl₃): δ 147.3 (2C, aromatic C-NO₂); 136.6, 132.0, 128.0 (6C, aromatic C-H); 131.9, 122.9 (4C, aromatic C). EI-mass spectrum: 401.9 (5 %). m/z calcd: 401.8674, HRMS: 399.8688 (0.6 %), 401.8677 (1.3 %), 403.8664 (0.6 %).

3,8-DIBROMOBENZO[C]CINNOLINE (7-7)

Method 1

Compound **7-6** (14 mmol, 5.63 g), concentrated hydrochloric acid (28 ml) and tin powder (57 mmol, 6.77g) were added in ethanol (180 ml) and refluxed for 30 minutes. The reaction mixture was poured into ice-water after it had cooled then basified with sodium hydroxide. The crude product was extracted with ether, washed with water, dried over

anhydrous sodium sulphate filtered then evaporated. The product was recrystallized using ethanol to yield paper-like yellow solid. *Yield: 3.75 g (79.2 %).*

Method 2

Compound **7-6** (40 mmol, 16.08 g), zinc powder (400 mmol, 26.16 g) and anhydrous calcium chloride (200 mmol, 22.20 g) were added in ethanol (180 ml) and refluxed for 2 hours. The reaction mixture was cooled then filtered. The filtrate was extracted with ether, washed with water, dried over anhydrous sodium sulphate filtered then evaporated. The product was recrystallized using ethanol to yield paper-like yellow solid. *Yield: 10.61 g (78.5 %).*

Melting point: 244.2 - 245.5 °C {lit. 242 - 243 °C}. ¹⁶ ¹H NMR (CDCl₃): δ 8.90 (d, 2H, 3 and 3' aromatic protons, ⁴J = 2.1 Hz), 8.40 (d, 2H, 5 and 5' aromatic protons, ³J = 8.7 Hz), 8.00 (dd, 2H, 6 and 6' aromatic protons, ³J = 8.7 Hz, ⁴J = 2.1 Hz). ¹³C {¹H} NMR (CDCl₃): δ 145.7 (2C, aromatic C-NO₂); 135.4, 133.8, 122.9 (6C, aromatic C-H); 123.4, 119.1 (4C, aromatic C). EI-mass spectrum: 335.7 (50 %), 337.7 (90 %), 339.7 (50 %). m/z calcd: 337.8877, HRMS: 335.8896 (30 %), 337.8872 (60 %), 339.8859 (40 %). Elemental Analysis (Calc.) for C₁₂H₆N₂Br₂: C, 42.64; H, 1.79; N, 8.29; Br, 47.23 % (Found): C, 42.85; H, 1.67; N, 8.30; Br, 46.93 %.

Crystal data of 7-7 grown in iodomethane: Crystal data: (C₁₃H₉Br₂IN₂)_n. M = 479.94 Triclinic. P-1, a = 7.2912(7) Å, b = 10.0409(10) Å, c = 10.8935(11) Å, α = 103.731(2)°, β = 103.127(2)°, γ = 107.400(2)°, V = 700.00(12) Å³, Z = 2, d_{calc} = 2.277 mg/m³, μ = 7.978 mm⁻¹, θ_{max} = 27.50 °, 9116 reflections collected, 3219 independent reflections, R_{int} =

0.0233, 3219 reflections with $I > 2\sigma(I)$, 164 parameters, $R1$ (all data) = 0.0243, $wR2$ (all data) = 0.0551.

2,2'-DINITROBIPHENYL (7-1)

Refer to the procedure on synthesis of **7-6**. 2-Bromonitrobenzene (**7-13**) (10 mmol, 2.02 g) was used as starting material for the synthesis of **7-2**. Recrystallization in ethanol yield pink needle-like crystals of the pure product.

Yield: 3.50 g (87 %). Melting point: 128.8 - 129.4 °C {lit. 127 - 128 °C}.¹⁷ ¹H NMR (CDCl₃): δ 8.22 (dd, 2H, 3 and 3' aromatic protons, ³J = 8.0 Hz, ⁴J = 1.4 Hz), 7.69 (td, 2H, 5 and 5' aromatic protons, ³J = 7.3 Hz, ⁴J = 1.4 Hz), 7.59 (td, 2H, 4 and 4' aromatic protons, ³J = 8.0 Hz, ⁴J = 1.4 Hz), 7.30 (dd, 2H, 6 and 6' aromatic protons, ³J = 7.7 Hz, ⁴J = 1.7 Hz). ¹³C {¹H} NMR (CDCl₃): δ 147.2 (2C, aromatic C-NO₂); 133.4, 130.9, 129.1, 124.8 (8C, aromatic C-H); 134.2 (2C, aromatic C). FAB-mass spectrum: 244.0 (100 %). m/z calcd: 244.0484, HRMS: 244.0495 (20 %).

BENZO[C]CINNOLINE (7-2)

Refer to the procedure for the synthesis of **7-7**. Compound **7-1** (8 mmol, 2.05 g) was used as starting material for the synthesis of **7-2**. The product was recrystallized using ethanol then flushed down a short column of silica gel (60 - 250 mesh) using CH₂Cl₂ as eluent to yield bright yellow solid products.

Yield: 0.25 g (17 %). Melting point: 159.2 - 159.9 °C {lit. 157 - 158 °C}¹⁸. ¹H NMR (CDCl₃): δ 8.76 (m, 2H, aromatic protons), 8.60 (m, 2H, aromatic protons), 7.93 (m, 4H,

aromatic protons). ^{13}C $\{^1\text{H}\}$ NMR (CDCl_3): δ 145.3 (2C, aromatic **C-NO₂**); 131.5, 131.3, 129.2, 121.4 (8C, aromatic **C-H**); 120.9 (2C, aromatic **C**). *El-mass spectrum*: 180.0 (85 %). *m/z calcd*: 180.0678, *HRMS*: 180.0690 (80 %).

4,4'-DICHLORO-2,2'-DINITROBIPHENYL (7-3)

Refer to the procedure on synthesis of **7-6**. 2-Bromo-5-chloronitrobenzene **7-14** (9 mmol, 2.13 g) was used as starting material for the synthesis of **7-3**. Recrystallization in ethanol yield dull yellow crystals of the pure product.

Yield: 0.76 g (27 %). *Melting point*: 140.5 - 142.0 °C {lit. 138 - 139 °C}. ^{19}F ^1H NMR (CDCl_3): δ 8.24 (d, 2H, 3 and 3' aromatic protons, $^4\text{J} = 2.1$ Hz), 7.68 (dd, 2H, 5 and 5' aromatic protons, $^3\text{J} = 8.4$ Hz, $^4\text{J} = 2.1$ Hz), 7.24 (d, 2H, 6 and 6' aromatic protons, $^3\text{J} = 8.4$ Hz). ^{13}C $\{^1\text{H}\}$ NMR (CDCl_3): δ 147.4 (2C, aromatic **C-NO₂**); 133.7, 131.9, 125.2 (6C, aromatic **C-H**); 135.5, 131.5 (4C, aromatic **C**). *El-mass spectrum*: 311.9 (5 %). *m/z calcd*: 313.9675, *HRMS*: 311.9715 (20 %), 313.9688 (12 %).

4,4'-DICHLOROBENZO[C]CINNOLINE (7-4)

Refer to the procedure for the synthesis of **7-7**. 4,4'-Dichloro-2,2'-dinitrobiphenyl (1 mmol, 0.31 g) was used as starting material for the synthesis of **7-4**. The product was recrystallized using ethanol to yield bright yellow paper-like solid. *Yield*: 0.11 g (45 %).

Melting point: 263.0 - 265.0 °C. ^1H NMR (CDCl_3): δ 8.73 (d, 2H, 3 and 3' aromatic protons, $^4\text{J} = 1.4$ Hz), 8.47 (d, 2H, 5 and 5' aromatic protons, $^3\text{J} = 8.7$ Hz), 7.93 (dd, 2H,

6 and 6' aromatic protons, $^3J = 8.7$ Hz, $^4J = 1.4$ Hz). ^{13}C $\{^1\text{H}\}$ NMR (CDCl_3): δ 145.3 (2C, aromatic C-NO₂), 135.4 (2C, aromatic C-Cl); 132.8, 130.4, 123.0 (6C, aromatic C); 118.8 (2C, aromatic C). EI-mass spectrum: 247.9 (100 %), 249.9 (75 %), 251.9 (15 %). m/z calcd: 247.9908, HRMS: 247.9902 (100 %), 249.9879 (63 %), 251.9821 (11 %).

2,7-DIBROMO-9,9'-DIHEXYLFLUORENE (7-11)

2,7-Dibromofluorene (2.00 g, 6 mmol) and 1-bromohexane (12.2 mmol, 1.8 ml) were dissolved in 50 ml dry DMSO and potassium *tert*-butoxide (12.2 ml, 1M in THF) was added dropwise to the solution under inert condition. The reaction mixture was allowed to stir for additional 24 hours then poured into ice water. The crude product was extracted with hexane, washed with water then dried using anhydrous sodium sulphate. The solvent was evaporated *in vacuo*. After purification via column chromatography over silica gel (60 - 250 mesh) using hexane as eluent, the solvent was removed and white crystals of the pure product were obtained.

Yield: 1.89 g (62 %). Melting point: 68.0 - 69.0 °C {65 - 66 °C}.²⁰ ^1H NMR (CDCl_3): δ 7.45 - 7.54 (m, 6H, aromatic protons), 1.93 (t, 4H, benzylic protons, $^3J = 7.7$ Hz), 0.60-1.15 (m, 22H, -(CH₂)₄CH₃ protons). ^{13}C $\{^1\text{H}\}$ NMR (CDCl_3): δ 152.5, 139.0, 121.5 (6C, aromatic C); 130.1, 126.2, 121.1 (6C, aromatic CH); 55.7(1C, benzylic C), 40.2 (2C, -CCH₂), 31.4, 29.5, 23.6, 22.5, 14.0 (10C, -(CH₂)₄CH₃). EI-mass spectrum: 490.1 (40 %), 492.1 (80 %), 494.1 (40 %).

POLYMERS 7-12a-e

Compounds **7-7** (z mmol), **7-10** (x mmol), **7-11** (y mmol), catalytic amount of tetrabutylammonium bromide, aqueous potassium carbonate (2 M), degassed toluene (2.5 ml) and 1.0 - 1.5 mol % (with respect to brominated monomers) of Pd(PPh₃)₄ were stirred for 48 hours under Ar at 100 °C. The mixture was then poured into a stirred methanol/water (1:1) mixture to generate yellow precipitates. The precipitates were filtered, redissolved in CHCl₃ and precipitated into methanol for washing. These residues were then filtered, redissolved in CHCl₃ and precipitated into acetone. The yellow solids were then vacuum-dried.

Table 10.1 Summary of the quantities of the monomers **7-7**, **7-10** and **7-11** used to synthesize the polymers **7-12a-e**, reaction yields, M_n , PDI, T_d (°C), Φ_{eff} (%), elemental analyses as well as ^1H and $^{13}\text{C}\{^1\text{H}\}$ results

Polymer	Percentage of benzo[c]cinnoline in polymer product from elemental analyses studies (calculated from N content)	Ratio			Yield (%)	M_n	PDI	T_d (°C)	Φ_{eff} (%)
		Fluorene		Benzo[c]cinnoline					
		7-10 (x mmol)	7-11 (y mmol)	7-7 (z mmol)					
7-12a	6.3	5	4	1	64	10556	1.91	356	1.05
7-12b	20.2	5	3	2	54	20123	1.71	329	0.57
7-12c	27.6	5	2	3	60	39728	1.38	358	0.45
7-12d	43.4	5	1	4	47	14565	1.26	347	0.26
7-12e	50.5	1	0	1	51	6765	1.05	325	0.19

Polymer	Elements [Expected (%) / Found (%)]			^1H NMR (CDCl_3 , δ)	^{13}C NMR (CDCl_3 , δ)
	C	H	N		
7-12a	89.77 / 89.86	9.35 / 8.51	0.88 / 0.55	9.05, 8.65, 8.26 (br, $\text{C}_{12}\text{H}_6\text{N}_2$ aromatic protons); 7.40 - 7.90 (m, $\text{C}_{25}\text{H}_{32}$ aromatic protons); 0.72, 1.07, 1.52, 2.06 (br, $\text{C}_{25}\text{H}_{32}$ alkyl protons)	152.2, 151.8, 145.9, 142.6, 141.0, 140.5, 140.0, 139.6, 138.1, 131.2, 128.8, 127.2, 126.1, 122.0, 121.8, 121.5, 120.4, 120.3, 120.0 (aromatic C); 55.3 (benzylic C); 40.4, 31.4, 29.7, 23.8, 22.5, 14.0 (alkyl C)
7-12b	89.19 / 90.36	8.95 / 8.08	1.86 / 1.88	9.13, 8.73, 8.34 (br s, $\text{C}_{12}\text{H}_6\text{N}_2$ aromatic protons); 7.50 - 7.93 (m, $\text{C}_{25}\text{H}_{32}$ aromatic protons); 0.80, 1.15, 1.26, 1.68, 2.14 (br, $\text{C}_{25}\text{H}_{32}$ alkyl protons)	152.4, 151.8, 145.9, 142.5, 141.2, 141.0, 140.5, 140.0, 139.6, 138.1, 132.2, 132.1, 128.8, 128.5, 128.4, 127.2, 126.1, 122.1, 121.9, 121.5, 120.7, 120.4, 120.0 (aromatic C); 55.5, 55.3 (benzylic C); 40.4, 31.4, 29.7, 23.8, 22.5, 14.0 (alkyl C)

7-12c	88.54 / 90.59	8.52 / 8.65	2.94 / 2.70	9.13, 8.73, 8.33 (<i>br s</i> , $C_{12}H_6N_2$ aromatic protons); 7.69 - 7.92 (<i>m</i> , $C_{25}H_{32}$ aromatic protons); 0.80, 1.14, 1.25, 1.57, 2.14 (<i>br</i> , $C_{25}H_{32}$ alkyl protons)	152.4, 152.2, 151.9, 151.8, 145.9, 142.6, 142.5, 141.2, 140.8, 140.6, 140.1, 140.0, 138.6, 131.1, 128.9, 127.2, 126.5, 126.4, 126.2, 122.0, 121.9, 121.5, 120.7, 120.4, 120.2, 119.9, 119.8 (aromatic C); 55.7, 55.5, 55.3 (benzylic C); 40.4, 31.4, 29.6, 23.8, 22.4, 13.9 (alkyl C)
7-12d	87.82 / 87.36	8.04 / 7.64	4.14 / 4.49	9.14 (<i>s</i>), 8.74 (<i>d</i>), 8.33 (<i>d</i>) ($C_{12}H_6N_2$ aromatic protons); 7.50 - 7.80 (<i>m</i> , $C_{25}H_{32}$ aromatic protons); 0.79, 1.14, 1.25, 1.60, 2.18 (<i>br</i> , $C_{25}H_{32}$ alkyl protons)	152.4, 145.9, 142.5, 140.8, 138.6, 131.1, 128.8, 126.5, 122.1, 121.9, 120.7, 119.8 (aromatic C); 55.7 (benzylic C); 40.5, 31.5, 29.7, 24.0, 22.6, 13.9 (alkyl C)
7-12e^{xv}	87.02 / 87.39	7.50 / 7.42	5.49 / 5.55	9.31 (<i>s</i>), 8.85 (<i>d</i>), 8.51 (<i>d</i>) ($C_{12}H_6N_2$ aromatic protons); 7.90 - 7.99 (<i>m</i> , $C_{25}H_{32}$ aromatic protons); 0.78, 1.14, 1.88, 2.17 (<i>br</i> , $C_{25}H_{32}$ alkyl protons)	152.4, 145.9, 142.6, 140.9, 138.6, 131.2, 128.8, 126.6, 122.1, 121.9, 120.8, 119.9 (aromatic C); 55.7 (benzylic C); 40.6, 31.6, 29.8, 29.7, 24.0, 22.6, 14.0 (alkyl C)

^{xv} ¹³C NMR was carried out on the Bruker AMX500 (500MHz)

COMPOUND 8-1a

Compound **6-8** (100 mg, 0.1 mmol) and excess $\text{Zn}(\text{OAc})_2 \cdot x\text{H}_2\text{O}$ were dissolved in THF and stirred for 5 days. Excess CHCl_3 was added to the mixture which was washed twice with brine and lastly with minimal deionized water. The salt was recrystallized using CHCl_3 /hexane mixture then dried.

Yield: 105 mg (70 %). ^1H NMR (CDCl_3): δ 10.03, 10.05 (2s, 2H, meso protons); 9.05, 9.01, 8.47, 8.31, 8.09 (5d, 8H, pyrrolic protons); 6.62 - 7.67 (m, 38H, Ph-H protons), 4.65 - 4.76 (m, 4H, Ph- CH_2P - protons). ^{13}C $\{^1\text{H}\}$ NMR (CDCl_3): δ 149.6, 136.2, 134.9, 134.5, 134.0, 133.9, 133.5, 133.3, 132.5, 132.1, 130.3, 130.2, 130.0, 129.7, 129.6, 129.1, 129.0, 128.0, 128.0, 126.8, 126.7, 117.3, 117.1, 116.2, 115.9, 114.8, 114.6 (62C, meso C, pyrrolic C and phenyl C); 106.6 (2C, aromatic Ph CH_2P -). ESI-mass spectrum: 539.3 [(M-2Br) $^{2+}$, 100 %]. m/z calcd: 1074.2959, HRMS: 1077.287 [(M-2Br) $^+$, 48 %]. Elemental Analysis (Calc.): C, 68.00; H, 4.24; N, 4.53; Zn, 5.29 % (Found): C, 67.99; H, 4.08; N, 4.70; Zn, 4.71 %.

COMPOUND 8-1b

Refer to procedure on **8-1a**. Compound **6-6** was used as starting material for the synthesis of **8-1b** to yield purple crystals.

Yield: 105 mg (70 %). ^1H NMR (CDCl_3): δ 10.08 (s, 2H, meso protons); 9.08, 8.45, 8.35 (3d, 8H, pyrrolic protons), 6.63 - 7.72 (m, 38H, Ph-H protons), 4.62 (d, 4H, Ph- CH_2P - protons). ^{13}C $\{^1\text{H}\}$ NMR (CDCl_3): δ 149.7, 149.6, 136.2, 134.4, 133.9, 133.8, 133.4, 133.3,

132.6, 131.1, 130.6, 130.1, 129.9, 129.6, 129.4, 128.1, 126.8, 117.4, 116.3, 115.2 (62C, meso C, pyrrolic C and phenyl C); 106.6 (2C, PhCH₂P-). ESI-mass spectrum: 539.2 [(M-2Br)²⁺, 60 %]. *m/z* calcd: 1074.2959, HRMS: 1077.287 [(M-2Br)⁺, 18 %]. Elemental Analysis (Calc.): C, 68.00; H, 4.24; N, 4.53; Br, 12.93; P, 5.01; Zn, 5.29 % (Found): C, 66.93; H, 4.53; N, 4.47; Br, 14.66; P, 3.65; Zn, 5.40 %.

1-BROMOMETHYL-4-METHOXYMETHYLBENZENE (8-3)²¹

Refer to procedure for 1-bromomethyl-2-methoxymethylbenzene **4-9**. Compound **8-3** was synthesized from 1,4-bisbromomethylbenzene **8-2** (22.12 g, 84 mmol) to yield pale yellow oil as product.

Yield: 8.13 g (45 %). ¹H NMR (CDCl₃): δ 7.37, 7.30 (2 overlapping d, 4H, Ph-H protons), 4.48 (s, 2H, Ph-CH₂O- protons), 4.44 (s, 2H, PhCH₂Br protons), 3.38 (s, 3H, -OCH₃ protons). ¹³C {¹H} NMR (CDCl₃): δ 138.6 (1C, aromatic C-CH₂O), 137.1 (1C, aromatic C-CH₂Br); 129.1, 128.0 (4C, aromatic CH), 74.2 (1C, Ph-CH₂O-), 58.2 (1C, -OCH₃), 33.3 (1C, Ph-CH₂Br). EI-mass spectrum: 213.9 (50 %), 215.9 (50 %). *m/z* calcd: 213.9993, HRMS: 213.9986 (100 %), 215.9970 (100 %).

4-METHOXYMETHYLBENZALDEHYDE (8-4)⁸

Refer to procedure for 2-methoxymethylbenzaldehyde **4-4**. Compound **8-4** was synthesized from **8-3** (33 mmol, 7.10 g) to yield yellow oil as product.

Yield: 2.50 g (38 %). ^1H NMR (CDCl_3): δ 10.01 (s, 1H, -CHO proton), 7.87 (d, 2H, Ph-H protons, $^3\text{J} = 6.6$ Hz), 7.50 (d, 2H, Ph-H protons, $^3\text{J} = 7.0$ Hz), 4.54 (s, 2H, Ph- CH_2 - protons), 3.43 (s, 3H, - OCH_3 protons). ^{13}C $\{^1\text{H}\}$ NMR (CDCl_3): δ 192.0 (1C, -CHO); 129.8, 127.6 (4C, aromatic CH); 145.3, 135.7 (2C, aromatic C); 73.9 (Ph- CH_2O -); 58.4 (- OCH_3). EI-mass spectrum: 150.1 (90 %). m/z calcd: 150.1775, HRMS: 150.0677 (12 %).

5,15-DI(4-METHOXYMETHYLPHENYL)PORPHYRIN (8-5).

Refer to procedure for **4-6** and **4-7**. Compound **8-5** was synthesized from compounds **8-4** and **4-5** to yield purple crystals after purification over silica gel (60 - 250 mesh) using CH_2Cl_2 as eluent.

Yield: 12 mg (13 %). ^1H NMR (CDCl_3): δ 10.34 (s, 2H, meso protons), 9.45 (d, 4H, pyrrolic protons, $^3\text{J} = 4.5$ Hz), 9.15 (d, 4H, pyrrolic protons, $^3\text{J} = 4.5$ Hz), 8.26 (d, 4H, Ph-H protons, $^3\text{J} = 8.0$ Hz), 7.76 (d, 4H, Ph-H protons, $^3\text{J} = 8.0$ Hz), 4.82 (s, 4H, Ph- CH_2O - protons), 3.65 (s, 6H, - OCH_3 protons), unobserved (br s, NH protons). ^{13}C $\{^1\text{H}\}$ NMR (CDCl_3): δ 147.2, 145.2, 140.8, 137.7, 134.9, 131.6, 131.0, 126.3, 118.8, 105.2 (32C, meso C, pyrrolic C and phenyl C); 74.8 (2C, Ph CH_2O -); 58.6 (2C, - OCH_3). EI-mass spectrum: 550.2 (100 %). MALDI-TOF m/z : 550.3492 (100 %).

5,15-DI(4-BROMOMETHYLPHENYL)PORPHYRIN (8-6).

Refer to procedure on **6-5**. Compound **8-6** was synthesized from **8-5** to yield purple crystals.

Yield: 400 mg (68 %). ^1H NMR (CDCl_3): δ 10.33 (s, 2H, meso protons), 9.42 (d, 2H, pyrrolic protons, $^3\text{J} = 4.8$ Hz), 9.09 (d, 2H, pyrrolic protons, $^3\text{J} = 4.5$ Hz), 8.26 (d, 4H, Ph-H protons, $^3\text{J} = 7.7$ Hz), 7.86 (d, 4H, Ph-H protons, $^3\text{J} = 8.0$ Hz), 4.89 (s, 4H, Ph- CH_2Br protons), -3.12 (s, 2H, NH protons). ^{13}C $\{^1\text{H}\}$ NMR (d_7 -DMF): δ 147.8, 146.2, 141.9, 139.1, 136.0, 135.8, 133.4, 131.5, 129.1, 127.9, 120.5, 106.6 (32C, meso C, pyrrolic C and phenyl C); overlapped by deuterated solvent peak (2C, Ph CH_2Br). EI-mass spectrum: 648. m/z calcd: 648.3892, MALDI-TOF m/z : 647.1842 (55 %), 649.1978 (100 %), 651.2018 (65 %). Elemental Analysis (Calc.) for $\text{C}_{34}\text{H}_{24}\text{N}_4\text{Br}_2$: C, 62.98; H, 3.73; N, 8.64 % (Found): C, 62.67; H, 3.45; N, 8.40 %.

COMPOUND 8-7

Refer to procedure for **6-6**. Compound **8-7** was synthesized from **8-6** to yield purple crystals.

Yield: 452 mg (50 %). ^1H NMR (CD_3OD): δ 10.43 (s, 2H, meso protons), 9.50 (d, 4H, pyrrolic protons, $^3\text{J} = 4.9$ Hz), 8.90 (d, 4H, pyrrolic protons, $^3\text{J} = 4.9$ Hz), 7.80 - 8.00 (m, 38H, Ph-H protons), 7.38 (2d, 4H, Ph- CH_2P - protons), unobserved (2H, NH protons). ^{13}C $\{^1\text{H}\}$ NMR (DMF and CD_3OD): δ 147.8, 146.2, 141.7, 136.8, 136.0, 135.8, 134.7, 133.4, 131.7, 131.6, 130.9, 130.7, 129.1, 127.9, 127.9 (62C, meso C, pyrrolic C and phenyl C); 119.4 (2C, Ph CH_2P -). ESI-mass spectrum: 1011.1 [(M-2Br) $^+$, 30 %]. m/z calcd: 1012.3824, HRMS: 1011.3736 [(M-2Br) $^+$, 100 %]. Elemental Analysis (Calc.) for $\text{C}_{70}\text{H}_{54}\text{N}_4\text{P}_2\text{Br}_2$: C, 71.68; H, 4.64; N, 4.78; Br, 13.62 % (Found): C, 67.94; H, 4.78; N, 4.88; Br, 13.93 %

COMPOUND 8-1c

Refer to procedure on **8-1a**. Compound **8-1c** was synthesized from **8-7** to yield purple crystals.

Yield: 102mg (68 %). ^1H NMR (CD_3OD): δ 10.26, 10.44 (2s, 2H, meso protons); 9.50, 9.41, 8.89, 8.83 (4d, 8H, pyrrolic protons; $^3\text{J} = 4.9, 4.5, 4.5, 4.2$ Hz respectively), 7.24 - 7.97 (m, 38H, Ph-H protons); 7.25, 7.35 (2d, 4H, Ph- CH_2P - protons). ^{13}C $\{^1\text{H}\}$ NMR (CD_3OD): δ 150.3, 150.1, 135.9, 135.3, 134.8, 134.7, 132.2, 131.6, 130.8, 130.7, 130.0, 129.4, 119.1, 118.4, 118.0 (62C, meso C, pyrrolic C and phenyl C); 106.3 (2C, Ph CH_2P -). ESI-mass spectrum: 537.3 [$(\text{M}-2\text{Br})^{2+}$, 100 %]. m/z calcd: 1074.2959, HRMS: 1077.286 [$(\text{M}-2\text{Br})^+$]. Elemental Analysis (Calc.): C, 68.00; H, 4.24; N, 4.53; Br, 12.93; P, 5.01; Zn, 5.29 % (Found): C, 63.09; H, 3.58; N, 5.13; Br, 16.18; P, 4.20; Zn, 4.12 %.

10.4 REFERENCES

- ¹ Silverstein R.M.; Bassler, G.C.; Morrill, T.C. "Spectroscopic Identification of Organic Compounds", 5th ed., John Wiley & Sons, Inc., 1991, Chapter 3, 91.
- ² Silverstein R.M.; Bassler, G.C.; Morrill, T.C. "Spectroscopic Identification of Organic Compounds", 5th ed., John Wiley & Sons, Inc., 1991, Chapter 4, 165.
- ³ Kroschwitz, J.I. "Polymer Characterization and Analysis", Wiley-Interscience, 1990, 1.
- ⁴ Silverstein R.M.; Bassler, G.C.; Morrill, T.C. "Spectroscopic Identification of Organic Compounds", 5th ed., John Wiley & Sons, Inc., 1991, Chapter 2,3.
- ⁵ Boyer, R.F. "Encyclopedia of Polymer Science and Technology", Suppl. Vol. 2, Wiley-Interscience, 1977. 753.

- ⁶ Cheremisinoff, N.P. *“Polymer Characterization – Lab Techniques and Analysis”*, Noyes Publication, Chapter 1, 1996, 9.
- ⁷ Aldrich MSDS [22115-41-9].
- ⁸ Nace, M. *J. Org. Chem.* **1959**, *24*, 1792.
- ⁹ Weast, R.C.; Grasselli, J.G. *“CRC Handbook of Data on Organic Compounds”*, Vol 2, 2nd ed, CRC Press, Inc., 1989.
- ¹⁰ Plater, M.J.; Sinclair, J.P.; Aiken, S.; Gelbrich, T.; Hursthouse, M.B. *Tetrahedron* **2004**, *60* (30), 6385.
- ¹¹ Sigma Aldrich 2005-2006 Catalogue, [152269-98-2].
- ¹² Takagi, K.; Nishikawa, Y.; Nishioka, N.; Kunisada, H.; Yuki, Y. *J. Polymer Sci., Part A: Polymer Chem.* **2002**, *40* (22), 3927.
- ¹³ Zhang, D.; Tessier, C.A.; Youngs, W.J. *Chem. Mater.* **1999**, *11*, 3050.
- ¹⁴ Zhou, Q.; Carroll, P.J.; Swager, T.M. *J. Org. Chem.* **1994**, *59*, 1294.
- ¹⁵ Shaw, F.R.; Turner, E.E. *J. Chem. Soc. Abs.* **1932**, 285.
- ¹⁶ Patrick, D.A.; Boykin, D.W.; Wilson, W.D.; Tanious, F.A.; Sychala, J.; Bender, B.C.; Hall, J.E.; Dykstra, C.C.; Ohemeng, K.A.; Tidwell, R.R. *Eur. J. Med. Chem.* **1997**, *32*, 781.
- ¹⁷ Barlas, H. *Chemiker-Zeitung*, **1985**, *109* (9), 311.
- ¹⁸ Hou, Z.; Fujiwara, Y.; Taniguchi, H. *J. Org. Chem.* **1988**, *53*, 3118.
- ¹⁹ Kornblum, N.; Kendall, D.L. *J. Am. Chem. Soc.* **1952**, *74*, 5782.
- ²⁰ Wang W. PhD Thesis, *“From Conjugated Linear to Conjugated Transannular Chromophore Paracyclophane-based Co-Polymers”*, NUS, Department of Chemistry, 2004.
- ²¹ Nobuyuki, N.; Koji, N. *Jpn. Kokai Tokkyo Koho* **2001**, 2001163815.

APPENDIX

Crystal data and structure refinement for 4-6

Empirical formula	C ₃₆ H ₃₀ N ₄ O ₂	
Formula weight	550.64	
Temperature	223(2) K	
Wavelength	0.71073 Å	
Crystal system	Monoclinic	
Space group	P2(1)/n	
Unit cell dimensions	a = 8.3509(6) Å	α = 90°
	b = 15.5894(12) Å	β = 98.646(2)°
	c = 11.0918(8) Å	γ = 90°
Volume	1427.58(18) Å ³	
Z	2	
Density (calculated)	1.281 Mg/m ³	
Absorption coefficient	0.081 mm ⁻¹	
F(000)	580	
Crystal size	0.34 x 0.10 x 0.10 mm ³	
Theta range for data collection	2.27 to 30.04 °	
Index ranges	-11<=h<=11, -21<=k<=19, -15<=l<=14	
Reflections collected	11517	
Independent reflections	4081 [R(int) = 0.0374]	
Completeness to theta = 30.04 °	97.7 %	
Absorption correction	Sadabs, (Sheldrick, 1996)	
Max. and min. transmission	0.9920 and 0.9731	
Refinement method	Full-matrix least-squares on F ²	
Data / restraints / parameters	4081 / 0 / 250	
Goodness-of-fit on F ²	0.913	
Final R indices [I>2sigma(I)]	R1 = 0.0535, wR2 = 0.1184	
R indices (all data)	R1 = 0.0838, wR2 = 0.1304	
Largest diff. peak and hole	0.306 and -0.210 e.Å ⁻³	

Selected bond lengths [Å] and angles [°] for 4-6

O(1)-C(17)	1.4058(19)
O(1)-C(18)	1.411(2)
N(1)-C(11)	1.3666(17)

N(1)-C(8)	1.3770(17)
N(2)-C(15)	1.3691(18)
N(2)-C(12)	1.3754(17)
C(1)-C(2)	1.401(2)
C(1)-C(6)	1.404(2)
C(1)-C(17)	1.501(2)
C(2)-C(3)	1.376(3)
C(3)-C(4)	1.378(3)
C(4)-C(5)	1.391(2)
C(5)-C(6)	1.391(2)
C(6)-C(7)	1.5047(19)
C(7)-C(12)	1.398(2)
C(7)-C(8)	1.400(2)
C(8)-C(9)	1.450(2)
C(9)-C(10)	1.343(2)
C(10)-C(11)	1.453(2)
C(11)-C(16)#1	1.393(2)
C(12)-C(13)	1.426(2)
C(13)-C(14)	1.360(2)
C(14)-C(15)	1.4294(19)
C(15)-C(16)	1.386(2)
C(16)-C(11)#1	1.393(2)
C(17)-O(1)-C(18)	113.53(15)
C(11)-N(1)-C(8)	105.03(11)
C(15)-N(2)-C(12)	110.20(12)
C(2)-C(1)-C(6)	118.71(15)
C(2)-C(1)-C(17)	119.83(14)
C(6)-C(1)-C(17)	121.45(13)
C(3)-C(2)-C(1)	121.26(16)
C(2)-C(3)-C(4)	120.13(16)
C(3)-C(4)-C(5)	119.57(18)
C(6)-C(5)-C(4)	121.10(16)
C(5)-C(6)-C(1)	119.21(13)
C(5)-C(6)-C(7)	119.12(13)
C(1)-C(6)-C(7)	121.66(14)

C(12)-C(7)-C(8)	124.32(12)
C(12)-C(7)-C(6)	116.72(12)
C(8)-C(7)-C(6)	118.93(13)
N(1)-C(8)-C(7)	125.16(12)
N(1)-C(8)-C(9)	110.45(13)
C(7)-C(8)-C(9)	124.39(13)
C(10)-C(9)-C(8)	107.09(14)
C(9)-C(10)-C(11)	106.29(14)
N(1)-C(11)-C(16)#1	126.29(13)
N(1)-C(11)-C(10)	111.13(12)
C(16)#1-C(11)-C(10)	122.58(14)
N(2)-C(12)-C(7)	124.64(13)
N(2)-C(12)-C(13)	106.57(12)
C(7)-C(12)-C(13)	128.79(13)
C(14)-C(13)-C(12)	108.41(13)
C(13)-C(14)-C(15)	107.93(13)
N(2)-C(15)-C(16)	126.43(13)
N(2)-C(15)-C(14)	106.88(12)
C(16)-C(15)-C(14)	126.61(13)
C(15)-C(16)-C(11)#1	128.16(14)
O(1)-C(17)-C(1)	109.73(14)

Crystal data and structure refinement for 4-13

Empirical formula	C ₃₆ H ₃₀ N ₄ O ₂	
Formula weight	550.64	
Temperature	223(2) K	
Wavelength	0.71073 Å	
Crystal system	Monoclinic	
Space group	P2(1)/n	
Unit cell dimensions	a = 8.7154(19) Å	α = 90°
	b = 13.750(3) Å	β = 108.057(5)°
	c = 12.896(3) Å	γ = 90°
Volume	1469.3(5) Å ³	
Z	2	
Density (calculated)	1.245 Mg/m ³	

Absorption coefficient	0.078 mm ⁻¹
F(000)	580
Crystal size	0.16 x 0.14 x 0.10 mm ³
Theta range for data collection	2.23 to 25.00 °
Index ranges	-10<=h<=9, -10<=k<=16, -14<=l<=15
Reflections collected	8200
Independent reflections	2587 [R(int) = 0.0692]
Completeness to theta = 25.00 °	99.8 %
Absorption correction	Sadabs, (Sheldirck 2001)
Max. and min. transmission	0.9922 and 0.9876
Refinement method	Full-matrix least-squares on F ²
Data / restraints / parameters	2587 / 0 / 195
Goodness-of-fit on F ²	1.020
Final R indices [I>2sigma(I)]	R1 = 0.0811, wR2 = 0.1824
R indices (all data)	R1 = 0.1500, wR2 = 0.2113
Largest diff. peak and hole	0.318 and -0.184 e.Å ⁻³

Selected bond lengths [Å] and angles [°] for 4-13

O(1)-C(17)	1.378(7)
O(1)-C(18)	1.439(6)
N(1)-C(6)	1.362(4)
N(1)-C(9)	1.384(4)
N(2)-C(4)	1.366(4)
N(2)-C(1)	1.372(4)
C(1)-C(10)#1	1.406(5)
C(1)-C(2)	1.444(5)
C(2)-C(3)	1.330(5)
C(3)-C(4)	1.439(5)
C(4)-C(5)	1.376(5)
C(5)-C(6)	1.396(5)
C(6)-C(7)	1.423(5)
C(7)-C(8)	1.358(5)
C(8)-C(9)	1.425(5)
C(9)-C(10)	1.395(5)
C(10)-C(1)#1	1.406(5)

C(10)-C(11)	1.501(5)
C(11)-C(12)	1.387(6)
C(11)-C(16)	1.391(6)
C(12)-C(13)	1.409(7)
C(13)-C(14)	1.356(8)
C(14)-C(15)	1.364(8)
C(15)-C(16)	1.398(6)
C(15)-C(17)	1.493(8)

C(17)-O(1)-C(18)	113.9(5)
C(6)-N(1)-C(9)	109.7(3)
C(4)-N(2)-C(1)	105.9(3)
N(2)-C(1)-C(10)#1	125.1(3)
N(2)-C(1)-C(2)	109.7(3)
C(10)#1-C(1)-C(2)	125.1(3)
C(3)-C(2)-C(1)	106.9(4)
C(2)-C(3)-C(4)	107.6(3)
N(2)-C(4)-C(5)	126.9(3)
N(2)-C(4)-C(3)	109.8(3)
C(5)-C(4)-C(3)	123.3(3)
C(4)-C(5)-C(6)	128.9(3)
N(1)-C(6)-C(5)	126.0(3)
N(1)-C(6)-C(7)	107.3(3)
C(5)-C(6)-C(7)	126.7(3)
C(8)-C(7)-C(6)	108.1(3)
C(7)-C(8)-C(9)	108.2(3)
N(1)-C(9)-C(10)	124.7(3)
N(1)-C(9)-C(8)	106.6(3)
C(10)-C(9)-C(8)	128.7(3)
C(9)-C(10)-C(1)#1	124.2(3)
C(9)-C(10)-C(11)	117.4(3)
C(1)#1-C(10)-C(11)	118.5(3)
C(12)-C(11)-C(16)	119.3(4)
C(12)-C(11)-C(10)	120.4(4)
C(16)-C(11)-C(10)	120.3(4)
C(11)-C(12)-C(13)	119.1(5)

C(14)-C(13)-C(12)	120.0(6)
C(13)-C(14)-C(15)	122.2(6)
C(14)-C(15)-C(16)	118.4(6)
C(14)-C(15)-C(17)	121.7(6)
C(16)-C(15)-C(17)	119.9(7)
C(11)-C(16)-C(15)	121.0(5)
O(1)-C(17)-C(15)	112.0(5)

Crystal data and structure refinement for 4-15 grown in CHCl₃/cyclohexane

Empirical formula	C ₃₆ H ₂₈ N ₄ O ₂ Zn	
Formula weight	613.99	
Temperature	223(2) K	
Wavelength	0.71073 Å	
Crystal system	Tetragonal	
Space group	I4(1)/a	
Unit cell dimensions	a = 22.812(3) Å	α = 90°
	b = 22.812(3) Å	β = 90°
	c = 11.423(3) Å	γ = 90°
Volume	5944.3(18) Å ³	
Z	8	
Density (calculated)	1.372 Mg/m ³	
Absorption coefficient	0.866 mm ⁻¹	
F(000)	2544	
Crystal size	0.10 x 0.10 x 0.04 mm ³	
Theta range for data collection	1.79 to 25.00 °	
Index ranges	-27 ≤ h ≤ 20, -27 ≤ k ≤ 26, -13 ≤ l ≤ 13	
Reflections collected	16293	
Independent reflections	2613 [R(int) = 0.1324]	
Completeness to theta = 25.00 °	100.0 %	
Absorption correction	Sadabs, (Sheldrick 2001)	
Max. and min. transmission	0.9662 and 0.9184	
Refinement method	Full-matrix least-squares on F ²	
Data / restraints / parameters	2613 / 0 / 196	
Goodness-of-fit on F ²	1.020	
Final R indices [I > 2σ(I)]	R1 = 0.0593, wR2 = 0.1184	

R indices (all data)
Largest diff. peak and hole

R1 = 0.1022, wR2 = 0.1338
0.513 and -0.303 e.Å⁻³

Selected bond lengths [Å] and angles [°] for 4-15 grown in CHCl₃/cyclohexane

Zn(1)-N(2)#1	2.037(3)
Zn(1)-N(2)	2.037(3)
Zn(1)-N(1)#1	2.062(3)
Zn(1)-N(1)	2.062(3)
Zn(1)-O(1)#2	2.434(3)
Zn(1)-O(1)#3	2.434(3)
O(1)-C(18)	1.423(5)
O(1)-C(17)	1.423(5)
O(1)-Zn(1)#4	2.434(3)
N(1)-C(4)	1.366(5)
N(1)-C(1)	1.369(5)
N(2)-C(6)	1.369(5)
N(2)-C(9)	1.379(5)
C(1)-C(10)#1	1.406(6)
C(1)-C(2)	1.439(6)
C(2)-C(3)	1.337(6)
C(3)-C(4)	1.433(6)
C(4)-C(5)	1.399(6)
C(5)-C(6)	1.386(6)
C(6)-C(7)	1.437(6)
C(7)-C(8)	1.346(6)
C(8)-C(9)	1.443(6)
C(9)-C(10)	1.401(6)
C(10)-C(1)#1	1.406(6)
C(10)-C(11)	1.493(6)
C(11)-C(12)	1.390(6)
C(11)-C(16)	1.398(6)
C(12)-C(13)	1.380(6)
C(13)-C(14)	1.369(6)
C(14)-C(15)	1.392(6)
C(15)-C(16)	1.393(6)

C(16)-C(17)	1.523(6)
N(2)#1-Zn(1)-N(2)	180.00(3)
N(2)#1-Zn(1)-N(1)#1	90.99(13)
N(2)-Zn(1)-N(1)#1	89.01(13)
N(2)#1-Zn(1)-N(1)	89.01(13)
N(2)-Zn(1)-N(1)	90.99(13)
N(1)#1-Zn(1)-N(1)	180.0(3)
N(2)#1-Zn(1)-O(1)#2	87.58(12)
N(2)-Zn(1)-O(1)#2	92.42(12)
N(1)#1-Zn(1)-O(1)#2	90.89(12)
N(1)-Zn(1)-O(1)#2	89.11(12)
N(2)#1-Zn(1)-O(1)#3	92.42(12)
N(2)-Zn(1)-O(1)#3	87.58(12)
N(1)#1-Zn(1)-O(1)#3	89.11(12)
N(1)-Zn(1)-O(1)#3	90.89(12)
O(1)#2-Zn(1)-O(1)#3	180.00(15)
C(18)-O(1)-C(17)	112.6(4)
C(18)-O(1)-Zn(1)#4	126.7(3)
C(17)-O(1)-Zn(1)#4	120.1(3)
C(4)-N(1)-C(1)	106.7(3)
C(4)-N(1)-Zn(1)	125.7(3)
C(1)-N(1)-Zn(1)	127.6(3)
C(6)-N(2)-C(9)	106.9(3)
C(6)-N(2)-Zn(1)	125.6(3)
C(9)-N(2)-Zn(1)	127.4(3)
N(1)-C(1)-C(10)#1	124.9(4)
N(1)-C(1)-C(2)	109.2(4)
C(10)#1-C(1)-C(2)	125.8(4)
C(3)-C(2)-C(1)	107.2(4)
C(2)-C(3)-C(4)	107.6(4)
N(1)-C(4)-C(5)	124.3(4)
N(1)-C(4)-C(3)	109.3(4)
C(5)-C(4)-C(3)	126.3(4)
C(6)-C(5)-C(4)	128.0(4)
N(2)-C(6)-C(5)	125.3(4)

N(2)-C(6)-C(7)	109.6(4)
C(5)-C(6)-C(7)	125.2(4)
C(8)-C(7)-C(6)	107.2(4)
C(7)-C(8)-C(9)	107.7(4)
N(2)-C(9)-C(10)	125.7(4)
N(2)-C(9)-C(8)	108.7(4)
C(10)-C(9)-C(8)	125.7(4)
C(9)-C(10)-C(1)#1	125.2(4)
C(9)-C(10)-C(11)	117.1(4)
C(1)#1-C(10)-C(11)	117.7(4)
C(12)-C(11)-C(16)	118.7(4)
C(12)-C(11)-C(10)	120.1(4)
C(16)-C(11)-C(10)	121.2(4)
C(13)-C(12)-C(11)	121.5(4)
C(14)-C(13)-C(12)	119.6(4)
C(13)-C(14)-C(15)	120.5(4)
C(14)-C(15)-C(16)	120.0(4)
C(15)-C(16)-C(11)	119.7(4)
C(15)-C(16)-C(17)	120.2(4)
C(11)-C(16)-C(17)	120.1(4)
O(1)-C(17)-C(16)	112.4(4)

Crystal data and structure refinement for 4-15 grown in ethyl acetate

Empirical formula	C ₃₆ H ₂₈ N ₄ O ₂ Zn	
Formula weight	613.99	
Temperature	223(2) K	
Wavelength	0.71073 Å	
Crystal system	Monoclinic	
Space group	P2(1)/c	
Unit cell dimensions	a = 9.2323(8) Å	α = 90°
	b = 10.3641(10) Å	β = 101.860(2)°
	c = 15.0985(14) Å	γ = 90°
Volume	1413.9(2) Å ³	
Z	2	
Density (calculated)	1.442 Mg/m ³	

Absorption coefficient	0.910 mm ⁻¹
F(000)	636
Crystal size	0.20 x 0.10 x 0.06 mm ³
Theta range for data collection	2.25 to 27.50 °
Index ranges	-11<=h<=9, -11<=k<=13, -18<=l<=19
Reflections collected	9655
Independent reflections	3228 [R(int) = 0.0508]
Completeness to theta = 27.50 °	99.8 %
Absorption correction	Sadabs, (Sheldrick 2001)
Max. and min. transmission	0.9474 and 0.8389
Refinement method	Full-matrix least-squares on F ²
Data / restraints / parameters	3228 / 0 / 197
Goodness-of-fit on F ²	1.108
Final R indices [I>2sigma(I)]	R1 = 0.0598, wR2 = 0.1243
R indices (all data)	R1 = 0.0799, wR2 = 0.1327
Largest diff. peak and hole	0.589 and -0.313 e.Å ⁻³

Selected bond lengths [Å] and angles [°] for 4-15 grown in ethyl acetate

Zn(1)-N(1)#1	2.028(2)
Zn(1)-N(1)	2.028(2)
Zn(1)-N(2)#1	2.030(2)
Zn(1)-N(2)	2.030(2)
N(1)-C(1)	1.369(4)
N(1)-C(4)	1.382(4)
N(2)-C(9)	1.369(4)
N(2)-C(6)	1.389(4)
O(1)-C(17)	1.372(4)
O(1)-C(18)	1.400(5)
C(1)-C(10)	1.386(4)
C(1)-C(2)	1.437(4)
C(2)-C(3)	1.346(4)
C(3)-C(4)	1.437(4)
C(4)-C(5)	1.397(4)
C(5)-C(6)	1.391(4)
C(5)-C(16)	1.512(4)

C(6)-C(7)	1.443(4)
C(7)-C(8)	1.335(5)
C(8)-C(9)	1.444(4)
C(9)-C(10)#1	1.386(4)
C(10)-C(9)#1	1.386(4)
C(11)-C(16)	1.392(4)
C(11)-C(12)	1.395(4)
C(11)-C(17)	1.495(4)
C(12)-C(13)	1.382(5)
C(13)-C(14)	1.378(5)
C(14)-C(15)	1.383(4)
C(15)-C(16)	1.393(4)
N(1)#1-Zn(1)-N(1)	180.00(15)
N(1)#1-Zn(1)-N(2)#1	88.92(10)
N(1)-Zn(1)-N(2)#1	91.08(10)
N(1)#1-Zn(1)-N(2)	91.08(10)
N(1)-Zn(1)-N(2)	88.92(10)
N(2)#1-Zn(1)-N(2)	180.0
C(1)-N(1)-C(4)	106.1(3)
C(1)-N(1)-Zn(1)	125.62(19)
C(4)-N(1)-Zn(1)	128.1(2)
C(9)-N(2)-C(6)	106.4(2)
C(9)-N(2)-Zn(1)	125.71(19)
C(6)-N(2)-Zn(1)	127.8(2)
C(17)-O(1)-C(18)	113.9(3)
N(1)-C(1)-C(10)	125.4(3)
N(1)-C(1)-C(2)	110.0(3)
C(10)-C(1)-C(2)	124.6(3)
C(3)-C(2)-C(1)	107.1(3)
C(2)-C(3)-C(4)	107.5(3)
N(1)-C(4)-C(5)	124.7(3)
N(1)-C(4)-C(3)	109.3(3)
C(5)-C(4)-C(3)	125.9(3)
C(6)-C(5)-C(4)	125.4(3)
C(6)-C(5)-C(16)	117.6(3)

C(4)-C(5)-C(16)	116.9(3)
N(2)-C(6)-C(5)	124.9(3)
N(2)-C(6)-C(7)	109.1(3)
C(5)-C(6)-C(7)	126.1(3)
C(8)-C(7)-C(6)	107.3(3)
C(7)-C(8)-C(9)	107.9(3)
N(2)-C(9)-C(10)#1	125.3(3)
N(2)-C(9)-C(8)	109.3(3)
C(10)#1-C(9)-C(8)	125.4(3)
C(9)#1-C(10)-C(1)	126.9(3)
C(16)-C(11)-C(12)	119.0(3)
C(16)-C(11)-C(17)	122.7(3)
C(12)-C(11)-C(17)	118.4(3)
C(13)-C(12)-C(11)	121.1(3)
C(14)-C(13)-C(12)	119.9(3)
C(13)-C(14)-C(15)	119.7(3)
C(14)-C(15)-C(16)	121.0(3)
C(11)-C(16)-C(15)	119.4(3)
C(11)-C(16)-C(5)	121.9(3)
C(15)-C(16)-C(5)	118.7(3)
O(1)-C(17)-C(11)	110.6(3)

Crystal data and structure refinement for 4-15 grown in nitrobenzene

Empirical formula	C ₃₆ H ₂₈ N ₄ O ₂ Zn	
Formula weight	613.99	
Temperature	223(2) K	
Wavelength	0.71073 Å	
Crystal system	Monoclinic	
Space group	P2(1)/c	
Unit cell dimensions	a = 9.236(6) Å	α = 90°
	b = 10.424(6) Å	β = 102.302(13)°
	c = 15.167(10) Å	γ = 90°
Volume	1426.6(15) Å ³	
Z	2	
Density (calculated)	1.429 Mg/m ³	

Absorption coefficient	0.902 mm ⁻¹
F(000)	636
Crystal size	0.14 x 0.12 x 0.08 mm ³
Theta range for data collection	2.26 to 27.50 °
Index ranges	-9<=h<=11, -12<=k<=13, -19<=l<=19
Reflections collected	9531
Independent reflections	3264 [R(int) = 0.0593]
Completeness to theta = 27.50 °	99.8 %
Absorption correction	Sadabs, (Sheldrick 2001)
Max. and min. transmission	0.9313 and 0.8841
Refinement method	Full-matrix least-squares on F ²
Data / restraints / parameters	3264 / 0 / 196
Goodness-of-fit on F ²	1.031
Final R indices [I>2sigma(I)]	R1 = 0.0569, wR2 = 0.1336
R indices (all data)	R1 = 0.0864, wR2 = 0.1465
Largest diff. peak and hole	0.861 and -0.554 e.Å ⁻³

Selected bond lengths [Å] and angles [°] for 4-15 grown in nitrobenzene

Zn(1)-N(1)#1	2.023(3)
Zn(1)-N(1)	2.023(3)
Zn(1)-N(2)	2.039(3)
Zn(1)-N(2)#1	2.039(3)
N(1)-C(2)	1.369(4)
N(1)-C(5)	1.392(4)
N(2)-C(10)	1.368(4)
N(2)-C(7)	1.388(4)
O(1)-C(17)	1.361(5)
O(1)-C(18)	1.398(5)
C(1)-C(10)#1	1.389(4)
C(1)-C(2)	1.396(4)
C(2)-C(3)	1.445(4)
C(3)-C(4)	1.345(5)
C(4)-C(5)	1.437(5)
C(5)-C(6)	1.393(5)
C(6)-C(7)	1.394(5)

C(6)-C(11)	1.516(4)
C(7)-C(8)	1.438(5)
C(8)-C(9)	1.343(5)
C(9)-C(10)	1.437(4)
C(10)-C(1)#1	1.389(4)
C(11)-C(12)	1.386(5)
C(11)-C(16)	1.398(5)
C(12)-C(13)	1.391(4)
C(13)-C(14)	1.378(5)
C(14)-C(15)	1.373(5)
C(15)-C(16)	1.399(4)
C(16)-C(17)	1.493(5)

N(1)#1-Zn(1)-N(1)	180.00(11)
N(1)#1-Zn(1)-N(2)	91.56(11)
N(1)-Zn(1)-N(2)	88.44(11)
N(1)#1-Zn(1)-N(2)#1	88.44(11)
N(1)-Zn(1)-N(2)#1	91.56(11)
N(2)-Zn(1)-N(2)#1	180.0
C(2)-N(1)-C(5)	105.9(3)
C(2)-N(1)-Zn(1)	125.5(2)
C(5)-N(1)-Zn(1)	128.4(2)
C(10)-N(2)-C(7)	106.3(3)
C(10)-N(2)-Zn(1)	125.4(2)
C(7)-N(2)-Zn(1)	128.1(2)
C(17)-O(1)-C(18)	114.0(4)
C(10)#1-C(1)-C(2)	127.4(3)
N(1)-C(2)-C(1)	125.1(3)
N(1)-C(2)-C(3)	110.0(3)
C(1)-C(2)-C(3)	125.0(3)
C(4)-C(3)-C(2)	107.2(3)
C(3)-C(4)-C(5)	107.5(3)
N(1)-C(5)-C(6)	124.9(3)
N(1)-C(5)-C(4)	109.5(3)
C(6)-C(5)-C(4)	125.6(3)
C(5)-C(6)-C(7)	125.0(3)

C(5)-C(6)-C(11)	117.5(3)
C(7)-C(6)-C(11)	117.5(3)
N(2)-C(7)-C(6)	124.9(3)
N(2)-C(7)-C(8)	109.3(3)
C(6)-C(7)-C(8)	125.8(3)
C(9)-C(8)-C(7)	107.0(3)
C(8)-C(9)-C(10)	107.9(3)
N(2)-C(10)-C(1)#1	124.9(3)
N(2)-C(10)-C(9)	109.4(3)
C(1)#1-C(10)-C(9)	125.7(3)
C(12)-C(11)-C(16)	119.4(3)
C(12)-C(11)-C(6)	118.8(3)
C(16)-C(11)-C(6)	121.8(3)
C(11)-C(12)-C(13)	121.1(3)
C(14)-C(13)-C(12)	119.8(4)
C(15)-C(14)-C(13)	119.3(3)
C(14)-C(15)-C(16)	122.1(3)
C(11)-C(16)-C(15)	118.2(3)
C(11)-C(16)-C(17)	122.6(3)
C(15)-C(16)-C(17)	119.1(3)
O(1)-C(17)-C(16)	110.5(3)

Crystal data and structure refinement for 4-16 grown in CHCl₃

Empirical formula	C ₃₆ H ₂₈ N ₄ O ₂ Zn	
Formula weight	613.99	
Temperature	223(2) K	
Wavelength	0.71073 Å	
Crystal system	Monoclinic	
Space group	P2(1)/n	
Unit cell dimensions	a = 14.3395(11) Å	α = 90°
	b = 10.2698(8) Å	β = 99.468(2)°
	c = 19.7425(14) Å	γ = 90°
Volume	2867.8(4) Å ³	
Z	4	
Density (calculated)	1.422 Mg/m ³	

Absorption coefficient	0.898 mm ⁻¹
F(000)	1272
Crystal size	0.08 x 0.06 x 0.04 mm ³
Theta range for data collection	1.91 to 25.00 °
Index ranges	-12<=h<=17, -12<=k<=12, -23<=l<=23
Reflections collected	16389
Independent reflections	5043 [R(int) = 0.1086]
Completeness to theta = 25.00 °	99.9 %
Absorption correction	Sadabs, (Sheldrick 2001)
Max. and min. transmission	0.9650 and 0.9317
Refinement method	Full-matrix least-squares on F ²
Data / restraints / parameters	5043 / 0 / 390
Goodness-of-fit on F ²	0.982
Final R indices [I>2sigma(I)]	R1 = 0.0606, wR2 = 0.1053
R indices (all data)	R1 = 0.1187, wR2 = 0.1222
Largest diff. peak and hole	0.416 and -0.398 e.Å ⁻³

Selected bond lengths [Å] and angles [°] for 4-16 grown in CHCl₃

Zn(1)-N(2)	2.028(4)
Zn(1)-N(4)	2.041(4)
Zn(1)-N(1)	2.055(4)
Zn(1)-N(3)	2.058(4)
Zn(1)-O(1)#1	2.209(3)
N(1)-C(4)	1.374(5)
N(1)-C(1)	1.376(6)
N(2)-C(6)	1.364(5)
N(2)-C(9)	1.378(6)
N(3)-C(11)	1.364(6)
N(3)-C(14)	1.367(5)
N(4)-C(16)	1.371(5)
N(4)-C(19)	1.374(6)
O(1)-C(28)	1.427(5)
O(1)-C(27)	1.435(5)
O(1)-Zn(1)#1	2.209(3)
O(2)-C(36)	1.416(7)

O(2)-C(35)	1.421(6)
C(1)-C(20)	1.403(6)
C(1)-C(2)	1.444(6)
C(2)-C(3)	1.336(6)
C(3)-C(4)	1.430(6)
C(4)-C(5)	1.390(6)
C(5)-C(6)	1.400(6)
C(6)-C(7)	1.423(6)
C(7)-C(8)	1.345(6)
C(8)-C(9)	1.451(6)
C(9)-C(10)	1.409(6)
C(10)-C(11)	1.393(6)
C(10)-C(29)	1.505(6)
C(11)-C(12)	1.445(6)
C(12)-C(13)	1.343(6)
C(13)-C(14)	1.441(6)
C(14)-C(15)	1.382(6)
C(15)-C(16)	1.397(6)
C(16)-C(17)	1.441(6)
C(17)-C(18)	1.352(6)
C(18)-C(19)	1.438(6)
C(19)-C(20)	1.408(6)
C(20)-C(21)	1.500(6)
C(21)-C(26)	1.393(6)
C(21)-C(22)	1.397(6)
C(22)-C(23)	1.367(7)
C(23)-C(24)	1.376(7)
C(24)-C(25)	1.383(7)
C(25)-C(26)	1.403(6)
C(26)-C(27)	1.506(6)
C(29)-C(34)	1.386(6)
C(29)-C(30)	1.401(6)
C(30)-C(31)	1.382(7)
C(31)-C(32)	1.359(8)
C(32)-C(33)	1.377(7)
C(33)-C(34)	1.398(7)

C(34)-C(35)	1.517(7)
N(2)-Zn(1)-N(4)	170.36(15)
N(2)-Zn(1)-N(1)	90.41(14)
N(4)-Zn(1)-N(1)	88.79(15)
N(2)-Zn(1)-N(3)	88.52(15)
N(4)-Zn(1)-N(3)	90.50(14)
N(1)-Zn(1)-N(3)	169.42(15)
N(2)-Zn(1)-O(1)#1	93.17(14)
N(4)-Zn(1)-O(1)#1	96.47(13)
N(1)-Zn(1)-O(1)#1	95.84(14)
N(3)-Zn(1)-O(1)#1	94.72(14)
C(4)-N(1)-C(1)	106.4(4)
C(4)-N(1)-Zn(1)	125.9(3)
C(1)-N(1)-Zn(1)	126.8(3)
C(6)-N(2)-C(9)	105.6(4)
C(6)-N(2)-Zn(1)	126.2(3)
C(9)-N(2)-Zn(1)	127.5(3)
C(11)-N(3)-C(14)	107.1(4)
C(11)-N(3)-Zn(1)	127.5(3)
C(14)-N(3)-Zn(1)	125.4(3)
C(16)-N(4)-C(19)	106.2(4)
C(16)-N(4)-Zn(1)	126.2(3)
C(19)-N(4)-Zn(1)	127.5(3)
C(28)-O(1)-C(27)	111.8(4)
C(28)-O(1)-Zn(1)#1	117.3(3)
C(27)-O(1)-Zn(1)#1	121.3(3)
C(36)-O(2)-C(35)	112.9(5)
N(1)-C(1)-C(20)	125.4(4)
N(1)-C(1)-C(2)	109.0(4)
C(20)-C(1)-C(2)	125.7(4)
C(3)-C(2)-C(1)	107.4(4)
C(2)-C(3)-C(4)	107.6(4)
N(1)-C(4)-C(5)	124.2(4)
N(1)-C(4)-C(3)	109.6(4)
C(5)-C(4)-C(3)	126.2(4)

C(4)-C(5)-C(6)	127.4(4)
N(2)-C(6)-C(5)	125.0(4)
N(2)-C(6)-C(7)	110.8(4)
C(5)-C(6)-C(7)	124.2(4)
C(8)-C(7)-C(6)	107.5(4)
C(7)-C(8)-C(9)	106.4(4)
N(2)-C(9)-C(10)	124.8(4)
N(2)-C(9)-C(8)	109.7(4)
C(10)-C(9)-C(8)	125.5(4)
C(11)-C(10)-C(9)	124.9(4)
C(11)-C(10)-C(29)	117.4(4)
C(9)-C(10)-C(29)	117.5(4)
N(3)-C(11)-C(10)	125.5(4)
N(3)-C(11)-C(12)	109.2(4)
C(10)-C(11)-C(12)	125.3(5)
C(13)-C(12)-C(11)	107.2(4)
C(12)-C(13)-C(14)	107.2(4)
N(3)-C(14)-C(15)	125.4(4)
N(3)-C(14)-C(13)	109.3(4)
C(15)-C(14)-C(13)	125.3(4)
C(14)-C(15)-C(16)	127.6(4)
N(4)-C(16)-C(15)	124.5(4)
N(4)-C(16)-C(17)	109.9(4)
C(15)-C(16)-C(17)	125.6(4)
C(18)-C(17)-C(16)	107.0(4)
C(17)-C(18)-C(19)	107.1(4)
N(4)-C(19)-C(20)	125.4(4)
N(4)-C(19)-C(18)	109.9(4)
C(20)-C(19)-C(18)	124.7(4)
C(1)-C(20)-C(19)	124.8(4)
C(1)-C(20)-C(21)	118.0(4)
C(19)-C(20)-C(21)	117.3(4)
C(26)-C(21)-C(22)	118.1(5)
C(26)-C(21)-C(20)	121.8(4)
C(22)-C(21)-C(20)	120.1(4)
C(23)-C(22)-C(21)	121.7(5)

C(22)-C(23)-C(24)	120.3(5)
C(23)-C(24)-C(25)	119.6(5)
C(24)-C(25)-C(26)	120.3(5)
C(21)-C(26)-C(25)	119.9(5)
C(21)-C(26)-C(27)	122.5(4)
C(25)-C(26)-C(27)	117.4(4)
O(1)-C(27)-C(26)	112.6(4)
C(34)-C(29)-C(30)	119.9(5)
C(34)-C(29)-C(10)	122.6(4)
C(30)-C(29)-C(10)	117.5(4)
C(31)-C(30)-C(29)	119.9(5)
C(32)-C(31)-C(30)	120.6(6)
C(31)-C(32)-C(33)	119.8(6)
C(32)-C(33)-C(34)	121.4(6)
C(29)-C(34)-C(33)	118.3(5)
C(29)-C(34)-C(35)	121.6(5)
C(33)-C(34)-C(35)	120.1(5)
O(2)-C(35)-C(34)	112.9(5)

Crystal data and structure refinement for 4-16 grown in THF

Empirical formula	C ₄₄ H ₄₄ N ₄ O ₄ Zn	
Formula weight	758.20	
Temperature	295(2) K	
Wavelength	0.71073 Å	
Crystal system	Monoclinic	
Space group	P2(1)/c	
Unit cell dimensions	a = 17.8424(17) Å	α = 90°
	b = 18.7939(18) Å	β = 101.134(2)°
	c = 11.8706(11) Å	γ = 90°
Volume	3905.6(6) Å ³	
Z	4	
Density (calculated)	1.289 Mg/m ³	
Absorption coefficient	0.676 mm ⁻¹	
F(000)	1592	
Crystal size	0.60 x 0.44 x 0.08 mm ³	

Theta range for data collection	1.59 to 27.50 °
Index ranges	-20<=h<=23, -24<=k<=24, -15<=l<=15
Reflections collected	29735
Independent reflections	8969 [R(int) = 0.0493]
Completeness to theta = 27.50 °	99.9 %
Absorption correction	Sadabs, (Sheldrick 2001)
Max. and min. transmission	0.9479 and 0.6871
Refinement method	Full-matrix least-squares on F ²
Data / restraints / parameters	8969 / 13 / 493
Goodness-of-fit on F ²	1.030
Final R indices [I>2sigma(I)]	R1 = 0.0544, wR2 = 0.1449
R indices (all data)	R1 = 0.1012, wR2 = 0.1672
Largest diff. peak and hole	1.037 and -0.445 e.Å ⁻³

Selected bond lengths [Å] and angles [°] for 4-16 grown in THF

Zn(1)-N(3)	2.046(3)
Zn(1)-N(1)	2.047(2)
Zn(1)-N(4)	2.058(2)
Zn(1)-N(2)	2.059(3)
Zn(1)-O(1)	2.212(2)
N(1)-C(4)	1.362(4)
N(1)-C(1)	1.369(3)
N(2)-C(9)	1.373(4)
N(2)-C(6)	1.376(4)
N(3)-C(14)	1.358(4)
N(3)-C(11)	1.384(4)
N(4)-C(16)	1.354(4)
N(4)-C(19)	1.374(3)
O(1)-C(40)	1.422(4)
O(1)-C(37)	1.422(4)
C(1)-C(20)	1.406(4)
C(1)-C(2)	1.423(4)
C(2)-C(3)	1.347(4)
C(3)-C(4)	1.442(4)
C(4)-C(5)	1.398(4)

C(5)-C(6)	1.394(5)
C(5)-C(21)	1.494(5)
C(6)-C(7)	1.443(4)
C(7)-C(8)	1.328(5)
C(8)-C(9)	1.436(5)
C(9)-C(10)	1.374(5)
C(10)-C(11)	1.393(5)
C(11)-C(12)	1.418(5)
C(12)-C(13)	1.332(5)
C(13)-C(14)	1.458(4)
C(14)-C(15)	1.406(5)
C(15)-C(16)	1.407(4)
C(15)-C(27)	1.477(5)
C(16)-C(17)	1.452(4)
C(17)-C(18)	1.337(5)
C(18)-C(19)	1.427(4)
C(19)-C(20)	1.380(5)
C(21)-C(22)	1.374(6)
C(21)-C(26)	1.388(6)
C(22)-C(23)	1.389(7)
C(23)-C(24)	1.365(9)
C(24)-C(25)	1.377(9)
C(25)-C(26)	1.342(8)
C(26)-C(33)	1.499(7)
C(27)-C(28)	1.379(5)
C(27)-C(32)	1.400(6)
C(28)-C(29)	1.374(6)
C(29)-C(30)	1.359(7)
C(30)-C(31)	1.356(7)
C(31)-C(32)	1.383(7)
C(32)-C(35)	1.486(6)
C(37)-C(38)	1.507(6)
C(38)-C(39)	1.502(9)
C(39)-C(40)	1.495(6)
C(35)-O(3A)	1.300(8)
C(35)-O(3)	1.341(7)

O(3)-C(36)	1.386(10)
O(3A)-C(36A)	1.419(9)
C(33)-O(2)	1.307(8)
C(33)-O(2A)	1.307(9)
O(2)-C(34)	1.463(10)
O(1S)-C(1S)	1.364(9)
O(1S)-C(4S)	1.399(9)
C(1S)-C(2S)	1.464(9)
C(2S)-C(3S)	1.484(9)
C(3S)-C(4S)	1.494(9)
N(3)-Zn(1)-N(1)	166.48(9)
N(3)-Zn(1)-N(4)	88.40(10)
N(1)-Zn(1)-N(4)	90.50(9)
N(3)-Zn(1)-N(2)	90.02(11)
N(1)-Zn(1)-N(2)	88.01(10)
N(4)-Zn(1)-N(2)	166.92(9)
N(3)-Zn(1)-O(1)	97.44(9)
N(1)-Zn(1)-O(1)	96.09(8)
N(4)-Zn(1)-O(1)	95.03(9)
N(2)-Zn(1)-O(1)	98.06(9)
C(4)-N(1)-C(1)	106.5(2)
C(4)-N(1)-Zn(1)	127.61(18)
C(1)-N(1)-Zn(1)	125.6(2)
C(9)-N(2)-C(6)	106.7(3)
C(9)-N(2)-Zn(1)	125.1(2)
C(6)-N(2)-Zn(1)	127.9(2)
C(14)-N(3)-C(11)	106.8(3)
C(14)-N(3)-Zn(1)	127.5(2)
C(11)-N(3)-Zn(1)	125.4(2)
C(16)-N(4)-C(19)	107.1(2)
C(16)-N(4)-Zn(1)	127.43(19)
C(19)-N(4)-Zn(1)	125.2(2)
C(40)-O(1)-C(37)	103.6(3)
C(40)-O(1)-Zn(1)	120.3(2)
C(37)-O(1)-Zn(1)	120.4(2)
N(1)-C(1)-C(20)	124.3(3)

N(1)-C(1)-C(2)	109.9(3)
C(20)-C(1)-C(2)	125.7(3)
C(3)-C(2)-C(1)	107.3(3)
C(2)-C(3)-C(4)	106.9(3)
N(1)-C(4)-C(5)	126.1(3)
N(1)-C(4)-C(3)	109.4(3)
C(5)-C(4)-C(3)	124.5(3)
C(6)-C(5)-C(4)	124.8(3)
C(6)-C(5)-C(21)	117.4(3)
C(4)-C(5)-C(21)	117.9(3)
N(2)-C(6)-C(5)	125.0(3)
N(2)-C(6)-C(7)	108.8(3)
C(5)-C(6)-C(7)	126.2(4)
C(8)-C(7)-C(6)	107.6(3)
C(7)-C(8)-C(9)	107.8(3)
N(2)-C(9)-C(10)	125.3(3)
N(2)-C(9)-C(8)	109.1(3)
C(10)-C(9)-C(8)	125.5(3)
C(9)-C(10)-C(11)	127.6(3)
N(3)-C(11)-C(10)	124.5(3)
N(3)-C(11)-C(12)	109.0(3)
C(10)-C(11)-C(12)	126.4(3)
C(13)-C(12)-C(11)	108.5(3)
C(12)-C(13)-C(14)	106.7(3)
N(3)-C(14)-C(15)	126.4(3)
N(3)-C(14)-C(13)	108.9(3)
C(15)-C(14)-C(13)	124.6(3)
C(14)-C(15)-C(16)	123.6(3)
C(14)-C(15)-C(27)	118.0(3)
C(16)-C(15)-C(27)	118.4(3)
N(4)-C(16)-C(15)	126.1(3)
N(4)-C(16)-C(17)	108.9(3)
C(15)-C(16)-C(17)	125.0(3)
C(18)-C(17)-C(16)	107.2(3)
C(17)-C(18)-C(19)	107.4(3)
N(4)-C(19)-C(20)	124.7(3)

N(4)-C(19)-C(18)	109.4(3)
C(20)-C(19)-C(18)	125.9(3)
C(19)-C(20)-C(1)	128.2(3)
C(22)-C(21)-C(26)	119.4(4)
C(22)-C(21)-C(5)	118.6(4)
C(26)-C(21)-C(5)	122.0(4)
C(21)-C(22)-C(23)	120.4(5)
C(24)-C(23)-C(22)	119.7(6)
C(23)-C(24)-C(25)	118.7(6)
C(26)-C(25)-C(24)	122.7(6)
C(25)-C(26)-C(21)	119.1(5)
C(25)-C(26)-C(33)	120.7(5)
C(21)-C(26)-C(33)	120.2(4)
C(28)-C(27)-C(32)	118.0(4)
C(28)-C(27)-C(15)	119.1(3)
C(32)-C(27)-C(15)	122.9(3)
C(29)-C(28)-C(27)	121.8(4)
C(30)-C(29)-C(28)	119.5(5)
C(31)-C(30)-C(29)	120.2(5)
C(30)-C(31)-C(32)	121.4(5)
C(31)-C(32)-C(27)	119.1(4)
C(31)-C(32)-C(35)	120.1(4)
C(27)-C(32)-C(35)	120.9(4)
O(1)-C(37)-C(38)	105.2(4)
C(39)-C(38)-C(37)	104.3(4)
C(40)-C(39)-C(38)	103.9(4)
O(1)-C(40)-C(39)	106.0(4)
O(3A)-C(35)-O(3)	55.3(6)
O(3A)-C(35)-C(32)	115.8(7)
O(3)-C(35)-C(32)	111.0(5)
C(35)-O(3)-C(36)	115.7(8)
C(35)-O(3A)-C(36A)	115.1(12)
O(2)-C(33)-O(2A)	39.2(7)
O(2)-C(33)-C(26)	115.5(6)
O(2A)-C(33)-C(26)	117.3(7)
C(33)-O(2)-C(34)	110.7(7)

C(1S)-O(1S)-C(4S)	104.5(10)
O(1S)-C(1S)-C(2S)	103.9(10)
C(1S)-C(2S)-C(3S)	92.9(9)
C(2S)-C(3S)-C(4S)	88.1(9)
O(1S)-C(4S)-C(3S)	97.0(9)

Crystal data and structure refinement for 4-18

Empirical formula	C ₃₆ H ₂₆ Br ₂ N ₄ O ₂ Zn	
Formula weight	771.80	
Temperature	295(2) K	
Wavelength	0.71073 Å	
Crystal system	Monoclinic	
Space group	P2(1)/c	
Unit cell dimensions	a = 10.5664(15) Å	α = 90°
	b = 18.505(3) Å	β = 103.580(3)°
	c = 7.9175(11) Å	γ = 90°
Volume	1504.8(4) Å ³	
Z	2	
Density (calculated)	1.703 Mg/m ³	
Absorption coefficient	3.513 mm ⁻¹	
F(000)	772	
Crystal size	0.20 x 0.20 x 0.16 mm ³	
Theta range for data collection	1.98 to 27.50 °	
Index ranges	-13<=h<=13, -24<=k<=24, -10<=l<=10	
Reflections collected	19462	
Independent reflections	3455 [R(int) = 0.0241]	
Completeness to theta = 27.50 °	100.0 %	
Absorption correction	Sadabs, (Sheldrick 2001)	
Refinement method	Full-matrix least-squares on F ²	
Data / restraints / parameters	3455 / 0 / 206	
Goodness-of-fit on F ²	1.048	
Final R indices [I>2sigma(I)]	R1 = 0.0261, wR2 = 0.0666	
R indices (all data)	R1 = 0.0309, wR2 = 0.0689	
Largest diff. peak and hole	0.478 and -0.239 e.Å ⁻³	

Selected bond lengths [Å] and angles [°] for 4-18

Zn(1)-N(2)#1	2.0463(15)
Zn(1)-N(2)	2.0463(15)
Zn(1)-N(1)	2.0559(14)
Zn(1)-N(1)#1	2.0559(14)
Zn(1)-O(1)#2	2.4281(14)
Zn(1)-O(1)#3	2.4281(14)
Br(1)-C(10)	1.9054(17)
O(1)-C(18)	1.417(3)
O(1)-C(17)	1.426(2)
O(1)-Zn(1)#4	2.4281(14)
N(1)-C(4)	1.370(2)
N(1)-C(1)	1.371(2)
N(2)-C(6)	1.367(2)
N(2)-C(9)	1.372(2)
C(1)-C(10)	1.397(3)
C(1)-C(2)	1.443(3)
C(2)-C(3)	1.348(3)
C(3)-C(4)	1.442(3)
C(4)-C(5)	1.402(3)
C(5)-C(6)	1.403(3)
C(5)-C(11)	1.501(2)
C(6)-C(7)	1.445(3)
C(7)-C(8)	1.338(3)
C(8)-C(9)	1.441(3)
C(9)-C(10)#1	1.394(3)
C(10)-C(9)#1	1.394(3)
C(11)-C(16)	1.390(3)
C(11)-C(12)	1.395(3)
C(12)-C(13)	1.379(3)
C(13)-C(14)	1.376(4)
C(14)-C(15)	1.371(3)
C(15)-C(16)	1.398(3)
C(16)-C(17)	1.513(3)

N(2)#1-Zn(1)-N(2)	180.0
N(2)#1-Zn(1)-N(1)	89.50(6)
N(2)-Zn(1)-N(1)	90.50(6)
N(2)#1-Zn(1)-N(1)#1	90.50(6)
N(2)-Zn(1)-N(1)#1	89.50(6)
N(1)-Zn(1)-N(1)#1	180.00(8)
N(2)#1-Zn(1)-O(1)#2	88.11(6)
N(2)-Zn(1)-O(1)#2	91.89(6)
N(1)-Zn(1)-O(1)#2	92.36(6)
N(1)#1-Zn(1)-O(1)#2	87.64(6)
N(2)#1-Zn(1)-O(1)#3	91.89(6)
N(2)-Zn(1)-O(1)#3	88.11(6)
N(1)-Zn(1)-O(1)#3	87.64(6)
N(1)#1-Zn(1)-O(1)#3	92.36(6)
O(1)#2-Zn(1)-O(1)#3	180.0
C(18)-O(1)-C(17)	112.65(18)
C(18)-O(1)-Zn(1)#4	117.12(14)
C(17)-O(1)-Zn(1)#4	122.71(13)
C(4)-N(1)-C(1)	106.60(14)
C(4)-N(1)-Zn(1)	125.83(12)
C(1)-N(1)-Zn(1)	127.17(12)
C(6)-N(2)-C(9)	106.44(14)
C(6)-N(2)-Zn(1)	126.13(12)
C(9)-N(2)-Zn(1)	127.44(12)
N(1)-C(1)-C(10)	123.24(16)
N(1)-C(1)-C(2)	109.49(16)
C(10)-C(1)-C(2)	127.26(17)
C(3)-C(2)-C(1)	107.17(16)
C(2)-C(3)-C(4)	107.10(17)
N(1)-C(4)-C(5)	125.45(16)
N(1)-C(4)-C(3)	109.62(16)
C(5)-C(4)-C(3)	124.93(17)
C(4)-C(5)-C(6)	125.85(17)
C(4)-C(5)-C(11)	117.56(16)
C(6)-C(5)-C(11)	116.56(16)
N(2)-C(6)-C(5)	125.71(16)

N(2)-C(6)-C(7)	109.49(16)
C(5)-C(6)-C(7)	124.80(17)
C(8)-C(7)-C(6)	107.25(17)
C(7)-C(8)-C(9)	107.24(17)
N(2)-C(9)-C(10)#1	123.43(16)
N(2)-C(9)-C(8)	109.54(16)
C(10)#1-C(9)-C(8)	126.95(17)
C(9)#1-C(10)-C(1)	128.68(16)
C(9)#1-C(10)-Br(1)	115.41(13)
C(1)-C(10)-Br(1)	115.84(13)
C(16)-C(11)-C(12)	118.98(18)
C(16)-C(11)-C(5)	120.95(17)
C(12)-C(11)-C(5)	120.03(17)
C(13)-C(12)-C(11)	121.2(2)
C(14)-C(13)-C(12)	119.5(2)
C(15)-C(14)-C(13)	120.2(2)
C(14)-C(15)-C(16)	121.1(2)
C(11)-C(16)-C(15)	119.01(19)
C(11)-C(16)-C(17)	122.69(17)
C(15)-C(16)-C(17)	118.30(19)
O(1)-C(17)-C(16)	112.60(17)

Crystal data and structure refinement for 4-20

Empirical formula	C ₃₆ H ₂₈ BrN ₄ O ₂ Zn	
Formula weight	693.90	
Temperature	295(2) K	
Wavelength	0.71073 Å	
Crystal system	Monoclinic	
Space group	P2(1)/c	
Unit cell dimensions	a = 10.2123(8) Å	α = 90°
	b = 18.4943(15) Å	β = 104.387(2)°
	c = 8.0320(6) Å	γ = 90°
Volume	1469.4(2) Å ³	
Z	2	
Density (calculated)	1.568 Mg/m ³	

Absorption coefficient	2.237 mm ⁻¹
F(000)	706
Crystal size	0.20 x 0.10 x 0.10 mm ³
Theta range for data collection	2.06 to 25.00 °
Index ranges	-12<=h<=7, -21<=k<=21, -9<=l<=9
Reflections collected	8454
Independent reflections	2586 [R(int) = 0.0500]
Completeness to theta = 25.00 °	100.0 %
Absorption correction	Sadabs, (Sheldrick 2001)
Max. and min. transmission	0.8073 and 0.6632
Refinement method	Full-matrix least-squares on F ²
Data / restraints / parameters	2586 / 0 / 206
Goodness-of-fit on F ²	1.215
Final R indices [I>2sigma(I)]	R1 = 0.0588, wR2 = 0.1219
R indices (all data)	R1 = 0.0762, wR2 = 0.1268
Largest diff. peak and hole	0.358 and -0.530 e.Å ⁻³

Selected bond lengths [Å] and angles [°] for 4-20

Zn(1)-N(2)	2.047(4)
Zn(1)-N(2)#1	2.047(4)
Zn(1)-N(1)#1	2.058(4)
Zn(1)-N(1)	2.058(4)
Zn(1)-O(1)#2	2.417(3)
Zn(1)-O(1)#3	2.417(3)
Br(1)-C(5)	1.860(5)
N(1)-C(4)	1.365(6)
N(1)-C(1)	1.382(6)
N(2)-C(6)	1.358(6)
N(2)-C(9)	1.366(6)
O(1)-C(18)	1.415(6)
O(1)-C(17)	1.417(6)
O(1)-Zn(1)#4	2.417(3)
C(1)-C(10)#1	1.389(7)
C(1)-C(2)	1.450(7)
C(2)-C(3)	1.353(7)

C(3)-C(4)	1.427(7)
C(4)-C(5)	1.397(7)
C(5)-C(6)	1.397(7)
C(6)-C(7)	1.431(7)
C(7)-C(8)	1.339(8)
C(8)-C(9)	1.451(7)
C(9)-C(10)	1.412(7)
C(10)-C(1)#1	1.389(7)
C(10)-C(11)	1.495(7)
C(11)-C(12)	1.400(7)
C(11)-C(16)	1.406(7)
C(12)-C(13)	1.371(8)
C(13)-C(14)	1.369(8)
C(14)-C(15)	1.376(8)
C(15)-C(16)	1.386(7)
C(16)-C(17)	1.510(7)

N(2)-Zn(1)-N(2)#1	180.0(3)
N(2)-Zn(1)-N(1)#1	90.04(16)
N(2)#1-Zn(1)-N(1)#1	89.96(16)
N(2)-Zn(1)-N(1)	89.96(16)
N(2)#1-Zn(1)-N(1)	90.04(16)
N(1)#1-Zn(1)-N(1)	180.0(3)
N(2)-Zn(1)-O(1)#2	88.02(14)
N(2)#1-Zn(1)-O(1)#2	91.98(14)
N(1)#1-Zn(1)-O(1)#2	88.58(14)
N(1)-Zn(1)-O(1)#2	91.42(14)
N(2)-Zn(1)-O(1)#3	91.98(14)
N(2)#1-Zn(1)-O(1)#3	88.02(14)
N(1)#1-Zn(1)-O(1)#3	91.42(14)
N(1)-Zn(1)-O(1)#3	88.58(14)
O(1)#2-Zn(1)-O(1)#3	180.00(19)
C(4)-N(1)-C(1)	106.8(4)
C(4)-N(1)-Zn(1)	127.0(3)
C(1)-N(1)-Zn(1)	125.9(3)
C(6)-N(2)-C(9)	106.3(4)

C(6)-N(2)-Zn(1)	127.0(3)
C(9)-N(2)-Zn(1)	126.6(3)
C(18)-O(1)-C(17)	112.9(4)
C(18)-O(1)-Zn(1)#4	116.0(3)
C(17)-O(1)-Zn(1)#4	122.5(3)
N(1)-C(1)-C(10)#1	125.9(5)
N(1)-C(1)-C(2)	109.0(4)
C(10)#1-C(1)-C(2)	125.1(5)
C(3)-C(2)-C(1)	106.4(5)
C(2)-C(3)-C(4)	108.1(5)
N(1)-C(4)-C(5)	122.8(5)
N(1)-C(4)-C(3)	109.6(4)
C(5)-C(4)-C(3)	127.6(5)
C(6)-C(5)-C(4)	129.4(5)
C(6)-C(5)-Br(1)	112.9(4)
C(4)-C(5)-Br(1)	117.6(4)
N(2)-C(6)-C(5)	123.6(4)
N(2)-C(6)-C(7)	110.5(5)
C(5)-C(6)-C(7)	125.9(5)
C(8)-C(7)-C(6)	106.9(5)
C(7)-C(8)-C(9)	107.1(5)
N(2)-C(9)-C(10)	125.7(5)
N(2)-C(9)-C(8)	109.2(5)
C(10)-C(9)-C(8)	125.1(5)
C(1)#1-C(10)-C(9)	125.5(5)
C(1)#1-C(10)-C(11)	118.5(5)
C(9)-C(10)-C(11)	116.0(4)
C(12)-C(11)-C(16)	118.3(5)
C(12)-C(11)-C(10)	120.2(5)
C(16)-C(11)-C(10)	121.5(5)
C(13)-C(12)-C(11)	121.5(5)
C(14)-C(13)-C(12)	119.5(6)
C(13)-C(14)-C(15)	120.7(5)
C(14)-C(15)-C(16)	120.8(5)
C(15)-C(16)-C(11)	119.2(5)
C(15)-C(16)-C(17)	118.2(5)

C(11)-C(16)-C(17)	122.6(5)
O(1)-C(17)-C(16)	112.4(5)

Crystal data and structure refinement for 4-22 grown in CHCl₃/toluene

Empirical formula	C ₃₆ H ₂₆ Br ₂ N ₄ O ₂ Zn	
Formula weight	771.80	
Temperature	295(2) K	
Wavelength	0.71073 Å	
Crystal system	Triclinic	
Space group	P-1	
Unit cell dimensions	a = 11.636(3) Å	α = 61.526(4)°
	b = 12.421(3) Å	β = 83.202(4)°
	c = 12.520(3) Å	γ = 88.852(4)°
Volume	1578.1(6) Å ³	
Z	2	
Density (calculated)	1.624 Mg/m ³	
Absorption coefficient	3.350 mm ⁻¹	
F(000)	772	
Crystal size	0.26 x 0.06 x 0.06 mm ³	
Theta range for data collection	1.86 to 27.50 °	
Index ranges	-15 ≤ h ≤ 15, -16 ≤ k ≤ 16, -16 ≤ l ≤ 16	
Reflections collected	20559	
Independent reflections	7251 [R(int) = 0.1031]	
Completeness to theta = 27.50 °	99.9 %	
Absorption correction	Sadabs, (Sheldrick 2001)	
Max. and min. transmission	0.8243 and 0.4763	
Refinement method	Full-matrix least-squares on F ²	
Data / restraints / parameters	7251 / 0 / 408	
Goodness-of-fit on F ²	0.896	
Final R indices [I > 2σ(I)]	R1 = 0.0612, wR2 = 0.1291	
R indices (all data)	R1 = 0.1723, wR2 = 0.1583	
Largest diff. peak and hole	0.682 and -0.586 e.Å ⁻³	

Selected bond lengths [Å] and angles [°] for 4-22 grown in CHCl₃/toluene

Zn(1)-N(2)	2.039(5)
Zn(1)-N(1)	2.045(4)
Zn(1)-N(4)	2.048(5)
Zn(1)-N(3)	2.056(5)
Zn(1)-O(2)	2.252(4)
Br(1)-C(1)	1.911(5)
Br(2)-C(11)	1.908(6)
N(1)-C(5)	1.372(7)
N(1)-C(2)	1.380(7)
N(2)-C(7)	1.382(7)
N(2)-C(10)	1.385(7)
N(3)-C(15)	1.356(7)
N(3)-C(12)	1.377(7)
N(4)-C(20)	1.374(7)
N(4)-C(17)	1.375(7)
O(1)-C(28)	1.348(9)
O(1)-C(27)	1.399(9)
O(2)-C(29)	1.422(8)
O(2)-C(30)	1.426(7)
C(1)-C(2)	1.369(8)
C(1)-C(20)	1.402(8)
C(2)-C(3)	1.438(8)
C(3)-C(4)	1.342(9)
C(4)-C(5)	1.438(8)
C(5)-C(6)	1.388(8)
C(6)-C(7)	1.396(8)
C(6)-C(21)	1.501(8)
C(7)-C(8)	1.436(9)
C(8)-C(9)	1.344(9)
C(9)-C(10)	1.412(9)
C(10)-C(11)	1.403(8)
C(11)-C(12)	1.371(9)
C(12)-C(13)	1.440(8)
C(13)-C(14)	1.352(9)

C(14)-C(15)	1.443(8)
C(15)-C(16)	1.403(8)
C(16)-C(17)	1.404(8)
C(16)-C(32)#1	1.487(8)
C(17)-C(18)	1.422(8)
C(18)-C(19)	1.348(8)
C(19)-C(20)	1.425(8)
C(21)-C(22)	1.371(9)
C(21)-C(26)	1.388(9)
C(22)-C(23)	1.395(10)
C(23)-C(24)	1.360(10)
C(24)-C(25)	1.374(10)
C(25)-C(26)	1.379(9)
C(26)-C(27)	1.499(10)
C(30)-C(31)	1.504(8)
C(31)-C(36)	1.391(8)
C(31)-C(32)	1.396(8)
C(32)-C(33)	1.387(8)
C(32)-C(16)#1	1.487(8)
C(33)-C(34)	1.370(9)
C(34)-C(35)	1.386(9)
C(35)-C(36)	1.361(9)
N(2)-Zn(1)-N(1)	90.79(19)
N(2)-Zn(1)-N(4)	172.41(19)
N(1)-Zn(1)-N(4)	88.92(18)
N(2)-Zn(1)-N(3)	89.16(19)
N(1)-Zn(1)-N(3)	170.08(19)
N(4)-Zn(1)-N(3)	89.83(19)
N(2)-Zn(1)-O(2)	92.85(18)
N(1)-Zn(1)-O(2)	92.99(17)
N(4)-Zn(1)-O(2)	94.74(18)
N(3)-Zn(1)-O(2)	96.92(18)
C(5)-N(1)-C(2)	106.7(5)
C(5)-N(1)-Zn(1)	125.2(4)
C(2)-N(1)-Zn(1)	127.8(4)

C(7)-N(2)-C(10)	106.0(5)
C(7)-N(2)-Zn(1)	125.5(4)
C(10)-N(2)-Zn(1)	128.2(4)
C(15)-N(3)-C(12)	107.3(5)
C(15)-N(3)-Zn(1)	126.4(4)
C(12)-N(3)-Zn(1)	126.3(4)
C(20)-N(4)-C(17)	106.5(5)
C(20)-N(4)-Zn(1)	127.3(4)
C(17)-N(4)-Zn(1)	126.1(4)
C(28)-O(1)-C(27)	114.8(7)
C(29)-O(2)-C(30)	112.3(5)
C(29)-O(2)-Zn(1)	116.5(4)
C(30)-O(2)-Zn(1)	120.3(4)
C(2)-C(1)-C(20)	128.4(5)
C(2)-C(1)-Br(1)	116.5(4)
C(20)-C(1)-Br(1)	115.1(4)
C(1)-C(2)-N(1)	123.4(5)
C(1)-C(2)-C(3)	127.7(6)
N(1)-C(2)-C(3)	108.9(5)
C(4)-C(3)-C(2)	107.7(6)
C(3)-C(4)-C(5)	107.4(6)
N(1)-C(5)-C(6)	126.6(5)
N(1)-C(5)-C(4)	109.3(5)
C(6)-C(5)-C(4)	124.1(6)
C(5)-C(6)-C(7)	125.5(6)
C(5)-C(6)-C(21)	117.6(5)
C(7)-C(6)-C(21)	116.8(5)
N(2)-C(7)-C(6)	125.9(6)
N(2)-C(7)-C(8)	108.9(5)
C(6)-C(7)-C(8)	125.2(6)
C(9)-C(8)-C(7)	107.5(6)
C(8)-C(9)-C(10)	107.9(6)
N(2)-C(10)-C(11)	121.7(6)
N(2)-C(10)-C(9)	109.7(6)
C(11)-C(10)-C(9)	128.4(6)
C(12)-C(11)-C(10)	128.8(6)

C(12)-C(11)-Br(2)	116.6(5)
C(10)-C(11)-Br(2)	114.5(5)
C(11)-C(12)-N(3)	124.7(6)
C(11)-C(12)-C(13)	126.9(6)
N(3)-C(12)-C(13)	108.4(6)
C(14)-C(13)-C(12)	108.1(6)
C(13)-C(14)-C(15)	106.1(6)
N(3)-C(15)-C(16)	126.2(5)
N(3)-C(15)-C(14)	110.1(6)
C(16)-C(15)-C(14)	123.5(6)
C(15)-C(16)-C(17)	124.7(6)
C(15)-C(16)-C(32)#1	118.6(5)
C(17)-C(16)-C(32)#1	116.6(6)
N(4)-C(17)-C(16)	125.9(5)
N(4)-C(17)-C(18)	109.3(5)
C(16)-C(17)-C(18)	124.9(6)
C(19)-C(18)-C(17)	107.4(6)
C(18)-C(19)-C(20)	107.6(6)
N(4)-C(20)-C(1)	123.7(5)
N(4)-C(20)-C(19)	109.1(5)
C(1)-C(20)-C(19)	127.2(5)
C(22)-C(21)-C(26)	118.9(6)
C(22)-C(21)-C(6)	119.5(6)
C(26)-C(21)-C(6)	121.6(6)
C(21)-C(22)-C(23)	121.5(7)
C(24)-C(23)-C(22)	118.8(7)
C(23)-C(24)-C(25)	120.6(7)
C(24)-C(25)-C(26)	120.6(7)
C(25)-C(26)-C(21)	119.6(7)
C(25)-C(26)-C(27)	120.6(7)
C(21)-C(26)-C(27)	119.8(6)
O(1)-C(27)-C(26)	108.9(7)
O(2)-C(30)-C(31)	112.9(5)
C(36)-C(31)-C(32)	118.7(6)
C(36)-C(31)-C(30)	118.0(6)
C(32)-C(31)-C(30)	123.3(6)

C(33)-C(32)-C(31)	119.0(6)
C(33)-C(32)-C(16)#1	120.5(5)
C(31)-C(32)-C(16)#1	120.5(5)
C(34)-C(33)-C(32)	121.7(6)
C(33)-C(34)-C(35)	118.7(7)
C(36)-C(35)-C(34)	120.6(6)
C(35)-C(36)-C(31)	121.1(6)

Crystal data and structure refinement for 4-22 grown in THF

Empirical formula	C ₄₀ H ₃₄ Br ₂ N ₄ O ₃ Zn	
Formula weight	843.90	
Temperature	223(2) K	
Wavelength	0.71073 Å	
Crystal system	Monoclinic	
Space group	P2(1)/c	
Unit cell dimensions	a = 17.9019(8) Å	α = 90°
	b = 13.9986(6) Å	β = 111.3870(10)°
	c = 14.8998(6) Å	γ = 90°
Volume	3476.8(3) Å ³	
Z	4	
Density (calculated)	1.612 Mg/m ³	
Absorption coefficient	3.051 mm ⁻¹	
F(000)	1704	
Crystal size	0.50 x 0.50 x 0.10 mm ³	
Theta range for data collection	1.90 to 27.50 °	
Index ranges	-22<=h<=23, -10<=k<=18, -18<=l<=19	
Reflections collected	24329	
Independent reflections	7982 [R(int) = 0.0306]	
Completeness to theta = 27.50 °	99.9 %	
Absorption correction	Sadabs, (Sheldrick 2001)	
Max. and min. transmission	0.7501 and 0.3107	
Refinement method	Full-matrix least-squares on F ²	
Data / restraints / parameters	7982 / 0 / 453	
Goodness-of-fit on F ²	1.053	
Final R indices [I>2sigma(I)]	R1 = 0.0391, wR2 = 0.0966	

R indices (all data)
Largest diff. peak and hole

R1 = 0.0545, wR2 = 0.1025
1.060 and -0.565 e.Å⁻³

Selected bond lengths [Å] and angles [°] for 4-22 grown in THF

Zn(1)-N(1)	2.052(2)
Zn(1)-N(3)	2.058(2)
Zn(1)-N(4)	2.060(2)
Zn(1)-N(2)	2.061(2)
Zn(1)-O(3)	2.1611(19)
Br(1)-C(1)	1.903(2)
Br(2)-C(11)	1.903(2)
O(1)-C(27)	1.412(4)
O(1)-C(28)	1.413(5)
O(2)-C(36)	1.401(4)
O(2)-C(35)	1.422(3)
O(3)-C(40)	1.383(4)
O(3)-C(37)	1.398(4)
N(1)-C(2)	1.375(3)
N(1)-C(5)	1.377(3)
N(2)-C(10)	1.369(3)
N(2)-C(7)	1.369(3)
N(3)-C(15)	1.368(3)
N(3)-C(12)	1.377(3)
N(4)-C(17)	1.368(3)
N(4)-C(20)	1.373(3)
C(1)-C(20)	1.394(4)
C(1)-C(2)	1.395(4)
C(2)-C(3)	1.443(4)
C(3)-C(4)	1.342(4)
C(4)-C(5)	1.439(4)
C(5)-C(6)	1.398(4)
C(6)-C(7)	1.405(4)
C(6)-C(21)	1.494(4)
C(7)-C(8)	1.435(4)
C(8)-C(9)	1.350(4)

C(9)-C(10)	1.439(4)
C(10)-C(11)	1.395(4)
C(11)-C(12)	1.390(4)
C(12)-C(13)	1.439(4)
C(13)-C(14)	1.345(4)
C(14)-C(15)	1.439(4)
C(15)-C(16)	1.406(4)
C(16)-C(17)	1.398(4)
C(16)-C(29)	1.500(4)
C(17)-C(18)	1.442(4)
C(18)-C(19)	1.343(4)
C(19)-C(20)	1.441(4)
C(21)-C(22)	1.388(4)
C(21)-C(26)	1.400(4)
C(22)-C(23)	1.392(5)
C(23)-C(24)	1.364(5)
C(24)-C(25)	1.367(5)
C(25)-C(26)	1.387(4)
C(26)-C(27)	1.514(4)
C(29)-C(30)	1.384(4)
C(29)-C(34)	1.395(4)
C(30)-C(31)	1.380(4)
C(31)-C(32)	1.377(5)
C(32)-C(33)	1.359(5)
C(33)-C(34)	1.398(4)
C(34)-C(35)	1.506(4)
C(37)-C(38)	1.482(5)
C(38)-C(39)	1.481(6)
C(39)-C(40)	1.456(6)

N(1)-Zn(1)-N(3)	166.22(8)
N(1)-Zn(1)-N(4)	89.16(8)
N(3)-Zn(1)-N(4)	88.78(8)
N(1)-Zn(1)-N(2)	89.32(8)
N(3)-Zn(1)-N(2)	89.47(8)
N(4)-Zn(1)-N(2)	166.36(8)

N(1)-Zn(1)-O(3)	96.14(8)
N(3)-Zn(1)-O(3)	97.64(8)
N(4)-Zn(1)-O(3)	98.99(8)
N(2)-Zn(1)-O(3)	94.65(8)
C(27)-O(1)-C(28)	111.9(3)
C(36)-O(2)-C(35)	111.3(2)
C(40)-O(3)-C(37)	109.8(3)
C(40)-O(3)-Zn(1)	123.8(2)
C(37)-O(3)-Zn(1)	124.5(2)
C(2)-N(1)-C(5)	105.9(2)
C(2)-N(1)-Zn(1)	127.45(18)
C(5)-N(1)-Zn(1)	126.62(16)
C(10)-N(2)-C(7)	106.4(2)
C(10)-N(2)-Zn(1)	126.52(17)
C(7)-N(2)-Zn(1)	126.71(17)
C(15)-N(3)-C(12)	106.2(2)
C(15)-N(3)-Zn(1)	127.44(17)
C(12)-N(3)-Zn(1)	126.21(18)
C(17)-N(4)-C(20)	106.4(2)
C(17)-N(4)-Zn(1)	126.75(17)
C(20)-N(4)-Zn(1)	126.86(17)
C(20)-C(1)-C(2)	128.6(2)
C(20)-C(1)-Br(1)	115.62(19)
C(2)-C(1)-Br(1)	115.64(19)
N(1)-C(2)-C(1)	123.2(2)
N(1)-C(2)-C(3)	110.0(2)
C(1)-C(2)-C(3)	126.7(2)
C(4)-C(3)-C(2)	106.9(2)
C(3)-C(4)-C(5)	107.6(2)
N(1)-C(5)-C(6)	125.7(2)
N(1)-C(5)-C(4)	109.7(2)
C(6)-C(5)-C(4)	124.6(2)
C(5)-C(6)-C(7)	125.6(2)
C(5)-C(6)-C(21)	116.7(2)
C(7)-C(6)-C(21)	117.7(2)
N(2)-C(7)-C(6)	125.3(2)

N(2)-C(7)-C(8)	109.8(2)
C(6)-C(7)-C(8)	124.9(2)
C(9)-C(8)-C(7)	107.2(2)
C(8)-C(9)-C(10)	106.9(2)
N(2)-C(10)-C(11)	123.6(2)
N(2)-C(10)-C(9)	109.8(2)
C(11)-C(10)-C(9)	126.7(2)
C(12)-C(11)-C(10)	128.7(2)
C(12)-C(11)-Br(2)	115.26(19)
C(10)-C(11)-Br(2)	115.97(19)
N(3)-C(12)-C(11)	123.9(2)
N(3)-C(12)-C(13)	109.6(2)
C(11)-C(12)-C(13)	126.5(2)
C(14)-C(13)-C(12)	107.2(2)
C(13)-C(14)-C(15)	107.1(2)
N(3)-C(15)-C(16)	125.4(2)
N(3)-C(15)-C(14)	109.9(2)
C(16)-C(15)-C(14)	124.7(2)
C(17)-C(16)-C(15)	124.9(2)
C(17)-C(16)-C(29)	117.5(2)
C(15)-C(16)-C(29)	117.7(2)
N(4)-C(17)-C(16)	126.3(2)
N(4)-C(17)-C(18)	109.5(2)
C(16)-C(17)-C(18)	124.1(2)
C(19)-C(18)-C(17)	107.5(2)
C(18)-C(19)-C(20)	106.9(2)
N(4)-C(20)-C(1)	123.8(2)
N(4)-C(20)-C(19)	109.7(2)
C(1)-C(20)-C(19)	126.4(2)
C(22)-C(21)-C(26)	119.3(3)
C(22)-C(21)-C(6)	119.9(3)
C(26)-C(21)-C(6)	120.9(2)
C(21)-C(22)-C(23)	120.2(3)
C(24)-C(23)-C(22)	120.1(3)
C(23)-C(24)-C(25)	120.2(3)
C(24)-C(25)-C(26)	121.2(3)

C(25)-C(26)-C(21)	119.0(3)
C(25)-C(26)-C(27)	118.8(3)
C(21)-C(26)-C(27)	122.2(3)
O(1)-C(27)-C(26)	113.8(3)
C(30)-C(29)-C(34)	118.6(3)
C(30)-C(29)-C(16)	119.6(3)
C(34)-C(29)-C(16)	121.8(2)
C(31)-C(30)-C(29)	121.7(3)
C(32)-C(31)-C(30)	119.4(3)
C(33)-C(32)-C(31)	119.8(3)
C(32)-C(33)-C(34)	121.7(3)
C(29)-C(34)-C(33)	118.7(3)
C(29)-C(34)-C(35)	123.3(3)
C(33)-C(34)-C(35)	118.0(3)
O(2)-C(35)-C(34)	113.0(2)
O(3)-C(37)-C(38)	107.9(3)
C(39)-C(38)-C(37)	105.7(3)
C(40)-C(39)-C(38)	105.7(3)
O(3)-C(40)-C(39)	109.5(4)

Crystal data and structure refinement for 7-7 grown in CH₃I

Empirical formula	C ₁₃ H ₉ Br ₂ IN ₂	
Formula weight	479.94	
Temperature	223(2) K	
Wavelength	0.71073 Å	
Crystal system	Triclinic	
Space group	P-1	
Unit cell dimensions	a = 7.2912(7) Å	α = 103.731(2)°
	b = 10.0409(10) Å	β = 103.127(2)°
	c = 10.8935(11) Å	γ = 107.400(2)°
Volume	700.00(12) Å ³	
Z	2	
Density (calculated)	2.277 Mg/m ³	
Absorption coefficient	7.978 mm ⁻¹	
F(000)	448	

Crystal size	0.64 x 0.08 x 0.07 mm ³
Theta range for data collection	2.03 to 27.50 °
Index ranges	-9<=h<=9, -13<=k<=13, -14<=l<=14
Reflections collected	9116
Independent reflections	3219 [R(int) = 0.0233]
Completeness to theta = 27.50 °	99.9 %
Absorption correction	Sadabs, (Sheldrick 2001)
Max. and min. transmission	0.6051 and 0.0800
Refinement method	Full-matrix least-squares on F ²
Data / restraints / parameters	3219 / 0 / 164
Goodness-of-fit on F ²	1.078
Final R indices [I>2sigma(I)]	R1 = 0.0217, wR2 = 0.0540
R indices (all data)	R1 = 0.0243, wR2 = 0.0551
Largest diff. peak and hole	0.927 and -0.458 e.Å ⁻³

Selected bond lengths [Å] and angles [°] for 7-7 grown in CH₃I

Br(1)-C(3)	1.898(2)
Br(2)-C(10)	1.903(2)
N(1)-N(2)	1.294(3)
N(1)-C(1)	1.379(3)
N(1)-C(13)	1.476(3)
N(2)-C(12)	1.359(3)
C(1)-C(6)	1.410(3)
C(1)-C(2)	1.416(3)
C(2)-C(3)	1.353(4)
C(3)-C(4)	1.398(4)
C(4)-C(5)	1.363(4)
C(5)-C(6)	1.415(3)
C(6)-C(7)	1.427(3)
C(7)-C(8)	1.410(3)
C(7)-C(12)	1.416(3)
C(8)-C(9)	1.368(3)
C(9)-C(10)	1.408(4)
C(10)-C(11)	1.359(3)
C(11)-C(12)	1.422(3)

N(2)-N(1)-C(1)	124.90(19)
N(2)-N(1)-C(13)	114.32(19)
C(1)-N(1)-C(13)	120.78(19)
N(1)-N(2)-C(12)	118.08(19)
N(1)-C(1)-C(6)	118.9(2)
N(1)-C(1)-C(2)	120.2(2)
C(6)-C(1)-C(2)	120.9(2)
C(3)-C(2)-C(1)	118.0(2)
C(2)-C(3)-C(4)	122.5(2)
C(2)-C(3)-Br(1)	117.74(19)
C(4)-C(3)-Br(1)	119.72(19)
C(5)-C(4)-C(3)	120.0(2)
C(4)-C(5)-C(6)	120.4(2)
C(1)-C(6)-C(5)	118.2(2)
C(1)-C(6)-C(7)	118.0(2)
C(5)-C(6)-C(7)	123.8(2)
C(8)-C(7)-C(12)	118.2(2)
C(8)-C(7)-C(6)	125.2(2)
C(12)-C(7)-C(6)	116.6(2)
C(9)-C(8)-C(7)	120.3(2)
C(8)-C(9)-C(10)	120.5(2)
C(11)-C(10)-C(9)	121.9(2)
C(11)-C(10)-Br(2)	119.9(2)
C(9)-C(10)-Br(2)	118.22(18)
C(10)-C(11)-C(12)	118.0(2)
N(2)-C(12)-C(7)	123.4(2)
N(2)-C(12)-C(11)	115.4(2)
C(7)-C(12)-C(11)	121.2(2)